

Two new species of the mealybug genus *Paracoccus* from Jiangxi, South China (Hemiptera, Coccoomorpha, Pseudococcidae)

Jiang-tao Zhang^{1,2}, Chao-qun Li^{1,2}, Xing-ping Liu^{1,2}, Yan Wang^{1,2}

¹ Key Laboratory of National Forestry and Grassland Administration on Forest Ecosystem Protection and Restoration of Poyang Lake Watershed, College of Forestry, Jiangxi Agricultural University, Nanchang, 330045, China

² College of Forestry, Jiangxi Agricultural University, Nanchang, 330045, China

Corresponding author: Jiang-tao Zhang (jiang_tao_zhang@163.com)

Abstract

Two new mealybug species, *Paracoccus gillianwatsonae* Zhang, **sp. nov.** and *P. wui* Zhang, **sp. nov.**, collected from Jiangxi, South China, are described and illustrated based on the morphology of adult females. *Paracoccus gillianwatsonae* is similar to *P. burnerae* (Brain, 1915), but it differs in having fewer pairs of cerarii, and in lacking both ventral oral collar tubular ducts on the margins of the head and translucent pores on the hind femur. *Paracoccus wui* resembles *P. keralae* Williams, 2004 and *P. neocarens* (Lit, 1992), but it differs in lacking ventral oral collar tubular ducts on the margins of the head and in having multilocular disc-pores usually in double rows at the posterior edges of abdominal segments V and VI. A key to the *Paracoccus* species found in China is provided.

Key words: *Dalbergia hupeana*, key, *Pinus massoniana*, Sternorrhyncha, taxonomy



Academic editor: Takumasa Kondo

Received: 14 January 2024

Accepted: 27 February 2024

Published: 3 April 2024

ZooBank: <https://zoobank.org/A40A2566-3C7F-49CE-8F9A-780874DDB782>

Citation: Zhang J-t, Li C-q, Liu X-p, Wang Y (2024) Two new species of the mealybug genus *Paracoccus* from Jiangxi, South China (Hemiptera, Coccoomorpha, Pseudococcidae). ZooKeys 1197: 1–11. <https://doi.org/10.3897/zookeys.1197.118778>

Copyright: © Jiang-tao Zhang et al. This is an open access article distributed under terms of the Creative Commons Attribution License ([Attribution 4.0 International – CC BY 4.0](https://creativecommons.org/licenses/by/4.0/)).

Introduction

Members of the family Pseudococcidae (commonly known as mealybugs) are small sap-sucking insects. The Pseudococcidae is the second-largest family of scale insects, with about 2047 described species in 261 genera worldwide (García Morales et al. 2016). The mealybug genus *Paracoccus* was established by Ezzat and McConnell (1956) with *Pseudococcus burnerae* Brain, 1915 designated as the type species. Currently, the genus includes 94 species (García Morales et al. 2016) and has a wide distribution in temperate and tropical parts of the world (Moghaddam and Esfandiari 2014). However, molecular phylogenetic analyses by Hardy et al. (2008) and Choi and Lee (2022) have indicated that *Paracoccus* is not monophyletic. Further molecular and morphological studies on this genus are greatly needed.

In China, Chen et al. (2011) first reported the invasive *Paracoccus marginatus* Williams & Granara de Willink, 1992 from Taiwan; later, this species was found in many places in mainland China, e.g. Fujian (Lin et al. 2019), Guangdong (Ahmed et al. 2015), Hainan (Wang et al. 2018), Jiangxi (Liao et al. 2021), and Yunnan (Wu et al. 2014; Zhang and Wu 2015). In addition, Miller et al. (2014)

reported that three *Paracoccus* species originating from China had been intercepted at U.S. ports of entry between 1995 and 2012: *P. burnerae*, *P. interceptus* Lit, 1997, and *P. marginatus*. Together with the two new species described herein, there are now five *Paracoccus* species reported from China.

In this study, *Paracoccus gillianwatsonae* and *P. wui*, both collected from Jiangxi, South China, are described and illustrated based on the morphology of adult females. A key to the species of *Paracoccus* reported from China is provided.

Materials and methods

Adult female specimens were slide-mounted using the method described by Borchsenius (1950). The morphological terminology used follows that of Williams (2004). Body measurements are given in millimeters (mm) and measurements of other structures are given in micrometers (μm). Each taxonomic illustration of the adult female is arranged in the usual way for Coccoomorpha, with features of the dorsum shown on the left side and those of the venter on the right. Enlargements of some important characters, not drawn to scale, are arranged around the main illustration. The letters and abbreviations used on the illustrations are explained in the legend below each illustration.

Slides of the new species are deposited in the College of Forestry, Jiangxi Agricultural University, Nanchang, China (**CFJAU**) and the Insect Collection of the Southwest Forestry University, Yunnan, China (**SWFU**). The slide labels are written in Chinese. Under 'Materials examined', the collection data of each holotype is listed with '/' indicating the positions of the line breaks on the labels.

Taxonomy

Genus *Paracoccus* Ezzat & McConnell, 1956

Paracoccus Ezzat and McConnell 1956: 37. Type species: *Pseudococcus burnerae* Brain, by original designation.

Gossypina Salazar 1972: 293. Type species: *Gossypina glauca* Salazar, by monotypy and original designation. Synonymized by Williams and Granara de Willink 1992: 292.

Diagnosis. (adapted and slightly modified from Williams 2004): body of adult female usually broadly oval. Anal lobes usually developed, each with a partial or complete ventral anal lobe bar extending from either apical seta or from bar seta. Antennae each normally 8-segmented. Legs well developed, claw without a denticle; tarsal digitules knobbed; translucent pores usually present on hind coxa and tibia. Cerarii numbering as many as 18 pairs, each cerarius bearing 2 conical setae, except some on head and thorax each with 3 or 4 setae; auxiliary setae usually absent except in anal lobe cerarii. Circulus present or absent. Anterior and posterior ostioles present. Anal ring normally with 6 setae. Oral rim tubular ducts present on dorsum and sometimes on venter. Oral collar tubular ducts present. Multilocular disc-pores present, at least on venter. Trilocular pores present.

***Paracoccus gillianwatsonae* Zhang, sp. nov.**

<https://zoobank.org/E9FB2EE0-028A-4C6A-96B0-D23596F5EC01>

Figs 1, 2

Materials examined. Holotype: 1 ♀ (mounted singly on a slide), CHINA, Jiangxi, Yichun City, Fengxin County, Chi'an Town [28°39'55"N, 115°21'9"E] / on the needles of *Pinus massoniana* Lamb. (Pinaceae) / 22.ix.2022, coll. Jiang-tao Zhang (CFJAU). **Paratypes:** 4 ♀♀ (mounted singly on 4 slides), same data as holotype (3 CFJAU, 1 SWFU).

Etymology. The species is named after Dr Gillian W. Watson (Department of Life Sciences, the Natural History Museum, London, U.K.), who has selflessly helped the first author.

Description. Live adult female (Fig. 1). Body elongate-oval, covered with thin, pale grey, mealy wax and with short, white lateral filaments around posterior body margins; these becoming successively longer on posteriormost four segments, with caudal filaments longest, each about 1/3 as long as maximum body width.

Slide-mounted adult female (Fig. 2, $n = 5$). Body elongate-oval, 1.4–1.8 mm long and 0.8–1.0 mm wide. Anal lobes moderately developed, dorsal surface of each lobe with a small, slightly sclerotized area; ventral surface with long apical seta, each 180–200 μm long, and anal lobe bar present forwards from apical seta. Antennae each usually with 8 segments, sometimes with segments IV and V combined; each antenna 322–360 μm long, length of segments (in μm): I 35.0–37.5, II 42.5–47.5, III 42.5–50.0, IV 25.0–30.0, V 22.5–30.0, VI 30.0–37.5, VII 35.0–40.0 and VIII 85.0–95.0. Eye spot located on body margin lateral to antennal base. Clypeolabral shield 150–163 μm long and 120–140 μm wide. Labium 130–148 μm long and 80–95 μm wide, 0.87–0.98 times as long as clypeolabral shield. Legs well developed; claw stout, without a denticle; both tarsal digitules and claw digitules apically knobbed, longer than claw; with translucent pores present on hind coxa and tibia (Fig. 2D, E). Hind leg measurements (in μm): coxa 55–65, trochanter + femur 227–245, tibia + tarsus 242–278, claw 20.0–22.5. Ratio of lengths of hind tibia + tarsus to trochanter + femur 1: 1.10–1.19, ratio of lengths of hind tibia to tarsus 1: 1.67–1.85. Circulus nearly quadrate, 50–75 μm long and 65–85 μm wide, situated between abdominal segments III and IV, divided by an intersegmental line. Anterior and posterior ostioles present, each lip with 7–12 trilocular pores and 0–4 setae. Anal ring 65–80 μm wide, bearing 6 long setae, each seta 112–130 μm long. Cerarii usually numbering 6 or 7 pairs on abdomen, sometimes also with 1 pair present on thorax and 1 pair present on head. Anal lobe cerarii (C_{18}) (Fig. 2H) each bearing 2 conical setae, each seta 15–17 μm long and 6–7 μm wide at base, with 1 or 2 auxiliary setae and 10–12 trilocular pores, all situated on a small slightly sclerotized area. Other cerarii each containing 2 conical setae and 3–5 trilocular pores. Cerarii C_{12} , if present, usually each containing only 1 conical seta and 1 short seta. Cerarii on thorax, if present, usually each containing 2 slender conical setae. On head, usually the ocular cerarii (C_3) present, each containing 3 or 4 slender setae. Discoidal pores (Fig. 2C), each narrower than a trilocular pore, scattered on dorsum and venter.

Dorsum. Setae (Fig. 2I) short, stiff, sometimes spine-like, mostly each 20.0–32.5 μm long, accompanied by shorter setae, each 7.5–15.0 μm long; setal



Figure 1. Live adult female of *Paracoccus gillianwatsonae* Zhang, sp. nov. on a needle of *Pinus massoniana* Lamb. (Pinaceae).

bases not closely associated with trilocular pores. Trilocular pores (Fig. 2B), each 3.0–3.5 μm wide, evenly distributed. Oral rim tubular ducts (Fig. 2J) present, numbering 11–24 in total, each duct 11–12 μm long and about 4 μm wide, with rim 8–9 μm in diameter, usually present singly near margins of head, thorax, and close to cerarii on posterior abdominal segments, and others usually present in medial or submedial areas of thorax and abdominal segments II and III, or only on abdominal segment II.

Venter. Setae relatively long and flagellate, longest setae present on medial area of head and posterior abdominal segments, each 62.5–125.0 μm long, accompanied by shorter setae, each 20.0–32.5 μm long. Cisanal setae each 50–55 μm long; obanal setae each 45–50 μm long. Trilocular pores similar to those on dorsum, evenly distributed. Multilocular disc-pores (Fig. 2G), each 7–8 μm in diameter, present around vulva in more-or-less single rows at posterior edges of abdominal segments IV–VII, and scattered or in rows at anterior edges of abdominal segments VI–VII, sometimes with 2 pores on abdominal segment III; also sparsely present on margins of posterior abdominal segments, and occasionally in submedial areas of thorax. Oral collar tubular ducts of 2 main sizes present: larger type (Fig. 2A), each 6–7 μm long and about 3.5 μm wide, present on medial areas of abdominal segments III–VII, in marginal groups on all abdominal segments and opposite each anterior coxa; and smaller type (Fig. 2F), each 5–6 μm long and 2.0–2.5 μm wide, present on medial areas of abdominal segments III–VII, also sparsely present in marginal areas together with large ducts, and occasionally present in medial areas of thorax.

Host plant. Pinaceae: *Pinus massoniana* Lamb.

Distribution. China (Jiangxi).

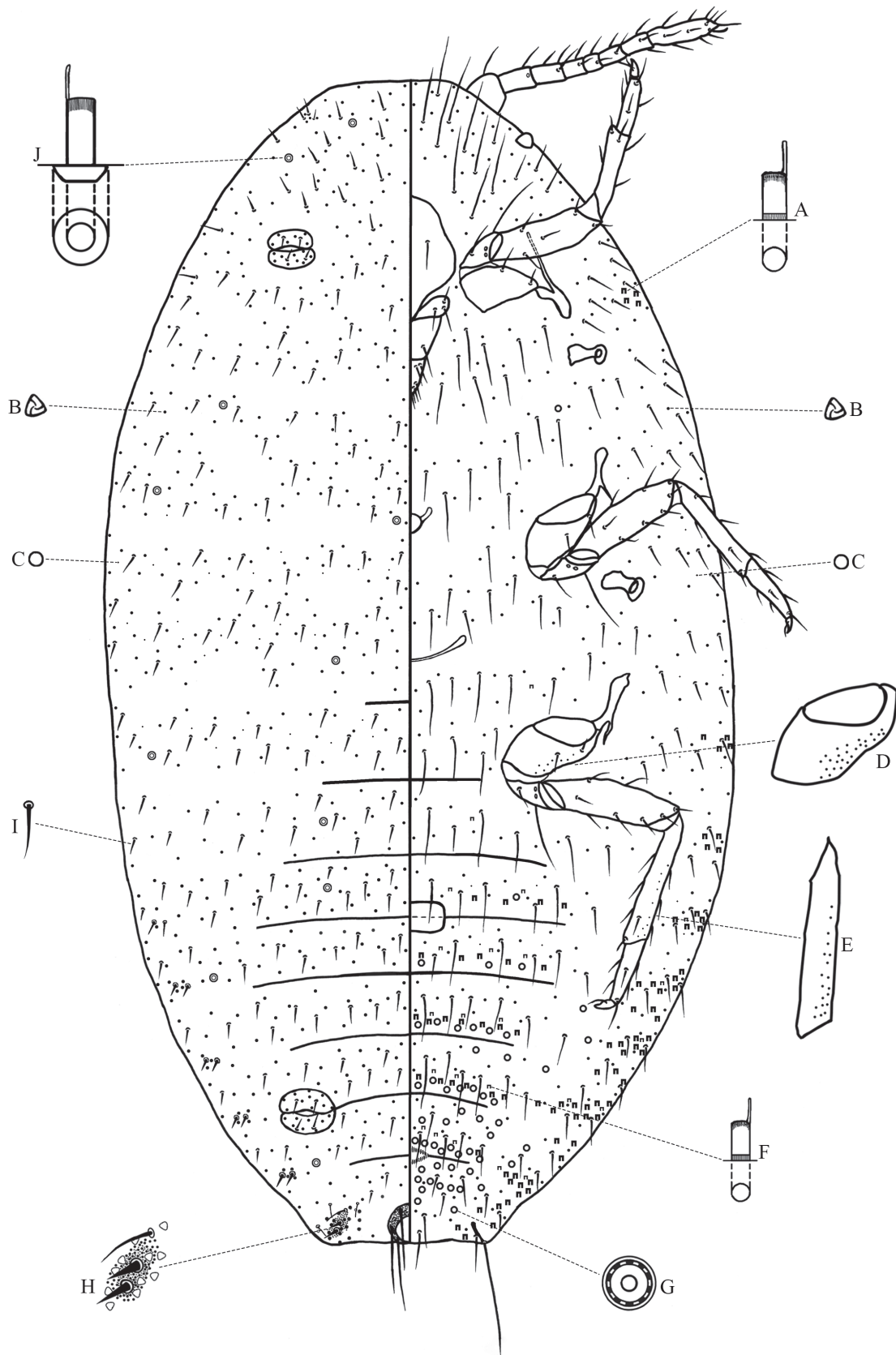


Figure 2. Adult female of *Paracoccus gillianwatsonae* Zhang, sp. nov. **A** large-type oral collar tubular duct **B** trilocular pore **C** discoidal pore **D** hind coxa **E** hind tibia **F** small-type oral collar tubular duct **G** multilocular disc-pore **H** anal lobe cerarius (C_{18}) **I** dorsal seta **J** oral rim tubular duct.

Remarks. *Paracoccus gillianwatsonae* sp. nov. is similar to *P. burnerae* (Brain, 1915) (morphological characteristics of *P. burnerae* based on the redescription and illustration by Williams (2004)) in having ventral multilocular disc-pores in single rows at the posterior edges of abdominal segments IV and V; it differs from the latter (character states of *P. burnerae* given in parentheses) by having: (i) ventral oral collar tubular ducts absent from margins of the head (present); (ii) cerarii numbering fewer than 18 pairs (18 pairs); and (iii) translucent pores absent from hind femur (present).

***Paracoccus wui* Zhang, sp. nov.**

<https://zoobank.org/150B72B5-4F10-4795-9FC4-C67A338FE302>

Figs 3, 4

Materials examined. Holotype: 1 ♀ (mounted singly on a slide), CHINA, Jiangxi, Lushan National Nature Reserve [29°33'N, 115°57'E] / under bark crack of *Dalbergia hupeana* Hance (Fabaceae) / 14.ix.2021, coll. Jiang-tao Zhang (CFJAU). **Paratypes:** 8 ♀♀ (mounted singly on 8 slides), same data as holotype (6 CFJAU, 2 SWFU).

Etymology. The species is named after Dr San-an Wu (Beijing Forestry University, Beijing, China), who has made important contributions to the study of Chinese scale insects and has selflessly helped the first author.

Description. Live adult female (Fig. 3). Body of mature adult female elongate-oval, covered with white, mealy wax; posterior of body with a short, white ovisac formed of tangled wax filaments.

Slide-mounted adult female (Fig. 4, $n = 5$). Body elongate-oval to broadly oval, 2.8–3.4 mm long and 1.9–2.5 mm wide. Anal lobes moderately developed, dorsal surface of each lobe with a small, slightly sclerotized area; ventral surface with long apical seta, each seta 225–240 μm long, and anal lobe bar present forwards from apical seta. Antennae each 355–458 μm long with 8 segments, length of segments (in μm): I 42.5–55.0, II 50.0–62.5, III 47.5–62.5, IV 25–35, V 27.5–50.0, VI 30.0–37.5, VII 37.5–50.0 and VIII 87.5–110.0. Eye spot located on body margin lateral to antennal base. Clypeolabral shield 163–213 μm long and 150–195 μm wide. Labium 178–225 μm long and 87.5–100.0 μm wide, 1.03–1.18 times as long as clypeolabral shield. Legs well developed; claw stout, without a denticle; both tarsal digitules and claw digitules apically knobbed, longer than claw; with translucent pores present on anterior and posterior surfaces of hind coxa (Fig. 4E) and on posterior surface of hind tibia (Fig. 4F). Hind leg measurements (in μm): coxa 80–113, trochanter + femur 275–378, tibia + tarsus 283–360, claw 27.5–32.5. Ratio of lengths of hind tibia + tarsus to trochanter + femur 1: 0.95–1.04, ratio of lengths of hind tibia to tarsus 1: 1.78–2.35. Circulus nearly quadrate, 115–145 μm long and 125–188 μm wide, situated between abdominal segments III and IV, divided by an intersegmental line. Anterior and posterior ostioles present, each lip with some trilobular pores and 1–5 setae. Anal ring 87.5–112.5 μm wide, bearing 6 long setae, each 120–145 μm long; occasionally 2 short setae present between long setae. Cerarii numbering 5–8 recognisable pairs on abdomen, sometimes also possibly 1–3 pairs discernible on thorax and head. Anal lobe cerarii (Fig. 4I) each containing 2 conical setae, each seta 16–20 μm long and 7–8 μm wide at base, 2–5 auxiliary setae and 22–26 trilobular pores, all situated on a small



Figure 3. Live adult female of *Paracoccus wui* Zhang, sp. nov. in bark crack of *Dalbergia hupeana* Hance (Fabaceae).

slightly sclerotized area. Anterior abdominal cerarii (Fig. 4J) each usually containing 2 smaller conical setae, 4–8 trilocular pores, and sometimes with small slightly sclerotized at setal bases; the setae in anterior abdominal cerarii sometimes widely spaced, or each reduced to only 1 conical seta, or replaced by 1 or 2 stout setae. Cerarii on thorax and head difficult to recognize because some marginal dorsal setae sometimes associated with 2–4 trilocular pores near setal bases, which can be confused with a cerarius; if cerarii present, each often with a pair of stout setae similar to those on dorsum, but recognisable as cerarius by a small concentration of trilocular pores, and sometimes the ocular cerarii (C_3) present, each with 3 or 4 slender setae. Discoidal pores (Fig. 4D) of varying sizes, with larger pores each usually wider than a trilocular pore (in one paratype most larger pores about same diameter as a trilocular pore and only a few pores wider than a trilocular pore), scattered on dorsum and venter.

Dorsum. Setae (Fig. 4K) stout with flagellate tips, sometimes bifurcate; larger setae, each 42.5–62.5 μm long and sometimes with 1 or 2 trilocular pores near setal base, and shorter setae, each 17.5–37.5 μm long. Trilocular pores (Fig. 4C), each 3–4 μm wide, evenly distributed. Multilocular disc-pores absent. Oral rim tubular ducts (Fig. 4L) very few, totaling 1–8 in available specimens, each about 9 μm long and 4–5 μm wide, with rim 8–9 μm in diameter, mainly present medially, submedially or submarginally on thorax and anterior abdominal segments, sometimes singly next to abdominal cerarii C_{11} , C_{15} and C_{17} , ducts usually absent from medially and submedially areas of abdominal segments IV–VIII. Oral collar tubular ducts usually absent from dorsum, occasionally 1 type of duct, similar to large type of oral collar tubular ducts on venter, singly present marginally or submarginally on thorax, or abdominal segment I, or abdominal segment IV.

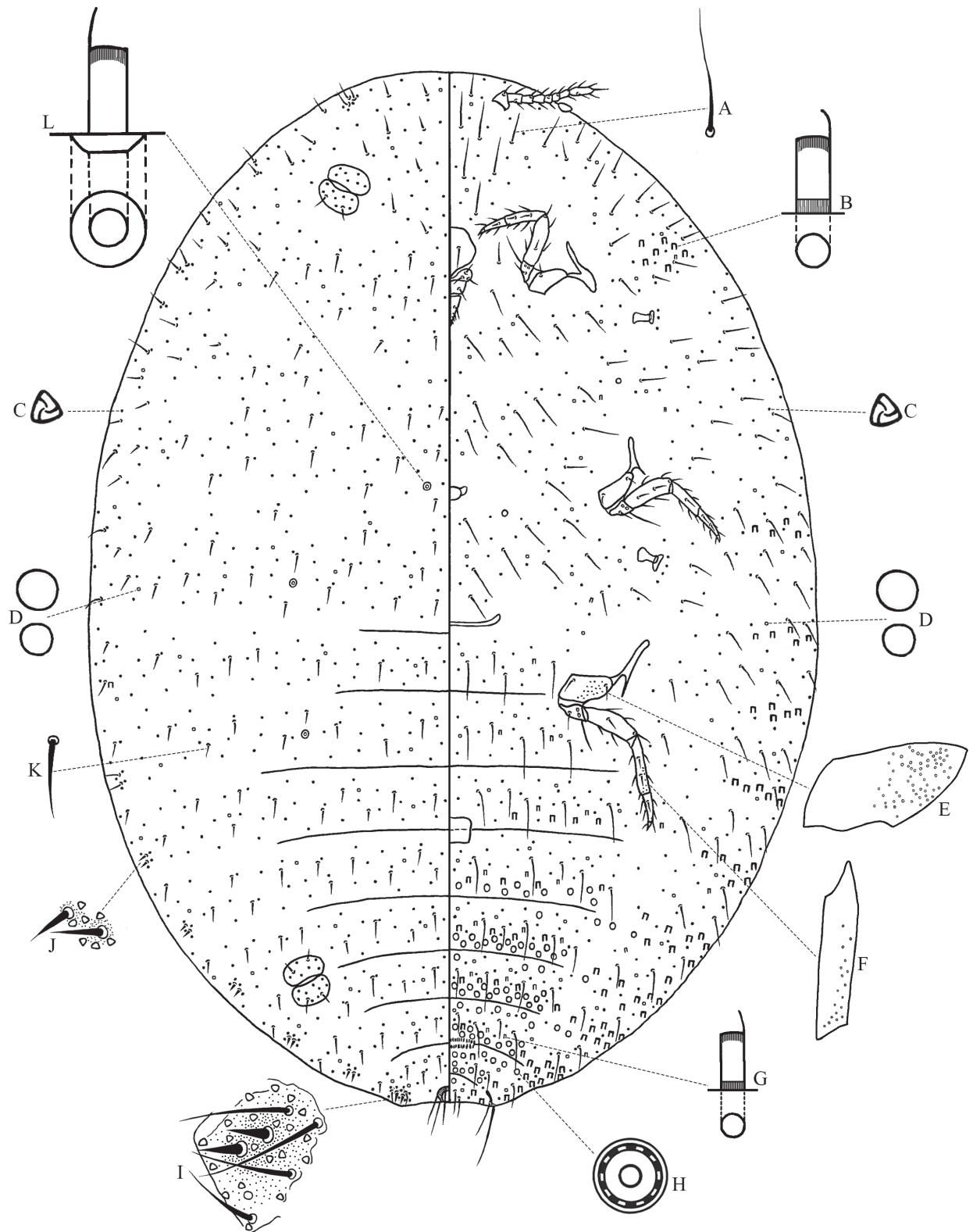


Figure 4. Adult female of *Paracoccus wui* Zhang, sp. nov. **A** ventral seta **B** large-type oral collar tubular duct **C** trilocular pore **D** discoidal pores **E** hind coxa **F** hind tibia **G** small-type oral collar tubular duct **H** multilocular disc-pore **I** anal lobe cerarius (C_{18}) **J** cerarius on abdomen **K** dorsal seta **L** oral rim tubular duct.

Venter. Setae (Fig. 4A) relatively long and flagellate, longest setae present on medial area of head and posterior abdominal segments, each 100–138 μm long, and shorter setae, each 30.0–62.5 μm long. Cisanal setae each 100–113 μm

long; obanal setae each 95–105 µm long. Trilocular pores similar to those on dorsum, evenly distributed. Multilocular disc-pores (Fig. 4H), each 7–8 µm in diameter, present around vulva, usually in double rows at posterior edges of abdominal segments V–VII, and in single or double rows at the posterior edge of abdominal segment IV; others distributed at anterior edges of abdominal segments V–VII; in addition, a few pores located on submargins of abdominal segments and sometimes also present on abdominal segment III; also scattered pores present on medial and submedial areas of thorax. Oral collar tubular ducts of 2 main sizes present: larger type (Fig. 4B), each about 8 µm long and 3.5–4.0 µm wide, present mainly on medial areas of abdominal segments III–VII, in marginal groups on thorax and abdomen, also opposite each anterior coxa; and smaller type (Fig. 4G), each about 6 µm long and 2.5–3.0 µm wide, present mainly on medial areas of abdominal segments II–VII, also sparsely present in marginal areas together with large ducts, and occasionally in medial areas of thorax.

Host plant. Fabaceae: *Dalbergia hupeana* Hance.

Distribution. China (Jiangxi).

Remarks. *Paracoccus wui* sp. nov. is similar to *P. keralae* Williams, 2004 in having only a few dorsal oral rim tubular ducts; it differs from the latter (character states of *P. keralae* given in parentheses) by having: (i) ventral oral collar tubular ducts absent from margins of the head (present); (ii) multilocular disc-pores usually in double rows at posterior edges of abdominal segments V and VI (in single rows); and (iii) larger discoidal pores usually each wider than a trilocular pore (narrower than a trilocular pore).

Paracoccus wui also resembles *P. neocarens* (Lit, 1992) (based on the redescription and illustration by Williams (2004)) in possessing some large discoidal pores and a reduced number of dorsal oral rim tubular ducts; it differs from the latter (character states of *P. neocarens* in parentheses) in having: (i) ventral oral collar tubular ducts absent from margins of the head (present between antennal bases); and (ii) multilocular disc-pores usually in double rows at posterior edges of abdominal segments V and VI (in single rows).

Key to adult females of *Paracoccus* known from China

- 1 Oral rim tubular ducts present on both dorsum and venter, near margins only ***P. marginatus* Williams & Granara de Willink**
- Oral rim tubular ducts present on dorsum only, with at least a few in submedian or median areas **2**
- 2 Ventral oral collar tubular ducts present on margins of the head ***P. burnerae* (Brain)**
- Ventral oral collar tubular ducts absent from margins of the head **3**
- 3 Abdominal segments IV and V with multilocular disc-pores present in single rows; labium shorter than clypeolabral shield ***P. gillianwatsonae* sp. nov.**
- Abdominal segments IV and V with multilocular disc-pores present usually in double rows; labium longer than clypeolabral shield **4**
- 4 Cerarii numbering 18 pairs; discoidal pores each narrower than a trilocular pore ***P. interceptus* Lit**
- Cerarii numbering fewer than 18 pairs; larger discoidal pores each usually wider than a trilocular pore ***P. wui* sp. nov.**

Acknowledgements

The first author is grateful to Dr San-an Wu (Beijing Forestry University, Beijing, China) and Dr Gillian W. Watson (Department of Life Sciences, the Natural History Museum, London, U.K.), for their help in species identification, reviewing earlier versions of the manuscript, and providing many valuable suggestions and comments.

Additional information

Conflict of interest

The authors have declared that no competing interests exist.

Ethical statement

No ethical statement was reported.

Funding

The project was supported by the National Natural Science Foundation of China (32000328).

Author contributions

Conceptualization: JZ. Data curation: JZ, CL. Writing – original draft: JZ. Writing – review and editing: JZ, XL, YW.

Author ORCIDs

Jiang-tao Zhang  <https://orcid.org/0000-0002-0007-3918>

Chao-qun Li  <https://orcid.org/0009-0004-5636-6906>

Xing-ping Liu  <https://orcid.org/0000-0003-1831-9290>

Yan Wang  <https://orcid.org/0009-0001-9347-6272>

Data availability







All of the data that support the findings of this study are available in the main text.

References

- Ahmed MZ, He RR, Wu MT, Gu YJ, Ren JM, Liang F, Li HL, Hu XN, Qiu BL, Mannion CM, Ma J (2015) First report of the papaya mealybug, *Paracoccus marginatus* (Hemiptera: Pseudococcidae), in China and genetic record for its recent invasion in Asia and Africa. *Florida Entomologist* 98(4): 1157–1162. <https://doi.org/10.1653/024.098.0420>
- Borchsenius NS (1950) Mealybugs and Scale Insects of USSR (Coccoidea). *Akademii Nauk SSSR, Zoological Institute, Moscow* 32: 1–250.
- Brain CK (1915) The Coccidae of South Africa. *Transactions of the Royal Society of South Africa*. Cape Town 5: 65–194. <https://doi.org/10.1080/00359191509519718>
- Chen SP, Wong JY, Wu WJ (2011) Preliminary report on the occurrence of papaya mealybug, *Paracoccus marginatus* Williams and Granara de Willink, in Taiwan. *Journal of Taiwan Agricultural Research* 60(1): 72–76. <https://doi.org/10.6156/jtar/2011.06001.07>
- Choi J, Lee S (2022) Higher classification of mealybugs (Hemiptera: Coccoomorpha) inferred from molecular phylogeny and their endosymbionts. *Systematic Entomology* 47(2): 1–17. <https://doi.org/10.1111/syen.12534>

- Ezzat YM, McConnell HS (1956) A classification of the mealybug tribe Planococcini (Pseudococcidae: Homoptera). Bulletin of the Maryland Agriculture Experiment Station A-84: 1–108.
- García Morales M, Denno BD, Miller DR, Miller GL, Ben-Dov Y, Hardy NB (2016) ScaleNet: a literature-based model of scale insect biology and systematics. Database. <http://scalenet.info> [Accessed 26 December 2023]
- Hardy NB, Gullan PJ, Hodgson CJ (2008) A subfamily-level classification of mealybugs (Hemiptera: Pseudococcidae) based on integrated molecular and morphological data. Systematic Entomology 33(1): 51–71. <https://doi.org/10.1111/j.1365-3113.2007.00408.x>
- Liao S, Liao WC, Li T, Lu HP, Wu M, Wang JG (2021) Invasive pest *Paracoccus marginatus* was first discovered in Jiangxi Province. Biological Disaster Science 44(1): 10–14.
- Lin LH, Zheng LZ, Shi MZ, Li JY, Wang QY, Li L, Fu JW, Wu MX (2019) A molecular detection and identification method for papaya mealybug (*Paracoccus marginatus*), the first recorded invasive pest in Fujian province of China. Journal of Fruit Science 36(9): 1130–1139.
- Lit IL (1992) A new genus and ten new species of Philippine mealybugs (Pseudococcidae, Coccoidea, Hemiptera). Philippine Entomologist 8: 1158–1181.
- Lit IL (1997) New records and additional notes on Philippine mealybugs (Pseudococcidae, Coccoidea, Hemiptera). Philippine Entomologist 11: 33–48.
- Miller D, Rung A, Parikh G, Venable G, Redford AJ, Evans GA, Gill RJ (2014) Identification tool for species of quarantine significance, 2nd edn. <http://idtools.org/scales/index.cfm> [Accessed 22 December 2023]
- Moghaddam M, Esfandiari M (2014) A new species of the genus *Paracoccus* (Hem.: Coccoomorpha: Pseudococcidae) from Iran. Journal of Entomological Society of Iran 34(3): 57–61.
- Salazar TJA (1972) Contribución al conocimiento de los Pseudococcidae del Perú. Revista Peruana de Entomología 15(2): 277–303.
- Wang YS, Zhou P, Tian H, Wan FH, Zhang GF (2018) First record of the invasive pest *Pseudococcus jackbeardsleyi* (Hemiptera: Pseudococcidae) on the Chinese mainland and its rapid identification based on species-specific polymerase chain reaction. Journal of Economic Entomology 111(5): 2120–2128. <https://doi.org/10.1093/jee/toy223>
- Williams DJ (2004) Mealybugs of southern Asia. The Natural History Museum, London. Southdene SDN. BHD., Kuala Lumpur, 896 pp.
- Williams DJ, Granara de Willink MC (1992) Mealybugs of Central and South America. C.A.B. International, Wallingford, 635 pp.
- Wu FZ, Liu ZH, Shen H, Yu F, Ma J, Hu XN, Zeng L (2014) Morphological and molecular identification of *Paracoccus marginatus* (Hemiptera: Pseudococcidae) in Yunnan, China. Florida Entomologist 97(4): 1469–1473. <https://doi.org/10.1653/024.097.0422>
- Zhang JT, Wu SA (2015) A new invasive mealybug, *Paracoccus marginatus* (Hemiptera: Coccoidea: Pseudococcidae), in mainland China. Journal of Environmental Entomology 37(2): 441–446.

Revisionary notes on the genus *Aulacocentrum* Brues (Hymenoptera, Braconidae, Macrocentrinae) from Vietnam

Thi Nhi Pham^{1,2}, Khuat Dang Long¹, Cornelis van Achterberg³, Thi Quynh Nga Cao¹,
Van Phu Pham¹, Thi Hoa Dang¹

1 Institute of Ecology & Biological Resources (IEBR), Vietnam Academy of Science & Technology (VAST), 18 Hoang Quoc Viet Road, Cau Giay, Ha Noi, Vietnam

2 Graduate University of Science & Technology, Vietnam Academy of Science & Technology (VAST), 18 Hoang Quoc Viet Road, Cau Giay, Ha Noi, Vietnam

3 Naturalis Biodiversity Centre, Postbus 9517, 2300 RA Leiden, Netherlands

Corresponding author: Khuat Dang Long (khuatdanglong@gmail.com)

Abstract

This paper contains descriptions and illustrations of five new species of the genus *Aulacocentrum* Brues, 1922, from Vietnam, viz. *Aulacocentrum assitum* Long & Pham, **sp. nov.**; *A. glabrum* Long, **sp. nov.**; *A. imparum* Long & van Achterberg, **sp. nov.**; *A. intermedium* Long & van Achterberg, **sp. nov.**; and *A. simulatum* Long, **sp. nov.** Additionally, *Aulacocentrum seticella* van Achterberg & He is newly recorded for Vietnam's braconid fauna. A checklist and a key to the Oriental and East Palaearctic *Aulacocentrum* species is provided and the in-country distribution of the Vietnamese species is given.

Key words: Australasian, Eastern Palaearctic, Ichneumonoidea, new record, new species, Oriental, parasitoid



Academic editor: Jose Fernandez-Triana

Received: 22 November 2023

Accepted: 29 February 2024

Published: 3 April 2024

ZooBank: <https://zoobank.org/E0B01863-8ABD-4D38-945E-ABDB465CE814>

Citation: Pham TN, Long KD, van Achterberg C, Cao TQN, Pham VP, Dang TH (2024) Revisionary notes on the genus *Aulacocentrum* Brues (Hymenoptera, Braconidae, Macrocentrinae) from Vietnam. ZooKeys 1197: 13–41. <https://doi.org/10.3897/zookeys.1197.116092>

Copyright: © Nhi Thi Pham et al.

This is an open access article distributed under terms of the Creative Commons Attribution License ([Attribution 4.0 International – CC BY 4.0](https://creativecommons.org/licenses/by/4.0/)).

Introduction

Macrocentrinae Foerster, 1863, is a relatively small subfamily of Braconidae Nees, 1811, comprising eight recognised genera. *Aulacocentrum* Brues, 1922 is a rather small genus distributed in the Old World tropics and southern part of the East Palaearctic region. Up to now, *Aulacocentrum* comprises nine valid species, of which four species are known from the Oriental region (but the position of one is uncertain) and one species additionally from the East Palaearctic region.

Aulacocentrum differs from other macrocentrine genera by having the first metasomal tergite with fine transverse striation and vein SC+R1 of hind wing strongly bent basally, both absent in *A. glabrum* sp. nov., but has typical narrowed marginal cell of hind wing (Fig. 4F). A detailed diagnosis of the genus *Aulacocentrum* was given by van Achterberg (1993b) and He and van Achterberg (1994). Previous records indicate that *Aulacocentrum* species are mainly endoparasitoids of pyralid larvae (Lepidoptera) (He and van Achterberg 1994; Yu et al. 2016). In this paper seven species of the genus are reported from Vietnam, of which five are new to science and one species is newly recorded for the fauna of Vietnam.

The species of the genus *Aulacocentrum* have been reported as a larval parasitoid of economically important pyralid moths; *Aulacocentrum philippinense*

(Ashmead), a widespread species, was reported from *Botyodes asialis* Guenée; *Chilo suppressalis* (Walker); *Cnaphalocrocis medinalis* (Guenée); *Crocidolomia pavonana* (Fabricius); *Diaphania pyloalis* (Walker); *Maruca vitrata* (Fabricius); *Palpita nigropunctalis* (Bremer); and *Spoladea recurvalis* (Fabricius) (Yu et al. 2016). In Vietnam, *A. philippinense* was previously reported as endoparasitoid reared from the rice leaf roller *Cnaphalocrocis medinalis* (Long and Belokobylskij 2003). In China, *A. confusum* He and van Achterberg was reported as parasitoid of several pyralid and crambid moths, such as *Ostrinia furnacalis* (Guenée), and *Diaphania pyloalis*; and *A. seticella* was recorded as a parasitoid of *Pachyzancla* sp. (He and van Achterberg 1994).

Materials and methods

All *Aulacocentrum* specimens, including holotypes and paratypes, are deposited in the Institute of Ecology & Biological Resources (**IEBR**) at Ha Noi, Vietnam. The collecting was by light traps in open spaces in the forest, but *A. seticella* was collected in Malaise traps.

We used an Olympus® SZ61 binocular microscope for this study; specimens were photographed by KDL using a Sony® 6000 digital camera attached to a Nikon® SMZ 800N binocular microscope and the figures were processed with Helicon Focus®8 stacking software and Adobe Photoshop CS5 to adjust the size and background. The distribution map for the two new species of *Aulacocentrum* was made using Paraview (<https://paraview.org>).

For terminology used in this paper, see van Achterberg (1993a), sculpture terms are based on Harris (1979), and vein terminology follows the modified Comstock-Needham system (van Achterberg 1993a). For a key to genera of Macrocentrinae in the Palaearctic region, see van Achterberg (1993b). For additional references and data, see Yu et al. (2016). Inside Vietnam, the distribution of the species follows the order of areas and provinces from north to south, and outside Vietnam, distribution of species follows an alphabetical order.

Abbreviations used in this paper are as follows:

POL	minimum postocellar line;
OOL	minimum ocular-ocellar line;
OD	maximum diameter of posterior ocellus;
"Macr.+number"	code number indexing for Macrocentrinae specimens in the collection at IEBR;
MT	Malaise trap;
NE	Northeastern;
S	South;
HTHCT	Department of Insect Systematics at IEBR;
IEBR	Institute of Ecology & Biological Resources, Vietnam Academy of Science and Technology, Ha Noi, Vietnam.

Results

Taxonomy

Class Hexapoda Blainville, 1816

Order Hymenoptera Linnaeus, 1758
Superfamily Ichneumonoidea Latreille, 1802
Family Braconidae Latreille, 1829
Subfamily Macrocentrinae Foerster, 1863

Genus *Aulacocentrum* Brues, 1922

Type species. *Aulacocentrum pedicellatum* Brues, 1922 (examined by CvA).

**Checklist and distribution of Oriental and East Palaearctic
Aulacocentrum species**

- Aulacocentrum assitum* Long & Pham, sp. nov. Oriental/Vietnam.
Aulacocentrum confusum He & van Achterberg, 1994. Eastern Palaearctic and Oriental/China.
Aulacocentrum glabrum Long, sp. nov. Oriental/Vietnam.
Aulacocentrum imparum Long & van Achterberg, sp. nov. Oriental/Vietnam.
Aulacocentrum intermedium Long & van Achterberg, sp. nov. Oriental/Vietnam.
Aulacocentrum longitergiae Sharma, 1978. Oriental/India.
Aulacocentrum nigrum Ku & Park, 1997. Eastern Palaearctic/Korea.
Aulacocentrum philippinense (Ashmead, 1904). Australasian/Indonesia-South Moluccas; Eastern Palaearctic/China, Japan, Korea; Oriental/India, Indonesia, Malaysia, Philippines, Vietnam.
Aulacocentrum seticella van Achterberg & He, 1994. Eastern Palaearctic/China, Japan, Korea; Oriental/China, India, Indonesia, Malaysia, Singapore, Vietnam.
Aulacocentrum simulatum Long, sp. nov. Oriental/Vietnam.

Key to Oriental and East Palaearctic *Aulacocentrum* species

- 1 Female.....**2**
– Male (as far as known)**10**
2 Vein SR of hind wing strongly bent basally, and near to or almost touching anterior wing margin at constriction (Figs 2I, 13D); first metasomal tergite flat basally (Fig. 2F).....**3**
– Vein SR of hind wing curved to moderately bent basally, remaining distinctly removed from anterior wing margin (Figs 4F, 6J, 8H, 10J); first metasomal tergite with basal depression (Figs 4G, 6F, 8I, 10K, 12I), rarely with shallow depression basally (*A. philippinense*).....**4**
3 Maxillary palp 2.2× height of head; fore wing vein 1-CU1 0.4× as long as vein cu-a (Fig. 2H); hind wing marginal cell parallel-sided apically (Fig. 2I); maximum length of second submarginal cell of fore wing 2.4× its apical width; vein 1r-m of hind wing 1.1× as long as vein 1-M and vein 1-M 0.6× as long as vein cu-a; notauli separated posteriorly by longitudinal carina-like rugosity (Fig. 2D); first metasomal tergite smooth basally; propleuron dark brown; hind coxa brown apically; first metasomal tergite black apically (Fig. 2F)..... ***A. assitum* Long & Pham, sp. nov.**
– Maxillary palp 1.6–1.7× height of head; fore wing vein 1-CU1 0.8× vein cu-a; hind wing marginal cell widened apically (Fig. 13D); maximum length of second submarginal cell of fore wing 3.0× its apical width; vein 1r-m of

- hind wing 0.9× as long as 1-M and 1-M 0.9× vein cu-a; notauli fused posteriorly into transverse rugulose area (Fig. 13B) or ending in a long carina; first metasomal tergite with sparse, convergent striations basally; propopleuron yellow (Fig. 13C); hind coxa and first metasomal tergite yellow
- **A. seticella van Achterberg & He**
- 4 Ocelli large, OOL = 0.5–0.6× OD (Figs 4A, 12A); first metasomal tergite with deep medio-basal depression (Figs 4G, 12I)..... **5**
- Ocelli small to medium-sized, OOL = 1.0–1.1× OD (Figs 6A, 10A; see van Achterberg 1993b: fig. 3); first metasomal tergite flat or with shallow medio-basal depression (Figs 6F, 10K)..... **6**
- 5 Vein SC+R1 of hind wing curved basally; basal cell apically and marginal cell basally of hind wing largely glabrous (Fig. 4F); marginal cell of hind wing distinctly narrowed medially and widened apically (Fig. 4F); first metasomal tergite with striation subapically (Fig. 4G)..... **A. glabrum Long, sp. nov.**
- Vein SC+R1 of hind wing distinctly bent basally; basal cell apically and marginal cell basally of hind wing setose (Fig. 12G); marginal cell of hind wing weakly narrowed medially and subparallel-sided apically (Fig. 12G); first metasomal tergite with transverse or curved transverse striation subapically (Fig. 12I)..... **A. simulatum Long, sp. nov.**
- 6 Antennal flagellum without median pale coloured (ivory) flagellomeres; all coxae and metasomal tergites mainly black; vein 1r-m of hind wing 0.6× as long as vein 1-M; scapus black ventrally; [first tergite ~ 3.7× its apical width]..... **A. nigrum Ku & Park**
- Antennal flagellum with median pale coloured (ivory) flagellomeres; fore and middle coxae yellow and hind coxa reddish yellow; basal 1/3 of first tergite and basal 2/3 of third tergite pale yellow (Figs 6F, 10K); vein 1r-m of hind wing 0.8–0.9× as long as vein 1-M; scapus whitish yellow or dark brown ventrally (Figs 6B, 10B)..... **7**
- 7 Clypeus basally less convex (He and van Achterberg 1994: figs 38, 39); malar space comparatively short (He and van Achterberg 1994: fig. 32); scapus dark brown, similarly coloured as first flagellomere or distinctly darker; hind trochantellus with 5–10 teeth, usually in two or three rows (He and van Achterberg 1994: figs 35, 42).....
- **A. confusum van Achterberg & He**
- Clypeus basally more convex (Figs 6B, 10B, 15B; He and van Achterberg 1994: figs 25, 26); malar space longer (Figs 6B, 10B, C; He and van Achterberg 1994: fig. 26); scapus at least partly ivory or pale yellowish ventrally, much paler than dark brown or blackish first flagellomere; teeth on hind trochantellus variable..... **8**
- 8 First metasomal tergite basally flat or near so (see Fig. 5 in van Achterberg 1993b); laterope more or less differentiated from glymma; second tergite distinctly constricted medio-laterally; hind coxa largely smooth with some transverse striae apically; hind femur mostly yellowish brown apically and yellow basally (but hind femur dark brown in males)..... **A. philippinense (Ashmead)**
- First metasomal tergite with basal depression (Figs 6F, 10K); laterope large, merged into deep groove posteriorly (Figs 6H, 10G); second tergite slightly constricted medio-laterally (Figs 6F, 10K); hind coxa punctate with transverse oblique striae apically (Fig. 6G); hind femur mostly dark to blackish brown and brownish yellow at extreme base..... **9**

- 9 First metasomal tergite with dorsal carinae (Fig. 6F); vein 1-SR+M of fore wing angularly bent medially (Fig. 6I); vein SC+R1 of hind wing less bent (Fig. 6J); vein 2-SC+R of hind wing quadrate (Fig. 6J); length of hind femur 8.4× its maximum width; hind coxa remotely punctate dorsally, with oblique striae dorso-apically (Fig. 6G); mesopleuron, metapleuron and propodeum black (Fig. 6C).....**A. imparum Long & van Achterberg, sp. nov.**
- First metasomal tergite without dorsal carinae (Fig. 10K); vein 1-SR+M of fore wing evenly curved medially (Fig. 10H); vein SC+R1 of hind wing more bent (Fig. 10J); vein 2-SC+R of hind wing longitudinal (Fig. 10J); length of hind femur 9.2× its maximum width; hind coxa densely punctate dorsally, with transverse striae dorso-apically (Fig. 10I); mesopleuron dark brown, metapleuron entirely, propodeum basally and laterally pale yellow (Fig. 10F)**A. intermedium Long & van Achterberg, sp. nov.**
- 10 Antennal flagellum unicoloured, without median pale flagellomeres; head and hind tibia reddish brown; length of first tergite 6.0× its apical width [marginal cell of hind wing strongly constricted subbasally; female unknown; India]..... **A. longitergiae Sharma**
- Antennal flagellum bicoloured, with median pale flagellomeres (Figs 7, 14); head entirely black (Figs 8A, 15A); hind tibia mostly blackish brown to black; length of first tergite 3.8–4.3× apical width..... **11**
- 11 Clypeus less convex; malar space rather short (Fig. 8C); first metasomal tergite parallel-sided, with rather deep basal depression (Fig. 8I); vein 1-SR+M of fore wing angularly bent medially (Fig. 8F); vein 1r-m of hind wing 0.7× 1-M; vein 2-SC+R of hind wing quadrate (Fig. 8H); hind coxa rather short, distinctly depressed dorso-apically, sparsely punctate dorsally and smooth apically (Fig. 8G); body length 7.8 mm....**A. imparum Long & van Achterberg, sp. nov.**
- Clypeus more convex; malar space longer (Fig. 15C); first metasomal tergite gradually widened posteriorly, with shallow medio-basal depression (Fig. 15H); vein 1-SR+M of fore wing evenly curved medially (Fig. 15I); vein 1r-m of hind wing 0.9× 1-M; vein 2-SC+R longitudinal (Fig. 15J); hind coxa elongate, sparsely punctate dorsally, weakly depressed dorso-apically and with some fine transverse striae apically (Fig. 15G); body length 7.5–9.0 mm **A. philippinense (Ashmead)**

The type species, *Aulacocentrum pedicellatum* Brues (described from Fiji but also known from the Australian region) is not included in the key because it has never been found in the Oriental region. *Aulacocentrum pedicellatum* Brues can be separated by the following characters: widened subbasal part of marginal cell of hind wing largely glabrous, rarely only medially glabrous (see He and van Achterberg 1994: figs 24, 37); length of first tergite 5.0–8.0× its apical width; apical 1/2 of wing membrane infuscate; mesosoma dark reddish brown; length of body usually more than 11.0 mm. The position of *A. longitergiae* Sharma, 1978 is uncertain because the holotype is unavailable for study. According to the author, the holotype was largely lost during handling (Sharma pers. comm. to CvA July 1985). *Aulacocentrum longitergiae* Sharma is provisionally included and may be distinguished as follows: widened subbasal part of marginal cell of hind wing completely setose; length of first tergite 6.0× its apical width; apical 1/2 of wing membrane hyaline; mesosoma reddish brown or infuscate; length of body less than 11.0 mm; flagellum unicoloured (in male, female unknown),

without pale flagellomeres; head and hind tibia reddish brown (Sharma 1978; He and van Achterberg 1994).

For the redescription of *A. philippinense* (Ashmead), see van Achterberg (1993b: 6–8) and figures therein; for the detailed descriptions of *A. confusum* and *A. seticella*, see He and van Achterberg (1994: 160–163 and of *A. nigrum* Ku and Park, see Ku and Park (1997: 212–213), and figures therein. For the key in this paper, we used the comparative characters of *A. philippinense* and *A. seticella* of specimens collected in Vietnam.

In Vietnam, *Aulacocentrum philippinense* (Ashmead) was previously reported by Long and Belokobylskij (2003) as solitary parasitoid of the rice leaf folder, *Cnaphalocrocis medinalis* (Pylalidae). All the species found in Vietnam have morphological characters that fit well to *Aulacocentrum* in the key to genera and the diagnosis of this genus provided by van Achterberg (1993b), except *A. glabrum* sp. nov.: marginal cell distinctly narrower medially than basally and more or less broadly widened apically; first metasomal tergite elongate, flat basally or with medio-basal depression, 3–6× as long as its apical width; antenna of both sexes often bicoloured (a variable character in *Aulacocentrum*).

Descriptions of species

Aulacocentrum assitum Long & Pham, sp. nov.

<https://zoobank.org/91B36A32-E69B-427B-9B30-715174C971E2>

Figs 1, 2, 16

Material. Holotype, ♀, “Macr.147” (IEBR), NE Vietnam: Ha Giang, Vi Xuyen, Phong Quang, forest, 22°54'00"N, 104°54'56"E; 650 m a.s.l.; light trap, 26.v.2022, PT Nhi, PV Phu.

Description. Holotype, female, body length 7.4 mm, fore wing length 6.2 mm, antenna 12.2 mm, ovipositor sheath 7.6 mm (Fig. 1).

Head. Antenna with 48 flagellomeres; flagellum densely setose; first flagellomere 1.4× second one; length of first and second flagellomeres 7.5 and 5.5× their widths, respectively; subapical antennomere 2.0× its width; apical flagellomere with long spine; in frontal view, width of face 1.2× its length (Fig. 2B); length of maxillary palp 2.2× height of head; face shiny, punctate; malar space as long as basal width of mandible; clypeus convex, finely punctate (Fig. 2B); distance between tentorial pits 1.8× distance from pit to eye margin; in lateral view, eye 3.5× temple medially; head transverse, in dorsal view, head 2.1× as wide as long; and width of head 0.6× median length; temple short, eye 13.5× as long as temple; ocelli large, OOL: OD: POL = 6: 8: 7 (Fig. 2A); frons, temple, and vertex coriaceous.

Mesosoma. Length of mesosoma 1.4× its height (Fig. 2E); pronotal trough crenulate medially, mostly smooth dorsally, sparsely punctate ventrally; propleuron densely punctate (Fig. 2E); middle lobe of mesoscutum without impressions anteriorly; notauli narrow, mostly smooth anteriorly, punctate posteriorly; notauli fused posteriorly, separating by mid-longitudinal rugosity (Fig. 2D); median lobe of mesoscutum smooth, with sparse fine punctures; lateral lobes of mesoscutum mostly smooth, with sparse punctures near notauli; scutellum convex, with dense fine punctures; mesopleuron densely punctate (Fig. 2E); metapleuron rugose-punctate; propodeum foveolate-rugose (Fig. 2C).



Figure 1. Habitus of *Aulacocentrum assitum* Long & Pham, sp. nov., holotype, female, lateral, “Macr.147” (IEBR).

Wings. Length of fore wing $2.9\times$ its maximum width (Fig. 2H); length of pterostigma $4.0\times$ its width; fore wing vein SR1 $2.3\times$ as long as vein 3-SR; vein r originating behind middle of pterostigma, r: 3-SR: SR1 = 11: 25: 57; cu-a slightly inclivous (Fig. 2H), cu-a: 1-CU1: 2-CU1 = 9: 4: 33; 2-SR: 3-SR: r-m = 17: 25: 7; second submarginal cell of fore wing narrowed distally; hind wing vein cu-a: 1-M: 1r-m = 15: 12: 13; vein 2-SC+R vertical; vein SR strongly bent basally, at constriction mostly touching the frontal wing margin (Fig. 2I).

Legs. Hind coxa sparsely setose; length of femur, tibia, and basitarsus of hind leg 7.8 , 17.8 , and $14.0\times$ their maximum widths, respectively; left hind trochantellus with two teeth apically (Fig. 2G); tibial spurs straight, setose, length of hind inner and outer tibial spurs $0.4\times$ and $0.3\times$ hind basitarsus combined; length of hind basitarsus $0.4\times$ hind tibia and $1.1\times$ second–fifth tarsal segments.

Metasoma. Length of metasoma $1.5\times$ head and mesosoma combined; first tergite parallel-sided, flat medio-basally, length $5.1\times$ its apical width; mostly smooth anterior of spiracle, transversely rugose from spiracle to apex; median length of second tergite $1.2\times$ third tergite; second tergite narrowed medio-laterally (Fig. 2F), with fine convergent striae; third tergite with fine parallel stri-



Figure 2. *Aulacocentrum assitum* Long & Pham, sp. nov., holotype, female, "Macr.147" (IEBR) A head, dorsal B head, frontal C propodeum, dorsal D mesonotum E mesopleuron F first–third metasomal tergites G hind femur H fore wing I hind wing.

ae basally; finely punctate apically; fourth–sixth metasomal tergites punctate, densely setose (Fig. 2F); length of ovipositor sheath 1.2× fore wing.

Colour. Head black; scapus dark brown, cream-white ventrally; pedicel yellow; flagellum brown with flagellomeres 9th–18th ivory; mandible yellow; palpi whitish yellow; propleuron brown; middle lobe of mesoscutum and scutellum yellowish brown; lateral lobes of mesoscutum, mesopleuron, metapleuron, and propodeum reddish yellow; fore and middle legs yellow; hind coxa yellow basally, brown apically; hind trochanter and trochantellus infuscate; hind femur dark brown; hind tibia mostly brown, pale yellow basally, cream-white apically; hind tibial and tarsus cream-white; tegula brownish yellow; wing membrane hyaline; veins yellowish brown, except vein 1-R1 and parastigma whitish yellow; pterostigma brown, pale yellow apically; metasoma brown, except first tergite basally, second and third metasomal tergites laterally and ventrally pale yellow; ovipositor sheath brown; ovipositor yellow.

Male. Unknown.

Biology. Unknown.

Etymology. From *assitus* (Latin for “near”), because this new species is close to *A. seticella* van Achterberg & He, 1994, from China.

Distribution. NE Vietnam (Ha Giang province) (Fig. 16).

Notes. This new species is close to *A. seticella* van Achterberg & He, but differs from the latter by the following characters: 1) length of maxillary palp 2.2× height of head (1.6–1.7× in *A. seticella*); 2) marginal cell of hind wing as wide basally as apically (Fig. 2I) (strongly widened basally in *A. seticella*, see He and van Achterberg 1994: fig. 18); and 3) second metasomal suture distinct, basal 1/3 of third tergite finely striate (second suture indistinct, more than basal 1/2 of third tergite finely striate in *A. seticella*).

***Aulacocentrum glabrum* Long, sp. nov.**

<https://zoobank.org/798AD0C1-3AFB-4C60-8329-8DDC4FB2DB5C>

Figs 3, 4, 16

Material. Holotype, ♀, “Macr.050” (IEBR), S Vietnam: Dong Nai, Vinh Cuu, Phu Ly, forest, 11°22'52.3"N, 107°03'43.6"E; 107 m a.s.l., light trap, 03.viii.2008, HV Tru.

Description. Holotype, female, body length 12.0 mm, fore wing length 9.4 mm, antenna 17.6 mm, ovipositor sheath 13.4 mm (Fig. 3).

Head. Antenna with 51 flagellomeres; first flagellomere 1.3× second one; length of first and second flagellomeres 3.8 and 4.4× their widths, respectively; length of subapical antennomere 2.7× its width; in frontal view, width of face 0.8× its length (Fig. 4B); length of maxillary palp 2.0× height of head; face densely punctate medially, sparsely punctate laterally (Fig. 4B); malar space 0.9× as long as basal width of mandible; clypeus slightly convex ventrally, sparsely finely punctate (Fig. 4B); distance between tentorial pits 1.3× distance from pit to eye margin; in dorsal view, width of head 2.2× median length; temple short, smooth, eye 15.5× temple; ocelli large, OOL: OD: POL = 6: 9: 9 (Fig. 4A); frons smooth.

Mesosoma. Length of mesosoma 1.4× its height (Fig. 4E); pronotal trough finely and densely crenulate medially, shiny smooth dorsally, finely punctate ventrally; propleuron densely punctate (Fig. 4E); middle and lateral lobes of mesoscutum mostly coriaceous, with sparse fine punctures; notauli crenulate an-



Figure 3. Habitus of *Aulacocentrum glabrum* Long, sp. nov., holotype, female, lateral, "Macr.050" (IEBR).

teriorly, strongly converging posteriorly in a sharp V-shaped depression, divided by mid-longitudinal rugosity (Fig. 4D); scutellar sulcus wide, with one median carina, 0.5× as long as scutellum; scutellum convex, rugose-punctate; mesopleuron densely punctate (Fig. 4E); metapleuron rugulose; propodeum reticulate-rugulose (Fig. 4C).

Wings. Length of fore wing 5.2× its maximum width; length of pterostigma 5.2× its width; fore wing vein SR1 2.2× as long as vein 3-SR; r: 3-SR: SR1 = 12: 37: 80; vein 1-CU1 quadrate; cu-a: 2-CU1 = 11: 52; 2-SR: 3-SR: r-m = 21: 37: 10; second submarginal cell of fore wing narrowed distally; hind wing vein 2-SC+R thick, nearly quadrate; vein 1-M weakly curved basally; hind wing vein cu-a: 1-M: 1r-m = 22: 22: 16; vein SR strongly bent basally (Fig. 4F), and marginal cell largely glabrous basally, wider medially than basally and apically, parallel-sided medially and distinctly widened apically (Fig. 4F).

Legs. Hind coxa densely setose latero-ventrally, but without setae dorso-apically; length of femur, tibia, and basitarsus of hind leg 9.1, 17.0, and 12.3× their maximum widths, respectively; left hind trochantellus with four teeth apically (Fig. 4H); length of hind inner and outer tibial spurs 0.4× and 0.3× hind basitarsus, respectively; length of hind basitarsus 0.4× hind tibia and as long as second–fifth tarsal segments combined.

Metasoma. Length of metasoma 1.6× head and mesosoma combined; first tergite deeply concave medio-basally (Fig. 4G), length of first tergite 3.6× its



Figure 4. *Aulacocentrum glabrum* Long, sp. nov., holotype, female, "Macr.050" (IEBR) **A** head, dorsal **B** head, frontal **C** propodeum **D** mesonotum **E** mesopleuron **F** hind wing **G** first–third metasomal tergites **H** left hind femur, outer side.

apical width; median length of second tergite $1.1\times$ third tergite; first metasomal tergite transversely striate basally, transverse-obliquely striate medio-subapically, obliquely striate at apex; second tergite with convergent striae on most part of tergite, but with parallel striae apically (Fig. 4G); third tergite with fine striae, mostly smooth apically; remaining metasomal tergites sparsely punctate, with sparse long setae; length of ovipositor sheath $1.4\times$ fore wing.

Colour. Head dark brown; palpi yellow; scapus and pedicellus dark brown; flagellum brown with flagellomeres 8th–18th yellow; mesosoma brown; wing veins yellowish brown; tegula yellow; parastigma, pterostigma basally and apically yellow; wing membrane hyaline; fore and middle legs yellow; hind coxa (except apically brown), trochanter and trochantellus yellow; hind tibia brown, except yellow at base; hind tarsus and tibial spurs yellow; metasoma blackish brown, except basal 1/2 of first and third tergites pale yellow; ovipositor sheath brown; ovipositor yellow.

Male. Unknown.

Biology. Unknown.

Etymology. From *glaber* (Latin for hairless), referring to the hind wing with both the basal cell apically and the marginal cell basally glabrous.

Distribution. S Vietnam (Dong Nai province) (Fig. 16).

Notes. This new species can be distinguished from other species by the following characters: marginal cell of hind wing largely glabrous basally, and vein 1-CU1 of fore wing quadrate.

***Aulacocentrum imparum* Long & van Achterberg, sp. nov.**

<https://zoobank.org/3C625000-324F-452E-98A5-3C510B6E3672>

Figs 5–8, 16

Material. *Holotype*, ♀, “Macr.172” (IEBR), NE Vietnam: Tuyen Quang, Lam Binh, Thac Nghien, forest, 22°34.334'N, 105°16.762'E; 114 m, light trap, 21.ix.2017, HTHCT. Paratype, 1♂, “Macr.170” (IEBR), NE Vietnam: topotypic.

Description. Holotype, female, body length 9.8 mm, fore wing length 7.5 mm, ovipositor sheath 10.5 mm (Fig. 5).

Head. Antenna incomplete, with six flagellomeres remaining; first flagellomere $1.5\times$ second; length of first and second flagellomeres 6.5 and $4.2\times$ their widths, respectively; in frontal view, width of face $0.9\times$ its length (Fig. 6B); length of maxillary palp $1.7\times$ height of head; face densely punctate medially, sparsely punctate laterally (Fig. 6B); malar space $1.1\times$ as long as basal width of mandible; clypeus straight ventrally, sparsely, finely punctate; distance between tentorial pits $1.2\times$ distance from pit to eye margin; in dorsal view, width of head $2.8\times$ median length (Fig. 6A); eye $9.3\times$ as long as temple; ocelli medium-sided, OOL: OD: POL = 9: 9: 10 (Fig. 6A); frons, vertex and temple smooth.

Mesosoma. Length of mesosoma $1.4\times$ its height (Fig. 6E); pronotal trough largely crenulate medially, mostly smooth ventrally and dorsally; propleuron densely punctate (Fig. 6E); middle lobe of mesoscutum rugulose dorsally; punctate ventrally; notauli sparsely crenulate anteriorly, narrowly fused posteriorly with median rugosity (Fig. 6D); scutellar sulcus with five median carina, $0.5\times$ scutellum; scutellum densely punctate; mesopleuron and metapleuron largely rugose-punctate (Fig. 6E); propodeum mostly transversely rugulose medially (Fig. 6C).



Figure 5. Habitus of *Aulacocentrum imparum* Long & van Achterberg, sp. nov., holotype, female, lateral, "Macr.172" (IEBR).

Wings. Length of fore wing 3.0× its maximum width (Fig. 6I); length of pterostigma 3.2× its width; vein SR1 of fore wing 2.1× as long as vein 3-SR; r: 3-SR: SR1 = 10: 29: 60; vein 1-SR+M of fore wing angularly bent medially (Fig. 6I); cu-a: 1-CU1: 2-CU1 = 14: 4: 60; 2-SR: 3-SR: r-m = 18: 29: 10; second submarginal cell of fore wing narrowed distally; hind wing with vein 2-SC+R quadrate (Fig. 6J); vein of hind wing cu-a: 1-M: 1r-m = 15: 13: 10; marginal cell sparsely setose, slightly widened apically.

Legs. Hind coxa densely setose latero-ventrally, densely punctate dorsally, with fine oblique striation apically (Fig. 6G); length of femur, tibia, and basitarsus of hind leg 8.4, 16.4, and 8.0× their maximum widths, respectively; left hind trochantellus with three teeth apically; length of hind inner and outer tibial spurs 0.4× and 0.3× hind basitarsus, respectively; length of hind basitarsus 0.3× hind tibia and 1.3× second–fifth tarsal segments combined.

Metasoma. Length of metasoma 1.4× head and mesosoma combined; first tergite slightly concave medio-basally (Fig. 6F), length of first tergite 3.8× its apical width; laterope large (Fig. 6H); second tergite slightly longer than third tergite medially; first metasomal tergite mostly transversely striate; second tergite weakly constricted medio-laterally, with convergent striae on basal 2/3 of tergite, parallel striation on apical third of tergite (Fig. 6F); third tergite finely striate on basal 2/3 of tergite; remaining metasomal tergites coriaceous, with dense setae (Fig. 6F); length of ovipositor 1.4× fore wing.

Colour. Head and mesosoma black; scapus pale yellow, brown dorsally; palpi yellow; fore leg pale yellow, except fore tarsus brownish yellow; middle leg yellow, except middle tarsus brownish yellow; hind coxa brownish yellow,

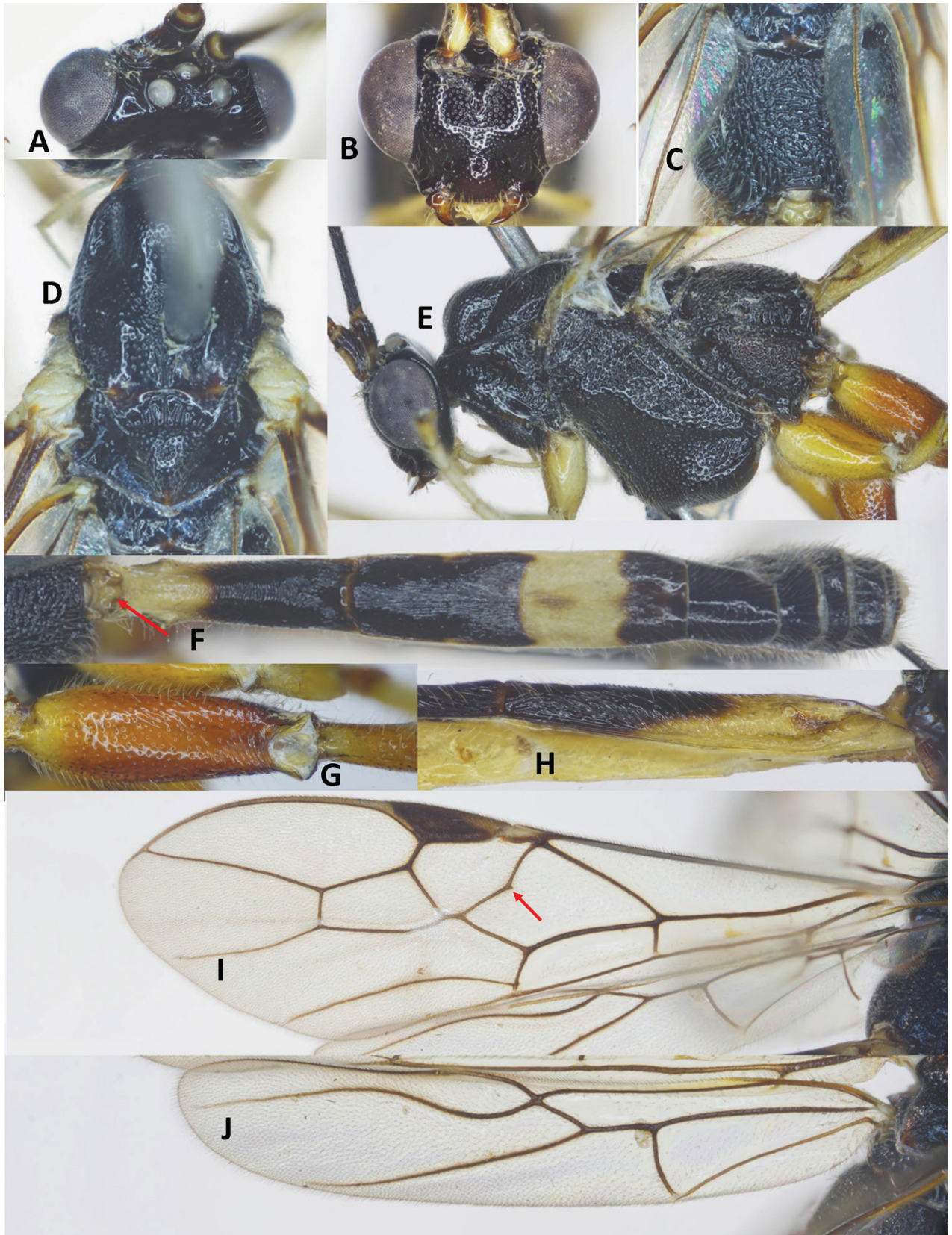


Figure 6. *Aulacocentrum imparum* Long & van Achterberg, sp. nov., holotype, female, “Macr.172” (IEBR) **A** head, dorsal **B** head, frontal **C** propodeum **D** mesonotum **E** mesopleuron **F** first-third metasomal tergites, arrow indicates medio-basal depression **G** hind coxa, dorsal **H** first metasomal tergite, lateral **I** fore wing, arrow indicates vein 1-SR+M of fore wing angularly bent medially **J** hind wing.



Figure 7. Habitus of *Aulacocentrum imparum* Long & van Achterberg, sp. nov., paratype, male, lateral, “Macr.170” (IEBR).

trochanter and trochantellus; hind femur blackish brown, yellow at extreme base; hind tibia blackish brown apically, cream-white basally; hind tibial spurs and tarsus cream-white; tegula cream-white; wing veins brown; parastigma yellow; pterostigma brown, yellow basally and apically; wing membrane hyaline; basal 1/2 of first metasomal tergite pale yellow; apical 1/2 of first tergite and second tergite black; basal 2/3 of third tergite pale yellow, apical 1/3 black; first–third sternites pale yellow and remainder black; ovipositor sheath brown; ovipositor yellow.

Variation male. Paratype, “Macr.170” (IEBR), body length 7.5 mm, fore wing length 5.5 mm (Fig. 7).

Head. Antenna with 41 flagellomeres; first flagellomere 1.3× second; length of first and second flagellomeres 6.7 and 5.0× their widths, respectively; in frontal view, width of face 0.9× its length (Fig. 8B); length of maxillary palp 1.4× height of head; face densely punctate medially, sparsely punctate laterally (Fig. 8B); malar space 1.1× as long as basal width of mandible; clypeus weakly convex in lateral view (Fig. 8C); straight ventrally, sparsely punctate; distance between tentorial pits 1.4× distance from pit to eye margin; in dorsal view, width of head 2.7× median length; eye 7.7× as long as temple; OOL: OD: POL = 6: 6: 9 (Fig. 8A); frons, vertex and temple coriaceous.

Mesosoma. Length of mesosoma 1.5× its height; pronotal trough largely crenulate medially, mostly smooth ventrally and dorsally; propleuron rugose-punctate (Fig. 8E); notauli sparsely crenulate anteriorly, narrowly fused posteriorly with median rugosity (Fig. 8D); middle lobe of mesoscutum rugulose dorsally; punctate ventrally; median lobes of mesoscutum sparsely punctate; scutellar sulcus 0.4× scutellum, with one median carina; scutellum densely punctate; me-

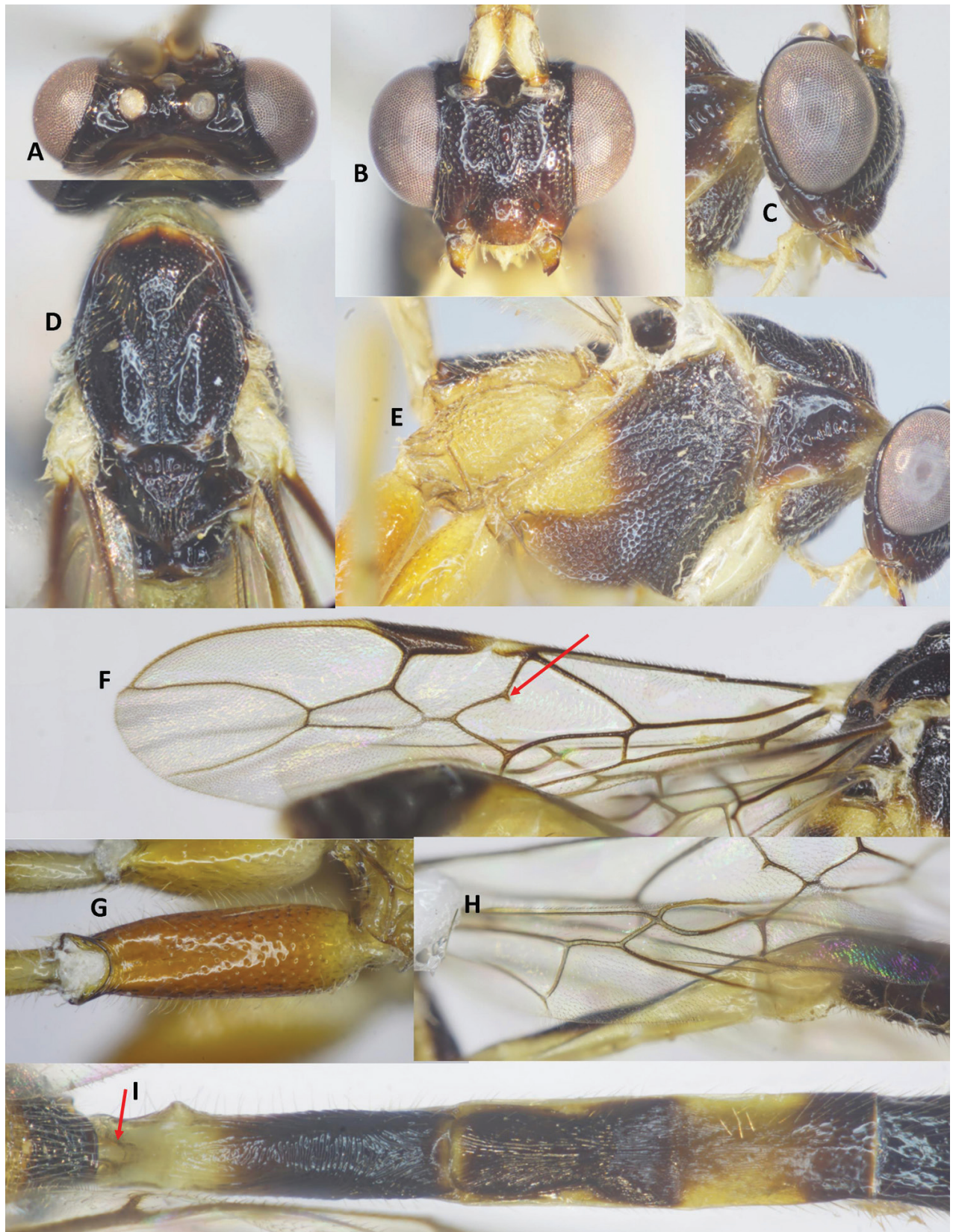


Figure 8. *Aulacocentrum imparum* Long & van Achterberg, sp. nov., paratype, male, "Macr.170" (IEBR) **A** head, dorsal **B** head, frontal **C** head, lateral **D** mesonotum **E** mesopleuron **F** fore wing, arrow indicates angular curve of vein 1-SR+M **G** hind coxa, dorsal **H** hind wing (part) **I** first-third metasomal tergites, arrow indicates medio-basal depression.

sopleuron rugose-punctate medially, densely punctate ventrally (Fig. 8E); metapleuron rugose-punctate; propodeum mostly transversely rugulose medially.

Wings. Length of fore wing 3.5× its maximum width (Fig. 8F); length of pterostigma 4.8× its width; vein SR1 of fore wing 2.1× as long as vein 3-SR; r: 3-SR: SR1 = 10: 25: 52; vein 1-SR+M of fore wing angularly bent medially (Fig. 8F); cu-a: 1-CU1: 2-CU1 = 6: 3: 37; 2-SR: 3-SR: r-m = 14: 25: 10; second submarginal cell of fore wing narrowed distally; hind wing vein 2-SC+R quadrate (Fig. 8H); vein of hind wing cu-a: 1-M: 1r-m = 16: 12: 10; marginal cell sparsely setose.

Legs. Hind coxa with discrete punctures dorsally, distinctly depressed dorso-apically and mostly smooth (Fig. 8G); length of femur, tibia, and basitarsus of hind leg 8.5, 16.8, and 9.0× their maximum widths, respectively; left hind trochantellus with three teeth apically; length of hind inner and outer tibial spurs 0.4× and 0.3× hind basitarsus, respectively; length of hind basitarsus 0.4× hind tibia and 1.2× second–fifth tarsal segments combined.

Metasoma. Length of metasoma 1.5× head and mesosoma combined; first metasomal tergite parallel-sided, with deep medio-basal depression (Fig. 8I), length 4.0× its apical width; second tergite 1.2× third tergite medially; first metasomal tergite mostly transversely striate; second tergite with convergent striae on basal 2/3 of the tergite, parallel striation on apical 1/3 of tergite (Fig. 8I); third tergite finely striate on basal 2/3 of tergite; remaining metasomal tergites coriaceous, with dense setae.

Colour. Head black; scapus whitish yellow, brown dorsally; palpi whitish yellow; antenna brown basally and apically, with 11th–19th flagellomeres ivory; pronotum whitish yellow; mesoscutum blackish brown to black; mesopleuron tricoloured, dark brown dorso-anteriorly, brown ventrally and yellow posteriorly; metapleuron entirely yellow (Fig. 8E); propodeum dark brown posteriorly, yellow anteriorly and laterally; fore and middle legs pale yellow; hind coxa reddish yellow (Fig. 8G); trochanter and trochantellus pale yellow; hind femur dark brown, yellow basally; hind tibia blackish brown in apical 3/4 of the tibia, cream-white in basal 1/4; hind tibial spurs and tarsus cream-white; tegula cream-white; wing veins brown; vein 1-R1 and parastigma yellow; pterostigma brown, yellow basally; wing membrane hyaline; basal 1/3 of first metasomal tergite pale yellow; apical 1/2 of first tergite and second tergite blackish brown; basal 2/3 of third tergite yellow, apical 1/3 brown; its remainder black.

Biology. Unknown.

Etymology. From *impar* Latin for unequal, odd, different, because in both sexes, left fore wing with vein 1-SR+M angularly bent medially.

Distribution. NE Vietnam (Tuyen Quang province) (Fig. 16).

Notes. This new species (both sexes) is closely related to *A. philippinense* (Ashmead) but can be separated from the latter by the following characters: 1) first metasomal tergite with basal depression (vs flat in *A. philippinense*); 2) second metasomal tergite (female) weakly constricted medio-laterally (vs distinctly constricted medio-laterally in *A. philippinense*); 3) OOL equal to OD; stemmaticum coriaceous (OOL slightly longer than OD, and stemmaticum rugulose in *A. philippinense*) and 4) vein 1-SR+M of fore wing angularly bent medially (vs evenly curved in *A. philippinense*).

***Aulacocentrum intermedium* Long & van Achterberg, sp. nov.**

<https://zoobank.org/4800309E-1E86-4407-B01E-39A20A0938EE>

Figs 9, 10, 16

Material. *Holotype*, ♀, “Macr.174” (IEBR), NE Vietnam: Cao Bang, Ha Quang, Yen Son, forest, 22°47'11.2"N, 104°54'06"E, 987 m, light trap, 12.vi.2023, Pham TN, Pham VP, Dang TH.

Description. Holotype, female, body length 8.9 mm; fore wing length 7.8 mm; ovipositor 9.0 mm (Fig. 9).

Head. Antenna with 47 flagellomeres; first flagellomere 1.2× second one; length of first and second flagellomeres 6.0 and 4.8× their widths, respectively; in frontal view, width of face 0.9× its length (Fig. 10B); length of maxillary palp 1.4× height of head; face densely punctate; malar space as long as basal width of mandible (Fig. 10C); clypeus less convex (Fig. 10C); straight ventrally, sparsely, finely punctate; distance between tentorial pits 1.6× distance from pit to eye margin; in dorsal view, width of head 2.6× median length (Fig. 10A); eye 8.5× as long as temple; OOL: OD: POL = 7: 8: 10 (Fig. 10A); frons, vertex and temple shiny, smooth.

Mesosoma. Length of mesosoma 1.5× its height (Fig. 10E); pronotal trough largely crenulate medially, mostly smooth ventrally and dorsally; propleuron with fine dense punctures (Fig. 10E); middle lobe of mesoscutum densely punctate; lateral lobes of mesoscutum sparsely punctate; notauli narrow, sparsely crenulate anteriorly, narrowly fused posteriorly with median rugosity (Fig. 10D); scutellar sulcus with three median carina, 0.5× scutellum; scutellum densely punctate; mesopleuron and metapleuron largely rugose-punctate (Fig. 10E); propodeum mostly irregularly rugulose (Fig. 10F).

Wings. Length of fore wing 4.1× its maximum width (Fig. 10H); length of pterostigma 4.9× its width; fore wing vein SR1 2.2× as long as vein 3-SR; r: 3-SR: SR1 = 10: 28: 63; cu-a: 1-CU1: 2-CU1 = 4: 9: 50; 2-SR: 3-SR: r-m = 13: 28: 9; second submarginal cell of fore wing narrowed distally; hind wing with vein 2-SC+R horizontal (= longitudinal); vein SC+R1 evenly curved (Fig. 10J); cu-a: 1-M: 1r-m = 10: 15: 15; marginal cell sparsely setose.

Legs. Hind coxa densely setose latero-ventrally, rugose-punctate dorsally, without striation apically (Fig. 10I); length of femur, tibia, and basitarsus of hind leg 9.8, 17.7, and 8.0× their maximum widths, respectively; left hind trochantellus with four teeth in one row; length of hind inner and outer tibial spurs 0.4× and 0.3× hind basitarsus, respectively; length of hind basitarsus 0.3× hind tibia and 1.1× second–fifth tarsal segments combined.

Metasoma. Length of metasoma 1.3× head and mesosoma combined; laterope large, fused into a groove posteriorly (Fig. 10G); first tergite evenly widened apically, with medio-basal depression (Fig. 10K); length of first tergite 4.1× its apical width (Fig. 10K); first metasomal tergite parallel-sided, with curved striation medially; second tergite 1.1× third tergite medially (Fig. 10K); second tergite weakly constricted medially, with convergent striae on basal 2/3 of tergite, with parallel striation apically; third tergite mostly coriaceous, with superficial micro-striae basally; remaining metasomal tergites coriaceous, with dense setae.

Colour. Scapus largely whitish yellow, pale brown dorso-apically; flagellum dark brown, with 9th–18th middle flagellomeres ivory; palpi cream-white; fore



Figure 9. Habitus of *Aulacocentrum intermedium* Long & van Achterberg, sp. nov., holotype, female, lateral, “Macr.174” (IEBR).

leg yellow except coxa, trochanter and trochantellus whitish yellow; middle leg yellow, except basitarsus and second brown; hind coxa reddish yellow, hind trochanter and trochantellus yellow, hind femur blackish brown to black, reddish yellow at extreme base; apical 1/2 of hind tibia blackish brown, pale yellow basally; hind tibial spurs and tarsus cream-white; pronotum yellow; mesonotum black; metapleuron yellow; propodeum black medio-posteriorly, yellow basally and ventrally; tegula whitish yellow; wing veins brown; parastigma yellow; pterostigma dark brown, yellow basally and apically; wing membrane hyaline; basal 2/3 of first metasomal tergite pale yellow, apical 1/3 black; second tergite entirely black; basal 2/3 of third tergite whitish yellow, black apically; the remainder blackish brown to black; hypopygium brown; ovipositor sheath brown; ovipositor yellow.

Male. Unknown.

Biology. Unknown.

Etymology. From *inter* in Latin meaning “between”, because this new species is intermediate between *A. imparum* sp. nov. and *A. philippinense*.

Distribution. NE Vietnam (Cao Bang) (Fig. 16).

Notes. This new species is similar to *A. philippinense* (Ashmead) but can be separated from the latter by the following characters: 1) first metasomal tergite with basal depression (vs flat in *A. philippinense*); 2) second metasomal tergite weakly constricted medio-laterally (vs distinctly constricted medio-laterally in *A. philippinense*); 3) stemmaticum coriaceous (vs stemmaticum rugulose in *A. philippinense*); and 4) hind coxa rugose-punctate dorsally with oblique striation dorso-laterally (vs nearly smooth with transverse striation dorso-apically in *A. philippinense*).

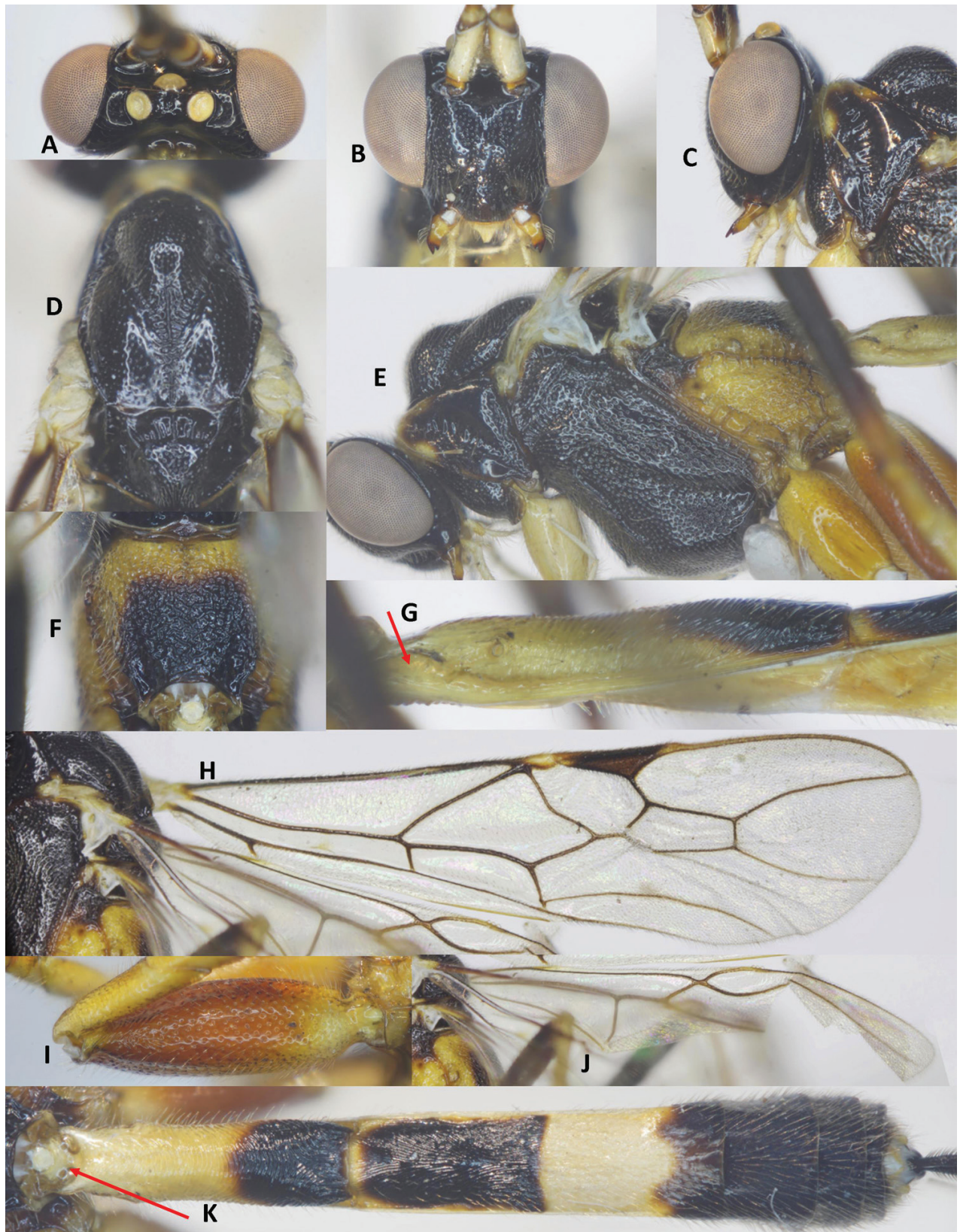


Figure 10. *Aulacocentrum intermedium* Long & van Achterberg, sp. nov., holotype, female, "Macr.174" (IEBR) **A** head, dorsal **B** head, frontal **C** propodeum, lateral **D** mesonotum **E** mesopleuron **F** propodeum, dorsal **G** first metasomal tergite, lateral, arrow indicates laterope **H** fore wing **I** hind coxa, dorsal **J** hind wing (part) **K** first-third metasomal tergites, dorsal, arrow indicates medio-basal depression.

***Aulacocentrum simulatum* Long, sp. nov.**

<https://zoobank.org/EE45A15F-983B-4EA8-A99B-5B8D9B2C2AA2>

Figs 11, 12, 16

Material. *Holotype*, ♀, "Macr.011" (IEBR), NC Vietnam: Thua Thien-Hue, A Luoi, A Roang forest, 16°06'36.0"N, 107°24'30.7"E, 700 m, light trap, 7.vi.2006, HV Tru.

Description. Holotype, female, body length 10.3 mm, fore wing length 7.7 mm, antenna 15.0 mm, ovipositor 8.3 mm (Fig. 11).

Head. Antenna incomplete, with 44 flagellomeres remaining, with 13 middle flagellomeres ivory; first flagellomere 1.3× second one; length of first and second flagellomeres 6.7 and 5.0× their widths, respectively; length of subapical antennomere 2.7× its width; in frontal view, width of face 0.9× its length (Fig. 12B); length of maxillary palp 1.5× height of head; face plough, with rather dense punctures; malar space 0.8× as long as basal width of mandible; clypeus with fine sparse punctures (Fig. 12B); distance between tentorial pits 2.0× distance from pit to eye margin; in lateral view, eye 5.3× temple; in dorsal view, head transverse, 2.3× as wide as long dorsally (Fig. 12A); eye 7.0× as long as temple; ocelli large, OOL: OD: POL = 4: 8: 8 (Fig. 12A); frons smooth, with median groove; stemmaticum rugose-punctate; vertex and temple punctate.

Mesosoma. Length of mesosoma 1.4× its height (Fig. 12E); pronotal trough largely crenulate medially, punctate ventrally, smooth medio-dorsally; prop-

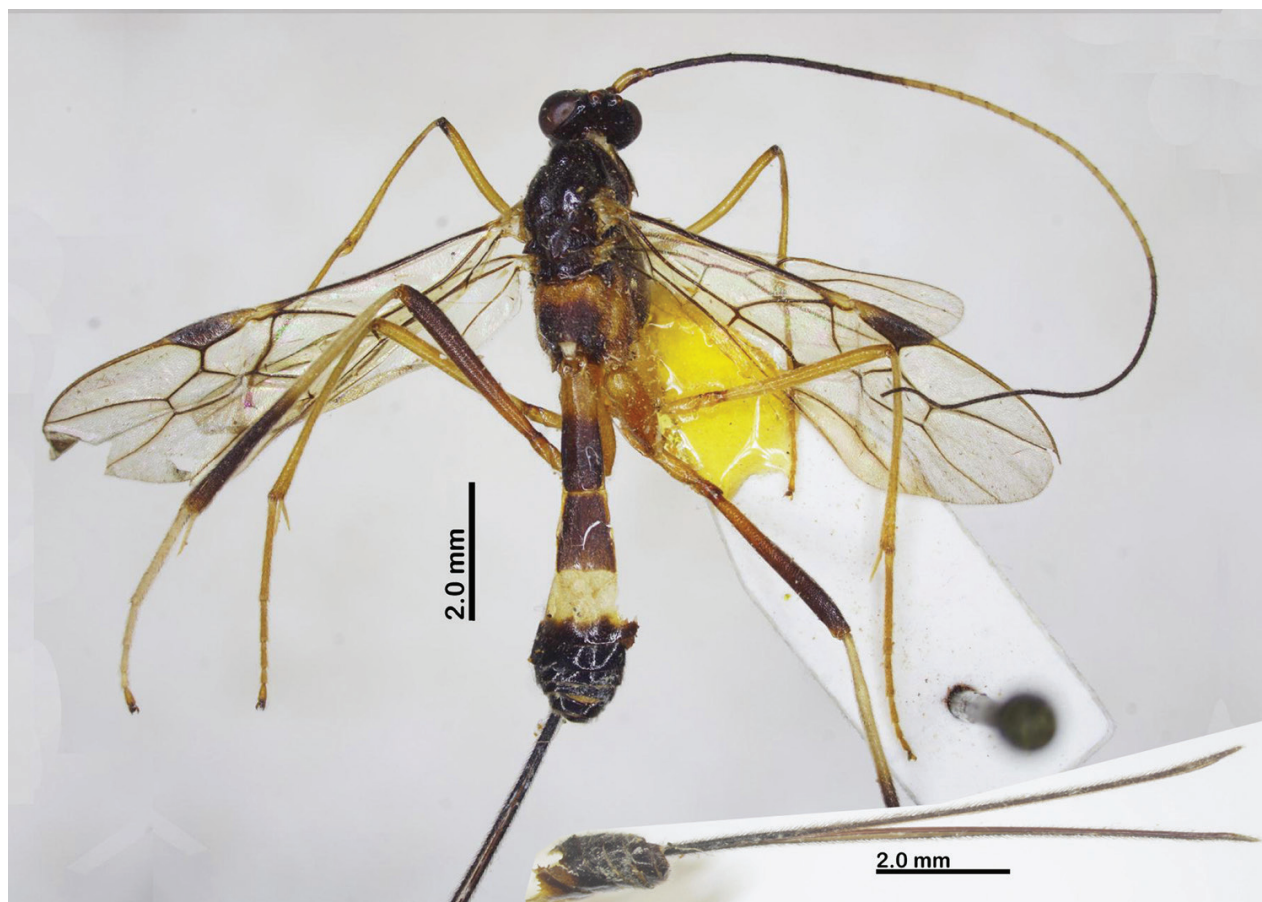


Figure 11. Habitus of *Aulacocentrum simulatum* Long, sp. nov., holotype, female, dorsal, "Macr.011" (IEBR).

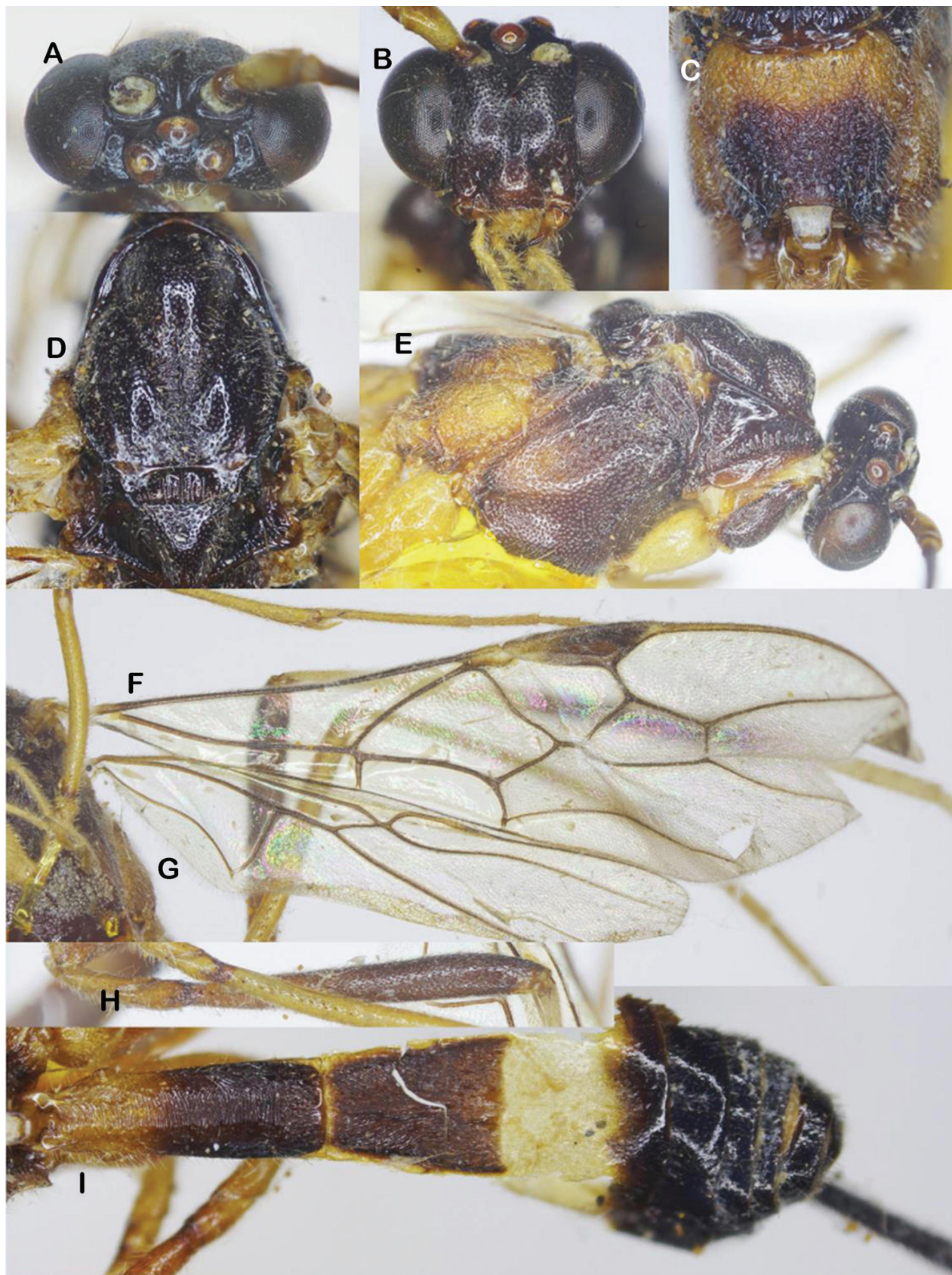


Figure 12. *Aulacocentrum simulatum* Long, sp. nov., holotype, female, "Macr.011" (IEBR) **A** head, dorsal **B** head, frontal **C** propodeum, dorsal **D** mesonotum **E** mesopleuron **F** fore wing **G** hind wing **H** hind trochanter, trochantellus and femur **I** metasoma.

leuron rugose-punctate (Fig. 12E); middle lobe of mesoscutum mostly rugose-punctate; lateral lobes densely punctate; notauli sparsely punctate anteriorly, converging posteriorly in a V-shaped depression, transverse rugose area separated by median carina-like rugosity (Fig. 12D); scutellar sulcus deep, with six carinae, 0.5× as long as scutellum; scutellum densely punctate; mesopleuron and metapleuron largely rugose; propodeum rugose-punctate basally and ventrally; coarsely rugulose medio-posteriorly (Fig. 12C).

Wings. Length of fore wing 3.2× its maximum width (Fig. 12F); pterostigma rather broad, length of pterostigma 3.5× as long as width medially; fore wing vein SR1 2.5× as long as vein 3-SR; r: 3-SR: SR1 = 10: 25: 63; vein cu-a vertical; cu-a: 1-CU1: 2-CU1 = 10: 3: 46 (Fig. 12F); vein r-m oblique; 2-SR: 3-SR: r-m = 17: 25: 9; second submarginal cell of fore wing narrowed apically; hind wing with vein 2-SC+R horizontal (= longitudinal) (Fig. 12G); vein SC+R1 distinctly bent (Fig. 12G); cu-a: 1-M: 1r-m = 25: 22: 15; marginal cell of hind wing weakly widened basally, slightly narrowed medially, nearly parallel-sided posteriorly (Fig. 12G).

Legs. Length of femur, tibia, and basitarsus of hind leg 8.3, 14.3, and 7.7× their maximum widths, respectively; left hind trochantellus with seven teeth in two rows apically (Fig. 12H); length of hind inner and outer tibial spurs 0.3 and 0.2× hind basitarsus, respectively; length of hind basitarsus 0.4× hind tibia and 1.2× second–fifth tarsal segments combined.

Metasoma. Length of metasoma 1.3× head and mesosoma combined; first tergite deeply concave medio-basally (Fig. 12I), length of first tergite 3.1× its apical width; median length of second tergite 1.1× third tergite; first metasomal tergite with transverse striation on most of tergite, irregular striation at apex (Fig. 12I); second tergite with convergent striation on basal 2/3 of tergite, parallel striation on apical 1/3 of tergite; third tergite with fine parallel striation on basal 4/5 of tergite, apical 1/5 of tergite smooth and sparsely setose; remaining metasomal tergites smooth with sparse setae; length of ovipositor 1.1× fore wing.

Colour. Head blackish brown; scapus nearly pale yellow entirely, except outer side brownish yellow; flagellum brown basally and apically, 8th–19th middle flagellomeres ivory; palpi yellow; mesonotum dark brown to black; metapleuron, propodeum basally yellow, dark brown apically; fore and middle legs yellow; hind leg yellow, except hind femur apically, hind tibia apically brown; tegula yellow; wing veins brown; wing membrane yellow, parastigma and pterostigma basally yellow; ovipositor sheath brown; ovipositor yellow.

Male. Unknown.

Biology. Unknown.

Etymology. From *simulo* (Latin for “imitate, copy”), because this new species is similar to *A. glabrum* sp. nov.

Distribution. NC Vietnam (Thua Thien-Hue province) (Fig. 16).

Notes. The new species is closely related to *A. glabrum* sp. nov., but differs from the latter by the following characters: 1) hind wing vein cu-a distinctly longer vein 1-M (25: 22) (vein cu-a as long as 1-M in *A. glabrum*); 2) left hind trochantellus with six teeth (four teeth in *A. glabrum*); 3) marginal cell of hind wing sparsely setose (largely glabrous in *A. glabrum*); and 4) first metasomal tergite transversely striate (partly obliquely striate in *A. glabrum*).

Newly recorded species

***Aulacocentrum seticella* van Achterberg & He, 1994**

Figs 13, 16

Aulacocentrum seticella van Achterberg & He, 1994: 160, figs 2–23, 40.

Material examined. ♀, “Bracn.056” (IEBR), NE Vietnam: Tuyen Quang, Na Hang, Thanh Tuong, forest, 22°19'01.0"N, 105°24'02"E, 162 m, MT, 15.x.2016, KD Long.

Diagnostic characters. Based on specimen collected in Vietnam, female, body length 7.5 mm; antenna with 50 antennomeres, with nine middle flagellomeres ivory; fore wing 6.0 mm; ovipositor 7.9 mm (Fig. 13A); length of maxillary palp 1.6× height of head; ratio of length of fore wing veins r: 3-SR: SR1 = 10: 23: 41, and 2-SR: 3-SR: r-m = 13: 23: 6; notauli converging posteriorly in distinct V-shaped depression (Fig. 13B); mesopleuron widely depressed medio-posteriorly (Fig. 13C); hind wing with vein 2-SC+R vertical; vein 1-M curved basally; vein SR mostly touching anterior margin of the wing (Fig. 13D); metasoma 1.5× as long as head and mesosoma combined; first metasomal tergite nearly parallel-sided; length of first tergite 5.2× its apical width; second tergite distinctly constricted medially, with convergent striation; more than basal 1/2 of third tergite finely, longitudinally striate; the remainder coriaceous, densely setose; ovipositor 1.7× metasoma in lateral view, and 1.3× as long as fore wing.

Male. Unknown.

Biology. Unknown.

Distribution. Eastern Palaearctic: Japan; Korea; Oriental: China (Guangxi, Guizhou); India, Indonesia (Java, Sumatra), Malaysia (Sabah), Singapore, NE Vietnam (Tuyen Quang province: Na Hang NP) (Fig. 16).

Previously recorded species

***Aulacocentrum philippinense* (Ashmead, 1904)**

Figs 14–16

Macrocentrus philippinensis Ashmead, 1904: 145.

Material examined. 1♀, “Macr.088” (IEBR), S Vietnam: Dong Nai, Vinh Cuu, Phu Ly, TWC, forest, 11°22.612'N, 107°03.594'E, 82 m, light trap, 7.vi.2020, PT Nhi; 2♀, “Macr.112”, “Macr.113” (IEBR), NE Vietnam: Ha Giang, Bac Me, Minh Ngoc, forest, 22°43'47.2"N, 105°12'21.3"E; 207 m, light trap, 21.vii.2019, DT Hoa; 1♀, “Macr.168” (IEBR), NW Vietnam: Son La, Thuan Chau, Chieng Bom, forest, 21°21'11"N, 103°36'24"E, 1100 m, light trap, 01.v.2016, HV Tru; 1♀, “Macr.169” (IEBR), NE Vietnam: Tuyen Quang, Na Hang, Trung Phin, forest, 22°30'13.68"N, 105°23'23.82"E, light trap, 18.ix.2017, HTHCT; 1♀, “Macr.175” (IEBR), NE Vietnam: Ha Giang, Dong Van, Pho Bang, light trap, 12.vi–17.vi.2023, Dinh Dieu Thuy; 1♂, “Macr.126” (IEBR), S Vietnam: Dong Nai, Vinh Cuu, Phu Ly, Suoi Rong, forest, 11°29'10.3"N, 107°09'58.8"E, 285 m, light trap, 12.vii.2020, PV Phu.

Description. Male, “Macr.126” (IEBR), body length 8.4 mm, fore wing length 5.9 mm (Fig. 14).

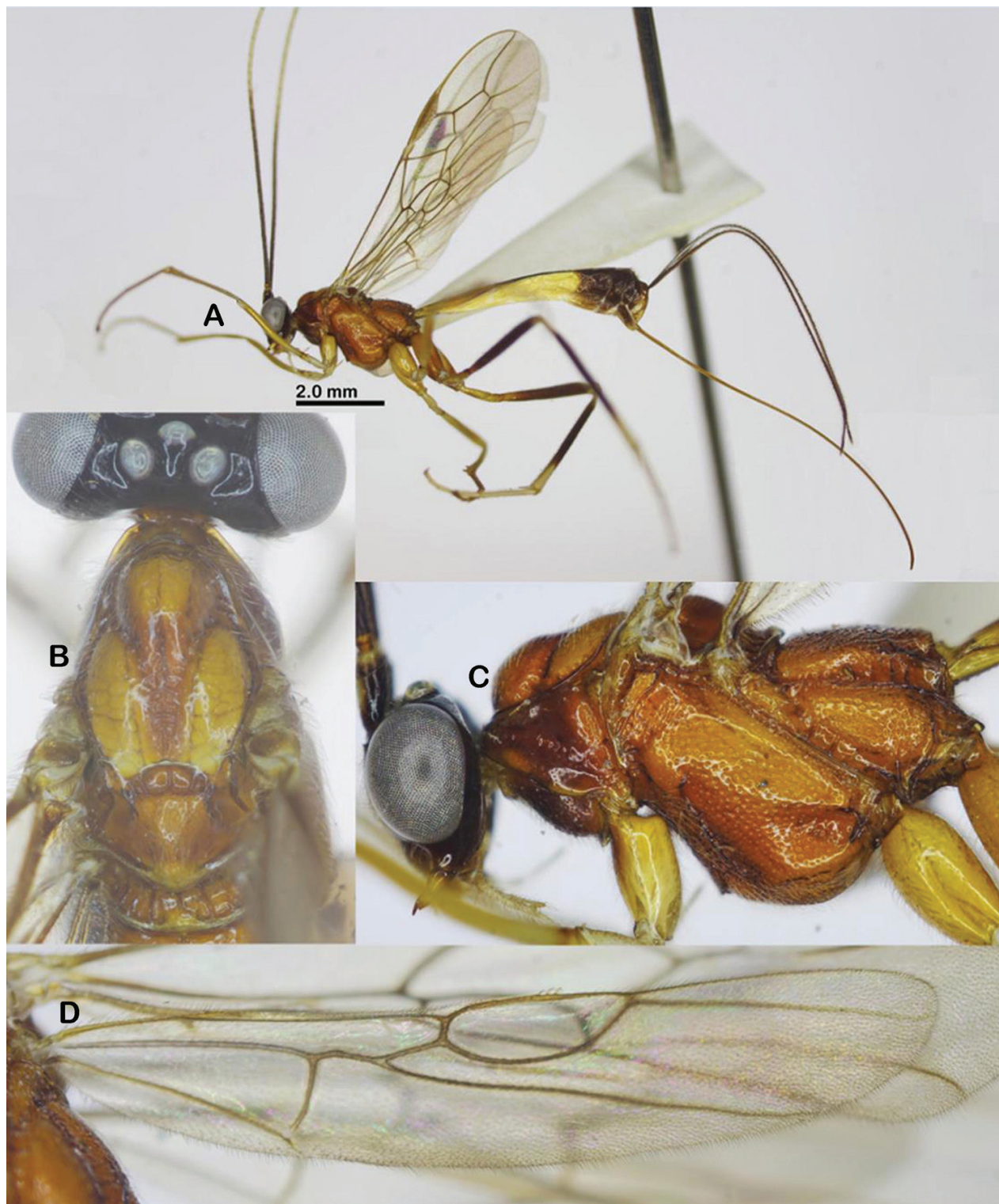


Figure 13. *Aulacocentrum seticella* van Achterberg & He, 1994, "Macr.056" (IEBR) **A** habitus, female, lateral **B** mesonotum **C** mesopleuron **D** hind wing.

Head. Antenna incomplete, with 31 flagellomeres remaining; first flagellomere 1.4× second one; length of first and second flagellomeres 6.8 and 5.0× their widths, respectively; in frontal view, width of face 0.9× its length (Fig. 15B); length of maxillary palp 1.7× height of head; face densely punctate medially, sparsely punctate laterally; malar space as long as basal width of mandible;

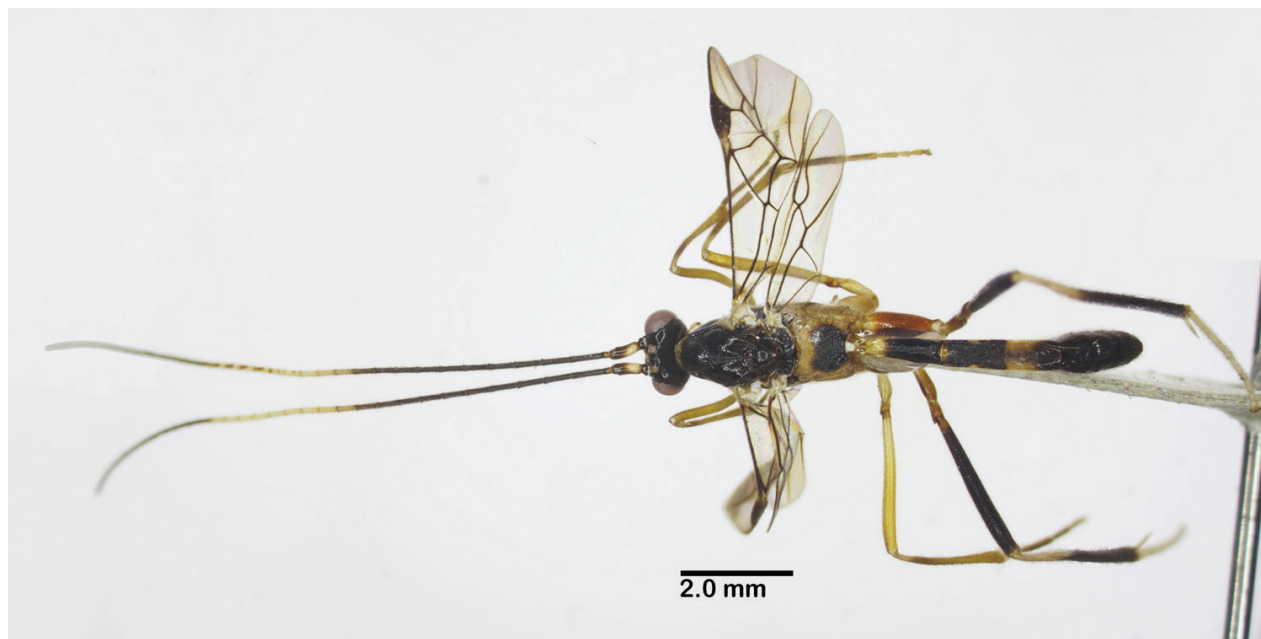


Figure 14. Habitus of *Aulacocentrum philippinense* (Ashmead), male, dorsal, "Macr.126" (IEBR).

clypeus straight ventrally, sparsely, finely punctate; distance between tentorial pits $1.5\times$ distance from pit to eye margin; in dorsal view, width of head $2.4\times$ median length (Fig. 15A); eye $8.3\times$ as long as temple; ocelli medium-sided, OOL: OD: POL = 8: 8: 10 (Fig. 15A); frons, vertex, and temple shiny, smooth; stemmaticum rugose-punctate.

Mesosoma. Length of mesosoma $1.3\times$ its height (Fig. 15E); pronotal trough largely crenulate medially, mostly smooth ventrally and dorsally; propleuron densely punctate (Fig. 15E); middle lobe of mesoscutum rugulose dorsally; punctate ventrally; notauli sparsely crenulate anteriorly, narrowly fused posteriorly with median rugosity (Fig. 15D); scutellar sulcus $2.6\times$ scutellum; scutellum densely punctate; mesopleuron and metapleuron largely rugose-punctate (Fig. 15E); propodeum mostly transversely rugulose (Fig. 15F).

Wings. Length of fore wing $3.3\times$ its maximum width (Fig. 15I); length of pterostigma $3.6\times$ its width; fore wing vein SR1 $2.1\times$ as long as vein 3-SR; r: 3-SR: SR1 = 10: 25: 53; cu-a inclivous (Fig. 15I), cu-a: 1-CU1: 2-CU1 = 11: 5: 47; 2-SR: 3-SR: r-m = 16: 25: 8; second submarginal cell of fore wing narrowed distally; hind wing with vein 2-SC+R horizontal (= longitudinal); vein 1-M weakly curved basally (Fig. 15J); cu-a: 1-M: 1r-m = 15: 10: 10; marginal cell sparsely setose.

Legs. Hind coxa elongate, densely setose latero-ventrally, but without setae dorso-apically; length of femur, tibia, and basitarsus of hind leg 8.2, 14.4, and $8.7\times$ their maximum widths, respectively; left hind trochantellus with four teeth in one row (Fig. 15G); length of hind inner and outer tibial spurs $0.6\times$ and $0.3\times$ hind basitarsus, respectively; length of hind basitarsus $0.4\times$ hind tibia and $1.1\times$ second–fifth tarsal segments combined.

Metasoma. Length of metasoma $1.4\times$ head and mesosoma combined; first tergite nearly flat medio-basally (Fig. 15H); length of first tergite $3.8\times$ its apical width; second tergite $1.1\times$ third tergite medially (Fig. 15H); first metasomal tergite mostly transversely striate; second tergite with convergent striae on basal $2/3$ of the tergite, parallel striation on $1/3$ apical of tergite; third tergite finely

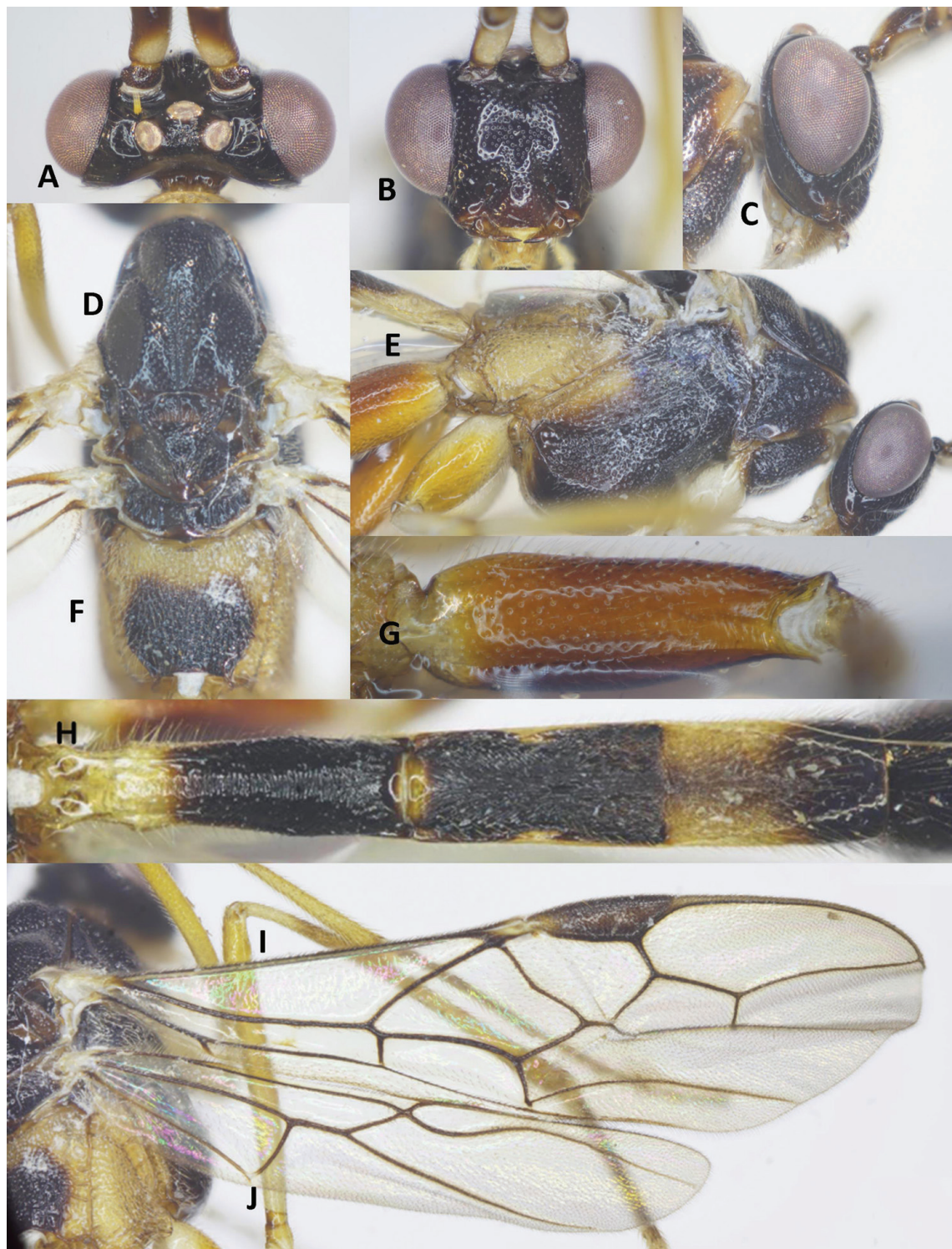


Figure 15. *Aulacocentrum philippinense* (Ashmead), male, "Macr.126" (IEBR) **A** head, dorsal **B** head, frontal **C** head, lateral **D** mesonotum **E** mesopleuron **F** propodeum, dorsal **G** hind coxa **H** first-third metasomal tergites, dorsal **I** fore wing **J** hind wing.

striate on 2/3 basal of tergite; remaining metasomal tergites coriaceous, with long setae.

Colour. Pale-yellow; scapus largely whitish yellow, brown dorsally and outer side laterally; flagellum brown, with 11th–19th middle flagellomeres cream-white; palpi cream-white; fore leg pale yellow except coxa, trochanter and trochantel-



Figure 16. Distribution map of *Aulacocentrum* species.

lus cream-white; middle leg yellow, except coxa basally, trochanter and trochantellus paler; hind coxa yellow, hind trochanter and trochantellus dirty yellow, hind femur entirely, apical 2/3 of hind tibia blackish brown; 1/3 of hind tibia and tarsus cream-white to whitish yellow; pronotum brown, whitish yellow dorsally; mesonotum blackish brown to black; propodeum black, pale yellow basally and ventrally; metapleuron whitish yellow; wing veins brown; tegula whitish yellow; wing membrane hyaline; basal 1/3 of first metasomal tergite pale yellow, apical 2/3, and second tergite entirely black; third tergite whitish yellow basally, blackish brown apically; remainder black; ovipositor sheath brown; ovipositor yellow.

Distribution. NE Vietnam (Ha Giang, Tuyen Quang); NW Vietnam (Son La); S Vietnam (Dong Nai) (Fig. 16).

Acknowledgements

This research is funded by the Vietnam Academy of Sciences and Technology (Project No. UQĐTCB.07/22-24) to the first author. Thanks are due to Mr Hoang Vu Tru (IEBR) for providing some specimens, and to Mr. Nguyen Hoang Vu, Indochina Institute of Biological and Environmental Sciences, Ha Noi, Vietnam, for his help in making the distribution map. The authors are also very grateful to the reviewers for their corrections and useful suggestions on the manuscript.

Additional information

Conflict of interest

The authors have declared that no competing interests exist.

Ethical statement

No ethical statement was reported.

Funding

This research is funded by the Vietnam Academy of Sciences and Technology (Project No. UQĐT.CB.07/22-24) to the first author.

Author contributions


All authors have contributed equally.

Author ORCIDs

Nhi Thi Pham  <https://orcid.org/0000-0001-9304-9863>

Khuat Dang Long  <https://orcid.org/0000-0002-9237-7344>

Cornelis van Achterberg  <https://orcid.org/0000-0002-6495-4853>

Cao Thi Quynh Nga  <https://orcid.org/0000-0001-9369-6649>

Pham Van Phu  <https://orcid.org/0009-0006-0108-5976>

Dang Thi Hoa  <https://orcid.org/0000-0002-8312-2825>



Data availability

All of the data that support the findings of this study are available in the main text.

References

- Ashmead WH (1904) Descriptions of new genera and species of Hymenoptera from the Philippine Islands. *Proceedings of the United States National Museum* 28(1387): 127–158. <https://doi.org/10.5479/si.00963801.28-1387.127>
- Harris RA (1979) A glossary of surface sculpturing. *Occasional Papers in Entomology, California Department of Food and Agriculture* 28: 1–33. https://antcat.s3.amazonaws.com/1631/Harris_1979_Occasional_Papers_in_Entomology_A_glossary_of_surface_sculpturing.pdf
- He J, van Achterberg C (1994) A revision of the genus *Aulacocentrum* Brues (Hymenoptera: Braconidae: Macrocentrinae) from China. *Zoologische Verhandelingen Leiden* 68(15): 159–171. <https://repository.naturalis.nl/pub/318760/ZM1994068015.pdf>
- Ku DS, Park JS (1997) A taxonomic study of the genus *Aulacocentrum* Brues (Hymenoptera, Braconidae, Macrocentrinae) from Korea. *Korean Journal of Systematic Zoology* 13(3): 211–220. <https://koreascience.kr/article/JAKO199711920828729.page>
- Long KD, Belokobylskij SA (2003) A preliminary list of the Braconidae (Hymenoptera) of Vietnam. *Russian Entomological Journal* 12(4): 385–398. <https://www.elibrary.ru/item.asp?id=9170418>
- Sharma V (1978) Taxonomic studies on Indian Braconidae (Hymenoptera). *Oriental Insects* 12(1): 123–132. <https://www.tandfonline.com/doi/abs/10.1080/00305316.1978.10434561>
- van Achterberg C (1993a) Illustrated key to the subfamilies of the Braconidae (Hymenoptera, Ichneumonoidea). *Zoologische Verhandelingen Leiden* 283: 1–189.
- van Achterberg C (1993b) Revision of the subfamily Macrocentrinae Foerster (Hymenoptera, Braconidae) from the Palaearctic region. *Zoologische Verhandelingen Leiden* 286: 1–110.
- Yu DS, van Achterberg C, Horstmann K (2016) *World Ichneumonoidea 2015. Taxonomy, biology, Morphology and Distribution*. Nepean, Ottawa. [database on flash-drive]

Mitochondrial genome data provide insights into the phylogenetic relationships within *Triplophysa dalaica* (Kessler, 1876) (Cypriniformes, Nemacheilidae)

Hao Meng¹, Yingnan Wang², Ge-Xia Qiao^{1,2}, Jun Chen^{1,2}

¹ Key Laboratory of Zoological Systematics and Evolution, Institute of Zoology, Chinese Academy of Sciences, Beijing 100101, China

² National Animal Collection Resource Center, Institute of Zoology, Chinese Academy of Sciences, Beijing 100101, China

Corresponding authors: Ge-Xia Qiao (qiaogx@ioz.ac.cn); Jun Chen (chenj@ioz.ac.cn)

Abstract

Due to the detrimental effect of formaldehyde on DNA, ethanol has replaced formalin as the primary preservative for animal specimens. However, short-term formalin fixation of specimens might be applied during field collection. In an increasing number of studies, DNA extraction and sequencing have been successfully conducted from formalin-fixed specimens. Here the DNA from five specimens of *Triplophysa dalaica* (Kessler, 1876) were extracted and performed high-throughput sequencing. Four of the specimens underwent short-term fixation with formalin and were subsequently transferred to ethanol. One was continuously stored in ethanol. No significant difference of DNA quality and amount were observed among these samples. Followed by assembly and annotation, five mitochondrial genomes ranging in length from 16,569 to 16,572 bp were obtained. Additionally, previously published data of other individuals or species were included to perform phylogenetic analyses. In the reconstructed trees, all eight individuals of *T. dalaica* form a monophyletic group within the *Triplophysa* branch. The group is divided into three clades: (1) samples from the Yellow River, (2) those from the Yangtze River, and (3) those from the Haihe River, and the Lake Dali Nur. This study sheds initial light on the phylogeographic relationships among different populations of *T. dalaica*, and will support the research about its evolutionary history in the future.

Key words: High-throughput sequencing, mitogenome assembly, phylogeny, stone loach



Academic editor: Maria Elina Bichuette

Received: 27 November 2023

Accepted: 14 March 2024

Published: 3 April 2024

ZooBank: <https://zoobank.org/4C6DF6D7-A9CB-4D56-BABB-1E206F3E84EB>

Citation: Meng H, Wang Y, Qiao G-X, Chen J (2024) Mitochondrial genome data provide insights into the phylogenetic relationships within *Triplophysa dalaica* (Kessler, 1876) (Cypriniformes, Nemacheilidae). ZooKeys 1179: 43–55. <https://doi.org/10.3897/zookeys.1179.116342>

Copyright: © Hao Meng et al. This is an open access article distributed under terms of the Creative Commons Attribution License ([Attribution 4.0 International – CC BY 4.0](https://creativecommons.org/licenses/by/4.0/)).

Introduction

Biological specimens preserved in museums represent a reservoir of valuable data. They provide information required in various fields such as taxonomy, geographic distribution, population dynamics, and climate change (Suarez and Tsutsui 2004; Wen et al. 2015). With the progression of historic DNA (hDNA) extraction and sequencing, genetic material contained in specimens of varying ages, taxa, and preservation methods have been more adequately explored (Hartley et al. 2006; Hartnup et al. 2011; Tin et al. 2014; Blaimer et al. 2016; Hawkins et al. 2016; Kehlmaier et al. 2019; Lalonde and Marcus 2020; Cong et al. 2021).

Formalin, an aqueous solution of formaldehyde, has been widely used as a preservative for specimens of invertebrates, fish, amphibians, and reptiles. However, it is a formidable challenge to extract hDNA from formalin-fixed specimens due to formalin's propensity to induce three forms of DNA damage in specimens: (1) fragmentation, (2) cross-linking between DNA and protein molecules, and (3) modification of DNA bases (Quach et al. 2004; Campos and Gilbert 2012; Do and Dobrovic 2012; Wong et al. 2014). In recent studies, hDNA in formalin-fixed specimens have been successfully sequenced (e.g. Hykin et al. 2015; Ruane and Austin 2017; Silva et al. 2017; Kehlmaier et al. 2020; Appleyard et al. 2021; Straube et al. 2021; Agne et al. 2022; Bernstein and Ruane 2022; O'Connell et al. 2022). Most of the modified extraction protocols focus on removal of residual formaldehyde and digestion. The approaches include replacing formaldehyde with ethanol at varying concentrations, pre-treating with high temperature, adding extra proteinase K, and extending digestion time.

Owing to the deleterious impact on genetic material and the inherent toxicity of formaldehyde, ethanol has been used as a preferred preservative instead of formalin. An increasing number of museums have transferred historical specimens preserved in formalin to ethanol. Moreover, due to limitations during fieldwork, specimens may undergo a temporary fixation in formalin and later transferred to ethanol for preservation. This study attempts to process these formalin-to-ethanol samples and conduct high-throughput sequencing (HTS).

Triplophysa is one of the most diverse genera within the family Nemacheilidae, with over 140 documented species in FishBase (Froese and Pauly 2023). In China, species of *Triplophysa* are predominantly distributed across the Qinghai-Tibet Plateau and adjacent regions, with a few occurrences in North China (Zhu 1989). Due to their widespread distribution, species of *Triplophysa* exhibit adaptability to diverse habitats, including cold environments, hypoxia, and saline waters. In recent years, multiple aspects including the phylogenetic relationships among *Triplophysa* species (Wang et al. 2016, 2023; Chen et al. 2019; Wu et al. 2020), phylogeography (Hu et al. 2020, 2022; Zhong et al. 2022; Du et al. 2023), patterns of population differentiation (Zhou et al. 2021b; Jin et al. 2022), and the adaptations to various habitats (Chen et al. 2020b, 2020a; Zhang et al. 2023) have been studied.

Within the genus, *Triplophysa dalaica* (Kessler, 1876) is an endemic species in China. It was initially described and collected from the Lake Dali Nur, which is an alkaline lake located in Inner Mongolia, China (43.38°N, 116.72°43'E). In addition to the Lake Dali Nur and its surrounding lakes and rivers, *T. dalaica* is also distributed in fresh water such as the Yellow River (Zhu 1989; Zhou et al. 2021a), the Haihe River (Zhu 1989; Wang et al. 2001; Zhou et al. 2020), and the Yangtze River (Chen et al. 1987). Recently, a chromosome-level reference genome of the *T. dalaica* was assembled using a sample from the Lake Dali Nur (Zhou et al. 2021a). Other research has primarily focused on its adaptation in response to factors such as hypoxia and salinity fluctuations (Wang et al. 2015; Zhou et al. 2022). Moreover, several analyses related to the phylogeny of loaches within the family Nemacheilidae or the genus *Triplophysa* have included this species (Wang et al. 2016, 2023; Chen et al. 2019; Wu et al. 2020). Nevertheless, the genetic relationships among populations from different water systems remain unknown.

Current study involves five mitogenomes obtained through HTS from *T. dalaica* specimens, and three *T. dalaica* mitogenomes published or assembled from released HTS data, along with 16 published mitogenomes of other species as outgroups. The analyses aim to confirm the taxonomic status of *T. dalaica*, and reconstruct the phylogenetic relationship of populations residing different geographic origins.

Materials and methods

Sample selection and DNA extraction

In this study, five specimens of *Triplophysa dalaica* were selected from the National Animal Collection Resource Center, representing individuals originating from three distinct rivers (Fig. 1; Table 1). Among these, four individuals collected in 2013 underwent formalin fixation for approximately 30 days, while one individual collected in 2019 has been continuously preserved in ethanol with a concentration exceeding 90%. These specimens were chosen to investigate the effects of short-term formalin fixation on the quality and suitability of the preserved material for molecular experiments.

To minimize the potential contamination, the entire DNA extraction process was conducted in a laboratory that had not previously been exposed to fish samples. Fin clips, approximately 5 mm in length from the tip of the right pectoral fin, were utilized. For formalin-fixed samples, a modified version of the protocol outlined by a previous study (Xia et al. 2007) was employed to pre-treat the samples for the removal of any residual formalin. Following the pre-treatment steps, the DNA was extracted using the DNeasy Blood & Tissue Kit (Qiagen, Shanghai, China) and the MinElute PCR Purification Kit (Qiagen, Shanghai, China) to maximize the recovery of fragmented DNA fragments. The protocols for DNA extraction have been uploaded to protocols.io (<https://www.protocols.io/private/FE16637289CE11EE83B20A58A9FEAC02>). The concentration and fragmentation of DNA were assessed by agarose gel electrophoresis or the Agilent 5400 system (Agilent, Palo Alto, USA).

High-throughput sequencing data acquisition

High-throughput sequencing (HTS) was conducted on a Illumina platform with PE150 strategy at Berry Genomics (Beijing, China) and Novogene Bioinformatics Technology Co., Ltd (Beijing, China). In addition to the five individuals sequenced for this study, HTS data for two *T. dalaica* individuals from the Lake Dali Nur and the Haihe River (Fig. 1; Table 1) were obtained from Sequence Read Archive (SRA) on the National Center for Biotechnology Information (NCBI) database using the SRA toolkit v 3.0.5 (<https://github.com/ncbi/sra-tools/>). Approximately 40 million reads were extracted from each individual for subsequent assembly of mitochondrial genomes.

The reads were subjected to quality control using fastp v. 0.23.4 (Chen et al. 2018; Chen 2023). This process involved the removal of reads with an overall quality score lower than 20, elimination of redundant duplicate reads, and trimming of adapter fragments from both ends.

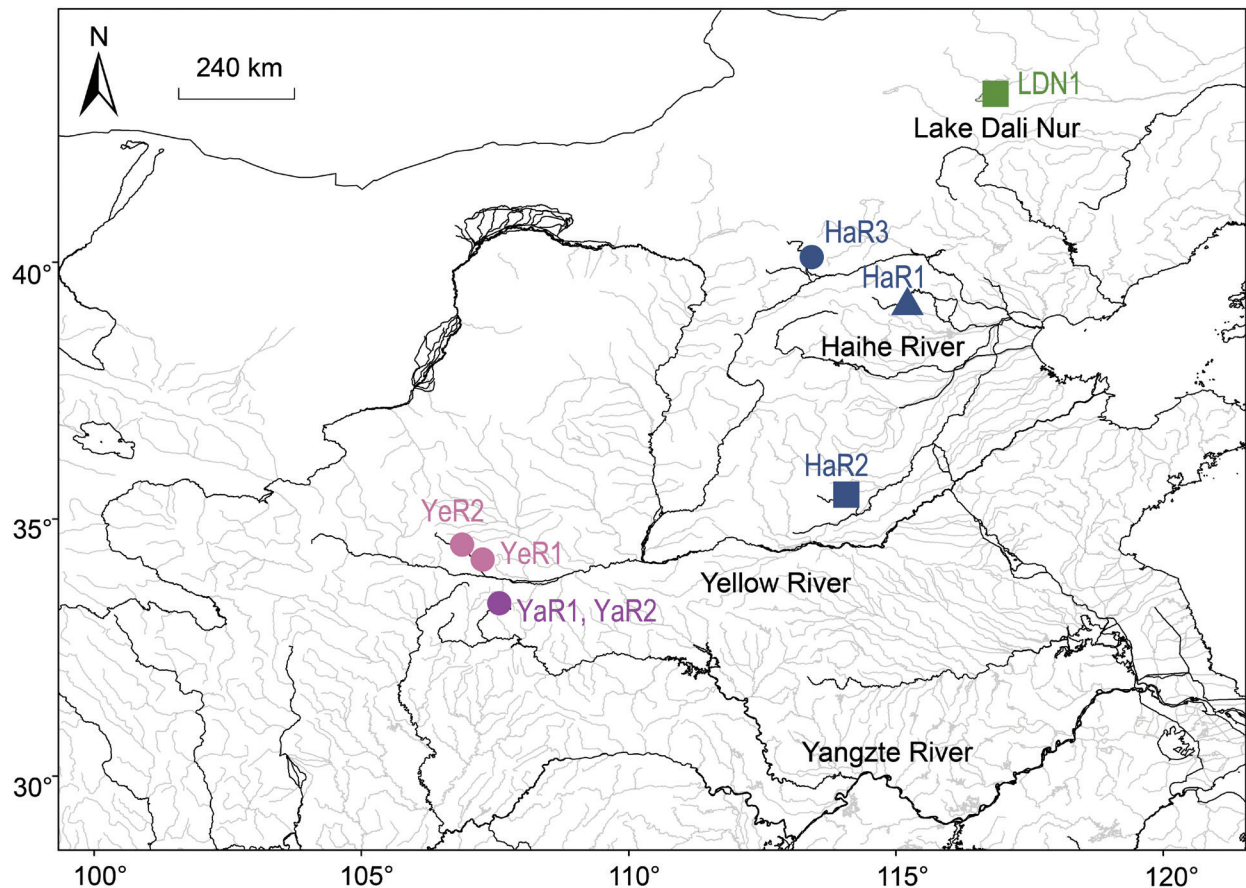


Figure 1. Geographic distribution of the eight *Triplophysa dalaica* samples. Circles: samples sequenced in this research. Triangle: sample with mitochondrial genome available in NCBI. Squares: samples for which mitochondrial genome assembled using released HTS data from NCBI.

Table 1. Information of the eight *Triplophysa dalaica* samples.

ID	Location	Water System	Data Acc. No.	Source
YeR1	34.66°N, 107.04°E	Yellow River	OR857523	This study
YeR2	34.94°N, 106.72°E	Yellow River	OR857524	This study
YaR1	33.85°N, 107.46°E	Yangtze River	OR857525	This study
YaR2	33.85°N, 107.46°E	Yangtze River	OR857526	This study
HaR3	40.32°N, 113.30°E	Haihe River	OR857527	This study
HaR1	Hebei Province	Haihe River	KY945353	Submitted by Feng et al.
HaR2	35.91°N, 113.86°E	Haihe River	SRX8097844	Zhou et al. 2021a
LDN1	43.38°N, 116.66°E	Lake Dali Nur	SRX8097848	Zhou et al. 2021a

Mitogenome assembly and annotation

The reads were mapped to the reference mitogenome of *T. dalaica* in NCBI (accession number KY945353) using Geneious v. 9.1.8 (Biomatters Ltd, Auckland, New Zealand) with 10 iterations in medium-low sensitivity. To eliminate nuclear mitochondrial DNA segments (NUMTs), the mapped reads were subjected to *de novo* assembly using Geneious assembler. This approach yielded a contig approximately 16 kb in length. Subsequently, a manual inspection and

sequence concatenation process was performed at both ends of the contig, resulting in the circular mitochondrial genome.

Following the assembly, the mitogenome was annotated on GeSeq (Tillich et al. 2017) using mitochondrial genomes of *Triplophysa* species available on NCBI as reference sequences. The annotation results also underwent rigorous manual verification.

Phylogenetic reconstruction

In addition to the five mitogenomes obtained in our study and the two assembled from published HTS data, an additional mitogenome of *T. dalaica* from the Haihe River (Fig. 1; Table 1, Suppl. material 1: tables S2, S3) was downloaded from NCBI. Published mitogenomes from another 13 species of *Triplophysa*, two species of Cobitidae, and one species of Gastromyzontidae were also included as outgroups in the phylogenetic analysis (Suppl. material 1: table S3).

The sequences for 13 protein-coding genes (PCGs) without stop codon from the mitogenomes were extracted and aligned based on their translated amino acid sequences with Geneious v. 9.1.8. These alignments were concatenated and indels were preserved, resulting in a total alignment length of 11,427 bp. Subsequently, the optimal partitioning scheme and substitution model for different genes and codon positions were determined by PartitionFinder 2 (Lanfear et al. 2012). Based on 13 PCGs and the positions of three codons, the alignment was partitioned into 39 segments. A “greedy” algorithm was employed to determine the best-fitting partition scheme, estimated by the Bayesian information criterion (BIC). At the same time, the optimal nucleotide substitution model for each partition was determined.

The phylogenetic analysis was performed using both maximum-likelihood (ML) and Bayesian-inference (BI) methods based on the best-fitting partition strategy. For the ML analysis, 1,000 fast bootstrap replicates were conducted with the GTR+I+G substitution model to assess the support values using RAXML v. 8.2.12 (Stamatakis 2014). The BI analysis was conducted using MrBayes v. 3.2.6 (Ronquist et al. 2012). For each partition, the best-fitting model estimated by PartitionFinder 2 was applied. The analysis was performed with four independent runs, each comprising 50 million generations, and the tree was sampled every 1,000 generations. Then the average standard deviation of split frequency and Tracer v. 1.7.2 software was used to assess the convergence of the BI analysis. After discarding the first 12,500 trees as conservative burn-in, the final consensus tree was obtained, and branch-support values were evaluated using Bayesian posterior probabilities (BPP) under a majority-rule criterion.

Divergence time estimation for the three *T. dalaica* clades

With the alignments of the 13 PCGs, the divergence time for three main clades of *T. dalaica* was estimated by a Markov chain Monte Carlo (MCMC) approach using BEAST v. 2.7.6 (Bouckaert et al. 2019). The Yule model was set as tree prior and the random local clock model was used. The nucleotide substitution model was set as suggested by PartitionFinder 2.

Because there is no solid fossil record of *Triplophysa*, a fossil of the genus *Cobitis* was used as time calibration for the tree (Suppl. material 1: fig. S1). The

fossil was estimated to be 13.8–15.9 Ma (Zhou 1992). Three parallel runs were conducted with 100 million generations and the trees were logged every 1,000 generations. The convergence of the parameters was assessed by Tracer v. 1.7.2 (Rambaut et al. 2018) with ESS value. The maximum clade credibility tree was obtained by TreeAnnotator v. 2.7.6 (Bouckaert et al. 2019).

Results

DNA was successfully extracted from the specimens of five *Triplophysa dalaica*. Agarose gel electrophoresis and fragment analysis by Agilent 5400 revealed varying degrees of degradation in the DNA from all these samples, with most fragments shorter than 4 kb. When utilizing nearly equal amounts of fin tissue samples, the DNA concentrations obtained from all five samples fell within the range of 10–30 ng/μL (Suppl. material 1: table S1).

High-throughput sequencing of the five samples yielded an average of approximately 5 Gb of data per sample (Suppl. material 1: table S2). Following quality control and *de novo* assembly, the lengths of mitochondrial genomes ranged from 16,569 to 16,572 bp, and the depth coverage spanning from 16.8-fold to 275.9-fold. Additionally, from published SRA files from two *T. dalaica* individuals collected in the Lake Dali Nur and Haihe River, 36–40 million reads were selected for each individual. After quality control and *de novo* assembly, these reads resulted in two mitochondrial genomes of 16,569 bp in length, with depths of 821.9-fold and 347.8-fold, respectively. Furthermore, a mitogenome for a *T. dalaica* sample from the Haihe River was downloaded from NCBI, which length is 16,569 bp.

The above eight mitochondrial genomes displayed an average base composition of A: 28.13%, T: 28.14%, G: 18.04%, C: 25.63%, and the GC content was 43.67%. These compositions exhibited no significant differences among each other (Chi-squared test, $df = 6$, $p = 0.634$). Following *de novo* assembly, seven mitochondrial genomes were annotated with GeSeq. These mitochondrial genomes included 22 transfer RNA (tRNA) genes, two ribosomal RNA (rRNA) genes, 13 protein-coding genes (PCGs), and one non-coding control region. The 13 PCGs in these eight *T. dalaica* mitochondrial genomes spanned 11,421 bp (including stop codons), encoding a total of 3,800 amino acids. Among these, 1,754 nucleotide and 149 amino acid variable sites were observed. All nucleotide mutations were found to be substitutions, and no insertions or deletions were detected (Suppl. material 1: table S4).

The coding sequences (CDS) without stop codon of the 13 mitochondrial PCGs from these eight *T. dalaica* individuals, along with 13 other *Triplophysa* species, two Cobitidae species, and one Gastromyzontidae species, yielded a total alignment with length of 11,427 bp. This alignment was divided into 39 user-defined partitions based on the three different codon positions of the 13 PCGs. The best scheme consisted of four partitions with its own best-fitting substitution model according to PartitionFinder 2 (Suppl. material 1: table S5).

Subsequently, employing the best-fitting partitioning scheme, phylogenetic trees for all 24 taxa were reconstructed using both RaXML (with a unified GTR + I + G model) and MrBayes (with individual partition-specific best-fitting substitution models). The resulting majority rule consensus trees (Fig. 2) exhibited nearly identical topology. In the trees, all *T. dalaica* individuals clustered together in a well-supported clade, sharing the same branch with other *Triplophysa* species (Fig. 2A).

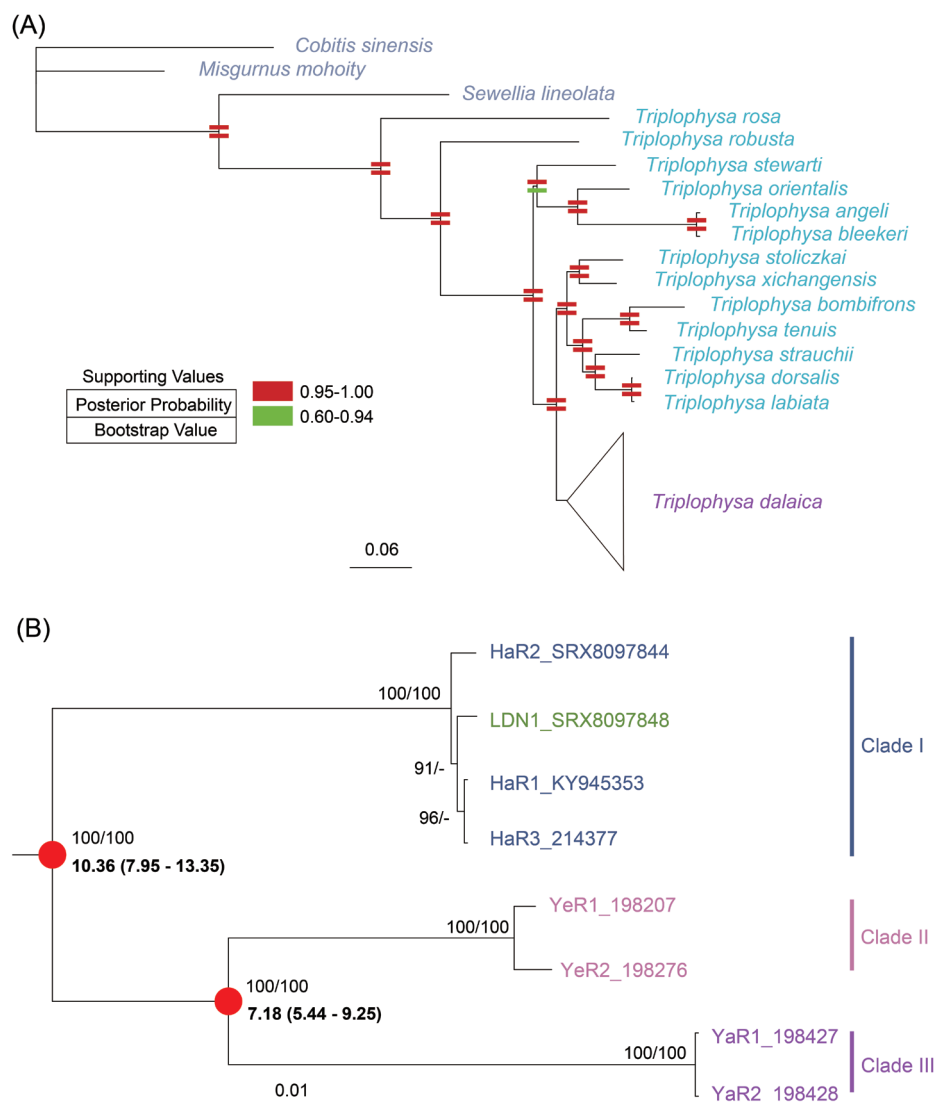


Figure 2. A The majority rule consensus tree constructed using MrBayes based on the CDS of 13 mitochondrial PCGs (excluding stop codons) of eight *Triplophysa dalaica* individuals and outgroup species, totaling 11,427 bp. The topology of the tree closely resembles that constructed by RAxML. Posterior probabilities (from MrBayes) and bootstrap values (from RAxML) for branches are depicted as two different colored rectangles, one above the other **B** details of the clade containing the eight *T. dalaica* individuals in the phylogenetic tree. Numerical values on branches represent posterior probabilities and bootstrap values, respectively. The dashes represent values less than 50. The red dots indicate divergence time estimated by MCMC approach with 95% HPD.

Within the branch of *T. dalaica* (Fig. 2B), three distinct lineages were observed: (I) individuals from the Yangtze River (YaR1 and YaR2); (II) samples from the Yellow River (YeR1 and YeR2); and (III) individuals from the Lake Dali Nur (LDN1) and the Haihe River (HaR1, HaR2, and HaR3). Furthermore, individuals from the Yangtze River and the Yellow River are reciprocally sister groups. Within clade III, the individuals from disconnected water systems did not exhibit significant genetic differentiation.

The divergence time between the *T. dalaica* and its sister clade containing *T. dorsalis* and *T. stoliczkai* was estimated at 11.35 Ma (95% HPD: 8.75–14.6 Ma;

Suppl. material 1: fig. S1), which is close to the time estimated by previous studies (Wang et al. 2016; Wu et al. 2020). Within *T. dalaica*, the divergence time between clade I and MRCA of clades II and III was estimated at approximately 10.36 Ma (95% HPD: 7.95–13.35 Ma), and the clades II and III diverged at about 7.18 Ma (95% HPD: 5.44–9.25 Ma).

Discussion

In this study, DNA was extracted from four samples that underwent short-term formalin fixation and one sample continuously preserved in ethanol. Notably, there were no significant differences in DNA concentration or fragmentation among these samples, and mitogenomic sequences were successfully assembled. It suggests that short-term formalin fixation (for around 30 days) may not significantly contribute to DNA degradation. Therefore, when ethanol is unavailable due to acquisition or transportation in the field, short-term formalin fixation may be considered an acceptable approach. However, prolonged immersion in formalin would lead to irreversible DNA damage. (Quach et al. 2004; Campos and Gilbert 2012; Do and Dobrovic 2012; Wong et al. 2014). It is advisable to promptly transfer samples into preservation solutions like ethanol following the completion of sampling, to mitigate any potential long-term DNA degradation.

The *Triplophysa dalaica* has been reported to inhabit the Lake Dali Nur, surrounding rivers and lakes of Inner Mongolia, as well as the Yellow River, the Haihe River, and the Yangtze River. The geographic sources of the samples analyzed in this study encompass all four of mentioned regions. All *T. dalaica* individuals form a monophyletic branch. This suggests that these eight individuals are the same taxon which belongs to the genus *Triplophysa*. Within the clade, the individuals from the Yangtze River (YaR1 and YaR2) and the Yellow River (YeR1 and YeR2) form two well-supported clusters, signifying the genetic distinctiveness of these two populations. They exhibit a sister relationship, suggesting their most common ancestor diverged from the clade III. Additionally, the sampling sites of the Yangtze and the Yellow Rivers are geographically adjacent, with a straight-line distance of approximately 100 km on the map. Their closer spatial distance correlates their genetic distance.

Clade III includes individuals from the Haihe River (HaR1, HaR2, and HaR3), and the Lake Dali Nur (LDN1), indicating close relationships among these individuals. The divergence-time estimation with mitochondrial PCGs also suggested they differentiated recently. However, a prior study conducted demographic history analysis using whole-genome resequencing data with the software PSMC for these two individuals, and the change of effective population size implied that populations from the Lake Dali Nur and the Haihe River might diverge approximately 1 million years ago (Zhou et al. 2021a). The inconsistency might be caused by mitochondrial introgression or another process. To address the evolutionary history of these two populations, more individuals from Lake Dali Nur and the Haihe River should be collected, and a broader set of nuclear genomic loci should be employed.

In the divergence-time analysis, these three clades were estimated to diverged 7–10 Ma. The divergence is relatively deep compared to the intraspecies differentiation in other *Triplophysa* species (Hu et al. 2020, 2022; Wu et al. 2020; Du et al. 2023), suggesting they might be divided into several potential subspecies, or even species, which need extra analyses including morphology

and phylogeny with more samples. These results offer insights into the evolutionary history of *T. dalaica*, as well as the correlation between the change of population and historical climate and geological events.

Acknowledgements

We thank the collectors of the specimens, Drs Yahui Zhao, Yingchun Xing, Haibo Liu, Xuejian Li, Chengyi Niu, and Jie Bai. They also provided information about specimens collecting and preserving. Yongqiang Wang, Zhiyun Chen, Huanshan Wang, Bo Cai, and other staff of museums and institutes were interviewed for the current status of wet specimen preservation. We thank Dr Baocheng Guo and his group for valuable suggestions on this study.

Additional information

Conflict of interest

The authors have declared that no competing interests exist.

Ethical statement

No ethical statement was reported.

Funding

This research was supported by the National Science & Technology Fundamental Resources Investigation Program of China (grant no. 2019FY101800), and the National Animal Collection Resource Center, China.

Author contributions

Conceptualization: HM. Data curation: HM. Formal analysis: HM, YW. Funding acquisition: JC, GXQ. Investigation: HM. Methodology: HM, YW. Project administration: JC. Resources: GXQ, YW, JC. Supervision: JC. Visualization: HM. Writing – original draft: HM. Writing – review and editing: YW, GXQ, JC.

Author ORCIDs

Hao Meng  <https://orcid.org/0000-0002-9672-9706>

Jun Chen  <https://orcid.org/0000-0002-0325-2532>

Data availability

All of the data that support the findings of this study are available in the main text or Supplementary Information.

References

- Agne S, Preick M, Straube N, Hofreiter M (2022) Simultaneous barcode sequencing of diverse museum collection specimens using a mixed RNA bait set. *Frontiers in Ecology and Evolution* 10: 909846. <https://doi.org/10.3389/fevo.2022.909846>
- Appleyard SA, Maher S, Pogonoski JJ, Bent SJ, Chua XY, McGrath A (2021) Assessing DNA for fish identifications from reference collections: The good, bad and ugly shed light on formalin fixation and sequencing approaches. *Journal of Fish Biology* 98(5): 1421–1432. <https://doi.org/10.1111/jfb.14687>

- Bernstein JM, Ruane S (2022) Maximizing molecular data from low-quality fluid-preserved specimens in natural history collections. *Frontiers in Ecology and Evolution* 10: 893088. <https://doi.org/10.3389/fevo.2022.893088>
- Blaimer BB, Lloyd MW, Guillory WX, Brady SG (2016) Sequence capture and phylogenetic utility of genomic ultraconserved elements obtained from pinned insect specimens. *PLoS One* 11(8): e0161531. <https://doi.org/10.1371/journal.pone.0161531>
- Bouckaert R, Vaughan TG, Barido-Sottani J, Duchêne S, Fourment M, Gavryushkina A, Heled J, Jones G, Kühnert D, De Maio N, Matschiner M, Mendes FK, Müller NF, Ogilvie HA, Du Plessis L, Popinga A, Rambaut A, Rasmussen D, Siveroni I, Suchard MA, Wu CH, Xie D, Zhang C, Stadler T, Drummond AJ (2019) BEAST 2.5: An advanced software platform for Bayesian evolutionary analysis. *PLoS Computational Biology* 15(4): e1006650. <https://doi.org/10.1371/journal.pcbi.1006650>
- Campos PF, Gilbert TMP (2012) DNA extraction from formalin-fixed material. In: Shapiro B, Hofreiter (Eds) *Ancient DNA: Methods and Protocols*. Humana Press, Totowa, 81–85. <https://doi.org/10.1007/978-1-61779-516-9>
- Chen S (2023) Ultrafast one-pass FASTQ data preprocessing, quality control, and deduplication using fastp. *iMeta* 2(2): e107. <https://doi.org/10.1002/imt2.107>
- Chen JX, Xu TQ, Fang S, Song SL, Wang X (1987) *Fishes in Qinling Mountain area*. Science Press, Beijing, 260 pp.
- Chen S, Zhou Y, Chen Y, Gu J (2018) Fastp: An ultra-fast all-in-one FASTQ preprocessor. *Bioinformatics (Oxford, England)* 34(17): i884–i890. <https://doi.org/10.1093/bioinformatics/bty560>
- Chen W, Yang J, Li Y, Li X (2019) Exploring taxonomic diversity and biogeography of the family Nemacheilinae (Cypriniformes). *Ecology and Evolution* 9(18): 10343–10353. <https://doi.org/10.1002/ece3.5553>
- Chen J, Shen Y, Wang J, Ouyang G, Kang J, Lv W, Yang L, He S (2020a) Analysis of multiplicity of hypoxia-inducible factors in the evolution of *Triplophysa* fish (Osteichthyes: Nemacheilinae) reveals hypoxic environments adaptation to Tibetan Plateau. *Frontiers in Genetics* 11: 1–15. <https://doi.org/10.3389/fgene.2020.00433>
- Chen SA, Hou J, Yao N, Xie C, Li D (2020b) Comparative transcriptome analysis of *Triplophysa yarkandensis* in response to salinity and alkalinity stress. *Comparative Biochemistry and Physiology. Part D, Genomics & Proteomics* 33: 100629. <https://doi.org/10.1016/j.cbd.2019.100629>
- Cong Q, Shen J, Zhang J, Li W, Kinch LN, Calhoun JV, Warren AD, Grishin NV (2021) Genomics reveals the origins of historical specimens. *Molecular Biology and Evolution* 38(5): 2166–2176. <https://doi.org/10.1093/molbev/msab013>
- Do H, Dobrovic A (2012) Dramatic reduction of sequence artefacts from DNA isolated from formalin-fixed cancer biopsies by treatment with uracil-DNA glycosylase. *Oncotarget* 3(5): 546–558. <https://doi.org/10.18632/oncotarget.503>
- Du YY, Zhang YP, Lou ZY, Wang T (2023) Unrecognized diversity, genetic structuring, and phylogeography of the genus *Triplophysa* (Cypriniformes: Nemacheilidae) sheds light on two opposite colonization routes during Quaternary glaciation that occurred in the Qilian Mountains. *Ecology and Evolution* 13(4): e10003. <https://doi.org/10.1002/ece3.10003>
- Froese R, Pauly D (2023) FishBase. <https://fishbase.org> [Accessed on: 2024-3-21]
- Hartley CJ, Newcomb RD, Russell RJ, Yong CG, Stevens JR, Yeates DK, La Salle J, Oakeshott JG (2006) Amplification of DNA from preserved specimens shows blowflies were preadapted for the rapid evolution of insecticide resistance. *Proceedings of the National Academy of Sciences of the United States of America* 103(23): 8757–8762. <https://doi.org/10.1073/pnas.0509590103>

- Hartnup K, Huynen L, Te Kanawa R, Shepherd LD, Millar CD, Lambert DM (2011) Ancient DNA recovers the origins of mori feather cloaks. *Molecular Biology and Evolution* 28(10): 2741–2750. <https://doi.org/10.1093/molbev/msr107>
- Hawkins MTR, Leonard JA, Helgen KM, McDonough MM, Rockwood LL, Maldonado JE (2016) Evolutionary history of endemic Sulawesi squirrels constructed from UCEs and mitogenomes sequenced from museum specimens. *BMC Evolutionary Biology* 16(1): 80. <https://doi.org/10.1186/s12862-016-0650-z>
- Hu J, Liu M, He D (2020) Phylogeography of *Triplophysa stenura* (Nemacheilidae): Responded to the Mid-Pleistocene climate transition in the Qinghai-Tibetan Plateau. *Zoological Studies (Taipei, Taiwan)* 59: 67. <https://doi.org/10.6620/ZS.2020.59-67>
- Hu J, Zhao J, Sui X, Zhu R, He D (2022) Across the highest mountain on earth: Discordant phylogeographic patterns and recent dispersal of Tibetan stone loaches (*Triplophysa*) in the Himalayas. *Journal of Fish Biology* 104(2): 374–386. <https://doi.org/10.1111/jfb.15296>
- Hykin SM, Bi K, McGuire JA (2015) Fixing formalin: A method to recover genomic-scale DNA sequence data from formalin-fixed museum specimens using high-throughput sequencing. *PLoS One* 10(10): e0141579. <https://doi.org/10.1371/journal.pone.0141579>
- Jin L, Li Z, Wang C, Wang Y, Li X, Yang J, Zhao Y, Guo B (2022) Contrasting population differentiation in two sympatric *Triplophysa* loaches on the Qinghai-Tibet Plateau. *Frontiers in Genetics* 13: 1–16. <https://doi.org/10.3389/fgene.2022.958076>
- Kehlmaier C, Zhang X, Georges A, Campbell PD, Thomson S, Fritz U (2019) Mitogenomics of historical type specimens of Australasian turtles: Clarification of taxonomic confusion and old mitochondrial introgression. *Scientific Reports* 9(1): 5841. <https://doi.org/10.1038/s41598-019-42310-x>
- Kehlmaier C, Zinenko O, Fritz U (2020) The enigmatic Crimean green lizard (*Lacerta viridis magnifica*) is extinct but not valid: Mitogenomics of a 120-year-old museum specimen reveals historical introduction. *Journal of Zoological Systematics and Evolutionary Research* 58(1): 303–307. <https://doi.org/10.1111/jzs.12345>
- Kessler KF (1876) Fishes. Mongoliya i strana tangutov. Trekhletnee puteshestvie v vostochnoi Nagornoj Azii N. Przheval'skogo [Mongolia and the Tangut Country: the Three-Year Expedition of N. Przewalski to the Mountain Asia]. Vol. II. Imperatorskoe Russkoe Geograficheskoe Obshchestvo, St. Petersburg, 1–36.
- Lalonde MML, Marcus JM (2020) How old can we go? Evaluating the age limit for effective DNA recovery from historical insect specimens. *Systematic Entomology* 45(3): 505–515. <https://doi.org/10.1111/syen.12411>
- Lanfear R, Calcott B, Ho SYW, Guindon S (2012) PartitionFinder: Combined selection of partitioning schemes and substitution models for phylogenetic analyses. *Molecular Biology and Evolution* 29(6): 1695–1701. <https://doi.org/10.1093/molbev/mss020>
- O'Connell KA, Mulder KP, Wynn A, de Queiroz K, Bell RC (2022) Genomic library preparation and hybridization capture of formalin-fixed tissues and allozyme supernatant for population genomics and considerations for combining capture- and RADseq-based single nucleotide polymorphism data sets. *Molecular Ecology Resources* 22(2): 487–502. <https://doi.org/10.1111/1755-0998.13481>
- Quach N, Goodman MF, Shibata D (2004) *In vitro* mutation artifacts after formalin fixation and error prone translesion synthesis during PCR. *BMC Clinical Pathology* 4(1): 1–5. <https://doi.org/10.1186/1472-6890-4-1>
- Rambaut A, Drummond AJ, Xie D, Baele G, Suchard MA (2018) Posterior summarization in Bayesian phylogenetics using Tracer 1.7. *Systematic Biology* 67(5): 901–904. <https://doi.org/10.1093/sysbio/syy032>

- Ronquist F, Teslenko M, Van Der Mark P, Ayres DL, Darling A, Höhna S, Larget B, Liu L, Suchard MA, Huelsenbeck JP (2012) MrBayes 3.2: Efficient bayesian phylogenetic inference and model choice across a large model space. *Systematic Biology* 61(3): 539–542. <https://doi.org/10.1093/sysbio/sys029>
- Ruane S, Austin CC (2017) Phylogenomics using formalin-fixed and 100+ year-old intrac-table natural history specimens. *Molecular Ecology Resources* 17(5): 1003–1008. <https://doi.org/10.1111/1755-0998.12655>
- Silva PC, Malabarba MC, Malabarba LR (2017) Using ancient DNA to unravel taxonomic puzzles: the identity of *Deuterodon pedri* (Ostariophysi: Characidae). *Neotropical Ichthyology* 15(1): e160141. <https://doi.org/10.1590/1982-0224-20160141>
- Stamatakis A (2014) RAxML version 8: A tool for phylogenetic analysis and post-analysis of large phylogenies. *Bioinformatics (Oxford, England)* 30(9): 1312–1313. <https://doi.org/10.1093/bioinformatics/btu033>
- Straube N, Lyra ML, Paijmans JLA, Preick M, Basler N, Penner J, Rödel MO, Westbury MV, Haddad CFB, Barlow A, Hofreiter M (2021) Successful application of ancient DNA extraction and library construction protocols to museum wet collection specimens. *Molecular Ecology Resources* 21(7): 2299–2315. <https://doi.org/10.1111/1755-0998.13433>
- Suarez A, Tsutsui N (2004) The value of museum collections for research and society. *Bioscience* 54(1): 66–74. [https://doi.org/10.1641/0006-3568\(2004\)054\[0066:T-VOMCF\]2.0.CO;2](https://doi.org/10.1641/0006-3568(2004)054[0066:T-VOMCF]2.0.CO;2)
- Tillich M, Lehwark P, Pellizzer T, Ulbricht-Jones ES, Fischer A, Bock R, Greiner S (2017) GeSeq – Versatile and accurate annotation of organelle genomes. *Nucleic Acids Research* 45(W1): W6–W11. <https://doi.org/10.1093/nar/gkx391>
- Tin MMY, Economo EP, Mikheyev AS (2014) Sequencing degraded DNA from non-destructively sampled museum specimens for RAD-tagging and low-coverage shotgun phylogenetics. *PLoS One* 9(5): e96793. <https://doi.org/10.1371/journal.pone.0096793>
- Wang SA, Wang ZM, Li GL, Cao YP (2001) *The Fauna of Hebei, China: Pisces*. Hebei Science and Technology Publishing House, Shijiazhuang, 169 pp.
- Wang Y, Yang L, Wu B, Song Z, He S (2015) Transcriptome analysis of the plateau fish (*Triplophysa dalaica*): Implications for adaptation to hypoxia in fishes. *Gene* 565(2): 211–220. <https://doi.org/10.1016/j.gene.2015.04.023>
- Wang Y, Shen Y, Feng C, Zhao K, Song Z, Zhang Y, Yang L, He S (2016) Mitogenomic perspectives on the origin of Tibetan loaches and their adaptation to high altitude. *Scientific Reports* 6(1): 1–10. <https://doi.org/10.1038/srep29690>
- Wang X, Song Y, Xie H, Zi F, Chen S, Luo S (2023) Complete mitogenome of the *Triplophysa bombifrons*: Comparative analysis and phylogenetic relationships among the members of *Triplophysa*. *Genes* 14(1): 128. <https://doi.org/10.3390/genes14010128>
- Wen J, Ickert-Bond SM, Appelhans MS, Dorr LJ, Funk VA (2015) Collections-based systematics: Opportunities and outlook for 2050. *Journal of Systematics and Evolution* 53(6): 477–488. <https://doi.org/10.1111/jse.12181>
- Wong SQ, Li J, Tan AYC, Vedururu R, Pang JMB, Do H, Ellul J, Doig K, Bell A, Macarthur GA, Fox SB, Thomas DM, Fellowes A, Parisot JP, Dobrovic A (2014) Sequence artefacts in a prospective series of formalin-fixed tumours tested for mutations in hotspot regions by massively parallel sequencing. *BMC Medical Genomics* 7(1): 1–10. <https://doi.org/10.1186/1755-8794-7-23>
- Wu H, Gu Q, Zhou C, Tang Y, Husemann M, Meng X, Zhang J, Nie G, Li X (2020) Molecular phylogeny and biogeography of *Triplophysa* stone loaches in the Central Chinese Mountains. *Biological Journal of the Linnean Society. Linnean Society of London* 130(3): 563–577. <https://doi.org/10.1093/biolinnean/blaa060>

- Xia YZ, Zhang CG, Chen YY, Sheng Y, Sun YH (2007) Discussing on the feasibility of large fragments DNA extraction from formalin-fixed fish specimens. *Shui Sheng Sheng Wu Hsueh Bao* 31: 485–491. <https://doi.org/10.3321/j.issn:1000-3207.2007.04.006>
- Zhang X, Wang T, Zhai D, Liu H, Xiong F, Wang Y (2023) Transcriptome analysis and gene expression analysis related to salinity-alkalinity and low temperature adaptation of *Triplophysa yarkandensis*. *Frontiers in Genetics* 13: 1089274. <https://doi.org/10.3389/fgene.2022.1089274>
- Zhong H, Sun Y, Wu H, Li S, Shen Z, Yang C, Wen M, Chen P, Gu Q (2022) Pleistocene climate and geomorphology drive the evolution and phylogeographic pattern of *Triplophysa robusta* (Kessler, 1876). *Frontiers in Genetics* 13: 955382. <https://doi.org/10.3389/fgene.2022.955382>
- Zhou J (1992) A new *Cobitis* from the middle Miocene of Shanwang, Shandong. *Vertebrata Palasiatica* 30: 71–76.
- Zhou C, Hu B, Ma W, Yang C, Zhao W, Li B, Meng X, Tang Y, Nie G (2020) A new fish record of the genus *Triplophysa* In Henan Province – *Triplophysa dalaica*. *Henan Shifan Daxue Xuebao. Ziran Kexue Ban* 48: 113–124.
- Zhou C, Hu B, Tang Y, Yang C, Ma W, Wang X, Liu R, Yan X, Dong J, Wang X, Nie G (2021a) The chromosome-level genome of *Triplophysa dalaica* (Cypriniformes: Cobitidae) provides insights into its survival in extremely alkaline environment. *Genome Biology and Evolution* 13(8): evab153. <https://doi.org/10.1093/gbe/evab153>
- Zhou X, Yi S, Zhao W, Zhou Q, Shen J, Li D, Huo B, Tang R (2021b) Genetic diversity and population differentiation of kashgarian loach (*Triplophysa yarkandensis*) in xinjiang tarim river basin. *Biology (Basel)* 10(8): 734. <https://doi.org/10.3390/biology10080734>
- Zhou C, Hu B, Tang Y, Chen X, Ma Z, Ding Q, Nie G (2022) Genome-wide characterization of the *Triplophysa dalaica slc4* gene family and expression profiles in response to salinity changes. *BMC Genomics* 23(1): 284. <https://doi.org/10.1186/s12864-022-09057-8>
- Zhu SQ (1989) The loaches of the subfamily Nemacheilinae in China (Cypriniformes: Cobitidae). Jiangsu Science and Technology Publishing House, Nanjing, 82 pp.

Supplementary material 1

Supplementary data

Authors: Hao Meng, Yingnan Wang, Ge-Xia Qiao, Jun Chen





Data type: pdf

Explanation note: **table S1**. Collecting and extraction information of the five *Triplophysa dalaica* samples; **table S2**. Summary of reads used for the mitochondrial genome assembly; **table S3**. Summary of the published mitogenomes used in phylogenetic analyses; **table S4**. Variable sites of the 13 PCGs in eight *T. dalaica* mitochondrial genomes; **table S5**. The best partition scheme and substitution model by Partition-Finder 2; **figure S1**. Divergence time among mitogenomes in this study with MCMC approach.

Copyright notice: This dataset is made available under the Open Database License (<http://opendatacommons.org/licenses/odbl/1.0/>). The Open Database License (ODbL) is a license agreement intended to allow users to freely share, modify, and use this Dataset while maintaining this same freedom for others, provided that the original source and author(s) are credited.

Link: <https://doi.org/10.3897/zookeys.1179.116342.suppl1>

Hidden in the riffles: A new suckermouth catfish (Mochokidae, *Chiloglanis*) from the middle Zambezi River system, Zimbabwe

Tadiwa I. Mutizwa^{1,2}, Wilbert T. Kadye^{1,2}, Pedro H. N. Bragança^{2,3}, Taurai Bere⁴, Albert Chakona^{1,2}

1 Department of Ichthyology and Fisheries Science, Faculty of Science, Rhodes University, Prince Alfred Street, PO Box 94, Makhanda, 6140, South Africa

2 NRF-South African Institute for Aquatic Biodiversity, Somerset Street, Private Bag 1015, Makhanda, 6140, South Africa

3 Department of Ichthyology, American Museum of Natural History, Central Park West at 79th Street, New York, NY 10024, USA

4 School of Wildlife, Ecology and Conservation, Chinhoyi University of Technology, Private Bag 7724, Chinhoyi, Zimbabwe

Corresponding author: Tadiwa I. Mutizwa (timutizwa@gmail.com)

Abstract

The recent surge in the discovery of hidden diversity within rheophilic taxa, particularly in West and East Africa, prompted a closer examination of the extent to which the current taxonomy may obscure the diversity of riffle-dwelling suckermouth catfishes in the genus *Chiloglanis* in southern Africa. Currently, the region comprises eight valid species within this genus. Seven of them have relatively narrow geographic distribution ranges except for *C. neumanni*, which is considered to be widely distributed, occurring from the Buzi River system in the south, and its northern limit being the eastward draining river systems in Tanzania. Recent surveys of the middle Zambezi River system revealed *Chiloglanis* specimens that were distinguishable from the known species of the genus from southern Africa. Integration of molecular and morphological data indicated that these specimens from the Mukwadzi River represent a new species to science, herein described as *Chiloglanis carnatus* Mutizwa, Bragança & Chakona, **sp. nov.** This species is readily distinguished from its southern African congeners by the possession of a distinctive extended dermal tissue covering the base of the dorsal fin and the possession of ten mandibular teeth (vs 8, 12, or 14 in the other taxa). Results from this study add to the growing evidence of a high level of undocumented diversity within riffle-dwelling taxa in southern Africa.

Key words: Diversity, freshwater, integrative taxonomy, rheophilic taxa, southern Africa



Academic editor: Maria E. Bichuette

Received: 24 October 2023

Accepted: 22 January 2024

Published: 4 April 2024

ZooBank: <https://zoobank.org/9146C6EC-E8DA-46E9-8595-70067C65ABF9>

Citation: Mutizwa TI, Kadye WT, Bragança PHN, Bere T, Chakona A (2024) Hidden in the riffles: A new suckermouth catfish (Mochokidae, *Chiloglanis*) from the middle Zambezi River system, Zimbabwe. ZooKeys 1197: 57–91. <https://doi.org/10.3897/zookeys.1197.114679>

Copyright: © Tadiwa I. Mutizwa et al. This is an open access article distributed under terms of the Creative Commons Attribution License ([Attribution 4.0 International – CC BY 4.0](https://creativecommons.org/licenses/by/4.0/)).

Introduction

Rheophilic habitats are characterised by fast flowing water and rocky substratum, which provide a wide range of specialised niches for distinct aquatic taxa adapted to these environments (Thompson 2013; Hrbek et al. 2018). Delimitation of species boundaries in rheophilic taxa using only morphological traits has previously presented challenges due to their superficially similar morphology, which is shaped by exposure to similar environmental drivers (Seegers 2008). However, integrative taxonomy as well as recent collections in under-sampled areas within the African continent have changed the previous perception that rheophilic habitats were depauperate (Schmidt et al. 2015, 2016, 2017, 2023; Thomson et al.

2015; Schmidt and Barrientos 2019; Kashindye et al. 2021; Mazungula and Chakona 2021; Day et al. 2023). These studies, which implemented integrative taxonomic approaches, have allowed the discovery of hidden diversity, particularly within the catfish genera *Chiloglanis* Peters, 1868 and *Amphilius* Günther, 1864, from different regions of the continent. An emerging pattern shows that species that were previously perceived to have broad geographic ranges represent species complexes comprising distinct lineages confined to specific river basins (Chakona et al. 2018; Mutizwa et al. 2021). Recently, a careful examination of the once broadly distributed catfish species, *C. occidentalis* Pellegrin, 1933 and *C. micropogon* Poll, 1952 from West Africa and *A. natalensis* Boulenger, 1917 from southern Africa, resulted in the description of 15 new species (Schmidt et al. 2017, 2023; Mazungula and Chakona 2021). Following these findings, rheophilic habitats have been identified as a new frontier for the discovery of hidden diversity of freshwater fishes in southern Africa and other poorly explored regions on the continent (Morris et al. 2016; Schmidt et al. 2016; Chakona et al. 2018).

The Mochokidae is the most species-rich freshwater catfish family that is endemic to Africa (Vigliotta 2008). Currently, this family has 228 valid species that are distributed across several river systems in sub-Saharan Africa, with the highest diversity occurring in the Congo River (Seegers 2008; Vigliotta 2008; Fricke et al. 2024). The Mochokidae is sister to a clade containing families Auchenoglanididae, Claroteidae, Malapteruridae, and Schilbeidae (Sullivan et al. 2006; Schedel et al. 2022). The genera within Mochokidae have been split into two subfamilies: the first is Chiloglanidinae, characterised by lips and barbels that are modified into an oral disc (suckermouth), a structure that is absent in the second subfamily Mochokinae. Chiloglanidinae contains the genera *Chiloglanis* Peters, 1868, *Atopodontus* Friel & Vigliotta, 2008, *Atopochilus* Sauvage, 1879, and *Euchilichthys* Boulenger, 1900, whereas Mochokinae includes the genera *Mochokus* Joannis, 1835, *Mochokiella* Howes, 1980, *Acanthocleithron* Nichols & Griscom, 1917, *Microsynodontis* Boulenger, 1903, and *Synodontis* Cuvier, 1816. Some of the intergeneric (e.g., the monophyly of Mochokinae) and the intrageneric (e.g., the monophyly of *Synodontis*) relationships within Mochokidae are not well supported and require broader species sampling to resolve (Sullivan et al. 2006; Vigliotta 2008; Day et al. 2013; Pinton et al. 2013; Schedel et al. 2022). Currently, in southern Africa *Chiloglanis* has eight recognised species: *C. bifurcus* Jubb & Le Roux, 1969, *C. emarginatus* Jubb & Le Roux, 1969, *C. anoterus* Crass, 1960, *C. paratus* Crass, 1960, *C. fasciatus* Pellegrin, 1936, *C. pretoriae* Van der Horst, 1931, *C. swierstrai* Van der Horst, 1931, and *C. neumanni* Boulenger, 1911. Except for *C. neumanni*, all these species are narrow range endemics (Fig. 1). For example, *C. bifurcus* is confined to a relatively small geographical range, occurring between 900 and 1200 metres above sea level in the Inkomati River system (Roux and Hoffman 2017a).

Uncertainties about the identity of the broadly distributed *C. neumanni* in southern Africa have persisted for decades. This species was described from the Bubu River, a tributary of the Great Ruaha River basin in Tanzania, and was considered to be distributed across several eastern, central, and southern African river systems (Daget et al. 1986; Bell-Cross and Minshull 1988). However, following extensive surveys of river systems in east Africa and comprehensive examination of specimens from this region, Seegers (1996) did not record *C. neumanni* from localities outside the Great Ruaha River system, indicating that this species was not as widely distributed as previously thought. Although

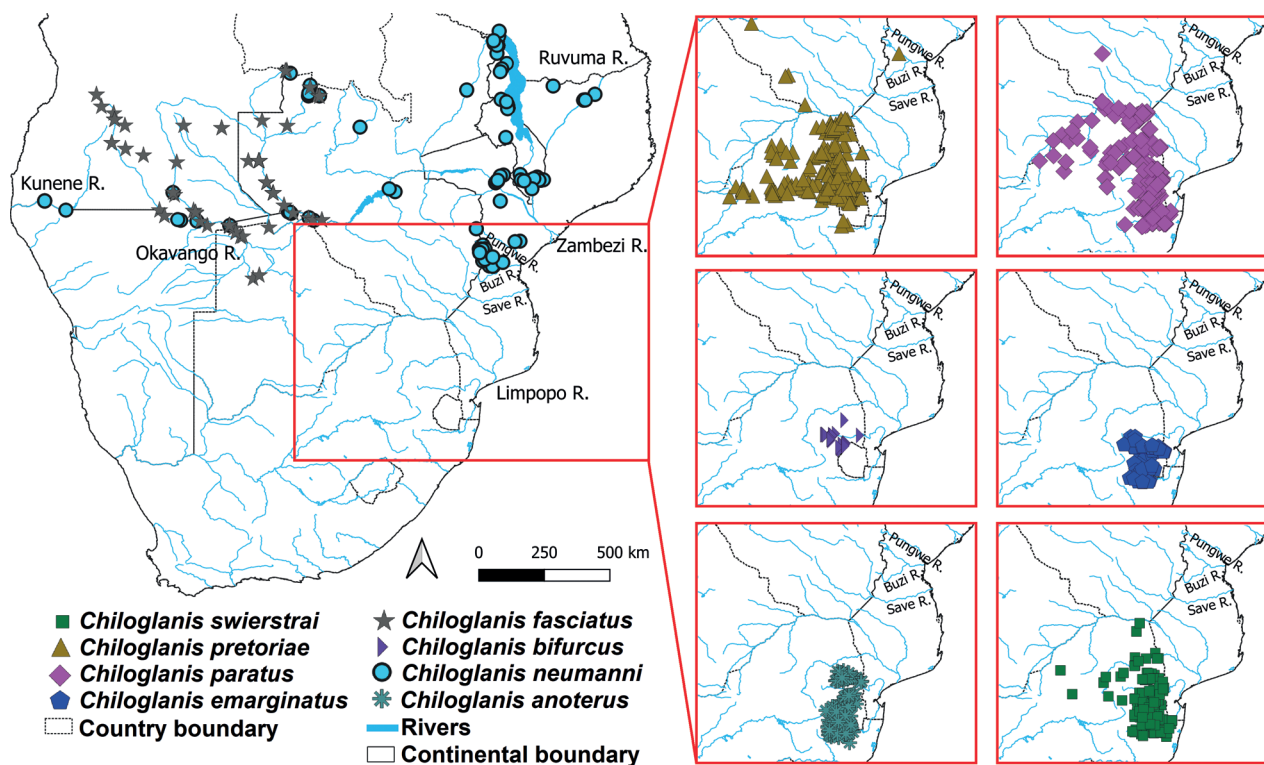


Figure 1. Distribution of *Chiloglanis* species in southern Africa based on data from the National Research Foundation-South African Institute for Aquatic Biodiversity extracted from the GIBF database (<https://www.gbif.org>).

the name *C. neumanni* has persisted in subsequent literature from southern Africa, ichthyologists have consistently made remarks that the suckermouth catfishes of this region required detailed taxonomic investigation to determine their identity (Marshall 2011). In recent years, there has been general consensus among southern African ichthyologists that the species currently referred to as *C. neumanni* in this region actually represents an undescribed species or even a species complex, including several undescribed species. This assertion is based on the extensive geographic distance between southern Africa and the Bubu River, as well as the emerging patterns of undescribed diversity within other species with similar distribution ranges as *C. neumanni*. For example, studies of *A. uranoscopus* (Pfeffer, 1889) and *Zaireichthys rotundiceps* (Hilgendorf, 1905) led to the resurrection of two synonyms and the description of nine new species (Thomson and Page 2010; Eccles et al. 2011). Indeed, a genetic study by Chakona et al. (2018) identified six unique lineages within the genus *Chiloglanis* from the Eastern Zimbabwe Highlands ecoregion, a result that is consistent with Marshall's (2011) postulation that the continued use of the name *C. neumanni* in southern Africa potentially obscures the actual diversity of this group of fishes in this region. A total of four new species to science are currently being described from the Eastern Zimbabwe Highlands ecoregion, with two of them being endemic to this region (Chakona et al., pers. obs.).

During surveys of the southern tributaries of the middle Zambezi River system in 2016 and 2019, morphologically distinct suckermouth catfishes were collected from the Mukwadzi River that drains the western margin of the Great Dyke in Zimbabwe. These specimens could not be attributed to any of the currently described species or recently identified lineages of *Chiloglanis* from this region. The present work represents the first in a series of studies that aim to resolve the

taxonomy of suckermouth catfishes of southern Africa. This study applied integrative taxonomic approaches combining genetic and morphological data to determine the taxonomic distinctiveness of the recently collected specimens from the middle Zambezi River. The significance and implications of incomplete documentation of the diversity of rheophilic species in a region where their unique habitats are under threat from multiple environmental impacts are discussed.

Materials and methods

Collections

Specimens were collected from two sites in the Mukwadzi River, a tributary of the Manyame River, a south bank affluent of the middle Zambezi River, during surveys in 2016 and 2019. Samples were collected using a battery-powered Samus 725GN backpack electric fisher with a block net placed downstream to capture dislodged animals in the fast-flowing current. The specimens were photographed to document the live colour pattern then euthanized with clove oil. Muscle tissue from the right side of the specimens was cut out and preserved in 99% ethanol for molecular analysis. Voucher specimens for morphological studies were fixed in 10% formalin in the field and subsequently transferred to 70% ethanol for long term preservation. Additional tissue samples and voucher specimens used in the present study were obtained from the National Fish Collection at the National Research Foundation-South African Institute for Aquatic Biodiversity (NRF-SAIAB) in Makhanda (Tables 1, 2).

Table 1. List of 80 COI sequences used in the present study including six new sequences of the specimens from the Mukwadzi River. The new sequences (in bold) include the hologenotype identified by an asterisk (*) and paragenotypes identified by a plus (+).

Species name	River system	GPS coordinates (Latitude, Longitude)	COI sequence ID
<i>Atopochilus savorgnani</i>	Congo	–	MK073983
	Congo	–	MK073984
<i>Chiloglanis anoterus</i>	Mlumati	-25.7567, 31.4386	LN610269
	Mlumati	-25.7692, 31.3367	LN610270
	Mlumati	-25.7692, 31.3367	LN610271
	Mlumati	-25.8672, 31.3347	LN610272
<i>Chiloglanis bifurcus</i>	Mlumati	–	MH432062
	Mlumati	–	SB8458
	Mlumati	–	SB8462
<i>Chiloglanis fasciatus</i>	Okavango	-13.5943, 16.8805	ANGFW077-12
	Okavango	-12.6713, 16.1114	ANGFW131-12
	Okavango	-12.6713, 16.1114	ANGFW132-12
	Okavango	-12.6713, 16.1114	ANGFW133-12
	Okavango	-12.6713, 16.1114	ANGFW134-12
<i>Chiloglanis paratus</i>	Phongolo	–	MPUMA025
	Phongolo	–	SB8459
<i>Chiloglanis pretoriae</i>	Limpopo	-23.9904, 31.8258	LN610341
<i>Chiloglanis</i> sp. 'dwarf'	Honde	-18.4337, 32.8969	MH432047
	Honde	-18.5992, 32.729	MH432054
	Makanga	-18.5438, 32.8013	MH432044
	Mupenga	-18.5725, 32.8038	MH432042
	Mupenga	-18.5725, 32.8038	MH432048
	Mutarazi	-18.5324, 32.8075	MH432018

Species name	River system	GPS coordinates (Latitude, Longitude)	COI sequence ID
<i>Chiloglanis</i> sp. 'dwarf'	Mutarazi	-18.5324, 32.8075	MH432019
	Mutarazi	-18.5324, 32.8075	MH432032
	Nyamhingura	-18.3696, 32.9354	MH432025
	Nyamhingura	-18.3696, 32.9354	MH432026
	Nyamhingura	-18.3696, 32.9354	MH432027
	Phalombe	-15.81, 35.646	MAFW097
	Pungwe	-18.3955, 32.9707	MH432030
	Pungwe	-18.3955, 32.9707	MH432031
	Pungwe	-18.45, 32.8968	MH432046
	Pungwe	-18.45, 32.8968	MH432057
	Pungwe	-18.3955, 32.9707	MH432061
<i>Chiloglanis</i> sp. 'Shire'	Ruo	-16.0403, 35.6633	MAFW029
<i>Chiloglanis</i> sp. 'Shire'	Shire	-15.061, 35.219	MAFW119
<i>Chiloglanis carnatus</i> sp. nov.	Manyame	-17.4249, 30.5854	PP156890*
	Manyame	-17.4249, 30.5854	PP156891*
	Manyame	-17.4249, 30.5854	PP156892*
	Manyame	-17.4249, 30.5854	PP156893*
	Manyame	-17.4249, 30.5854	PP156894*
	Manyame	-17.4249, 30.5854	PP156895*
<i>Chiloglanis</i> sp. 'Nyangombe'	Chidya	-18.2653, 32.5903	MH432020
	Chidya	-18.2653, 32.5903	MH432021
	Chidya	-18.2653, 32.5903	MH432022
	Chidya	-18.2653, 32.5903	MH432033
<i>Chiloglanis</i> sp. 'Pungwe'	Chiyengwa	-18.6878, 32.922	MH432040
	Honde	-18.5992, 32.729	MH432049
	Pungwe	-18.3955, 32.9707	MH432028
	Pungwe	-18.3955, 32.9707	MH432029
<i>Chiloglanis</i> sp. 'roughskin'	Buzi	-19.932, 33.826	SAFW910
	Chiyengwa	-18.6878, 32.922	MH432045
	Chiyengwa	-18.6878, 32.922	MH432051
	Honde	-18.5438, 32.8044	MH432036
	Makanga	-18.5438, 32.8013	MH432043
	Mupenga	-18.5725, 32.8038	MH432038
	Mupenga	-18.5725, 32.8038	MH432039
	Mupenga	-18.5725, 32.8038	MH432041
	Mupenga	-18.5725, 32.8038	MH432060
	Ngarura	-18.5474, 32.8718	MH432052
	Ngarura	-18.5474, 32.8718	MH432053
	Ngarura	-18.5474, 32.8718	MH432059
	Nyamukombe	-18.3821, 33.0327	MH432034
	Nyamukombe	-18.3821, 33.0327	MH432035
	Nyamukombe	-18.3821, 33.0327	MH432058
	Nyamukwara	-18.6918, 32.9236	MH432055
	Nyamukwara	-18.6918, 32.9236	MH432056
	Pungwe	-18.4414, 32.8875	MH432050
	Rwera	-18.5434, 32.8044	MH432037
	<i>Chiloglanis</i> sp. 'Zambezi'	Zambezi	-15.656, 30.953
Nyangombe		-18.0829, 32.5819	MH432023
Nyangombe		-18.0829, 32.5819	MH432024
Okavango		-14.9397, 17.7188	ANGFW015-12
Okavango		-13.5943, 16.8805	ANGFW078-12
Okavango		-14.6497, 16.9066	ANGFW211-12
<i>Chiloglanis swierstrai</i>	Phongolo	–	SB8457
	Phongolo	–	SB8460
	Phongolo	–	SB8461
<i>Euchilichthys boulengeri</i>	Dipumu	-6.0045, 22.3905	HM418085
<i>Euchilichthys royauxi</i>	Epulu	–	KT192823

Table 2. List of 184 specimens examined in this study including 19 specimens collected from the Mukwadzi River.

Species	Type status	Catalogue No.	No. specimens	River system	Latitude, Longitude
<i>Chiloglanis anoterus</i>	Holotype	SAIAB 186246	1	Phongola	-27.5, 30.4667
<i>Chiloglanis bifurcus</i>	Holotype	SAIAB 120160	1	Incomati	-25.4333, 30.7167
	Paratype	SAIAB 120161	6	Incomati	-25.4333, 30.7167
	Paratype	SAIAB 120529	3	Incomati	-25.3833, 30.35
<i>Chiloglanis emarginatus</i>	Holotype	SAIAB 120117	1	Incomati	-25.9833, 30.6833
	Paratype	SAIAB 120118	9	Incomati	-25.85, 30.2
<i>Chiloglanis fasciatus</i>	–	SAIAB 204928	6	Okavango	-14.3872, 16.2876
	–	SAIAB 204916	4	Okavango	-14.387, 16.2873
<i>Chiloglanis carnatus</i> sp. nov.	Holotype	SAIAB 236631	1	Manyame	-17.4249, 30.5854
	Paratype	SAIAB 211349	13	Manyame	-17.4244, 30.5845
	Paratype	SAIAB 211346	5	Manyame	-17.4249, 30.5854
<i>Chiloglanis paratus</i>	Holotype	SAIAB 186248	1	Phongola	-27.3833, 31.5
	Paratype	SAIAB 120050	1	Incomati	–
<i>Chiloglanis swierstrai</i>	Paratype	SAIAB 30013	1	Phongola	-25.6667, 27.8333
	Paratype	SAIAB 21805	5	Phongola	-27.4333, 31.5167
	Holotype	SAIAB 186247	1	Phongola	-27.4167, 31.1833
<i>Chiloglanis pretoriae</i>	–	SAIAB 82972	10	Limpopo	-23.0105, 30.4785
	–	SAIAB 70603	3	Incomati	-25.8478, 27.7836
	–	SAIAB 70822	3	Limpopo	-25.3883, 28.3117
<i>Chiloglanis neumanni</i>	Lectotype	BMNH190575249	1	Bubu	–
	Paralectotype	BMNH190575250	1	Bubu	–
	Paralectotype	BMNH190575250	1	Bubu	–
<i>Chiloglanis</i> sp. 'rough skin'	–	SAIAB 201075	4	Pungwe	-18.4414, 32.8875
	–	SAIAB 201095	2	Chiyengwa	-18.6878, 32.922
	–	AC14CL10	11	Mupenga	-18.5725, 32.8038
	–	SAIAB 200955	5	Ngarura	-18.5474, 32.8718
	–	SAIAB 200933	9	Nyamukombe	-18.3821, 33.0327
	–	SAIAB 201035	15	Rwera	-18.5434, 32.8044
	–	SAIAB 201047	3	Nyamukombe	-18.3821, 33.0327
	–	SAIAB 201088	8	Nyamukwara	-18.6918, 32.9236
	–	SAIAB 201026	8	Honde	-18.5438, 32.8044
<i>Chiloglanis</i> sp. 'dwarf'	–	AC14CL10	10	Mupenga	-18.5725, 32.8038
	–	SAIAB 200940	3	Pungwe	-18.45, 32.8968
	–	SAIAB 200923	1	Pungwe	-18.3955, 32.9707
	–	SAIAB 205087	5	Mutarazi	-18.5324, 32.8075
	–	SAIAB 205074	3	Nyamhingura	-18.3696, 32.9354
	–	AC13BL04	3	Pungwe	-18.3955, 32.9707
<i>Chiloglanis</i> sp. 'Pungwe'	–	AC13BL04	2	Pungwe	-18.3955, 32.9707
	–	SAIAB 201095	1	Chiyengwa	-18.6878, 32.922
	–	SAIAB 201067	1	Honde	-18.5992, 32.729
<i>Chiloglanis</i> sp. 'Nyangombe'	–	SAIAB 210408	6	Chidya	-18.2653, 32.5903
<i>Chiloglanis</i> sp. 'Zambezi'	–	SAIAB 200517	2	Nyangombe	-18.0829, 32.5819
	–	SAIAB 81243	2	Lower Zambezi	-15.656, 30.953
	–	SAIAB 186643	1	Okavango	-14.9397, 17.7188
	–	SAIAB 186709	1	Okavango	-13.5943, 16.8805

DNA extraction, amplification, and sequencing

A total of six new COI sequences of *Chiloglanis carnatus* sp. nov. were generated for this study. Preparation and sequencing of genetic material was done in the Aquatic Genomics Research Platform at the NRF-SAIAB. Genomic DNA was extracted from preserved tissues using the salting-out method (Sunnucks and Hales 1996). The mitochondrial DNA cytochrome c oxidase subunit I (COI) gene was amplified by polymerase chain reaction (PCR) using the universal fish DNA barcoding primer set FishF1 and FishR1 (Ward et al. 2005). PCRs were performed with a Veriti 96 well thermal cycler (Applied Biosystems, USA) and each reaction mixture (25 μ L) contained 50–100 ng of template DNA, 6.5 μ L of water, 0.5 μ L of each primer (10 μ M), and 12.5 μ L Taq DNA polymerase 2 \times master mix red (Amplicon PCR enzymes and reagents, Denmark). The PCR amplification profile had an initial denaturation step of 3 min at 94 $^{\circ}$ C followed by 38 cycles of 30 sec at 94 $^{\circ}$ C, annealing at 55 $^{\circ}$ C for 30 sec, and extension at 72 $^{\circ}$ C for 50 sec, and final extension at 72 $^{\circ}$ C for 7 min. The amplicons were purified using an Exonuclease I-Shrimp Alkaline Phosphate (Exo/SAP, Thermo Fisher Scientific, USA) protocol (Werle et al. 1994), sequenced using standard fluorescent BigDye v. 3.1 (Applied Biosystems, USA) terminator chemistry in the forward direction, and analysed on a 3500 Genetic Analyser (Applied Biosystems, USA) at the NRF-SAIAB. Additional sequences were obtained from the public databases GenBank (<https://www.ncbi.nlm.nih.gov/genbank/>) and Barcode of Life Data Systems (BOLD) (<http://www.boldsystems.org/>) (Table 1).

Phylogenetic analyses

Phylogenetic analyses included genetic sequences generated from *Chiloglanis carnatus* sp. nov., six of the seven nominal species from southern Africa, six candidate species of *Chiloglanis* identified by Chakona et al. (2018) (*Chiloglanis* sp. 'roughskin', *Chiloglanis* sp. 'Zambezi', *Chiloglanis* sp. 'Nyangombe', *Chiloglanis* sp. 'Pungwe', *Chiloglanis* sp. 'Shire', *Chiloglanis* sp. 'dwarf'), and three outgroup species (*Euchilichthys boulengeri* Nichols & LaMonte, 1934; *Euchilichthys royauxi* Boulenger, 1902; *Atopochilus savorgnani* Sauvage, 1879) (Table 1). Genetic material for *C. neumanni* from its type locality and *C. emarginatus* could not be accessed before finalising this study. Mitochondrial DNA sequences were edited, aligned, and trimmed in MEGA-X (Kumar et al. 2016). The sequences were translated into amino acid sequences in MEGA-X to check for stop codons and gaps to ensure that they were copies of functional mitochondrial protein coding sequences. Haplotype groups were identified using DNASP 6 (Rozas et al. 2017). The most suitable model for nucleotide substitution was selected using the Akaike Information Criterion (AIC) (Akaike 1974) as implemented in the program jModelTest 0.1.1 (Darriba et al. 2012). Bayesian phylogenetic inference was performed in MrBayes 3.2.6 (Ronquist et al. 2012) using the TIM3+I+G evolutionary model identified using jModeltest. The phylogenetic tree and posterior probabilities were inferred using four Markov chain Monte Carlo (MCMC) chains which were run for 2×10^6 generations with tree sampling every 1000 generations. The program Tracer 1.7 (Rambaut et al. 2018) was used to analyse the quality of the trace files generated by MrBayes and to determine the number of trees to be discarded as burn-in. The first 25%

of the sampled trees for each analysis was discarded as burn-in, and the remaining trees were used to calculate a majority rule consensus tree. Maximum likelihood (ML) analysis of the same dataset was performed in RAxML v. 8 (Stamatakis 2014) through the graphical user interface raxmlGUI v. 2 (Silvestro and Michalak 2012). A total of 10 ML searches were performed in raxmlGUI and support values for the ML tree nodes were estimated by 1000 non-parametric bootstrap inferences (Felsenstein 1985). Bootstrap values equal to or higher than 70% (Hillis and Bull 1993), and posterior probability values at 0.95 or higher (Alfaro and Holder 2006), were considered strong support.

Molecular species delimitation

Four molecular species delimitation methods were used to delineate candidate species within the suckermouth catfishes of southern Africa using the same dataset used for the phylogenetic analysis. The first two methods, Automatic Barcode Gap Discovery (ABGD; Puillandre et al. 2012) and Assemble Species by Automatic Partitioning (ASAP; Puillandre et al. 2021) infer the barcode gap from the data to partition sequences into proposed candidate species. These methods were performed on their respective web servers (<https://bioinfo.mnhn.fr/abi/public/abgd/> and <https://bioinfo.mnhn.fr/abi/public/asap/asapweb.html>). The intra-specific diversity priors were set at $P_{\min} = 0.001$ and $P_{\max} = 0.1$ for both methods. The Kimura (K80) TS/TV distance model was used and the remaining settings were left at their default parameters. The second pair of species delimitation methods included the Bayesian implementation of the Poisson Tree Processes (bPTP) (Zhang et al. 2013) and the General Mixed Yule Coalescent (GMYC) (Pons et al. 2006; Fujisawa and Barraclough 2013). Both GMYC and bPTP require a phylogenetic tree as input and from this tree they estimate rates of branching events to infer which parts of the tree are likely to follow a speciation model (interspecific variation) and which parts follow a coalescent model (intraspecific variation). The bPTP was performed on the web server (<http://species.h-its.org/ptp/>) using the same tree generated for phylogenetic reconstruction and a MCMC run for 1×10^6 generations with 10% burn-in. For the GMYC analysis a fully resolved ultrametric tree was inferred in Bayesian evolutionary analysis by sampling trees (BEAST) 2.4.6 (Bouckaert et al. 2014) using a strict clock and Yule model and the MCMC was ran for 1×10^7 generations with tree sampling every 1000 generations. The program Tracer 1.7.2 was used to analyse the quality of the trace files generated by BEAST. TreeAnnotator (Helfrich et al. 2018) was used to summarise the trees sampled by BEAST into a single maximum credibility tree with a burn-in of 25%. The species' limits by threshold Statistics (splits) package (<http://r-forge.r-project.org/projects/splits>) in R 3.5.0 (R Core Team 2018) was used to identify the candidate species from the maximum credibility tree produced by TreeAnnotator. Model corrected intraspecific and interspecific genetic distances of the molecular taxonomic units identified by the species delimitation methods were calculated in PAUP* 4.0a163 (Swofford 2003).

Morphological analyses

A total of 19 specimens of *Chiloglanis carnatus* sp. nov. collected from the Mukwadzi River were examined in the present study. Comparative material included

the lectotype of *C. neumanni*, holotypes of six valid species from southern Africa and five candidate species identified by Chakona et al. (2018) (Table 2). Because type material for *C. fasciatus* could not be accessed before finalising this study, 10 conspecific specimens collected from close to the type locality of this species and identified using the species description by Pellegrin (1936) and the key in Skelton (2001) were used as topotypes. The syntypes of *C. pretoriae* were severely deformed, thus only their meristic counts were included for comparison in this study, but 16 specimens collected from near the type locality of *C. pretoriae* and identified using the key in Skelton (2001) were used as topotypes for this species. Formulae and terminology of morphometric and meristic characters followed Schmidt et al. (2015), Friel and Vigliotta (2008), and Skelton and White (1990). A total of 49 morphometric characters were measured to the nearest 0.1 mm using digital Vernier callipers following Friel and Vigliotta (2008) (Table 3, Fig. 2A–D). External meristic counts were performed under a stereo microscope. Vertebrae counts were made from radiographs taken at the NRF-SAIAB using an Inspex 20i Digital X-ray Imaging System (Kodex Inc., New Jersey, USA). Radiographs for the lectotype and paralectotypes of *C. neumanni* were taken at the Royal Museum for Central Africa in Tervuren, Belgium (MRAC) using a VisiX-MedexLoncin (www.medex.be). A total of nine meristic characters were examined: number of mandibular teeth, pre-maxillary teeth, pectoral-fin rays, pelvic-fin rays, dorsal-fin rays, anal-fin rays, abdominal vertebrae, caudal vertebrae, and total vertebrae (Fig. 3). Following Roberts (1989), vertebrae counts excluded the Weberian structures and began from the fifth vertebra which was identified by a pair of large but slender ribs, and included the hypural complex which was counted as one vertebra. The abdominal vertebrae were defined as the vertebrae that occurred anterior to the first anal fin ray pterygiophore. Caudal vertebrae were defined as those that occurred posterior to the first anal fin ray pterygiophore and included the hypural complex which was counted as one vertebra (Roberts 1989) (Fig. 3). The genital papillae were examined to determine the sex of the specimens following Friel and Vigliotta (2008). Morphological measurements were standardised by transforming body measurements into percentages of the standard length (**SL**) and head measurements into percentages of the head length (**HL**). Principal component analyses (PCA) were performed in PAST v. 3.12 (Hammer et al. 2001) using the covariance matrix for the morphometric data in order to identify morphological characters that contributed the most to distinguishing *Chiloglanis carnatus* sp. nov. from the other *Chiloglanis* species from southern Africa.

Results

Phylogenetic analyses

The COI alignment of 80 sequences had 534 base pairs and 176 variable sites. A total of 47 unique haplotypes were identified. Although the Bayesian phylogenetic tree was not fully resolved, it showed genetic structuring that supported the monophyly of suckermouth catfishes from southern Africa (Fig. 4). *Chiloglanis carnatus* sp. nov. was recovered as an exclusive group that is genetically divergent (2.8–15.0% genetic distances) from other *Chiloglanis* species and lineages from southern Africa (Figs 4, 5; Table 4). With the exception of *C. pretoriae* and *Chiloglanis* sp. 'Shire', all recovered clades were well-support-

Table 3. Morphological characters examined in the present study.

Morphological characters	Abbreviation
Adipose fin to caudal peduncle length	AD-CPL
Adipose-fin base length	ADFBL
Adipose-fin height	ADFH
Anal-fin base length	ANFBL
Anal-fin length along longest ray	ANFL
Anterior nare interspace	ANI
Body depth at anus	BDA
Body depth at dorsal-fin insertion	BDDF
Caudal fork length	CFKL
Caudal peduncle depth	CPD
Caudal peduncle length	CPL
Dorsal fin to adipose fin length	DF-ADFL
Dorsal-fin base length	DFBL
Dorsal-fin length along longest ray	DFL
Dorsal-spine length	DSL
Eye diameter (horizontal axis)	EDH
Eye diameter (vertical axis)	EDV
Head depth	HD
Head length to opercular membrane margin	HL
Lateral mandibular barbel length	LMBL
Length of post-cleithral process	LCP
Lower caudal-fin lobe length	LCFL
Lower lip length	LLL
Mandibular tooth row width	MTRW
Maxillary barbel length	MXBL
Medial mandibular barbel length	MMBL
Mouth width	MW
Occipital shield width	OSW
Oral disc length	ODL
Oral disc width	ODW
Orbital interspace	OBI
Pectoral-fin length	PFL
Pectoral-spine length	PSL
Pelvic-fin interspace	PVI
Pelvic-fin length	PVFL
Post-cleithral process to occipital shield length	CP-OSL
Posterior nares interspace	PNI
Pre-anal length	PANL
Pre-dorsal length	PDL
Pre-maxillary tooth-patch length	PMXL
Pre-maxillary tooth-patch width	PMXW
Pre-pectoral length	PPTL
Pre-pelvic length	PPVL
Snout length	SNL
Standard length	SL
Total length	TL
Upper caudal-fin lobe length	UCFL
Upper lip length	ULL
Width at pectoral-fin insertion	WPTFI
Abdominal vertebrae	-
Anal fin-ray count	-

Morphological characters	Abbreviation
Caudal vertebrae	–
Dorsal fin-ray count	–
Mandibular tooth count	–
Pectoral fin-ray count	–
Pelvic fin-ray count	–
Pre-maxillary tooth count	–
Total vertebrae	–

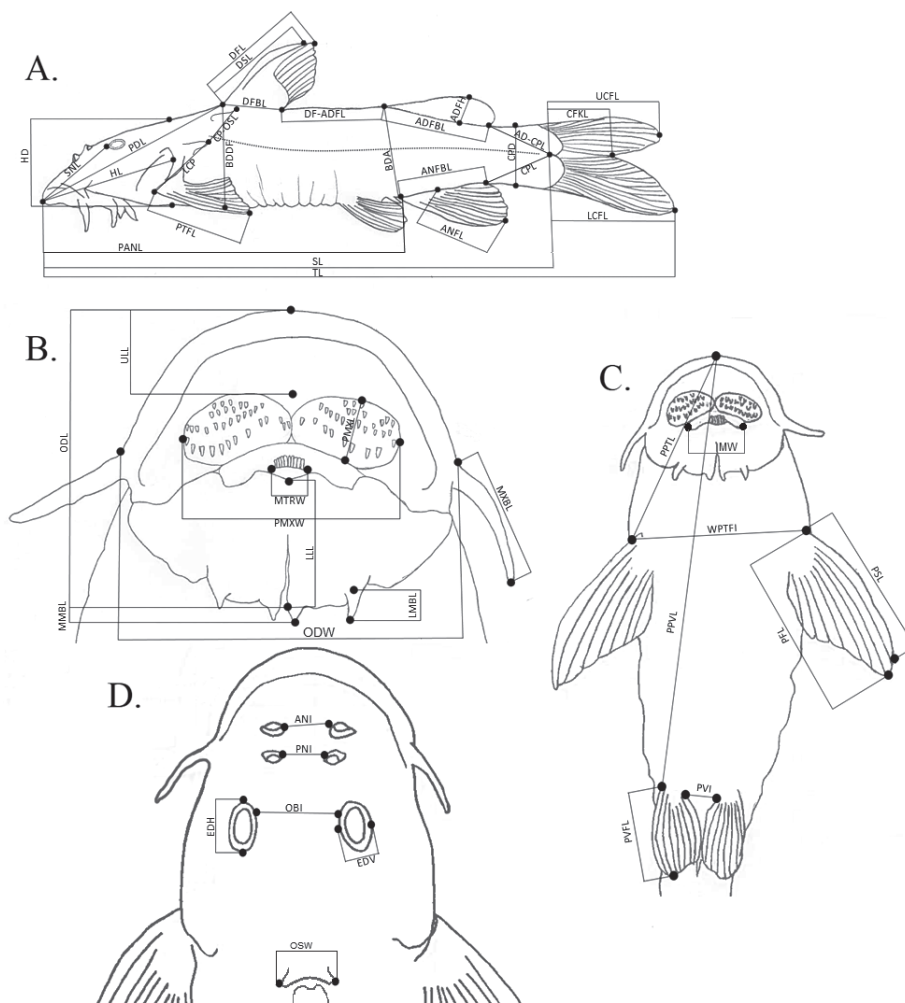


Figure 2. Illustrations depicting linear measurements recorded from *Chiloglanis* specimens **A** lateral view **B** ventral view of the Oral disc **C** ventral view **D** dorsal view of the head. Abbreviations: AD-CPL-adipose fin to caudal peduncle length, ADF-BL-adipose-fin base length, ADFH-adipose-fin height, ANFBL-anal-fin base length, ANFL-anal-fin length along longest ray, ANI-anterior nares interspace, BDA-body depth at anus, BDDF-body depth at dorsal-fin insertion, CFKL-caudal fork length, CPD-caudal peduncle depth, CPL-caudal peduncle length, CP-OSL- post-cleithral process to occipital shield length, DF-AD-FL-dorsal fin to adipose fin length, DFBL-dorsal-fin base length, DFL-dorsal-fin length along longest ray, DSL-dorsal-spine length, EDH-eye diameter (horizontal axis), EDV-eye diameter (vertical axis), HD-head depth, HL-head length to opercular membrane margin, LCFL-Lower caudal-fin lobe length, LCP-length of post-cleithral process, LLL-lower lip length, LMBL-Lateral mandibular barbel length, MMBL-Medial mandibular barbel length, MTRW-mandibular tooth row width, MXBL-maxillary barbel length, MW-mouth width, OBI-orbital interspace, ODL-oral disc length, ODW-oral disc width, OSW-occipital shield width, PANL-pre-anal length, PDL-pre-dorsal length, PMXL-pre-maxillary tooth-patch length, PMXW- pre-maxillary tooth patch width, PNI-posterior nares interspace, PPTL-pre-pectoral length, PPVL-pre-pelvic length, PSL-pectoral-spine length, PFL-pectoral-fin length, PVFL-pelvic-fin length, PVI-pelvic-fin interspace, SL-standard length, SNL-snout length, TL-total length, UCFL–Upper caudal-fin lobe length, ULL-upper lip length, WPTFI-width at pectoral-fin insertion.

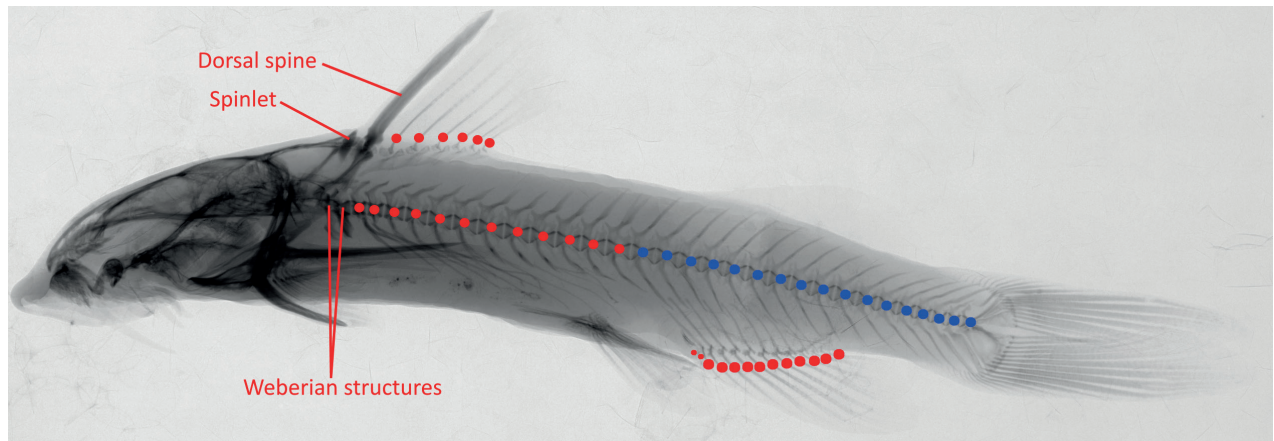


Figure 3. Illustration showing how fin rays and vertebrae were counted using x-ray radiographs. The red dots along the vertebra represent the abdominal vertebrae and the blue dots represent the caudal vertebrae.

ed (posterior probability > 0.95). Genetic divergences within valid and candidate species ranged from 0–1.5% and interspecific divergences ranged from 1.3–15.7% (Table 4). *Chiloglanis paratus* from the Phongolo River was recovered as the most basal clade that is sister species to all the southern African suckermouth catfishes included in the present study. The relationships among the remaining taxa were not well resolved as they were recovered within five polytomous clades with weak support between them (Fig. 4). The first clade contained *Chiloglanis carnatus* sp. nov. from the Manyame River and *C. fasciatus* from the Okavango River. The second clade contained *C. anoterus* and *C. bifurcus* from the Incomati River system as well as *C. pretoriae* from the Limpopo River system. The third clade contained *Chiloglanis* sp. 'Nyangombe' from the Nyangombe River and *Chiloglanis* sp. 'dwarf' from the Pungwe and Ruo rivers. The fourth clade contained *Chiloglanis swierstrai* from the Limpopo River system. The fifth clade contained the *Chiloglanis* sp. 'Zambezi', *Chiloglanis* sp. 'Pungwe', *Chiloglanis* sp. 'roughskin', and *Chiloglanis* sp. 'Shire' lineages. The *Chiloglanis* sp. 'roughskin' lineage occurs in the Buzi and Pungwe rivers, whereas *Chiloglanis* sp. 'Pungwe' is endemic to the Pungwe River. *Chiloglanis* sp. 'Shire' and *Chiloglanis* sp. 'Zambezi' lineages were found in the lower Zambezi River system with the latter lineage also occurring in the Okavango River. The phylogenetic tree inferred using the ML approach had similar topology to the Bayesian inference tree (Fig. 5).

Molecular species delimitation

All four molecular species delimitation methods identified *Chiloglanis carnatus* sp. nov., *Chiloglanis* sp. 'Shire', *Chiloglanis* sp. 'Nyangombe', *C. swierstrai*, *C. anoterus*, *C. pretoriae*, *C. bifurcus*, *C. fasciatus*, and *C. paratus* as unique molecular taxonomic units (Fig. 4). The Assemble Species by Automatic Partitioning method recovered the least number of candidate species, this method grouped *Chiloglanis* sp. 'roughskin', *Chiloglanis* sp. 'Pungwe', and *Chiloglanis* sp. 'Zambezi' into a single molecular taxonomic unit. The General Mixed Yule Coalescent method recovered the highest number of molecular taxonomic units. This method identified additional molecular taxonomic units within *Chiloglanis* sp. 'roughskin' and *Chiloglanis* sp. 'dwarf'. The Automatic Barcode Gap Discovery and bPPT

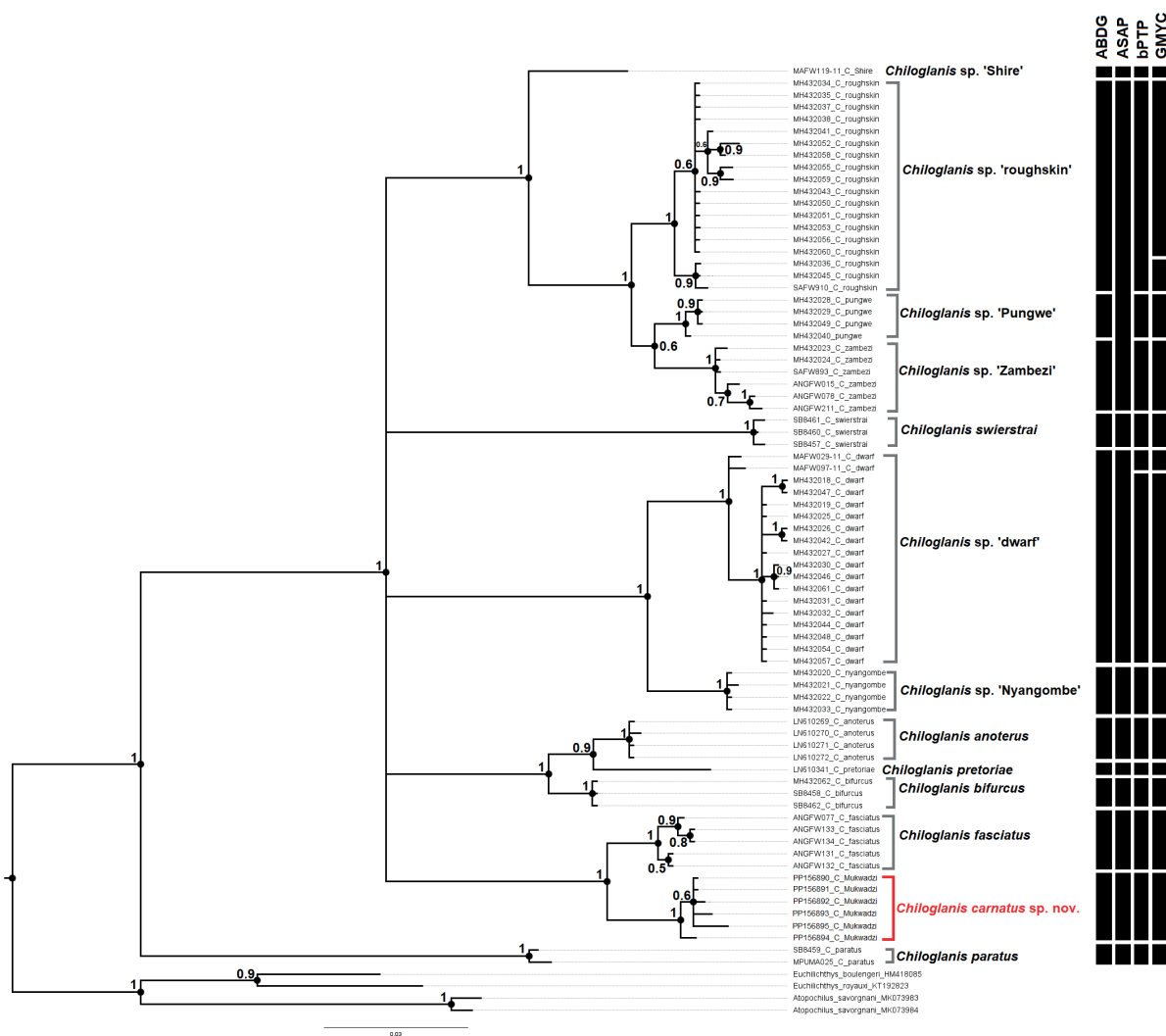


Figure 4. Bayesian inference tree of the species and lineages of the genus *Chiloglanis* found in southern African. The numbers at the nodes represent the Bayesian posterior probabilities. The black bars represent candidate species proposed by four molecular species delimitation methods: Automatic Barcode Gap Discovery (ABGD), Automatic Partitioning (ASAP), Bayesian implementation of the Poisson Tree Processes (bPTP), and General Mixed Yule Coalescent (GMYC).

inferred similar molecular taxonomic units with the exception of *Chiloglanis* sp. 'dwarf' which was split into two molecular taxonomic units by the latter method.

Morphological analyses

Principal component analysis (PCA) of the morphometric characters showed that *Chiloglanis carnatus* sp. nov. is separated from *C. swierstrai* and *C. anoterus* along principal component 1 (PCI) (Fig. 6). This separation was associated with maxillary barbel length (Table 6). *Chiloglanis carnatus* sp. nov. (20.3–28.8%HL) has relatively shorter maxillary barbels compared to *C. swierstrai* (44.2–66.8%HL) and *Chiloglanis* sp. 'Zambezi' (31.3–37.0%HL, Table 5, Fig. 7A, B). *Chiloglanis carnatus* sp. nov. is separated from *C. swierstrai*, *C. anoterus*, and *C. neumanni* along principal component 2 (PCII) (Fig. 6). Separation along PCII is associated with the oral disc width (Table 6). *Chiloglanis carnatus* sp. nov. has a relatively smaller oral disc width (51.1–64.6%HL) compared to *C. anoterus* (69.1%HL, Table 5, Fig. 7C).

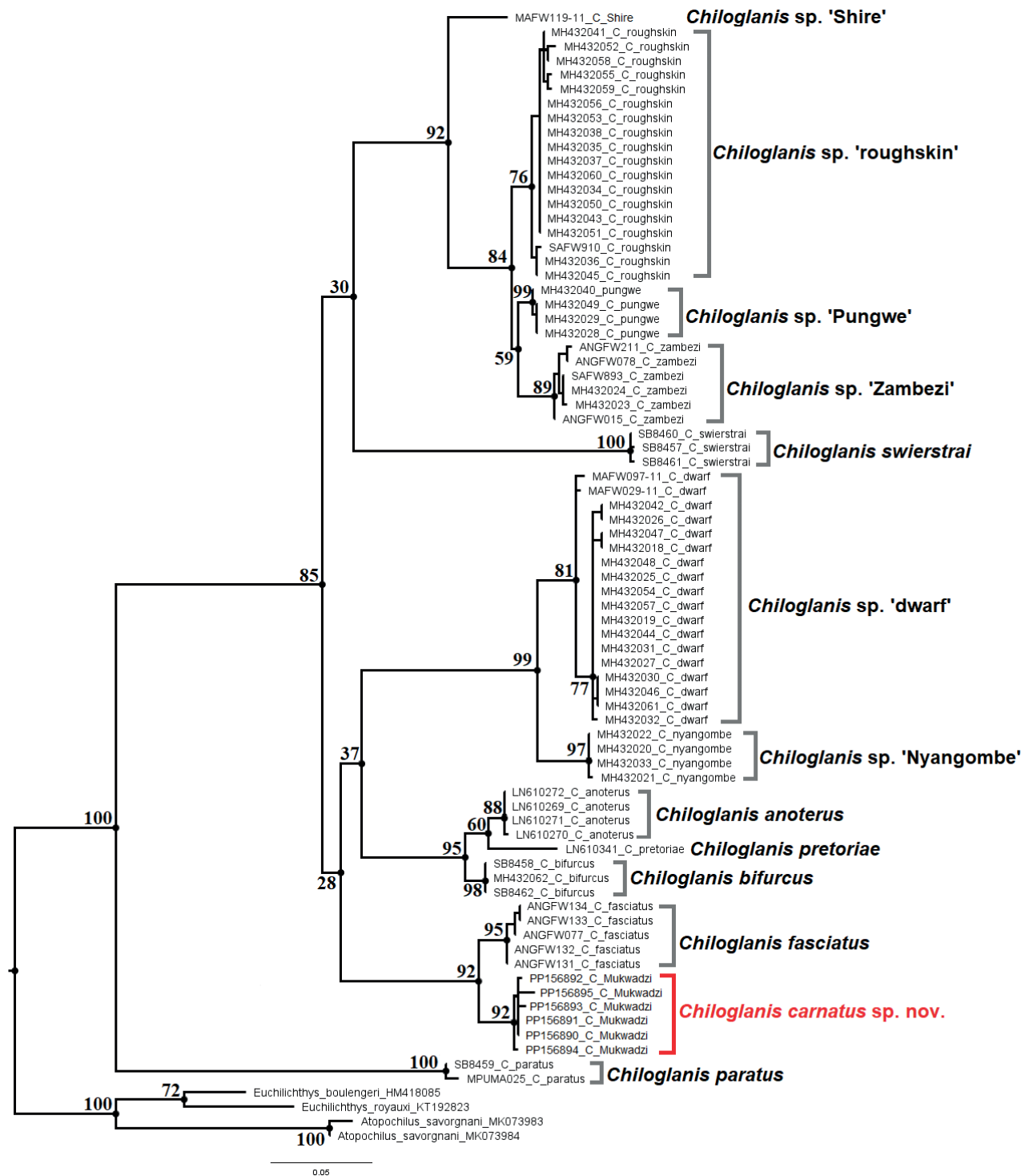


Figure 5. Maximum likelihood tree of the species and lineages of the genus *Chiloglanis* found in southern African. The numbers at the nodes represent the bootstrap values.

Additional scatterplots were generated to explore the characters that further distinguish the *Chiloglanis carnatus* sp. nov. specimens. The *Chiloglanis carnatus* sp. nov. specimens have a narrower mandibular tooth row width (4.6–8.1%HL) compared to *C. pretoriae* (16.0–25.6%HL), *C. swierstrai* (10.0–16.6%HL), *C. neumanni* (9.9–13.5%HL), *C. emarginatus* (9.6–13.5%HL), *C. bifurcus* (10.4–17.3%HL), *C. anoterus* (10.5%HL), *Chiloglanis* sp. 'dwarf'

Table 4. Ranges of cytochrome oxidase I (COI) genetic distances (%) between the *Chiloglanis* species included in the present study.

		1	2	3	4	5	6	7	8	9	10	11	12	13	14	15	16
1	<i>Chiloglanis</i> sp. 'dwarf'	0–1.5															
2	<i>Chiloglanis</i> sp. 'Nyangombe'	3.6–4.5	0–0.2														
3	<i>Chiloglanis</i> sp. 'Zambezi'	10.7–11.4	9.0–9.7	0–0.9													
4	<i>Chiloglanis</i> sp. 'Pungwe'	11.0–11.8	9.9–10.3	2.1–3.0	0–0.2												
5	<i>Chiloglanis</i> sp. 'roughskin'	10.5–11.6	9.4–10.3	2.2–3.9	1.3–2.6	0–1.3											
6	<i>Chiloglanis</i> sp. 'Shire'	11.4–11.9	10.1–10.3	5.1–5.6	5.0–5.2	4.1–5.2	–										
7	<i>Chiloglanis carnatus</i> sp. nov.	12.0–13.7	12.9–13.9	10.7–12.0	11.0–12.0	10.1–11.2	10.3–11.0	0–1.1									
8	<i>Chiloglanis anoterus</i>	11.0–11.4	11.0–11.2	9.5–10.1	9.7–10.7	9.6–9.9	9.7	9.7–11.4	0–0.2								
9	<i>Chiloglanis pretoriae</i>	9.9–10.3	10.1–10.3	10.7–11.0	10.7–10.8	11.0–11.4	10.1	10.7–11.4	3.4–3.6	–							
10	<i>Chiloglanis fasciatus</i>	10.9–12.0	12.0–12.4	10.9–11.4	11.2–11.6	10.3–10.9	10.3	2.8–3.9	9.0–9.2	9.6–9.7	0–0.6						
11	<i>Chiloglanis swierstrai</i>	12.4–13.9	13.7–14.2	11.4–11.8	11.4–11.8	11.2–11.8	10.1–11.0	12.4–13.3	11.4–11.8	12.4–12.7	9.0–12.5	0.2–0.4					
12	<i>Chiloglanis bifurcus</i>	9.9–10.3	10.5–10.7	9.9–10.3	10.5–10.7	10.3–10.7	9.4	9.8–10.5	2.4–2.6	4.1	9.0–9.2	11.8–12.2	0				
13	<i>Chiloglanis paratus</i>	15.0–15.5	14.4–14.8	14.2–14.8	14.8–15.2	15.0–15.7	13.9–14.0	14.0–15.0	13.3–13.7	13.7–13.9	13.7–14.4	15.4–15.7	13.1–13.5	0.6			
14	<i>Atopochilus savognnani</i>	15.7–16.1	15.5–16.3	15.0–15.9	15.5–16.1	15.0–15.5	14.2–14.4	15.5–16.9	15.0–15.7	14.8–15.0	15.0–15.5	16.5–16.9	15.2–15.7	15.0–15.5	1.1		
15	<i>Euchilichthys boulengeri</i>	15.2–15.4	15.0–15.2	15.2–15.4	14.4	14.0–14.2	14.2	15.4–16.1	14.6–15.4	14.8	15.0–15.4	13.7–13.9	14.6–15.4	13.3–13.5	11.2–11.4	–	
16	<i>Euchilichthys royauxi</i>	16.5–17.0	16.3–16.5	16.3–16.9	15.7	15.4–16.1	14.8	15.7–16.5	16.3–16.5	16.5	15.2–15.5	15.4–15.5	16.3	13.5–3.9	10.7	6.6	–

(13.6–25.0%HL), *Chiloglanis* sp. 'Nyangombe' (19.0–25.5%HL), *Chiloglanis* sp. 'Pungwe' (17.6–27.8%HL), *Chiloglanis* sp. 'roughskin' (11.9–22.2%HL), and *Chiloglanis* sp. 'Zambezi' (20.5–25.4%HL; Fig. 7D, E). *Chiloglanis carnatus* sp. nov. has an oral disc with relatively longer lower lips (18.3–26.6%HL) compared to *Chiloglanis* sp. 'roughskin' (9.6–16.8%HL, Fig. 7F). *Chiloglanis carnatus* sp. nov. has a relatively deeper caudal peduncle (11.3–13.2%SL) compared to *C. neumanni* (9.5–9.9%SL), *C. paratus* (9.6–9.9%SL), *C. fasciatus* (7.5–8.8%SL), *C. swierstrai* (7.2–8.7%SL), and *Chiloglanis* sp. 'Zambezi' (10.0–11.1%SL, Fig. 7G, H). A longer adipose-fin base length distinguishes *Chiloglanis carnatus* sp. nov. (17.0–23.3%SL) from *C. bifurcus* 9.2–13.6%SL) (Fig. 7I). Larger adipose fin height (4.1–6.8%SL) and shorter anal fin rays (11.7–17.9%SL) further distinguish *Chiloglanis carnatus* sp. nov. from *C. neumanni* (adipose fin height: 2.7–3.1%SL; anal fin ray length: 19.2–20.9%SL; Fig. 7J, K). A shorter distance between the anterior nares of *Chiloglanis carnatus* sp. nov. (9.5–15.5%HL) separates it from *C. bifurcus* (19.5–21.2%HL), *C. emarginatus* (16.5–22.4%HL), and *C. swierstrai* (15.7–22.4%HL, Fig. 7L). *Chiloglanis carnatus* sp. nov. has a relatively longer head (30.5–34.9%SL vs 24.8–28.0%SL), relatively wider body at pectoral-fin insertion (23.0–25.3%SL vs 17.6–21.5%SL), and relatively longer

Table 5. Summary of morphological characters examined in the present study. All values except standard length (SL) and Head length (HL) are given as percentages of the HL or SL. For the meristics the mode is given alongside the range of the counts in parentheses where the counts varied.

Species	<i>Chiloglanis carnatus</i> sp. nov.	<i>Chiloglanis pretoriae</i>	<i>Chiloglanis anoterus</i>	<i>Chiloglanis bifurcus</i>	<i>Chiloglanis emarginatus</i>	<i>Chiloglanis fasciatus</i>	<i>Chiloglanis neumanni</i>	<i>Chiloglanis paratus</i>	<i>Chiloglanis swierstrai</i>	<i>Chiloglanis sp. 'dwarf'</i>	<i>Chiloglanis sp. 'Nyangombe'</i>	<i>Chiloglanis sp. 'Pungwe'</i>	<i>Chiloglanis sp. 'roughskin'</i>	<i>Chiloglanis sp. 'Zambezi'</i>
Number of specimens	19	16	1	10	10	10	3	2	7	25	6	4	65	6
Total length	45.3–62.2	31.7–67.1	80.1	68.7–84.9	50.2–66.6	37.7–53.3	0–42.7	44–51.9	45.2–65.7	31.4–51.1	33.1–48.2	34.4–62.9	39.8–87.6	55.2–62.6
Standard length	35.5–48.9	26.5–54.6	61.7	51.4–63.9	40.3–55.6	30.3–41.7	33.4–39.8	35.8–42.4	34.9–51.9	26.0–41.6	26.0–38.5	24.6–48.6	31.6–66.6	43.7–50.6
Head length	12.1–15.6	8.8–19.4	20.3	15.7–19.5	12.3–15.7	10.0–13.7	10.1–12.6	11.1–13.8	9.2–13.6	8.0–12.8	8.9–13.1	6.6–15.6	10.3–22.8	13.9–16.8
% Standard length														
Pre-pectoral length	26.9–30.0	26.3–32.7	30.9	27.4–31.1	24.5–27.3	29.5–32.4	26.1–27.8	28.4–30.0	25.0–27.0	24.3–33.1	29.6–32.3	30.2–35.9	25.7–32.4	25.8–31.4
Pre-dorsal length	39.9–43.7	40.7–48.7	38.6	38.9–42.9	37.7–42.7	40.4–44.9	38.6–41.5	39.2–42.3	34.5–36.7	36.6–50.5	39.0–46.8	35.4–44.7	36.0–44.1	36.2–46.3
Pre-pelvic length	56.0–59.3	53.6–58.4	59.7	52.5–58.1	51.3–56.8	56.1–59.7	55.6–57.5	55.2–58.6	49.1–54.8	50.7–58.6	51.7–64.2	57.2–65.1	53.6–61.6	55.3–60.7
Pre-anal length	67.6–73.3	66.4–72.8	73.3	63.4–69.3	63.0–68.2	67.7–73.3	70.7–72.4	67.6–71.3	64.1–69.5	64.1–75.3	65.2–80.1	56.7–80.2	64.3–77.6	58.7–76.5
Dorsal fin to adipose fin length	18.2–22.6	18.1–25.8	25.5	21.4–29.1	20.2–24.4	21.4–24.1	21.6–26.9	23.9–28	18.7–26.8	21.5–28.6	20.2–28.4	21.9–29.1	19.2–30.2	20.5–21.6
Pectoral-spine length	15.0–19.8	13.5–19.8	11.5	17.8–22.4	17.2–22	17.5–21.5	16.8–22.4	19.7–22.7	19.0–23.1	13.7–20	13.7–20.2	18.2–19.9	13.8–26.6	14.7–22.0
Pectoral-fin length	19.3–23.6	14.1–22.6	19	22.9–26.6	19.5–24.3	21.4–25.1	21.9–24.5	22.6–26.4	23.2–25.5	15.4–24.3	18.2–21.1	22.1–25.9	17.6–27.4	20.5–26.1
Width at pectoral-fin insertion	23.0–25.3	24.4–29.8	24.3	24.7–27.9	23.9–26.5	23.7–26.1	21.4–24.9	23.8–25.8	17.6–21.5	21.7–25.7	22.3–26.1	23.9–27.0	21.0–27.6	23.6–25.7
Pelvic-fin length	10.8–14.2	12.2–15.9	12.9	14.6–17.2	10.8–14.6	11.6–14.6	13.6–14	13.0–13.1	12.3–15.4	11.7–15.3	11.7–13.3	13.8–16.0	10.2–17.5	13.4–15.7
Pelvic-fin interspace	3.0–5.1	2.1–4.7	4.3	4.4–6.2	2.8–4.7	2.5–4.7	3.0–3.9	4.4–4.7	2.7–4.9	1.8–6.0	2.0–4.2	2.7–5.4	2.6–8.2	3.8–5.0
Body depth at dorsal-fin insertion	15.5–20.7	16.0–21.0	19.1	16.2–21.8	17.3–22.4	15.4–19.3	17.7–22.1	15.2–18.1	12.2–19.2	16.8–22.7	15.7–19.3	17.2–20.8	17.2–25.3	17.3–20.2
Body depth at anus	13.9–17.6	15.3–18.7	18	16.7–21.2	15.5–18.6	11.9–14.5	13.5–16.1	12.9–15.4	11.3–14.6	14.3–19.9	13.1–16.2	13.8–17.8	12.5–20.4	14.0–15.6
Dorsal-spine length	13.2–18.0	13.3–20.9	11.3	13–17.5	14.0–17.4	15.8–20.5	17.1–20.4	18.4–21.3	14.0–15.0	11.6–20.1	14.5–17.9	13.8–20.6	12.5–25.4	11.9–17.8
Dorsal-fin base length	10.7–14.1	12.8–18.0	8.6	9.5–13.2	8.8–12.9	10.4–13.7	8.5–10.2	12.8–14.6	7.5–9.6	11.5–23.7	12.8–16.6	20.6–28	11.8–30.6	15.4–24.7
Adipose fin to caudal peduncle length	12.9–17.0	13.3–17.7	15.2	14.9–18.5	13.1–17.0	13.1–16.8	11.9–14.1	13.6–15.6	14.0–15.9	14.4–19.8	15.1–20.9	11.3–16.1	13.3–21.6	15.7–17.2
Adipose-fin base length	17.0–23.3	16.2–25.2	16.5	9.2–13.6	14.6–19.6	12.4–17.8	15.5–17.4	13.7–15.4	17.0–22.5	13.2–17	11.3–17.3	13.2–19.6	10.4–19.3	14.9–17.4
Adipose-fin height	4.1–6.8	4.2–5.8	3.5	2.9–4.6	2.3–5.0	3.3–5.2	2.7–3.1	3.0–3.9	3.5–5.2	2.8–5.4	3.2–5.3	3.3–5.6	3.3–8.7	5.0–6.2
Anal-fin length along longest ray	11.7–17.9	13.7–18.3	15.5	14.1–17.8	11.6–14.6	11.5–16.6	19.2–20.9	12.8–14.6	10.1–15.5	11.8–18.7	13.0–17.2	11.0–17.5	10.9–20.5	13.2–16.9
Anal-fin base length	10.5–13.5	11.7–15.4	12.9	11.5–15.3	10.9–14.9	8.9–11.4	11.1–12.1	10.6–11.0	11.7–15	10.6–16.4	11.9–15.5	11.3–19.4	8.2–15.6	11.8–14.2
Caudal peduncle depth	11.3–13.2	11–13.8	12.2	11.1–14.1	10.2–11.9	7.5–8.8	9.5–9.9	9.6–9.9	7.2–8.7	10.9–12.6	10.0–11.9	9.6–12.8	9.8–14.9	10.0–11.1
Caudal peduncle length	15.9–19.7	15.8–22.6	18.6	19.9–22.7	19.1–23.7	18.8–21.7	16.0–18.8	17.7–18.9	19.6–22.0	17.4–24.5	20.3–22.9	13.6–15.8	13.9–21.9	16.2–17.9
Head length	30.5–34.9	33.3–38.6	32.9	29.5–31.3	26.5–30.7	30.4–35.2	30.2–31.7	31.0–32.6	24.8–28.0	27.8–34.9	32.8–39.4	25.9–33.7	28.3–36.3	31.4–34.1

Species	<i>Chiloglanis carnatus</i> sp. nov.	<i>Chiloglanis pretoriae</i>	<i>Chiloglanis anoterus</i>	<i>Chiloglanis bifurcus</i>	<i>Chiloglanis emarginatus</i>	<i>Chiloglanis fasciatus</i>	<i>Chiloglanis neumanni</i>	<i>Chiloglanis paratus</i>	<i>Chiloglanis swierstrai</i>	<i>Chiloglanis sp. 'dwarf'</i>	<i>Chiloglanis sp. 'Nyangombe'</i>	<i>Chiloglanis sp. 'Pungwe'</i>	<i>Chiloglanis sp. 'roughskin'</i>	<i>Chiloglanis sp. 'Zambezi'</i>
% Head length														
Eye diameter (vertical axis)	9.9–13.8	11.6–18.3	10.6	12.1–16.6	11.9–16.5	9.4–13.1	9.1–14.9	10.6–12.5	13.2–18.6	11.8–16.1	12.6–13.9	10.9–20.4	7.4–15.3	11.5–15.1
Orbital interspace	21.5–28.7	22.6–28.9	23.4	19.5–24.6	18.3–24.4	18.5–25.4	25.7–30.2	22.2–23.9	15.3–22.7	23.3–38.5	20.9–25.2	23.8–38.4	18.0–38.9	22.7–30.4
Anterior nares interspace	9.5–15.5	12.4–16.6	11.9	19.5–21.2	16.5–22.4	11.5–17.6	13.9–19.8	13.3–15.5	15.7–22.4	10.9–18.4	13.0–14.7	13.7–23.0	11.0–21.6	13.5–16.7
Posterior nares interspace	10.3–15.5	11–15.5	11.8	15.3–21.9	13.8–20.9	9.9–16.1	14.9–22.2	9.3–10.9	12.6–18.2	12.9–16.7	12.6–14.7	8.9–13.0	7.5–18.4	10.2–13.0
Snout length	54.0–66.2	55.7–65.7	65	58.2–64.8	49.5–59.9	58.9–69.3	51.5–56.2	56.9–59.0	51.5–57.5	52.3–66.1	51.4–67.3	54.7–84	51.1–68.0	53.4–66.2
Pre-maxillary tooth-patch length	8.2–12.3	8.2–13.9	11.7	7.0–9.3	6.3–8.2	7.5–9.5	9.9–12.9	9.2–11.8	8.5–11.6	6.8–10.3	6.1–9.9	7.5–11.5	5.4–14.3	9.9–12.1
Pre-maxillary tooth-patch width	36.8–47.9	30.7–46.8	51.5	44.1–50.2	39.9–46.2	40.3–46.7	36.4–38.9	41.3–44.2	39.5–47.1	35.9–45.3	39.6–47.8	31.7–44.5	29.7–50.1	37.2–45.1
Mandibular tooth row width	4.6–8.1	16.0–25.6	10.5	10.4–17.3	9.6–13.5	4.8–6.6	9.9–13.5	7.2–7.7	10.0–16.6	13.6–25.0	19.0–25.5	17.6–27.8	11.9–22.2	20.5–25.4
Maxillary barbel length	20.3–28.8	21.3–36.8	22.7	23.8–41.8	29.1–41.8	26.4–31.2	21.8–30.2	24.3–27.5	44.2–66.8	17.4–34.3	20.1–28.1	19.7–32.1	20.2–45.7	31.3–37.0
Upper lip length	11.1–16.2	11.7–18.8	16.7	8.4–12.3	6.6–10.6	8.8–15.5	9.1–10.0	12.3–12.4	7.0–10.5	6.9–14.3	8.4–13.5	11.3–19.5	10.2–19.5	12.5–17.2
Lower lip length	18.3–26.6	22.4–27.7	25.1	17.7–25.6	23.5–28.8	18.8–24.9	19.8–27.0	22.8–27.6	19.2–26.0	12.6–22.9	20.7–29.3	19.7–27.8	9.6–16.8	20.7–24.7
Mouth width	23.9–33.8	24.8–32.6	39.6	30.9–39.1	25.7–36.2	25.6–32.1	20.6–22.8	28.0–35.9	27.9–34.0	20.4–33.4	27.1–33.8	25.2–37.8	17.5–32.8	24.7–31.1
Oral disc width	51.1–64.6	48.4–70.3	69.1	59.3–69.3	58.9–66.3	51.4–64.1	47.6–53.5	60.8–64.8	51.8–63.0	44.4–57.3	45.8–56.1	63.4–69.7	35.7–69.2	54.4–63.3
Oral disc length	48.6–57	46.0–61.1	63.8	53.7–61.3	43.3–54.7	48.4–59.7	41.6–53.2	55.7–57.8	48.6–62.4	40.7–53.9	41.9–58.2	46.5–57.4	38.6–57.1	47.9–57.3
Meristics														
Mandibular tooth count	10	12	12	8	8 (6–8)	8	8	12	11 (11–14)	-	-	-	-	-
Pre-maxillary tooth count	60 (43–69)	51–59	86	54 (50–64)	36–54	64 (51–65)	55–60	39–51	50 (34–59)	-	-	-	-	-
Pectoral-fin ray count	8 (6–8)	8	8	8 (7–8)	7	8	8	8	8	-	-	-	-	-
Pelvic-fin ray count	7 (6–7)	7	7	7	7 (7–8)	7	7	7	7	-	-	-	-	-
Dorsal-fin ray count	6 (5–7)	6	5	5 (5–6)	6 (5–6)	6 (5–6)	5	5	5 (5–6)	-	-	-	-	-
Anal-fin ray count	12 (12–13)	10	13	12 (9–13)	10 (10–12)	9 (8–12)	10 (10–12)	9	12 (9–13)	-	-	-	-	-
X-rays														
Number of specimens	9	2	1	4	6	7	5	1	6	-	-	-	-	-
Abdominal vertebrae	13 (11–13)	12–13	13	11 (10–11)	10 (10–12)	13 (12–13)	13 (12–13)	12	12 (11–13)	-	-	-	-	-
Caudal vertebrae	17 (16–18)	18–19	17	20 (18–20)	19 (17–19)	16 (16–17)	16 (16–18)	16	20 (16–20)	-	-	-	-	-
Total vertebrae	29 (29–30)	28	30	30 (29–30)	29 (28–30)	29 (28–29)	28	27	32 (31–32)	-	-	-	-	-

Table 6. The PCA loadings for the first two principal components for the measured characters of *Chiloglanis* species and lineages from southern Africa.

Principal component	1	2
Eigenvalue	90.91	70.84
% variance	22.46	17.50
Adipose fin to caudal peduncle length	-0.02	-0.02
Adipose-fin base length	0.05	-0.01
Adipose-fin height	-0.04	0.00
Anal-fin base length	0.03	-0.05
Anal-fin length along longest ray	-0.03	-0.06
Body depth at anus	-0.02	-0.04
Body depth at dorsal-fin insertion	-0.09	-0.06
Caudal peduncle depth	-0.05	-0.02
Caudal peduncle length	0.08	-0.10
Dorsal-fin to adipose fin length	-0.02	-0.02
Dorsal-fin base length	-0.17	0.08
Dorsal-spine length	-0.06	0.04
Pre-anal length	-0.16	0.17
Pre-dorsal length	-0.10	0.11
Pre-pectoral length	-0.08	0.10
Pre-pelvic length	-0.12	0.15
Pectoral-spine length	0.04	0.01
Pectoral-fin length	0.04	0.03
Pelvic-fin length	0.00	0.02
Width at pectoral-fin insertion	-0.04	0.06
Pelvic-fin interspace	0.00	0.02
Head length	-0.18	0.07
Anterior nares interspace	0.14	-0.08
Eye diameter (vertical axis)	0.11	-0.03
Lower lip length	0.02	0.37
Mandibular tooth row width	-0.16	-0.05
Maxillary barbel length	0.60	-0.41
Mouth width	0.35	0.21
Orbital interspace	-0.18	-0.14
Oral disc length	0.22	0.34
Oral disc width	0.39	0.41
Pre-maxillary tooth-patch length	0.00	0.09
Pre-maxillary tooth-patch width	0.23	0.24
Posterior nares interspace	0.13	-0.13
Snout length	-0.05	0.35
Upper lip length	-0.09	0.15

pre-pelvic (56.0–59.3%SL vs 49.1–54.8%SL) and pre-dorsal distances (39.9–43.7%SL vs 34.5–36.7%SL) that readily separated them from *C. swierstrai* (Fig. 7M–P).

Comparison of meristic characters revealed consistent differences between *Chiloglanis carnatus* sp. nov. specimens and the other species from southern Africa. *Chiloglanis carnatus* sp. nov. specimens have ten closely packed mandibular teeth that separate them from *C. bifurcus*, *C. emarginatus*, *C. fasciatus*, and *C. neumanni* that have eight mandibular teeth as well as from *C. anoterus*, *C. pretoriae*, *C. paratus*, and *C. swierstrai* that have > 10 mandibular teeth (Fig. 8A). A higher number of anal-fin rays separates *Chiloglanis carnatus* sp. nov. specimens (12–13) from *C. paratus* (9) and *C. pretoriae* (10) (Fig. 8B).

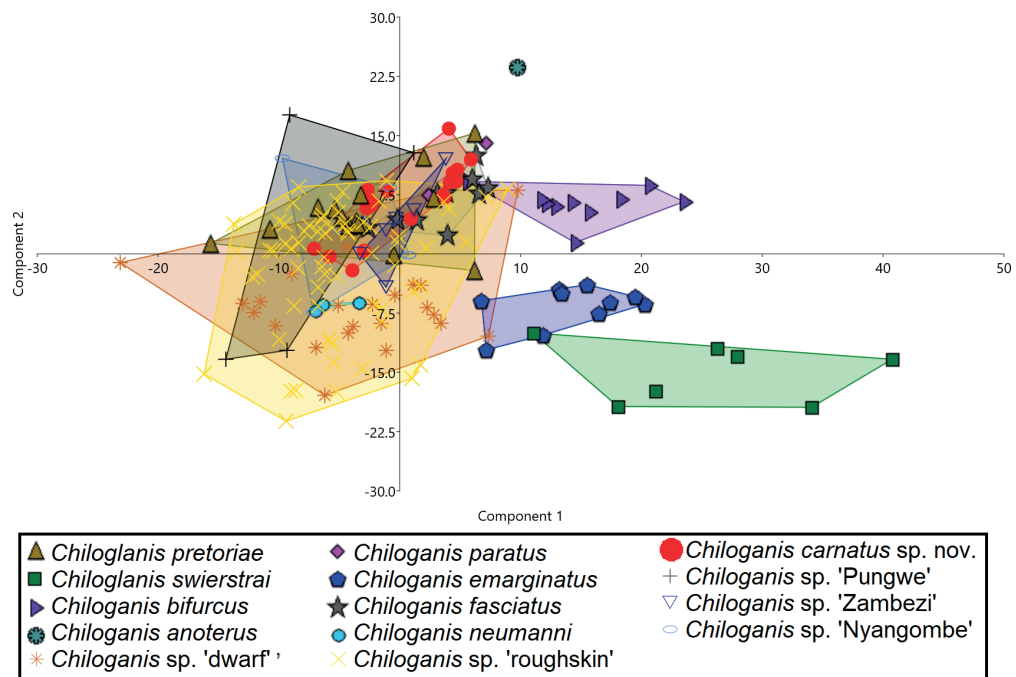


Figure 6. Scatter plot of the first two principal components of the morphometric characters of *Chiloglanis* species and lineages from southern African.

Chiloglanis carnatus sp. nov. specimens have a higher number of total vertebrae (29–30) compared to *C. neumanni* (28), *C. pretoriae* (28), and *C. paratus* (27) (Fig. 8C).

The integrated approach used in this study provided genetic and morphological characters that clearly and consistently distinguish *Chiloglanis carnatus* sp. nov. from the known species and lineages from this region. This study has thus provided evidence that supports the description of the *Chiloglanis carnatus* sp. nov. as a new species.

Taxonomic account

Chiloglanis carnatus Mutizwa, Bragança & Chakona, sp. nov.

<https://zoobank.org/E1F0912C-986F-450F-9B90-400D86F5F3BC>

Material examined. Holotype. ZIMBABWE • ♂, stored in 70% ethanol, 46.8 mm SL, Fig. 9A–E; Mukwadzi River near bridge on the road to Mutorashanga, Manyame River sub-catchment, middle Zambezi River system, Mashonaland West Province, 17.42485°S, 30.58542°E; 30 Jun. 2016; A. Chakona, W. Kadye and T. Bere; SAIAB 236631; genseq-1 COI PP156890. **Paratypes.** ZIMBABWE • 5 ♀, stored in 70% ethanol, 36.5–45.5 mm SL; near bridge on the road to Mutorashanga, Mukwadzi River, Manyame River sub-catchment, middle Zambezi River system, Mashonaland West Province, 17.42485°S, 30.58542°E; 30 Jun. 2016; A. Chakona, W. Kadye and T. Bere; SAIAB 211346; genseq-2 COI PP156891 to PP156895. ZIMBABWE • 6 ♀, 35.5–45.1 mm SL, 7 ♂, 36.5–48.9 mm SL, stored in 70% ethanol; near bridge on the road to Mutorashanga, Mukwadzi River, Manyame River system, middle Zambezi Basin, Mashonaland West Province, 17.42444°S, 30.58453°E; 11 Apr. 2019; A. Chakona, W. Kadye and T. Bere; SAIAB 211349.

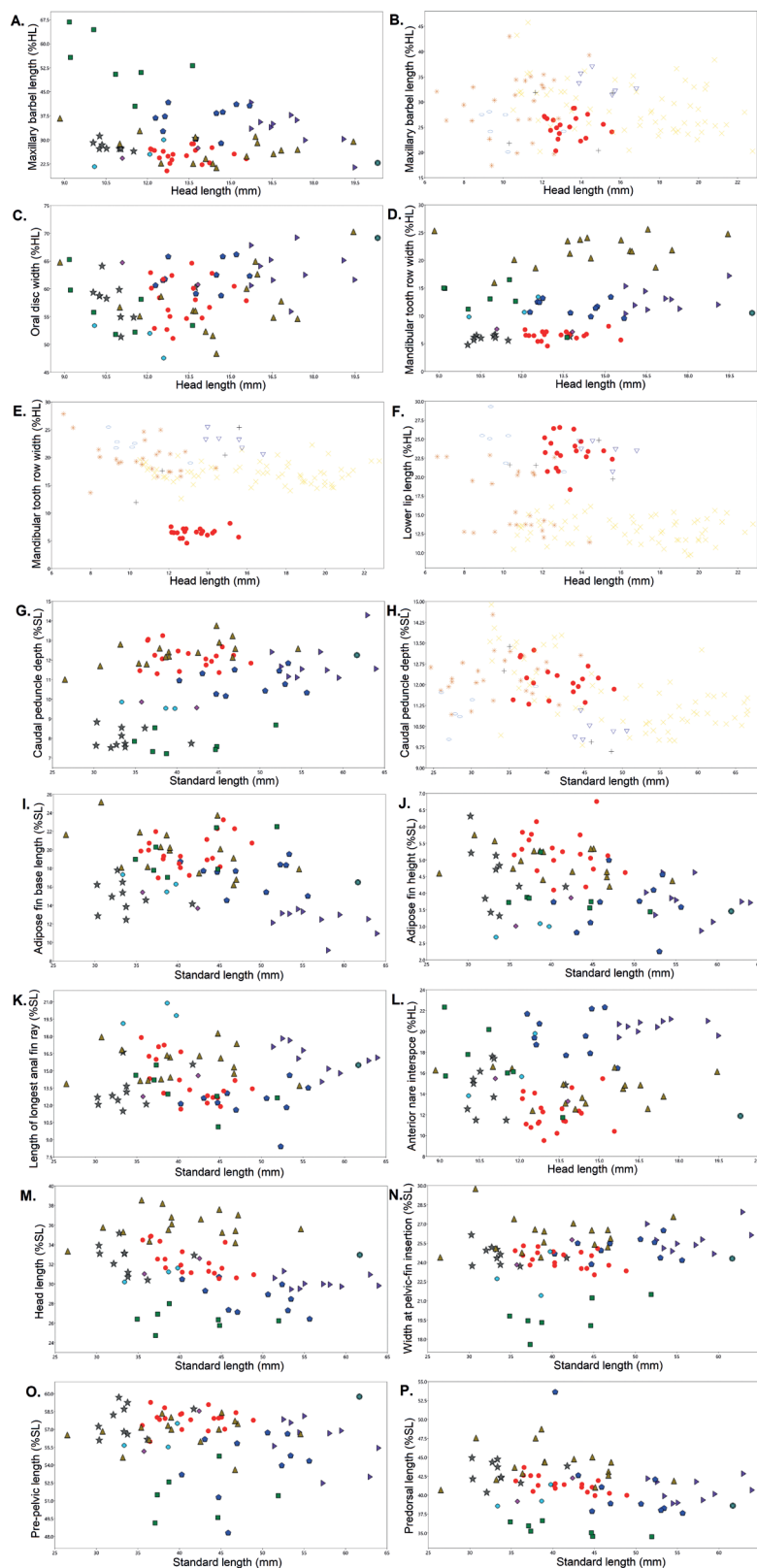


Figure 7. Scatterplots of the morphometric characters of the *Chiloglanis* species and lineages from southern African. Key: *Chiloglanis carnatus* sp. nov. (red circle), *C. pretoriae* (brown triangle), *C. swierstrai* (dark green square), *C. bifurcus* (purple right-pointing triangle), *C. anoterus* (green heavy asterisk), *C. paratus* (pink diamond), *C. emarginatus* (Blue pentagon), *C. fasciatus* (grey star), *C. neumanni* (light blue circle), *Chiloglanis* sp. 'dwarf' (orange eight spoked asterisk), *Chiloglanis* sp. 'roughskin' (yellow multiplication sign), *Chiloglanis* sp. 'Pungwe' (black plus sign), *Chiloglanis* sp. 'Zambezi' (blue down-pointing hollow triangle), *Chiloglanis* sp. 'Nyangombe' (light blue hollow circle).

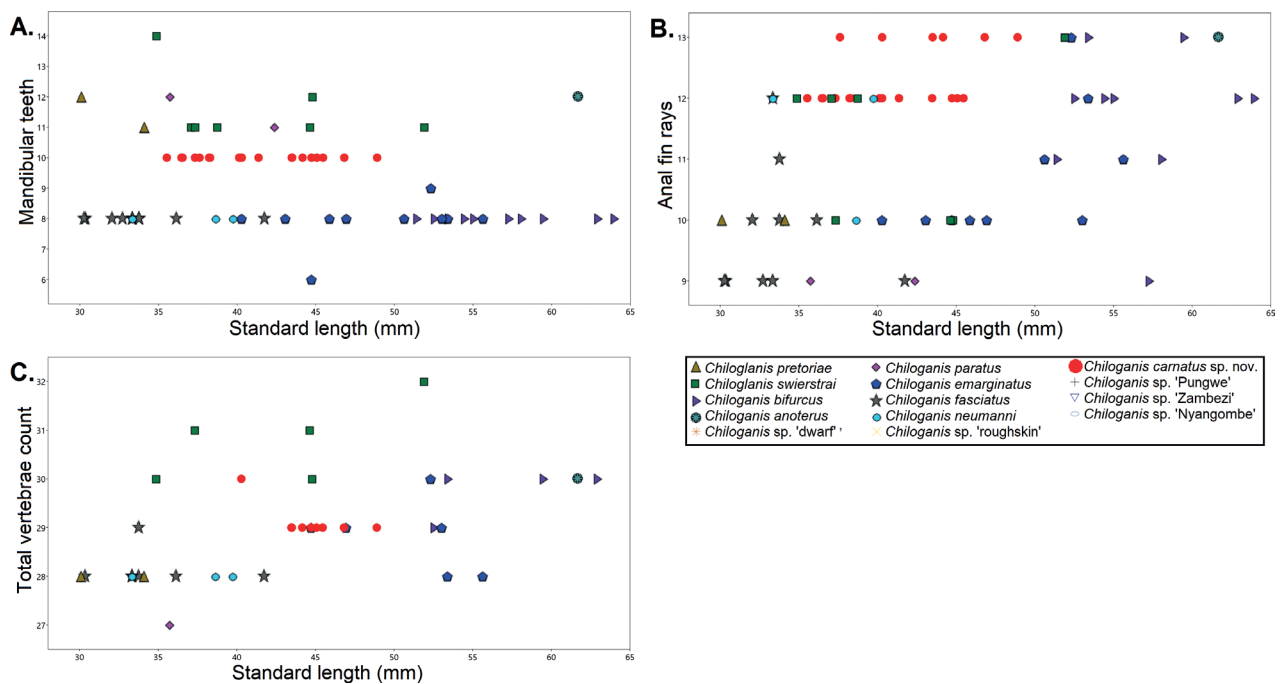


Figure 8. Scatterplots of the meristic characters of the *Chiloglanis* species from southern African.

Diagnosis. *Chiloglanis carnatus* sp. nov. is readily distinguished from its congeners in southern Africa (i.e. *C. anoterus*, *C. bifurcus*, *C. emarginatus*, *C. fasciatus*, *C. paratus*, *C. pretoriae* and *C. swierstrai*) by the presence of a dorsal fin that has a basal portion covered by a fleshy skin, a character which is absent in the other species. *Chiloglanis carnatus* possesses ten closely packed mandibular teeth, that further distinguishes it from *C. fasciatus* that has eight closely packed mandibular teeth; *C. bifurcus* and *C. emarginatus* that have eight widely spaced mandibular teeth; *C. anoterus*, *C. paratus*, and *C. pretoriae* that have 12 closely packed mandibular teeth; and *C. swierstrai* that has 14 closely packed mandibular teeth. *Chiloglanis carnatus* possesses a deeply forked caudal fin that readily separates it from *C. pretoriae* and *C. emarginatus* that have emarginate caudal fins, and from *C. anoterus* that has a caudal fin with extended median rays in males and emarginate in females. *Chiloglanis carnatus* possesses a caudal fin with an upper lobe that is shorter than the lower lobe. This distinguishes it from *C. bifurcus* that has a caudal fin with an upper lobe that is longer than the lower lobe. *Chiloglanis carnatus* has an oral disc with a well-developed mid-ventral cleft that distinguishes it from *C. swierstrai* that possesses an oral disc without a mid-ventral cleft. *Chiloglanis carnatus* possesses a smooth skin with a few tubercles occasionally found on the head that separates it from *C. fasciatus* that has its entire dorsal and lateral body surfaces mostly covered by small tubercles. *Chiloglanis carnatus* has a dorsal spine with crenate anterior and posterior margins that distinguish it from *C. paratus* that has a dorsal spine with a serrated posterior margin.

Description. Morphometric proportions and meristics are summarised in Table 7. Holotype meristic counts are given in parentheses.

Body shape. Anterior portion of body slightly compressed dorsally, becoming laterally compressed from pelvic fin insertion to caudal peduncle. Body greatest depth at dorsal-fin insertion. Pre-dorsal profile convex, sharply sloping from snout to posterior nostril, gently from nostril to dorsal-fin origin. Post-dorsal profile about straight from dorsal-fin base to adipose-fin origin, becoming

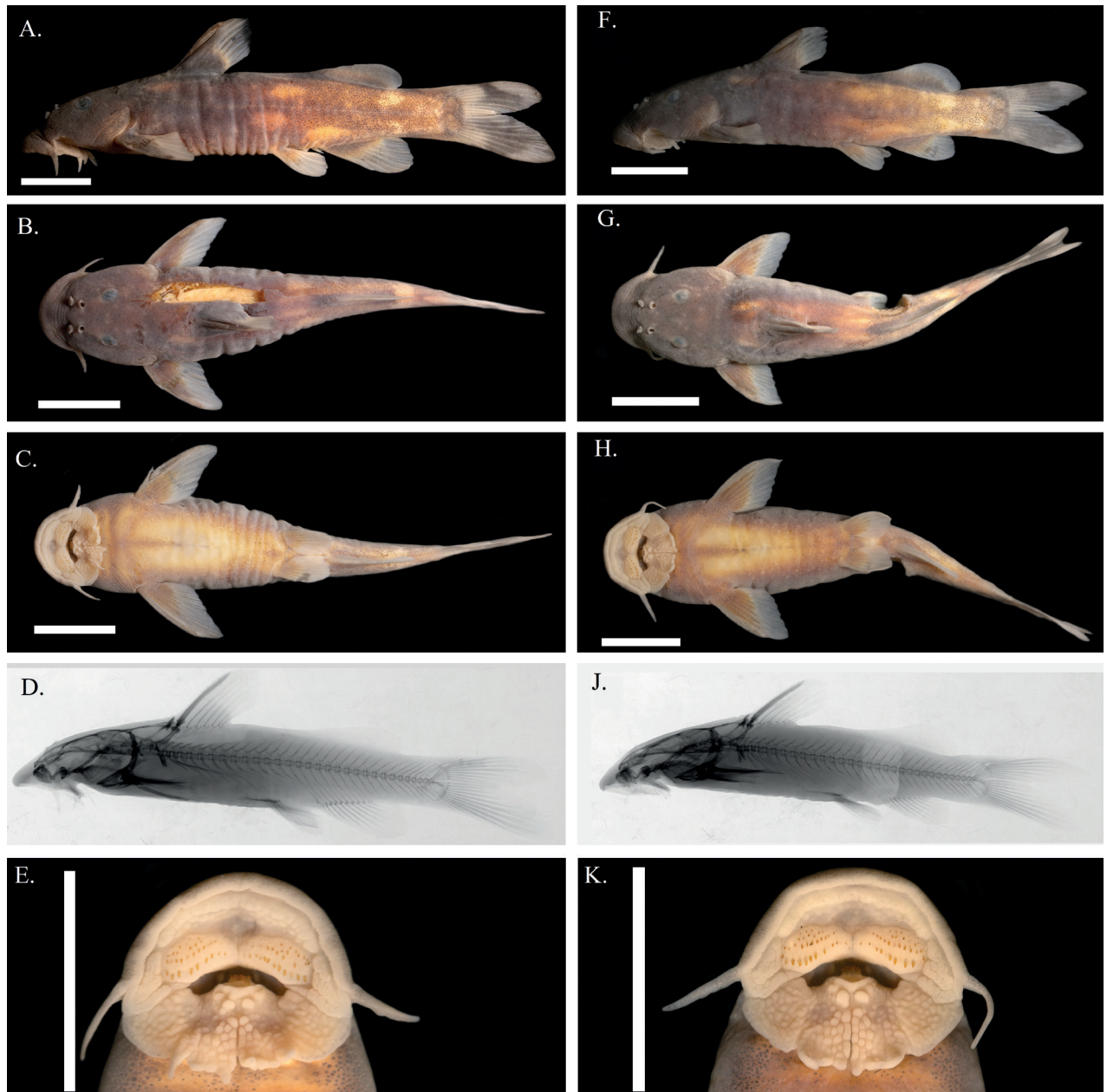


Figure 9. Holotype of *Chiloglanis carnatus* sp. nov., SAIAB 236631 male (A–E) and female paratype specimen SAIAB 211346 (F–K). Scale bars: 1 cm.

gently concave from adipose-fin origin to caudal fin. Ventral profile gently convex from region just posterior to oral disc to anal-fin origin, becoming gently concave from anal-fin origin to caudal fin.

Head. slightly depressed dorsally. Oval eye dorsally positioned, $\sim 1/2$ distance between snout and gill opening. Interorbital distance greater than distance between nostrils. Anterior and posterior nostrils closer to the eye than snout. Distance between anterior nostrils slightly greater than distance between posterior nostrils. Posterior nostril medially positioned relative to orbit. Anterior nostril with posterior flap; posterior nostril with anterior flap. Occipital-nuchal shield not visible through skin. Gill opening above pectoral fin insertion.

Oral disc. Mouth inferior; large upper and lower lips combined to form oral disc (see Fig. 9E, K). Oral disc width greater than length. Upper and lower lips with

Table 7. Summary of morphological characters for *Chiloglanis carnatus* sp. nov. All values except standard length (SL) and Head length (HL) are given as percentages of the HL or SL.

	Holotype	Paratypes			
	Male	Males		Females	
Number of specimens		7		11	
		Range	Mean	Range	Mean
Total length	58.2	45.3–62.2	49.8	45.3–56.1	52.2
Standard length	46.8	36.5–48.9	39.6	35.5–45.5	41.8
Head length	14.3	12.1–15.1	13.0	12.3–15.6	13.5
% Standard length					
Pre-pectoral length	28.1	26.9–30.0	28.9	27.1–29.1	28.3
Pre-dorsal length	40.2	40.0–42.6	41.6	39.9–43.7	41.3
Pre-pelvic length	58.4	56.0–58.8	57.8	56.9–59.3	57.9
Pre-anal length	71.1	67.6–70.8	69.1	67.9–73.3	70.6
Dorsal fin to adipose fin length	20.9	18.4–22.2	20.6	18.2–22.6	20.6
Pectoral-spine length	18.6	15.6–19.8	17.7	15.0–18.6	16.5
Pectoral-fin length	20.9	20.9–23.6	22.4	19.3–22.2	20.9
Width at pectoral-fin insertion	23.8	23.3–25.2	24.3	23.0–25.3	24.3
Pelvic-fin length	12.2	13.3–14.2	13.7	10.8–14.1	12.3
Pelvic-fin interspace	4.6	3.3–4.6	4.0	3.0–5.1	3.9
Body depth at dorsal-fin insertion	18.9	15.5–20.7	18.0	16.2–20.1	17.8
Body depth at anus	17.6	15.3–16.9	15.8	13.9–17.0	15.9
Dorsal-spine length	15.7	13.6–18.0	16.1	13.2–17.7	15.9
Dorsal-fin length along longest ray	17.9	15.2–20.7	18.5	16.2–20.0	17.4
Dorsal-fin base length	11.0	12.1–14.1	13.1	10.7–13.8	12.3
Adipose fin to caudal peduncle length	13.5	12.9–17.0	15.0	10.3–16.4	13.8
Adipose-fin base length	22.3	17.0–22.0	19.6	17.2–23.3	19.8
Adipose-fin height	5.1	4.1–6.1	5.2	4.2–6.8	5.3
Anal-fin length along longest ray	14.2	13.1–17.2	15.7	11.7–17.9	13.4
Anal-fin base length	12.1	11.8–15.3	13.2	11.1–13.4	12.5
Caudal peduncle depth	12.2	11.3–13.2	12.1	11.4–13.1	12.1
Caudal peduncle length	16.8	16.0–19.2	18.3	15.9–19.7	17.5
Caudal fork length	12.3	9.8–14.5	11.4	9.2–14.4	11.7
Head length	30.6	30.9–34.8	32.9	30.5–34.9	32.2
% Head length					
Head depth	57.4	43.9–57.6	51.2	48.2–57.3	51.2
Eye diameter (vertical axis)	11.9	10.6–13.2	11.7	9.9–13.8	11.9
Eye diameter (horizontal axis)	15.7	13.0–16.4	14.1	12.9–16.8	15.0
Orbital interspace	25.1	22.3–28.7	24.1	21.5–26.8	24.5
Anterior nares interspace	12.1	9.5–15.5	12.1	10.4–14.6	12.2
Posterior nares interspace	12.6	11.0–15.5	13.5	10.3–15.4	12.7
Snout length	61.1	54.3–63.8	58.7	54.0–66.2	60.7
Pre-maxillary tooth-patch length	9.9	8.2–11.0	9.9	8.8–12.3	10.4
Pre-maxillary tooth-patch width	44.3	36.8–44.7	41.1	38.4–47.9	42.1
Mandibular tooth row width	6.7	4.6–8.1	6.4	5.4–7.1	6.4
Maxillary barbel length	27.6	20.3–27.2	25	22.3–28.8	25.3
Upper lip length	15.1	11.1–14.5	13.1	11.3–16.2	13.9
Lower lip length	23.4	18.3–25.2	22.7	20.7–26.6	23.8
Mouth width	29.2	25.3–30.8	27.3	23.9–33.8	28.1

	Holotype	Paratypes			
	Male	Males		Females	
	Number of specimens	7		11	
		Range	Mean	Range	Mean
Oral disc width	62.8	51.1–62.9	57.2	52.9–64.6	58.2
Oral disc length	54.3	48.6–57.0	53.1	50.2–56.4	53.3
Postcleithral process to occipital shield	37.8	29.5–36.3	33.1	32.2–38.3	35.5
Length of postcleithral process	29.6	23.4–28.9	25.5	22.9–27.8	25.9
Occipital shield width	23.6	14.6–19.5	16.9	14.9–24.2	18.8
Lower caudal-fin lobe length	13.4	9.3–13.0	10.6	10.0–12.7	11.2
Upper caudal-fin lobe length	10.8	8.7–12.1	9.8	9.1–11.7	10.4
Medial mandibular barbel length	0.6	0.2–0.6	0.4	0.4–0.9	0.6
Lateral mandibular barbel length	1.3	1.0–1.8	1.4	1.1–1.8	1.4
Meristics		Range	Mode	Range	Mode
Mandibular tooth count	10	8–10	10	8–10	10
Pre-maxillary tooth count	59	43–69	–	49–68	60
Pectoral fin-ray count	8	7–8	8	6–8	8
Pelvic fin-ray count	7	7	7	6–7	7
Dorsal fin-ray count	6	6	6	5–7	6
Anal fin-ray count	13	12–13	12	12–13	12
Abdominal vertebrae	12	12	–	11–13	13
Caudal vertebrae	17	17	–	16–18	16
Total vertebrae	29	29	–	29–30	29

pronounced roundish papillae, largest papillae concentrated around mid-ventral cleft of lower lip. Three pairs of barbels. Maxillary barbel unbranched, originating from lateral region of oral disc, extending to posterior region of oral disc. Lateral mandibular barbel longer than medial mandibular barbel, both incorporated into lower lip. Shallow cavity above lower lip.

Dentation. Pre-maxillary teeth arranged in three or four rows; variable number of teeth (43–69). Up to 5+5 closely packed mandibular teeth; central teeth projecting higher than outer teeth forming a gentle arc; replacement tooth row emerges anteriorly to the functional row.

Fins. Dorsal-fin ray count 5–7 (6), originating in anterior 1/3 of body, posterior to pectoral-fin origin. Dorsal fin basal portion covered by a fleshy skin prominent in large adult males and females with $\sim \frac{3}{4}$ of the dorsal spine and the first two rays also covered by fleshy skin (Fig. 10). Dorsal spine length \sim 80% of longest dorsal fin ray length. Dorsal spine with dentate anterior and posterior margins. Pectoral-fin ray count 6–8 (8), origin anterior to gill opening; pectoral spine anterior margin smooth; dentate posterior margin; pectoral spine length \sim 80% of pectoral fin length. Adipose fin origin preceded by anterior tissue flange; rounded (Fig. 10). Caudal fin forked, lower lobe longer than upper lobe. Anal-fin ray count 12 or 13 (13), origin posterior to origin of adipose fin; terminating just before end of adipose-fin; rounded. Pelvic-fin ray count 6 or 7 (7), origin posterior to midpoint between end of dorsal-fin and adipose-fin origin; rounded.

Skin. Skin smooth with occasional tubercles present, concentrated on dorsal and lateral surface of head. Lateral line complete; originating anterior to dorsal fin at same horizontal level of orbit and sloping ventrally until it lies mid-laterally along body.

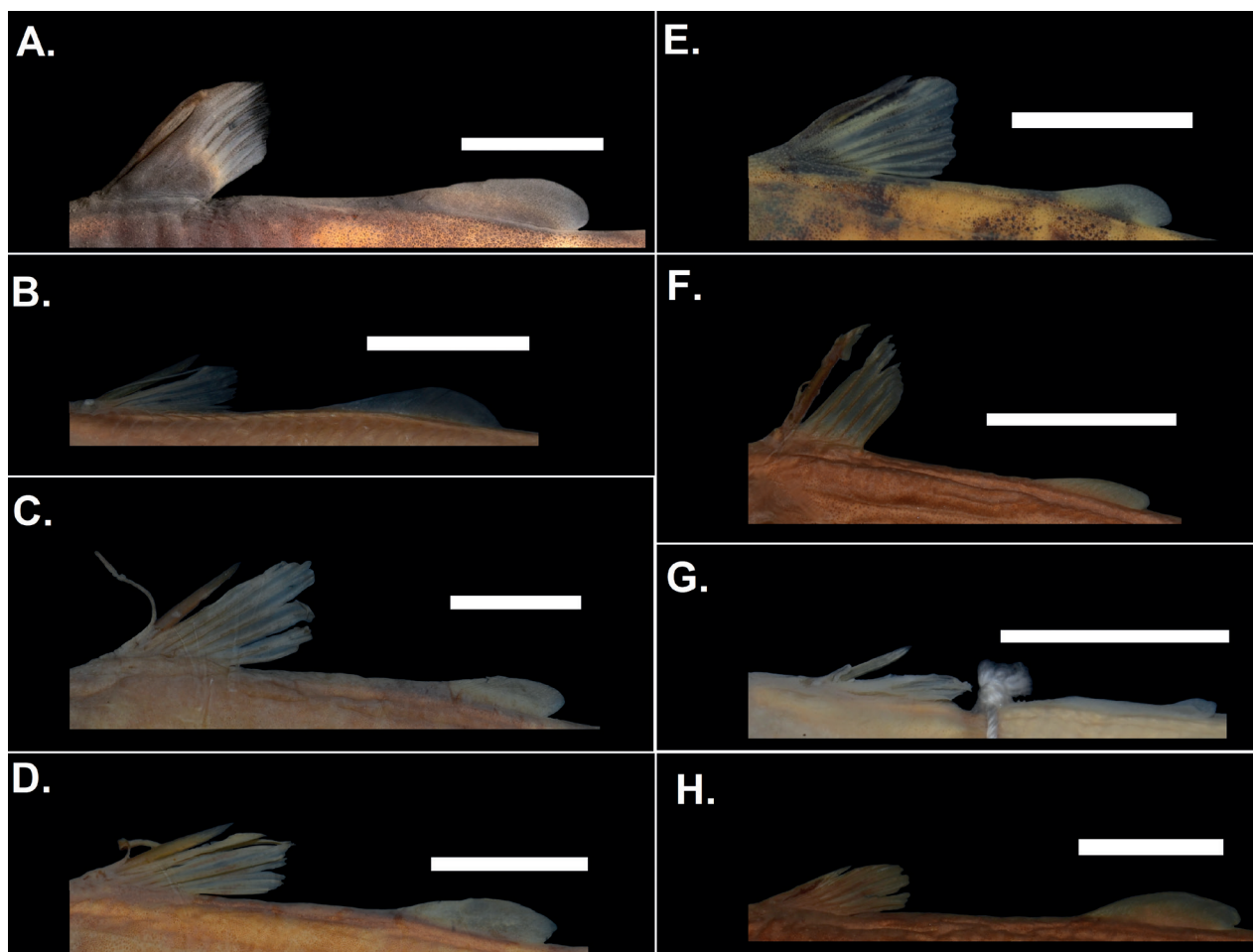


Figure 10. Comparison of the dorsal and adipose fins of *Chiloglanis carnatus* sp. nov. and the type specimens of the valid southern African species **A** *Chiloglanis carnatus* sp. nov. (SAIAB 236631) specimens have an extended dermal tissue covering the base of the dorsal fin that distinguishes them from **B** *C. swierstrai* (SAIAB 186247) **C** *C. bifurcus* (SAIAB 120160) **D** *C. emarginatus* (SAIAB 120117) **E** *C. fasciatus* (SAIAB 204928) **F** *C. paratus* (SAIAB 186248) **G** *C. pretoriae* (SAIAB 30011) **H** *C. anoterus* (SAIAB 186246). Scale bars: 1 cm.

Sexual dimorphism. Urogenital opening situated adjacent to origin of anal fin. Urogenital papillae sexually dimorphic; elongated in males; reduced and separated from anus by shallow invagination in females.

Colouration. Overall body background colouration brown with yellowish ventral surface. Anterior portion of body dark brown becoming paler towards posterior. Small dark melanophores scattered across entire dorsal and lateral sides. Six yellowish brown blotches on lateral surface of body; two vertically arranged posterior to end of adipose fin; one above origin of anal fin; two above pelvic fin origin; and one below dorsal fin origin. Basal 1/3 of fins pale to dark brown with medium and posterior portion of fins gradually becoming translucent. Dark blotch cuts vertically across caudal peduncle lobes.

Vertebral counts. Total vertebrae 29 or 30 (29), abdominal vertebrae 11–13 (12), caudal vertebrae 16–18 (17).

Etymology. The specific epithet *carnatus* means fleshy, referring to the dermal tissue covering the base of the dorsal fin of some of the larger specimens of this species and the general robust body structure of this species compared to its regional congeners.

Distribution. *Chiloglanis carnatus* was collected from two sites in the Mukwadzi River near the bridge on the Mutorashanga Road. The Mukwadzi River is a perennial river that originates from wetlands (dambos) on the eastern side of the Great Dyke. This river flows in a north-western direction cutting through the Great Dyke before it joins the Manyame River. The Great Dyke is a major intrusion of mafic and ultramafic rocks that have vast ore deposits, including gold, silver, chromium, platinum, nickel, and asbestos. The rich mineral deposits have resulted in the establishment of many mines along the Great Dyke. The sites where *C. carnatus* was collected were in a communal area surrounded by rural communities on the western slope of the Great Dyke. The substratum at the sites was composed of bedrock, cobbles and gravel, and the riparian vegetation was dominated by *Syzygium* Gaertner, 1788 and *Phragmites* Adanson, 1763. At these sites *C. carnatus* co-occurred with native fish species that include *Labeo cylindricus* Peters, 1852, *Opsaridium zambezense* (Peters, 1852), *Enteromius trimaculatus* (Peters, 1852), *Tilapia sparrmanii* Smith, 1840, *Clarias gariepinus* (Burchell, 1822), and *Labeobarbus marequensis* (Smith, 1841) as well as the non-native species *Serranochromis jallae* (Boulenger, 1896) and *Micropterus salmoides* (Lacepède, 1802).

Discussion

This study integrated molecular and morphological data to evaluate the taxonomic distinctiveness of specimens of suckermouth catfishes that were collected from the middle Zambezi River system in Zimbabwe. Based on substantial genetic differentiation as well as consistent meristic, morphometric, and qualitative differences from its southern African congeners, a new species of *Chiloglanis* is described. This is the first description more than five decades after the last comprehensive review of *Chiloglanis* species from southern Africa (see Jubb and Le Roux 1969). This study adds to the growing body of literature that demonstrates the value of integrative taxonomic approaches in the discovery and description of new species within this region (Maake et al. 2014; Morris et al. 2016; Riddin et al. 2016; Kambikambi et al. 2021; Mazungula and Chakona 2021). As evidenced from this study and work by Chakona et al. (2018), additional species of suckermouth catfishes from southern Africa remain to be formally described. It is anticipated that ongoing taxonomic studies on this group of fishes will result in the description of at least ten new species from this region. These species were all previously included under a single species, *C. neumanni*, but this study and ongoing work by researchers from the NRF-SAIAB indicates that this species does not occur in southern Africa. Updated taxonomic information of *Chiloglanis* species from this region will improve our understanding of biogeographic and phylogeographic patterns as well as drainage evolution in the region.

The dentition of species in the genus *Chiloglanis*, like that of most members of the family Mochokidae, is highly specialised (Roberts 1989). *Chiloglanis carnatus* possesses ten closely packed mandibular teeth, a number not found in any other *Chiloglanis* species in southern Africa. Variation in the number of mandibular teeth in individual specimens can be observed due to tooth loss from the functional row, delayed exposure of some teeth in the replacement row, or early advancement of some replacement row teeth (Roberts 1989). However, by examining both the functional and replacement rows, it was possible to determine the diagnostic number of teeth for this species. Outside southern Africa, the presence

of ten mandibular teeth has been reported in west African species such as *C. kolente* Schmidt et al., 2017, *C. kabaensis* Schmidt et al., 2017, *C. nzerekore* Schmidt et al., 2017, *C. occidentalis* Pellegrin, 1933, and *C. normani* Pellegrin, 1933 (Paugy et al. 2003; Schmidt et al. 2017). In addition to dentation, there were several morphometric characters associated with the oral disc (e.g., maxillary barbel length, oral disc width, lower lip length and mandibular tooth row width) that distinguish *C. carnatus* from congeners in southern Africa. Considering the importance of the oral disc in the ecology of the species in this genus, these differences warrant further study, particularly assessing potential differences in trophic ecology.

Rheophilic habitats form 'islands' with suitable environmental conditions for specialised taxa such as those in the genus *Chiloglanis*. The disjunct distribution of these habitats within a river may play an important role in promoting genetic and morphological diversity within rheophilic taxa. Some rheophilic species have very narrow distribution ranges such that significant differences have been found in the fish communities occurring at different rapids within the same river system (Hrbek et al. 2018). In southern Africa high genetic and morphological diversity within *C. anoterus* has been reported from geographically isolated populations in the upper sections of the Phongolo and Inkomati river systems, highlighting the importance of the rheophilic habitats in headwater streams (Morris et al. 2016). The close association of *Chiloglanis* species with rheophilic habitats probably promotes diversification; however, this has yet to be explicitly tested within this region. The discovery of the *C. carnatus* from a small section of the Mukwadzi River as well as other undescribed species within southern Africa (Chakona et al. 2018) emphasises the need for accelerating inventory of the diversity found in rheophilic habitats as these may harbour a considerable number of species which are still unknown to science.

A number of southern African freshwater fish species in the genera *Enteromius* Cope, 1867, *Nothobranchius* Peters, 1868, *Pseudobarbus* Smith, 1841, *Sandelia* Castelnau, 1861, *Galaxias* Cuvier, 1816, and *Oreochromis* Günther, 1889 are threatened with extinction due to their narrow geographic ranges, the introduction of invasive species, and habitat degradation (Marshall and Tweddle 2007; Jordaan and Chakona 2017; Roux and Hoffman 2017b; Nagy and Watters 2019). Among the *Chiloglanis* species from southern Africa, *C. bifurcus* and *C. emarginatus* are under threat with the former classified as Critically Endangered and the latter as Vulnerable in the IUCN Red List of threatened species (Roux and Hoffman 2017a, 2018). *Chiloglanis bifurcus* is a narrow-range endemic species that is confined to the upper sections of the Inkomati River system, whereas *C. emarginatus*' range in the Phongolo River system has declined substantially over the past decades (Roux and Hoffman 2017a, 2018). Habitat loss through flow regulation, pollution, and sedimentation has been attributed as the main driver of population decline in both these species (Roux and Hoffman 2017a, 2018). *Chiloglanis carnatus* was collected from two sites in the Mukwadzi River. The section downstream of these sites as well as other tributaries of the Mukwadzi River are heavily impacted by anthropogenic activities. There are at least 13 small impoundments in the Mukwadzi River before its confluence with the Manyame River. Largemouth bass (*Micropterus salmoides*) and the nembwe (*Serranochromis jallae*) were also introduced into this river system, and this combination of flow modification, water abstraction, and non-native species is likely to negatively impact populations of native spe-

cies (Gratwicke and Marshall 2001; Gratwicke et al. 2003; Kadye et al. 2013; Kadye and Booth 2020). In addition to the modification of this river and the non-native species, the rich mineral resources found within the Great Dyke attract formal and informal mining operations which also threaten the species living within these rivers through increased sedimentation/siltation which may cause habitat loss. Although little is known about the distribution of *C. carnatus* beyond the sites sampled in this study, multiple anthropogenic activities in the Mukwadzi River catchment raise concerns about the conservation status of this species.

The description of *C. carnatus* contributes towards clarifying the taxonomic uncertainty surrounding species of the genus *Chiloglanis* found within the geographic range formerly attributed to *C. neumanni* within southern Africa. The discovery of *C. carnatus* follows the common pattern found among recent taxonomic studies within the region whereby comprehensive sampling across poorly explored regions and the use of integrated taxonomic approaches has identified unique diversity within species previously thought to have wide distribution ranges (Bragança et al. 2020; Kambikambi et al. 2021; Mazungula and Chakona 2021). This pattern is likely to be consistent across southern Africa suggesting underestimation of the region's biodiversity. In particular, species such as those from the genus *Chiloglanis* are likely to be more diverse since they occur in disjunct distributions in rheophilic habitats, which are likely to be associated with allopatric speciation. This study also raises the awareness of the potential unique riverine diversity of the rivers that flow through the Great Dyke, an important geological feature where 20 endemic plant species that are adapted to the unique serpentine soils have been recorded (Wild 1965). Further exploration of the aquatic fauna of this poorly surveyed region is likely to uncover additional new species for science.

Acknowledgements

We would like to thank the NRF-SAIAB personnel including Paul Skelton, Roger Bills, Maditaba Meltaf, Nkosinathi Mazungula, Nonkoliso Mgibntaka, Amanda Gura, Zinzi Somana, Siphamandla Mceleli, Gwynneth Matcher, and Taryn Bodil for the support during this study.

Additional information

Conflict of interest

The authors have declared that no competing interests exist.

Ethical statement

Ethical clearance for the approaches used for sample collection and processing was approved by the National Research Foundation-South African Institute for Aquatic Biodiversity (NRF-SAIAB) Animal Ethics Committee (Ref#: 2014/03 and REF#: 25/4/1/7/5_2022-02).


Funding


This research was supported by the Rhodes University Sandisa Imbewu Grant, the NRF-Research Development Grant (CSRP190416431023), NRF-SAIAB Refresh project (FBIP-211006643719) and NRF-SAIAB Topotypes project (IBIP-BS 13100251309).

Author contributions

Conceptualization: WK, PB, TB, AC. Data curation: TIM. Formal analysis: TIM. Funding acquisition: WK, AC. Investigation: TIM. Methodology: PB, AC, WK, TIM. Project administration: AC, WK. Resources: AC, TB. Supervision: AC, WK, PB. Visualization: PB, TIM. Writing – original draft: TIM. Writing – review and editing: TIM, PB, AC, TB, WK.

Author ORCIDs

Tadiwa I. Mutizwa  <https://orcid.org/0000-0003-4017-1720>

Wilbert T. Kadye  <https://orcid.org/0000-0002-5273-8360>

Pedro H. N. Bragança  <https://orcid.org/0000-0002-8357-7010>

Taurai Bere  <https://orcid.org/0000-0002-8603-5137>

Albert Chakona  <https://orcid.org/0000-0001-6844-7501>

Data availability

All of the data that support the findings of this study are available in the main text.

References

- Adanson M (1763) Familles des Plantes. Vincent, Paris, 640 pp. <https://doi.org/10.5962/bhl.title.271>
- Akaike H (1974) A new look at the statistical model identification. *IEEE Transactions on Automatic Control* 19(6): 716–723. <https://doi.org/10.1109/TAC.1974.1100705>
- Alfaro ME, Holder MT (2006) The posterior and the prior in Bayesian phylogenetics. *Annual Review of Ecology, Evolution, and Systematics* 37(1): 19–42. <https://doi.org/10.1146/annurev.ecolsys.37.091305.110021>
- Bell-Cross G, Minshull JL (1988) The Fishes of Zimbabwe. National Museums and Monuments of Zimbabwe, Harare, 294 pp.
- Bouckaert R, Heled J, Kühnert D, Vaughan T, Wu CH, Xie D, Suchard MA, Rambaut A, Drummond AJ (2014) BEAST 2: a software platform for Bayesian evolutionary analysis. *PLoS Computational Biology* 10(4): e1003537. <https://doi.org/10.1371/journal.pcbi.1003537>
- Boulenger GA (1896) Liste des poissons recueillis par le R. P. Louis Jalla a Kazungula, Haut Zambese. *Bollettino dei Musei di Zoologia ed Anatomia* 11(260): 1–2.
- Boulenger GA (1900) Matériaux pour la Faune du Congo. Poissons Nouveaux du Congo. Sixième Partie. *Annales du musée du congo publiées par ordre du secrétaire d'état*, Bruxelles, 520–529.
- Boulenger GA (1902) Additions à la faune ichthyologique de bassin du Congo. Matériaux pour la faune du Congo. *Annales du Musée du Congo (Ser. Zoology)* 2: 19–57.
- Boulenger GA (1903) On the fishes collected by Mr. G. L. Bates in southern Cameroon. *Proceedings of the Zoological Society of London* 1(3): 21–29. <https://doi.org/10.1111/j.1469-7998.1903.tb08256.x>
- Boulenger GA (1911) Catalogue of the Fresh-Water Fishes of Africa in the British Museum (Natural History), London, 481–482.
- Bragança PHN, Smith TG, Vreven EJWMN, Chakona A (2020) Integrative taxonomy reveals hidden diversity in the southern African darters genus *Nannocharax* Günther 1867 (Characiformes: Distichodontidae). *Journal of Fish Biology* 97(6): 1713–1723. <https://doi.org/10.1111/jfb.14535>
- Burchell WJ (1822) Travels in the Interior of Southern Africa. Longman, London, 280 pp. <https://doi.org/10.5962/bhl.title.100911>

- Castelnau FL (1861) Mémoire sur les poissons de l'Afrique australe. Paris 1–3: 1–78. <https://doi.org/10.5962/bhl.title.3819>
- Chakona A, Kadye WT, Bere T, Mazungula DN, Vreven EJWMN (2018) Evidence of hidden diversity and taxonomic conflicts in five stream fishes from the Eastern Zimbabwe Highlands freshwater ecoregion. *ZooKeys* 768: 69–95. <https://doi.org/10.3897/zookeys.768.21944>
- Cope ED (1867) Supplement on some new species of American and African fishes. *Transactions of the American Philosophical Society* 13(3): 400–407.
- Crass RS (1960) Notes on the freshwater fishes of Natal with descriptions of four new species. *Annals of the Natal Museum* 14(3): 446–456.
- Cuvier G (1816) Le Règne Animal distribué d'après son organisation pour servir de base à l'histoire naturelle des animaux et d'introduction à l'anatomie comparée. Les reptiles, les poissons, les mollusques et les annélides. A. Belin, Paris, Edition 1 v 2: 1–532.
- Daget J, Gosse JP, Van den Audenaerde DT (1986) CLOFFA 2 Check-List of the Freshwater Fishes of Africa. ORSTOM, Paris, 111 pp.
- Darriba D, Taboada GL, Doallo R, Posada D (2012) JModelTest 2: More models, new heuristics and parallel computing. *Nature Methods* 9(8): e772. <https://doi.org/10.1038/nmeth.2109>
- Day JJ, Peart CR, Brown KJ, Friel JP, Bills RI, Moritz T (2013) Continental diversification of an African catfish radiation (Mochokidae: *Synodontis*). *Systematic Biology* 62(3): 351–365. <https://doi.org/10.1093/sysbio/syt001>
- Day JJ, Steell EM, Vigliotta TR, Withey LA, Bills R, Friel JP, Genner MJ, Stiasny MLJ (2023) Exceptional levels of species discovery ameliorate inferences of the biogeography and diversification of an Afrotropical catfish family. *Molecular Phylogenetics and Evolution* 107754: e107754. <https://doi.org/10.1016/j.ympev.2023.107754>
- Eccles DH, Tweddle D, Skelton PH (2011) Eight new species in the dwarf catfish genus *Zaireichthys* (Siluriformes: Amphiliidae). *Smithiana. Bulletin* 13(4): 3–28.
- Felsenstein J (1985) Confidence limits on phylogenies: An approach using the bootstrap. *Evolution; International Journal of Organic Evolution* 39(4): e783. <https://doi.org/10.2307/2408678>
- Fricke R, Eschmeyer WN, Van der Laan R [Eds] (2024) Eschmeyer's catalog of fishes: genera, species, references. <http://researcharchive.calacademy.org/research/ichthyology/catalog/fishcatmain.asp> [Accessed 20 January 2024]
- Friel JP, Vigliotta TR (2008) *Atopodontus adriaensi*, a new genus and species of African suckermouth catfish from the Ogooué and Nyanga River systems of Gabon (Siluriformes: Mochokidae). *Proceedings of the Academy of Natural Sciences of Philadelphia* 157(1): 13–23. [https://doi.org/10.1635/0097-3157\(2008\)157\[13:AAANGA\]2.0.CO;2](https://doi.org/10.1635/0097-3157(2008)157[13:AAANGA]2.0.CO;2)
- Fujisawa T, Barraclough TG (2013) Delimiting species using single-locus data and the Generalized Mixed Yule Coalescent approach: A revised method and evaluation on simulated data sets. *Systematic Biology* 62(5): 707–724. <https://doi.org/10.1093/sysbio/syt033>
- Gaertner J (1788) *Syzygium*. *De Fructibus et Seminibus Plantarum* 1: e166. <https://doi.org/10.5962/bhl.title.102753>
- Gratwicke B, Marshall BE (2001) The relationship between the exotic predators *Micropoterus salmoides* and *Serranochromis robustus* and native stream fishes in Zimbabwe. *Journal of Fish Biology* 58(1): 68–75. <https://doi.org/10.1111/j.1095-8649.2001.tb00499.x>
- Gratwicke B, Marshall BE, Nhwatiwa T (2003) The distribution and relative abundance of stream fishes in the upper Manyame River, Zimbabwe, in relation to land use, pol-

- lution and exotic predators. *African Journal of Aquatic Science* 28(1): 25–34. <https://doi.org/10.2989/16085914.2003.9626596>
- Günther A (1864) Catalogue of the Physostomi, containing the families Siluridae, Characinae, Haplochitonidae, Sternoptychidae, Scopelidae, Stomiatidae in the collection of the British Museum. *Catalogue of the fishes in the British Museum* 5: 315–316.
- Günther DA (1889) On Some Fishes from the Kilimanjaro District. *Proceedings of the Zoological Society of London* 57 No. 1. Blackwell Publishing Ltd., Oxford, 70–72. <https://doi.org/10.1111/j.1469-7998.1889.tb06752.x>
- Hammer Ø, Harper DAT, Ryan PD (2001) PAST: Paleontological statistics software package for education and data analysis. *Palaeontologia Electronica* 4(1): 1–9.
- Helfrich P, Rieb E, Abrami G, Lücking A, Mehler A (2018) TreeAnnotator: versatile visual annotation of hierarchical text relations. *Proceedings of the eleventh international conference on language resources and evaluation (LREC 2018)*.
- Hilgendorf F (1905) Fische von Deutsch und Englisch Ost-Afrika. Gesammelt von Oscar Neumann 1893–1895. *Zoologische Jahrbucher. Systematik* 22: 405–420.
- Hillis DM, Bull JJ (1993) An empirical test of bootstrapping as a method for assessing confidence in phylogenetic analysis. *Systematic Biology* 42(2): 182–192. <https://doi.org/10.1093/sysbio/42.2.182>
- Howes GJ (1980) A New Catfish from Sierra Leone. *Bulletin of the British Museum, Natural History. Zoology* 38: 165–170. <https://doi.org/10.5962/p.12613>
- Hrbek T, Meliciano NV, Zuanon J, Farias IP (2018) Remarkable geographic structuring of rheophilic fishes of the lower Araguaia River. *Frontiers in Genetics* 9(8): 1–12. <https://doi.org/10.3389/fgene.2018.00295>
- Joannis L de (1835) Observations sur les poissons du Nil, et description de plusieurs espèces 24 nouvelles. *Magasin de zoologie*, 53 pp.
- Jordaan M, Chakona A (2017) *Pseudobarbus burchelli*. The IUCN Red List of Threatened Species 2017: e.T107649398A100170338. <https://dx.doi.org/10.2305/IUCN.UK.2017-3.RLTS.T107649398A100170338.en> [Accessed on 17 October 2023]
- Jubb RA, Le Roux P (1969) Revision of the *Chiloglanis* (Pisces: Mochokidae) of Southern Africa and descriptions of two new species. *Annals of the Cape Provincial Museums* 8(2): 13–23. [Natural History]
- Kadye WT, Booth AJ (2020) Environmental niche patterns of native and non-native fishes within an invaded African river system. *Journal of Fish Biology* 96(5): 1269–1277. <https://doi.org/10.1111/jfb.13988>
- Kadye WT, Chakona A, Marufu LT, Samukange T (2013) The impact of non-native rainbow trout within Afro-montane streams in eastern Zimbabwe. *Hydrobiologia* 720(1): 75–88. <https://doi.org/10.1007/s10750-013-1624-4>
- Kambikambi MJ, Kadye WT, Chakona A (2021) Allopatric differentiation in the *Enteromius anoplus* complex in South Africa, with the revalidation of *Enteromius cernuus* and *Enteromius oraniensis*, and description of a new species, *Enteromius mandelai* (Teleostei: Cyprinidae). *Journal of Fish Biology* 99(3): 931–954. <https://doi.org/10.1111/jfb.14780>
- Kashindy BB, Manda BK, Friel JP, Chakona A, Vreven EJWMN (2021) A new species of African suckermouth catfish (Teleostei: Mochokidae), from the Upper Congo basin. *Ichthyological Exploration of Freshwaters* 9902(11): 1–14.
- Kumar S, Stecher G, Tamura K (2016) MEGA7: Molecular evolutionary genetics analysis Version 7.0 for bigger datasets. *Molecular Biology and Evolution* 33(7): 1870–1874. <https://doi.org/10.1093/molbev/msw054>
- Lacepède BGE (1802) *Histoire Naturelle des Poissons* 4. Chez Plassan Imprimeur-Libraire, Paris, 324–329.









- Maake PA, Gon O, Swartz ER (2014) Descriptions of three new species of *Marcusenius* Gill, 1862 (Teleostei: Mormyridae) from South Africa and Mozambique. *Zootaxa* 3780(3): 455–480. <https://doi.org/10.11646/zootaxa.3780.3.2>
- Marshall BE, Tweddle D (2007). *Oreochromis mortimeri*. The IUCN Red List of Threatened Species 2007: e.T63337A12659594. <https://doi.org/10.2305/IUCN.UK.2007.RLTS.T63337A12659594.en> [Accessed 17 October 2023]
- Marshall BE (2011) The Fishes of Zimbabwe and Their Biology. Smithania Monograph 3. South African Institute for Aquatic Biodiversity (private), Grahamstown, South Africa, 169–175.
- Mazungula DN, Chakona A (2021) An integrative taxonomic review of the Natal mountain catfish, *Amphilius natalensis* Boulenger 1917 (Siluriformes, Amphiliidae), with description of four new species. *Journal of Fish Biology* 99(1): 1–21. <https://doi.org/10.1111/jfb.14714>
- Morris J, Ford AGP, Ali JR, Peart CR, Bills R, Day JJ (2016) High levels of genetic structure and striking phenotypic variability in a sexually dimorphic suckermouth catfish from the African Highveld. *Biological Journal of the Linnean Society. Linnean Society of London* 117(3): 528–546. <https://doi.org/10.1111/bij.12650>
- Mutizwa TI, Kadye WT, Chakona A (2021) Deep genetic and morphological divergence in the *Hippopotamyrus ansorgii* species complex (Teleostei: Mormyridae) in southern Africa. *Journal of Fish Biology* 99(2): 1–14. <https://doi.org/10.1111/jfb.14743>
- Nagy B, Watters B (2019) *Nothobranchius mkuziensis*. The IUCN Red List of Threatened Species 2019: e.T131471491A131471537. <https://dx.doi.org/10.2305/IUCN.UK.2019-3.RLTS.T131471491A131471537.en> [Accessed 17 October 2023]
- Nichols JT, Griscom L (1917) Freshwater fishes of the Congo Basin obtained by the American Museum Congo Expedition, 1909–1915. *Bulletin of the American Museum of Natural History* 37: 64–83.
- Nichols JT, La Monte FR, Callewaert R (1934) More new fishes from the Kasai District of the Belgian Congo. *American Museum novitates* 723: 1–6.
- Paugy D, Lévêque C, Teugels GG (2003) Poissons d'eaux douces et saumâtres de l'Afrique de l'Ouest, édition complète. (IRD-MNHN-M, Vol. 815). Paris-Turvuren.
- Pellegrin J (1933) Voyage de Ch. Alluaud et PA Chappuis en Afrique occidentale Française (Dec. 1930-Mars 1931). Poissons. *Archiv für Hydrobiologie* 26: 101–120.
- Pellegrin J (1936) Contribution à l'ichthyologie de l'Angola. *Arquivos do Museu Bocage* 7: 45–62.
- Peters WCH (1852) Diagnosen von neuen Flussfischen aus Mossambique. Bericht Über Die Zur Bekanntmachung Geeigneten Verhandlungen Der Königlichen Preussischen Akademie Der Wissenschaften Zu Berlin, 681–685.
- Peters WCH (1868) Ueber eine von dem Baron Carl von der Decken entdeckte neue Gattung von Welsen, *Chiloglanis deckenii*, und einige andere Süßwasserfische aus Ostafrika. *Monatsberichte der Königlichen Preussischen Akademie der Wissenschaften zu Berlin* 1868: 598–602.
- Pinton A, Agnèse JF, Paugy D, Otero O (2013) A large-scale phylogeny of *Synodontis* (Mochokidae, Siluriformes) reveals the influence of geological events on continental diversity during the Cenozoic. *Molecular Phylogenetics and Evolution* 66(3): 1027–1040. <https://doi.org/10.1016/j.ympev.2012.12.009>
- Pfeffer GJ (1889) Übersicht der von Herrn Dr. Franz Stuhlmann in Ägypten, auf Sansibar und dem gegenüberliegenden Festlande gesammelten Reptilien, Amphibien, Fische, Mollusken und Krebse. *Jahrbuch Der Hamburgischen Wissenschaftlichen Anstalten* 6(4): 1–36.

- Poll M (1952) Poissons de rivières de la région des lacs Tanganika et Kivu recueillis par G. Marlier. *Revue de Zoologie et de Botanique Africaines* 46(3–4): 221–236.
- Pons J, Barraclough TG, Gomez-Zurita J, Cardoso A, Duran DP, Hazell S, Hazell S, Kamoun S, Sumlin WD, Vogler AP (2006) Sequence-based species delimitation for the DNA taxonomy of undescribed insects. *Systematic Biology* 55(4): 595–609. <https://doi.org/10.1080/10635150600852011>
- Puillandre N, Lambert A, Brouillet S, Achaz G (2012) ABGD, Automatic Barcode Gap Discovery for primary species delimitation. *Molecular Ecology* 21(8): 1864–1877. <https://doi.org/10.1111/j.1365-294X.2011.05239.x>
- Puillandre N, Brouillet S, Achaz G (2021) ASAP: assemble species by automatic partitioning. *Molecular Ecology Resources* 21(2): 609–620. <https://doi.org/10.1111/1755-0998.13281>
- R Core Team (2018) R: A language and environment for statistical computing. R Foundation for Statistical Computing, Vienna. <https://www.R-project.org/>
- Rambaut AR, Drummond AJ, Dong X, Baele G, Suchard MA (2018) Posterior Summarization in Bayesian Phylogenetics Using Tracer 1.7. *Systematic Biology* 67(5): 901–904. <https://doi.org/10.1093/sysbio/syy032>
- Riddin MA, Bills R, Villet MH (2016) Phylogeographic, morphometric and taxonomic re-evaluation of the river sardine, *Mesobola brevianalis* (Boulenger, 1908) (Teleostei, Cyprinidae, Chedrini). *ZooKeys* 641: 121–150. <https://doi.org/10.3897/zookeys.641.10434>
- Roberts TR (1989) Systematic revision and description of new species of suckermouth catfishes (*Chiloglanis*, Mochokidae) from Cameroun. *Proceedings of the California Academy of Sciences* 46(6): 151–178.
- Ronquist F, Teslenko M, Van Der Mark P, Ayres DL, Darling A, Höhna S, Larget B, Liu L, Suchard MA, Huelsenbeck JP (2012) Mrbayes 3.2: Efficient bayesian phylogenetic inference and model choice across a large model space. *Systematic Biology* 61(3): 539–542. <https://doi.org/10.1093/sysbio/sys029>
- Roux F, Hoffman A (2017a) *Chiloglanis bifurcus*. The IUCN Red List of Threatened Species 2017: e.T4632A100193958. <http://dx.doi.org/10.2305/IUCN.UK.2017-3.RLTS.T4632A100193958.en>
- Roux F, Hoffman A (2017b) *Enteromius treurensis*. The IUCN Red List of Threatened Species 2017: e.T2572A100159826. <https://dx.doi.org/10.2305/IUCN.UK.2017-3.RLTS.T2572A100159826.en> [Accessed 17 October 2023]
- Roux F, Hoffman A (2018) *Chiloglanis emarginatus*. The IUCN Red List of Threatened Species 2018: e.T63366A100194297. <https://doi.org/10.2305/IUCN.UK.2018-1.RLTS.T63366A100194297.en>
- Rozas J, Ferrer-Mata A, Sánchez-DelBarrio JC, Guirao-Rico S, Librado P, Ramos-Onsins SE, Sánchez-Gracia A (2017) DnaSP 6: DNA Sequence Polymorphism Analysis of Large Data Sets. *Molecular Biology and Evolution* 34(12): 3299–3302. <https://doi.org/10.1093/molbev/msx248>
- Sauvage HE (1879) Notice sur la faune ichthyologique de l'Ogôoué. *Bulletin de la Société philomathique de Paris (7th Série)* 3: 90–103.
- Schedel FDB, Chakona A, Sidlauskas BL, Popoola MO, Wingi NU, Neumann D, Vreven EJWMN, Schliewen UK (2022) New phylogenetic insights into the African catfish families Mochokidae and Austroglanididae. *Journal of Fish Biology* 100(5): 1171–1186. <https://doi.org/10.1111/jfb.15014>
- Schmidt RC, Bart HL, Nyingi WD (2015) Two new species of African suckermouth catfishes, genus *Chiloglanis* (Siluriformes: Mochokidae), from Kenya with remarks on

- other taxa from the area. *Zootaxa* 4044(1): 45–64. <https://doi.org/10.11646/zootaxa.4044.1.2>
- Schmidt RC, Bart Jr HL, Pezold F (2016) High levels of endemism in suckermouth catfishes (Mochokidae: *Chiloglanis*) from the Upper Guinean forests of West Africa. *Molecular Phylogenetics and Evolution* 100: 199–205. <https://doi.org/10.1016/j.ympev.2016.04.018>
- Schmidt RC, Bart Jr HL, Pezold F, Friel JP (2017) A Biodiversity hotspot heats up: nine new species of suckermouth catfishes (Mochokidae: *Chiloglanis*) from Upper Guinean Forest streams in West Africa. *Copeia* 105(2): 301–338. <https://doi.org/10.1643/CI-16-474>
- Schmidt RC, Barrientos C (2019) A new species of suckermouth catfish (Mochokidae: *Chiloglanis*) from the Rio Mongo in Equatorial Guinea. *Zootaxa* 4652(3): 507–519. <https://doi.org/10.11646/zootaxa.4652.3.7>
- Schmidt RC, Bragança PH, Friel JP, Pezold F, Tweddle D, Bart HL (2023) Two New Species of Suckermouth Catfishes (Mochokidae: *Chiloglanis*) from Upper Guinean Forest Streams in West Africa. *Ichthyology & Herpetology* 111(3): 376–389. <https://doi.org/10.1643/i2022067>
- Seegers L (2008) The catfishes of Africa: a handbook for identification and maintenance. Aqualog.
- Seegers L (1996). The fishes of the Lake Rukwa drainage. *Annales-Musee Royal de l'Afrique Centrale. Sciences Zoologiques (Belgium)* ISSN 0770-4666, 213–236.
- Silvestro D, Michalak I (2012) RaxmlGUI: A graphical front-end for RAXML. *Organisms, Diversity & Evolution* 12(4): 335–337. <https://doi.org/10.1007/s13127-011-0056-0>
- Skelton PH (2001) A Complete Guide To The Freshwater Fishes Of Southern Africa. Struik, Cape Town, South Africa, 241–242.
- Skelton PH, White PN (1990) Two new species of *Synodontis* (Pisces: Siluroidei: Mochokidae) from southern Africa. *Ichthyological Exploration of Freshwaters* 1(3): 277–287.
- Smith A (1840) Pisces. In *Illustrations of the zoology of South Africa; consisting chiefly of figures and descriptions of the objects of natural history collected during an expedition into the interior of South Africa in 1834–36*. *Journal of the Society for the Bibliography of Natural History* 2(6): 187–189.
- Smith A (1841) Pisces. In *Illustrations of the zoology of South Africa; consisting chiefly of figures and descriptions of the objects of natural history collected during an expedition into the interior of South Africa in 1834–36*. *Journal of the Society for the Bibliography of Natural History* 2(6): 187–189.
- Stamatakis A (2014) RAXML Version 8: A tool for Phylogenetic Analysis and Post-Analysis of Large Phylogenies. <https://doi.org/10.1093/bioinformatics/btu033>
- Swofford DL (2003) PAUP*. Phylogenetic Analysis Using Parsimony (*and other Methods) Version 4. Sinauer Associates, Sunderland.
- Sullivan JP, Lundberg JG, Hardman MA (2006) A phylogenetic analysis of the major groups of catfishes (Teleostei: Siluriformes) using rag1 and rag2 nuclear gene sequences. *Molecular Phylogenetics and Evolution* 41(3): 636–662. <https://doi.org/10.1016/j.ympev.2006.05.044>
- Sunnucks P, Hales DF (1996) Numerous transposed sequences of mitochondrial cytochrome oxidase I-II in aphids of the genus *Sitobio* (Hemiptera: Aphidae). *Molecular Biology and Evolution* 13(3): 510–524. <https://doi.org/10.1093/oxfordjournals.molbev.a025612>
- Thompson DM (2013) Pool-Riffle. In *Treatise on Geomorphology* 9: 364–378. <https://doi.org/10.1016/B978-0-12-374739-6.00246-3>

- Thomson AW, Page LM (2010) Taxonomic revision of the *Amphilius uranoscopus* group (Teleostei: Siluriformes) in Kenya, with the description of a new species from the Athi River. *Bulletin of the Florida Museum of Natural History* 49(2): 45–66.
- Thomson AW, Page LM, Hilber SA (2015) Revision of the *Amphilius jacksonii* complex (Siluriformes: Amphiliidae), with the descriptions of five new species. *Zootaxa* 3986(1): 61–87. <https://doi.org/10.11646/zootaxa.3986.1.3>
- Van der Horst CJ (1931) Some South African siluroid fishes. *Annals of the Transvaal Museum* XIV(3): 245–250.
- Vigliotta TR (2008) A phylogenetic study of the African catfish family Mochokidae (Osteichthyes, Ostariophysi, Siluriformes), with a key to genera. *Proceedings of the Academy of Natural Sciences of Philadelphia* 157(1): 73–136. [https://doi.org/10.1635/0097-3157\(2008\)157\[73:APSOTA\]2.0.CO;2](https://doi.org/10.1635/0097-3157(2008)157[73:APSOTA]2.0.CO;2)
- Ward RD, Zemlak TS, Innes BH, Last PR, Hebert PDN (2005) DNA barcoding Australia's fish species. *Philosophical Transactions of the Royal Society of London, Series B, Biological Sciences* 360(1462): 1847–1857. <https://doi.org/10.1098/rstb.2005.1716>
- Werle E, Schneider C, Renner M, Volker M, Fiehn W (1994) Convenient single-step, one tube purification of PCR products for direct sequencing. *Nucleic Acids Research* 22(20): 4354–4355. <https://doi.org/10.1093/nar/22.20.4354>
- Wild H (1965) The flora of the Great Dyke of Southern Rhodesia with special reference to the serpentine soils. *Kirkia* 5(1): 49–86.
- Zhang J, Kapli P, Pavlidis P, Stamatakis A (2013) A general species delimitation method with applications to phylogenetic placements. *Bioinformatics* 29(22): 2869–2876. <https://doi.org/10.1093/bioinformatics/btt499>

Zhangixalus thaoae sp. nov., a new green treefrog species from Vietnam (Anura, Rhacophoridae)

Tao Thien Nguyen¹, Huy Hoang Nguyen¹, Hoa Thi Ninh¹, Linh Tu Hoang Le¹, Hai Tuan Bui¹, Nikolai Orlov², Chung Van Hoang³, Thomas Ziegler^{4,5}

1 Institute of Genome Research, Vietnam Academy of Science and Technology, 18 Hoang Quoc Viet Road, Hanoi, Vietnam

2 Department of Herpetology, Zoological Institute, Russian Academy of Sciences, 199034, St. Petersburg, Russia

3 Forest Resources and Environment Centre, 300 Ngoc Hoi Road, Thanh Tri, Hanoi, Vietnam

4 AG Zoologischer Garten Köln, Riehler Strasse 173, D-50735 Cologne, Germany

5 Institute of Zoology, University of Cologne, Zùlpicher Straße 47b, D-50674 Cologne, Germany

Corresponding author: Tao Thien Nguyen (nguyenthientao@gmail.com)

Abstract

We describe a new treefrog species from Lao Cai Province, northwestern Vietnam. The new species is assigned to the genus *Zhangixalus* based on a combination of the following morphological characters: (1) dorsum green, smooth; body size medium (SVL 30.1–32.2 in males); (2) fingers webbed; tips of digits expanded into large disks, bearing circum-marginal grooves; (3) absence of dermal folds along limbs; (4) absence of supraclavical fold and tarsal projection. The new species can be distinguished from its congeners by: (1) dorsal surface of the head and body green without spots; (2) axilla and groin cream with a black blotch; (3) ventral cream without spot; (4) chin creamy with grey marbling; anterior part of the thigh and ventral surface of tibia orange without spots; posterior parts of thigh orange with a large black blotch; (5) ventral side of webbing orange with some grey pattern (6) iris red-bronze, pupils black; (7) finger webbing formula $I1\frac{1}{4}-1\frac{1}{4}II1-2III1-1IV$, toe webbing formula $I\frac{1}{2}-\frac{1}{2}II0-1\frac{1}{2}III\frac{1}{4}-1\frac{3}{4}IV1\frac{3}{4}-\frac{1}{2}V$. Phylogenetically, the new species is nested in the same subclade as *Z. jodiae*, *Z. pinglongensis*, and *Z. yaoshanensis*, with genetic distances ranging from 3.23% to 4.68%. The new species can be found in evergreen montane tropical forests at an elevation of about 1,883 m a.s.l. This new discovery brings the number of known genus *Zhangixalus* species to 42 and the number of species reported from Vietnam to 10.

Key words: 16S rRNA gene, Lao Cai Province, molecular phylogeny, morphology, new species



Academic editor: Angelica Crottini

Received: 11 April 2023

Accepted: 10 March 2024

Published: 8 April 2024

ZooBank: <https://zoobank.org/E33270AB-994B-4438-974C-1BE11A4FF3A4>

Citation: Nguyen TT, Nguyen HH, Ninh HT, Le LTH, Bui HT, Orlov N, Hoang CV, Ziegler T (2024) *Zhangixalus thaoae* sp. nov., a new green treefrog species from Vietnam (Anura, Rhacophoridae). ZooKeys 1197: 93–113. <https://doi.org/10.3897/zookeys.1197.104851>

Copyright: © Tao Thien Nguyen et al. This is an open access article distributed under terms of the Creative Commons Attribution License ([Attribution 4.0 International – CC BY 4.0](https://creativecommons.org/licenses/by/4.0/)).

Introduction

The genus *Zhangixalus* Li, Jiang, Ren & Jiang, 2019 currently contains 42 species, with a wide distribution in northeastern India, Nepal, Bhutan, southern China, Myanmar, northern Thailand, Laos, northern Vietnam, Taiwan, and Japan, and south to Indonesia, Brunei, and Malaysia (Frost 2024). Brakels et al. (2023) revealed two major clades in the genus *Zhangixalus* in their phylogenetic

analysis of the group; these include a continental Southeast Asian and East Asian species group and a Sundaland group. Brakels et al. (2023) also included six species in the *Z. chenfui* group, distributed in China, Vietnam, and Laos, including *Zhangixalus chenfui* (Liu, 1945), *Z. jodiae* (Nguyen, Ninh, Orlov, Nguyen & Ziegler, 2020), *Z. melanoleucus* Brakels, Nguyen, Pawangkhanant, Idiatullina, Lorphengsy, Suwannapoom & Poyarkov, 2023, *Z. nigropunctatus* (Liu, Hu & Yang, 1962), *Z. pinglongensis* (Mo, Chen, Liao & Zhou, 2016), and *Z. yaoshanensis* (Liu & Hu, 1962).

Among the nine *Zhangixalus* species reported from Vietnam, *Z. dennysi* (Blanford, 1881) has been reported from southeastern China to northeastern Vietnam, *Z. dorsoviridis* (Bourret, 1937) from northwestern Vietnam and southern China; *Z. duboisi* (Ohler, Marquis, Swan & Grosjean, 2000) from the Hoang Lien range in Vietnam and China; *Z. feae* (Boulenger, 1893) from Myanmar to the Tay Nguyen Plateau, Vietnam; *Z. franki* Ninh, Nguyen, Orlov, Nguyen & Ziegler, 2020 exclusively from Ha Giang Province, Vietnam; *Z. hungfuensis* (Liu & Hu, 1961) from Lao Cai Province, Vietnam, and Sichuan and Guangxi provinces, China; *Z. jodiae* Nguyen, Ninh, Orlov, Nguyen & Ziegler, 2020 from Ha Giang Province, Vietnam; *Z. pachyproctus* Yu, Hui, Hou, Wu, Rao & Yang, 2019 from northern Vietnam, Yunnan Province, China, and Prachuap Khiri Khan, Thailand; and *Z. puerensis* (He, 1999) from Lao Cai and Ha Giang provinces, Vietnam, and Yunnan, China (Frost 2024).

During our 2019 fieldwork in Y Ty Commune, Bat Xat District, Lao Cai Province, Vietnam, we collected a series of tree frogs that morphologically resembled *Z. yaoshanensis*, a species known from Guangxi Province, China (Liu and Hu 1962). However, the newly discovered population from Vietnam differs from *Z. yaoshanensis* by the following distinct morphological characteristics: size medium (SVL 30.1–32.2 mm in males); dorsum green without spots, venter cream without spots; flank, axilla, and posterior thigh cream with large black blotches. Furthermore, our phylogenetic analysis shows that the Lao Cai Province population is nested in the same subclade with *Z. jodiae*, *Z. pinglongensis*, and *Z. yaoshanensis* in the *Z. chenfui* group.

The pairwise distance from the newly collected species to the congeners of *Zhangixalus* species ranges from 3.23% (compared to *Z. pinglongensis*) to 10.83% (compared to *Z. smaragdinus*). Meanwhile, the genetic distance among species of *Zhangixalus* ranges from 0.49% (*Z. dugritei* and *Z. hui*) to 11.89% (*Z. pachyproctus* and *Z. yaoshanensis*). This demonstrates that the treefrog from Y Ty Commune is a distinct taxon, with a genetic distance of at least 3.23% from other *Zhangixalus* species.

Based on the morphological characters and molecular information, we describe here the unnamed *Zhangixalus* species from Lao Cai Province, Vietnam, as a new species.

Materials and methods

Repositories, Institutional acronyms, or Institutional abbreviations

IEBR Institute of Ecology and Biological Resources
ROM Royal Ontario Museum

Sampling

The field survey was conducted from 25 April to 1 May 2019 by C.V. Hoang and A.M. Luong in Y Ty Commune, Bat Xat District, Lao Cai Province, northwestern Vietnam. Geographic coordinates and elevations were obtained using a Garmin GPSMAP 76CSX (using the WGS84 datum). After the frogs were photographed alive, three specimens of the new species (IEBR A 5136, IEBR A 5137 and IEBR A 5138) (Table 1) were anaesthetized and euthanized in a closed vessel with a piece of cotton wool containing ethyl acetate (Simmons 2002), fixed in 80% ethanol for 5 h, and then transferred to 70% ethanol for permanent storage. Liver-tissue samples were preserved separately in 96% ethanol before fixation and subsequently deposited in the collection of IEBR.

Molecular data and phylogenetic analyses

We used the protocols of Kuraishi et al. (2013), modified by Nguyen et al. (2015a), for DNA extraction, amplification, and sequencing. Fragments of the 16S rRNA mitochondrial DNA gene were amplified using the same primers used by Kuraishi et al. (2013).

For the phylogenetic analyses, 55 sequences of 26 *Zhangixalus* species were combined with two sequences of *Rhacophorus kio* as outgroups (Table 1).

Chromas Pro software (Technelysium Pty Ltd, Tewantin, Australia) was used to edit the sequences, which were aligned using MAFFT v. 7 (Kato and Standley 2013) with default settings. We then checked the initial alignments by eye and adjusted them slightly. Phylogenetic trees were constructed using IQ-TREE v. 1.6.12 (Nguyen et al. 2015b) while maximum-likelihood bootstrap support (MLBS) was evaluated by ultrafast bootstrap approximation with 1000 replicates (Hoang et al. 2018) (ML). Prior to Bayesian analyses, we chose the optimum substitution models for entire sequences by using ModelFinder implemented in IQ-TREE based on the Bayesian information criterion (BIC) (Kalyaanamoorthy et al. 2017). According to ModelFinder, the best-fit model for ML analysis was TIM2+F+I+G4. Because the TIM2 model and F parameter are not implemented in MrBayes, we selected the next best-fit model for our Bayesian-inference (BI) analysis, which was the general time reversible model (GTR; Tavaré 1986) with a proportion of invariable sites and a gamma shape parameter (Alpha 0.215). The BI phylogenetic construction was done in MrBayes v. 3.2.7a (Ronquist et al. 2012) with two independent runs of four Markov Chains for 10,000,000 generations. A tree was sampled every 100 generation, and a consensus topology was calculated for 75,001 trees after discarding the first 25,000 trees using the relative burn-in option (25% of trees discarded). We checked parameter estimates and convergence using TRACER v. 1.5 (Rambaut and Drummond 2009). We regarded tree nodes in the ML tree with bootstrap values of 95% or greater as sufficiently resolved (Hoang et al. 2018), and nodes with a BPP of 95% or greater as significant in the BI analysis (Leaché and Reeder 2002).

Morphological characters

A total of 34 measurements were taken with digital calipers to the nearest 0.1 mm (Nguyen et al. 2016). Abbreviations are as follows: **SVL**: snout–vent

Table 1. Samples of *Zhangixalus* and other species were used for DNA analysis in this study.

No.	Scientific name	Voucher	Locality	GenBank no.	Source
1.	<i>Rhacophorus kio</i>	VN.2018.84	Kon Tum, Vietnam		This study
2.	<i>R. kio</i>	VN.2018.83	Kon Tum, Vietnam		This study
3.	<i>Zhangixalus chenfui</i>	RaoZT0806013	Zhaotong, Yunnan, China	JX219431	Li et al. 2012b
4.	<i>Z. chenfui</i>	Li05	Mt. Omei, Sichuan, China	JX219432	Li et al. 2012b
5.	<i>Z. dennysi</i>	ML.2019.1	Vinh Phuc, Vietnam		This study
6.	<i>Z. dennysi</i>	ML.2019.2	Vinh Phuc, Vietnam		This study
7.	<i>Z. dorsovirens</i>	YN080446	Jinping, Yunnan	JX219425	Li et al. 2012b
8.	<i>Z. dorsovirens</i>	Yt.2018.16	Lao Cai, Vietnam		This study
9.	<i>Z. dorsovirens</i>	YT 2018 6	Lao Cai, Vietnam		This study
10.	<i>Z. duboisi</i>	VNMN7079	Ha Giang, Vietnam		This study
11.	<i>Z. duboisi</i>	VNMN010243	Lai Chau, Vietnam		This study
12.	<i>Z. dugritei</i>	LJT 051002	Sichuan, China	JN688872	Li et al. 2012a
13.	<i>Z. dugritei</i>	LJT 051008	Sichuan, China	JN688873	Li et al. 2012a
14.	<i>Z. feae</i>	HB.2014.28	Hoa Binh, Viet Nam		This study
15.	<i>Z. feae</i>	VNMN05859	Lai Chau Viet Nam		This study
16.	<i>Z. franki</i>	VNMN 011686	Ha Giang, Vietnam	LC548745	Ninh et al. 2020
17.	<i>Z. franki</i>	VNMN 011687	Ha Giang, Vietnam	LC548746	Ninh et al. 2020
18. L	<i>Z. hongchibaensis</i>	CIB 097696	Chongqing, China	JN688882	Li et al. 2012a
19.	<i>Z. hongchibaensis</i>	CIB 097687	Chongqing, China	JN688883	Li et al. 2012a
20.	<i>Z. hui</i>	SCUM 0504111 L	Sichuan, China	JN688877	Li et al. 2012a
21.	<i>Z. hui</i>	SCUMLI 01	Sichuan, China	JN688878	Li et al. 2012a
22.	<i>Z. hungfuensis</i>	SCUM 060425L	Sichuan, China	EU215538	Li et al. 2008
23.	<i>Z. hungfuensis</i>	SCUM 060424 L	Sichuan, China	JN688879	Li et al. 2012a
24.	<i>Z. jodiae</i>	VNMN 07121	Ha Giang, Vietnam	LC545594	Nguyen et al. 2020
25.	<i>Z. jodiae</i>	VNMN 07122	Ha Giang, Vietnam	LC545595	Nguyen et al. 2020
26.	<i>Z. lishuiensis</i>	YPX47794	Lishui, Zhejiang, China	KY653719	Liu et al. 2017
27.	<i>Z. lishuiensis</i>	YPX47792	Lishui, Zhejiang, China	KY653720	Liu et al. 2017
28.	<i>Z. melanoleucus</i>	BEI 01010	Phou Samsoum Mt., Xiengkhoang, Laos	OQ305233	Brakels et al. 2023
29.	<i>Z. melanoleucus</i>	BEI 01011	Phou Samsoum Mt., Xiengkhoang, Laos	OQ305235	Brakels et al. 2023
30.	<i>Z. melanoleucus</i>	ZMMU A7781	Phou Samsoum Mt., Xiengkhoang, Laos	OQ305234	Brakels et al. 2023
31.	<i>Z. nigropunctatus</i>	GZ070658	Weining, Guizhou, China	JX219430	Li et al. 2012b
32.	<i>Z. nigropunctatus</i>	Li06	Weining, Guizhou, China	JX219433	Li et al. 2012b
33.	<i>Z. omeimontis</i>	Li02	Sichuan, China	JX219420	Li et al. 2012b
34.	<i>Z. omeimontis</i>	RaoZT0806010	Sichuan, China	JX219419	Li et al. 2012b
35.	<i>Z. pachyproctus</i>	TQ.2018.72	Tuyen Quang, Viet Nam		This study
36.	<i>Z. pachyproctus</i>	VNMN:1299	Nghe An, Vietnam	LC545592	This study
37.	<i>Z. pinglongensis</i>	NHMG201002011	Guangxi, China	KU170684	Mo et al. 2016
38.	<i>Z. pinglongensis</i>	NHMG201002003	Guangxi, China	KU170683	Mo et al. 2016
39.	<i>Z. puerensis</i>	VNMN 010284	Lai Chau, Viet Nam		This study
40.	<i>Z. puerensis</i>	SCUM 060648 L	Yunnan, ChinaYunnan, China	JN688884	Li et al. 2012a
41.	<i>Z. schlegelii</i>	KUHE 44531	Okayama, Japan	LC369670	Matsui et al. 2018
42.	<i>Z. schlegelii</i>	Genbank	Hiroshima, Japan	NC007178	Sano et al. 2005
43.	<i>Z. smaragdinus</i>	RAO6241	Tibet, China	JX219411	Li et al. 2012b
44.	<i>Z. smaragdinus</i>	CAS 224708	Nagmung, Putao District, Kachin, Myanmar	MN613214	Yu et al. 2019
45.	<i>Z. wui</i>	CIB 097685	Hubei, China	JN688881	Li et al. 2012a
46.	<i>Z. wui</i>	CIB 097690	Hubei, China	JN688880	Li et al. 2012a
47.	<i>Z. yaoshanensis</i>	NHMG150408	Guangxi, China	MG322122	Chen et al. 2018
48.	<i>Z. yaoshanensis</i>	NHMG150404	Guangxi, China	MG322121	Chen et al. 2018
49.	<i>Z. yinggelingsis</i>	HN2018002	Hainan, China	MW192130	Genbank

No.	Scientific name	Voucher	Locality	GenBank no.	Source
50.	<i>Z. yunnanensis</i>	Rao3494	Longling, Yunnan, China	JX219429	Li et al. 2012b
51.	<i>Z. yunnanensis</i>	Rao3496	Longling, Yunnan, China	JX219428	Li et al. 2012b
52.	<i>Z. zhokaiyae</i>	AHURhaDb-150420-03	Anhui, China	KU601499	Pan et al. 2017
53.	<i>Z. zhokaiyae</i>	AHURhaDb-150420-01	Anhui, China	KU601500	Pan et al. 2017
54.	<i>Zhangixalus thaoae</i> sp. nov.	ROM38011	Lao Cai, Vietnam	JX219427	Li et al. 2012b
55.	<i>Zhangixalus thaoae</i> sp. nov.	IEBR A 5136	Lao Cai, Vietnam	LC762092	This study
56.	<i>Zhangixalus thaoae</i> sp. nov.	IEBR A 5137	Lao Cai, Vietnam	LC762093	This study
57.	<i>Zhangixalus thaoae</i> sp. nov.	IEBR A 5138	Lao Cai, Vietnam	LC762094	This study

length, **HW**: head width (across angle of jaws), **HL**: head length (from back of mandible to tip of snout), **MND**: distance from jaw angle to nostril, **MFED**: distance from back of mandible to front of the eye, **MBED**: distance from back of mandible to back of the eye, **SNL**: snout length (from anterior corner of eye to tip of snout), **ED**: eye diameter, **UEW**: maximum width of upper eyelid, **IND**: internarial distance, **IOD**: interorbital distance (minimal distance between orbits), **AED**: distance between anterior corners of eyes, **PED**: distance between posterior corners of eyes, **NS**: distance from nostril to tip of snout, **EN**: distance from anterior corner of eye to nostril, **TYD**: maximal tympanum diameter, **TED**: distance from anterior margin of tympanum to posterior corner of eye, **Ua**: upper arm length (from axilla to elbow), **Fa**: lower arm and hand length (from elbow to tip of third finger), **NPL**: nuptial pad length, **F1–4**: length of fingers I–IV (from basis of finger to tip of finger), **FeL**: thigh length from vent to knee, **TbL**: tibia length from knee to tarsus, **TbW**: maximal tibia width, **FL**: foot length from tibiotarsal joint to tip of fourth toe, **T1–5**: length of toes I–V, **IML**: inner metatarsal tubercle length. Terminology for describing the webbing formula followed Glaw and Vences (2007). Sex was determined by the presence of nuptial pads and gonadal inspection.

Results

Phylogenetic analyses

The aligned 16S sequences yielded a total of 1,033 characters. Of 1033 nucleotide sites, 309 were variable and 295 were parsimony informative within the analysed *Zhangixalus* species. Nucleotide frequencies were A = 37.7%, T = 24.4%, C = 20.7%, and G = 17.2% (data for ingroup only). Our phylogenetic analyses employing ML and BI methods yielded identical topologies, and only the BI tree is presented in Fig. 1.

Phylogenetically, the undescribed species of *Zhangixalus* from Y Ty Commune, Bat Xat District, Lao Cai Province, Vietnam was clustered with seven species in the *Z. chenfui* group with a well-supported node (both 100% in the ML and BI analyses). Furthermore, the undescribed *Zhangixalus* species was found to be most closely related to a clade consisting of *Z. pinglongensis* and *Z. yaoshanensis*, with significantly high support value in the BI analysis (99%) and a high support value from ML analysis (94%). The genetic distance among the examined sequences ranges from 3.23% (between *Zhangixalus* sp. from Lao Cai Province and *Z. pinglongensis*) to 8.10% (between *Z. chenfui* and *Z. yaoshanensis*) (Table 2).

Table 2. Uncorrected pairwise distances (β -distance) among *Zhangixalus* species analysed.

	1.	2.	3.	4.	5.	6.	7.	8.	9.	10.	11.	12.	13.	14.	15.	16.	17.	18.	19.	20.	21.	22.	23.	24.	25.	26.				
1. <i>Zhangixalus thaoae</i> sp. nov.	0.00-0.19																													
2. <i>Z. chenfui</i>	7.42	0.00																												
3. <i>Z. dennysi</i>	10.72	11.12-11.32	0.19																											
4. <i>Z. dorsoviridis</i>	8.59-8.69	9.29-9.38	9.76-40.15	0.39-0.78																										
5. <i>Z. duboisi</i>	7.62-7.91	8.69-8.89	9.07-9.27	4.88-5.27	0.29																									
6. <i>Z. dugritei</i>	8.02-8.81	8.22-9.00	9.86-8.30	6.05-8.31	4.40-8.02	0.11																								
7. <i>Z. feae</i>	8.99	9.09	8.50	9.38	8.40	8.21																								
8. <i>Z. franki</i>	7.81-7.97	8.50-8.70	9.07-9.51	5.18-5.69	2.73-2.90	4.88-5.18	8.21-8.70	0.00																						
9. <i>Z. hongchibaensis</i>	8.71-8.90	9.21-9.30	10.95-11.24	6.55-7.04	5.09-5.38	3.62-3.81	8.72-8.90	5.57-5.91	0.10																					
10. <i>Z. hui</i>	8.21-8.31	8.22	9.86-10.06	6.35-6.54	4.50-4.59	0.49-0.59	8.12-8.21	4.79-4.87	3.91-4.01	0.00																				
11. <i>Z. hungfuensis</i>	8.62-8.72	9.21	10.08-10.27	5.97-6.16	5.09-5.19	3.71-3.81	8.81-8.90	5.19-5.50	3.52-3.62	3.62	0.00																			
12. <i>Z. jodiae</i>	3.90	7.32	10.32-10.52	8.98-9.27	7.41-7.61	7.81-7.91	8.31-8.40	7.71-7.76	8.90-8.99	8.01	8.90	0.00																		
13. <i>Z. lishuiensis</i>	9.09-9.19	8.61	9.47	4.00-4.20	4.50-4.59	5.87-5.96	7.93-8.02	4.69-4.97	6.56-6.65	5.87	5.48	9.08	0.00																	
14. <i>Z. melanoleucus</i>	6.43	7.22	10.81-11.00	8.29-8.68	8.20-8.39	7.71-7.81	8.80-8.89	7.61-7.86	8.70-8.80	7.91	8.71	7.21	8.89	0.00																
15. <i>Z. nigropunctatus</i>	5.56-5.76	6.93	10.33-10.53	9.08-9.28	8.11-8.30	8.11-8.20	8.41-8.50	7.71-7.96	9.29-9.38	8.30	9.00	5.65	8.90	5.46	0.00															
16. <i>Z. ormeimontis</i>	7.91-8.11	8.79-8.89	9.17-9.56	4.98-5.18	1.27-1.37	4.50-4.59	8.21-8.30	3.03-3.11	5.38-5.58	4.40	4.99-5.09	7.32	4.40-4.59	8.19-8.59	8.30	0.20														
17. <i>Z. pachyproctus</i>	10.54-10.83	10.94-11.13	10.04	9.76-10.34	9.46-9.66	10.25	7.82	10.13	10.65	9.86-10.06	10.18	10.82-11.01	9.28-9.47	11.11	10.44-10.63	9.37-9.56	0.19													
18. <i>Z. pinglongensis</i>	3.23-3.33	7.24	10.36	8.80-8.90	7.72-7.82	8.02-8.12	8.62-8.71	7.83-7.88	8.81-8.91	8.22	8.42	4.01	8.61	6.74	5.68	7.82-7.92	10.65-10.85	0.00												
19. <i>Z. puerensis</i>	7.92-8.71	8.22-8.62	9.29-9.77	6.35-6.74	4.89-5.28	3.42-3.61	7.73-8.12	5.08-5.59	3.82-4.79	3.32-3.42	3.62-3.82	7.81-8.21	5.68-6.16	8.21-8.30	8.69-8.90	4.79-4.89	9.58-9.86	2.83												
20. <i>Z. schlegelii</i>	8.50-9.20	9.00-10.11	10.25-10.65	7.32-7.43	5.87-6.16	6.05-6.65	7.92-8.32	5.96-6.53	6.16-6.56	5.57-6.06	6.07-6.17	8.69-9.38	6.84-7.14	8.20-9.38	8.89-9.40	5.87-6.26	9.28-9.58	9.00-9.40	5.86-6.36	1.17										
21. <i>Z. smaragdinus</i>	10.73-10.83	10.94	10.33	10.93-11.32	10.54	10.74-10.84	8.79-8.80	10.63-11.07	11.44-11.53	10.84	11.06	10.43	10.35	10.82	10.54	10.44	8.38	10.75	10.36-10.45	9.96-10.17	0.00									
22. <i>Z. wui</i>	8.61-8.81	9.01-9.11	9.87-10.17	6.65-6.94	4.99-5.09	3.52-3.71	8.91-9.10	5.18-5.49	3.91-4.10	3.23-3.32	2.84-2.94	8.90-8.99	6.56-6.65	8.41-8.50	8.99-9.09	4.99-5.09	10.39-10.65	8.91-9.01	4.11-4.30	6.26-6.56	11.53-11.63	0.10								
23. <i>Z. yaoshanensis</i>	3.80-4.68	7.62-8.10	10.53-11.10	9.07-9.85	7.90-8.68	8.50-9.28	7.90-9.77	9.68-9.88	9.30-9.36	8.69-9.38	9.30-9.88	4.68-5.36	9.18-9.67	6.82-7.79	5.95-6.53	8.29-8.88	11.21-11.89	3.62-4.30	8.69-9.58	9.18-9.97	10.82-11.40	9.38-10.07	0.88							
24. <i>Z. yinggelingensis</i>	8.81-8.91	8.42	10.76-10.86	7.34-7.44	6.17	5.97-6.07	8.54-8.63	6.37-6.54	7.90-8.68	6.07	6.67	9.20	7.05	8.71	8.52	6.07-6.17	10.37-10.57	8.43	6.08-6.17	7.84-8.83	11.06-11.40	7.06-9.10	8.81-9.10							
25. <i>Z. yunnanensis</i>	6.54	6.93	10.23-10.43	8.40-8.50	8.49-8.68	7.82-7.92	8.20-8.21	8.01-8.39	8.90-9.00	7.82	8.71	6.43	8.50	4.97	5.46	8.20-8.29	10.73-10.93	6.74	8.31-8.41	8.31-8.61	9.85-9.85	8.71-8.81	8.52							
26. <i>Z. zhoukaiyae</i>	8.61-8.81	8.52-8.62	9.68-9.78	3.81-4.01	4.40-4.60	5.68-5.87	8.04-8.23	4.79-5.19	6.56-6.76	5.58-5.68	5.39-5.49	8.41-8.50	1.56-1.66	8.60-8.70	8.61-8.71	4.21-4.50	8.90-9.19	8.42-8.52	5.68-6.07	6.65-6.86	9.68-9.78	6.56-6.66	8.90-9.48	8.32-8.41	0.10					

Taxonomic account

Zhangixalus thaoae sp. nov.

<https://zoobank.org/DB9E5E8E-3E66-4AB1-B837-8FB8D485E982>

Fig. 2

Material examined. Holotype: VIETNAM • ♂; Y Ty Commune, Bat Xat District, Lao Cai Province, Northwestern Vietnam; 22°37'17.6"N, 103°37'23.5"E; 1883 m a.s.l.; 01 May 2019; C. V. Hoang and A. M. Luong leg.; IEBR A 5136; GenBank: LC762092.1. **Paratypes:** VIETNAM • 2 ♂; same locality as for holotype; same geo-coordinates; same altitude; same collection date; same collectors; IEBR A 5137, 5138; GenBank: LC762093.1, LC762094.1.

Diagnosis. The new species is placed in the genus *Zhangixalus* based on some morphological characters: dorsum green and smooth; body size medium (SVL 30.1–32.2 in males); fingers webbed; tips of digits expanded into large disks, bearing circum-marginal grooves; absence of dermal folds along limbs; absence of supraclacal fold and tarsal projection (Fig. 2).

The new species is distinguished from its congeners by a combination of the following characteristics: 1) dorsal surface of head and body green without spots; 2) axilla and groin cream with a black blotch; 3) ventrum cream-colored without spots; 4) chin cream, with grey marbling; anterior part of thigh and ventral surface of tibia orange, without blotch; posterior parts of thigh orange with a large, black blotch; 5) ventral side of webbing orange, with some grey; 6) iris red-bronze, pupils black. 7) finger webbing formula $I1\frac{1}{4}-1\frac{1}{4}II1-2III1-1IV$, and toe webbing formula $I\frac{1}{2}-\frac{1}{2}II0-1\frac{1}{2}III\frac{1}{4}-1\frac{3}{4}IV1\frac{3}{4}-\frac{1}{2}V$.

Description of the holotype (male). Size medium (SVL 32.2 mm), body robust; head slightly compressed, head length nearly equal to the width (HW 12.1 mm, HL 11.7 mm), convex above; snout round, slightly protruding beyond lower jaw in lateral view, and longer than the horizontal diameter of eye (SNL 5.4 mm, ED 4.2 mm); canthus rostralis round, loreal region oblique, concave; interorbital distance wider than internarial distance and upper eyelid (IOD 4.3 mm, IND 3.1 mm, UEW 3.0 mm); distance between anterior corners of eyes about 69.30% of the distance between posterior corners of eyes; nostrils round, without lateral flap of skin, closer to tip of snout than to eye; pupil oval, horizontal; tympanum distinct, round, about half the size of eye diameter, and twice greater than distance between tympanum and eye (TYD 2.1, TYE 1.0); pineal ocellus and spinules on upper eyelid absent; vomerine teeth well developed, in two oblique ridges; choanae round; tongue deeply notched posteriorly; supratympanic fold weakly.

Forelimbs robust, upper arm short, nearly one-half of hand length (Ua 6.2 mm, Fa 14.6 mm), dermal fringe along the outer edge of forearm absent; relative finger lengths $I < II < V < III$; tips of fingers with enlarged discs with distinct circum-marginal grooves; disc of finger III approximately 1.5 times of the width of finger III ($fd3/fw3$ 1.5), greater than tympanum diameter ($fd3/TYD$ 1.27); webbing formula $I1\frac{1}{4}-1\frac{1}{4}II1-2III1-1IV$, subarticular tubercles distinct, blunt, round, formula 1, 1, 2, 2; nuptial pads prominent, oval, smooth.

Hindlimbs long and thin, heels overlapping when held at right angles to the body; tibia length about four times greater than tibia width (TbL 13.9 mm, TbW 3.1 mm), longer than thigh length (FeL 13.3 mm), shorter than foot length (FL 19.0 mm); relative toe lengths $I < II < III < V < IV$; tips of toes with enlarged discs with



Figure 2. Adult male holotype (IEBR A 5136) of *Zhangixalus thaoae* sp. nov., in life, from Y Ty Commune, Bat Xat District, Lao Cai Province, northwestern Vietnam.

distinct circum-marginal grooves, discs slightly smaller than those of fingers; webbing formula $I\frac{1}{2}-\frac{1}{2}II0-1\frac{1}{2}III\frac{1}{4}-1\frac{3}{4}IV1\frac{3}{4}-\frac{1}{2}V$; subarticular tubercles distinct, blunt, round, formula 1, 1, 2, 3, 2; inner metatarsal tubercle small (IML 1.6 mm); dermal ridge along the outer edge of tibia and tarsus absent; dermal projection at tibiotarsal articulation absent.

Skin texture: dorsal surface of head and body smooth; supratympanic fold weakly developed, throat and chest smooth, belly rough; ventral surface of fore- and hindlimbs smooth.

Coloration in life: iris red-bronze, pupil black; dorsal surface of head and body green without spots; dorsal surface of fore and hind limbs green, upper side of fingers II and II and toes I, II, and III yellow, all tip of fingers and toes yellow; axilla cream and groin cream with a black blotch; anterior part of thigh and ventral surface of tibia orange without spots; posterior parts of thigh orange with a large black blotch; lower jaw cream, with grey marbling, and throat region white; ventral side of webbing orange with some gray pattern, nuptial pads grey.

Coloration in preservative: As in life, but with green dorsal surface fading to dark blue; and ventral side of body, limbs, and upper side of fingers I and II, upper side of toes I, II, and III fading to light yellow.

Variation. Ground color of dorsum light green; ventral surface cream, without spots. The size of blotches in the axilla, groin, and posterior thigh region of the paratype is smaller than in the holotype (Fig. 3). For measurements of the type series, see Table 3.

Etymology. The species is named after the first author's wife, Nguyen Thi Thanh Thao, as a token of gratitude for her understanding and strong support of his research activity. We recommend Thao's Tree Frog as the English common name andẾch cây thảo as the Vietnamese common name.

Male secondary sexual characters. Male specimens with nuptial pad present on base of the finger I and external single subgular vocal sac.

Natural history notes. Specimens were collected between 19:00 and 24:00h on a branch about 1 m above the ground. The ground consisted of mountain soil and puddles, and there was a small stream about 2 m away (Fig. 4A). The habitat was an undisturbed evergreen forest on a granite mountain (Fig. 4B).



Figure 3. The variation of morphological characteristic of *Zhangixalus thaoae* sp. nov. IEBR A 5136 is the holotype, and the two remaining samples are paratypes.

Other tree frogs that were found at the site were *Polypedates* sp., of the *P. leucomystax* species complex; *Zhangixalus duboisi* (Ohler, Marquis, Swan & Grosjean, 2000); *Hyla annectans* (Jerdon, 1870); and *Gracixalus gracilipes* (Bourret, 1937). Females, larval stages, and eggs of the new species are unknown.

Distribution. *Zhangixalus thaoae* sp. nov. is currently known only from the type locality (Fig. 5). The species was recorded at an elevation of approximately 1,880 m a.s.l.

Conservation status. The new species is expected to be found in the evergreen forest of Guangxi Province, southern China, because the terrain there consists mostly of granite mountains, but in Yunnan Province, China, which contains mostly limestone terrain, the species is not expected. However, the geographic distribution of the species needs to be confirmed by further studies. Because there is a lack of information on the species' abundance and distribution, we suggest that it be considered as Data Deficient following IUCN Red List categories (IUCN 2023).

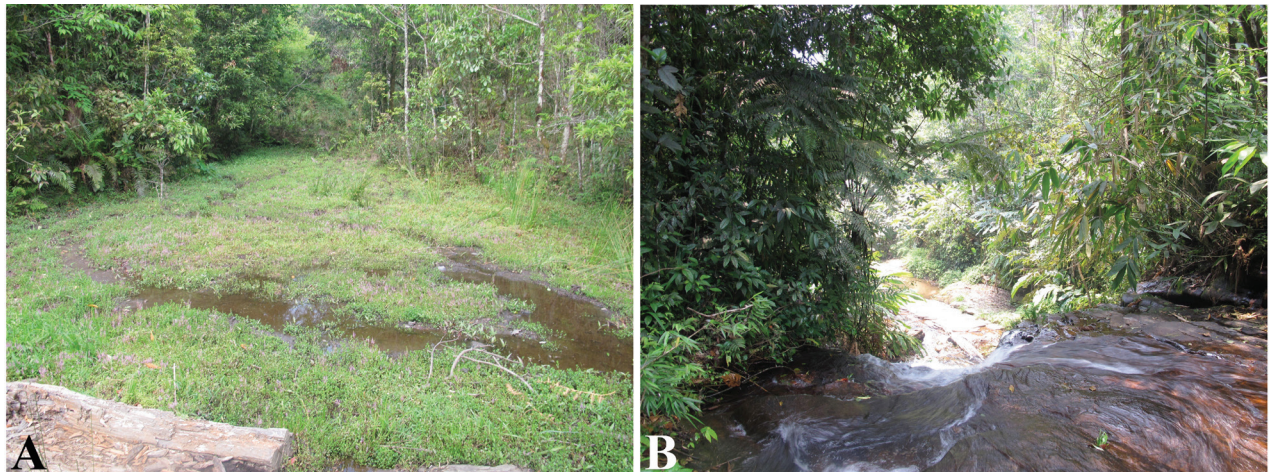


Figure 4. Habitat of the new species in Y Ty Commune, Bat Xat District, Lao Cai Province **A** collection site with a small puddle **B** the stream near the biotope of the holotype.

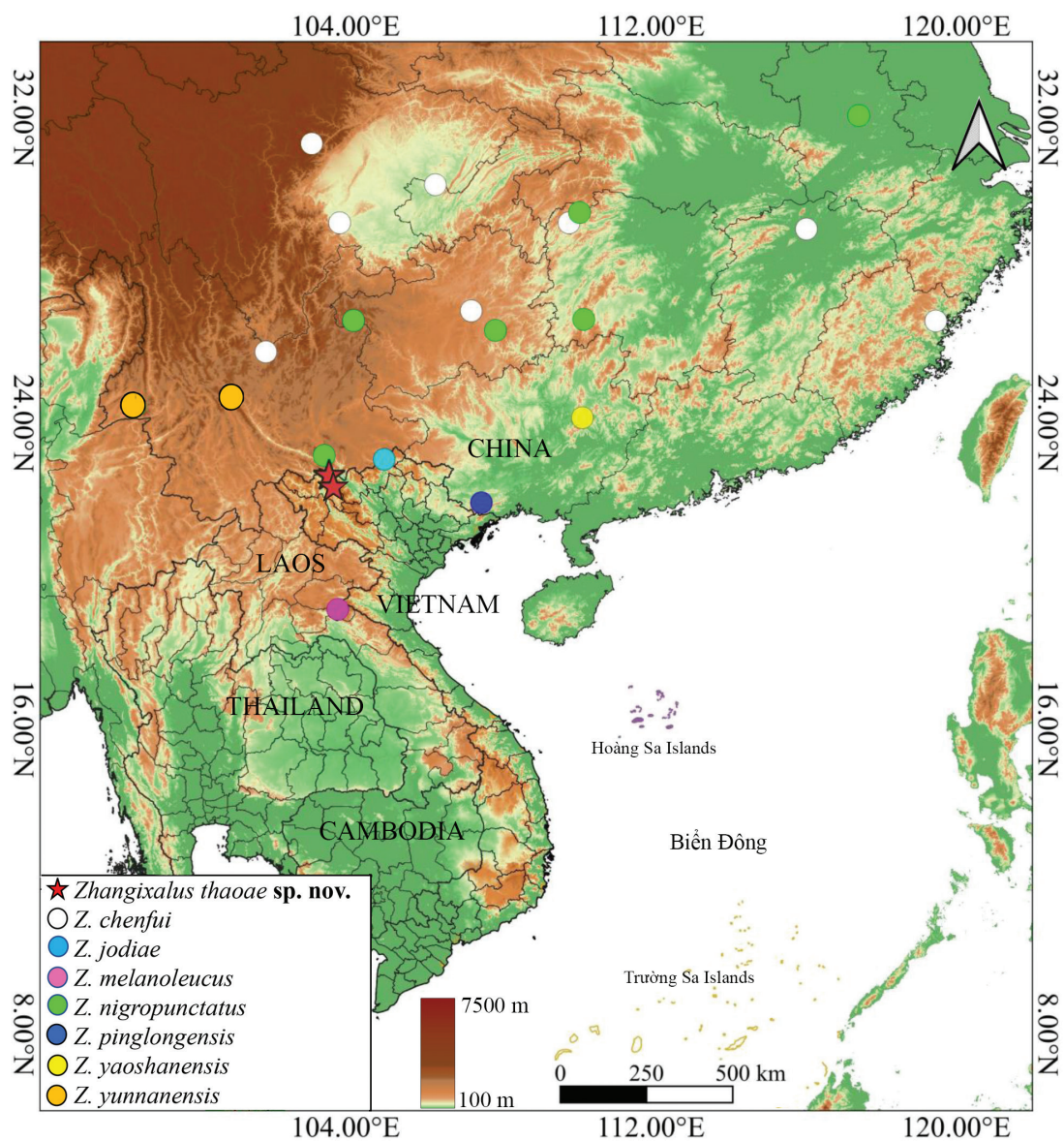


Figure 5. The distribution of species of the *Zhangixalus chenfui* group.

Table 3. Measurements (in mm) of *Zhangixalus thaoae* sp. nov.

Number	IEBR A 5136	IEBR A 5137	IEBR A 5138
Sex	Male (holotype)	Male	Male
SVL	32.2	32.0	30.1
HW	12.1	11.7	12.8
HL	11.7	11.3	13.1
MND	9.5	9.8	10.8
MFED	7.5	7.2	10.6
MBED	3.8	4.5	4.1
SNL	5.4	5.1	5.4
ED	4.2	3.4	3.9
UEW	3.0	3.0	3.5
IND	3.1	3.9	4.0
IOD	4.3	4.6	4.7
AED	7.0	7.1	7.5
PED	10.1	10.4	11.5
NS	3.1	2.8	3.2
EN	2.9	2.6	3.2
TYD	2.1	2.0	2.5
TED	1.0	1.2	1.4
Ua	6.2	6.1	7.0
Fa	14.6	16.1	16.6
F1	3.0	4.0	3.1
F2	4.2	5.2	5.4
F3	6.1	6.4	7.2
F4	4.8	5.7	5.3
FeL	13.3	13.2	14.0
TbL	13.9	13.9	14.0
TbW	3.4	3.1	3.3
FL	19.0	20.3	21.8
T1	3.6	5.0	4.5
T2	6.2	7.4	6.8
T3	9.2	10.3	10.7
T4	11.8	13.5	13.6
T5	10.0	10.9	11.3
IML	1.6	1.8	1.7
HW/HL	1.03	1.04	0.97
SNL/HW	0.44	0.43	0.43
NS/EN	1.08	1.07	0.99
ED/SNL	0.78	0.66	0.72
TYE/TYD	0.46	0.62	0.57
TYD/ED	0.50	0.59	0.64
HAL/FLL	2.36	2.64	2.37
TBL/TL	1.05	1.05	1.01

Comparisons. We compare *Zhangixalus thaoae* sp. nov. with other species of *Zhangixalus* occurring in Vietnam and elsewhere.

The new species mostly resembles *Z. yaoshanensis* by the combination of the following characteristics: head as long as wide in *Zhangixalus thaoae* sp. nov. (HL/HW 0.96–1.02), posterior parts of thigh orange with a large black blotch, ventral surface of tibia orange, iris red-bronze with black pupil in *Zhangixalus thaoae* sp. nov. vs head wider than long (HL/HW = 0.83); posterior thigh surface and ventral surface of tibia red-orange without spot, iris pale yellowish gold with a network of fine dark gold reticulations in *Z. yaoshanensis* (Chen et al. 2018).

Zhangixalus thaoae sp. nov. can be distinguished from other species in the genus *Zhangixalus* by its smaller size (SVL 30.1–32.2 mm) vs SVL >50 mm in the following species: 47.0–70.5 (Wilkinson and Rao 2004; Ohler 2009; Jiang et al. 2016) in *Z. burmanus*; 68–92 mm (Fei et al. 2010) in *Z. dennysi*; 53.1–67.2 mm (Ohler et al. 2000; Orlov et al. 2001; Ziegler et al. 2014) in *Z. duboisi*; 68–116 mm (Fei et al. 2010) in *Z. feae* (Boulenger, 1893); 77.9–85.8 mm (Ninh et al. 2020) in *Z. franki*; 52–66 mm (Fei et al. 2010), 52–65 mm (Liu 1950) in *Z. omeimontis*; 74.2 mm (Luu and Calame 2014), 73.4–78.2 mm in *Z. pachyproctus* (Yu et al. 2019); and 76.3–79.6 mm in *Z. smaragdinus* (Yu et al. 2019).

Zhangixalus thaoae sp. nov. can be distinguished from other *Zhangixalus* species of a similar size in having a different coloration pattern: dorsum green without blotches or spots in the new species vs light or dark green with many white or brown spots or blotches in various sizes in *Z. dugritei* (David 1872; Li et al. 2012a), *Z. hongchibaensis* (Li et al. 2012a), *Z. hui* (Liu 1945), and *Z. wui* (Li et al. 2012a).

Zhangixalus arboreus has a green dorsum with numerous dark spots (Okada and Kawano 1924), which is absent in *Zhangixalus thaoae* sp. nov.

Zhangixalus achantharrhena has a green dorsum, without spots, and a cream venter, without the brown flecks of the new species (Harvey et al. 2002).

Zhangixalus arvalis has a white line along flanks, which is absent in *Z. thaoae* sp. nov. (Lue et al. 1995).

Zhangixalus chenfui has a brown ventrum, with a dark-brown pattern, not cream-colored, without a dark-brown pattern, as in *Zhangixalus thaoae* sp. nov. (Liu 1945).

Zhangixalus dorsoviridis has cream flanks with many black blotches and the anterior thigh is orange with some irregularly sized black circles (Bourret 1937) (Figs 6C, D, 7C, D). In *Z. thaoae* sp. nov., the flanks are cream with one single black spot and the posterior thigh is orange with a single large black blotch (Figs 6A, B, 7A, B).

Zhangixalus dulitensis is pea-green dorsally with some white dots, the head and back have purplish dots, there is purplish line from eye to eye around the snout and passing through the nostrils, and there is reddish-brown patch on each eyelid (Boulenger 1892; Haas et al. 2012). *Zhangixalus thaoae* sp. nov. does not have this color pattern.

Zhangixalus jarujini has a reddish-brown dorsum with irregular dark-brown markings, while *Z. thaoae* sp. nov. has a green dorsum without any markings.

Zhangixalus jodiae has black and orange blotches interposed on anterior, posterior part of thighs and ventral surface of tibia (Figs 6E, F, 7E, F); *Z. thaoae* sp. nov. does not have this color pattern, but rather a large, black blotch on an orange background (Figs 6A, B, 7A, B).

Zhangixalus leucofasciatus exhibits a cream axilla without dark spots, in contrast to a black blotch on the cream axilla of *Z. thaoae* sp. nov.; additionally, *Z. leucofasciatus* possesses a white stripe along the upper lip, body and limbs, a feature that is absent in *Z. thaoae* sp. nov. (Liu and Hu 1962; Fei et al. 2010).

Zhangixalus pinglongensis has flanks, anterior and posterior surfaces of the thigh covered with black blotches and white spots (Mo et al. 2016). In contrast, *Z. thaoae* sp. nov. lacks similar black blotches with white spots on its flanks, anterior and posterior surfaces of the thighs.

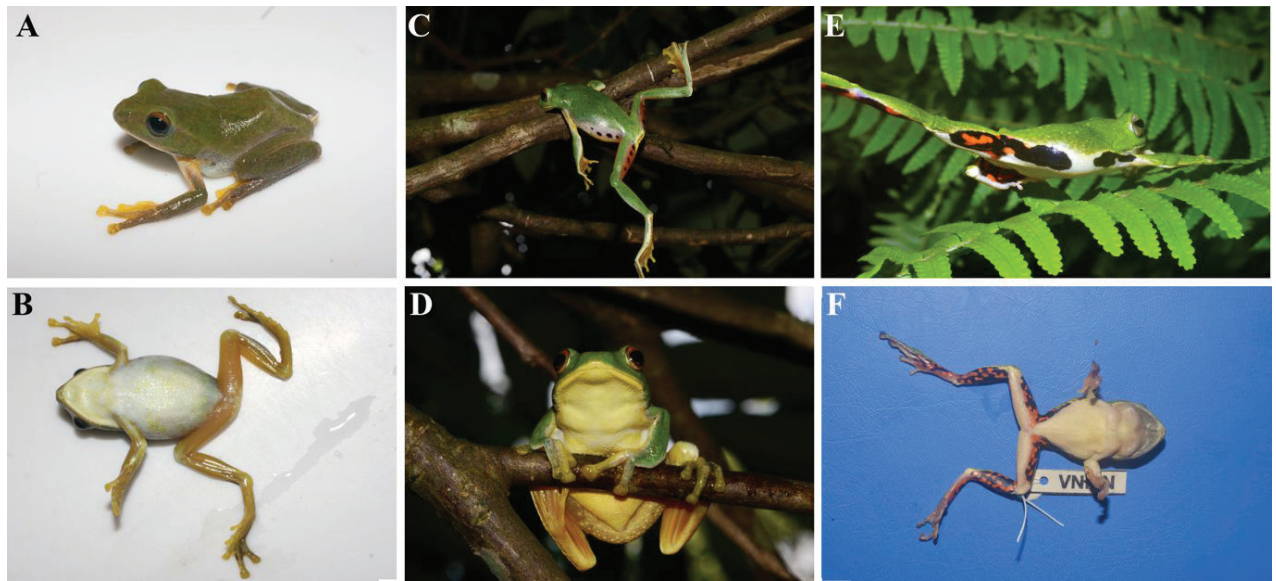


Figure 6. Dorsal and ventral views of three *Zhangixalus* species in life (except for F, which was immediately photographed after the specimen was anesthetized) **A, B** *Zhangixalus thaoae* sp. nov. IEBR.A 5136 **C, D** *Z. dorsovirens* VNMN 06156 **E, F** *Z. jodiae* VNMN 07122.



Figure 7. Dorsal and ventral views of three *Zhangixalus* species in preservative **A, B** *Zhangixalus thaoae* sp. nov. IEBR.A 5136 **C, D** *Z. dorsovirens* VNMN 06156 **E, F** *Z. jodiae* VNMN 07122.

Zhangixalus minimus is characterized by a dark-brown mottling pattern on its hands and feet, which is absent in *Z. thaoae* sp. nov. (Rao et al. 2006).

Zhangixalus melanoleucus is whitish cream with an irregular black pattern on the ventral surface of its thighs, shanks, dorsal surfaces of the feet and fingers I, II, and III (Brakels et al. 2023). Meanwhile, in *Z. thaoae* sp. nov., the ventral surface of the thighs, shanks, dorsal surfaces of the feet and fingers I, II, and III are orange, without any irregular black pattern.

Zhangixalus moltrechti has a red-orange anterior and posterior thigh with multiple dark spots, while the thigh in *Z. thaoae* sp. nov. has an orange anterior with no spots and an orange posterior with a single large blotch (Boulenger 1908; Fei et al. 2010). Furthermore, the webbings of the foot in *Z. moltrechti* are red-orange, with dark spots, while those in *Z. thaoae* sp. nov. are yellow with no spots.

Zhangixalus nigropunctatus has yellow flanks and posterior thigh with some black blotches, in contrast to *Z. thaoae* sp. nov., in which the flank is cream-colored and the posterior thigh is orange, both featuring a single black spot (Liu et al. 1962; Fei et al. 2010). In *Z. nigropunctatus*, there is also a white stripe along the flanks and limbs, separating the dorsal and ventral sides, which is a feature that is absent in *Z. thaoae* sp. nov.

Zhangixalus schlegelii has flanks and groin without spots, while in *Z. thaoae* sp. nov. these each have a large black blotch (Günther 1858). A white stripe along the flanks and limbs, separating the dorsal and ventral sides, is present in *Z. schlegelii* but absent in *Z. thaoae* sp. nov. Furthermore, there is a prominent supratympanic fold in *Z. schlegelii*, which is only weakly visible in *Z. thaoae* sp. nov.

Zhangixalus yinggelingsis has green dorsal head, body and limbs, adorned with a small number of very fine white spots (Chou et al. 2007), which are absent in *Z. thaoae* sp. nov. In addition, the supratympanic fold in *Z. yinggelingsis* is prominent, whereas it is weakly visible in *Z. thaoae* sp. nov.

Zhangixalus yunnanensis has greyish webbings and yellowish-brown iris, which are respectively orange and red-bronze in *Z. thaoae* sp. nov. (Pan et al. 2024). Furthermore, *Z. yunnanensis* exhibits a somewhat broader head (IND/IOD 0.96-1), which is proportionally smaller relative to the body (HL/SVL 0.31-0.33) compared to the head of *Z. thaoae* sp. nov. (IND/IOD 0.72-0.85, HL/SVL 0.37-0.43).

Zhangixalus zhokaiyae has yellowish posterior thigh with irregular greyish blotching, whereas the posterior thigh of *Z. thaoae* sp. nov. is orange without spots. In *Z. zhokaiyae*, the pupil is dark charcoal-grey and the iris is golden-yellow, while in *Z. thaoae* sp. nov. the pupil is black, and the iris is red-bronze (Pan et al. 2017).

A more detailed comparison of morphological differences between *Z. thaoae* and other members in the *Z. chenfui* group can be found in Table 4.

Discussion

Zhangixalus nigropunctatus was first recorded in Weining District, Guizhou Province, China by Liu et al. (1962) in 1962. Based Orlov et al. (2001) study of a series of specimens collected from Fan Si Pan Mountain, in the northern part of the Hoang Lien Mountains, Sa Pa district, Lao Cai Province, they suggested that *Z. nigropunctatus* might be a junior synonym of *Z. dorsovireidis*, a species originally described by Bourret (1937) from Sa Pa District, Lao Cai Province,

Table 4. Comparison of morphology character of species within *Z. chenfui* group.

Species	SVL	Dorsum color	Vomerine teeth	Ventral color	Flank coloration	Snout shape	The color pattern of the thigh	Fingers web formula	Toes web formula	Source
<i>Zhangixalus thaoae</i> sp. nov.	30-32.2 (M)	Smooth, and green without spots	Present	Lower jaw cream with grey and throat region white belly cream without spots	Flank cream with a black blotch	Rounded	The anterior part of the thigh is orange without spots; the posterior part of the thigh is orange with a large black blotch	I1 ^{1/2} -1 ^{1/4} I1 ¹ -2III1-1IV	I ^{1/2} - ^{1/2} II0-1 ^{1/2} III ^{1/2} -1 ^{1/4} IV1 ^{3/4} - ^{1/2} V	This study
<i>Z. chenfui</i>	33-41 (M) 48-55 (F)	Skin with granules above	Present	Ventral brown with dark-brown pattern	Flanks orange with blotches, have a black strip along flank isolated upper and lower part of the body	Rounded	Anterior of thigh orange with blotches	–	–	Liu et al. 1945; Fei et al. 2009
<i>Z. jodiae</i>	36.1 – 39.8 (M)	Dorsal surface of the head and body green without spots	Present	Lower jaw region greyish, chest and belly cream	Flank cream, axilla, and groin with large black blotches	Rounded	The dorsal surface is green without spots, the front-rear parts of the thigh, and the ventral surface of the tibia black with orange blotches	I1-1III1-1III2-1IV	I1-1III ^{1/2} -1III0-1 ^{1/2} IV1- ^{1/2} V	Nguyen et al. 2021
<i>Z. melanoleucus</i>	34.4-36.3 (M) 53.7 (F)	Dorsum smooth and uniform green with several dark and light-green spots	Present	Throat grey with dark grey margins, chest and belly immaculate white	Flank white, covered by an irregular black pattern, groin cream	Rounded	The anterior and posterior surfaces of the thighs are white cream covered with an irregular black pattern, ventral surfaces of the thighs cream	I2 ^{1/2} -3III2-3 III2 ^{1/4} -2IV	I2-2 ^{1/2} II1-2III1-2 IV2-1V	Brakels et al. 2023
<i>Z. nigropunctatus</i>	32.0 – 37.0 (M) 44-45(F)	Dorsum smooth and green	–	Lower jaw grey, chest and belly white	Flanks orange with blotches has a white strip along isolated dorsal and ventral side	Rounded	Dorsal surface green, anterior and posterior surfaces of thighs orange and has some black blotches on posterior of thigh	–	–	Fei et al. 2009
<i>Z. pinglongensis</i>	32.0 – 38.5 (M)	Dorsum smooth and green	Present	Lower jaw grey, chest and belly cream	Flank covered with black blotches with white spots or white spots with a faint orange tint	Rounded	The anterior and posterior surfaces of the thigh covered with black blotches with white spots or white spots with a faint orange tint	I 1 – 1-II 1* – 1*III2 – 2IV	I1* – 1II 2* – 2III 2* – 3IV 3 – 2*V	Mo et al. 2016
<i>Z. yaoshanensis</i>	31.6 – 36.4 (M) 51.1 (F)	The dorsal surface is smooth and green, with or without faint spots,	Present	Throat grey in males, ventral green without spots	The posterior surface of the flanks is orange-red without spots	Point	Dorsal surface green with or without faint green spots, anterior and posterior surface of thighs orange-red without spots	I1 – 1II1 – 1III1* – 2IV	I 1* – 1II1* – 1III 2* – 2IV2* – 2*V	Chen et al. 2018
<i>Z. yunnanensis</i>	31.3-36.0 (M) 47.6-48.6 (F)	Smooth and green	Present	Throat black	Cream mottled with greyish brown	Rounded	Black blotches in axilla, groin, and posterior part of thigh	I1 – 1II1 – 2III1 – 1IV	I1 – 1II0.5 – 2.5III1 – 2IV2 – 0.5IV	Pan et al. 2024

Vietnam. Li et al. (2012b) investigated the phylogenetic relationships of the genus *Rhacophorus* sensu lato and showed that a specimen identified as *Z. nigropunctatus* in the collection of Orlov et al. (2001; ROM 38011) was nested in the same subclade as *Z. nigropunctatus* from China (Weining, Guizhou) (Pan et al. 2024). Although the genetic distance between them was greater than 5% and there was no specimen description, Orlov et al. (2001) concluded that both *Z. dorsovirens* and *Z. nigropunctatus* occur in Sa Pa, Lao Cai Province (see also Pan et al. 2017).

The phylogenetic results of our study reveal that the specimen JX219427 from (ROM 38011; Orlov et al. 2001), which was originally classified as belonging in the *Z. nigropunctatus* clade of Li et al. (2012b), is in fact *Z. thaoae* with a genetic distance of only 0.19 compared with the three other newly found specimens. Furthermore, *Z. thaoae*, *Z. dorsovirens*, and *Z. nigropunctatus* show high genetic distance of at least 5.5%. This large genetic distance makes it unlikely that by using genetic data, the taxonomic assignment of a specimen into the three aforementioned species can be confused. Although molecular data indicates that ROM 38011 belongs to *Z. thaoae*, detailed morphological data to support such assignment is not available; neither Orlov et al. (2001) nor Li et al. (2012b) provided a detailed description of that specimen, and Orlov et al. (2001) did not provide a figure of ROM 38011. However, Orlov et al. (2001), noted that ROM 38011 had an “obviously darkened” median vocal sac which differed from the other specimens they examined.

Overall, there is evidence that the specimen ROM 38011 had been misidentified as either *Z. dorsovirens* or *Z. nigropunctatus* and that *Z. thaoae* is a valid new taxon. Based on our reclassification of ROM 38011 as *Z. thaoae* and lack of other known records, we herein formally exclude *Z. nigropunctatus* from the amphibian fauna of Vietnam. *Zhangixalus nigropunctatus* is only known from Yunnan Province (Pingbian), Anhui Province (Yuei), Guizhou Province, (Weining and Leishan), and Hunan Province (Sangzhi and Chengbu), China (Li et al. 2012b; Pan et al. 2017, 2024).

In addition to the new species described in this paper, Nguyen et al. (2020) previously described *Z. jodiae* and assigned earlier records of *Z. dorsovirens* from Ha Giang Province to *Z. jodiae*. Thus, two species belonging to the *Z. chen-fui* group of green treefrogs, *Z. jodiae* and *Zhangixalus thaoae*, are currently known from Vietnam.

Acknowledgements

We are grateful to the directorates of the Forest Protection Department of Lao Cai Province for their support of our fieldwork and for issuing relevant permits. We thank MA. Luong (IEBR) for supporting in the field and TN. Nguyen for supporting in laboratory. This research was partially funded by the State Themes of ZISP 122031100282-2 and grant no.075-15-2021-1069 by the Ministry of Science and Higher Education of the Russian Federation to Nikolai Orlov.

Additional information

Conflict of interest

The authors have declared that no competing interests exist.

Ethical statement

No ethical statement was reported.

Funding

This research is funded by the Vietnam Academy of Science and Technology (VAST) under grant number NCXS.01.03/23–25.

Author contributions


Writing – original draft: TTN. Writing – reviewing and editing: TTN, NO, TZ. Funding acquisition & Supervision: HHN, TTN. Investigation – sample collection: CVH. Formal analysis – phylogenetic & morphological analysis: HTN, LTHL, HTB.

Author ORCIDs

Tao Thien Nguyen  <https://orcid.org/0000-0002-5640-4536>

Huy Hoang Nguyen  <https://orcid.org/0000-0002-6284-5813>


Hoa Thi Ninh  <https://orcid.org/0009-0002-8133-432X>

Linh Tu Hoang Le  <https://orcid.org/0009-0003-0887-2786>

Hai Tuan Bui  <https://orcid.org/0000-0003-4065-7229>

Nikolai Orlov  <https://orcid.org/0000-0003-4401-348X>

Chung Van Hoang  <https://orcid.org/0000-0002-0709-974X>

Thomas Ziegler  <https://orcid.org/0000-0002-4797-609X>

Data availability

All of the data that support the findings of this study are available in the main text.

References

- Blanford WT (1881) On a collection of reptiles and frogs chiefly from Singapore. *Proceedings of the Zoological Society of London* 1881(1): 215–226. <https://doi.org/10.1111/j.1096-3642.1881.tb01281.x>
- Boulenger GA (1892) An account of the reptiles and batrachians collected by Mr. C. Hose on Mt. Dulit, Borneo. *Proceedings of the Zoological Society of London* 1892: 505–508. [2 pl.]
- Boulenger GA (1893) Concluding report on the reptiles and batrachians obtained in Burma by Signor L. Fea dealing with the collection made in Pegu and the Karin Hills in 1887–88. *Annali del Museo Civico di Storia Naturale di Genova* 2(13): 304–347.
- Boulenger GA (1908) Descriptions of a new frog and a new snake from Formosa. *Annals & Magazine of Natural History* 8(2): 221–222. <https://doi.org/10.1080/00222930808692472>
- Bourret R (1937) Notes herpétologiques sur l'Indochine française. XIV. Les batraciens de la collection du Laboratoire des Sciences Naturelles de l'Université. *Descriptions de quinze espèces ou variétés nouvelles. Annexe au Bulletin Général de l'Instruction Publique. Hanoi*, 5–56.
- Brakels P, Nguyen VT, Pawangkhanant P, Idiatullina S, Lorphengsy S, Suwannapoom C, Poyarkov NA (2023) Mountain jade: A new high-elevation microendemic species of the genus *Zhangixalus* (Amphibia: Anura: Rhacophoridae) from Laos. *Zoological Research. Kunming* 44: 374–379. <https://doi.org/10.24272/j.issn.2095-8137.2022.382>

- Chen W, Liao X, Zhou S, Mo Y, Huang Y (2018) Rediscovery of *Rhacophorus yaoshanensis* and *Theloderma kwangsiensis* at their type localities after five decades. *Zootaxa* 4379(4): 484–496. <https://doi.org/10.11646/zootaxa.4379.4.2>
- Chou W-h, Lau MW-n, Chan BPL (2007) A new treefrog of the genus *Rhacophorus* (Anura: Rhacophoridae) from Hainan Island, China. *Raffles Bulletin of Zoology*. Singapore 55: 157–165.
- David A (1872) [1871] Rapport adressé a MM. les Professeurs-Administrateurs du Muséum d'histoire naturelle. *Nouvelles Archives du Muséum d'Histoire Naturelle*, Paris 7: 75–100.
- Fei L, Ye CY, Jiang JP (2010) *Colored Atlas of Chinese Amphibians*. Sichuan Publishing House of Science and Technology, Chengdu.
- Frost DR (2024) *Amphibian Species of the World: an Online Reference*. Version 6.2. <http://research.amnh.org/herpetology/amphibia/index.html> [Accessed 12 January 2024]
- Glaw F, Vences M (2007) *A Field Guide to the Amphibians and Reptiles of Madagascar*. Third Edition, Frosch Verlag, Cologne.
- Günther ACLG (1858) Neue Batrachier in der Sammlung des britischen Museums. *Archiv für Naturgeschichte* 24: 319–328. <https://doi.org/10.5962/bhl.part.5288>
- Haas A, Hertwig ST, Krings W, Braskamp E, Dehling JM, Min PY, Jankowski A, Schweizer M, Das I (2012) Description of three *Rhacophorus* tadpoles (Lissamphibia: Anura: Rhacophoridae) from Sarawak, Malaysia (Borneo). *Zootaxa* 3328(1): 1–19. <https://doi.org/10.11646/zootaxa.3328.1.1>
- Harvey MB, Pemberton AJ, Smith EN (2002) New and poorly known parachuting frogs (Rhacophoridae: *Rhacophorus*) from Sumatra and Java. *Herpetological Monograph* 16(1): 46–92. [https://doi.org/10.1655/0733-1347\(2002\)016\[0046:NAPKPF\]2.0.CO;2](https://doi.org/10.1655/0733-1347(2002)016[0046:NAPKPF]2.0.CO;2)
- He XR (1999) A new species of the family Rhacophoridae from Yunnan - *Polypedates puerensis*. *Sichuan Journal of Zoology*. *Sichuan Journal of Zoology* 18: 99–100. [In Chinese with English abstract]
- Hoang DT, Chernomor O, Haeseler AV, Bui QM, Le SV (2018) UFBoot2: Improving the ultrafast bootstrap approximation. *Molecular Biology and Evolution* 35(2): 518–522. <https://doi.org/10.1093/molbev/msx281>
- IUCN (2023) *The IUCN Red List of Threatened Species*. Version 2023-1. <https://www.iucnredlist.org> [Accessed on 20.03.2024]
- Jiang K, Wang K, Yang J, Jin J, Zou D, Yan F, Pan H, Che J (2016) Two new records of amphibia from Tibet, China, with description of *Rhacophorus burmanus*. *Sichuan Journal of Zoology* 35(2): 210–216. [In Chinese with English abstract]
- Kalyaanamoorthy S, Minh BQ, Wong TK, Von Haeseler A, Jermini LS (2017) ModelFinder: Fast model selection for accurate phylogenetic estimates. *Nature Methods* 14(6): 587–589. <https://doi.org/10.1038/nmeth.4285>
- Katoh K, Standley DM (2013) MAFFT multiple sequence alignment software version 7: Improvements in performance and usability. *Molecular Biology and Evolution* 30(4): 772–780. <https://doi.org/10.1093/molbev/mst010>
- Kuraishi N, Matsui M, Hamidy A, Belabut DM, Ahmad N, Panha S, Sudin A, Yong HS, Jiang JP, Ota H, Thong HT, Nishikawa K (2013) Phylogenetic and taxonomic relationships of the *Polypedates leucomystax* complex (Amphibia). *Zoologica Scripta* 42(1): 54–70. <https://doi.org/10.1111/j.1463-6409.2012.00562.x>
- Leaché AD, Reeder TW (2002) Molecular systematics of the eastern fence lizard (*Sceloporus undulatus*): A comparison of parsimony, likelihood, and Bayesian approaches. *Systematic Biology* 51(1): 44–68. <https://doi.org/10.1080/106351502753475871>

- Li JT, Liu J, Chen YY, Wu JW, Murphy RW, Zhao EM, Wang YZ, Zhang YP (2012a) Molecular phylogeny of treefrogs in the *Rhacophorus dugritei* species complex (Anura: Rhacophoridae), with descriptions of two new species. *Zoological Journal of the Linnean Society* 165(1): 143–162. <https://doi.org/10.1111/j.1096-3642.2011.00790.x>
- Li JT, Li Y, Murphy RW, Rao DQ, Zhang YP (2012b) Phylogenetic resolution and systematics of the Asian tree frogs, *Rhacophorus* (Rhacophoridae, Amphibia). *Zoologica Scripta* 41(6): 557–570. <https://doi.org/10.1111/j.1463-6409.2012.00557.x>
- Liu C (1945) New frogs from West China. *Journal of the West China Border Research Society B* 15: 28–44.
- Liu CC (1950) Amphibians of western China. *Fieldiana. Zoology Memoirs* 2: 1–397. <https://doi.org/10.5962/bhl.part.4737>
- Liu CC, Hu SQ (1961) Tailless Amphibians of China. Science Press, Beijing. [In Chinese]
- Liu CC, Hu SQ (1962) A herpetological report of Kwangsi. *Acta Zoologica Sinica. Dong Wu Xue Bao* 14(Supplement): 73–104.
- Liu CC, Hu SQ, Yang FH (1962) Preliminary report of Amphibia from western Kweichow. *Acta Zoologica Sinica. Acta Zoologica Sinica* 14: 381–392.
- Liu B-q, Wang Y-f, Jiang K, Chen H-m, Zhou J-j, Xu J-n, Wu C-h (2017) A new tree-frog species of the genus *Rhacophorus* found in Zhejiang, China (Anura: Rhacophoridae). *Dongwuxue Zazhi* 52: 361–372. [In Chinese with English abstract]
- Lue KY, Lai JS, Chen SL (1995) A new species of *Rhacophorus* (Anura: Rhacophoridae) from Taiwan. *Journal of Herpetology* 29(3): 338–345. <https://doi.org/10.2307/1564982>
- Luu VQ, Calame T (2014) First records of *Gracixalus supercornutus* (Orlov, Ho & Nguyen, 2004) and *Rhacophorus maximus* Günther, 1858 from Laos. *Herpetology Notes* 7: 419–423.
- Matsui M, Kawahara Y, Eto K, Hamidy A, Ahmad N, Hossman MYB (2018) Distinct species status of *Kurixalus chaseni* (Rhacophoridae, Anura) as revealed by mitochondrial phylogeny. *Alytes* 36: 170–177. <https://doi.org/10.1080/00222933.2020.1728411>
- Mo YM, Chen WC, Liao XW, Zhou SC (2016) A new species of the genus *Rhacophorus* (Anura: Rhacophoridae) from southern China. *Asian Herpetological Research* 7(3): 139–150. <https://doi.org/10.16373/j.cnki.ahr.150070>
- Nguyen TT, Matsui M, Eto K (2015a) Mitochondrial phylogeny of an Asian tree frog genus *Theلودerma* (Anura: Rhacophoridae). *Molecular Phylogenetics and Evolution* 85: 59–67. <https://doi.org/10.1016/j.ympev.2015.02.003>
- Nguyen TL, Heiko A, Schmidt AH, Bui QM (2015b) IQ-TREE: A fast and effective stochastic algorithm for estimating maximum-likelihood phylogenies. *Molecular Biology and Evolution* 32(1): 268–274. <https://doi.org/10.1093/molbev/msu300>
- Nguyen QT, Pham TC, Nguyen TT, Ngo NH, Ziegler T (2016) A new species of *Theلودerma* (Amphibia: Anura: Rhacophoridae) from Vietnam. *Zootaxa* 4168(1): 171–186. <https://doi.org/10.11646/zootaxa.4168.1.10>
- Nguyen TT, Ninh HT, Orlov NL, Nguyen TQ, Ziegler T (2020) A new species of the genus *Zhangixalus* (Amphibia: Rhacophoridae) from Vietnam. *Journal of Natural History* 54(1–4): 257–273. <https://doi.org/10.1080/00222933.2020.1754484>
- Ninh HT, Nguyen TT, Orlov NL, Nguyen TQ, Ziegler T (2020) A new species of the genus *Zhangixalus* (Amphibia: Rhacophoridae) from Vietnam. *European Journal of Taxonomy* 688(688): 1–8. <https://doi.org/10.5852/ejt.2020.688>
- Ohler A (2009) *Rhacophorus burmanus* (Anderson, 1939) the valid nomen for *Rhacophorus taronensis* Smith, 1940 and *Rhacophorus gongshanensis* Yang & Su, 1984. *Herpetozoa* (Wien) 21: 179–182.

- Ohler A, Marquis O, Swan S, Grosjean S (2000) Amphibian biodiversity of Hoang Lien Nature Reserve (Lao Cai Province, northwestern Vietnam) with description of two new species. *Herpetozoa (Wien)* 13(1/2): 71–87.
- Okada Y, Kawano U (1924) On the ecological distribution of two new varieties of *Rhacophorus* in Japan. *Dōbutsugaku zasshi/ Zoological Magazine*. Tokyo 36: 104–109, 144–153. [In Japanese]
- Orlov NL, Lathrop A, Murphy RW, Ho CT (2001) Frogs of the family Rhacophoridae (Anura: Amphibia) in the northern Hoang Lien Mountains (Mount Fan Si Pan, Sa Pa District, Lao Cai Province), Vietnam. *Russian Journal of Herpetology* 8: 17–44.
- Pan T, Zhang YN, Wang H, Wu J, Kang X, Qian LF, Li K, Zhang Y, Chen JY, Rao DQ, Jiang JP, Zhang BW (2017) A new species of the genus *Rhacophorus* (Anura: Rhacophoridae) from Dabie Mountains in East China. *Asian Herpetological Research* 8: 1–13. <https://doi.org/10.16373/j.cnki.ahr.160064>
- Pan Y, Hou M, Yu G, Liu S (2024) A new species of *Zhangixalus* (Anura, Rhacophoridae) from Yunnan, China. *Zoosystematics and Evolution* 100(1): 183–197. <https://doi.org/10.3897/zse.100.113850>
- Rambaut A, Drummond A (2009) TRACER. Version 1.5. <http://beast.bio.ed.ac.uk/Tracer>
- Rao DQ, Wilkinson JA, Liu HN (2006) A new species of *Rhacophorus* (Anura: Rhacophoridae) from Guangxi Province, China. *Zootaxa* 1258(1): 17–31. <https://doi.org/10.11646/zootaxa.1258.1.2>
- Ronquist F, Teslenko M, Mark P, Ayres DL, Darling A, Höhna S, Larget B, Liu L, Suchard MA, Huelsenbeck JP (2012) MrBayes 3.2: Efficient Bayesian phylogenetic inference and model choice across a large model space. *Systematic Biology* 61(3): 539–542. <https://doi.org/10.1093/sysbio/sys029>
- Sano N, Kurabayashi A, Fujii T, Yonekawa H, Sumida M (2005) Complete nucleotide sequence of the mitochondrial genome of Schlegel's tree frog *Rhacophorus schlegelii* (family Rhacophoridae): Duplicated control regions and gene rearrangements. *Genes & Genetic Systems* 80(3): 213–224. <https://doi.org/10.1266/ggs.80.213>
- Simmons JE (2002) *Herpetological Collecting and Collection Management*. Revised Edition. Society for the Study of Amphibian and Reptile. *Herpetological Circular* 31: 1–153.
- Tavaré S (1986) Some probabilistic and statistical problems in the analysis of DNA sequences. *Lectures on Mathematics in the Life Sciences* 17: 57–86.
- Wilkinson JA, Rao DQ (2004) Taxonomic status of *Rhacophorus taronensis* Smith, 1940. *Proceedings of the California Academy of Sciences* 55(25): 451–457.
- Yu GH, Hui H, Hou M, Wu ZH, Rao DQ, Yang JX (2019) A new species of *Zhangixalus* (Anura: Rhacophoridae), previously confused with *Zhangixalus smaragdinus* (Blyth, 1852). *Zootaxa* 4711(2): 275–292. <https://doi.org/10.11646/zootaxa.4711.2.3>
- Ziegler T, Tran DTA, Nguyen TQ, Perl RGB, Wirk L, Kulisc M, Lehmann T, Rauhaus A, Nguyen TT, Le QK, Vu TN (2014) New amphibian and reptile records from Ha Giang Province, northern Vietnam. *Herpetology Notes* 7: 185–201.

Primitive new termites (Blattodea, Termitoidae) in Cretaceous amber from Myanmar

Yurong Jiang^{1,2}, Xinru Deng^{1,2}, Chungkun Shih^{2,3}, Yunyun Zhao², Dong Ren², Zhipeng Zhao¹

1 Fishery Resource and Environment Research Center, Chinese Academy of Fishery Sciences, Beijing, China

2 College of Life Sciences, Capital Normal University, Beijing, China

3 Department of Paleobiology, National Museum of Natural History, Smithsonian Institution, Washington, DC, USA

Corresponding author: Zhipeng Zhao (zhaozhipeng@cafs.ac.cn)

Abstract

Mastotermitidae, the first-diverging extant family of termites, has only one relic extant species; however, this family had greater richness during the Mesozoic and Cenozoic eras. Fossil termites from the Cretaceous provide information on the early evolution of termites and the transition between extinct families. Herein, two new Mastotermitidae species found in upper Cretaceous (Cenomanian) Kachin amber are reported. One is a female imago described as *Angustitermes reflexus* **gen. et sp. nov.** and assigned to the subfamily Mastotermitinae. The other is *Mastotermes reticulatus* **sp. nov.**, which is described from an isolated forewing. With the comparison especially of the antenna and venation, these new mastotermitids further increase our knowledge of the diversity and morphology of Mastotermitidae during the Mesozoic.

Key words: Fossil termites, Isoptera, Mastotermitidae, social insects, taxonomy



Academic editor: Eliana Canello

Received: 21 October 2023

Accepted: 15 February 2024

Published: 10 April 2024

ZooBank: <https://zoobank.org/AA02946C-E345-4997-85E0-D5B7B7308A57>

Citation: Jiang Y, Deng X, Shih C, Zhao Y, Ren D, Zhao Z (2024) Primitive new termites (Blattodea, Termitoidae) in Cretaceous amber from Myanmar. ZooKeys 1197: 115–126. <https://doi.org/10.3897/zookeys.1197.114452>

Copyright: © Yurong Jiang et al.

This is an open access article distributed under terms of the Creative Commons Attribution License ([Attribution 4.0 International – CC BY 4.0](https://creativecommons.org/licenses/by/4.0/)).

Introduction

Termites are social insects with the support of mutualistic protists or cellulose-digesting bacteria (Breznak and Brune 1994; Sanderson 1996; Sugimoto et al. 2000; Krishna et al. 2013a; Zhao et al. 2020, 2021). The enormous biomass of termites largely contributes to the global carbon cycle, while occupying an important ecological position in the biosphere (Tuma et al. 2020). The rank of termites has been controversial. Inward et al. (2007) indicated that the rank of termites should be a family, however, some termitologists proposed to continue using “Isoptera” (Lo et al. 2007), and the current compromise is to use “epifamily Termitoidae” (Eggleton et al. 2007; Bignell et al. 2011; Xiao et al. 2012; Beccaloni and Eggleton 2013; Zhao et al. 2019) or “infraorder Isoptera”.

As the first-diverging extant family in Termitoidae (Thompson et al. 2000; Legendre et al. 2015; Bucek et al. 2019; Zhao et al. 2019), Mastotermitidae

shares many characters with cockroaches, for example, a large anal lobe in the hind wing and vestigial ootheca or egg pod (Nalepa and Lenz 2000; Krishna et al. 2013a). The most obvious morphological differences from other termite families are that the hind wings have large anal lobes and Sc, R, Rs, and M veins are thick and more sclerotized than CuA. Mastotermitidae was divided into two subfamilies, Mastotermitinae Desneux, 1904 and Idanotermitinae Engel, 2021, based on the presence or absence of ocelli (Jiang et al. 2021).

Besides the sole relic species, *Mastotermes darwiniensis* Froggatt, 1897, living in northern Australia and southern New Guinea (Froggatt 1897; Nalepa and Lenz 2000; Engel et al. 2009), nine genera and 33 extinct species have been documented. Among them, 21 species were documented from compression fossils, one from Cretaceous deposits, and others from Cenozoic deposits (e.g. Wappler and Engel 2006; Krishna et al. 2013b; Vršanský and Aristov 2014; Engel et al. 2015; Bezerra et al. 2020). In addition, 12 species were reported in amber, among which seven species were reported from the Cretaceous, including five species from Kachin amber (Zhao et al. 2019; Jouault et al. 2021, 2022): *Anisotermes bourguignoni* Jouault, Engel, Huang & Nel, 2022, *Anisotermes xiai* Zhao, Eggleton & Ren, 2019, *Magnifitermes krishnai* Jouault, Engel & Nel, 2022, *Mastotermes monostichus* Zhao, Eggleton & Ren, 2019, *Mastotermes myanmarensis* Jouault, 2022, *Milesitermes engeli* Jouault & Nel, 2021, one species from amber of Sagaing Region, Myanmar: *Mastotermes myanmarensis* Jouault, 2022 (Jouault et al. 2022). One species was described from France: *Mastotermes sarthensis* Schlüter, 1989 (Schlüter 1989). The other five species were reported from the Cenozoic (Krishna and Emerson 1983; Krishna and Grimaldi 1991; Nel and Bourguet 2006; Engel et al. 2007; Engel 2008).

Materials and methods

The two specimens studied here were collected from amber mines located in the Hukawng Valley in Kachin State of northern Myanmar. Determined by U-Pb dating of Zircon, the deposit age of the amber mine was 98.79 ± 0.62 Ma which means it comes from early Cenomanian of the upper Cretaceous (Shi et al. 2012). The amber specimens involved in this study were acquired by Mr Fangyuan Xia before 2015 and donated for this study in 2016. Both specimens are deposited in the Key Laboratory of Insect Evolution and Environmental Changes, College of Life Sciences, Capital Normal University, Beijing, China (**CNUB**, curator: Dong Ren).

The amber is cut and polished. The specimens are examined, measured, and photographed with a Nikon SMZ25 microscope system. To help reduce picture distortion caused by refraction and internal cracks, the amber was placed in a properly sized crystallizing dish, with a proper amount of water, and the capture angle and area of interest was adjusted when viewing; the amber was affixed with plasticine when measurements and photographs were taken.

All images are stacked using the software Helicon Focus v. 8 for better depth of field. Simplified drawings were prepared using Adobe Illustrator CC and further modified using Adobe Photoshop CC.

Systematic paleontology

Family Mastotermitidae Desneux, 1904

Subfamily Mastotermitinae Engel, 2021

Genus *Angustitermes* Jiang, Z. Zhao & Ren, gen. nov.

<https://zoobank.org/FA73A948-C6EE-43D2-86E9-09485B5F7970>

Type species. *Angustitermes reflexus* Jiang, Z. Zhao & Ren, gen. et sp. nov. (Figs 1–3).

Etymology. *Angusti-* is a Latin adjective, reflecting the fact that the medial field of this genus is narrow, and *termes* is the usual noun for the generic name in Termitoidae. The gender is masculine.

Diagnosis. Imago: ocelli oval; fontanelle absent; Y-suture absent; mandibles not exceeding labrum; antenna moniliform with 22 articles; compound eyes lying in middle position on head; pronotum saddle-shaped. Wings heavily reticulated, with “cross-veins” present. **Forewing:** scale large, overlapping hind wing base, humeral suture convex; all major veins origin in scale; veins Sc, R₁, R₂, Rs, and M more pigmented than CuA; Sc simple; Rs with about three main branches, terminating on costal margin anterior to wing apex; radial field narrow, parallel to costal margin; M closer to Rs than CuA, lying more or less parallel to Rs as a simple vein for the greater part of its length, first branching in apical 1/5 of wing length, medial field narrow, encompassing wing apex; CuA branched, lying above the mid-longitudinal line of wing; CuP (claval suture) arched, meeting basal suture before posterior margin. **Hind wing:** basal suture not visible, large anal lobe present. **Legs:** tibial spines of all legs present; tibial spur formula 3–4–4; tarsi pentamerous; arolium present. **Abdomen:** cerci short, trimerous; abdominal styli absent.

Remarks. Based on the sclerotized vein M, presence of the anal lobe, saddle-shaped pronotum, pentamerous tarsi, etc., *Angustitermes* gen. nov. is considered to belong to the Mastotermitidae and is assigned to the subfamily Mastotermitinae because of the ocelli (Fig. 1C). Besides the new genus and *Mastotermes*, there are two other genera in Mastotermitinae: *Garmitermes* Engel, Grimaldi & Krishna, 2007 and *Magnifitermes* Jouault, Engel & Nel, 2022. Termites in both *Angustitermes* gen. nov. and *Garmitermes* have a rounded head, but unlike *Angustitermes* gen. nov., *Garmitermes* has 26 antennal articles, the arolium is greatly vestigial or absent, and the tibial spur formula of *Garmitermes* is 3–5–4 (Engel et al. 2007). Both *Angustitermes* gen. nov. and *Magnifitermes* have arolium, and their tibial spur formula is the same. However, the shape of the head of *Magnifitermes* is relatively long and with about 28 antennal articles (Jouault et al. 2022). Although in different subfamilies, *Angustitermes* gen. nov. and *Anisotermes* share many similarities, such as the rounded head and the tibial spur formula. However, the M vein of *Anisotermes* is located halfway between Rs and CuA, and the first inferior branch of the M vein on the hind wings gradually fades away, ultimately terminating in the center of the hind wings of *Anisotermes* (Zhao et al. 2019; Jouault et al. 2022).

The major feature of *Angustitermes* gen. nov. is that the M vein is a simple vein for the greater part of its length, first branch branching in the apical 1/5 of wing length, and the medial field is narrow (Fig. 2B). The simple M and narrow medial field of *Angustitermes* gen. nov. is similar to *Blattotermes* Riek, 1952. However, *Angustitermes* gen. nov. has sparser veins than *Blattotermes*; the

branches of R and secondary branches of CuA are fewer, and tertiary branch is absent; its forewings are much shorter, so that the difference in wing lengths between these two genera is more than 10 mm. Besides, the specimen of the new *Angustitermes* species is from the upper Cretaceous while the three *Blattotermes* species are from the Cenozoic: *Blattotermes neoxenus* Riek, 1952 and *Blattotermes wheeleri* (Collins, 1925) are from Eocene, and *Blattotermes massiliensis* Nel, 1986 is from Oligocene (Collins 1925; Riek 1952; Nel 1986; Thorne et al. 2000; Krishna et al. 2013b).

***Angustitermes reflexus* Jiang, Z.Zhao & Ren, gen. et sp. nov.**

<https://zoobank.org/A0343631-5430-4D81-9F18-F3E5AECB4071>

Figs 1–3

Type material. Holotype. Myanmar • Imago♀; Kachin State, Hukawng Valley; one imago (abdomen fragmentary); Kachin amber; CNU-TER-BU-2017005 (Figs 1–3).

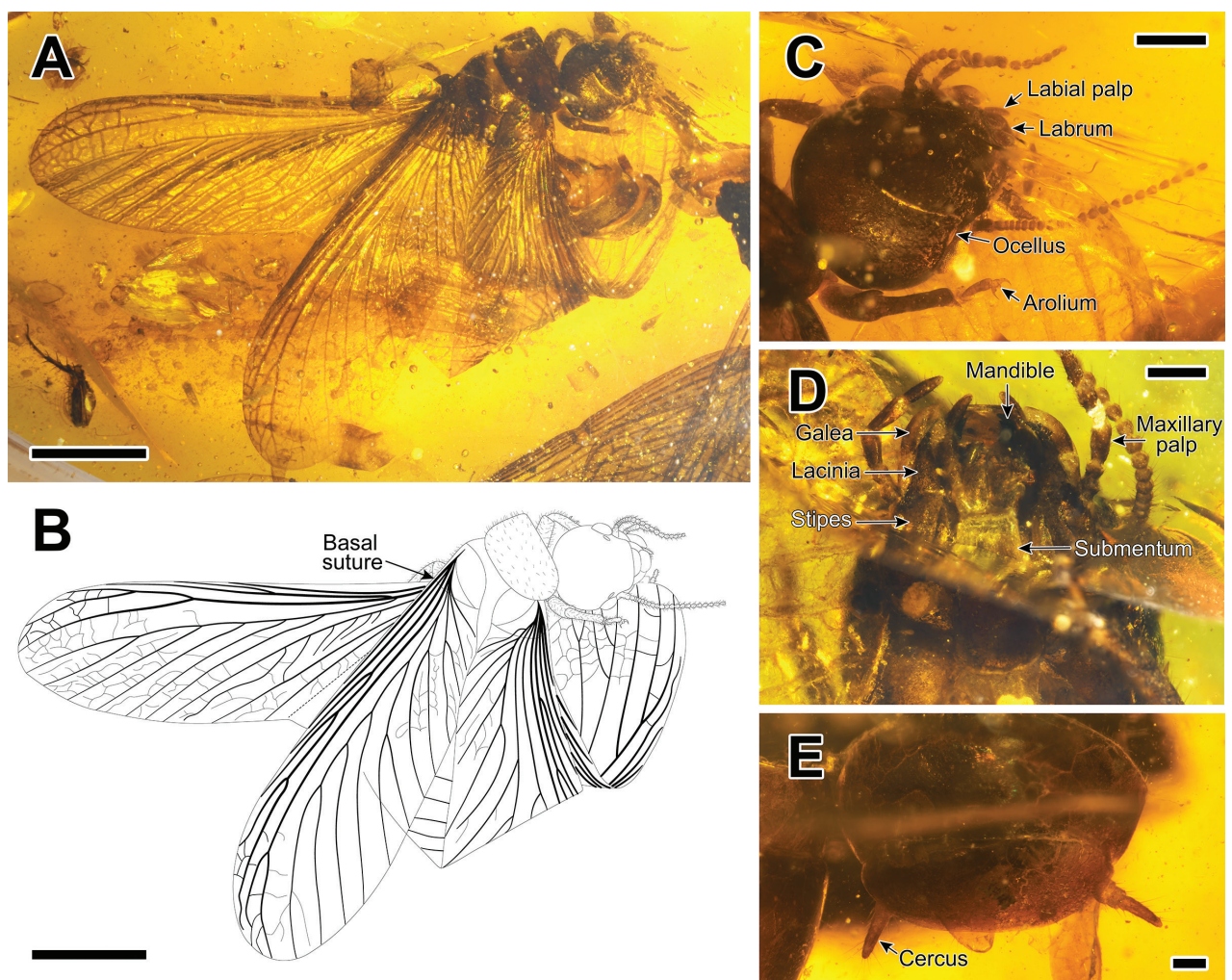


Figure 1. Photographs and drawing of *Angustitermes reflexus* gen. et sp. nov., holotype specimen CNU-TER-BU-2017005 (female imago) **A** habitus (dorsal view) **B** drawing of habitus (dorsal view) **C** head in dorsal view **D** head in ventral view **E** cerci in dorsal view. Scale bars: 4.0 mm (**A**, **B**); 1.0 mm (**C**); 0.5 mm (**D**); 0.2 mm (**E**).

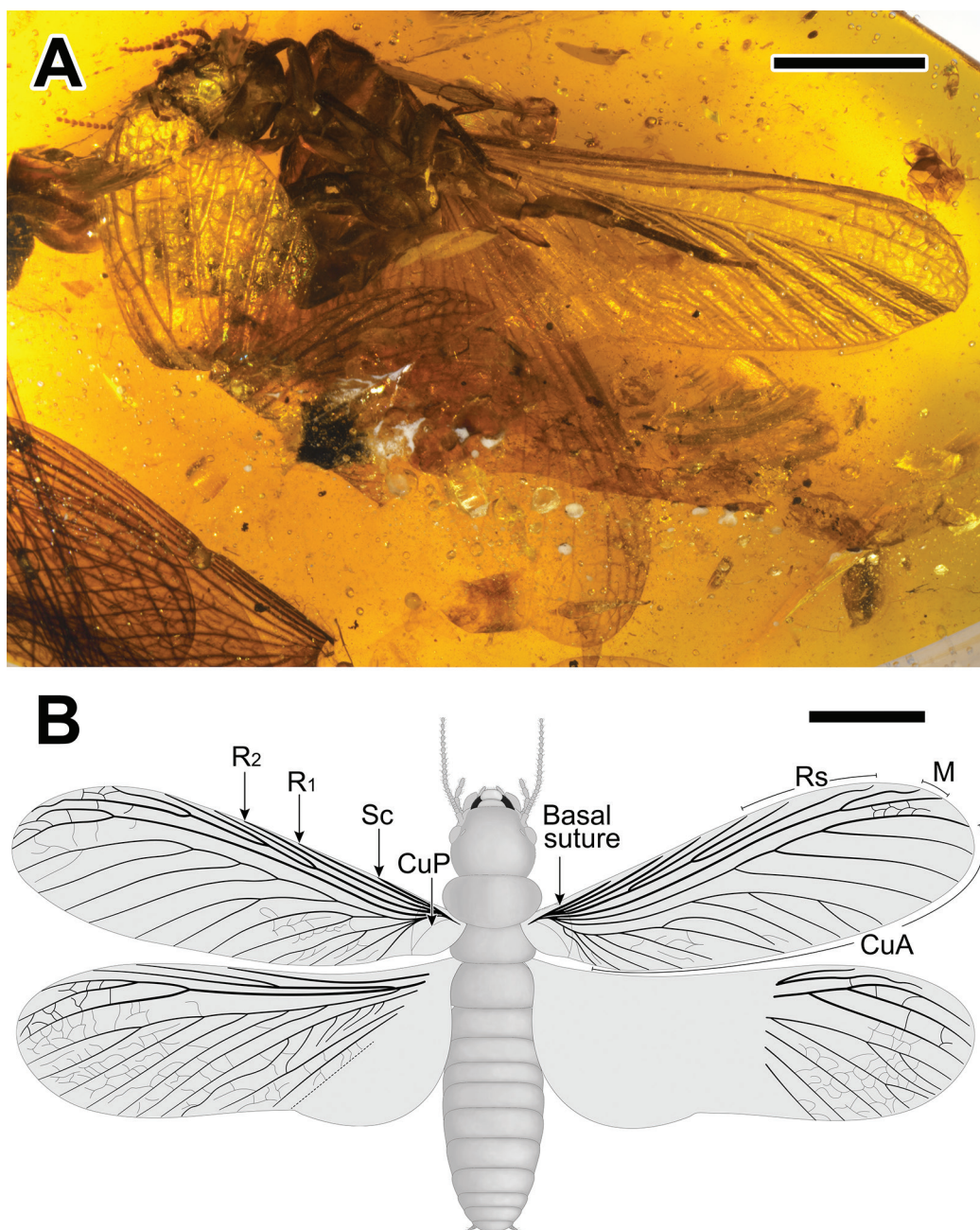


Figure 2. Photograph and drawing of *Angustitermes reflexus* gen. et sp. nov., holotype specimen CNU-TER-BU-2017005 (female imago) **A** habitus (ventral view) **B** partial reconstruction with wings unfolded. Scale bars: 4.0 mm (**A**); 4.0 mm (**B**).

Etymology. The specific name, *reflexus*, means “fold”, which is in reference to the fact that the right forewing and right hindwing of the holotype are folded. The gender is masculine to match gender of the genus.

Locality. The specimen was collected from the upper Cretaceous (Gennomanian) deposits of the Hukawng Valley, Kachin State, northern Myanmar.

Diagnosis. As for the genus.

Description. Imago: head length 3.38 mm, width 2.99 mm (excluding sizes of compound eyes), with sparse setae; labrum sclerotized, connecting to anteclypeus, width longer than length, anterior margin with short setae; apical tooth of mandibles not reaching the apex of labrum, first marginal tooth and apical tooth of left mandible divided in acute angle, other marginal teeth not visible; width of

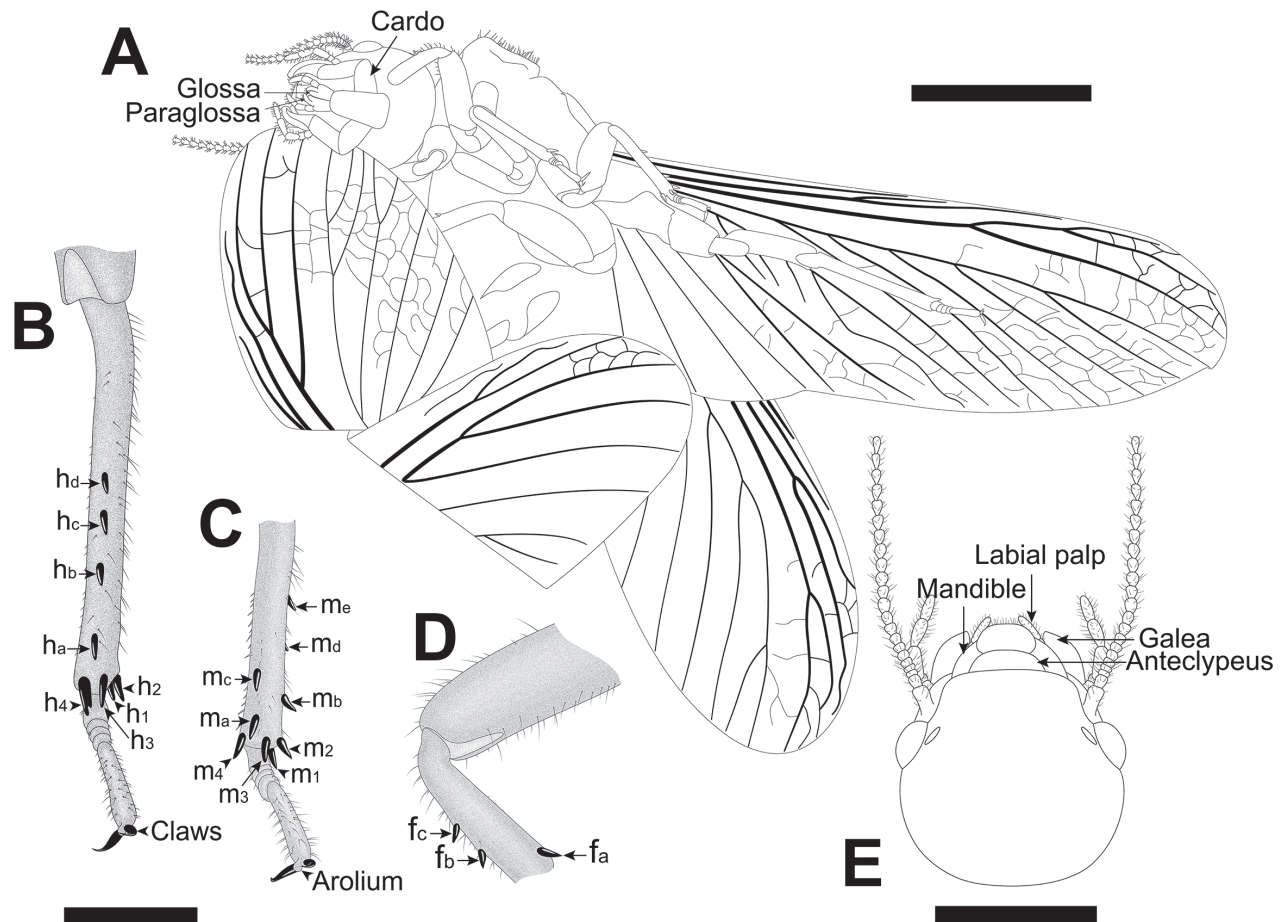


Figure 3. Drawings of *Angustitermes reflexus* gen. et sp. nov., holotype specimen CNU-TER-BU-2017005 (female imago) **A** drawing of habitus (ventral view) **B–D** drawings of femur, tibia, tarsi, arolium and claw of left hind leg, mid-leg and fore-leg, respectively **E** drawing of head in dorsal view. Scale bars: 4.0 mm (**A**); 0.5 mm (**B, C, D**); 2.0 mm in (**E**).

anteclypeus and postclypeus much longer than length; antenna with 22 articles; compound eyes hemispheric, slightly flat, diameter about 0.67 mm, lying on the middle position of the head, ommatidia diameter about 0.02 mm. Pronotum pilous, width about 3.35 mm, centronal length 1.97 mm, almost breaking away from the head. Wings long and broad with apex rounded, length 13.91 mm (excluding forewing scale), scale length 2.17 mm, wing width 5.02 mm; reticulated veins obviously pigmented among radial field and medial field, basal 5/8 of right hind wing hidden under right forewing. **Forewing:** scales with sparse setae, humeral margin convex, with weakly arched lobe present, basal suture curved; Sc simple, terminating on basal quarter of wing length; R with two branches in scale, terminating along anterior wing margin at half wing length; Radial field occupying about 1/8 wing area, left forewing with four branches, first branching at basal 1/3 of wing length, right forewing with three branches, first branching at basal 1/4 of wing length; M with two branches, branching at apical 1/5 of forewing; right CuA first branching in scale, occupying about 3/4 right forewing with three main branches, the branch near M vein branching at 1/2 of the wing length, the next branch branching near the middle of the wing to the base, and the branch near posterior margin branching in scale. **Hind wing:** basal suture not visible; large anal lobe present; left Rs with two branches branching from M at base; M with three branches. **Legs:** different degrees of damages to the legs, the left pro-

tarsus not preserved and the distal part of protibia not visible, the right mesotrochanter expanded and ruptured, and the large area of the left metacoxa broken; tibial spurs and spines not serrated. **Abdomen:** abdomen fragmentary, some of the detached abdominal segments can be observed, including the distal abdominal segments with a pair of cerci. Cerci trimerous; abdominal styli absent.

Genus *Mastotermes* Froggatt, 1897

***Mastotermes reticulatus* Jiang, Z. Zhao & Ren, sp. nov.**

<https://zoobank.org/E9A4A732-D930-4B28-B22E-41507EA2C357>

Fig. 4

Type material. Holotype. Myanmar • Kachin State, Hukawng Valley; forewing (margin partly missing) only; Kachin amber; CNU-TER-BU-2017006 (Fig. 4).

Etymology. Latin, *reticulatus*, meaning “reticulate”, which is in reference to the well-developed and clearly recognizable reticulated veins of holotype.

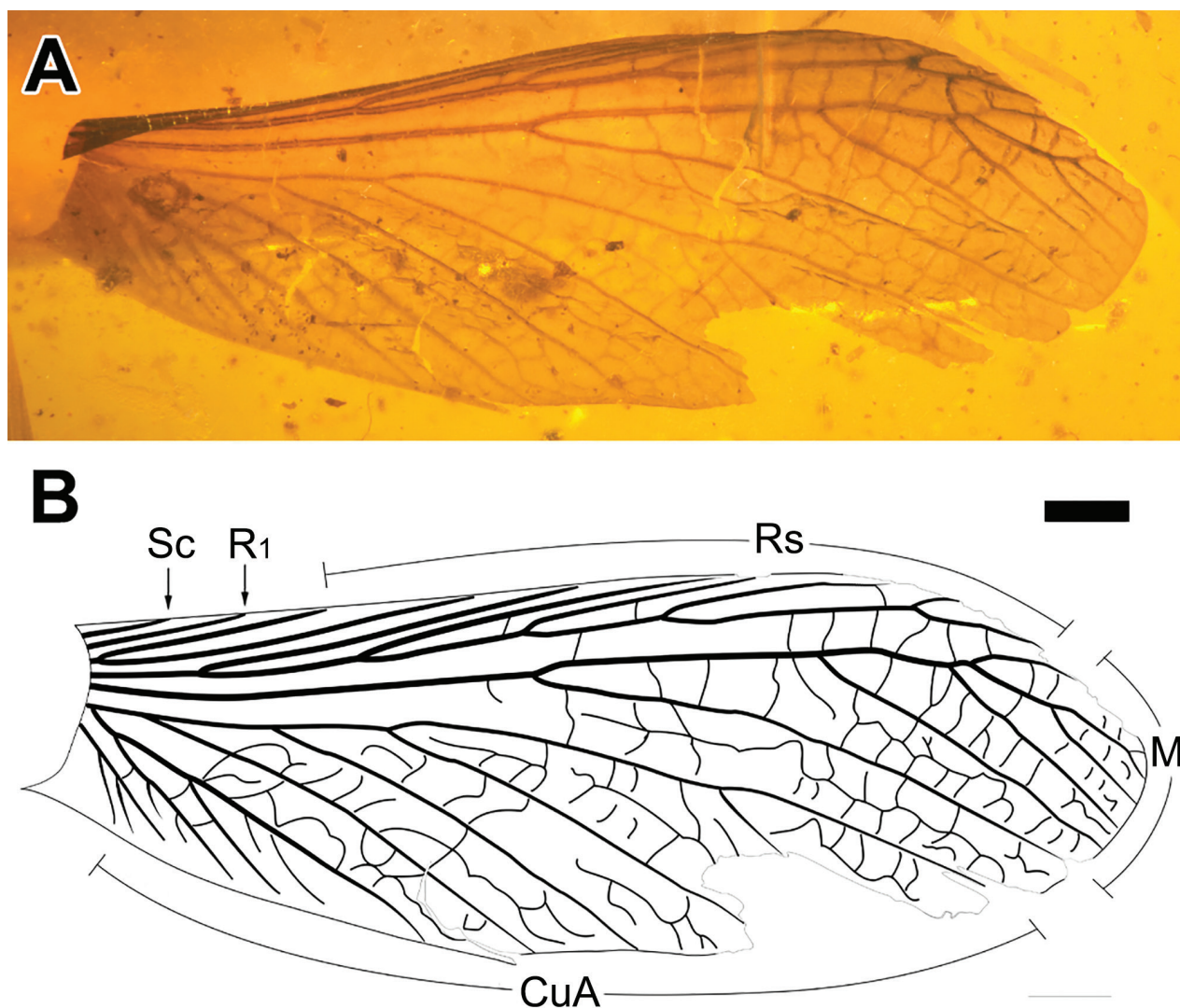


Figure 4. Photograph and drawing of *Mastotermes reticulatus* sp. nov., holotype specimen CNU-TER-BU-2017006 (isolated forewing) **A** photograph of forewing **B** drawing of forewing (with upturned part flattened). Scale bar: 1.0 mm (**A, B**).

Locality. The specimen was collected from the upper Cretaceous (Cenomanian) deposits of the Hukawng Valley, Kachin State, northern Myanmar.

Diagnosis. Forewing: wing length (excluding forewing scale) about three times as long as wide; forewing scale large; heavily reticulated, irregular bilayer structure in M and CuA, cross veins between Rs and M obvious; Sc, R, Rs, and M thickened, strongly sclerotized and obviously pigmented; Sc and R₁ simple and short; Rs with seven or eight branches, with secondary branches, running parallel to costal margin; M with six branches, first branch of M arising at forewing mid-length, secondary branches present, medial field encompassing wing apex, angle of branches and main vein gradually increasing.

Description. Forewing: forewing length (excluding forewing scale) 13.2 mm, width about 4.7 mm; suture length about 2.3 mm, strongly arched, making a sharp angle with posterior margin; distal costal margin slightly missing, posterior margin partially missing because of abrasion of the amber; base of costal margin rolled up, making the Sc and R poorly visible; Sc length 1.0 mm; R₁ length 2.0 mm, Rs with eight branches; M slightly closer to Rs than to CuA, encompassing wing apex, six branches visible, angle of branches and main vein gradually increasing, so that branches terminate closely on margin, first branch of M arising at forewing mid-length, second branch arising at about distal third of forewing length, and base of third branch close to fourth branch with secondary branch.

Remarks. The forewing of *Mastotermes reticulatus* sp. nov. is similar to that of *Mastotermes monostichus* Zhao, Eggleton & Ren, 2019, but there are some differences; the Sc, R, and Rs of *Mastotermes reticulatus* sp. nov. are closer, and there are fewer secondary branches, which makes the Rs veins parallel to the costal margin, instead of gradually narrowing as in *M. monostichus*. Compared with *M. monostichus*, the M vein of *M. reticulatus* sp. nov. is even more irregular and with fewer branches (Fig. 4). These different characteristics indicate that they are not the same species.

Discussion

The number of antennal articles in *Angustitermes reflexus* gen. et sp. nov. is only 22 (Fig. 2B), which is fewer than in most mastotermitids, especially the range of 29–32 of the extant *Mastotermes darwiniensis* (Krishna et al. 2013a), even though the antennae of many fossil termites are incompletely preserved. Another mastotermitid, *Mastotermes minutus* Nel & Bourguet, 2006 (Nel and Bourguet 2006), which was described from Early Eocene amber of Oise (France), has the fewest antennal articles, with only 20. Other mastotermitids that have been reported with complete antennae have more than 24 antennal articles. In addition to the antennae and the synapomorphies of mastotermitids, there are many similarities between *Mastotermes minutus* and *Angustitermes reflexus* gen. et sp. nov.: an ocellus is present, which indicates that they belong to the same subfamily; M of the hind wing branches from Rs, close to the wing scale; meso- and metatibiae have at least three lateral spines; tibial spurs are 3–4–4; and an arolium is present. However, these species also have some differences: the M vein of *Angustitermes reflexus* gen. et sp. nov. is closer to Rs than Cu (Fig. 2B), while the M vein of *Mastotermes minutus* is closer to Cu than to Rs. In terms of geological time, the number of antennal articles within Mastotermitidae seems to

change from many (plesiomorphic state) to few and then back to many. Further phylogenetic analysis with more fossil mastotermitids may clarify the specific trend of the evolution of the number of antennal articles in Mastotermitidae.

The sclerotized vein M of the forewings in *Angustitermes reflexus* gen. et sp. nov. are relatively simple, with only two branches and the medial fields, located in the anterior third, compressed. Concurrently, the distal-most branches of CuA, which end at the wing apex, are also thick and sclerotized, similar to M, and stronger than the other branches of CuA (Figs 2, 3A). This is opposite in the wings of *Mastotermes reticulatus* sp. nov., *Anisotermes xiai*, and *Mastotermes monostichus*, which have multibranching M in the forewing, with the basal-most branches gradually tapering and unsclerotized. Mastotermitids share a synapomorphy: the Sc, R, Rs, and M veins are thicker and much sclerotized than CuA (Engel et al. 2009; Zhao et al. 2019). The synapomorphy tends to indicate the overall degree of sclerotization present in each vein, and some branches with different locations may show different degrees of thickness and sclerotization.

Acknowledgements

We thank the editorial board of ZooKeys and express our gratitude to Prof. Scheffrahn and an anonymous reviewer for their critical and valuable reviews of the manuscript. We thank Xiaomin Yang for her kind help in the preparation of this study. We also thank Guoyi Zhang, Wei Gao, and Dawei Guo for the technical support and some useful comments.

Additional information

Conflict of interest

The authors have declared that no competing interests exist.

Ethical statement

No ethical statement was reported.

Funding

This work was supported by grants from the National Natural Science Foundation of China [nos. 32101239, 42288201, 32020103006]; Support Project of High-level Teachers in Beijing Municipal Universities in the Period of 14th Five-year Plan [no. BPHR20220114]; and Central Public-interest Scientific Institution Basal Research Fund, CAFS [no. 2023TD12].

Author contributions

Yurong Jiang: data curation, formal analysis, methodology, writing-original draft; Xinru Deng: data curation, formal analysis, methodology; Chungkun Shih: formal analysis, writing-review and editing; Yunyun Zhao: formal analysis, writing-review and editing; Dong Ren: data curation, writing-review, supervision; Zhipeng Zhao: writing-review and editing, project administration, supervision.

Author ORCIDs

Yurong Jiang  <https://orcid.org/0000-0002-7249-1377>

Chungkun Shih  <https://orcid.org/0000-0002-3434-2477>

Dong Ren  <https://orcid.org/0000-0001-8660-0901>

Zhipeng Zhao  <https://orcid.org/0000-0002-6665-8943>

Data availability

All of the data that support the findings of this study are available in the main text.

References

- Beccaloni G, Eggleton P (2013) Order Blattodea. In: Zhang Z-Q (Ed.) *Animal Biodiversity: An Outline of Higher-level Classification and Survey of Taxonomic Richness* (Addenda 2013). *Zootaxa* 3703(1): 46–48. <https://doi.org/10.11646/zootaxa.3703.1.10>
- Bezerra FI, Mendes M, De Souza O (2020) New record of Mastotermitidae from Fonseca Basin, Eocene-Oligocene boundary of southeastern Brazil. *Biologia* 75(11): 1881–1890. <https://doi.org/10.2478/s11756-020-00441-x>
- Bignell DE, Roisin Y, Lo N [Eds] (2011) *Biology of Termites: a Modern Synthesis*. Springer Science+Business Media, Springer Dordrecht, [xiv +] 576 pp. <https://doi.org/10.1007/978-90-481-3977-4>
- Breznak JA, Brune A (1994) Role of microorganisms in the digestion of lignocellulose by termites. *Annual Review of Entomology* 39(1): 453–487. <https://doi.org/10.1146/annurev.en.39.010194.002321>
- Bucek A, Šobotník J, He S, Shi M, McMahon DP, Holmes EC, Roisin Y, Lo N, Bourguignon T (2019) Evolution of termite symbiosis informed by transcriptome-based phylogenies. *Current Biology* 29(21): 3728–3734. <https://doi.org/10.1016/j.cub.2019.08.076>
- Collins RL (1925) A lower Eocene termite from Tennessee. *American Journal of Science* 5(53): 406–410. <https://doi.org/10.2475/ajs.s5-9.53.406>
- Eggleton P, Beccaloni G, Inward D (2007) Response to Lo et al. *Biology Letters* 3(5): 564–565. <https://doi.org/10.1098/rsbl.2007.0367>
- Engel MS (2008) Two new termites in Baltic amber (Isoptera). *Journal of the Kansas Entomological Society* 81(3): 194–203. <https://doi.org/10.2317/JKES-0802.01.1>
- Engel MS, Grimaldi DA, Krishna K (2007) A synopsis of Baltic amber termites (Isoptera). *Stuttgarter Beiträge zur Naturkunde. Serie B, Geologie und Palaontologie* 372: 1–20.
- Engel MS, Grimaldi DA, Krishna K (2009) Termites (Isoptera): Their phylogeny, classification, and rise to ecological dominance. *American Museum Novitates* 3650(3650): 1–27. <https://doi.org/10.1206/651.1>
- Engel MS, Currano ED, Jacobs BF (2015) The first mastotermitid termite from Africa (Isoptera: Mastotermitidae): a new species of *Mastotermes* from the early Miocene of Ethiopia. *Journal of Paleontology* 89(6): 1038–1042. <https://doi.org/10.1017/jpa.2015.73>
- Froggatt WW (1897) Australian Termitidae. Part II. *Proceedings of the Linnean Society of New South Wales* 21(4)[1896]: 510–552[+ 2 pls]. <https://doi.org/10.5962/bhl.part.8483>
- Inward D, Beccaloni G, Eggleton P (2007) Death of an order: A comprehensive molecular phylogenetic study confirms that termites are eusocial cockroaches. *Biology Letters* 3(3): 331–335. <https://doi.org/10.1098/rsbl.2007.0102>
- Jiang RX, Zhang HR, Eldredge KT, Song XB, Li YD, Tihelka E, Huang DY, Wang S, Engel MS, Cai CY (2021) Further evidence of Cretaceous termitophily: description of new termite hosts of the trichopseniine *Cretotrichopsenius* (Coleoptera: Staphylinidae), with emendations to the classification of lower termites (Isoptera). *Palaeoentomology* 4(4): 374–389. <https://doi.org/10.11646/palaeoentomology.4.4.13>

- Jouault C, Legendre F, Grandcolas P, Nel A (2021) Revising dating estimates and the antiquity of eusociality in termites using the fossilized birth–death process. *Systematic Entomology* 46(3): 592–610. <https://doi.org/10.1111/syen.12477>
- Jouault C, Engel MS, Legendre F, Huang D, Grandcolas P, Nel A (2022) Incrementing and clarifying the diversity and early evolution of termites (Blattodea: Isoptera). *Zoological Journal of the Linnean Society* 196(2): 608–629. <https://doi.org/10.1093/zoolinnean/zlac064>
- Krishna K, Emerson AE (1983) A new fossil species of termite from Mexican amber, *Mastotermes electromexicus* (Isoptera, Mastotermitidae). *American Museum Novitates* 2767: 1–8.
- Krishna K, Grimaldi DA (1991) A new fossil species from Dominican amber of the living Australian termite genus *Mastotermes* (Isoptera, Mastotermitidae). *American Museum Novitates* 3021: 1–10.
- Krishna K, Grimaldi DA, Krishna V, Engel MS (2013a) Treatise on the Isoptera of the world: Basal families. *Bulletin of the American Museum of Natural History* 377(7): 1–196. <https://doi.org/10.1206/377.1>
- Krishna K, Grimaldi DA, Krishna V, Engel MS (2013b) Treatise on the Isoptera of the world: Basal families. *Bulletin of the American Museum of Natural History* 377(7): 223–246. <https://doi.org/10.1206/377.2>
- Legendre F, Nel A, Svenson GJ, Robillard T, Pellens R, Grandcolas P (2015) Phylogeny of Dictyoptera: Dating the origin of cockroaches, praying mantises and termites with molecular data and controlled fossil evidence. *PLOS ONE* 10(7): e0130127. <https://doi.org/10.1371/journal.pone.0130127>
- Lo N, Engel MS, Cameron S, Nalepa CA, Tokuda G, Grimaldi D, Kitade O, Krishna K, Klass KD, Maekawa K, Miura T, Thompson GJ (2007) Save Isoptera: A comment on Inward et al. *Biology Letters* 3(5): 562–563. <https://doi.org/10.1098/rsbl.2007.0264>
- Nalepa CA, Lenz M (2000) The ootheca of *Mastotermes darwiniensis* Froggatt (Isoptera: Mastotermitidae): homology with cockroach oothecae. *Proceedings of the Royal Society B, Biological Sciences* 267(1454): 1809–1813. <https://doi.org/10.1098/rspb.2000.1214>
- Nel A (1986) Sur trois espèces nouvelles de termites fossiles du Stampien d’Aix-en-Provence (Bouches-du-Rhône) (Dictyoptera, Hodotermitidae, Mastotermitidae). *Entomologiste (Paris)* 42(5): 271–278.
- Nel A, Bourguet E (2006) Termite of the Early Eocene amber of France (Isoptera: Mastotermitidae, Kalotermitidae). *Neues Jahrbuch für Geologie und Paläontologie. Monatshefte* 2006(2): 101–115. <https://doi.org/10.1127/njgpm/2006/2006/101>
- Riek EF (1952) Fossil insects from the Tertiary sediments at Dinmore, Queensland. *Papers from the Department of Geology, University of Queensland* 4(2): 17–22.
- Sanderson MG (1996) Biomass of termites and their emissions of methane and carbon dioxide: A global database. *Global Biogeochemical Cycles* 10(4): 543–557. <https://doi.org/10.1029/96GB01893>
- Schlüter T (1989) Neue Daten über harzkonservierte Arthropoden aus dem Cenomanium NW-Frankreichs. *Documenta Naturae (München)* 56(5): 59–70[+ 6 pls].
- Shi GH, Grimaldi DA, Harlow GE, Wang J, Wang J, Yang MC, Lei WY, Li QL, Li XH (2012) Age constraint on Myanmar amber based on U-Pb dating of zircons. *Cretaceous Research* 37: 155–163. <https://doi.org/10.1016/j.cretres.2012.03.014>
- Sugimoto A, Bignell DE, MacDonald JA (2000) Global impact of termites on the carbon cycle and atmospheric trace gases. In: Abe T, Bignell DE, Higashi M (Eds) *Termites: evolution, sociality, symbioses, ecology*, 409–435. Kluwer Academic Publishers, Dordrecht, [xxii +] 466 pp. https://doi.org/10.1007/978-94-017-3223-9_19

- Thompson GJ, Kitade O, Lo N, Crozier RH (2000) Phylogenetic evidence for a single ancestral origin of a “true” worker caste in termites. *Journal of Evolutionary Biology* 13(6): 869–881. <https://doi.org/10.1046/j.1420-9101.2000.00237.x>
- Thorne BL, Grimaldi DA, Krishna K (2000) Early Fossil History of the Termites. In: Abe T, Bignell DE, Higashi M (Eds) *Termites: Evolution, Sociality, Symbioses, Ecology*. Springer, Dordrecht, 77–93. https://doi.org/10.1007/978-94-017-3223-9_4
- Tuma J, Eggleton P, Fayle TM (2020) Ant-termite interactions: An important but under-explored ecological linkage. *Biological Reviews of the Cambridge Philosophical Society* 95(3): 555–572. <https://doi.org/10.1111/brv.12577>
- Vršanský P, Aristov D (2014) Termites (Isoptera) from the Jurassic/Cretaceous boundary: Evidence for the longevity of their earliest genera. *European Journal of Entomology* 111(1): 137–141. <https://doi.org/10.14411/eje.2014.014>
- Wappler T, Engel MS (2006) A new record of *Mastotermes* from the Eocene of Germany (Isoptera: Mastotermitidae). *Journal of Paleontology* 80(2): 380–385. [https://doi.org/10.1666/0022-3360\(2006\)080\[0380:ANROMF\]2.0.CO;2](https://doi.org/10.1666/0022-3360(2006)080[0380:ANROMF]2.0.CO;2)
- Xiao B, Chen AH, Zhang YY, Jiang GF, Hu CC, Zhu CD (2012) Complete mitochondrial genomes of two cockroaches, *Blattella germanica* and *Periplaneta americana*, and the phylogenetic position of termites. *Current Genetics* 58(2): 65–77. <https://doi.org/10.1007/s00294-012-0365-7>
- Zhao ZP, Eggleton P, Yin XC, Gao TP, Shih CK, Ren D (2019) The oldest known mastotermitids (Blattodea: Termitoidae) and phylogeny of basal termites. *Systematic Entomology* 44(3): 612–623. <https://doi.org/10.1111/syen.12344>
- Zhao ZP, Yin XC, Shih CK, Gao TP, Ren D (2020) Termite colonies from mid-Cretaceous Myanmar demonstrate their early eusocial lifestyle in damp wood. *National Science Review* 7(2): 381–390. <https://doi.org/10.1093/nsr/nwz141>
- Zhao ZP, Shih CK, Gao TP, Ren D (2021) Termite communities and their early evolution and ecology trapped in Cretaceous amber. *Cretaceous Research* 117: 104612. <https://doi.org/10.1016/j.cretres.2020.104612>

Development of a multi-entry identification key for economically important fruit fly larvae (Diptera, Tephritidae, Dacinae)

Welma Pieterse¹, Marc De Meyer², Massimiliano Virgillio², Pia Addison¹

¹ Department of Conservation Ecology and Entomology, Stellenbosch University, Stellenbosch, 7600, South Africa

² Biology Department, Royal Museum for Central Africa, Leuvensesteenweg 13, Tervuren, 3080, Belgium

Corresponding author: Pia Addison (pia@sun.ac.za)

Abstract

Identification of fruit fly larvae is difficult due to the limited morphological characteristics present. However, this is the stage at which fruit flies are intercepted at ports of entry through horticultural imports. Molecular tools are useful but are time-consuming and expensive compared to morphological identifications. This project aims to use available information from the literature and our own research to build a multi-entry identification key for thirteen tephritid species and species groups that are of economic concern for the European Union. Third-instar larvae were obtained from different regions and hosts. Thirteen species or representatives of species groups were obtained, including *Ceratitis*, *Dacus*, *Bactrocera* and *Zeugodacus* spp. The cephalopharyngeal skeletons were dissected out, cleared in a 10% NaOH solution, dehydrated and mounted in Euparal on glass slides. Images of at least 20 larvae/species were captured using a compound microscope fitted with a camera. Measurements were taken of the mounted mandibles and the number of tubules and their position in the anterior spiracles in relation to the cephalic skeleton were noted. Differences between morphometric parameters were tested via ANOVA and verified using discriminant function analysis. A matrix was compiled including nine characters for which significant inter-specific differentiation was preliminarily detected. The key was converted into a mobile application by LucID.

Key words: Identification tool, interactive key, larvae, LucID, mandible



Academic editor: Vera Silva

Received: 5 December 2023

Accepted: 7 March 2024

Published: 10 April 2024

ZooBank: <https://zoobank.org/9D1740FB-E52D-4A9A-8048-4619491EBB81>

Citation: Pieterse W, De Meyer M, Virgilio M, Addison P (2024) Development of a multi-entry identification key for economically important fruit fly larvae (Diptera, Tephritidae, Dacinae). ZooKeys 1197: 127–136. <https://doi.org/10.3897/zookeys.1197.116887>

Copyright: © Welma Pieterse et al. This is an open access article distributed under terms of the Creative Commons Attribution License ([Attribution 4.0 International – CC BY 4.0](https://creativecommons.org/licenses/by/4.0/)).

Introduction

The family Tephritidae has more than 4000 species distributed globally (White and Elson-Harris 1992). The larvae of about 35% of the species attack fruit, including horticultural crops of economic importance (White and Elson-Harris 1992). Fruit flies are among the most destructive pests of these crops and are of quarantine importance for export markets (Ekesi et al. 2006, 2016). As the larvae feed inside fruit, this is the life stage detected during inspection for import or export. However, larvae are difficult to identify morphologically (Frías et al. 2008; Dutra et al. 2012). In the absence of an identification tool to identify the larvae rapidly and quickly, the consignments are usually rejected.

The majority of the thirteen species studied here are at risk of being intercepted when entering Europe through imported fruit, namely, *Ceratitis rosa* s.l. Karsch (Natal fruit fly), *Ceratitis cosyra* (Walker) (Mango fruit fly), *Bactrocera dorsalis* (Hendel) (Oriental fruit fly), *Zeugodacus cucurbitae* (Coquillett) (Melon fruit fly) and *Bactrocera zonata* (Saunders) (Peach fruit fly). All are considered potential quarantine pests for the European Union (EU) and are listed as such in the Commission Implementing Regulation 2019/2072 and amending Implementing Regulation 2021/2285. In addition, *B. dorsalis* and *B. zonata* have also been included in the list of priority pests in EU regulation 2019/1702. *Zeugodacus cucurbitae*, *Bactrocera minax* (Enderlein) (Chinese citrus fly), *Bactrocera tryoni* (Froggatt) (Queensland fruit fly), *B. dorsalis* and *C. rosa* are listed as A1 quarantine pests in the European and Mediterranean Plant Protection Organization (EPPO) countries (EPPO 2022a). *Bactrocera zonata*, *Ceratitis capitata* (Wiedemann) (Mediterranean fruit fly) and *Dacus ciliatus* Loew (Ethiopian fruit fly) are listed on the A2 EPPO list (EPPO 2022b). *Zeugodacus tau* Walker (Pumpkin fruit fly) is mainly a pest of Cucurbitaceae and occurs in Asia and Oceania (Jaleel et al. 2018). Guava and Mango are the main hosts for *Bactrocera correcta* (Bezzi) (Guava fruit fly), which occurs mainly in Asia (Liu et al. 2019).

Being able to make a correct identification of insect species in the shortest possible period of time is essential to comply with international biosecurity measures, since not all species are of quarantine importance in all countries (Boykin et al. 2012). Several keys for the identification of adult specimens are available (White and Elson-Harris 1992; Virgilio et al. 2014). Descriptions of larvae of some species are given by White and Elson-Harris 1992, but other authors give more detailed descriptions of the larvae of some species (Elson-Harris 1988; Carroll and Wharton 1989; Carroll 1998; Carroll et al. 2004 onwards; Frías et al. 2008; Lasserre et al. 2009; Steck and Ekesi 2015; Balmes and Mouttet 2017; Dutra et al. 2018a, b; Kamayev et al. 2020; Rodriguez et al. 2021). However, this information is not always easy to access, and the keys are difficult to follow unless specialized expertise is available.

The presence or absence of a preapical tooth on the mandible can be used as a distinguishing characteristic in a taxonomic key, but since the characteristics of the mouthparts of tephritid species are not known for all species, it could be a controversial character to use. White and Elson-Harris (1992) state that the preapical tooth is absent in third-instar larvae of *C. capitata*, while Carroll et al. (2004) indicate that it might be present in only some specimens. The presence of a preapical tooth on the mandibles is also variable according to Steck and Ekesi (2015), while Balmes and Mouttet (2017) use the presence/absence of the preapical tooth as a diagnostic characteristic in their key. Kamayev et al. (2020) argue that the preapical tooth is too variable to use as a taxonomic characteristic.

According to Pieterse et al. (2017), the shape of the mandibles of fruit fly larvae of *B. dorsalis*, *C. capitata*, *C. rosa* s.s. and *C. cosyra* can be used to distinguish between the third-instar larvae of the species studied. Since shape analysis (which was used in the aforementioned article) is an involved process not suitable for use in a routine diagnostic laboratory, a set of measurements of the cephalic skeleton of third-instar tephritid larvae was designed in the current study that can be used in a robust taxonomic multi-entry key.

Lucid® (<https://keys.lucidcentral.org/search/>) was developed at the University of Queensland (Norton et al. 2000) and is a multimedia identification and

training tool. It is a multi-entry key, as opposed to a traditional dichotomous key, making it more user-friendly for scientists who do not have expert knowledge of the taxonomy of Tephritidae larvae. Multi-entry keys allow the user to choose the characteristics they want to use based on the availability of characters on each specimen. The characters used are also illustrated or imaged for ease of reference. Multi-entry keys have been developed using the LucID platform for adult fruit flies, such as the keys to African frugivorous flies by Virgilio et al. (2014) and the key to adult fruit flies of *Bactrocera* and related genera developed by Doorenweerd et al. (2022).

Multi-entry keys have several benefits over molecular identification tools, namely, they are more accessible and cost-effective; they can be used anywhere without specialised equipment, and the answer is obtained quickly. The key developed here is converted into a mobile application by LucID, for both Android and Apple devices, making it freely available. Multi-entry keys can, furthermore, be used on specimens that are too degraded to be used for DNA analysis. Larval mouth hooks are heavily sclerotized and can still be used even when a specimen is degraded. The aim of the key is to provide a practical identification tool for third-instar fruit fly larvae that are commonly intercepted in the EU.

Materials and methods

Preparation of slides. Larvae from 13 species were obtained from colonies from various laboratories around the world and were preserved in 70% ethanol. The heads of the larvae were cut off and cleared by heating in 10% NaOH. The cephalopharyngeal skeletons (Fig. 1) of the larvae of all species were removed, dehydrated with alcohol (70–100%) and mounted in Euparal (Agar Scientific) on glass slides. Images of the slides were captured using a Zeiss compound microscope (MZ 16A) fitted with an Axiocam digital camera (DFC 295). Measurements were taken using ZEN imaging software from the Zeiss MZ 16A.

Fig. 2 shows the various measurements for parameters without (Fig. 2A) and with (Fig. 2B) a preapical tooth.

Images of the cephaloskeleton and anterior spiracles of ten larvae per species were taken in the same way. The position of the anterior spiracles in relation to the cornua and the number of tubules were recorded for each species (Fig. 3).

Data analysis

Discriminant function analysis with classification functions was carried out to statistically allocate the specimens to the species studied using the recorded mandible measurements in Statistica v. 14.1.0 (TIBCO Software Inc, Palo Alto, CA, USA). Measurements for all the specimens of the same species were pooled for these analyses.

Results and discussion

A total of 873 mandibles from thirteen species were mounted on slides and examined (Table 1). The raw data of all measurements are listed in the Suppl. material 1.

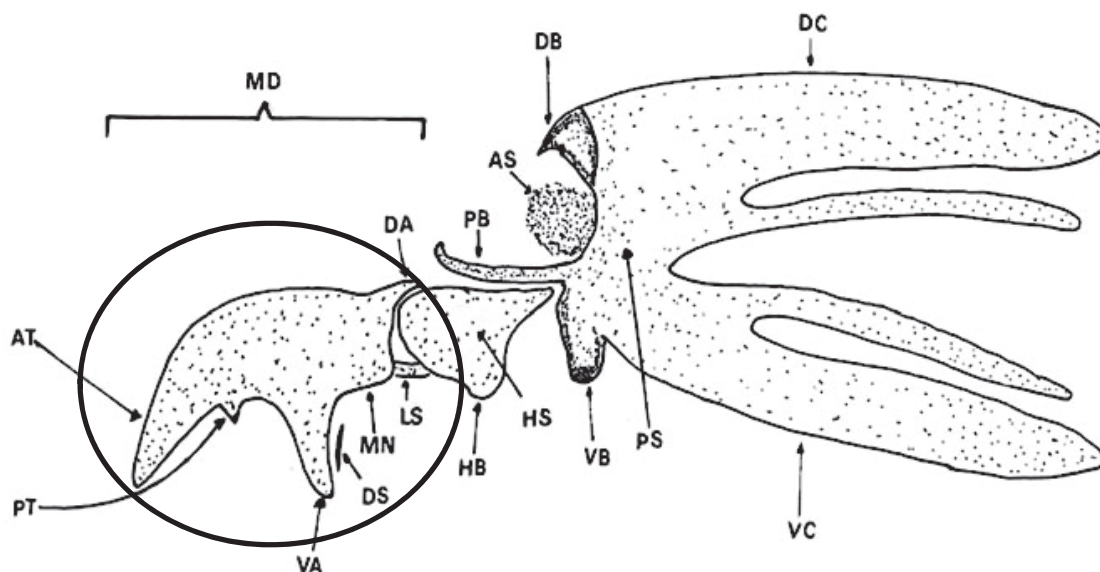


Figure 1. Cephalopharyngeal skeleton of 3rd instar larva, lateral view. Region of interest circled. Abbreviations used in LucID key: AT = Apical Tooth; DA = Dorsal Apodeme; DS = Dental Sclerite; MD = Mandible; MN = Mandibular Neck; PT = Preapical Tooth; VA = Ventral Apodeme (from: Frías et al. 2006).

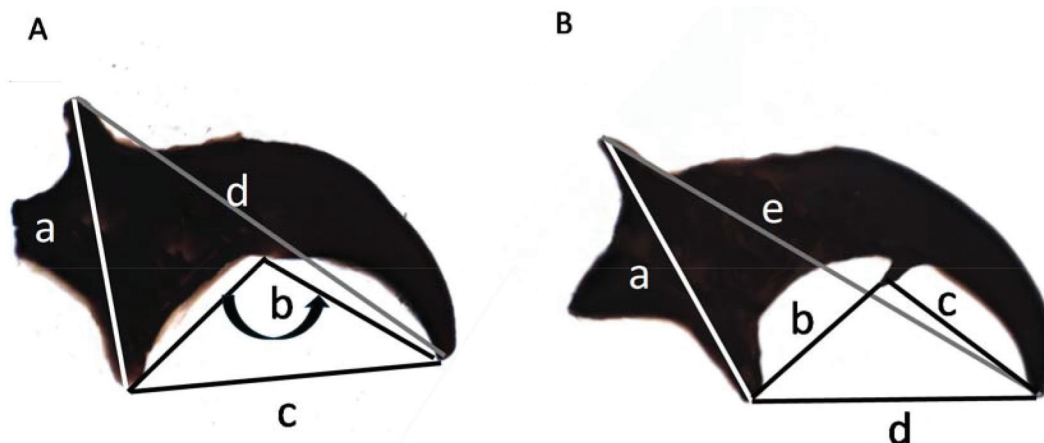


Figure 2. **A, B** Images of a typical tephritid mandible indicating the areas measured. Image **(A)** indicates the measurements for the mandibles without a preapical tooth and **(B)** indicates the measurements for the mandibles where the preapical tooth is present. Measurements are as follows for **A**: (a) the distance between the dorsal apodeme and the ventral apodeme; (b) the ventral angle between the apical tooth and the ventral apodeme; (c) the distance between the ventral apodeme and the apical tooth; (d) the distance between the dorsal apodeme and the apical tooth. Measurements are as follows for **B**: (a) the distance between the dorsal apodeme and the ventral apodeme; (b) the distance between the ventral apodeme and the preapical tooth; (c) the distance between the apical tooth and the preapical tooth; (d) the distance between the ventral apodeme and the apical tooth; (e) the distance between the dorsal apodeme and the apical tooth. Measurements were recorded in μm (distances) and degrees (angles).

We did not see a prominent preapical tooth in any of the mandibles of *C. capitata* third-instar larvae that we examined, so we used the presence/absence of the preapical tooth as one of the distinguishing characteristics in the key. The characteristics and measurements (Table 2), as well as the geographical distribution, the number of tubules and the position of the anterior spiracles in relation to the cornua, were used to compile a LucID key that can be used to identify the third-instar larvae of the species listed in Table 1.

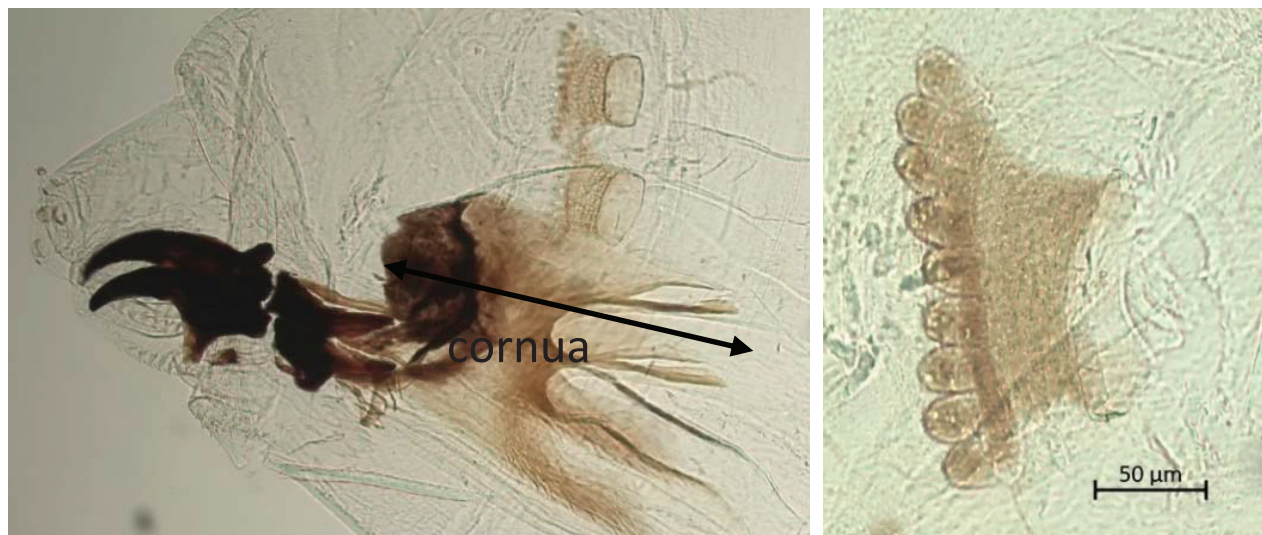


Figure 3. Lateral view of the cephaloskeleton and anterior spiracles of *Bactrocera correcta* indicating the position of the front spiracles in relation to the cornua (left) and image of the anterior spiracle of *Bactrocera dorsalis* showing 9 tubules (right).

Table 1. Species, origin, and sample size of mandibles used to develop a multi-entry key of tephritid larvae of economic importance to the European Union.

Species	Origin	Number of mandibles measured
<i>Bactrocera correcta</i>	IAEA Vienna colony	51
<i>Bactrocera dorsalis</i>	Quarantine Station Stellenbosch colony	18
<i>Bactrocera dorsalis</i>	Atomic Energy Research Establishment Baipayl, Bangladesh colony	13
<i>Bactrocera dorsalis</i>	IAEA Vienna colony	24
<i>Bactrocera dorsalis</i>	CRI Nelspruit South Africa colony	24
<i>Bactrocera dorsalis</i>	University of Pretoria colony	20
<i>Bactrocera minax</i>	Changsa, Hunan, China colony	17
<i>Bactrocera oleae</i>	IAEA Vienna, colony	29
<i>Bactrocera oleae</i>	Madrid, Spain, olives	18
<i>Zeugodacus tau</i>	IAEA Vienna, colony	20
<i>Zeugodacus tau</i>	Atomic Energy Research Establishment Baipayl, Bangladesh, colony	22
<i>Bactrocera tryoni</i>	Queensland University of Technology, Brisbane, Australia, colony	16
<i>Bactrocera tryoni</i>	IAEA Vienna, colony	37
<i>Bactrocera zonata</i>	The "Israel Cohen" Institute for Biological Control, Yehud-Monosson, Israel, colony	24
<i>Bactrocera zonata</i>	Atomic Energy Research Establishment Baipayl, Bangladesh, colony	18
<i>Bactrocera zonata</i>	IAEA Vienna, colony	14
<i>Bactrocera zonata</i>	CIRAD La Réunion, colony	45
<i>Ceratitis capitata</i>	The "Israel Cohen" Institute for Biological Control, Yehud-Monosson, Israel, colony	19
<i>Ceratitis capitata</i>	Plant Quarantine Station, Stellenbosch, South Africa, colony	21
<i>Ceratitis capitata</i>	CRI Nelspruit South Africa, colony	11
<i>Ceratitis capitata</i>	Citrus, Plant Quarantine Station, Stellenbosch, South Africa	4
<i>Ceratitis capitata</i>	Nectarine, Plant Quarantine Station, Stellenbosch, South Africa	8
<i>Ceratitis capitata</i>	CIRAD La Réunion colony	19
<i>Ceratitis capitata</i>	Greece, Bitter orange	11
<i>Ceratitis capitata</i>	CIRAD La Réunion, wild host	18
<i>Ceratitis cosyra</i>	CRI Nelspruit South Africa colony	74

Species	Origin	Number of mandibles measured
<i>Ceratitis quilicii</i>	CRI Nelspruit South Africa colony	63
<i>Ceratitis rosa</i>	CRI Nelspruit South Africa colony	67
<i>Dacus ciliatus</i>	Piketberg, South Africa, Pumpkin	19
<i>Dacus ciliatus</i>	Eduardo Mondlane University, Maputu, Mozambique, Cucumber	20
<i>Zeugodacus cucurbitae</i>	Atomic Energy Research Establishment Baipayl, Bangladesh colony	30
<i>Zeugodacus cucurbitae</i>	IAEA Vienna colony	20
<i>Zeugodacus cucurbitae</i>	CIRAD La Réunion colony	14

Table 2. Average, minimum, and maximum distances (µm) and angles (°) that were used to compile the LucID key for thirteen species of fruit fly larvae of economic importance to the European Union.

Prominent preapical tooth absent				
	<i>Bactrocera dorsalis</i>	<i>Bactrocera zonata</i>	<i>Ceratitis capitata</i>	<i>Bactrocera oleae</i>
Distance a (µm)	168 (144–195)	156 (131–171)	141 (130–154)	133 (113–151)
Angle b (°)	102 (87–117)	107 (96–129)	103 (94–116)	103 (93–120)
Distance c (µm)	174 (146–214)	152 (128–180)	130 (113–151)	115 (96–132)
Distance d (µm)	279 (241–326)	252 (203–329)	213 (186–236)	194 (152–215)
	<i>Bactrocera tryoni</i>	<i>Bactrocera correcta</i>	<i>Bactrocera minax</i>	
Distance a (µm)	156 (139–169)	148 (132–161)	278 (253–301)	
Angle b (°)	107 (96–116)	106 (77–120)	110 (101–121)	
Distance c (µm)	156 (144–172)	157 (134–188)	282 (265–303)	
Distance d (µm)	242 (222–262)	257 (232–285)	424 (398–456)	
	<i>Ceratitis rosa</i>	<i>Ceratitis quilicii</i>	<i>Ceratitis cosyra</i>	<i>Zeugodacus cucurbitae</i>
Distance a (µm)	149 (134–167)	161 (147–179)	151 (138–168)	194 (163–223)
Distance b (µm)	107 (96–119)	98 (86–110)	96 (82–106)	135 (105–169)
Distance c (µm)	73 (65–84)	74 (64–79)	79 (69–90)	85 (64–102)
Distance d (µm)	149 (132–171)	148 (127–160)	149 (132–146)	186 (150–225)
Distance e (µm)	233 (202–257)	241 (221–265)	239 (212–263)	299 (245–340)
	<i>Dacus ciliatus</i>	<i>Zeugodacus tau</i>		
Distance a (µm)	169 (153–188)	198 (169–224)		
Distance b (µm)	109 (93–121)	139 (112–160)		
Distance c (µm)	47 (40–60)	92 (83–101)		
Distance d (µm)	148 (129–164)	190 (167–211)		
Distance e (µm)	250 (230–267)	315 (279–357)		

Bactrocera zonata, *B. tryoni* and *B. correcta* could not be identified reliably without including distribution data as well as the position of the spiracle, indicating a percentage correct identification of below 61% based on the discriminant function analysis (Table 3). *Bactrocera correcta* was misidentified as *B. zonata* in 27% (14 out of 54) of cases, while *B. zonata* was only identified correctly in 56.43% of cases, often being confused with *B. correcta* and *B. tryoni* (Table 3). However, if the position of the spiracle relative to the cornua was included, *B. correcta* could be distinguished from *B. tryoni* and *B. zonata*. *Ceratitis rosa* and *C. quilicii* can be identified with more than 75% certainty based on the distance between the dorsal apodeme and the ventral apodeme as well as the distance between the ventral apodeme and the apical tooth (Table 4). Overall, it was found that species with a secondary tooth were identified with more accuracy than those without.

Table 3. Classification matrix of the species where a secondary tooth is absent on the mandibles. Rows: Observed classifications; Columns: Predicted classifications.

Species	Percent Correct	p-value	Bd	Cc	Bz	Bo	Bt	Bc	Bm
<i>Bactrocera dorsalis</i> (Bd)	93.12	0.2985	149	0	4	0	0	7	0
<i>Ceratitis capitata</i> (Cc)	97.19	0.1996	0	104	1	1	0	1	0
<i>Bactrocera zonata</i> (Bz)	56.43	0.1884	6	10	57	0	14	14	0
<i>Bactrocera oleae</i> (Bo)	80.85	0.0877	0	9	0	38	0	0	0
<i>Bactrocera tryoni</i> (Bt)	49.06	0.0989	0	1	25	0	26	1	0
<i>Bactrocera correcta</i> (Bc)	60.78	0.0951	5	1	14	0	0	31	0
<i>Bactrocera minax</i> (Bm)	100	0.0317	0	0	0	0	0	0	17
Total	78.73		160	125	101	39	40	54	17

Table 4. Classification matrix of the species where a secondary tooth is present on the mandibles. Rows: Observed classifications; Columns: Predicted classifications.

Species	Percent Correct	P-value	Cr	Cq	Cc	Zc	Dc	Bt
<i>Ceratitis rosa</i> (Cr)	94.03	0.1988	63	3	1	0	0	0
<i>Ceratitis quilicii</i> (Cq)	79.36	0.1869	6	50	7	0	0	0
<i>Ceratitis cosyra</i> (Cc)	66.13	0.1840	9	12	41	0	0	0
<i>Zeugodacus cucurbitae</i> (Zc)	75	0.1899	0	3	0	48	0	13
<i>Dacus ciliatus</i> (Dc)	100	0.1157	0	0	0	0	39	0
<i>Zeugodacus tau</i> (Zt)	76.19	0.1246	0	0	0	10	0	32
Total	81.01		78	68	49	58	39	45

Balmes and Mouttet (2017) combine morphological characteristics including the presence of a preapical tooth, the number of tubules in the anterior spiracle and the number of oral ridges in their key. We found that it was difficult to consistently produce slide-mounted mandibles of high enough quality to see all the characteristics used. In their description of the third-instar larvae of members of the *Ceratitis* FAR complex, Steck and Ekesi (2015) relied on electron microscope images, which are not practical for use in a routine diagnostic laboratory. Frías et al. (2006, 2008) also used electron microscope images to visualise some characteristics. The multi-entry key published by Carroll et al. (2004 onwards) uses a combination of characteristics that can be observed using a dissection microscope, slides prepared for visualising using a compound microscope and slides prepared to visualise using scanning electron microscopy (SEM). Using this key requires access to an SEM and specialist knowledge of larval morphology.

The LucID key was transformed to an app that can be downloaded from Google Play store (for Android) or Apple App store (for Apple phones). https://play.google.com/store/apps/details?id=com.lucidcentral.mobile.lucid.fruit_fly_larvae&hl=en-US&ah=RArn8-TSJV3KC1m-QBBa0Vfcz7s.

This is the first time a multi-entry key for tephritid larvae of economic significance has been developed in app format. While the characters rely mostly on measurements, it does require some knowledge of how to prepare the mouthparts so that measurements of specific distances can be made. However, it will be a valuable tool for enabling non-molecular identifications of fruit fly larval pests in fruit.

Acknowledgements

We are grateful to Anthony Clarke, Australia; Domingos Cugala Mozambique; Hélène Delatte, CIRAD, Reunion; Marc de Meyer, Africa Museum, Belgium; Yoav Gazit, Israel; Manuel González Núñez, Spain; Minette Karsten, Pretoria, South Africa Mahfuza Khan, Bangladesh; Aruna Manrakhan, Nelspruit, South Africa, Rui Pereira, IAEA Vienna, Ronald Ramukhesa and Saadiek Rosenberg, DALRRD, South Africa who sent us the larval specimens used in this project. Thank you to the Entomological Society of Israel for permission to use the image of the cephalopharyngeal skeleton in Fig. 1. This manuscript has received the general approval of the committee (John Terblanche, Hélène DeLatte and Nikos Papadopoulos) on 1 December 2023

Additional information

Conflict of interest

The authors have declared that no competing interests exist.

Ethical statement

No ethical statement was reported.

Funding

This study was funded by the European Union's Horizon 2020 Research and Innovation Program FFIPM (grant agreement No 818184) and the Standards and Trade Development Facility's project Fruit Fly Free STDF/PG/567.


Author contributions

Conceptualization: MDM, PA. Data curation: WP. Formal analysis: WP. Funding acquisition: MV. Methodology: MDM, PA. Software: MV. Writing - original draft: WP. Writing - review and editing: MDM, MV, PA.

Author ORCIDs

Welma Pieterse  <https://orcid.org/0000-0002-1290-8636>

Marc De Meyer  <https://orcid.org/0000-0003-0755-2898>

Massimiliano Virgillio  <https://orcid.org/0000-0002-1323-6886>

Pia Addison  <https://orcid.org/0000-0002-8227-339X>

Data availability

The raw data supporting the conclusions of this article will be made available by the authors, without undue reservation.

References

- Balmes V, Mouttet R (2017) Development and validation of a simplified morphological identification key for larvae of tephritid species most commonly intercepted at import in Europe. *Bulletin OEPP. EPPO Bulletin. European and Mediterranean Plant Protection Organisation* 47(1): 91–99. <https://doi.org/10.1111/epp.12369>
- Boykin LM, Armstrong KF, Kubatko L, De Barro P (2012) Species delimitation and global biosecurity. *Evolutionary Bioinformatics Online* 8: 1–37. <https://doi.org/10.4137/EBO.S8532>

- Carroll LE (1998) Description of the third instar larva of *Ceratitis rosa* Karsch (Diptera: Tephritidae). *Proceedings of the Entomological Society of Washington* 100(1): 88–94. <http://www.biodiversitylibrary.org/item/54709>
- Carroll LE, Wharton RA (1989) Morphology of the immature stages of *Anastrepha ludens* (Diptera: Tephritidae). *Annals of the Entomological Society of America* 82(2): 201–214. <https://doi.org/10.1093/aesa/82.2.201>
- Carroll LE, Norrbom AL, Dallwitz MJ, Thompson FC (2004) [onwards] Pest fruit flies of the world – larvae. Version: 9th April 2019. www.delta-intkey.com
- Doorenweerd C, Anderson CT, Leblanc L, San Jose M, Rubinoff D, Geib S, Barr N (2022) Adult fruit fly identification of *Bactrocera* and allied genera using the Lucid multi-entry key platform (Diptera: Tephritidae: Dacinae: Dacini). <https://idtools.org/tools/2103/> [Last accessed: 21/08/2023]
- Dutra VS, Ronchi-Teles B, Steck GJ, Silva JG (2012) Description of larvae of *Anastrepha* spp. (Diptera: Tephritidae) in the *fraterculus* group. *Annals of the Entomological Society of America* 105(4): 529–538. <https://doi.org/10.1603/AN11180>
- Dutra VS, Ronchi-Teles B, Steck GJ, Rodriguez EJ, Norrbom AL, Sutton BD, Silva JG (2018a) Description of the Larvae of *Anastrepha curitis*, *Anastrepha pickeli* and *Anastrepha pulchra* (Diptera: Tephritidae). *Proceedings of the Entomological Society of Washington* 120(1): 9–24. <https://doi.org/10.4289/0013-8797.120.1.9>
- Dutra VS, Ronchi-Teles B, Steck GJ, Araujo EL, Souza-Filho MF, Raga A, Silva JG (2018b) Description of larvae of three *Anastrepha* species in the *fraterculus* group (Diptera: Tephritidae). *Proceedings of the Entomological Society of Washington* 120(4): 708–724. <https://doi.org/10.4289/0013-8797.120.4.708>
- Ekesi S, Nderitu PW, Rwomushana I (2006) Field infestation, life history and demographic parameters of the fruit fly *Bactrocera invadens* (Diptera: Tephritidae) in Africa. *Bulletin of Entomological Research* 96(4): 379–386. <https://doi.org/10.1079/BER2006442>
- Ekesi S, De Meyer M, Mohamed SA, Virgilio M, Borgemeister C (2016) Taxonomy, ecology, and management of native and exotic fruit fly species in Africa. *Annual Review of Entomology* 61(1): 219–238. <https://doi.org/10.1146/annurev-ento-010715-023603>
- Elson-Harris MM (1988) Morphology of the immature stages of *Dacus tryoni* (Froggatt) (Diptera: Tephritidae). *Australian Journal of Entomology* 27(2): 91–98. <https://doi.org/10.1111/j.1440-6055.1988.tb01153.x>
- EPPO (2022a) A1 List of pests recommended for regulation as quarantine pests - version 2022-09. https://www.eppo.int/ACTIVITIES/plant_quarantine/A1_list#insects
- EPPO (2022b) A2 List of pests recommended for regulation as quarantine pests - version 2022-09. https://www.eppo.int/ACTIVITIES/plant_quarantine/A2_list#insects
- Frías D, Hernández-Ortiz V, Vaccaro NC, Bartolucci AF, Salles LA (2006) Comparative morphology of immature stages of some frugivorous species of fruit flies (Diptera: Tephritidae). *Israel Journal of Entomology* 35(36): 423–457.
- Frías D, Selivon D, Hernández-Ortiz V (2008) Taxonomy of immature stages: new morphological characters for Tephritidae larvae identification. In *Fruit Flies of Economic Importance from Basic to Applied Knowledge*. *Proceedings of the 7th International Symposium on Fruit Flies of Economic Importance, Salvador (Brazil), July 2005*, 29–44.
- Jaleel W, Lu L, He Y (2018) Biology, taxonomy, and IPM strategies of *Bactrocera tau* Walker and complex species (Diptera; Tephritidae) in Asia: A comprehensive review. *Environmental Science and Pollution Research International* 25(20): 19346–19361. <https://doi.org/10.1007/s11356-018-2306-6>
- Kamayev IO, Galinskaya TV, Ovtshinnikova OG (2020) Variability of the mandibular sclerite and its value in diagnostics of the third instar larvae of the Mediterranean Fruit Fly

- Ceratitis capitata* (Wiedemann, 1824) (Diptera, Tephritidae). Entomological Review 100(9): 1254–1264. <https://doi.org/10.1134/S0013873820090055>
- Lasserre DF, Ortiz VH, Muñoz LL (2009) Description of the third-instar of *Anastrepha leptozona* Hendel (Diptera: Tephritidae). Neotropical Entomology 38(4): 491–496. <https://doi.org/10.1590/S1519-566X2009000400008>
- Liu X, Zhang L, Haack RA, Liu J, Ye H (2019) A noteworthy step on a vast continent: new expansion records of the guava fruit fly, *Bactrocera correcta* (Bezzi, 1916)(Diptera: Tephritidae), in mainland China. BiolInvasions Records 8(3): 530–539. <https://doi.org/10.3391/bir.2019.8.3.08>
- Norton GA, Patterson DJ, Schneider M (2000) LucID: A multimedia educational tool for identification and diagnostics. International Journal of Innovation in Science and Mathematics Education 4(1): 1–8. <https://openjournals.library.sydney.edu.au/CAL/article/view/6141>
- Pieterse W, Manrakhan A, Ramukhesa HR, Rosenberg SM, Addison P (2017) The use of shape analysis to differentiate between the mandibles of four economically important tephritid species. Journal of Applied Entomology 141(6): 450–457. <https://doi.org/10.1111/jen.12368>
- Rodriguez EJ, Steck GJ, Moore MR, Norrbom AL, Sutton BD, Branham MA (2021) Description of larvae of *Anastrepha amplidentata* and *Anastrepha durantae* with review of larval morphology of the *Fraterculus* Group (Diptera: Tephritidae). Proceedings of the Entomological Society of Washington 123(1): 169–189. <https://doi.org/10.4289/0013-8797.123.1.169>
- Steck GJ, Ekesi S (2015) Description of third instar larvae of *Ceratitis fasciventris*, *C. anonae*, *C. rosa* (FAR complex) and *C. capitata* (Diptera, Tephritidae). In: De Meyer M, Clarke AR, Vera MT, Hendrichs J (Eds) Resolution of Cryptic Species Complexes of Tephritid Pests to Enhance SIT Application and Facilitate International Trade. ZooKeys 540: 443–466. <https://doi.org/10.3897/zookeys.540.10061>
- Virgilio M, White I, De Meyer M (2014) A set of multi-entry identification keys to African frugivorous flies (Diptera, Tephritidae). ZooKeys 428: 97–108. <https://doi.org/10.3897/zookeys.428.7366>
- White IM, Elson-Harris MM (1992) Fruit flies of economic significance: their identification and bionomics. CAB international. <https://doi.org/10.1079/9780851987903.0000>

Supplementary material 1

Raw data of all measurements

Authors: Welma Pieterse, Marc De Meyer, Massimiliano Virgillio, Pia Addison

Data type: xlsx

Copyright notice: This dataset is made available under the Open Database License (<http://opendatacommons.org/licenses/odbl/1.0/>). The Open Database License (ODbL) is a license agreement intended to allow users to freely share, modify, and use this Dataset while maintaining this same freedom for others, provided that the original source and author(s) are credited.

Link: <https://doi.org/10.3897/zookeys.1197.116887.suppl1>

Description of the larva of *Cybister lewisianus* Sharp, 1873 (Coleoptera, Dytiscidae, Cybistrinae)

Kohei Watanabe¹, Masakazu Hayashi²

¹ Ishikawa Insect Museum, Hakusan, Ishikawa, 920–2113, Japan

² Hoshizaki Green Foundation, Izumo, Shimane, 691–0076, Japan

Corresponding author: Kohei Watanabe (koutarouhigasi@yahoo.co.jp)

Abstract

We describe for the first time, the larvae of *Cybister* (*Cybister*) *lewisianus* Sharp, 1873, an endangered species of diving beetle in Japan, emphasizing the chaetotaxy of the cephalic capsule, head appendages, legs, last abdominal segment, and urogomphi. *Cybister lewisianus* larvae are characterized by a longer third article of antenna 3 than the sum of the first and second articles; rounded apex of parietal setae 1–3; labium seta 8 absent; elongated trochanter seta 4, not multi-branched; rounded apex of abdominal setae 1, 12, and 13 (instar I); narrow lateral projections of the frontoclypeus; pronotum without two dark-brown longitudinal stripes dorsally (instar III); and the base of the thick row of small setae on the inner edge of the mandible angulate and projecting medially (all instars).

Key words: Chaetotaxy, diving beetle, larval morphology, larval stage, Red List, water beetle



Academic editor: Mariano Michat

Received: 25 January 2024

Accepted: 25 March 2024

Published: 10 April 2024

ZooBank: <https://zoobank.org/D3E447BD-A240-4FEC-B24D-D329E81A10B1>

Citation: Watanabe K, Hayashi M (2024) Description of the larva of *Cybister lewisianus* Sharp, 1873 (Coleoptera, Dytiscidae, Cybistrinae). ZooKeys 1197: 137–152. <https://doi.org/10.3897/zookeys.1197.119508>

Copyright: ©

Kohei Watanabe & Masakazu Hayashi.

This is an open access article distributed under terms of the Creative Commons Attribution

License ([Attribution 4.0 International – CC BY 4.0](https://creativecommons.org/licenses/by/4.0/)).

Introduction

Compared to adults, coleopteran larvae lack morphological information (Hammond et al. 2019). This trend is also present in Dytiscidae, in which information on larval morphology is generally limited (Alarie and Michat 2023). A nomenclature system of Dytiscidae larval chaetotaxy was developed to provide a detailed description and comparison of their larval morphology and to allow for phylogenetic analysis (Alarie and Michat 2023). Particularly, primary sensilla (setae and pores) have been important for the diagnosis and study of phylogenetic relationships among the species (Michat et al. 2017).

The genus *Cybister* Curtis, 1827 includes large diving beetles (adult length: 13–43 mm) and belongs to the subfamily Cybistrinae (Miller and Bergsten 2016). *Cybister* includes 97 species and is distributed in all major biogeographic regions (Miller and Bergsten 2016; Nilsson and Hájek 2023). Seven species are distributed in Japan (Nakajima et al. 2020; Watanabe and Yoshitomi 2022), and six of these species (approximately 86%) are on the national Red List and are threatened with extinction (Ministry of the Environment of Japan 2020).

Knowledge of the larval morphology of *Cybister* is particularly scarce in comparison to that of other diving beetle groups (Miller et al. 2024). Laboratory

experiments and field research have gradually unraveled their larval feeding habits in detail (e.g., Ohba 2009a, b; Ohba and Inatani 2012; Yamasaki et al. 2022; Fukuoka et al. 2023). Contrastingly, although the characteristics of larvae of some species have been described (Wilson 1923; Kamiya 1938; Fiori 1949; Morioka 1953; Nakagawa 1954; Fukuda et al. 1959; Watts 1964; Larson et al. 2000; Kamite 2008), information about the larval morphology of only four species can be found, i.e., *Cybister fimbriolatus* (Say, 1823), *C. lateralimarginalis* (De Geer, 1774), *C. tripunctatus* (Olivier, 1795) and *C. sugillatus* Erichson, 1834 (Michat 2010; Michat et al. 2015, 2017; Miller et al. 2024).

Cybister lewisianus Sharp, 1873 (adult length 21–26 mm) is listed as “Critically Endangered” on the Japanese Red List (Ministry of the Environment of Japan 2015) and is designated a “nationally endangered species of wild fauna and flora” by the Japanese “Conservation of Endangered Species of Wild Fauna and Flora” Act (Ministry of the Environment of Japan 2022). Identifying the larvae of Japanese *Cybister* to species level is challenging due to their similar body shape and length. They have not been described in detail, and morphological information is limited to third-instar larvae (Ichikawa 1984; Kamite 2008; Mitamura et al. 2017). Recently, Inoda et al. (2022) stated that the shape of the larval clypeus could be useful to identify these species. Similarly, Watanabe (2024) suggested color of the antennal segments, ratio of each antennal segment and article, and shape of the mandible are helpful for identification in the field. Herein, we describe in detail the morphometric and chaetotaxic characteristics of *C. lewisianus* larvae for the first time, according to the now generalized system used to describe aquatic Adephaga larvae (Alarie and Michat 2023).

Material and methods

All larvae used for description were obtained through rearing following the methods used by Watanabe et al. (2021, 2023). A wild individual (Fig. 4) was captured with official permission of the Wildlife Division, Chubu Regional Environmental Office, Ministry of the Environment of Japan (2303313) and the Ishikawa Prefecture, Japan (4-45), and was released at the site after it was photographed.

The larvae were fixed in boiling water, transferred to 70% ethanol in glass vials with caps and subsequently mounted on slides with 70% ethanol or euparal. The specimens were observed using an optical microscope (Nikon ECLIPSE E400) up to 1000-fold magnification and were sketched using a microscope equipped with a Nikon Y-IDT drawing tube. Figures of the line drawing were prepared using an iPad Pro 11-inch (4th generation) after scanning the sketch. Photographs of the living larvae were captured using a Nikon D500 digital camera equipped with a Nikon AF-S Micro NIKKOR 60 mm f/2.8G ED lens. The examined larvae were deposited in the larval collections of the Ishikawa Insect Museum (Ishikawa, Japan) and the Hoshizaki Green Foundation (Shimane, Japan).

Measurements were made using an optical microscope (Nikon ECLIPSE E400) with a glass slide including a microscale, a stereoscopic microscope (Leica M205C, Planapo 1.0X) with a Leica DFC420 camera, LAS version 3.3.1, and digital vernier calipers (to calculate total length only). The fine structures of the specimens were observed using a JEOL JCM-6000 Neoscope scanning electron microscope (SEM). Larvae were freeze-dried and coated with ultrathin

layers of gold through high-vacuum evaporation. The methods and terms used in this study were abbreviated following Alarie et al. (2011, 2023) and Michat et al. (2015, 2019): A and AN, antenna; AB and LAS, abdominal segment VIII (last abdominal segment); CL, longest claw; CO, coxa; COL, coronal line length; FE, femur; FR, frontoclypeus; FRL, frontoclypeus length; HL, head length; HW, maximum head width; L, leg; LA, labium; LP, labial palpi; MN, mandible; MNL, mandible length; MNW, mandible width; MP, maxillary palpi; MX, maxilla; OCW, occipital foramen width; PA, parietal; PPF, maxillary palpifer; PT, pretarsus; TA, tarsus; TI, tibia; TL, total length; TR, trochanter; U and UR, urogomphus. Primary setae and pores were coded following Alarie et al. (2011) and Alarie and Michat (2023).

Results

Description of larvae of *Cybister* (*Cybister*) *lewisianus* Sharp, 1873

Figs 1–30, Table 1

Material source. The description of larvae of *Cybister lewisianus* was based on four instar I, three instar II, and three instar III specimens, reared *ex ovo* in the laboratory at the Ishikawa Insect Museum from adults collected in Suzu-shi, Ishikawa Prefecture, with official permission for exhibition and research at the Ishikawa Insect Museum.

Diagnosis. Ratio HL/HW = 1.26–1.32 (instar I), 1.30–1.33 (instar II), and 1.32–1.34 (instar III) (Table 1). All instars with base of the thick row of small setae on MN inner edge angulate, projecting medially [not angulate and projecting in *C. brevis* Aubé, 1838, *C. chinensis* Motschulsky, 1854, *C. tripunctatus* (Watanabe 2024)]. Instar I larvae of *C. lewisianus* can be distinguished from those of other *Cybister* species by the following combination of characteristics: EB rounded [spiniform in *C. sugillatus* (Michat et al. 2015)]; first article of A2 pale-yellow [dark-brown in *C. brevis* (Watanabe 2024)]; third article of A3 longer than the sum of first and second articles of A3 [shorter in *C. brevis*, *C. chinensis*, *C. tripunctatus* (Watanabe 2024)]; setae PA1–3 with rounded apex [spiniform in *C. tripunctatus* (Alarie et al. 2011)]; seta FR10 broad [narrow in *C. tripunctatus* (Alarie et al. 2011)]; seta MX11 multi-branched [single in *C. tripunctatus* (Alarie et al. 2011)]; seta LA8 absent [present in *C. sugillatus* and *C. tripunctatus* (Alarie et al. 2011; Michat et al. 2015)]; seta TR4 not multi-branched [multi-branched in *C. tripunctatus* (Alarie et al. 2011)]; setae AB1, AB12, and AB13 with rounded apex [spiniform in *C. tripunctatus* (Alarie et al. 2011)]. In the instar III larva, lateral projections of FR narrow [broad in *C. chinensis*, *C. limbatus* (Fabricius, 1775), *C. rugosus* (MacLeay, 1833) and *C. tripunctatus* (Ichikawa 1984; Kamite 2008; Mitamura et al. 2017; Watanabe and Hayashi 2023)]; pronotum without two dark-brown longitudinal stripes dorsally [with two dark-brown longitudinal stripes in *C. brevis*, *C. sugillatus*, *C. rugosus* (Mitamura et al. 2017; Watanabe and Hayashi 2023)].

Description, instar I (Figs 1, 5–30). **Color** (Fig. 1). Head capsule pale-yellow; anterolateral part of frontoclypeus, coronal line, and lateral margin light-yellow-brown; several brown small maculae; stemmata dark-brown; antennae pale-yellow except for third article of A3 and A4 dark-brown; mandible pale-yellow except for distal portion light-red-brown and thick row of small setae on the inner margin dark-brown; maxilla pale-yellow except for third article of palpomere 3;

Table 1. Measurements and ratios for the larvae of *Cybister lewisianus* Sharp, 1873. *N* = number of specimens examined.

Measure	<i>C. lewisianus</i>			Measure	<i>C. lewisianus</i>		
	Instar I (<i>N</i> = 3)	Instar II (<i>N</i> = 3)	Instar III (<i>N</i> = 3)		Instar I (<i>N</i> = 3)	Instar II (<i>N</i> = 3)	Instar III (<i>N</i> = 3)
TL (mm)	20.19–20.31	30.37–32.63	50.85–53.36	PPF/MP1	0.36–0.37	0.41–0.42	0.43–0.47
HL (mm)	2.12–2.17	3.27–3.29	4.53–4.82	MP1/MP2	1.52–1.58	1.67–1.81	1.92–1.99
HW (mm)	1.64–1.68	2.46–2.51	3.37–3.61	MP3/MP2	1.28–1.43	1.15–1.22	1.01–1.04
FRL (mm)	0.91–1.07	1.35–1.38	1.74–1.79	MP/LP	2.06–2.25	1.85–2.10	1.92–1.97
OCW (mm)	0.69–0.74	1.14–1.31	1.75–1.98	LP2/LP1	0.76–0.82	0.61–0.66	0.46–0.48
HL/HW	1.26–1.32	1.30–1.33	1.32–1.34	L3 (mm)	5.16–5.43	7.29–7.53	10.23–10.77
HW/OCW	2.28–2.38	1.92–2.17	1.81–1.93	L3/L1	1.20–1.31	1.25–1.30	1.28–1.31
COL/HL	0.51–0.57	0.58–0.59	0.62–0.63	L3/L2	1.12–1.18	1.09–1.16	1.12–1.14
FRL/HL	0.43–0.49	0.41–0.42	0.37–0.38	L3/HW	3.06–3.25	2.96–3.01	2.93–3.03
A/HW	0.95–0.99	0.80–0.84	0.80–0.83	L3 (CO/FE)	1.00–1.02	1.02–1.05	0.98–1.01
A2/A1	0.86–0.94	0.79–0.89	0.75–0.78	L3 (TI/FE)	0.67–0.71	0.66–0.69	0.65–0.67
A3/A1	0.62–0.64	0.53–0.54	0.39–0.40	L3 (TA/FE)	0.74–0.77	0.68–0.69	0.60–0.64
A4/A3	0.17–0.20	0.12–0.14	0.10–0.13	L3 (CL/TA)	0.36–0.37	0.32–0.33	0.26–0.29
A3'/A4	0.81–0.85	0.73–0.96	0.52–0.82	LAS (mm)	4.03–4.26	5.93–6.26	8.30–8.91
MNL/MNW	3.09–3.27	3.16–3.19	3.17–3.30	LAS/HW	2.46–2.53	2.41–2.52	2.43–2.47
MNL/HL	0.49–0.51	0.48–0.50	0.48–0.50	U (mm)	0.02	0.03–0.05	0.04–0.05
A/MP	1.24–1.38	1.37–1.40	1.46–1.51				

labium pale-yellow; thoracic tergites light-yellow-brown except for pale-yellow membranous area, several small brown maculae, slightly larger pair of brown maculae on anterior quarter side of protergite; one pair of brown maculate on each side of membranous region of meso- and metathorax; abdominal tergites I–VI pale-yellow with several small brown maculae; one pair of slightly larger brown maculae on middle of dorsolateral margin of membranous region, five pairs of ventral brown maculae; abdominal tergites VII–VIII light-yellow-brown with several small brown maculae; four pairs of brown maculae on sterna of abdominal tergite VII; legs pale-yellow; urogomphus light-yellow-brown. Color as shown in Fig. 1 and in Watanabe (2024: figs 1B, 2C).

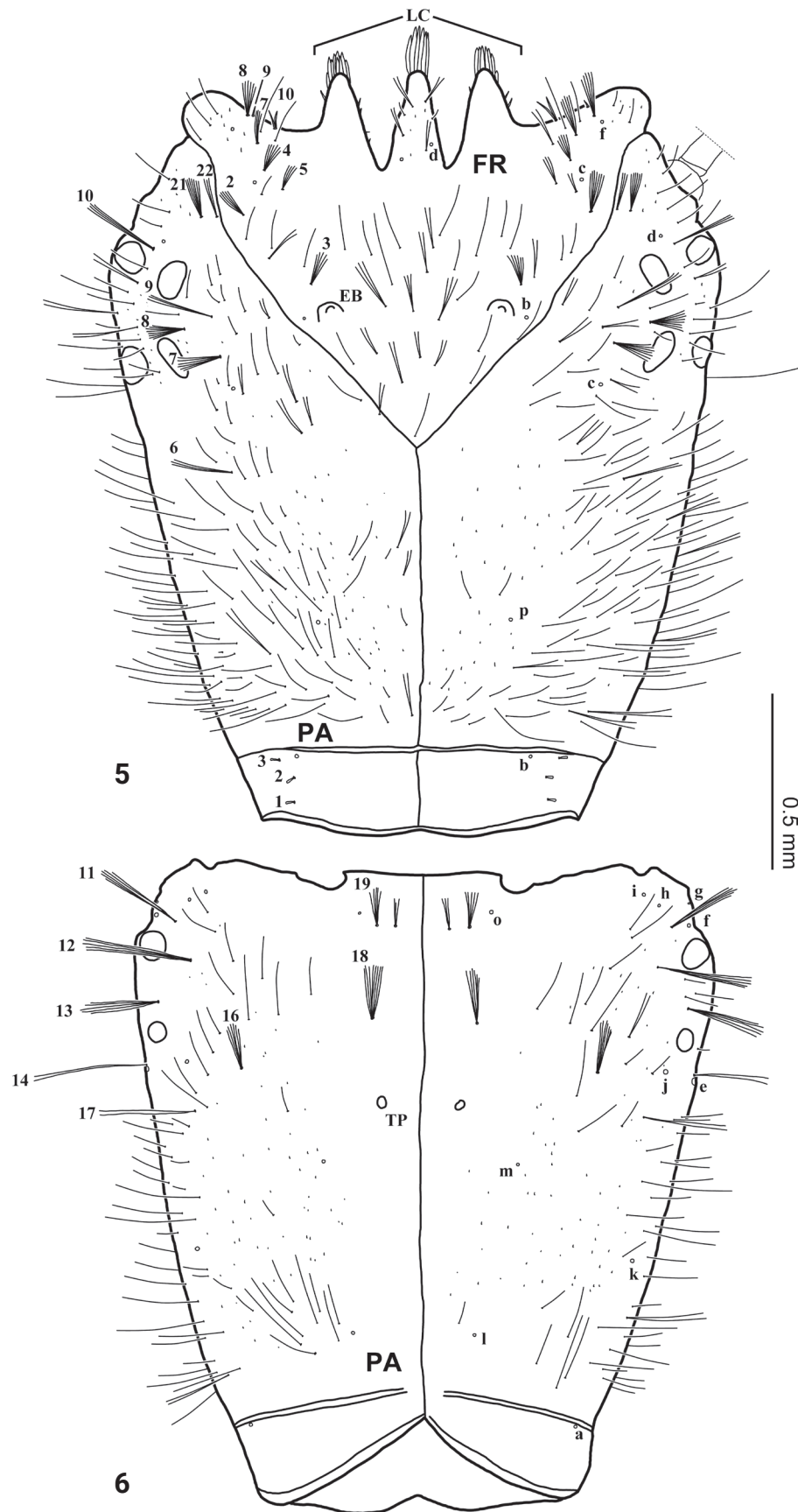
Body (Fig. 1). Elongate, subcylindrical; measurements and body shape ratios are shown in Table 1.

Head (Figs 5–13, 19–28). Cephalic capsule (Figs 5, 6, 19, 25). Flattened, sub-triangular, longer than broad; maximum width at level of anterior stemmata, constricted at level of occipital region, lacking temporal spiniform setae; occipital suture present; ecdysial line well marked, COL long; occipital foramen deeply emarginate ventrally (Figs 6, 25); tentorial pits visible slightly above middle of ventral midline (Figs 6, 25, 27); FR subtriangular, anterior margin projected forward, divided into three well developed and about equally long triangular projections, central projection narrow and with same length on both sides, lateral projections slightly broader and with inner length longer than outer length, notches between medial and lateral projections narrow; anterolateral lobes rounded, not projecting beyond lamellae clypeales; EB present, large, rounded (Figs 5, 19, 23), near ecdysial line at level of seta PA9; six stemmata on each side, four dorsal, and two ventral. Antennae (Figs 7, 8, 22). Elongate, slender, almost as

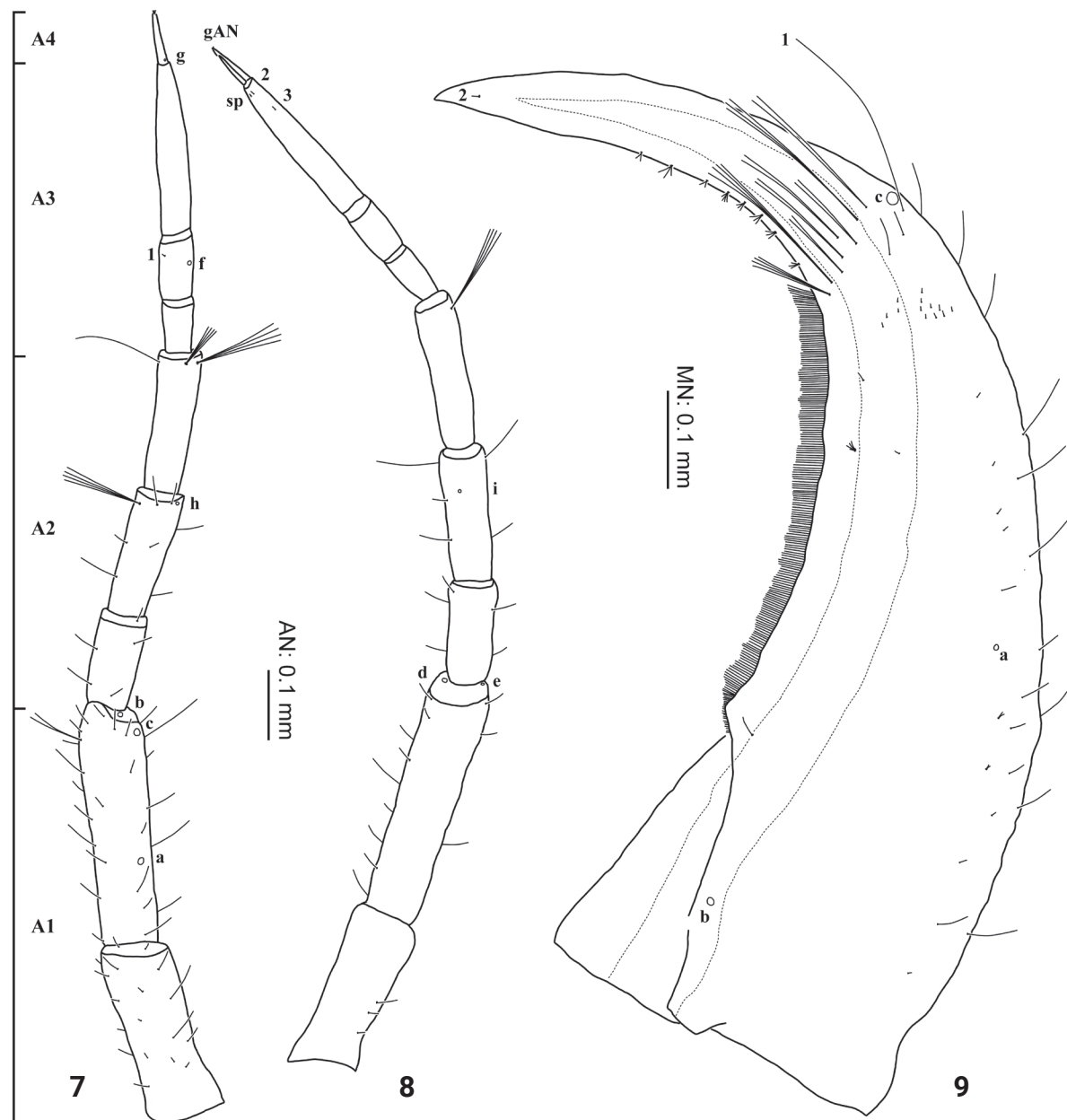


Figures 1–4. First to third-instar larva of *Cybister* (*Cybister*) *lewisianus* Sharp, 1873 1 instar I 2 instar II 3, 4 instar III 1–3 captive individuals 4 wild individual.

long or slightly shorter than HW, composed of four antennomeres; A1 longest, subdivided into two articles, distal article approximately < 1.5 longer than basal article; A2 shorter than A1, subdivided into three articles: first article shortest and third article longest; A3 shorter than A2, subdivided into three articles: first article shortest and third article longest; A3' shorter than A4, elongate, slender; A4 shortest. Mandible (Fig. 9). Strong, falciform, broadest at base, narrowing to apex, abruptly narrowed toward apex from pore MNC; base of the thick row of small setae on inner edge angulate and projecting medially; mandibular channel present. Maxilla (Figs 10, 11). Premaxillary lobes well developed; cardo well

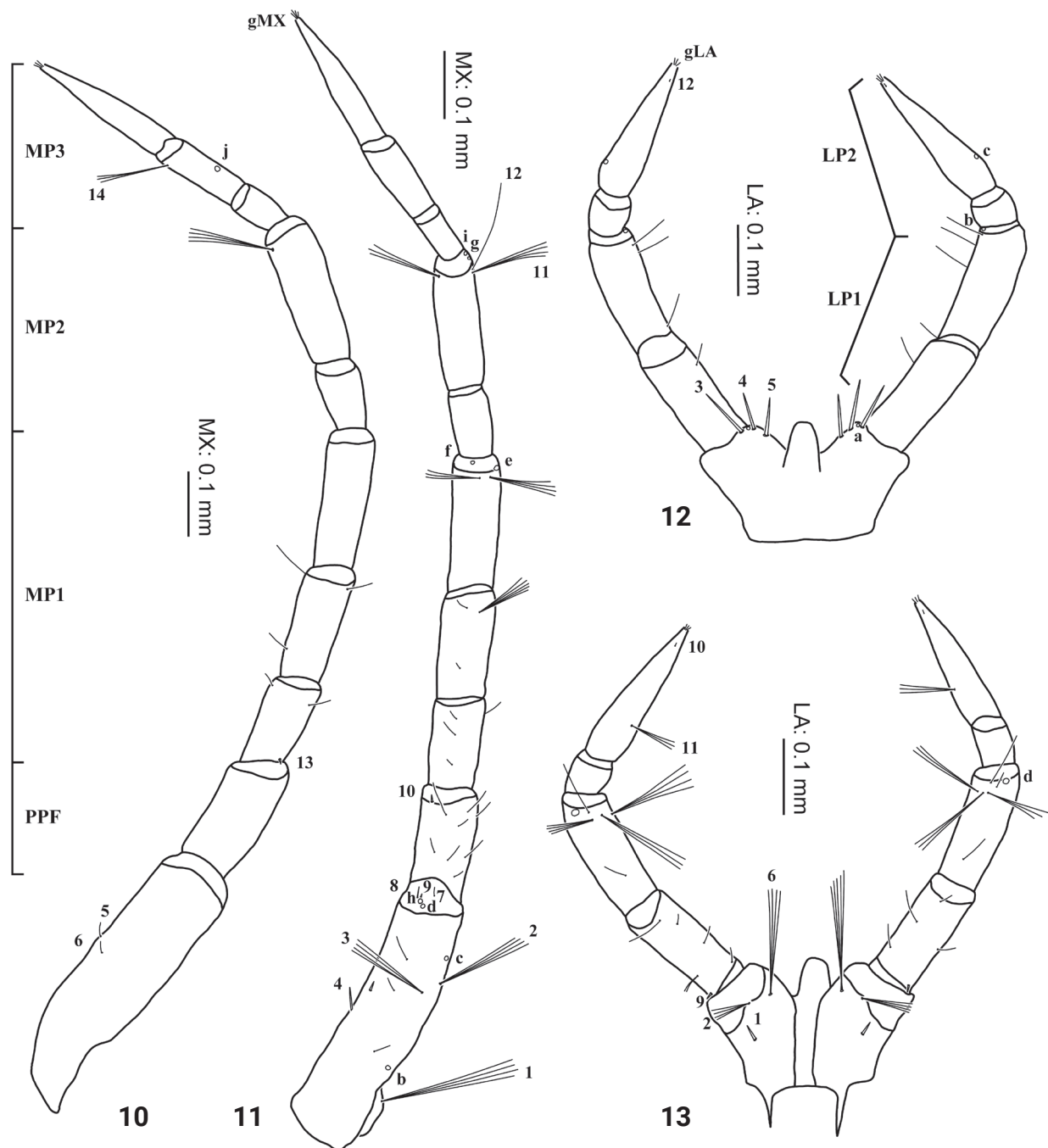


Figures 5, 6. First-instar larva of *Cybister (Cybister) lewisianus*, cephalic capsule **5** dorsal aspect **6** ventral aspect. EB, egg burster; LC, lamellae clypeales; TP, tentorial pit.



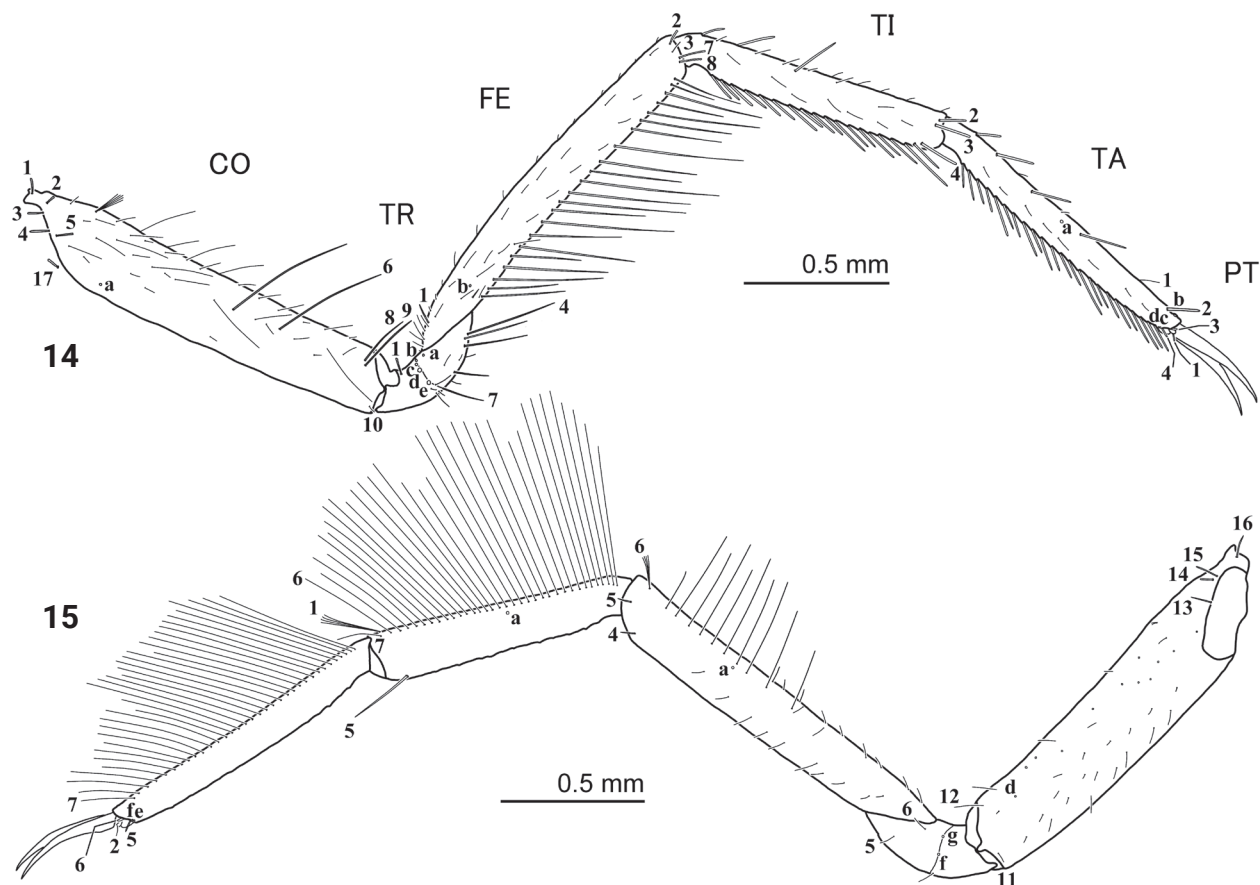
Figures 7–9. First-instar larva of *Cybister* (*Cybister*) *lewisianus* 7, 8 antenna 9 mandible 7, 9 dorsal aspect 8 ventral aspect. sp, spinula.

developed, subovate, stipes elongate, slender, subcylindrical; galea absent; PPF elongate, slender, palpomere-like; MP elongate, slender, shorter than antenna, composed of three palpomeres, MP1 longest and MP2 the shortest; MP1 subdivided into three articles, basal article shortest and third article longest, MP2 subdivided into two articles, distal article longer than first article; MP3 subdivided into three articles, first article shortest and third article longest. Labium (Figs 12, 13, 28). Prementum broader than long, not sclerotized ventromedially, anterodorsal margin well projected forward, median process with apex rounded, reaching approximately the level of anterior margin of prementum; LP much shorter than MP, composed of two palpomeres; LP1 longer than LP2; LP1 subdivided into two articles subequal in length; LP2 subdivided into two articles, distal article more than twice longer than basal article.



Figures 10–13. First-instar larva of *Cybister* (*Cybister*) *lewisianus* 10, 11 maxilla 12, 13 labium 10, 12 dorsal aspect 11, 13 ventral aspect.

Thorax (Figs 1, 14, 15, 29, 30). Pro-, meso-, and metanotum convex, length of pronotum twice that of mesonotum, metanotum and mesonotum with subequal length, pronotum, metanotum, and metanotum with subequal width; protergite longer than broad, subrectangular, lateral margins emarginate at about middle, anterior and posterior margins straight; meso- and metatergite small, broader than long, subtrapezoidal, posterior central margin emarginate; sagittal line present on all tergites; sternum of prothorax membranous except for one pair of small subtriangular sclerites, sterna of meso- and metathorax membranous; spiracles absent. Legs (Figs 14, 15, 29, 30). Long, composed of

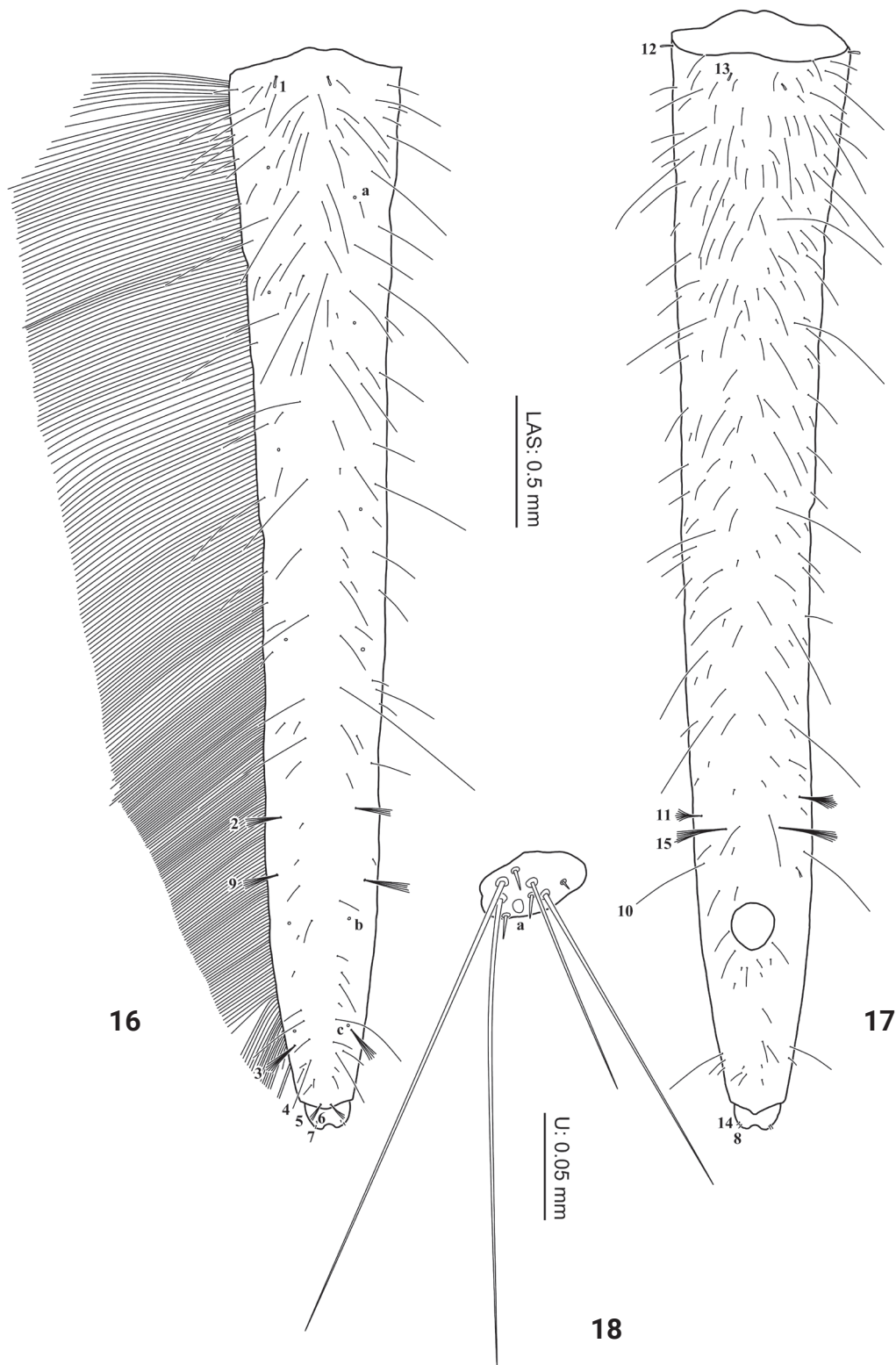


Figures 14, 15. First-instar larva of *Cybister (Cybister) lewisianus*, metathoracic leg **14** anterior aspect **15** posterior aspect.

six segments, L1 shortest and L3 longest; CO, FE, TI, and TA subcylindrical, elongate and slender; TR short, divided into two parts by an annulus; PT with two long curved claws.

Abdomen (Figs 1, 16–18). Eight-segmented; segments I–VI subequal in length, mostly membranous with a minute sclerite on anterodorsal region, tergites I–VI without anterior carina, sagittal line present; segments II–III slightly broader than the others; posterior part of sclerites I–VI and anterior part of sclerite VII densely covered with small spinulae; sterna of segments I–VI membranous; segment VII narrower, subtrapezoidal, without anterior carina, sagittal line absent; segments I–VII without spiracles; segment VIII longest and narrowest, sclerotized except anteroventrally and around anus. Urogomphus (Fig. 18). Strongly reduced, slightly broader than long, comprised of one urogomphomere.

Chaetotaxy. Similar to that of the generalized *Cybister* larva (Alarie et al. 2011; Alarie and Michat 2023) with the following remarks: lamellae clypeales drill-like (Figs 20, 21); seta PA1–3 apically rounded (Figs 5, 24); seta FR10 broad, bifid (Fig. 5); seta MX11 multi-branched (Fig. 11); seta LA8 absent (Fig. 12); setae CO1–5, CO14, and CO17 apically rounded (Figs 14, 15); seta TR1 apically rounded (Fig. 14); seta TR4 elongate, not multi-branched (Figs 14, 29); setae FE2, FE7, and FE8 apically rounded (Fig. 14); seta FE3 slenderer than FE2, FE7, and FE8 (Fig. 14); setae TI2–4 apically rounded (Fig. 14); setae TA2–5 apically rounded (Figs 14, 15); seta PT1 apically rounded (Fig. 14); setae AB1, AB12 and AB13 apically rounded (Figs 16, 17); and seta AB4 long (Fig. 16).



Figures 16–18. First-instar larva of *Cybister (Cybister) lewisianus* 16, 17 abdominal segment VIII 18 urogomphus 16 dorsal aspect 17, 18 ventral aspect.

Description, instar II (Fig. 2). As first-instar larva except as follows:

Color (Fig. 2). Head capsule with small brown maculae more numerous; thoracic tergites light yellow-brown except for pale-yellow membranous region with several gray maculae; abdominal tergites I–VI light-yellow-brown except

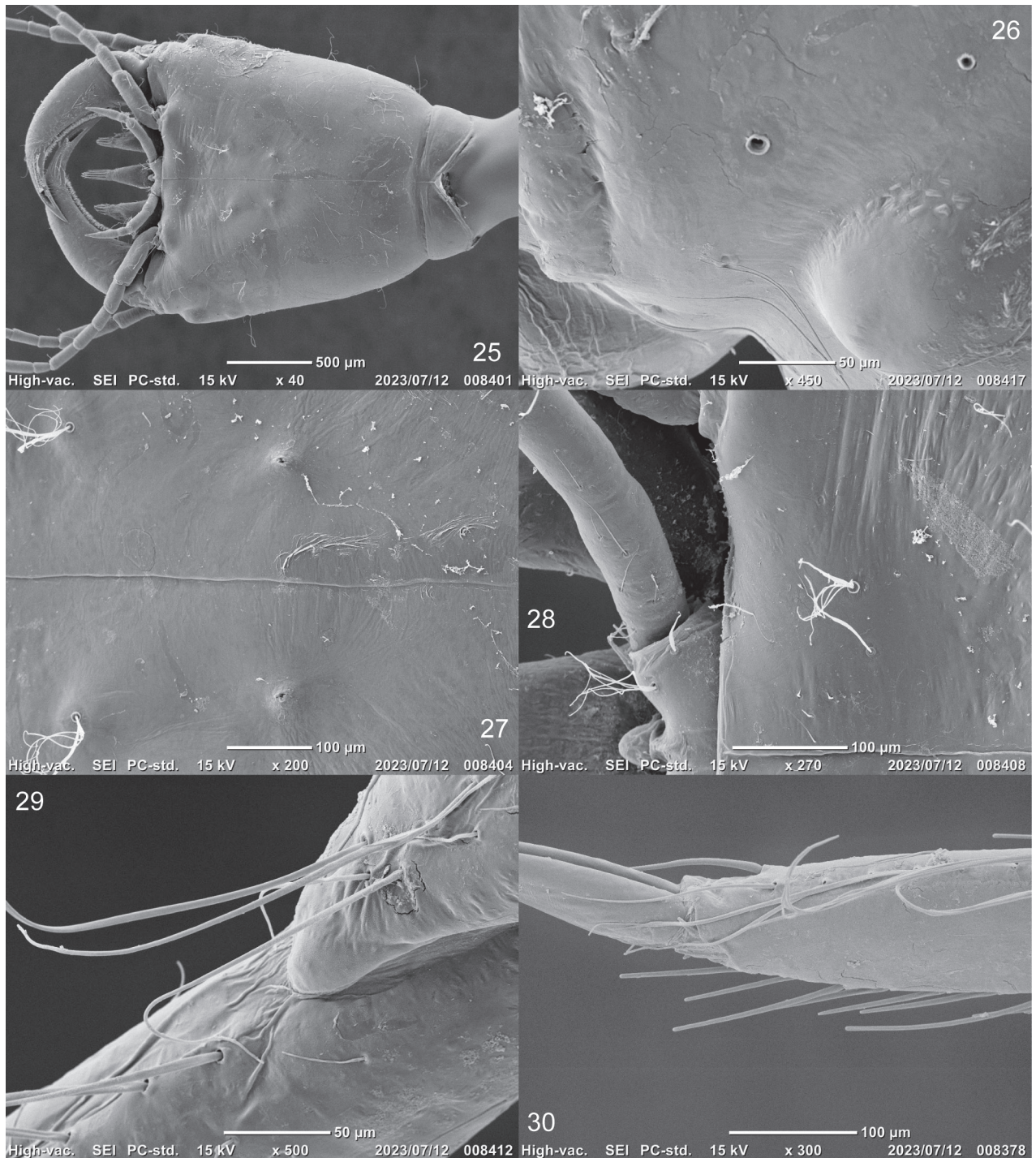


Figures 19–24. SEM photographs of first-instar larva of *Cybister* (*Cybister*) *lewisianus*, head, dorsal aspect **19** cephalic capsule **20** mandible and projections of lamellae clypeales **21** lamellae clypeales of central projection **22** apex of antenna **23** egg burster **24** setae PA1–3.

for pale-yellow membranous region with several gray maculae; abdominal tergites VII–VIII with several small brown maculae. Color as shown in Fig. 2 and in Watanabe (2024: figs 1F, 3B).

Body. Measurements and body shape ratios are shown in Table 1.

Head. Cephalic capsule. EB absent; HW/OCW = 1.92–2.17. Antennae. Shorter than HW; A3/A1 = 0.53–0.54. Maxilla. MP1/MP2 = 1.67–1.81; MP3/MP2 = 1.15–1.22. Labium. LP2/LP1 = 0.61–0.66.



Figures 25–30. SEM photographs of first-instar larva of *Cybister (Cybister) lewisianus* **25** cephalic capsule **26** pores PAF-i **27** tentorial pit **28** labium and cephalic capsule **29** trochanter and femur **30** tarsus and pretarsus **25–28** ventral aspect **29** antero-ventral aspect **30** posterior aspect.

Abdomen. Sclerites I–VII not covered with small spinulae.

Chaetotaxy. Identification of the secondary setae was difficult due to the large number of additional setae.

Description, instar III (Fig 3, 4). As second-instar larva except as follows:

Color (Fig 3, 4). Head capsule yellow-brown; thoracic tergites yellow-brown except for light-brown membranous region with several gray maculae; anterior

and posterior margin of protergite brown; abdominal tergites I–VI yellow-brown except for light-brown membranous region, one light-brown vitta on each side of abdominal tergites; abdominal tergites VII–VIII yellow-brown, tergite VII with several light-yellow-brown maculae. Color as shown in Figs 3, 4 and in Inoda et al. (2022: fig. 1), Watanabe and Hayashi (2023: fig. 4E), and Watanabe (2024: figs 1J, 4B).

Body. Thorax. Spiracles present on mesosternum; measurements and body shape ratios shown in Table 1.

Head. Antennae. A3 shorter than half of A1. Maxilla. MP1 about twice longer than MP2; MP3 almost same length as MP2. Labium. LP2 shorter than half of LP1.

Abdomen. Spiracles present on segments I–VII.

Remarks. A study on *Laccophilus yoshitomi* Watanabe & Kamite, 2018 reported that larvae raised in captivity differed in color from those collected in the field (Watanabe and Okada 2023); however, no pronounced differences in color were observed between captive and wild individuals of *Cybister lewisianus* in the present study (Figs 3, 4).

Acknowledgements

We express our sincere gratitude to Yves Alarie (Laurentian University) and Mariano C. Michat (University of Buenos Aires) for their important comments and suggestions, Tomoki Sumikawa (Ishikawa Insect Museum) for his cooperation with rearing, Hirokazu Fukutomi (Ishikawa Insect Museum) for his support with microscopic observations, Seidai Nagashima (Itami City Museum of Insects) for sharing the method of photographing the larvae, the Wildlife Division, Chubu Regional Environmental Office, Ministry of the Environment, Japan and the Ishikawa Prefecture, Japan for permission to conduct the sampling, and Daisuke Utsunomiya (Sustainable Society and Ecosystems Office, Suzu City) for supporting the survey. We would like to thank Editage (www.editage.jp) for English language editing.

Additional information

Conflict of interest

The authors have declared that no competing interests exist.

Ethical statement

No ethical statement was reported.

Funding

This research was supported by joint research expenses from the Hoshizaki Green Foundation.

Author contributions

Kohei Watanabe was involved in the study conception, rearing, sampling, observation and description. Masakazu Hayashi was involved in observation. The first draft of the manuscript was written by Kohei Watanabe and all authors have read and approved the final version of the manuscript.

Author ORCIDs

Kohei Watanabe  <https://orcid.org/0000-0002-8761-232X>

Masakazu Hayashi  <https://orcid.org/0000-0003-3708-9005>

Data availability

All of the data that support the findings of this study are available in the main text.

References

- Alarie Y, Michat MC (2023) Larval Chaetotaxy of World Dytiscidae (Coleoptera: Adephaga) and Implications for the Study of Hydradephaga. In: Yee DA (Ed.) Ecology, Systematics, and the Natural History of Predaceous Diving Beetles (Coleoptera: Dytiscidae). Springer, Cham, 17–53. https://doi.org/10.1007/978-3-031-01245-7_2
- Alarie Y, Michat MC, Miller KB (2011) Notation of primary setae and pores on larvae of Dytiscinae (Coleoptera: Dytiscidae), with phylogenetic considerations. *Zootaxa* 3087(1): 1–55. <https://doi.org/10.11646/zootaxa.3087.1.1>
- Alarie Y, Watanabe K, Michat MC (2023) The very rare Japanese endemic diving beetle *Japanolaccophilus niponensis* (Kamiya, 1939), (Coleoptera: Dytiscidae, Laccophilinae): larval morphology and phylogenetic comparison with other known Laccophilini. *Zootaxa* 5285(1): 116–132. <https://doi.org/10.11646/zootaxa.5285.1.4>
- Fiori G (1949) Contributi alla conoscenza morfologica ed etologica dei coleotteri. III. Le larve dell'*Acilius sulcatus* L. e del *Cybister lateralimarginalis* De Geer (Dytiscidae [sic]). *Bollettino dell'Istituto di Entomologia della Università degli Studi di Bologna* 17: 234–264.
- Fukuda A, Kurosa K, Hayashi N (1959) Coleoptera. In: Kawada A (Ed.) Illustrated Insect Larvae of Japan. Hokuryukan, Tokyo, 392–545. [In Japanese]
- Fukuoka T, Tamura R, Yamasaki S, Ohba SY (2023) Effects of different prey on larval growth in the diving beetle *Cybister sugillatus* Erichson, 1834 (Coleoptera: Dytiscidae). *Aquatic Insects* 44(3): 226–234. <https://doi.org/10.1080/01650424.2022.2141259>
- Hammond PM, Marshall JE, Cox ML, Jessop L, Garner BH, Barclay MVL (2019) British Coleoptera larvae. A guide to the families and major subfamilies. In: Barclay MVL, Garner BH (Eds) Royal Entomological Society/Field Studies Council, [viii +] 280 pp.
- Ichikawa N (1984) Notes on breeding water beetles. *Insectarium* 22(3): 8–10. [In Japanese]
- Inoda T, Watanabe K, Odajima T, Miyazaki Y, Yasui S, Kitano T, Konuma J (2022) Larval clypeus shape provides an indicator for quantitative discrimination of species and larval stages in Japanese diving beetles *Cybister* (Coleoptera: Dytiscidae). *Zoologischer Anzeiger* 296: 110–119. <https://doi.org/10.1016/j.jcz.2021.12.003>
- Kamite Y (2008) An explanation on the immature stages of subfamily Dytiscinae (Coleoptera: Dytiscidae) of Japan. *Bulletin of the Hoshizaki Green Foundation* 11: 125–141. [In Japanese]
- Kamiya K (1938) Family Dytiscidae Class Insecta Coleopteroidea-Coleoptera. *Fauna Nipponica* 10 (8/11). Sanseido, Tokyo, 137 pp. [In Japanese]
- Larson DJ, Alarie Y, Roughley RE (2000) Predaceous Diving Beetles (Coleoptera: Dytiscidae) of the Nearctic Region, with emphasis on the fauna of Canada and Alaska. National Research Council of Canada, Ottawa, 982 pp.
- Michat MC (2010) Descriptions of larvae of *Megadytes* (Coleoptera: Dytiscidae: Dytiscinae): The subgenera *Trifurcitus* and *Megadytes* s. str., ground plan of chaetotaxy

- of the genus and phylogenetic analysis. *European Journal of Entomology* 107(3): 377–392. <https://doi.org/10.14411/eje.2010.047>
- Michat MC, Alarie Y, Watts CHS (2015) Phylogenetic placement of the genus *Sternhydrus* (Coleoptera: Dytiscidae: Cybistrini) based on larval morphology, with description of *S. atratus*. *Annals of the Entomological Society of America* 108(5): 881–892. <https://doi.org/10.1093/aesa/sav067>
- Michat MC, Alarie Y, Miller KB (2017) Higher-level phylogeny of diving beetles (Coleoptera: Dytiscidae) based on larval characters. *Systematic Entomology* 42(4): 734–767. <https://doi.org/10.1111/syen.12243>
- Michat MC, Alarie Y, Watts CHS (2019) Dealing with a hairy beast—larval morphology and chaetotaxy of the Australian endemic diving beetle genus *Spencerhydrus* (Coleoptera, Dytiscidae, Cybistrini). *ZooKeys* 884: 53–67. <https://doi.org/10.3897/zookeys.884.38391>
- Miller KB, Bergsten J (2016) *Diving Beetles of the World. Systematics and Biology of the Dytiscidae*. Johns Hopkins University Press, Baltimore, 320 pp.
- Miller KB, Michat MC, Ferreira Jr N (2024) Reclassification of Cybistrinae Sharp, 1880 in the Neotropical Region (Coleoptera, Adephaga, Dytiscidae), with description of new taxa. *ZooKeys* 1188: 125–168. <https://doi.org/10.3897/zookeys.1188.110081>
- Ministry of the Environment of Japan (2015) *Red data book 2014 – Threatened wildlife of Japan, vol 5. Insecta*. Gyosei Corporation, Tokyo, 509 pp. [In Japanese]
- Ministry of the Environment of Japan (2020) *Red List 2020*. <https://www.env.go.jp/press/files/jp/114457.pdf> [Accessed 7 January 2024] [In Japanese]
- Ministry of the Environment of Japan (2022) *List of nationally endangered species of wild fauna and flora*. <https://www.env.go.jp/nature/kisho/domestic/list.html> [Accessed 7 January 2024] [In Japanese]
- Mitamura T, Hirasawa K, Yoshii S (2017) *The Handbook of Japanese Aquatic Insect, Volume 1: Coleoptera*. Bun-ichi Sogo Shuppan, Tokyo, 176 pp. [In Japanese]
- Morioka Y (1953) Observation of *Hydaticus bipunctatus* and *Cybister tripunctatus lateralis* larvae. *Shin Kontyu* 6(12): 9–11. [In Japanese]
- Nakagawa A (1954). Study of Japanese Dytiscidae larvae. *Shin Kontyu* 7(10): 2–6. [In Japanese]
- Nakajima J, Hayashi M, Ishida K, Kitano T, Yoshitomi H (2020) *Aquatic Coleoptera and Hemiptera of Japan*. Bun-ichi Sogo Shuppan, Tokyo, 352 pp. [In Japanese]
- Nilsson AN, Hájek J (2023) *A World Catalogue of the Family Dytiscidae, or the Diving Beetles (Coleoptera, Adephaga)*. Version 1.1.2023. http://www.waterbeetles.eu/documents/W_CAT_Dytiscidae_2024.pdf [Accessed 7 January 2024]
- Ohba S (2009a) Feeding habits of the diving beetle larvae, *Cybister brevis* Aubé (Coleoptera: Dytiscidae) in Japanese wetlands. *Applied Entomology and Zoology* 44(3): 447–453. <https://doi.org/10.1303/aez.2009.447>
- Ohba S (2009b) Ontogenetic dietary shift in the larvae of *Cybister japonicus* (Coleoptera: Dytiscidae) in Japanese rice fields. *Environmental Entomology* 38(3): 856–860. <https://doi.org/10.1603/022.038.0339>
- Ohba S, Inatani Y (2012) Feeding preferences of the endangered diving beetle *Cybister tripunctatus orientalis* Gschwendtner (Coleoptera: Dytiscidae). *Psyche* (Cambridge, Massachusetts) 139714: 1–3. <https://doi.org/10.1155/2012/139714>
- Watanabe K (2024) The characterization of four *Cybister* (Coleoptera: Dytiscidae) species larvae in Honshu, Japan. *Bulletin of the Hoshizaki Green Foundation* 27: 147–155. [In Japanese]

- Watanabe K, Hayashi M (2023) A review on Dytiscidae (Coleoptera) larvae in Shimane Prefecture, Japan. Special Bulletin of the Hoshizaki Green Foundation 32: 63–81. [In Japanese]
- Watanabe K, Okada R (2023) Description of the larvae of *Laccophilus yoshitomi* Watanabe and Kamite, 2018 (Coleoptera: Dytiscidae: Laccophilinae). The Coleopterists Bulletin 77(1): 93–100. <https://doi.org/10.1649/0010-065X-77.1.93>
- Watanabe K, Yoshitomi H (2022) Family Dytiscidae. In: Editorial Committee of Catalogue of the Insects of Japan (Ed.) Catalogue of the Insects of Japan. Vol. 6. Order Coleoptera, part 1. Touka Shobo, Fukuoka, 8–27.
- Watanabe K, Inoda T, Suda M, Yoshida W (2021) Larval rearing methods for two endangered species of diving beetle, *Cybister chinensis* Motschulsky, 1854 and *Cybister lewisianus* Sharp, 1873 (Coleoptera: Dytiscidae), using laboratory-bred food prey. The Coleopterists Bulletin 75(2): 440–444. <https://doi.org/10.1649/0010-065X-75.2.440>
- Watanabe K, Saiki R, Sumikawa T, Yoshida W (2023) Rearing method for the endangered species *Dineutus mellyi mellyi* Régimbart, 1882 (Coleoptera: Gyrinidae). Aquatic Insects 44(3): 195–204. <https://doi.org/10.1080/01650424.2022.2107676>
- Watts CHS (1964) The larvae of Australian *Cybister* spp. Curt., *Homoeodytes* spp. Reg. and *Hyderodes shuckardi* Hope. (Coleoptera: Dytiscidae.). Transactions of the Royal Society of South Australia 88: 145–156.
- Wilson CB (1923) Water beetles in relation to pondfish culture, with life histories of those found in fishponds at Fairport, Iowa. Bulletin of United States Bureau of Fisheries 39: 231–345.
- Yamasaki S, Watanabe K, Ohba SY (2022) Larval feeding habits of the large-bodied diving beetle *Cybister rugosus* (Coleoptera: Dytiscidae) under laboratory conditions. Entomological Science 25(2): e12510. <https://doi.org/10.1111/ens.12510>

Revision of the Chinese *Pachynotus* Kollar & L. Redtenbacher, 1844 (Coleoptera, Curculionidae), with descriptions of two new species

Jinliang Ren^{1,2}, Li Ren¹, Runzhi Zhang^{1,2}

¹ Key Laboratory of Zoological Systematics and Evolution, Institute of Zoology, Chinese Academy of Sciences, No.1 Beichen West Road, Chaoyang District, Beijing 100101, China

² College of Life Science, University of Chinese Academy of Sciences, Beijing 100049, China

Corresponding author: Runzhi Zhang (zhangrz@ioz.ac.cn)

Abstract

The Chinese species of the highland weevil genus *Pachynotus* is revised, including a single known species, *P. lampoglobus* Chao & Y.-Q. Chen, 1980, and the descriptions of two new species, *P. pilosus* **sp. nov.** and *P. arcuatus* **sp. nov.** All Chinese *Pachynotus* species occur in Xizang (Tibet), China, and a key to these species is presented. Additionally, the COI sequences of two species, *P. lampoglobus* and *P. pilosus* **sp. nov.**, are provided, with details of the genetic distance.

Key words: COI, Curculionidae, key, new species, *Pachynotus*, Xizang



Academic editor: M. Alonso-Zarazaga

Received: 31 October 2023

Accepted: 16 March 2024

Published: 10 April 2024

ZooBank: <https://zoobank.org/53C902B0-2308-42E4-907C-D5BAAD67ED54>

Citation: Ren J, Ren L, Zhang R (2024)

Revision of the Chinese *Pachynotus* Kollar & L. Redtenbacher, 1844

(Coleoptera, Curculionidae), with descriptions of two new species.

ZooKeys 1197: 153–169. <https://doi.org/10.3897/zookeys.1197.114969>

Copyright: © Jinliang Ren et al.

This is an open access article distributed under terms of the Creative Commons Attribution

License (Attribution 4.0 International – CC BY 4.0).

Introduction

Pachynotus Kollar & L. Redtenbacher, 1844, belonging to the tribe Tanymecini (Curculionidae, Entiminae), is mainly distributed in the Himalayas, such as Kashmir, Himachal Pradesh, Uttarakhand of India and Xizang of China (Alonso-Zarazaga et al. 2023; Appendix 1). Because of the Himalayas' high species richness and endemism, this mountain region has been identified as one of the 25 biodiversity hotspots in the world (Myers et al. 2000). The genus *Pachynotus* was established by Kollar and Redtenbacher (1844) for a single species, *P. globicollis* Kollar & L. Redtenbacher 1844, from India and Kashmir. Marshall (1916) redefined the genus and described *P. globicollis*, while synonymising *Cneorhinus obscurus* Kollar & L. Redtenbacher, 1844 with *P. globicollis*. Chao and Chen (1980) described *P. lampoglobus* Chao & Y.-Q. Chen, 1980 from China. Mahendiran and Ramamurthy (2013) reviewed this genus, described two new species, *P. mayarami* Mahendiran & Ramamurthy, 2013 and *P. kumaonensis* Mahendiran & Ramamurthy, 2013, and provided a key to all the species distributed in India.

Herein, we describe two new species and present a key to Chinese *Pachynotus*. Moreover, we provide the COI sequences of *P. lampoglobus* and *P. pilosus* and analyse the genetic distance of these two species based on COI sequences.

Materials and methods

All specimens, including types, examined for this study are collections of the Institute of Zoology, Chinese Academy of Sciences, Beijing, China (**IZCAS**), and the Natural History Museum, London, UK (**NHMUK**). The types of the new species are deposited in IZCAS. Label data are given as they are, verbatim, with pinyin romanisation and comments in square brackets if labels are in Chinese; labels are separated by double slashes and lines by slashes.

Specimens were dissected after soaking them in soapy water overnight for cleaning and softening, and the dissected parts were placed in a cold 10% KOH solution for 20 h to macerate the soft tissues. After dissection, all parts were photographed and stored in glycerine in microvials pinned beneath the specimen from which they were dissected.

The morphological terminology used in this study mainly follows Marshall (1916) and Aslam (1966). Measurements were made using an ocular micrometre as follows: standard length – dorsally from anterior margin of thorax to the apex of elytra along midline; pronotal length – dorsally from anterior margin to base along midline; pronotal width – dorsally across widest part; elytral length – dorsally along suture of elytra from base to apex; elytral width – dorsally across widest part; rostral length – dorsally in a straight line from apex to anterior margin of eye; rostral width – dorsally across base of rostrum. Measurements are made in millimetres.

All observations and dissections were performed using a Nikon SMZ1500 stereomicroscope. The habitus images were taken with a Canon-5D camera mounted on a Nikon SMZ1500 microscope. CombineZM and Helicon Focus software were used to combine the photos. Photoshop CC2019 was used to modify the photos if required.

DNA was extracted from all the specimens via DNeasy Blood & Tissue Kits (Qiagen, Germany). DNA was extracted from either 1, 3, or 6 legs or the whole body, depending on the size of specimen. Polymerase chain reaction (PCR) amplifications for COI sequences were conducted using the primers LCO1490 (GGTCAACAAATCATAAAGATATTGG) and HCO2198 (TAAACTTCAGGGTGACCAAAAATCA). PCR reaction mixes (25 µL) contained 12.5 µL 2× Taq PCR MasterMix (Tiangen Biotech Co., Ltd, Beijing, China), 1 µL of forward and reverse primer each (Sangon Biotech Co. Ltd, Shanghai, China), 2 µL total undiluted DNA template, and 8.5 µL dd H₂O. PCR profile as follows: 94 °C for 2 min, first cycle set (5 repeats): 94 °C for 40 s, 45 °C for 40 s and 72 °C for 60 s. Second cycle set (35 repeats): 94 °C for 40 s, 51 °C for 40 s and 72 °C for 60 s, followed by elongation at 75 °C for 5 min. PCR products were visualised through 1% agarose gel electrophoresis in TAE buffer. Successful PCR products were sent for sequencing in the Beijing Genomics Institute (BGI, Shenzhen, China). The raw data were assembled and edited via SeqMan v. 7.1. We failed to amplify the COI sequence of *P. arcuatus*. In order not to destroy the type specimen (only one specimen), we abandoned the idea of further amplification of the COI sequence. The intraspecific and interspecific K2P genetic distances of *P. lampoglobus* and *P. pilosus* were separately calculated using the MEGA v. 7.

Results

Taxonomic treatment

Pachynotus Kollar & L. Redtenbacher, 1844

Pachynotus Kollar & L. Redtenbacher 1844: 541. Type species: *P. globicollis* Kollar & L. Redtenbacher, 1844. Type locality: India and Kashmir.

Diagnosis. Head with eyes lateral, ovate, flat, or slightly prominent. Base of rostrum not or only slightly broader than forehead, with narrow or broad central furrow, reaching fore margin of forehead or head apex; antennal scrobes dilated and much shallower behind, upper edge touching eyes. Antennal with scape reaching the middle or posterior margin of the eyes at rest, clavate; funicle with the two basal desmomeres more elongate, desmomere III–VI subequal, desmomere VII subconical; club short, ovate, three-segmented. Pronotum with a central sulcus, fine, extremely shallow. Elytra ovate, with base raised as prominent flange or not, and the base bisinuate or not; odd interstriae more raised than even ones or not; metanepisternum fused with it behind, metanepisternal suture therefore distinct only in the cephalic 1/2. Corbels of hind tibiae open or narrowly enclosed; claws connate at base.

Pachynotus pilosus sp. nov.

<https://zoobank.org/37B015C6-3A67-4BD0-B8D7-F312C395791F>

Figs 1, 2, 3A, B, 4A, C, E, 5

Material examined. Holotype, ♂: (white, printed): 西藏山南曲松 [Xīzàng Shānnán Qǔsōng] 邱多江乡亚堆扎拉山垭口 [Qiūduōjiāngxiāng Yàduīzhāláshānyàkǒu] / 28.8307°N, 92.0507°E / 中科院动物所 [Zhōngkēyuàn Dòngwùsuǒ] / 4989.19 m / 2021.VII.12 / 任金梁 [Rén Jīnliáng]: IOZ(E)1965015 // **Paratypes** (2♂, 3♀): same data as holotype except IOZ(E)1965016–IOZ(E)1965020.

Description. Holotype, male. Measurements (in mm): standard length: 5.10; pronotal length: 1.70; pronotal width: 1.9; elytral length: 3.10; elytral width: 2.08; rostral length: 0.90; rostral width: 0.60.

Habitus and colour (Fig. 1A, B): body elongate-oval, small; integument dark reddish brown; antennae and legs reddish brown, with pale yellowish-brown scales; scales on dorsal and lateral surfaces of rostrum moderately dense, oval to elongate-oval; antennal scape and funicles without scales; pronotum with polygonal scales, moderately dense, not contiguous; scales on elytra polygonal, dense, not contiguous; scales on ventrites moderately dense, polygonal, elongate-oval; scales on legs dense; dorsal of tarsi surface without scales; body with erect to suberect and slightly longer setae; rostrum sparsely covered with suberect fine setae; antennal scape and desmomeres I–VII with long, fine, sparse setae; dorsal and lateral surfaces of pronotum with sparse, suberect setae; setae on interstriae long, erect to suberect, behind declivity slightly longer, erect, equal to 6 × diameter of one scale; setae on ventral surface moderately long, fine, erect.

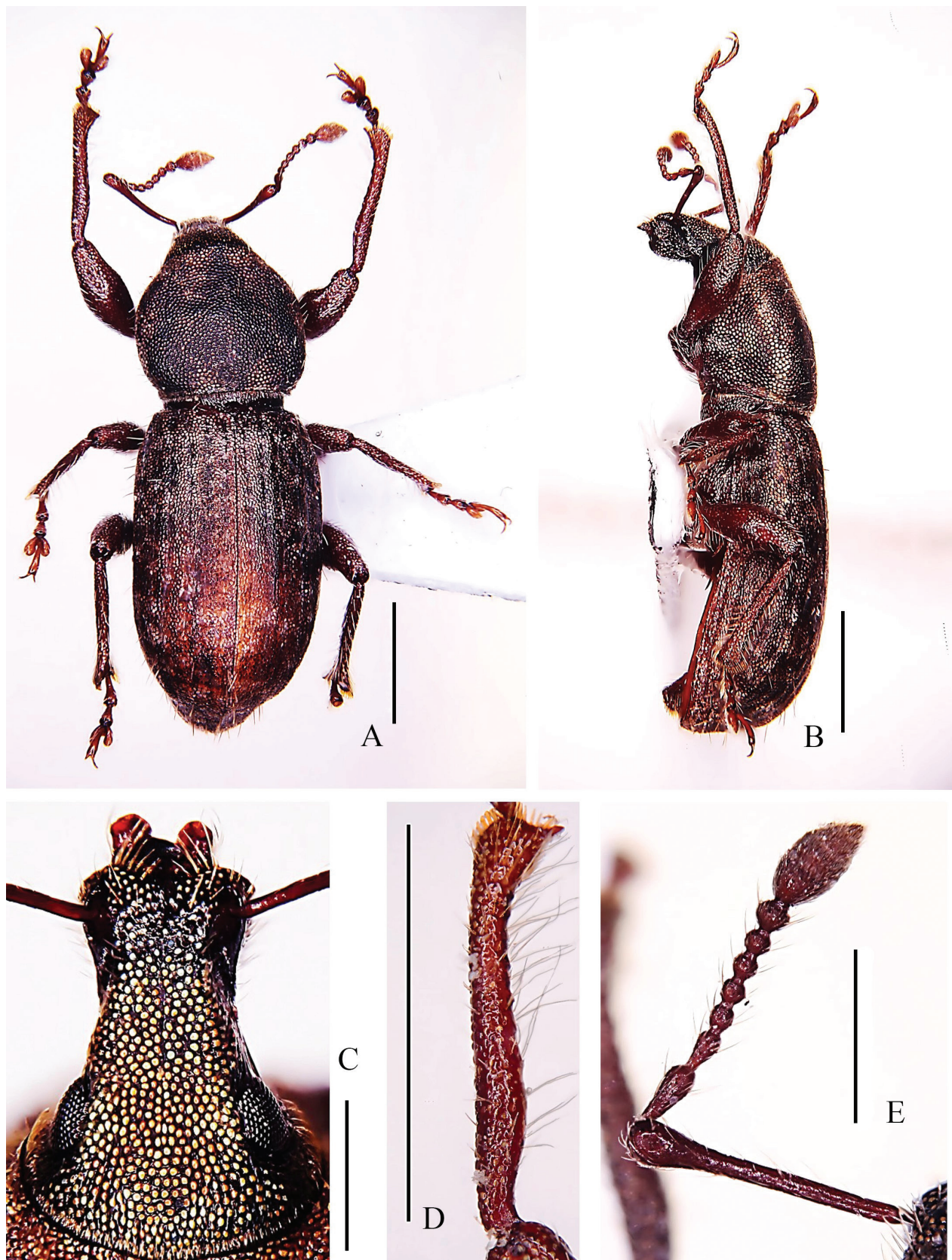


Figure 1. Habitus of *Pachynotus pilosus* sp. nov., holotype **A** dorsal view **B** lateral view **C** head and rostrum, dorsal view **D** left protibia, dorsal view **E** antenna, dorsal view. Scale bars: 1 mm (**A**, **B**, **D**); 0.5 mm (**C**, **E**).

Head (Fig. 1C): moderately convex; dorsal surface smooth; punctures small, moderately dense; eyes flat, oval; forehead weakly convex, moderately elevated than base of rostrum in lateral view.

Rostrum (Fig. 1C): in dorsal view $1.50 \times$ as long as wide, apex narrower than base; sides narrowed from base to middle, and then slightly broadened to apex; dorsal surface with a narrow and shallow median sulcus, reaching fore margin of forehead; epistome broad U-shaped, smooth, posterior angle of epistome $>90^\circ$; mandibular scars oval; ventral margin of antennal scrobes visible at apical half in dorsal view; in lateral view, without triangular depression positioned laterally between eyes and antennal scrobes; prementum with two setae.

Antennae (Fig. 1E): scape slender, clavate, reaching posterior margin of eyes at rest, $0.99 \times$ length of funicle; desmome I $1.40 \times$ length of II, both segments elongate clavate; desmome III short, clavate, $0.59 \times$ length of II; desmome IV $0.91 \times$ length of III, nearly equal width; desmomeres IV–VI moniliform, equal in length and width; desmome VII moniliform, $1.21 \times$ length, $1.24 \times$ width of VI; club elongate-oval, apical sharp, three-segmented, uniformly pubescent, segment I $1.25 \times$ length of II; segment II shorter than segment III.

Pronotum: $0.89 \times$ as long as wide; subquadrate in dorsal outline, strongly convex; sides strongly rounded, greatest width after midpoint, gradually narrowing towards both ends, fore margin shorter than posterior one; median sulcus fine, extremely shallow; dorsal surface smooth, punctures small, each puncture covered by a scale; postocular lobes absent, vibrissae fine, dense, yellow.

Scutellum: large and distinct, triangular, shiny, uncoated, reddish brown.

Elytra: $1.49 \times$ as long as wide, moderately convex, elongate-oval; base not raised as prominent flange, not bisinuate; sides subparallel before declivity, only slightly narrowed near the base; striae distinct, narrow, moderately deep, linear; punctures minute, spot like, moderately dense, space between punctures narrower than the diameter of punctures; interstriae wide, slightly flat, without tubercles, odd interstriae slightly raised than even ones.

Abdomen (Fig. 2A): sternite I depressed in middle, slightly convex at sides; suture between sternites I and II slightly curved forward in middle; sternite II slightly convex; sternite I longer than II, sternite II slightly shorter than III and IV combined; sternites III and IV equal in length; sternite V moderately convex, apex round, longer than sternites III and IV combined.

Legs: rather short; femora clavate; fore tibiae subcylindrical, slightly sinuate, slightly bent inwards at apical quarter, apex not projected inwards and outwards, with long and slender hairs, obviously different from other setae, somewhat sparse (Fig. 1D); inner margin of fore tibiae with several extremely small teeth; median and hind tibiae without teeth; corbels of hind tibiae closed.

Genitalia: sternite VIII (Fig. 2B) divided into two hemisternites, transversely oriented, subtrapeziform; each laterally acuminate. Sternite IX (Fig. 2B) with basal plate bilobed; spiculum gastrale $1.19 \times$ as long as aedeagus, strongly sclerotised, anterior third curved. Penis (Fig. 2C, D) in dorsal view with tube 0.97 mm in length, $4.8 \times$ length of wide, temones 0.62 mm long; in lateral view curved, more strongly so near base and at apex, greatest width at midpoint. Tegmen (Fig. 2E) $0.61 \times$ length of penis, with ring narrow, parameroid lobes developed with basal half more sclerotised; tegminal apodeme slender, forming a Y-shape with basal piece.

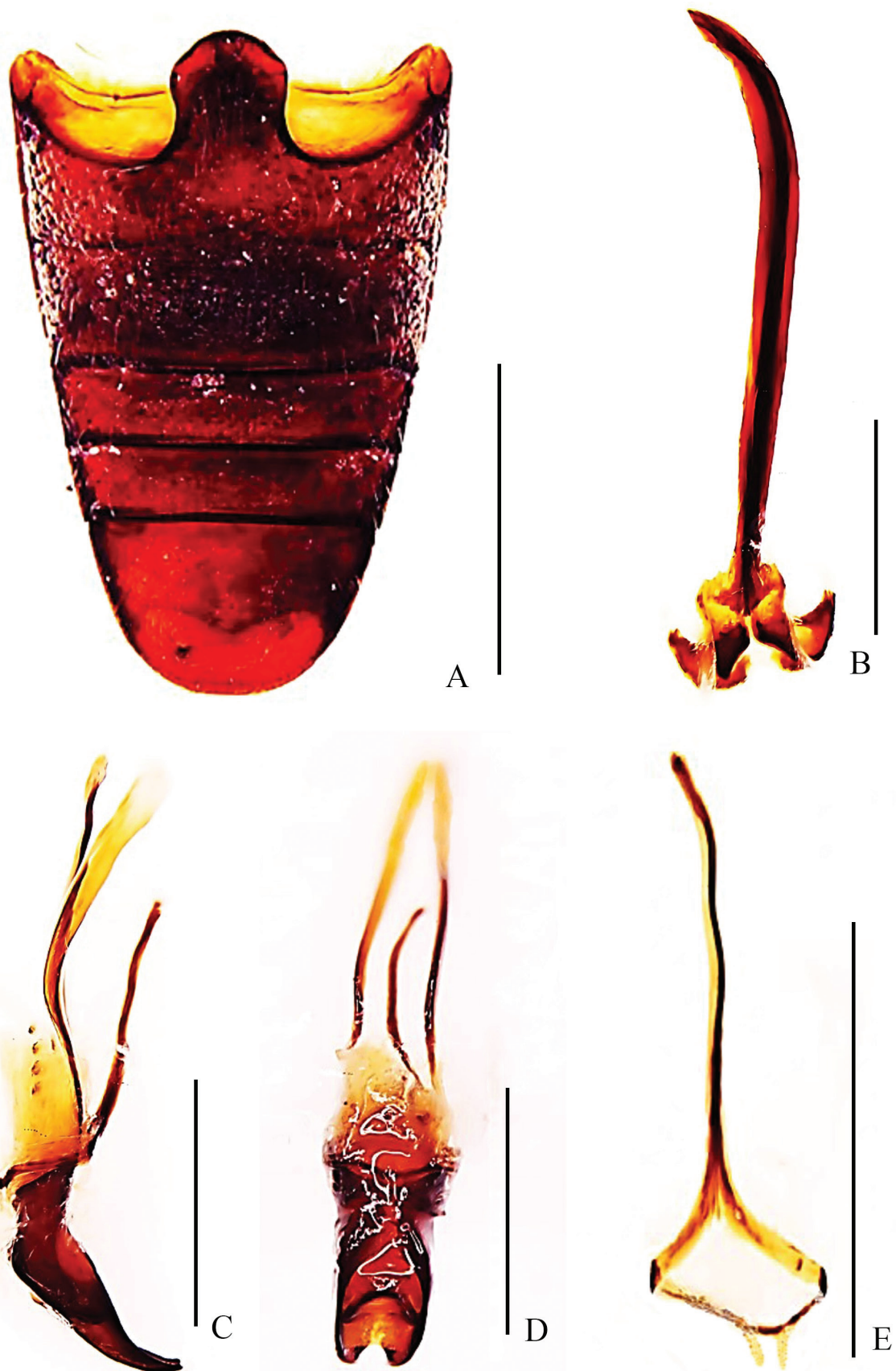


Figure 2. Abdominal and genital structures of *Pachynotus pilosus* sp. nov., holotype **A** ventrites, ventral view **B** sternites VIII and IX, dorsal view **C** aedeagus, lateral view **D** aedeagus, dorsal view **E** tegmen, dorsal view. Scale bars: 0.5 mm.

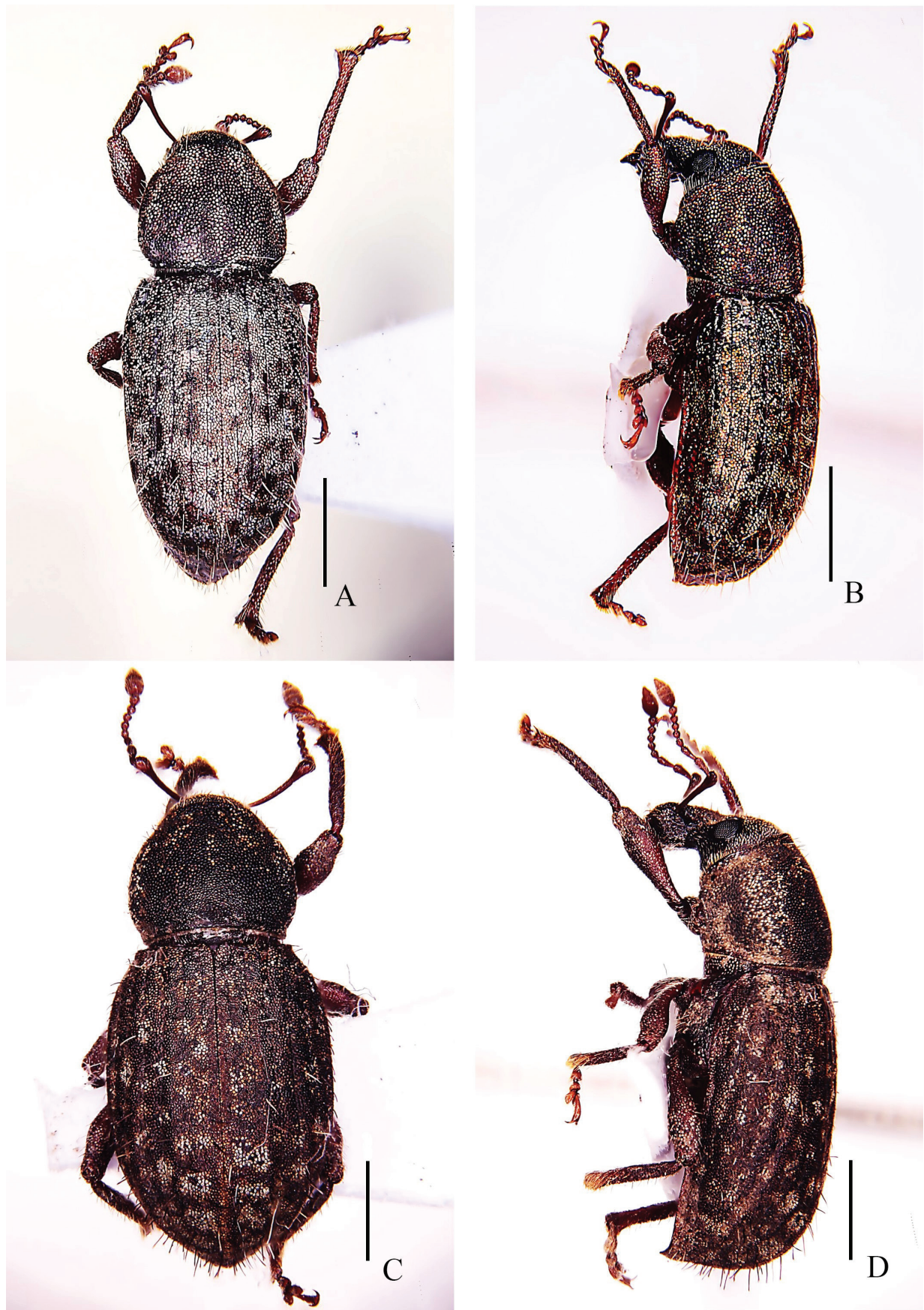


Figure 3. Habitus of *Pachynotus pilosus* sp. nov. paratype **A** dorsal view **B** lateral view. *Pachynotus arcuatus* sp. nov. holotype **C** dorsal view **D** lateral view. Scale bars: 1 mm.

Variation. Male paratypes. Measurements (in mm): standard length: 5.00–5.30; pronotal length: 1.7–1.9; pronotal width: 1.85–2.10; elytral length: 3.00–3.20; elytral width: 2.00–2.20; rostral length: 0.80–1.00; rostral width: 0.60–0.70.

Females. Measurements (in mm): standard length: 4.80–5.50; pronotal length: 1.70–1.80; pronotal width: 1.80–2.10; elytral length: 3.10–3.50; elytral width: 2.08–2.60; rostral length: 0.80–1.00; rostral width: 0.60–0.75. Fore tibiae with short and slender setae, same as other setae (Fig. 4C); ventrite V (Fig. 5A) parabolic, longer than ventrite II. Sternite VIII (Fig. 5C) with spiculum ventrale thin, rod-like and sinuate. Spermatheca (Fig. 5D) with corpus subquadrate; cornu widely curved, U-shaped, apically gradually narrowed; ramus subspherical, prominent and long.

Etymology. *Pilosus*, Latin adjective, meaning “hairy”, in reference to the significantly longer hair on the male fore tibiae than on other parts.

Distribution. China (Xizang).

***Pachynotus arcuatus* sp. nov.**

<https://zoobank.org/1D3535AB-C051-4DBE-9458-390738E4B13E>

Figs 3C, D, 4B, D, F, 6

Material examined. Holotype, ♀: (white, printed): 西藏山南地区 [Xīzàng Shānnándìqū] 羊措拉山 [Yángcuòlāshān] / 28.09708°N, 91.933395°E / 4685 m / 2018.VIII.15 / 周润 [Zhōu Rùn] / 中科院动物所 [Zhōngkēyuàn Dòngwùsuǒ]: IOZ(E)1965679.

Description. Holotype, female. Measurements (in mm): standard length: 5.90; pronotal length: 1.90; pronotal width: 2.20; elytral length: 3.90; elytral width: 3.00; rostral length: 1.15; rostral width: 0.85.

Habitus and colour (Fig. 3C, D): body elongate-oval, small; integument dark reddish brown; antennae and legs reddish brown, with light-grey scales; scales on dorsal and lateral surfaces of rostrum moderately dense, oval to elongate-oval; antennal scape and funicles without scales; pronotum with polygonal scales, moderately dense, not contiguous; scales on elytra polygonal, dense, not contiguous; scales on ventrites moderately dense, polygonal to elongate-oval; scales on legs dense; dorsal of tarsi surface without scales; body with erect to suberect and slightly longer setae, sparser; rostrum sparsely covered with suberect fine setae; antennal scape and desmomerer I–VII with long, fine and sparse setae; dorsal and lateral surfaces of pronotum with sparse, suberect setae; setae on interstriae long, erect to suberect, behind declivity slightly longer, erect, equal to 6 × diameter of one scale; setae on ventral surface moderately long, fine, erect.

Head (Fig. 4B): moderately flat; dorsal surface smooth; punctures small and dense; eyes flat, oval; forehead weakly convex, moderately elevated than base of rostrum in lateral view.

Rostrum (Fig. 4B): in dorsal view, 1.35 × as long as wide, apex narrower than base; sides narrowed from base to middle, and then slightly broadened to apex; dorsal surface with a broad, deep, median sulcus, reaching vertex of head; posterior angle of epistome 90°, smooth; mandibular scars oval; ventral margin of antennal scrobes visible at apical half in dorsal view; in lateral view, without triangular depression positioned laterally between eyes and antennal scrobes; prementum with two setae.

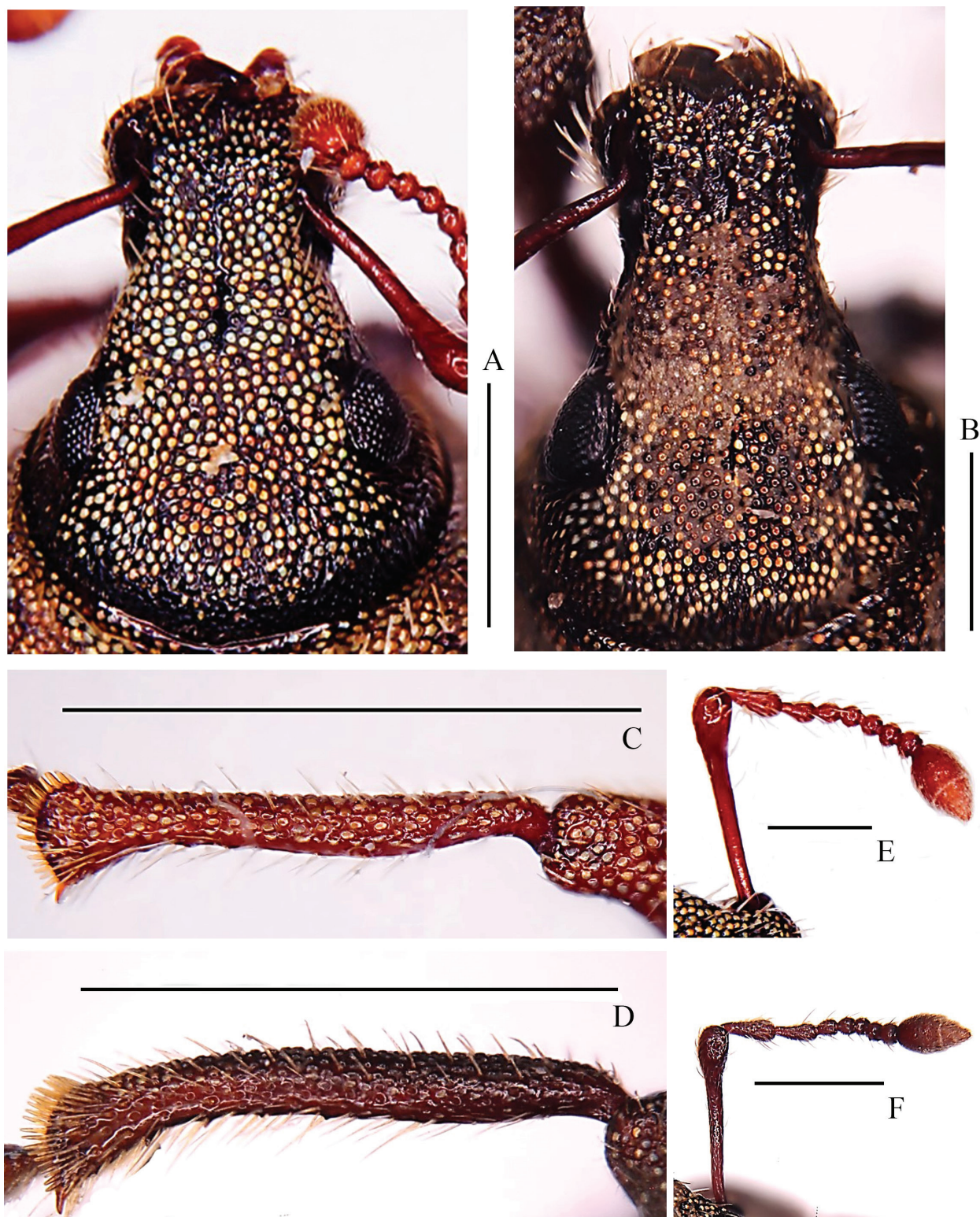


Figure 4. *Pachynotus pilosus* sp. nov. **A** head and rostrum, dorsal view **C** right protibia, anterior view **E** antenna, anterior view; *Pachynotus arcuatus* sp. nov. **B** head and rostrum, dorsal view **D** right protibia, anterior view **F** antenna, anterior view. Scale bars: 0.5 mm (**A**, **B**, **E**, **F**); 1 mm (**C**, **D**).

Antennae (Fig. 4F): scape slender, clavate, reaching posterior margin of eyes at rest, $0.98 \times$ length of funicle; desmommere I $1.43 \times$ length of II, both segments elongate clavate; desmommere III short, clavate, $0.51 \times$ length of II; desmommere

IV $0.93 \times$ length of III, nearly equal width; desmomerer IV–VI moniliform, equal in length and width; desmomerer VII moniliform, $1.08 \times$ length, $1.03 \times$ width of VI; club elongate-oval, apically sharp, three-segmented, uniformly pubescent, segment I $1.21 \times$ length of II; segment II shorter than segment III.

Pronotum: $0.86 \times$ as long as wide; subquadrate in dorsal outline, strongly convex; sides strongly rounded, greatest width after midpoint, gradually narrowing towards both ends, fore margin shorter than posterior one; median sulcus fine, extremely shallow; postocular lobes absent, vibrissae fine, dense, yellow.

Scutellum: large and distinct, U-shaped, shiny, uncoated, reddish brown.

Elytra: $1.30 \times$ as long as wide, moderately convex, elongate-oval; with base raised as prominent flange, not bisinuate; sides subparallel before declivity, only slightly narrowed near base; striae distinct, narrow, moderately deep, linear; puncture minute, spot-like, moderately dense, space between punctures narrower than diameter of punctures; interstriae wide, slightly flat, without tubercles, odd interstriae slightly raised than even ones.

Abdomen (Fig. 6A): sternite I depressed in middle, slightly convex at sides; suture between sternites I and II slightly bisinuate; sternite II slightly convex; sternite I longer than II, sternite II slightly shorter than III and IV combined; sternites III and IV equal in length; sternite V moderately convex, apical round, longer than sternites III and IV combined.

Legs: rather short; femora clavate; fore tibiae obviously bent inward at apical third, apex neither projected inwards nor outwards (Fig. 4D); inner margin of fore tibiae with several extremely small teeth; median- and hind tibiae without teeth; corbels of hind tibiae closed.

Genitalia: ventrite V (Fig. 6A) parabolic, longer than ventrite II. Sternite VIII (Fig. 6C) with spiculum ventrale thin, rod-like, and sinuate. Spermatheca (Fig. 6D) with corpus subquadrate; cornu elongate, widely curved, wide U-shaped, apically gradually narrowed; ramus quadrate.

Male. Unknown.

Remarks. This new species resembles *P. pilosus* sp. nov. but differs by the following characters: scutellum U-shaped; rostrum with a broad and deep median sulcus, reaching head vertex; elytra base raised as prominent flange; fore tibiae obviously bent inward at apical third.

Etymology. *Arcuatus*, Latin participle, meaning “curved”, in reference to the fore tibiae, which is bent inward at its apical third.

Distribution. China (Xizang).

Pachynotus lampoglobus Chao & Y.-Q. Chen, 1980

Fig. 7

Material examined. **Holotype**, ♂: (white, printed): 西藏普兰科加 [Xizàng Pǔlán Kējiā] / 3700公尺 [Gōng Chǐ] / 中国科学院 [Zhōngguó Kēxué Yuàn] / 14. VII 1976 / 黄复生 [Huáng Fùshēng]: IOZ(E)905056 // **Paratype** (1♂): same data as holotype except IOZ(E)905057.

Redescription. **Holotype, male.** Measurements (in mm): standard length: 5.60; pronotal length: 1.85; pronotal width: 2.10; elytral length: 3.70; elytral width: 3.00; rostral length: 1.10; rostral width: 1.00.

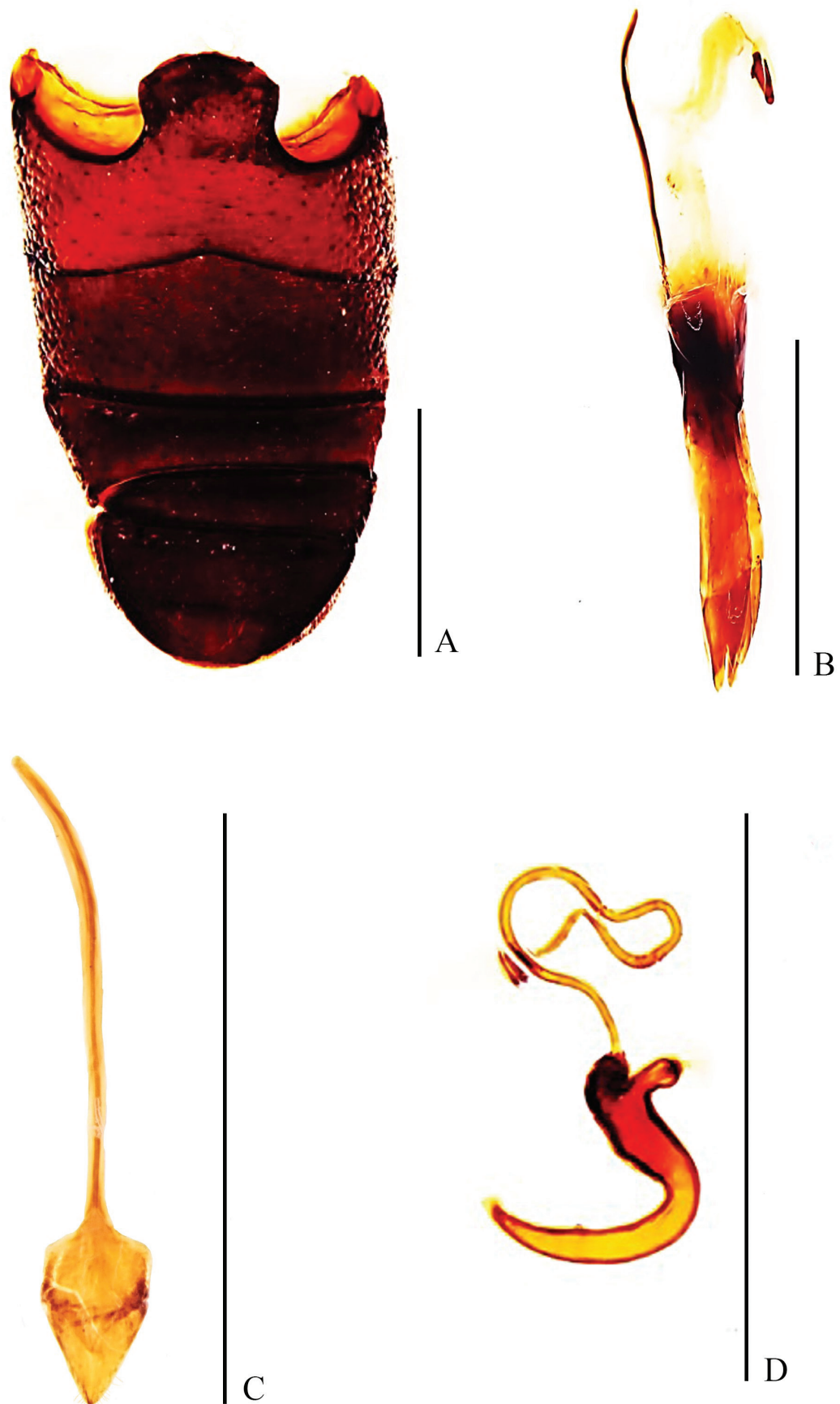


Figure 5. Abdominal and genital structures of *Pachynotus pilosus* sp. nov. **A** ventrites, ventral view **B** sternite VIII and female genitalia, lateral view **C** sternum VIII, dorsal view **D** spermatheca, lateral view. Scale bars: 0.5 mm.



Figure 6. Abdominal and genital structures of *Pachynotus arcuatus* sp. nov. **A** ventrites, ventral view **B** sternite VIII and female genitalia, lateral view **C** sternum VIII, dorsal view **D** spermatheca, lateral view. Scale bars: 0.5 mm.

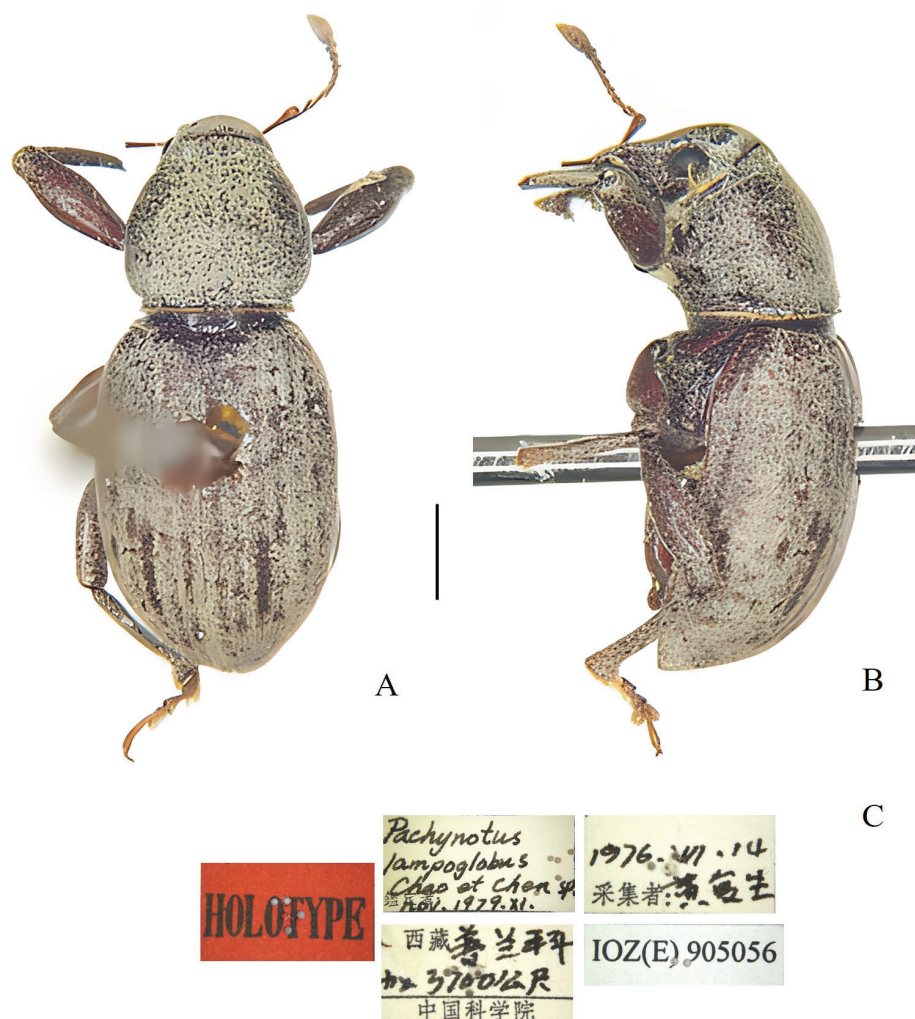


Figure 7. Habitus of *Pachynotus lampoglobus*, holotype. **A** dorsal view **B** lateral view **C** specimen label. Scale bars: 1 mm.

Habitus and colour (Fig. 7): body wide, ovate; blackish-reddish brown; antennae and legs reddish brown, with pale yellowish-brown scales with red-green metallic lustre; scales on dorsal and lateral surfaces of rostrum moderately dense, oval to elongate-oval; antennal scape and funicles without scales; pronotum with polygonal scales, moderately dense, not contiguous; scales on elytra polygonal, dense, but not contiguous; scales on ventrites moderately dense, polygonal to elongate-oval; scales on legs dense; dorsal of tarsi surface without scales; body with erect to suberect, short, sparse setae; rostrum sparsely covered with suberect, fine, short setae; antennal scape and desmomerer I–VII with long, fine, sparse setae; dorsal and lateral surfaces of pronotum with sparse, suberect setae; setae on interstriae short, erect to suberect, equal to $2 \times$ diameter of scale; setae on the ventral surface moderately long, fine, erect.

Head: convex; dorsal surface smooth; punctures small and dense; eyes moderately convex, oval; forehead convex, moderately elevated than base of rostrum in lateral view.

Rostrum: in dorsal view, $1.10 \times$ as long as wide; sides narrowed from base to apex; apex narrower than base; dorsal surface with a broad and deep median sulcus, reaching middle of forehead; posterior angle of epistome more than 90° , smooth; mandibular scars oval; ventral margin of antennal scrobes visible at

apical two-thirds in dorsal view; in lateral view, without triangular depression positioned laterally between eyes and antennal scrobes; prementum with four setae.

Antennae: scape slender, clavate, reaching middle of eyes at rest, $0.88 \times$ length of funicle; desmomere I $1.30 \times$ length of II, both segments elongate clavate; desmomere III short, clavate, $0.47 \times$ length of II; desmomere IV $0.88 \times$ length of III, nearly equal width; desmomeres IV–VI moniliform, equal in length and width; desmomere VII moniliform, $1.09 \times$ length, $1.06 \times$ width of VI; club elongate-oval, apical sharp, three-segmented, uniformly pubescent, segment I $1.35 \times$ length of II; segment II shorter than segment III.

Pronotum: $0.88 \times$ as long as wide; subquadrate in dorsal outline, strongly convex; sides strongly rounded, greatest width at midpoint, gradually narrowing towards both ends, fore margin shorter than posterior one; median sulcus, fine, extremely shallow; dorsal surface of pronotum smooth, punctures small, each puncture covered by a scale; postocular lobes absent, vibrissae fine, dense, yellow.

Scutellum: large and distinct, U-shaped, shiny, uncoated, reddish brown.

Elytra: $1.23 \times$ as long as wide, moderately convex, elongate-oval; base not raised as prominent flange, not bisinuate; sides subparallel before declivity, only slightly narrowed near the base; striae distinct, narrow, moderately deep, linear; punctures minute, spot-like, moderately dense, spaces between punctures narrower than diameter of punctures; interstriae wide, flat, without tubercles, odd interstriae not more raised than even ones.

Abdomen: sternite I depressed in middle, slightly convex at sides; suture between sternite I and II slightly bisinuate; sternite II slightly convex; sternite I longer than II, sternite II slightly shorter than III and IV combined; sternites III and IV equal in length; sternite V moderately convex, apical round, shorter than sternites III and IV combined.

Legs: slightly short; femora clavate, densely with scales; fore tibiae bent inward at apical half, apex projected inwards and outwards; inner margin of fore tibiae with several moderately large teeth; median- and hind tibiae with moderately small teeth; corbels of hind tibiae closed.

Variation. Male paratype. Measurements (in mm): standard length: 6.10; pronotal length: 1.90; pronotal width: 2.20; elytral length: 3.80; elytral width: 3.10; rostral length: 1.10; rostral width: 0.90.

Female. Unknown.

Distribution. China (Xizang).

Genetic distances

The intraspecific genetic distances of *P. lampoglobus* and *P. pilosus* are 0% and 1.38%, respectively (0.69%, average). The interspecific genetic distances are between 22.64% and 23.50% (23.07%, average) (Table 1).

Table 1. Genetic distance of *Pachynotus lampoglobus* and *P. pilosus* based on COI sequences.

	Species	GenBank Accession Number	1	2	3
1	<i>P. lampoglobus</i>	OR123593			
2		OR123594	0%		
3	<i>P. pilosus</i> sp. nov	OR123595	22.64%	22.64%	
4		OR123596	23.50%	23.50%	1.38%

Key to species of *Pachynotus* occurring in China

- 1 Prementum with two setae; scape reaching posterior margin of eyes at rest; inner margin of fore tibiae with extremely small teeth; mid and hind tibiae without teeth; elytral odd interstriae more raised than even ones.....**2**
- Prementum with four setae; scape reaching middle of eyes at rest; inner margin of fore tibiae with several moderately big teeth; mid and hind tibiae with moderately small teeth; elytral odd interstriae not more raised than even ones.....***P. lampoglobus***
- 2 Scutellum triangular; rostrum with a narrow and shallow median sulcus, reaching fore margin of forehead; posterior angle of epistome > 90°; elytral base not raised as prominent flange; fore tibiae slightly bent inward at apical quarter.....***P. pilosus* sp. nov.**
- Scutellum U-shaped; rostrum with a broad and deep median sulcus, reaching head vertex; posterior angle of epistome 90°; elytral base raised as prominent flange; fore tibiae obviously bent inward at apical third.....***P. arcuatus* sp. nov.**

Discussion

The three Chinese *Pachynotus* species occurring in Xizang are all endemic to China, and morphological variation and genetic differences among these species are conspicuous. In our study, the average interspecific genetic distance between *P. lampoglobus* and *P. pilosus* was 33 × that of the average intraspecific genetic distance. This confirms, by molecular means, the validity of the new species *P. pilosus* sp. nov. (Hebert et al. 2003, 2004). In addition, the COI sequences of *P. lampoglobus* and *P. pilosus* are provided for the first time, which will help promote further DNA barcoding studies of this genus.

Pachynotus species in China are quite different in size from other *Pachynotus* species. *P. globicollis* (length 9.63 mm, width 2.89 mm), *P. mayarami* (length 9.55 mm, width 3.10 mm), and *P. kumaonensis* (length 9.80 mm, width 3.25 mm) are larger than *P. lampoglobus* (average length 5.82 mm, average width 3.05 mm), *P. pilosus* (average length 5.12 mm, average width 2.21 mm), and *P. arcuatus* (length 5.90 mm, average width 3.00 mm). It is worth noting that *P. globicollis*, *P. mayarami*, and *P. kumaonensis* are distributed in Uttarakhand, India; *P. globicollis* was found at an altitude of 1753–2286 m in Uttarakhand (Mahendiran and Ramamurthy 2013), and the other two species have no altitudinal information. *P. lampoglobus*, *P. pilosus*, and *P. arcuatus* are found in Xizang of China at altitudes of 3700 m, 4989 m, and 4685 m, respectively. This phenomenon of extreme altitude could be attributed to the advantages that diminutive bodies offer in the face of the relatively harsh conditions of high-altitude environments. In such conditions, these smaller weevils can thrive on minimal food resources and easily seek refuge by burrowing into rock crevices, thus evading predators and harsh climatic conditions.

As flightless weevils, the genus *Pachynotus* is inherently predisposed to geographical isolation, leading to the emergence of new species as observed in previous studies (Chen 1991; Ren 2008) and this study. Therefore, our findings suggest that there may be more *Pachynotus* species awaiting discovery, considering the geographic isolation and the unique ecological niches that *Pachynotus* species inhabit.

Acknowledgements

Thanks are due to Run Zhou for collecting and providing specimens of the new species described in this study, and to Jing Xu and Yizhe Li for their kind help during this study.

Additional information

Conflict of interest

The authors have declared that no competing interests exist.

Ethical statement

No ethical statement was reported.

Funding


This research was supported by the National Natural Science Foundation of China (31872260).

Author contributions

Conceptualization, Runzhi Zhang, Li Ren and Jinliang Ren; methodology and formal analysis Jinliang Ren; data curation, Jinliang Ren field sampling, Jinliang Ren; writing – original draft, Jinliang Ren; writing – review and edit, Runzhi Zhang, Li Ren and Jinliang Ren. All authors have read and agreed to the published version of the manuscript.

Author ORCIDs

Jinliang Ren  <https://orcid.org/0009-0000-9847-1035>

Li Ren  <https://orcid.org/0000-0002-8597-0449>

Runzhi Zhang  <https://orcid.org/0000-0001-9001-0154>

Data availability

All of the data that support the findings of this study are available in the main text.

References

- Alonso-Zarazaga MA, Barrios H, Borovec R, Bouchard P, Caldara R, Colonnelli E, Gültekin L, Hlaváč P, Korotyaev B, Lyal CHC, Machado A, Meregalli M, Pierotti H, Ren L, Sánchez-Ruiz M, Sforzi A, Silfverberg H, Skuhrovec J, Trýzna M, Velázquez de Castro AJ, Yunakov NN (2023) Cooperative Catalogue of Palaearctic Coleoptera Curculionidae. Monografías electrónicas S.E.A. 8: 729 pp. <http://sea-entomologia.org/monoelec.html>
- Aslam NA (1966) Revision of Tanymecine genera, *Achlainomus* Waterhouse and *Hyperomias* Marshall and designation of type for *Stropohosomoides* Aslam (Coleoptera, Curculionidae). *Annals and Magazine of Natural History (Series 13)* 9: 405–416. <https://doi.org/10.1080/00222936608651663>
- Chao YC, Chen YQ (1980) Chinese *Leptomias* Faust and its allied genera in the Qinghai-Xizang plateau district (Coleoptera, Curculionidae). *Entomotaxonomia* 2(2): 85–107.
- Chen YQ (1991) A revision of *Leptomias* Faust and descriptions of new genera and new species from Xizang, China (Coleoptera, Curculionidae). *Sinozoologia* 8: 257–266.

- Hebert PDN, Cywinska A, Ball SL, deWaard JR (2003) Biological identifications through DNA barcodes. *Proceedings of the Royal Society B, Biological Sciences* 270(1512): 313–321. <https://doi.org/10.1098/rspb.2002.2218>
- Hebert PDN, Stoeckle MY, Zemlak TS, Francis CM (2004) Identification of Birds through DNA Barcodes. *PLoS Biology* 2(10): 1657–1663. <https://doi.org/10.1371/journal.pbio.0020312>
- Kollar V, Redtenbacher L (1844) Hugel, C. F. von Kaschmir and das Reich der Siek. Aufzählung und Beschreibung der von Freiherrn Carl v. Hugel auf seiner Reise durch Kaschmir und das Himalayagebirge gesammelten Insecten 4(2): 247–586.
- Mahendiran G, Ramamurthy VV (2013) The weevil genus *Pachynotus* Redtenbacher (Coleoptera: Curculionidae: Entiminae) from India. *Oriental Insects* 47(1): 76–85. <https://doi.org/10.1080/00305316.2012.757024>
- Marshall GAK (1916) Coleoptera. Rhynchophora: Curculionidae. *The Fauna of British India including Ceylon and Burma*. Taylor and Francis, London, 367 pp. <https://doi.org/10.5962/bhl.title.100762>
- Myers N, Mittermeier RA, Mittermeier CG, da Fonseca GAB, Kent J (2000) Biodiversity hotspots for conservation priorities. *Nature* 403(6772): 853–858. <https://doi.org/10.1038/35002501>
- Ren L (2008) Systematics of the *Leptomias* generic group from China (Coleoptera, Curculionidae). Ph.D. thesis, Institute of Zoology Chinese Academy of Sciences, Beijing, China.

Appendix 1

Checklist to species of the genus *Pachynotus*

***Pachynotus globicollis* Kollar & L. Redtenbacher, 1844: 544**

Cneorhinus obscurus Kollar & L. Redtenbacher, 1844: 544.

Distribution. India (Kashmir, Himachal Pradesh, Uttarakhand).

***Pachynotus kumaonensis* Mahendiran & Ramamurthy, 2013: 82**

Distribution. India (Uttarakhand).

***Pachynotus lampoglobus* Chao & Y.-Q. Chen, 1980: 88**

Distribution. China (Xizang).

***Pachynotus mayarami* Mahendiran & Ramamurthy, 2013: 82**

Distribution. India (Uttarakhand).

***Pachynotus pilosus* J.-L. Ren, Ren & Zhang, sp. nov.**

Distribution. China (Xizang).

***Pachynotus arcuatus* J.-L. Ren, Ren & Zhang, sp. nov.**

Distribution. China (Xizang).

Leptanilla voldemort sp. nov., a gracile new species of the hypogaeic ant genus *Leptanilla* (Hymenoptera, Formicidae) from the Pilbara, with a key to Australian *Leptanilla*

Mark K. L. Wong^{1,2}, Jane M. McRae³

1 School of Biological Sciences, The University of Western Australia, Crawley, WA 6009, Australia

2 Centre for Environment and Life Sciences, Commonwealth Scientific and Industrial Research Organization, Floreat, WA 6014, Australia

3 Bennelongia Environmental Consultants, 5 Bishop Street, Jolimont, WA 6014, Australia

Corresponding author: Mark K. L. Wong (mark.wong@uwa.edu.au)

Abstract

The genus *Leptanilla* Emery, 1870 of the family Formicidae, subfamily Leptanillinae, comprises miniscule, pale, blind ants that are rarely collected and poorly understood due to their hypogaeic (i.e. underground) lifestyles. Here we describe a new *Leptanilla* species from two workers collected via subterranean scraping in the arid Pilbara region of Western Australia. *Leptanilla voldemort* sp. nov. is the second leptanilline species documented in Australia after the elusive *Leptanilla swani* Wheeler, 1932. Workers of *L. voldemort* sp. nov. display a remarkably gracile morphology characterised by elongated legs, antennae, and mandibles, and they are easily differentiated from other *Leptanilla* species. We also provide new measurements for *L. swani* from two workers found proximally to the type locality of *L. voldemort* sp. nov. A key to the worker caste of *Leptanilla* species of the Australian continent is presented.

Key words: Australia, hypogaeic, *Leptanilla*, Milieu Souterrain Superficiel, subterranean



Academic editor: Matthew Prebus

Received: 12 October 2023

Accepted: 26 February 2024

Published: 11 April 2024

ZooBank: <https://zoobank.org/8305E70B-42A4-4E8C-86E6-63967D6A4DDD>

Citation: Wong MKL, McRae JM (2024) *Leptanilla voldemort* sp. nov., a gracile new species of the hypogaeic ant genus *Leptanilla* (Hymenoptera, Formicidae) from the Pilbara, with a key to Australian *Leptanilla*. ZooKeys 1197: 171–182. <https://doi.org/10.3897/zookeys.1197.114072>

Copyright: © Mark K. L. Wong & Jane M. McRae. This is an open access article distributed under terms of the Creative Commons Attribution License ([Attribution 4.0 International – CC BY 4.0](https://creativecommons.org/licenses/by/4.0/)).

Introduction

Although lacking the impressive colours, armoury and colony sizes seen in many of the world's ~14,000 ant species (Bolton 2024), the diminutive members of the genus *Leptanilla* Emery, 1870 (Formicidae, Leptanillinae) are darlings of myrmecologists, for they include some of the most elusive and bizarre ants on Earth. All known *Leptanilla* species are hypogaeic, living in small colonies that nest and forage exclusively underground (Griebenow 2024; Qian et al. 2024). As such, individuals of *Leptanilla* are rarely collected by conventional methods for sampling ants (e.g. pitfall traps), which tend to target surface habitats (Wong and Guénard 2017). In adaption to subterranean life, *Leptanilla* ants characteristically display cryptobiotic morphological traits; their workers are very small (often <2 mm), depigmented and blind (Bolton 1990; Wong and Guénard 2016). The few observations of live *Leptanilla* colonies have also revealed intriguing, specialised behaviours, such as specialised predation on geophilomorph centipedes (Masuko 1990), and adult feeding on haemolymph

(i.e. blood) of the larvae from a unique duct-like organ in the larval integument—the “larval haemolymph tap” (Masuko 1989). Moreover, recent phylogenomic analyses show that together with the monotypic Martialinae, the Leptanillinae constitute the sister group to all other extant ant species, making them especially significant for our understanding of ant evolution (Borowiec et al. 2019; Romiguier et al. 2022; but see Cai 2024).

The 61 described species of *Leptanilla* are found in tropical and temperate regions of the Old World (Bolton 1990; Griebenow 2024; Qian et al. 2024). The apparently patchy distribution of the genus may be an artefact of geographic biases in ant research in general (Kass et al. 2022) and the use of subterranean sampling techniques in particular (Wong and Guénard 2017). While multiple *Leptanilla* species have been documented in Africa, Europe, and Asia, only one species, *Leptanilla swani* Wheeler, 1932 has been described from Australia thus far. Moreover, few if any workers of *L. swani* have been found in the 90 years since it was first described (Wheeler 1932; Heterick 2022; AntWeb 2024). Although winged *Leptanilla* males have been collected in flight-interception traps throughout the continent, the identities of these are questionable, as none occur in sympatry with definitive workers of *L. swani* (AntWeb 2024; Zachary Griebenow pers. comm.).

Here, we describe a new *Leptanilla* species, *Leptanilla voldemort* sp. nov., from two workers collected in the arid Pilbara region of Western Australia. *Leptanilla voldemort* sp. nov. represents the second species of *Leptanilla* and second member of the subfamily Leptanillinae from the Australian continent. Notably, workers of *L. voldemort* sp. nov. display a distinctly gracile morphology, characterised by elongated legs, antennae, and mandibles. This remarkable phenotype is not seen in most other *Leptanilla* species – including the other Australian species, *L. swani*, for which new morphological measurements are hereby reported from two workers collected proximally to the type locality of *L. voldemort* sp. nov. A key to the worker caste of *Leptanilla* from Australia is also presented.

Methods

Photographs of specimens were obtained with an incorporated digital camera mounted on a Leica M205C dissecting microscope through the Leica Application Suite V4 software. A total of 33–72 images were taken and stacked together. Morphological measurements and indices were calculated following Griebenow et al. (2022). These are detailed below.

- HW** (head width): maximum width of cranium in full-face view.
- HL** (head length): maximum length of head in full-face view from anterior margin of head to cranial vertex.
- SL** (scape length): maximum length of scape in medial view, excluding bulbous.
- MaL** (mandible length): maximum length of mandible from view orthogonal to lateral mandibular margin, measured from ventral mandibular articulation to mandibular apex.
- WL** (Weber’s length): maximum diagonal length of mesosoma in profile view, measured from most anterior extent of pronotum excluding cervical shield to most posterior extent of propodeal lobes, when present.

- PrW** (pronotal width): maximum width of pronotum, measured in dorsal view.
- MW** (mesonotal width): maximum width of mesonotum in dorsal view, measured immediately anterior to mesocoxal foramen.
- PTL** (petiolar length): maximum length of petiole in dorsal view, not including presclerites.
- PTH** (petiolar height): maximum height of petiole in profile view, including sternal process and dorsal node, if distinct.
- PTW** (petiolar width): maximum width of petiole in dorsal view.
- PPL** (postpetiolar length): maximum length of postpetiole in dorsal view, not including presclerites.
- PPW** (postpetiolar width): maximum width of postpetiole in dorsal view.
- PPH** (postpetiolar height): maximum height of postpetiole in profile view, including sternal process and dorsal node, if distinct.
- CI** (cephalic index) = $HW \div HL \times 100$.
- SI** (scape index) = $SL \div HW \times 100$.
- MI** (mandibular index) = $MaL \div HW \times 100$.
- PI** (petiolar index) = $PTW \div PTL \times 100$.
- PPI** (postpetiolar index) = $PPW \div PPL \times 100$.
- PPHI** (postpetiolar height index) = $PPH \div PPL \times 100$.

Abbreviations of the type depositories are as follows:

- ANIC** Australian National Insect Collection;
WAM Western Australian Museum.

Results

Species accounts

***Leptanilla voldemort* Wong & McRae, sp. nov.**

<https://zoobank.org/6C23DA06-A060-4326-A318-991C7EB3C7A1>

Figs 1–4

Type material. Holotype. AUSTRALIA • 1 worker; Western Australia, Newman; 22°44'S, 119°02'E; ca 575 m a.s.l.; 8 Mar. 2023; Jane M. McRae leg.; collected via subterranean scraping; BENNSPECIMENID_746962.1; WAM.

Paratype. AUSTRALIA • 1 worker; same data as for holotype; BENNSPECIMENID_746962; WAM.

Unfortunately, both the holotype and paratype specimens were brittle and partially damaged during the mounting process. A photograph of the fully intact specimens in liquid prior to mounting is shown in Fig. 1. During mounting of the holotype, the postpetiole was disconnected from the petiole and gaster. The paratype was similarly disconnected at the petiole and gaster. Broken segments of each specimen were glued onto its respective mount. The full-body images of the mounted holotype in profile view (Fig. 2) and dorsal view (Fig. 3) are composites in which the postpetiole and gaster were imaged separately in the respective views, and subsequently reattached to the body digitally, while ensuring consistency of scale.

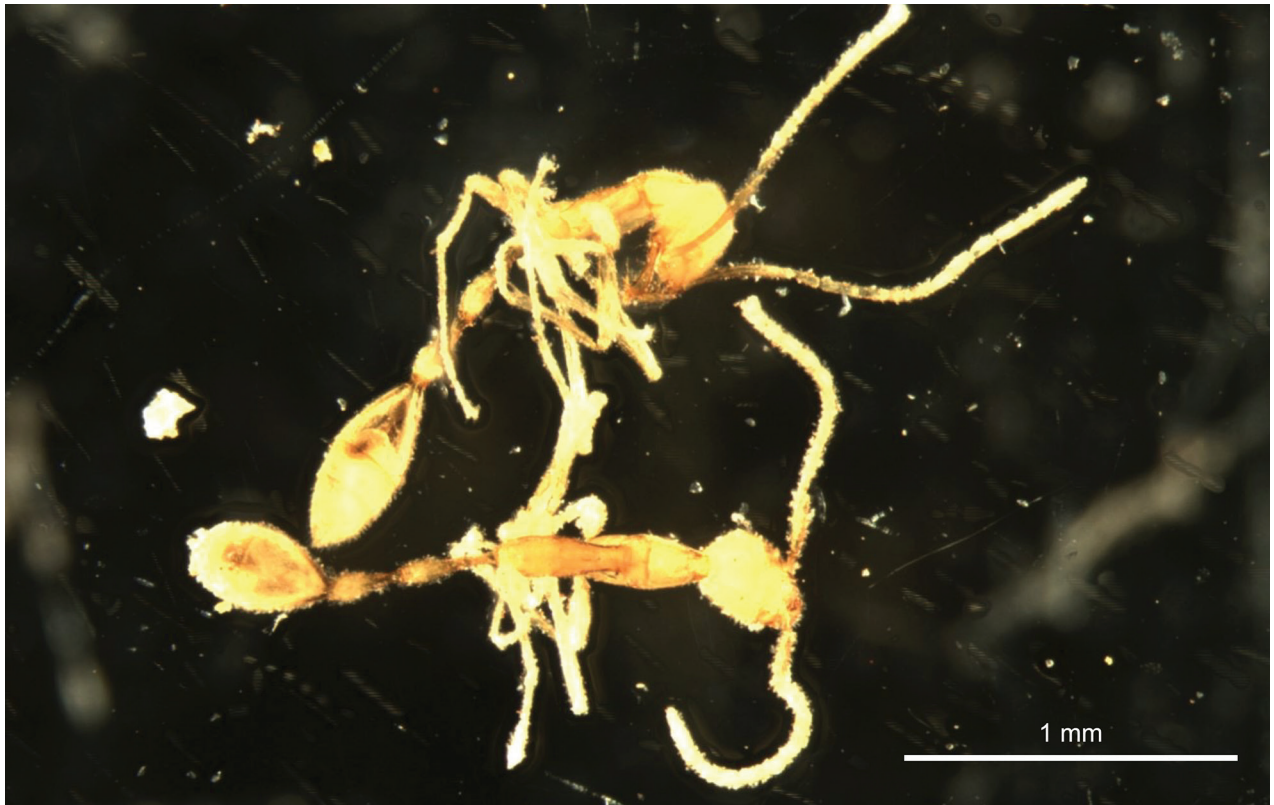


Figure 1. Workers of *Leptanilla voldemort* sp. nov. from Western Australia in ethanol.



Figure 2. Profile view of *Leptanilla voldemort* sp. nov. (holotype) from Western Australia. The postpetiole and gaster of the specimen, which were disconnected from the main body during mounting, were imaged separately and subsequently attached to the body digitally while ensuring consistency of scale.



Figure 3. Dorsal view of *Leptanilla voldemort* sp. nov. (holotype) from Western Australia. The postpetiole and gaster of the specimen, which were disconnected from the main body during mounting, were imaged separately and subsequently attached to the body digitally while ensuring consistency of scale.

Measurements and indices. All measurements are in millimetres (mm).

Holotype: HW 0.26; HL 0.35; SL 0.36; MaL 0.21; WL 0.59; PrW 0.16; MW 0.12; PTL 0.28; PTH 0.08; PTW 0.07; PPL 0.24; PPW 0.10; PPH 0.10; CI 73, SI 139, MI 81, PI 25, PPI 39, PPHI 42.

Paratype (n = 1): HW 0.27; HL 0.36; SL 0.35; MaL 0.20; WL 0.61; PrW 0.16; MW 0.12; CI 75, SI 128, MI 75.

Worker description. Head. Head longer than wide (CI = 73–75). In full-face view (Fig. 4), posterior margin of head slightly concave. Lateral margins of head slightly convex. Eyes absent. Anterior clypeal margin extending forward with two rounded lobes anterolaterally and slightly concave on its anteromedian portion. Median portion of clypeus raised; frontoclypeal process present and concealing labrum. Mandibles long relative to head (MI = 75–81) and armed with three teeth. Apical tooth acute and larger than subapical and basal teeth. Basal tooth larger than subapical tooth with tip approximately perpendicular to mandibular margin; margin distal to subapical tooth irregularly serrate. Antennal insertion exposed. Antennae with 12 segments. Scape elongated, extending well beyond mid-point of head (SI = 128–139); margins subparallel, expanding slightly before tapering at apex. Pedicel longer than broad and constricted at separation from scape; constriction separating pedicel from flagellum not pronounced. Flagellum filiform; all flagellomeres longer than broad. Antennomere 12 approximately double the length of previous flagellomeres with apex tapered.



Figure 4. Full-face view of *Leptanilla voldemort* sp. nov. (holotype) from Western Australia.

Mesosoma. In dorsal view, maximum width of pronotum ($PrW = 0.16$ mm) wider than posterior portions of mesosoma (Fig. 3). In lateral view, pronotal dorsum slightly convex, tapering along anterior margin, with posterior margin slightly elevated above mesonotal dorsum (Fig. 2). Promesonotal suture clearly visible in both lateral and dorsal view. In dorsal view, mesonotum constricted anteriorly, with lateral margins gently convex and approximating maximum width at fusion with propodeum. In dorsal view, propodeum not constricted anteriorly, with outline of posterior margin trapezoidal (Fig. 3). In lateral view, propodeal dorsum raised and strongly convex, with posterior forming a strongly convex propodeal declivity at an approximate 65° angle (Fig. 2). Metapleural gland bulla and propodeal spiracle visible. Coxae robust, pro- and mesocoxae well separated; distal leg articles elongated.

Metasoma. Metasoma elongated in both dorsal and lateral view ($PL + PPL \approx WL$). In dorsal view (Fig. 3), petiole four times as long as wide ($PI = 25$), with lateral margins subparallel at anterior and convex after mid-point to achieve maximum width; posterior margin convex and rounded. Postpetiole longer than wide ($PPI = 39$), with similar shape to petiole but wider and more rounded posteriorly. In lateral view (Fig. 2), petiole with dorsal and ventral margins subparallel at anterior and convex after mid-point to achieve maximum height; posterior margin slightly concave. Subpetiolar process absent. Postpetiole with dorsal and ventral margins subparallel at anterior and diverging near mid-point, after which dorsal margin is weakly convex and ventral margin is strongly concave; posterior margin concave.

Sculpture. Sculpture absent. Most of the body slick and shiny (i.e. not a result of glare from diffusing light when imaging).

Pubescence. Pubescence present on most of the body, especially antennae and legs, but sparse to absent on propodeum and metasoma. Numerous sub-erect to erect setae on dorsal and ventral surfaces of pronotum, cranium, and mandibles. Long basal and subapical setae on mandibles.

Colouration. Pale gold to amber. Colouration slightly lighter at extremities.

Castes. Male and gyne unknown.

Etymology. The species epithet pays tribute to the antagonist in the Harry Potter book series, Lord Voldemort, a terrifying wizard who, like the new ant, is slender, pale, and thrives in darkness. The species epithet is a noun, and thus invariant.

Distribution. Only known from the type locality within the Pilbara region of Western Australia.

Ecology. *Leptanilla voldemort* sp. nov. was collected from a hot grassland in the north-west Pilbara, a region characterised by very hot summers (average maximum 36–39 °C), low winter minima (average minimum 6–12 °C), low average annual rainfall (200–350 mm), and high evaporation (average annual potential evaporation 3200–4000 mm) (Eberhard et al. 2005). Both type specimens were collected from a 25 m deep mining exploration drill hole using a subterranean scraping method, whereby a weighted net was lowered to the base of the hole and dragged four times back to the surface against the wall of the hole (Halse and Pearson 2014). The drill hole was in a dry drainage line, with the subterranean substrate consisting of coarse alluvium near surface over banded iron formation at depth. Other organisms recorded from the drill hole include troglofaunal beetles of an unknown genus, troglofaunal flies of the genus *Allopnixia* Freeman, 1952 and troglofaunal centipedes assigned to the genus *Cryptops* Leach, 1814. We are presently unable to ascertain whether colonies of *L. voldemort* sp. nov. inhabit topsoil, the subsurface alluvium, or voids in the deeper weathered banded iron formation. The colony size and structure of *L. voldemort* sp. nov. is unknown.

Remarks. The worker of *L. voldemort* sp. nov. is easily distinguished from the other native Australian leptanilline species, *L. swani* Wheeler, 1932, which is evidently sympatric with *L. voldemort* sp. nov. (see new collection data below). First, *L. voldemort* sp. nov. has distinctly elongated mandibles (MI = 75–81) and antennae (SI = 128–139), while in *L. swani* these appendages are stouter and shorter (MI = 44–56, SI = 59–74). Second, *L. voldemort* sp. nov. possesses metasomal segments that are two to four times longer than wide (PI = 25, PPI = 39), while in *L. swani* these segments are almost as long as wide (PI = 56–70, PPI = 83–100). Finally, *L. voldemort* sp. nov. (WL = 0.59–0.61 mm) is larger in size than *L. swani* (WL = 0.35–0.45 mm). In general, the gracile phenotype of *L. voldemort* sp. nov. is distinctive among the genus *Leptanilla*, except for *Leptanilla laventa* Griebenow, Moradmand & Isaia, 2022, a species described from Iran. Specifically, the elongated antennae and petiole of workers in both *L. voldemort* sp. nov. (SI = 128–139, PI = 25) and *L. laventa* (SI = 160–163, PI = 29–32) are not observed in other *Leptanilla* species (SI < 100, PI > 31) (Griebenow et al. 2022; Griebenow 2024; Qian et al. 2024). Nonetheless, workers of *L. voldemort* sp. nov. can be distinguished from those of *L. laventa* based on several key morphological differences. First, in dorsal view, the shape of the petiole and postpetiole of *L. voldemort* sp. nov. is distinctly more elongated

(PI = 25; PPI = 39) than in *L. laventa* (PI = 29–32; PPI = 59–64.7). Second, in lateral view, the propodeal declivity of *L. voldemort* sp. nov. is strongly convex and distinctly angular, whereas that of *L. laventa* is weakly convex and gently rounded. Third, in full-face view, the axis of the basal mandibular tooth of *L. voldemort* sp. nov. extends almost perpendicular to the mandibular margin, with the tip of the tooth forming an 80–90° angle with the medial mandibular margin, whereas in *L. laventa*, the basal tooth is recurved, with the tip of the tooth forming a 60–70° angle with the medial mandibular margin. Finally, *L. voldemort* sp. nov. (WL = 0.59–0.61 mm) is smaller in size than *L. laventa* (WL = 0.74–0.85 mm).

***Leptanilla swani* Wheeler, 1932**

Notes. Below we provide measurements for three worker specimens of *L. swani*. Collection data for the first two specimens are as follows: AUSTRALIA; 2 workers; Western Australia, Newman; 22°47'S, 119°9'E; ca 537 m a.s.l.; 9 May 2022; Jane M. McRae leg.; collected via subterranean scraping; BENNSPECIMENID_735794 and BENNSPECIMENID_735840; WAM. Collection data for the third specimen, a paratype of the species, is as follows: **Paratype:** AUSTRALIA; 1 worker; Western Australia, Chittering; 31°27'S, 116°5'E; ca. 225 m a.s.l.; D. Swan leg.; CASENT0172006; ANIC.

BENNSPECIMENID_735794 (Fig. 5): HW 0.23; HL 0.31; SL 0.17; MaL 0.13; WL 0.44; PrW 0.15; MW 0.14; PTL 0.15; PTH 0.11; PTW 0.08; PPL 0.11; PPW 0.09; PPH 0.13; CI 72, SI 74, MI 56, PI 56, PPI 83, PPHI 117.

BENNSPECIMENID_735840: HW 0.22; HL 0.31; SL 0.16; MaL 0.12; WL 0.45; PrW 0.15; MW 0.12; PTL 0.15; PTH 0.11; PTW 0.09; PPL 0.12; PPW 0.10; PPH 0.12; CI 71, SI 72, MI 55, PI 59, PPI 87, PPHI 106.

CASENT0172006: HW 0.20; HL 0.28; SL 0.12; MaL 0.09; WL 0.35; PrW 0.13; MW 0.11; PTL 0.11; PTH 0.10; PTW 0.08; PPL 0.08; PPW 0.08; PPH 0.10; CI 69, SI 59, MI 44, PI 70, PPI 100, PPHI 125.

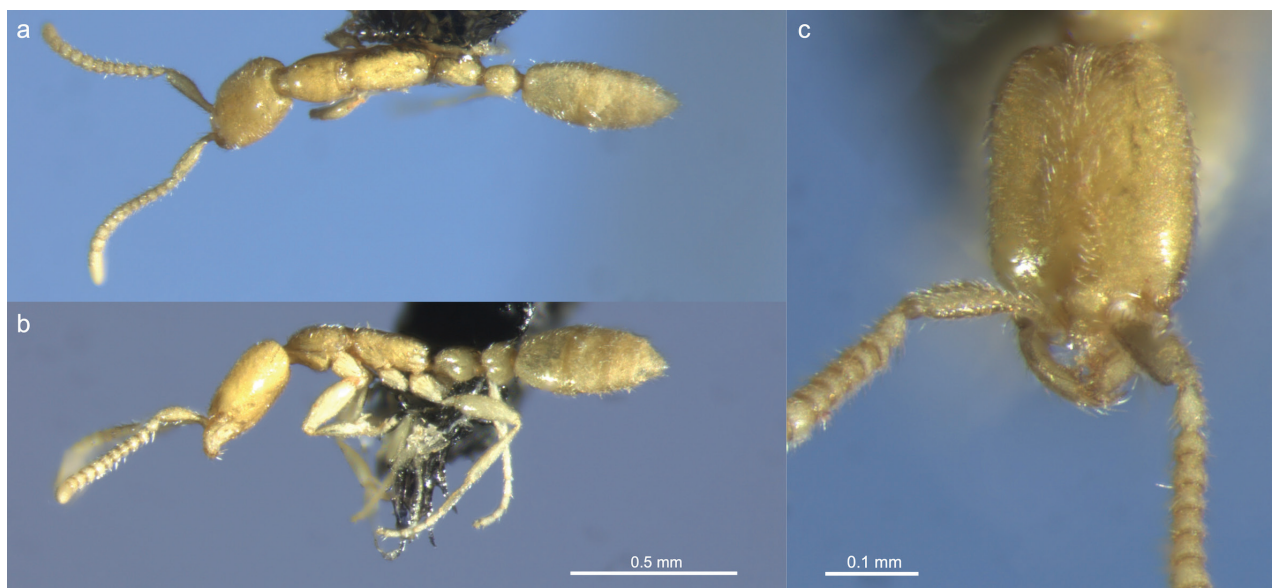


Figure 5. Worker of *Leptanilla swani* (BENNSPECIMENID_735794) **a** dorsal view **b** profile view **c** full-face view.

Synoptic species list of Australian *Leptanilla* species

Leptanilla swani Wheeler, 1932

Leptanilla voldemort sp. nov.

Key to Australian *Leptanilla* species based on the worker caste

- 1 Elongated mandibles (MI = 75–81), antennae (SI = 128–139), and metasoma (PI = 25, PPI = 39). Large body size (WL = 0.59–0.61) ***L. voldemort* sp. nov.**
- Stout mandibles (MI = 44–56), antennae (SI = 59–74), and metasoma (PI = 56–70, PPI = 83–100). Small body size (WL = 0.35–0.45) ***L. swani* Wheeler**

Discussion

Despite Australia being a global hotspot for ant diversity (Kass et al. 2022), *Leptanilla voldemort* sp. nov. is only the second species of *Leptanilla* and second member of the subfamily Leptanillinae known from the continent since the discovery of *L. swani* in 1932. To this end, it is envisaged that the targeted employment of currently underutilised techniques for collecting hypogaecic ant species such as subterranean scraping, subterranean pitfall traps, and soil extractions (Wong and Guénard 2017) may facilitate the discovery of additional Australian leptanilline species. The Pilbara region of north-western Australia, in particular, is one of the oldest land surfaces on Earth (Pepper et al. 2008). Due to multiple vicariant isolation and divergence events that have occurred with surface aridification, this region harbours globally significant levels of endemic diversity in subterranean invertebrate species (Mokany et al. 2019). The presence of both *L. swani* and *L. voldemort* sp. nov. in the Pilbara highlights the importance of this region for Australian leptanilline species.

Although we collected individuals of both *L. voldemort* sp. nov. and *L. swani* within the same general locality (sites <15 km apart) in the Pilbara, the two sympatric species clearly exhibit contrasting morphologies. Whereas *L. swani* is stout and compact (Fig. 5), *L. voldemort* sp. nov. is distinctly gracile (Fig. 2). We posit that these morphological differences may relate to the species' use of dissimilar microhabitats within the subterranean environment. Given that a colony of *L. swani* was collected from under a large stone (Wheeler 1932), it is reasonable to assume that *L. swani* inhabits the shallower layers of soil. Moreover, the generally compact body plan of *L. swani* resembles that of most other *Leptanilla* species that have been collected via the sifting of topsoil (10–20 cm depth) or via the installation of subterranean pitfall traps (10–50 cm depth) in the soil layer (Wong and Guénard 2016, 2017). In contrast, the distinctively gracile morphology of *L. voldemort* sp. nov. is unlike that of any other *Leptanilla* species except *L. laventa* from Iran. Interestingly, *L. laventa* was not collected from soil, but via subterranean pitfall traps buried 0.6–1 m belowground in the *Milieu Souterrain Superficiel*, an underground network of empty air-filled voids and cracks developing within multiple layers of rock fragments, located below the soil layer (Mammola et al. 2016; Griebenow et al. 2022). We can only presently speculate whether *L. voldemort* sp. nov. occupies a similar microhabitat; systematic sampling of the ants

from different vertical sections of the subterranean column (via subterranean pit-fall traps or excavations) coupled with measurements of climatic and structural parameters of the substrate should provide clarification on the matter. Finally, the elongated mandibles and large, sharp basal teeth of *L. voldemort* sp. nov. suggest that the ants are likely specialised predators; however, it remains to be seen whether they prey on geophilomorph centipedes, as in other species of *Leptanilla* (Masuko, 1990), or other hypogaeic taxa, such as centipedes of the family Cryptopidae (Chilopoda, Scolopendromorpha), hypogaeic cockroaches, and pauropods, all of which were collected from the same drill hole as *L. voldemort* sp. nov.

Acknowledgements

We are grateful to Stuart Halse, Melanie McGellin, and Melita Pennifold from Bennelongia Environmental Consultants for their assistance with the specimens and comments on the manuscript, and Nikolai Tataric from the Western Australian Museum for his assistance with deposition of the specimens. We also thank Zachary Griebenow and Francisco Hita Garcia for their comments on a previous version of the manuscript.

Additional information

Conflict of interest

The authors have declared that no competing interests exist.

Ethical statement

No ethical statement was reported.

Funding

M.K.L.W. is supported by a Forrest Fellowship from the Forrest Research Foundation.

Author contributions

M.K.L.W. studied, imaged and described the species, and wrote the manuscript. J.M.M. oversaw fieldwork and processing of specimens. Both authors proofread and edited all versions of the manuscript.

Author ORCIDs

Mark K. L. Wong  <https://orcid.org/0000-0002-6248-3103>

Data availability

All of the data that support the findings of this study are available in the main text.




References

- AntWeb (2024) California Academy of Science. <https://www.antweb.org> [Accessed 12 February 2024]
- Bolton B (1990) The higher classification of the ant subfamily Leptanillinae (Hymenoptera: Formicidae). *Systematic Entomology* 15(3): 267–282. <https://doi.org/10.1111/j.1365-3113.1990.tb00063.x>

- Bolton B (2024) An online catalog of the ants of the world. <https://antcat.org> [Accessed 24 February 2024]
- Borowiec ML, Rabeling C, Brady SG, Fisher BL, Schultz TR, Ward PS (2019) Compositional heterogeneity and outgroup choice influence the internal phylogeny of the ants. *Molecular Phylogenetics and Evolution* 134: 111–121. <https://doi.org/10.1016/j.ympev.2019.01.024>
- Cai C (2024) Ant backbone phylogeny resolved by modelling compositional heterogeneity among sites in genomic data. *Communications Biology* 7(1): 106. <https://doi.org/10.1038/s42003-024-05793-7>
- Eberhard SM, Halse SA, Scanlon MD, Cocking JS, Barron HJ (2005) Assessment and conservation of aquatic life in the subsurface of the Pilbara region, Western Australia. In: Gilbert J (Ed.) *Proceedings of an International Symposium on World Subterranean Biodiversity*. University of Lyon.
- Griebenow Z (2024) Systematic revision of the ant subfamily Leptanillinae (Hymenoptera, Formicidae). *ZooKeys* 1189: 83–184. <https://doi.org/10.3897/zookeys.1189.107506>
- Griebenow ZH, Isaia M, Moradmam M (2022) A remarkable troglomorphic ant, *Yavnella laventa* sp. nov. (Hymenoptera: Formicidae: Leptanillinae), identified as the first known worker of *Yavnella* Kugler by phylogenomic inference. *Invertebrate Systematics* 36(12): 1118–1138. <https://doi.org/10.1071/IS22035>
- Halse SA, Pearson GB (2014) Troglifauna in the vadose zone: Comparison of scraping and trapping results and sampling adequacy. *Subterranean Biology* 13: 17–34. <https://doi.org/10.3897/subtbiol.13.6991>
- Heterick BE (2022) A guide to the ants of Western Australia. Part II: Distribution and biology. *Records of the Western Australian Museum* 86(1, Supplement 86): 247–510. <https://doi.org/10.18195/issn.0313-122x.86.2022.247-510>
- Kass JM, Guénard B, Dudley KL, Jenkins CN, Azuma F, Fisher BL, Parr C, Gibb H, Longino JT, Ward PS, Chao A, Lubertazzi D, Weiser M, Jetz W, Guralnick R, Blatrix R, Des Lauriers J, Donoso DA, Georgiadis C, Gomez K, Hawkes PG, Johnson RA, Lattke JE, Macgown JA, Robson S, Sanders NJ, Dunn RR, Economo EP (2022) The global distribution of known and undiscovered ant biodiversity. *Science Advances* 8(31): eabp9908. <https://doi.org/10.1126/sciadv.abp9908>
- Mammola S, Giachino PM, Piano E, Jones A, Barberis M, Badino G, Isaia M (2016) Ecology and sampling techniques of an understudied subterranean habitat: The Milieu Souterrain Superficiel (MSS). *Naturwissenschaften* 103(11–12): 1–24. <https://doi.org/10.1007/s00114-016-1413-9>
- Masuko K (1989) Larval hemolymph feeding in the ant *Leptanilla japonica* by use of a specialized duct organ, the “larval hemolymph tap” (Hymenoptera: Formicidae). *Behavioral Ecology and Sociobiology* 24(2): 127–132. <https://doi.org/10.1007/BF00299644>
- Masuko K (1990) Behavior and ecology of the enigmatic ant *Leptanilla japonica* Baroni Urbani (Hymenoptera: Formicidae: Leptanillinae). *Insectes Sociaux* 37(1): 31–57. <https://doi.org/10.1007/BF02223813>
- Mokany K, Harwood TD, Halse SA, Ferrier S (2019) Riddles in the dark: Assessing diversity patterns for cryptic subterranean fauna of the Pilbara. *Diversity & Distributions* 25(2): 240–254. <https://doi.org/10.1111/ddi.12852>
- Pepper M, Doughty P, Arculus R, Keogh JS (2008) Landforms predict phylogenetic structure on one of the world’s most ancient surfaces. *BMC Evolutionary Biology* 8(1): 1–7. <https://doi.org/10.1186/1471-2148-8-152>

- Qian YH, Xu ZH, Man P, Liu GL (2024) Three new species of the ant genus *Leptanilla* (Hymenoptera: Formicidae) from China, with a key to the world species. *Myrmecological News* 34: 21–44. https://doi.org/10.25849/myrmecol.news_034:021
- Romiguier J, Borowiec ML, Weyna A, Helleu Q, Loire E, La Mendola C, Rabeling C, Fisher BL, Ward PS, Keller L (2022) Ant phylogenomics reveals a natural selection hotspot preceding the origin of complex eusociality. *Current Biology* 32(13): 2942–2947. <https://doi.org/10.1016/j.cub.2022.05.001>
- Wheeler WM (1932) An Australian *Leptanilla*. *Psyche* (Cambridge, Massachusetts) 39(3): 53–58. <https://doi.org/10.1155/1932/81860>
- Wong MKL, Guénard B (2016) *Leptanilla hypodracos* sp. n., a new species of the cryptic ant genus *Leptanilla* (Hymenoptera, Formicidae) from Singapore, with new distribution data and an updated key to Oriental *Leptanilla* species. *ZooKeys* 551: 129–144. <https://doi.org/10.3897/zookeys.551.6686>
- Wong MKL, Guénard B (2017) Subterranean ants: summary and perspectives on field sampling methods, with notes on diversity and ecology (Hymenoptera: Formicidae). *Myrmecological News* 25: 1–16. https://doi.org/10.25849/myrmecol.news_025:001

Divergence of the freshwater sleeper, *Neodontobutis hainanensis* (Chen, 1985) (Teleostei, Odontobutidae), in the Pearl River basin and on Hainan Island of southern China

Mingwei Zhou^{1,2}, Jianhong Xia³, Chenhong Li^{1,2}

¹ Shanghai Universities Key Laboratory of Marine Animal Taxonomy and Evolution, Shanghai Ocean University, Shanghai 201306, China

² Engineering Research Center of Environmental DNA and Ecological Water Health Assessment, Shanghai Ocean University, Shanghai 201306, China

³ Shanghai Natural History Museum, Branch of the Shanghai Science & Technology Museum, Shanghai 200041, China

Corresponding authors: Jianhong Xia (snhmichth@hotmail.com); Chenhong Li (chli@shou.edu.cn)

Abstract

Study of divergence of freshwater fish populations between island and adjacent mainland areas can shed light on the phylogeographical relationships of these regions. *Neodontobutis hainanensis* is a freshwater fish species restricted to Hainan Island and in Guangdong and Guangxi provinces in the southern mainland China. We examine the phylogenetic relationship and population structure of *N. hainanensis* based on 3,176 nuclear loci using a gene-capture method. STRUCTURE analysis and principal coordinate analyses (PCA) indicate that populations from Guangdong, Guangxi and Hainan are each distinct, except that some individuals of the Guangdong population share minor genetic components with individuals of the Guangxi population. In the concatenated gene tree, the Hainan population is grouped with the Guangdong population, but the coalescent tree groups the Hainan population as the sister to the Guangxi population. Finally, coalescent simulations confirmed the divergence pattern supported by the coalescent tree and revealed a one-way introgression from the Guangxi population to the Guangdong population, which can explain the discordant results supported by the concatenated and coalescent phylogenetic analyses. Due to recent decline of *N. hainanensis* populations and the genetic patterns in this species, as revealed in this study, the populations in the three areas should be treated as separate conservation units.

Key words: Gene flow, phylogeography, population structure, southern China



Academic editor: Maria Elina Bichuette

Received: 31 July 2023

Accepted: 14 March 2024

Published: 17 April 2024

ZooBank: <https://zoobank.org/358F9D8D-10B2-4783-8C23-70E54D3AB013>

Citation: Zhou M, Xia J, Li C (2024)

Divergence of the freshwater sleeper,

Neodontobutis hainanensis (Chen, 1985) (Teleostei, Odontobutidae),

in the Pearl River basin and on Hainan Island of southern China.

ZooKeys 1197: 183–196. <https://doi.org/10.3897/zookeys.1197.110314>

<https://doi.org/10.3897/zookeys.1197.110314>

Copyright: © Mingwei Zhou et al.

This is an open access article distributed under terms of the Creative Commons Attribution

License ([Attribution 4.0 International – CC BY 4.0](https://creativecommons.org/licenses/by/4.0/)).

Introduction

Hainan Island is the second largest island in China, with an area of 33,920 km², and is in the northernmost part of the South China Sea (Zhu 2020). The northern corner of Hainan Island is separated from the Leizhou Peninsula of mainland China by the Qiongzhou Strait, whereas the western coast of Hainan Island is separated from Guangxi Zhuang Autonomous Region of the southern China and the northern Vietnam by the Beibu Gulf. Besides the Qiongzhou Strait and the Beibu Gulf, other geographic barriers, such as the Yunkai-Shiwan Mountains may also played a role in shaping population patterns of the region's ichthyofauna. Hainan

Island lies at 108°36'43"–111°2'31"E and 18°10'04"–20°9'40"N (Zhu 2020) and has a typical tropical climate. The island is home to about 138 native freshwater fish species belonging to 90 genera and 26 families (Xiong et al. 2018). There are 14 species endemic to Hainan Island, but most native species are also distributed on the adjacent mainland, such as in Guangdong and Guangxi (Xiong et al. 2018). The study of the population structure and phylogeography of these species would shed light on the biogeographical events on Hainan Island that have shaped the patterns of its freshwater ichthyofauna.

Although the Qiongzhou Strait is much narrower than the Beibu Gulf, both geographical and biogeographical evidence support the hypothesis that Hainan Island might have originated as part of the northeastern Indo-China Peninsula and adjacent Guangxi, China, but not from southeastern China, and particularly Guangdong (Zhu 2020). For example, flora of Hainan Island was found more closely related to that of Guangxi and northern Vietnam than to that of Guangdong; 110 genera of plants are shared with Guangxi and Vietnam, but only seven genera are exclusively shared with Guangdong (Zhu 2020). This pattern also is supported by population genetics of freshwater fishes, such as dwarf snakehead, *Channa gachua* (Hamilton, 1822) (Wang et al. 2021) and white cloud mountain minnow, *Tanichthys albonubes* Lin, 1932 (Zhao et al. 2018). Nonetheless, the population genetics of other freshwater fish species, which usually have a wide distribution, may support alternative scenarios (Tsao et al. 2016; Chen et al. 2017) and complex population history. For this reason, the choice of fish species is important in revealing different facets of biogeographical events that shaped the ichthyofauna.

The genus *Neodontobutis* (Gobiiformes, Odontobutidae) has three to six species (Iwata 2011; Zhou et al. 2022). *Neodontobutis lani* Zhou, 2022 is reported only in Chongzuo City, southern Guangxi, China (Zhou et al. 2022). *Neodontobutis hainanensis* is distributed in southern China, including restricted areas in Guangdong and Guangxi, and on Hainan Island (Wu and Zhong 2008). The other species are distributed in the northern Indo-China Peninsula (Iwata 2011; Zhou et al. 2022). *Neodontobutis hainanensis* is a small, benthic species inhabiting hill streams and backwaters (Chen et al. 2002). Being a strict freshwater fish, of small size and with limited distribution and presumably low capacity for migration, *N. hainanensis* could be an appropriate species for testing phylogeographic relationships between Hainan Island and the adjacent mainland China.

We captured and sequenced 4,434 single-copy nuclear coding loci from the individuals of *N. hainanensis* collected from Hainan Island and Guangdong and Guangxi provinces, applied a target-gene enrichment method, and performed phylogenetic reconstruction, STRUCTURE analysis, principal coordinate analysis (PCA) and coalescent simulations to infer the relationships of the populations from these three areas and possible historical events shaping the current genetic patterns in this species.

Materials and methods

Taxon sampling

Sixteen individuals of *N. hainanensis* were collected in total. Five specimens from Haikou, Hainan Island (20.0°N, 110.2°E), 5 specimens from Chongzuo, Zhuang Autonomous Region of Guangxi (22.8°N, 107.2°E), and six specimens



Figure 1. Sampling sites (triangles) for three populations of *Neodontobutis hainanensis*: Yangjiang, Guangdong (blue), Chongzuo, Guangxi (red) and Haikou, Hainan (green).

Table 1. Sampling information and localities of *Neodontobutis hainanensis*.

Voucher number	Sample id	Location	Population id
SOU1801005-1	25461	Chongzuo, Guangxi	GX
SOU1801005-2	25462	Chongzuo, Guangxi	GX
SOU1801005-3	25463	Chongzuo, Guangxi	GX
SOU1801005-4	25464	Chongzuo, Guangxi	GX
SOU1801005-5	25465	Chongzuo, Guangxi	GX
SOU1801010-8	20278	Haikou, Hainan	HN
SOU1801010-9	20279	Haikou, Hainan	HN
SOU1801010-10	202710	Haikou, Hainan	HN
SOU1801010-11	202711	Haikou, Hainan	HN
SOU1801010-12	202712	Haikou, Hainan	HN
SOU1801011-2	CL1227_2	Yangjiang, Guangdong	GD
SOU1801011-3	CL1227_3	Yangjiang, Guangdong	GD
SOU1801013	CL1228	Yangjiang, Guangdong	GD
SOU1801014-1	CL1279_1	Yangjiang, Guangdong	GD
SOU1801014-3	CL1279_3	Yangjiang, Guangdong	GD
SOU1801014-4	CL1279_4	Yangjiang, Guangdong	GD
Outgroups	25913	Chongzuo, Guangxi	<i>Neodontobutis lani</i>
	CL632_1	Harbin, Heilongjiang	<i>Percottus glenii</i>
	CL1275_4	Dandong, Liaoning	<i>Odontobutis yaluensis</i>

from Yangjiang, Guangdong province (21.9°N, 112.1°E) (Table 1; Fig. 1). The specimens were deposited in the Fish Collection of Shanghai Ocean University (voucher numbers SOU1801005-1-5, SOU1801010-8-12, SOU1801011-2-3, SOU1801013, SOU1801014-1,-3,-4; contact person: Dr Ya Zhang, email: zhang-ya@shou.edu.cn). Fin clips or muscle tissue samples were preserved in etha-

nol for DNA extraction. Raw sequences of *Odontobutis yaluensis*, *Percottus glenii*, and *Neodontobutis lani* from previous studies (Li et al. 2018; Zhou et al. 2022) were used as outgroups (<https://www.ncbi.nlm.nih.gov/>, accessed February 2023, accession number SRP127338). Detailed sample information and sampling localities are shown in Table 1.

DNA extraction and target loci enrichment

Genomic DNA was extracted from tissue samples using an Ezup Column Animal Genomic DNA Purification Kit (Sangon, Shanghai, China). The concentration of extracted DNA was measured using a NanoDrop™ 3300 fluorescence spectrophotometer, and the integrity of extracted DNA was visually checked using gel electrophoresis. A cross-species target loci enrichment method was used to enrich 4,434 coding regions of single-copy nuclear loci (Li et al. 2013). A set of gobioid-specific capture probes targeting the 4,434 loci were adopted from Li et al. (2018). Briefly, 300–1000 ng DNA were used for library preparation for gene enrichment according to Meyer and Kircher (2010), involving steps of shearing, blunt ending, ligation, and gap filling. Specific short sequences called “inline index” were added on 3’ end of both P5 and P7 adaptors to allow pooling different samples from the same population before the follow-up target enrichment steps and to track potential cross-contamination (Wang et al. 2022). After target enrichment, all samples were pooled in equimolar ratio for 2× 150 bp paired-end sequencing on an Illumina HiSeq X10 lane at Genewiz (Suzhou, Jiangsu, China).

Data assemblage and multiple sequences alignment

Reads were assembled, aligned, and filtered following the ASSEXON pipeline, which includes a series of Perl scripts for processing target enrichment data (Yuan et al. 2019). Briefly, compressed raw reads were unzipped using `gunzip_Files.pl`. Reads from each sample were separated according to the combination of index sequences using `demultiplex.pl`. Adaptors and low-quality sequences were trimmed using `trim_adaptor.pl`, which invokes `trim_galore v. 0.4.1` (http://www.bioinformatics.babraham.ac.uk/projects/trim_galore/). A set of 4,434 nuclear coding sequences of *Oreochromis niloticus* was used as a reference (Yuan et al. 2019). Reads were parsed to each locus according to the reference sequence and then assembled by using `assemble.pl`. Assembled sequences were uploaded to Mendeley Data (<https://data.mendeley.com/datasets/8rgcmdx-rmk/1>). Output files include assembled coding regions of the loci were aligned by using `mafft_aln.pl`, which invokes `Mafft v. 7.294b` (Katoh and Standley 2013) for aligning. Finally, poorly aligned coding sequences were excluded by using `filter.pl`. Target enrichment results were summarized using `statistics.pl` (Yuan et al. 2019).

Phylogenetic analysis

Aligned sequences were concatenated using a Perl script `concat_loci.pl` in the ASSEXON package (Yuan et al. 2019), then a Perl script, `extract_DNAblocks.pl`, was used to generate a partition scheme file by codon position. A concatenated maximum-likelihood tree including *N. hainanensis* from the three populations and the outgroups was constructed using IQ-TREE v. 1.7 (Minh et al. 2020) with

1,000 bootstrap replicates. The -spp option in IQ-TREE was applied to select the best model for each part according to the partition scheme file.

To infer the species tree, maximum-likelihood gene trees of all loci were reconstructed by using the Perl script `construct_tree.pl` in the ASSEXON package, which generated gene trees for each loci using RAxML v. 8.0.0 (Stamatakis 2014) under the GTRGAMMA model. Then, ASTRAL v. 4.10.6 (Mirarab et al. 2014) was used to generate a coalescent species tree from all gene trees. The resulting trees were visualized in FigTree v. 1.4.0 (Rambaut 2013).

SNPs calling

Consensus sequences were generated from the aligned sequences of *N. hainanensis* using a Perl script `consensus.pl` in the ASSEXON package (Yuan et al. 2019). BWA v. 0.7.16 (Li and Durbin 2009) was used to build the index from the consensus sequence and align the trimmed raw reads of individual samples of *N. hainanensis* to the consensus sequence. GATK4 (McKenna et al. 2010) was used for SNP calling and filtering. VCFTOOLS v. 0.1.16 (Danecek et al. 2011) was used to exclude loci out of Hardy-Weinberg Equilibrium with a p -value < 0.001 . A custom Perl script (`vcftosnps.pl`) (Cheng et al. 2019) was used to convert the VCF file output from GATK4 into NEXUS file and STRUCTURE file for PCA and STRUCTURE analysis. To avoid linkage disequilibrium, one SNP was randomly selected for each gene locus.

Population structure analysis

Principal coordinate analyses (PCA) were conducted on the NEXUS file contained SNP data using TBTOOLS v. 2.03 (Chen et al. 2020). Values of PC1 and PC2 were plotted to show genetic clustering of individuals from different populations. Population structure was reconstructed using STRUCTURE v. 2.3.4 (Pritchard et al. 2000) with the STRUCTURE file contained SNP data. Length of burn-in period was set as 500. The number of MCMC reps after burn-in was set as 500,000. Candidate genetic cluster numbers (K value) was set from 1 to 3. Each run was repeated 40 times. The output result was compressed and uploaded to "STRUCTURE HARVESTER" (Earl and von Holdt 2012) to compute the best K value for plotting.

Testing hypotheses of divergence and migration events

FASTSIMCOAL v. 2.7 (Excoffier and Foll 2011) was used to test three possible divergence models of *N. hainanensis* as well as their divergence time (generations) and potential migration events (Fig. 2). FASTSIMCOAL v. 2.7 is versatile software that can estimate complex historical population events such as population resize, growth rates, and migration from site frequency spectrum (SFS). The VCF file (*.vcf) contains SNP data was converted to Arlequin file (*.arp) using PGDSPIDER v. 2.1.1.5 (Lischer and Excoffier 2012). ARLEQUIN v. 3.5 (Excoffier et al. 2007) was used to generate folded joint SFS (*.obs) from the Arlequin file. The model with the best likelihood was regarded as the optimal one to simulate the real divergent event. According to the PCA and STRUCTURE result, single-direction migration from Guangxi population to Guangdong population is proposed. Therefore, Migration matrix was added to the optimal model to estimate values of migration from Guangxi to Guangdong and the opposite direction respective-

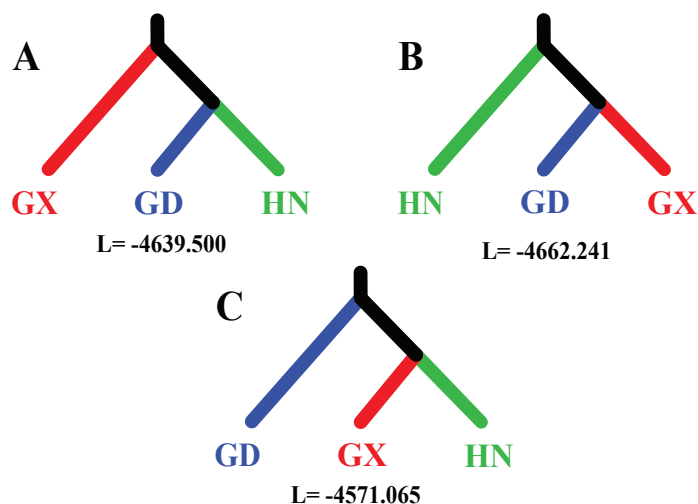


Figure 2. Three possible divergence models of *Neodontobutis hainanensis*. GD: Guangdong population; GX: Guangxi population; HN: Hainan Island population. L represents Log likelihood values estimated using FASTSIMCOAL 2.7 for the three non-migration models.

ly. All template files (*.tpl, see Suppl. material 1) that contain population parameters and estimation files (*.est, see Suppl. material 2) that contain unknown parameters for estimation were provided in Suppl. materials 1, 2.

Results

Read assembly and SNP calling

For each sample, 1,942–2,720 loci from the 4,434 targeted ones were obtained after assembling, aligning, and removing badly aligned sequences. A total of 3,176 loci were used for phylogenetic analysis and in the making of the consensus sequence. The length of the concatenated alignments was 583,539 bp with 29.13% gaps. A total of 3,493 SNP sites were detected through GATK calling and 996 sites were chosen subsequently for PCA, STRUCTURE analysis, and converted to SFS for FASTSIMCOAL 2 simulations.

Phylogenetic analysis

The concatenated maximum-likelihood tree is shown in Fig. 3. Individuals of the three populations form reciprocal monophyletic clades. The Guangdong population is sister to the Guangxi population, and then it is grouped with the population of Hainan Island. The ASTRAL coalescent species tree is shown in Fig. 4. In the coalescent tree, all three populations are monophyletic as well, but the Hainan Island population forms a clade with the Guangxi population, which is then sister to the Guangdong population.

Population structure

The PCA result was shown in Fig. 5A. All individuals from each population form a distinct cluster except for CL1228, which lies between the Guangdong population and Guangxi population. The STRUCTURE result is shown in

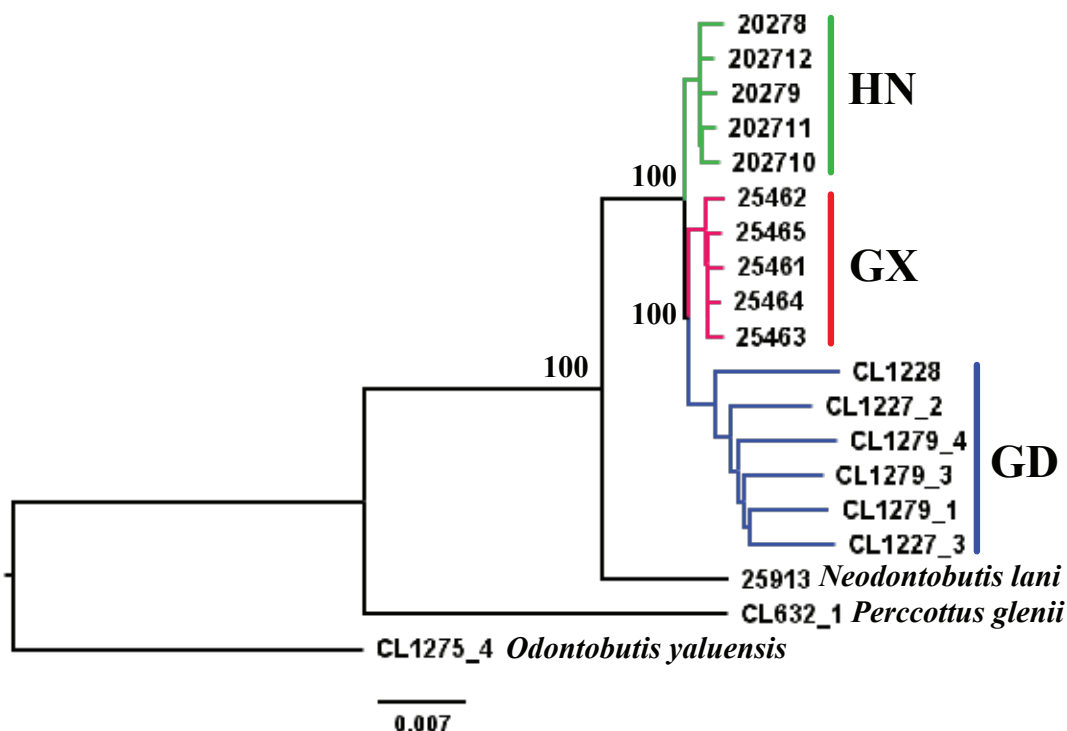


Figure 3. The concatenated maximum likelihood tree of *Neodontobutis hainanensis*. GD: Guangdong population; GX: Guangxi population; HN: Hainan Island population.

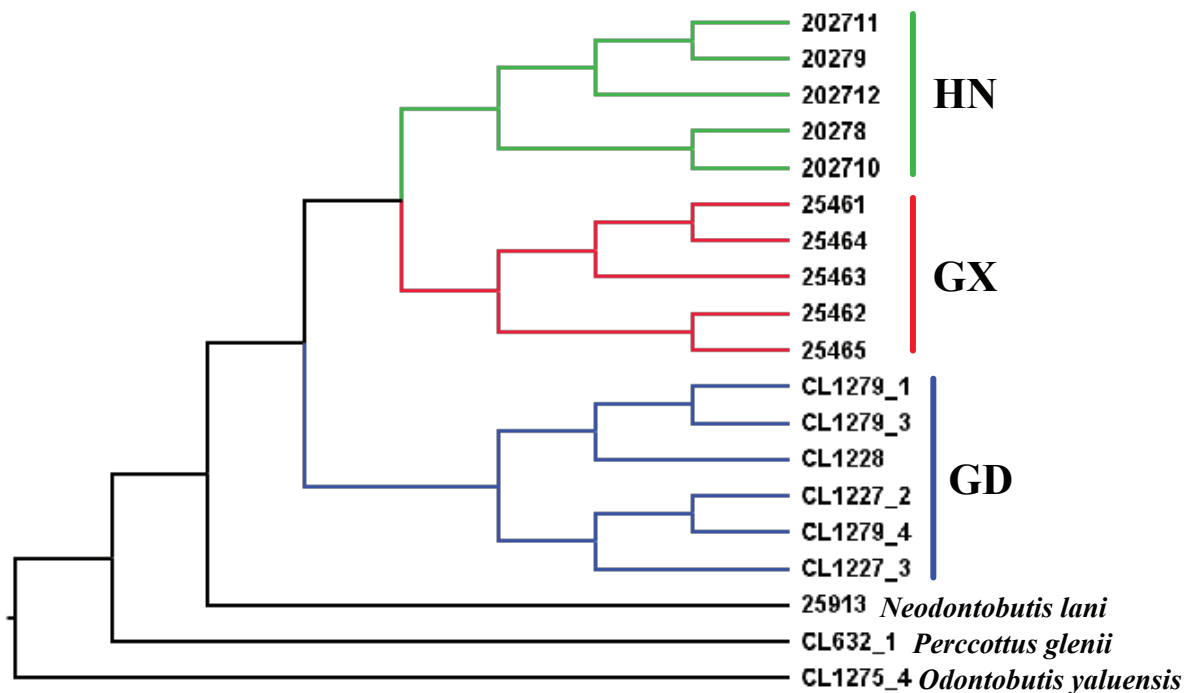


Figure 4. The ASTRAL coalescent tree of *Neodontobutis hainanensis*. GD: Guangdong population; GX: Guangxi population; HN: Hainan Island population.

Fig. 5B. Populations from Guangdong, Guangxi, and Hainan each formed distinct groups. However, some individuals in the Guangdong population, particularly CL1228 share some genetic components with individuals of Guangxi.

Estimation on population historical events

Log-likelihood values estimated by using FASTSIMCOAL v. 2.7 for the three non-migration models are shown in Fig. 2. The model which grouped the Guangxi population and the Hainan Island population as sister groups (Fig.2C) showed best likelihood, indicating that it was the optimal model to explain real divergent events. According to the result of the STRUCTURE analysis, introgression from the Guangxi population to the Guangdong population is obvious, so the relevant migration option is added to the best non-migration model. The final historical population events estimated by FASTSIMCOAL v. 2.7 is shown in Fig. 6. The Guangdong population diverged from the common ancestor of *Neodontobutis* 52,445 generations ago, then the Hainan Island population and the Guangxi population diverged around 31,855 generations ago. The migration value from Guangxi populations to Guangdong population and the opposite direction were 4.41820×10^{-4} and 1.54779×10^{-5} , respectively, indicating one-way introgression of *N. hainanensis* from the Guangxi population to the Guangdong population.

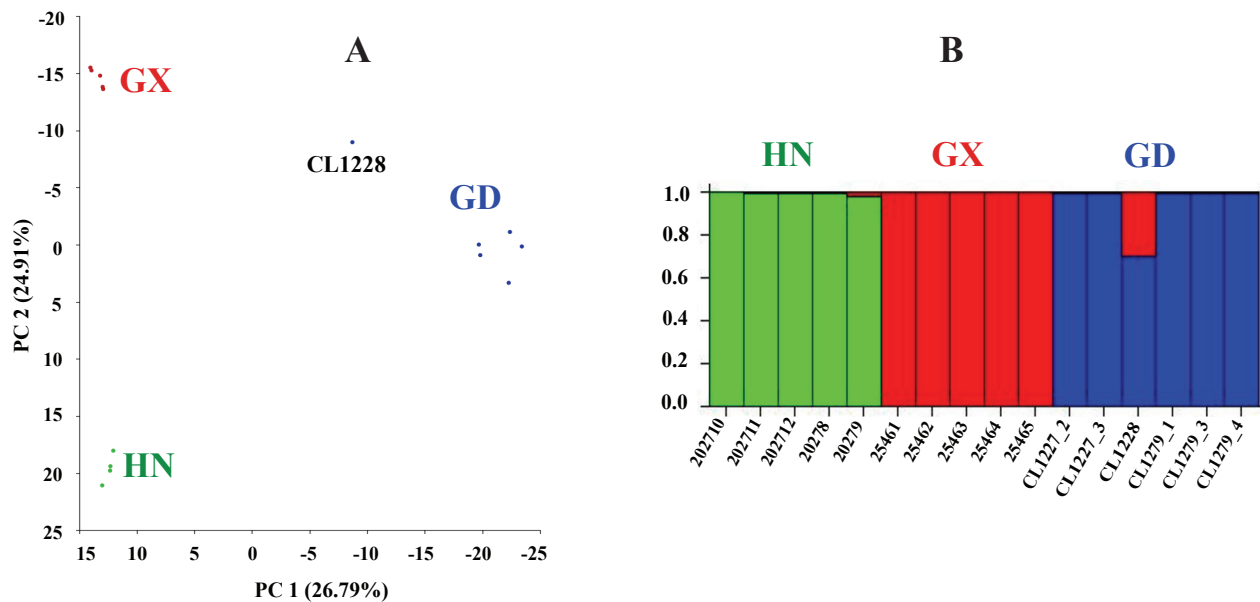


Figure 5. Result of principal component analysis (A) and population structure (B) on *Neodontobutis hainanensis*. GD: Guangdong population; GX: Guangxi population; HN: Hainan Island population.

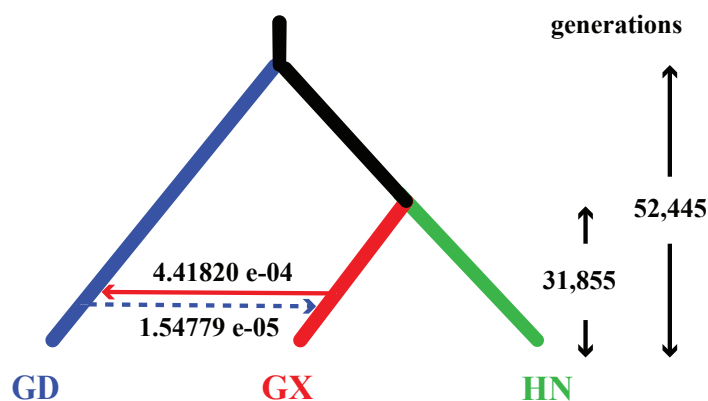


Figure 6. Historical population models simulate using FASTSIMCOAL 2.7. GD: Guangdong population; GX: Guangxi population; HN: Hainan Island population.

Discussion

High population differentiation of *Neodontobutis hainanensis*

Both concatenated tree and species tree show that the three *N. hainanensis* populations are monophyletic. The PCA and STRUCTURE results show that despite some mixture in the Guangdong population, genetic compositions of the three populations are largely distinct. All results indicate that the three populations of *N. hainanensis* are highly differentiated. Because *N. hainanensis* is strictly freshwater fish of small body size, with a benthic habit, and presumably lacks planktonic eggs or a larval stage (Iwata et al. 2001; Iwata 2011), its capacity for migration may be limited. Similar phenomenon was also found in *Perccottus glenii* Dybowski, 1877 in northeastern China (Zhang et al. 2021), *Channa gachua* around Beibu Gulf (Wang et al. 2021), and *Tanichthys albonubes* in southern China and northern Vietnam (Zhao et al. 2018). In contrast, populations of *Hemiculter leucisculus* (Basilewsky, 1855) in Guangdong, in Guangxi, and on Hainan Island (Chen et al. 2017) do not show evident differentiation. The different patterns might be due to that *H. leucisculus* is an active pelagic fish with wider distribution, indicating its relatively high migration ability or incomplete lineage sorting due to large effective population size.

Phylogenetic relationship of three populations of *Neodontobutis hainanensis*

Although the three *N. hainanensis* populations were found to be monophyletic in both the concatenated tree and the coalescent tree, their phylogenetic relationship shows discordance. In the concatenated tree, the Guangxi population is sister of Guangdong population, but in the coalescent tree the Guangxi population is the sister to Hainan Island population. The results of FASTSIMCOAL v. 2.7 analysis corroborates the divergent history shown by the coalescent tree. Both PCA and STRUCTURE analyses indicate that migration occurred from the Guangxi population to the Guangdong population, which was confirmed by the FASTSIMCOAL v. 2.7 analyses. The migration from the Guangxi population to the Guangdong population might explain the discrepancy between the concatenated tree and the coalescent tree.

Reconstruction of the divergent events in *Neodontobutis hainanensis*

According to the results of species tree, PCA, STRUCTURE analysis, and FASTSIMCOAL v. 2.7 simulation, Indo-China Peninsula and the adjacent Guangxi are supposed to be at the center of diversity of the genus *Neodontobutis*, with two species (*N. hainanensis*, *N. lani*) distributed in Guangxi and presumably four species, *N. auarmus* (Vidthayanon, 1995), *N. tonkinensis* (Mai, 1978), *N. ngheanensis* Nguyen & Nguyen, 2011, and *N. macropectoralis* (Mai, 1978), found on the Indo-China Peninsula (Vietnam, Laos, and Thailand) (Iwata 2011; Zhou et al. 2022). We postulate that *N. hainanensis* might have originated in Guangxi and probably adjacent Hainan Island, which was connected with Guangxi and northern Vietnam during last glacial period due to lower sea levels (Yao et al. 2009). From there, *N. hainanensis* dispersed

downstream of the Pearl River in Guangdong. Due to low migration ability of *N. hainanensis* and presumed vicariance events, the Guangdong population diverged from the common ancestor of Guangxi and Hainan population. After the sea level rose, Beibu Gulf formed, which resulted in divergence between the Guangxi population and the population of Hainan Island. A similar pattern of divergence is also observed in *Channa gachua*, *Tanichthys albonubes*, and *Opsariichthys hainanensis* Nichols & Pope, 1927, in which Hainan populations have closer relationships with Guangxi or Vietnamese populations than Guangdong populations (Zhao et al. 2018; Zhang et al. 2020; Wang et al. 2021). Nonetheless, populations of *Aphyocypris normalis* Nichols & Pope, 1927 and *Garra orientalis* Nichols, 1925 from northern Hainan Island are genetically closer to their Guangdong population (Chen and Jang-Liaw 2023; Yang et al. 2016), but the populations of southern or southwestern Hainan Island of these species were genetically distinct, indicating potentially independent origins, probably from the northern Indo-China Peninsula.

Besides the Qiongzhou Strait and the Beibu Gulf, the Yunkai-Shiwan Mountains may also be a significant barrier that shaped the genetic patterns of *N. hainanensis*. One-way introgression from the Guangxi population to the Guangdong population was detected from both STRUCTURE and FASTSIM-COAL v. 2.7 analyses. That may have caused by sporadic dispersal events, because the two populations are not in the same river system. Potential river-capture events await further study using species with similar distribution patterns.

Due to the recent population decline in *N. hainanensis*, we failed to collect more samples from each population. However, by utilizing genome-wide SNPs from thousands of loci in this study, we were able to mitigate the impact of having a limited number of individuals per population and still obtain valuable information. More samples from different populations of *N. hainanensis* as well as from other species of *Neodontobutis* from Vietnam would help to investigate the history of divergence in the genus. Excavating a complete fossil of the Odontobutidae also should help to precisely testing relevant geographical timeframe in southern China and on the Indo-China Peninsula. Because the recent decline of *N. hainanensis* and the distinct genetic patterns of the three populations revealed in this study, we recommend that the populations of *N. hainanensis* from Guangdong, Guangxi and Hainan should be treated as separate conservation units.

Conclusion

Neodontobutis hainanensis from Hainan Island, upstream and downstream of the Pearl River basin are distinct. The population of upstream Pearl River is sister group to the population of Hainan Island. One-way introgression from the population of upstream Pearl River to the population of downstream was supported by both population structure analysis and coalescent simulation.

Acknowledgements

The authors sincerely thank Jiahu Lan and Linxi Pan, who helped sampling for this research.

Additional information

Conflict of interest

The authors have declared that no competing interests exist.

Ethical statement

All animal procedures performed in this research were done in accordance with the “Ethical Standards of the Shanghai Ocean University (2020)”.


Funding

This work was supported by the Science and Technology Commission of Shanghai Municipality (19410740500; 19050501900) to CL.

Author contributions

C Li and J Xia conceived the research ideas. M Zhou collected the data and performed the analyses. M Zhou wrote the first draft. J Xia and M Zhou edited the manuscript. All authors revised and approved the final version of the manuscript.

Author ORCIDs

Mingwei Zhou  <https://orcid.org/0000-0002-1182-8466>

Jianhong Xia  <https://orcid.org/0009-0001-9615-4797>

Chenhong Li  <https://orcid.org/0000-0003-3075-1756>

Data availability

All of the data that support the findings of this study are available in the main text or Supplementary Information.

References

- Chen IS, Jang-Liaw NH (2023) Phylogeography of *Aphyocypris normalis* Nichols and Pope, 1927 at Hainan Island and adjacent areas based on mitochondrial DNA data. PLOS ONE 18(2): e0282460. <https://doi.org/10.1371/journal.pone.0282460>
- Chen IS, Kottelat M, Wu H (2002) A new genus of freshwater sleeper (Teleostei: Odontobutidae) from southern China and mainland Southeast Asia. Taiwan Shuichanxue Hui Kan 29: 229–235.
- Chen W, Zhong Z, Dai W, Fan Q, He S (2017) Phylogeographic structure, cryptic speciation and demographic history of the sharpbelly (*Hemiculter leucisculus*), a freshwater habitat generalist from southern China. BMC Evolutionary Biology 17(1): 216. <https://doi.org/10.1186/s12862-017-1058-0>
- Chen C, Chen H, Zhang Y, Thomas HR, Frank MH, He Y, Xia R (2020) TBtools: An integrative toolkit developed for interactive analyses of big biological data. Molecular Plant 13(8): 1194–1202. <https://doi.org/10.1016/j.molp.2020.06.009>
- Cheng F, Wang Q, Maisano Delser P, Li C (2019) Multiple freshwater invasions of the tapertail anchovy (Clupeiformes: Engraulidae) of the Yangtze River. Ecology and Evolution 9(21): 12202–12215. <https://doi.org/10.1002/ece3.5708>
- Danecek P, Auton A, Abecasis G, Albers CA, Banks E, DePristo MA, Handsaker RE, Lunter G, Marth GT, Sherry ST, McVean G, Durbin R (2011) The variant call format and VCFtools. Bioinformatics (Oxford, England) 27(15): 2156–2158. <https://doi.org/10.1093/bioinformatics/btr330>

- Earl DA, vonHoldt BM (2012) STRUCTURE HARVESTER: A website and program for visualizing STRUCTURE output and implementing the Evanno method. *Conservation Genetics Resources* 4(2): 359–361. <https://doi.org/10.1007/s12686-011-9548-7>
- Excoffier L, Foll M (2011) fastsimcoal: A continuous-time coalescent simulator of genomic diversity under arbitrarily complex evolutionary scenarios. *Bioinformatics (Oxford, England)* 27(9): 1332–1334. <https://doi.org/10.1093/bioinformatics/btr124>
- Excoffier L, Laval G, Schneider S (2007) Arlequin (version 3.0): An integrated software package for population genetics data analysis. *Evolutionary Bioinformatics Online* 1: 47–50. <https://doi.org/10.1177/117693430500100003>
- Iwata A (2011) Systematics of Odontobutidae. In: Patzner R, Tassell JLV, Kovacic M, Kapoor BG (Eds) *The Biology of Gobies*. Science Publishers, Enfield, 61–77.
- Iwata A, Sakai H, Shibukawa K, Jeon SR (2001) Developmental characteristics of a freshwater goby, *Micropercops swinhonis*, from Korea. *Zoological Science* 18(1): 91–97. <https://doi.org/10.2108/zsj.18.91>
- Katoh K, Standley DM (2013) MAFFT multiple sequence alignment software version 7: Improvements in performance and usability. *Molecular Biology and Evolution* 30(4): 772–780. <https://doi.org/10.1093/molbev/mst010>
- Li H, Durbin R (2009) Fast and accurate short read alignment with Burrows-Wheeler transform. *Bioinformatics (Oxford, England)* 25(14): 1754–1760. <https://doi.org/10.1093/bioinformatics/btp324>
- Li C, Hofreiter M, Straube N, Corrigan S, Naylor GJ (2013) Capturing protein-coding genes across highly divergent species. *BioTechniques* 54(6): 321–326. <https://doi.org/10.2144/000114039>
- Li H, He Y, Jiang J, Liu Z, Li C (2018) Molecular systematics and phylogenetic analysis of the Asian endemic freshwater sleepers (Gobiiformes: Odontobutidae). *Molecular Phylogenetics and Evolution* 121: 1–11. <https://doi.org/10.1016/j.ympev.2017.12.026>
- Lischer HE, Excoffier L (2012) PGDSpider: An automated data conversion tool for connecting population genetics and genomics programs. *Bioinformatics (Oxford, England)* 28(2): 298–299. <https://doi.org/10.1093/bioinformatics/btr642>
- McKenna A, Hanna M, Banks E, Sivachenko A, Cibulskis K, Kernytsky A, Garimella K, Altshuler D, Gabriel S, Daly M, DePristo MA (2010) The genome analysis toolkit: A MapReduce framework for analyzing next-generation DNA sequencing data. *Genome Research* 20(9): 1297–1303. <https://doi.org/10.1101/gr.107524.110>
- Meyer M, Kircher M (2010) Illumina sequencing library preparation for highly multiplexed target capture and sequencing. *Cold Spring Harbor Protocols* 2010(6): pdb.prot5448. <https://doi.org/10.1101/pdb.prot5448>
- Minh BQ, Schmidt HA, Chernomor O, Schrempf D, Woodhams MD, von Haeseler A, Lanfear R (2020) IQ-TREE 2: New models and efficient methods for phylogenetic inference in the genomic era. *Molecular Biology and Evolution* 37(5): 1530–1534. <https://doi.org/10.1093/molbev/msaa015>
- Mirarab S, Reaz R, Bayzid MS, Zimmermann T, Swenson MS, Warnow T (2014) ASTRAL: Genome-scale coalescent-based species tree estimation. *Bioinformatics (Oxford, England)* 30(17): i541–i548. <https://doi.org/10.1093/bioinformatics/btu462>
- Pritchard JK, Stephens M, Donnelly P (2000) Inference of population structure using multilocus genotype data. *Genetics* 155(2): 945–959. <https://doi.org/10.1093/genetics/155.2.945>

- Rambaut A (2013) Figtree v 1.4.2. <http://tree.bio.ed.ac.uk>
- Stamatakis A (2014) RAxML version 8: A tool for phylogenetic analysis and post-analysis of large phylogenies. *Bioinformatics (Oxford, England)* 30(9): 1312–1313. <https://doi.org/10.1093/bioinformatics/btu033>
- Tsao YF, Lin WW, Chang CH, Ueda T, Jang-Liaw NH, Zhao YH, Kao HW (2016) Phylogeography, Historical Demography, and Genetic Structure of the Rose Bitterling, *Rhodeus ocellatus* (Kner, 1866) (Cypriniformes: Acheilognathidae), in East Asia. *Zoological Studies (Taipei, Taiwan)* 55: e49. <https://doi.org/10.6620/zs.2016.55-49>
- Wang J, Li C, Chen J, Wang J, Jin J, Jiang S, Yan L, Lin HD, Zhao J (2021) Phylogeographic structure of the dwarf snakehead (*Channa gachua*) around Gulf of Tonkin: Historical biogeography and pronounced effects of sea-level changes. *Ecology and Evolution* 11(18): 12583–12595. <https://doi.org/10.1002/ece3.8003>
- Wang Y, Yuan H, Huang J, Li C (2022) Inline index helped in cleaning up data contamination generated during library preparation and the subsequent steps. *Molecular Biology Reports* 49(1): 385–392. <https://doi.org/10.1007/s11033-021-06884-y>
- Wu H, Zhong J (2008) *Fauna Sinica Ostichthyes Perciformes (V) Gobioidei*. Science Press, Beijing.
- Xiong W, Wang Q, Xie D, Fletcher DH, He D (2018) Factors influencing tropical Island freshwater fishes: Species, status, threats and conservation in Hainan Island. *Knowledge and Management of Aquatic Ecosystems* 419(419): 6. <https://doi.org/10.1051/kmae/2017054>
- Yang JQ, Hsu KC, Liu ZZ, Su LW, Kuo PH, Tang WQ, Zhou ZC, Liu D, Bao BL, Lin HD (2016) The population history of *Garra orientalis* (Teleostei: Cyprinidae) using mitochondrial DNA and microsatellite data with approximate Bayesian computation. *BMC Evolutionary Biology* 16(1): 73. <https://doi.org/10.1186/s12862-016-0645-9>
- Yao Y, Harff J, Meyer M, Zhan W (2009) Reconstruction of paleocoastlines for the northwestern South China Sea since the Last Glacial Maximum. *Science in China. Series D, Earth Sciences* 52(8): 1127–1136. <https://doi.org/10.1007/s11430-009-0098-8>
- Yuan H, Atta C, Tornabene L, Li C (2019) Assexon: Assembling exon using gene capture data. *Evolutionary Bioinformatics Online* 15: 1176934319874792. <https://doi.org/10.1177/1176934319874792>
- Zhang WJ, Wang JJ, Li C, Chen JQ, Li W, Jiang SY, Hsu KC, Zhao M, Lin HD, Zhao J (2020) Spatial genetic structure of *Opsariichthys hainanensis* in South China. *Mitochondrial DNA. Part A, DNA Mapping, Sequencing, and Analysis* 31(3): 98–107. <https://doi.org/10.1080/24701394.2020.1741564>
- Zhang Y, Sun J, Shi L, Yu H, Jia Z (2021) Population genetic pattern of the freshwater fish Amur sleeper (*Perccottus glenii*) across its native distribution area in China. *Conservation Genetics* 22(1): 125–131. <https://doi.org/10.1007/s10592-020-01323-0>
- Zhao J, Hsu K-C, Luo J-Z, Wang C-H, Chan B-P, Li J, Kuo P-H, Lin H-D (2018) Genetic diversity and population history of *Tanichthys albonubes* (Teleostei: Cyprinidae): implications for conservation. *Aquatic Conservation* 28(2): 422–434. <https://doi.org/10.1002/aqc.2840>
- Zhou M, He A, Wang F, Li Y, Li C (2022) *Neodontobutis lani*, a new sleeper fish of the family Odontobutidae (Teleostei: Gobiiformes) from Guangxi, southern China. *Zootaxa* 5134(1): 113–124. <https://doi.org/10.11646/zootaxa.5134.1.5>
- Zhu H (2020) On the biogeographical origin of Hainan Island in China. *Zhiwu Kexue Xuebao* 38(6): 839–843. <https://doi.org/10.11913/PSJ.2095-0837.2020.60839>

Supplementary material 1

A text file contains all template files (*.tpl) for FASTSIMCOAL2 simulations in this research

Authors: Mingwei Zhou, Jianhong Xia, Chenhong Li

Data type: txt

Copyright notice: This dataset is made available under the Open Database License (<http://opendatacommons.org/licenses/odbl/1.0/>). The Open Database License (ODbL) is a license agreement intended to allow users to freely share, modify, and use this Dataset while maintaining this same freedom for others, provided that the original source and author(s) are credited.

Link: <https://doi.org/10.3897/zookeys.1197.110314.suppl1>

Supplementary material 2

A text file contains all estimation files (*.est) for FASTSIMCOAL2 simulations in this research

Authors: Mingwei Zhou, Jianhong Xia, Chenhong Li

Data type: txt

Copyright notice: This dataset is made available under the Open Database License (<http://opendatacommons.org/licenses/odbl/1.0/>). The Open Database License (ODbL) is a license agreement intended to allow users to freely share, modify, and use this Dataset while maintaining this same freedom for others, provided that the original source and author(s) are credited.

Link: <https://doi.org/10.3897/zookeys.1197.110314.suppl2>

A new species of *Hemiphyllodactylus* (Squamata, Gekkonidae) from southwest Yunnan, China

Hongxin Zhou^{1,2}, Shimin Li^{2,3}, Ziqi Shen², Shuo Liu⁴, Dingqi Rao²

1 Key Laboratory for Forest Resources Conservation and Utilization in the Southwest Mountains of China, Ministry of Education Faculty of Biodiversity and Conservation, Southwest Forestry University, Kunming, Yunnan 650224, China

2 Kunming Institute of Zoology, Chinese Academy of Sciences, Kunming, Yunnan 650201, China

3 Anhui Normal University, Wuhu, Anhui 241000, China

4 Kunming Natural History Museum of Zoology, Kunming Institute of Zoology, Chinese Academy of Sciences, Kunming, Yunnan 650223, China

Corresponding authors: Dingqi Rao (raodq@mail.kiz.ac.cn); Shuo Liu (liushuo@mail.kiz.ac.cn)

Abstract

A new species of gekkonid, *Hemiphyllodactylus gengmaensis* **sp. nov.**, is described based on six specimens from Gengma Dai and Wa Autonomous County, Yunnan, China. The new species can be distinguished from its congeners by a significant genetic divergence of greater than 9.7% in the mitochondrial ND2 gene and a combination of the following characters: a maximum SVL of 43.24mm; 8 or 9 chin scales; six circumnasal scales; 2 or 3 internasal scales; 9–11 supralabial scales; 8 or 9 infralabial scales; 11–18 dorsal scales; 8–10 ventral scales; a manual lamellar formula of 5–5–5–4 or 5–6–5–4 and a pedal lamellar formula of 5–5–6–5; 20–25 precloacal and femoral pore-bearing scales contiguous in males; dark postorbital stripes or striping on body; dark dorsal transverse blotches present; and a brown postsacral mark bearing anteriorly projecting arms. The discovery of this new species brings the number of *Hemiphyllodactylus* species in China to 15.

Key words: Gengma Dai and Wa Autonomous County, *Hemiphyllodactylus gengmaensis* sp. nov., integrative taxonomy, molecular phylogeny, slender gecko



Academic editor: Anthony Herrel

Received: 14 December 2023

Accepted: 27 March 2024

Published: 17 April 2024

ZooBank: <https://zoobank.org/1188BAC9-B6BC-4298-A7F5-BFE237CED84F>

Citation: Zhou H, Li S, Shen Z, Liu S, Rao D (2024) A new species of *Hemiphyllodactylus* (Squamata, Gekkonidae) from southwest Yunnan, China. ZooKeys 1197: 197–213. <https://doi.org/10.3897/zookeys.1197.117359>

Copyright: © Hongxin Zhou et al.

This is an open access article distributed under terms of the Creative Commons Attribution

License (Attribution 4.0 International – CC BY 4.0).

Introduction

Species of the genus *Hemiphyllodactylus* Bleeker, 1860 are small nocturnal geckos (SVL < 63 mm) distributed in South Asia, Southeast Asia, South China, and the Indo-Pacific region (Zug 2010; Grismer et al. 2013, 2018a; Agarwal et al. 2019; Eliades et al. 2019; Agung et al. 2021, 2022). Furthermore, all *Hemiphyllodactylus* are well camouflaged, occur in low densities, are forest-dwelling, and have small populations (Zug 2010; Grismer et al. 2013, 2018a; Agarwal et al. 2019; Eliades et al. 2019; Agung et al. 2021, 2022). Hence, *Hemiphyllodactylus* was considered to a low-diversity taxon (Zug 2010) until

Grismer et al. (2013) revealed its high diversity using integrative taxonomy. In the following decade, the number of species within the group has increased from 12 to 54 (Uetz et al. 2023).

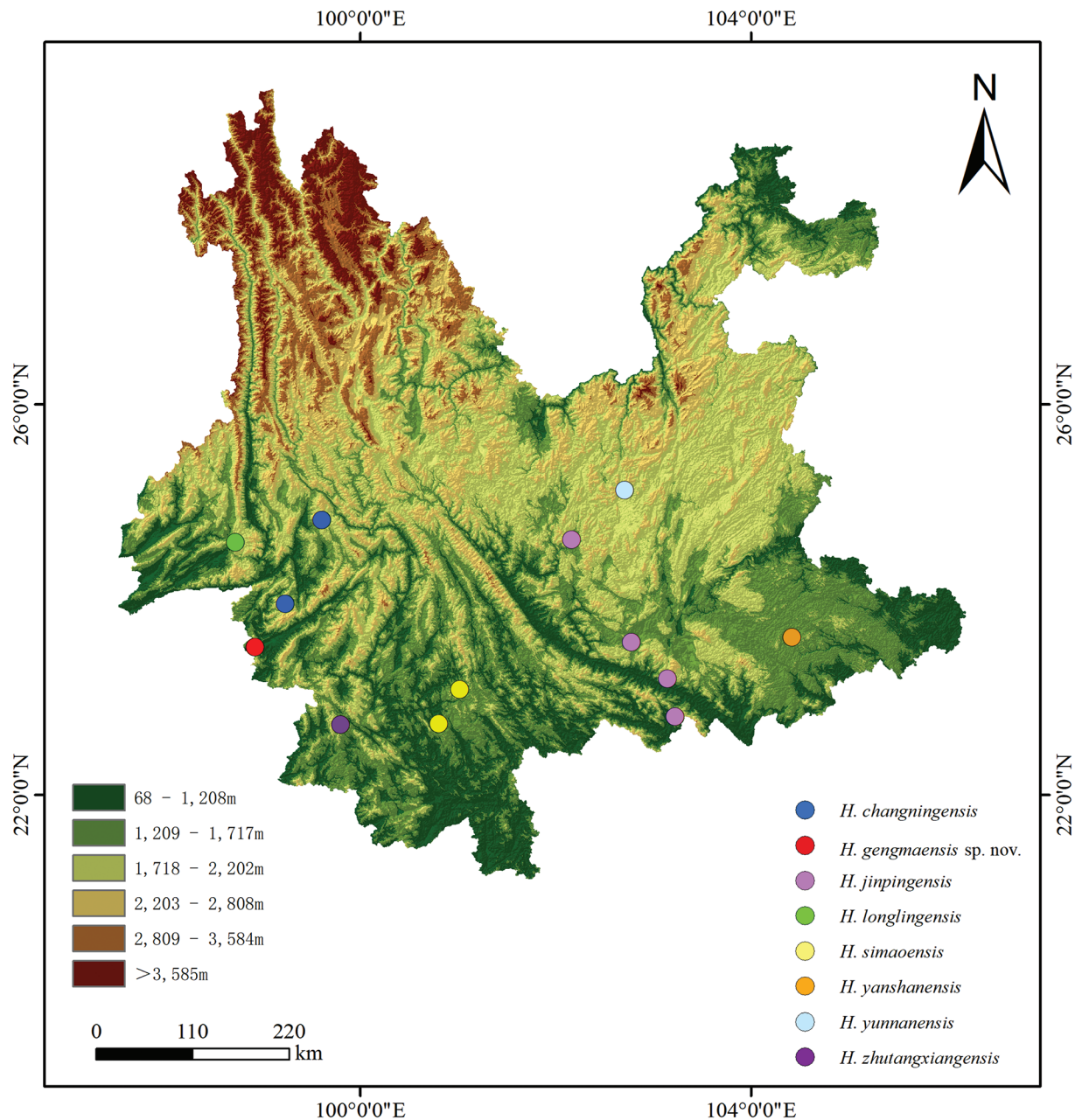
In China, *Hemiphyllodactylus* species have also been overlooked. The first species of slender geckos known from China is *Gehyra yunnanensis* (Boulenger, 1903), then “Smith revised its taxonomic status, placing it in the genus *Hemiphyllodactylus*” (Zug 2010). Zhou et al. (1981) recognized three subspecies of *H. yunnanensis* based on the digital lamellae patterns of specimens collected in Yunnan, Guizhou, and Guangxi Zhuang Autonomous Region, China: *H. y. dushanensis* Zhou & Liu, *H. y. jinpingensis* Zhou & Liu, and *H. y. longlingensis* Zhou & Liu. However, for the subsequent 32 years, most of Chinese slender geckos were regarded as simply *H. yunnanensis*, until Grismer et al. (2013) elevated these three subspecies to full species rank. Subsequently, nine additional species were incrementally recorded from China: *H. zugi* Nguyen, Lehmann, Le Duc, Duong, Bonkowski & Ziegler, 2013; *H. changningensis* Guo, Zhou, Yan & Li, 2015; *H. huishuiensis* Yan, Lin, Guo, Li & Zhou, 2016; *H. hongkongensis* Sung, Lee, Ng, Zhang & Yang, 2018; *H. zayuensis* Jiang, Wang & Che, 2020; *H. dupanglingensis* Zhang, Qian & Yang, 2020; *H. zhutangxiangensis* Agung, Grismer, Grismer, Quah, Chornelia, Lu & Hughes, 2021; *H. simaoensis* Agung, Chornelia, Grismer, Grismer, Quah, Lu, Tomlinson & Hughes, 2022; and *H. yanshanensis* Agung, Chornelia, Grismer, Grismer, Quah, Lu, Tomlinson & Hughes, 2022. The fourteenth species, *H. typus* Bleeker, 1860, as a widely distributed species, its actual coordinate data for distribution in China is unavailable (Agung et al. 2021; Uetz et al. 2023). According to recent genus-wide molecular phylogenetic studies, all *Hemiphyllodactylus* species in China belong to the *typus* group, and they are divided into four clades (Grismer et al. 2013, 2014a, 2014b, 2017, 2018a, 2020a, 2020b; Ngo et al. 2014; Agung et al. 2021, 2022): both clade 3 (*H. longlingensis*, *H. zhutangxiangensis*, *H. zayuensis*, and *H. changningensis*) and clade 4 (*H. jinpingensis* and *H. simaoensis*) of Agung et al. (2022) colonized China from western Indochina, and both clade 6 (*H. dushanensis*, *H. hongkongensis*, *H. dupanglingensis*, *H. zugi*, *H. huishuiensis*, and *H. yanshanensis*) and clade 7 (*H. yunnanensis*) of Agung et al. (2022) colonized China from eastern Indochina.

During our herpetological survey in Banxing Village, Gengma Dai and Wa Autonomous County, Yunnan, China, we collected six specimens belonging to the genus *Hemiphyllodactylus*. These specimens are distinguished from known species of *Hemiphyllodactylus* based on molecular and morphological data. Therefore, we describe them as a new species below.

Materials and methods

Sampling

Six specimens were collected from in Banxing Village, Gengma Dai and Wa Autonomous County of Yunnan Province in China on 15 May 2014 (Fig. 1). All specimens were preserved in 80% ethanol, and their muscle and liver tissues were preserved in 95% ethanol. Specimens were deposited in Kunming Institute of Zoology (KIZ), Chinese Academy of Sciences (CAS).



Molecular data and phylogenetic analyses

We used Trelief Hi-Pure Animal Genomic DNA Kit for genomic DNA extraction following the manufacturer's protocol (<https://www.tsingke.com.cn>). We amplified and sequenced the complete mitochondrial NADH dehydrogenase subunit 2 gene (ND2), totaling 1,038 bp using the primers L4437b and H5934 (Macey et al. 1997). The protocol for polymerase chain reaction (PCR) amplifications followed Agung et al. (2021). Genomic DNA extraction, PCR processes, and sequencing were executed at Beijing Tsingke Biotechnology Co., Ltd. All specimen sequences have been deposited in GenBank, with accession numbers from PP540021 to PP540025.

Table 1. List of specimens used for phylogenetic analyses in this study.

Species	GenBank no.	Locality	Voucher information
<i>H. harterti</i>	KF219760	Bukit Larut, Malaysia	LSUHC 10383
<i>H. harterti</i>	KF219761	Bukit Larut, Malaysia	LSUHC 10384
<i>H. indosobrinus</i>	JN393935	Champasak, Pakxong, Laos	FMNH 258695
<i>H. flaviventris</i>	MG322161	Chanthaburi, Thailand	ZMKU TM001204N
<i>H. flaviventris</i>	MG322162	Chanthaburi, Thailand	ZMKU TM001205N
<i>H. flaviventris</i>	MG322163	Chanthaburi, Thailand	ZMKU TM001206N
<i>H. flaviventris</i>	MG322164	Chanthaburi, Thailand	ZMKU TM001207N
<i>H. flaviventris</i>	MG322165	Chanthaburi, Thailand	ZMKU TM001208N
<i>H. arakuensis</i>	MK570109	Araku, Visakhapatnam District, Andhra Pradesh, India	BNHS 2275
<i>H. aurantiacus</i>	MK570110	Yercaud, Salem District, Tamil Nadu, India	AK 237
<i>H. aurantiacus</i>	MK570111	Yercaud, Salem District, Tamil Nadu, India	AMB s.n.
<i>H. jnana</i>	MK570112	Bangalore, Karnataka, India	CES G174
<i>H. jnana</i>	MK570113	Bangalore, Karnataka, India	CES G173
<i>H. jnana</i>	MK570114	Bangalore, Karnataka, India	CYL01
<i>H. jnana</i>	MK570115	Bangalore, Karnataka, India	CES G470
<i>H. kolliensis</i>	MK570116	Kolli Hills, Namakkal, Tamil Nadu, India	CES G138
<i>H. kolliensis</i>	MK570117	Kolli Hills, Namakkal, Tamil Nadu, India	AK 276
<i>H. zwegabinensis</i>	MT028174	Zwegabin Mountain, Kayin State, Myanmar	LSUHC 14184
<i>H. pinlaungensis</i>	MT028166	Pinlaung City, Shan State, Myanmar	LSUHC 14263
<i>H. pinlaungensis</i>	MT028167	Pinlaung City, Shan State, Myanmar	LSUHC 14264
<i>H. pinlaungensis</i>	MT028168	Pinlaung City, Shan State, Myanmar	LSUHC 14265
<i>H. kyaiktiyoensis</i>	MT028146	Mon State, Myanmar	LSUHC 14030
<i>H. kyaiktiyoensis</i>	MT028147	Mon State, Myanmar	LSUHC 14031
<i>H. kyaiktiyoensis</i>	MT028148	Mon State, Myanmar	LSUHC 14032
<i>H. kyaiktiyoensis</i>	MT028149	Mon State, Myanmar	LSUHC 14033
<i>H. khlonglanensis</i>	MG322153	Kamphaeng Phet, Thailand	ZMKU TM000999N
<i>H. khlonglanensis</i>	MG322154	Kamphaeng Phet, Thailand	ZMKU TM001000N
<i>H. khlonglanensis</i>	MG322155	Kamphaeng Phet, Thailand	ZMKU TM001001N
<i>H. khlonglanensis</i>	MG322156	Kamphaeng Phet, Thailand	ZMKU TM001002N
<i>H. zhutangxiangensis</i>	MW962150	Zhutangxiang town, Lancang Lahu, Yunnan, China	KIZ061163
<i>H. zhutangxiangensis</i>	MW962151	Zhutangxiang town, Lancang Lahu, Yunnan, China	KIZ061164
<i>H. zhutangxiangensis</i>	MW962152	Zhutangxiang town, Lancang Lahu, Yunnan, China	KIZ061165
<i>H. zhutangxiangensis</i>	MW962153	Zhutangxiang town, Lancang Lahu, Yunnan, China	KIZ061166
<i>H. zhutangxiangensis</i>	MW962154	Zhutangxiang town, Lancang Lahu, Yunnan, China	KIZ061167
<i>H. longlingensis</i>	FJ971045	Longyang District, Baoshan, Yunnan, China	isolate N30
<i>H. longlingensis</i>	FJ971046	Longyang District, Baoshan, Yunnan, China	NJNUh00104
<i>H. longlingensis</i>	FJ971047	Longyang District, Baoshan, Yunnan, China	isolate N32
<i>H. longlingensis</i>	FJ971048	Longyang District, Baoshan, Yunnan, China	isolate N33
<i>H. zalonicus</i>	MW039150	Zalon Taung National Forest, Ban Mauk, Sagaing, Myanmar	ZMMU R 16635
<i>H. changningensis</i>	ON676073	Yongde County, Yunnan, China	KIZ 061990
<i>H. changningensis</i>	ON676074	Yongde County, Yunnan, China	KIZ 061991
<i>H. changningensis</i>	ON676075	Yongde County, Yunnan, China	KIZ 061992
<i>H. changningensis</i>	ON676076	Yongde County, Yunnan, China	KIZ 061993
<i>H. changningensis</i>	ON676077	Yongde County, Yunnan, China	KIZ 061994
<i>H. changningensis</i>	ON676078	Yongde County, Yunnan, China	KIZ 061995
<i>H. changningensis</i>	ON676079	Yongde County, Yunnan, China	KIZ 061996
<i>H. changningensis</i>	ON676080	Yongde County, Yunnan, China	KIZ 061997
<i>H. gengmaensis</i> sp. nov.	PP540023	Gengma Dai and Wa Autonomous County, Yunnan, China	2014002297
<i>H. gengmaensis</i> sp. nov.	PP540024	Gengma Dai and Wa Autonomous County, Yunnan, China	2014002298
<i>H. gengmaensis</i> sp. nov.	PP540022	Gengma Dai and Wa Autonomous County, Yunnan, China	2014002299
<i>H. gengmaensis</i> sp. nov.	PP540021	Gengma Dai and Wa Autonomous County, Yunnan, China	2014002300
<i>H. gengmaensis</i> sp. nov.	PP540025	Gengma Dai and Wa Autonomous County, Yunnan, China	2014002302

A total of 47 ND2 sequences from GenBank, containing 2 ND2 sequences of outgroup taxa (*Hemiphyllodactylus harterti* Werner, 1900) and 45 sequences of extant *Hemiphyllodactylus* species, was downloaded; these with our five new sequences are listed in Table 1. Sequences were assembled and manual proof-read in SeqMan (DNASTAR, Inc., Madison, WI, USA), then aligned using Clustal W (Thompson et al. 1994) implemented in MEGA 7 (Kumar et al. 2016). For phylogenetic relationships analysis, we considered maximum likelihood (ML) and Bayesian inference (BI) using IQ-TREE v. 2.2.0 (Nguyen et al. 2015) and MrBayes v. 3.2.7a (Ronquist et al. 2012) in the Phylosuite application (Zhang D et al. 2020; Xiang et al. 2023), respectively. After alignment, we used Gblock 0.91b (Talavera and Castresana 2007) to remove misaligned positions. ModelFinder v. 2.2.0 (Kalyaanamoorthy et al. 2017) was used to select the best-fitting model of evolution based on the Bayesian Information Criterion (BIC). A maximum-likelihood (ML) analysis was conducted using TPM+F+G4 as the best-fit substitution model for codon position one, TPM+F+G4 for position two, and TIM+F+G4 for position three. We applied 1,000 bootstrap pseudoreplicates with the ultrafast bootstrap approximation algorithm (UFBoot) (Agung et al. 2021), where nodes having values 95 and above were considered highly supported (Minh et al. 2013). A Bayesian-inference (BI) analysis was conducted using GTR+I+G+F model following the methods by Agung et al. (2021), except that instead of discarding 10% of the trees, we discarded the first 25% of the sampled as burn-in. Nodes with Bayesian posterior probabilities (BPP) of 0.95 and above were considered highly supported (Huelsenbeck et al. 2001; Wilcox et al. 2002). Uncorrected pairwise divergences were calculated using MEGA 7 (Kumar et al. 2016).

Morphological data

Mensural data were taken with a digital calipers to the nearest 0.01 mm under a dissecting microscope (Jiangnan XTB-01) following Zug (2010), Grismer et al. (2013), and Agung et al. (2021): snout-vent length (**SVL**), taken from the tip of the snout to the vent; tail length (**TL**), taken from the vent to the tip of the tail; trunk length (**TrunkL**), taken from the posterior margin of the forelimb at its insertion point on the body to the anterior margin of the hind limb at its insertion point on the body; head length (**HL**), measured from the posterior margin of the retroarticular process of the lower jaw to the tip of the snout; head width (**HW**), measured at the angle of the jaws; eye diameter (**ED**), the greatest horizontal diameter of the eyeball; snout-eye length (**SnEye**), measured from anterior-most margin of the eyeball to the tip of snout; nares-eye length (**NarEye**), measured from the anterior margin of the eyeball to the posterior margin of the external nares; and snout width (**SnW**), measured between the external nares.

For meristic characters and color pattern, we measured and evaluated them according to the methods of Agung et al. (2021).

Results

Our results of ML and BI analyses were similar to those obtained by Agung et al. (2021): the specimens from Gengma County were recovered as members

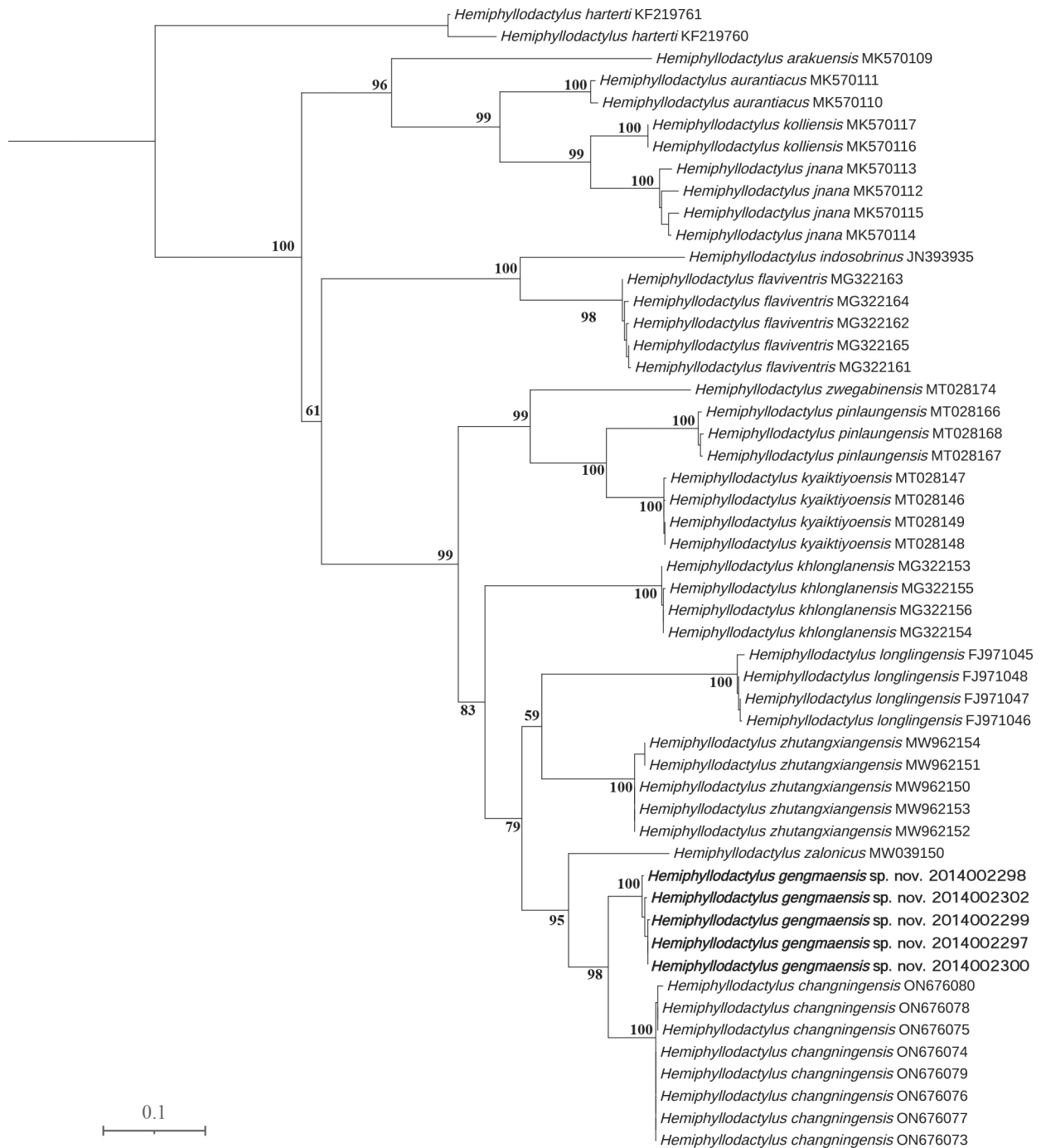


Figure 2. Maximum-likelihood consensus tree based on 1038 bp mitochondrial ND2 gene. Numbers by the nodes indicate ML bootstrap support values.

of Clade 3 in both ML and BI analyses (Figs 2, 3), which includes *Hemiphyllodactylus longlingensis*, *H. zaloncus*, *H. changningensis*, and *H. zhutangxiangensis*. The mean percentage of uncorrected pairwise distance between the Gengma County specimens and *H. changningensis* is 9.7% (Table 2). Furthermore, the new species also could be distinguished from its congeners by body proportions, CN, VS, Lamellar formulae hands and feet II–V, SL1T and total number of femoropreloacal pores. Therefore, we describe them here as a new species.

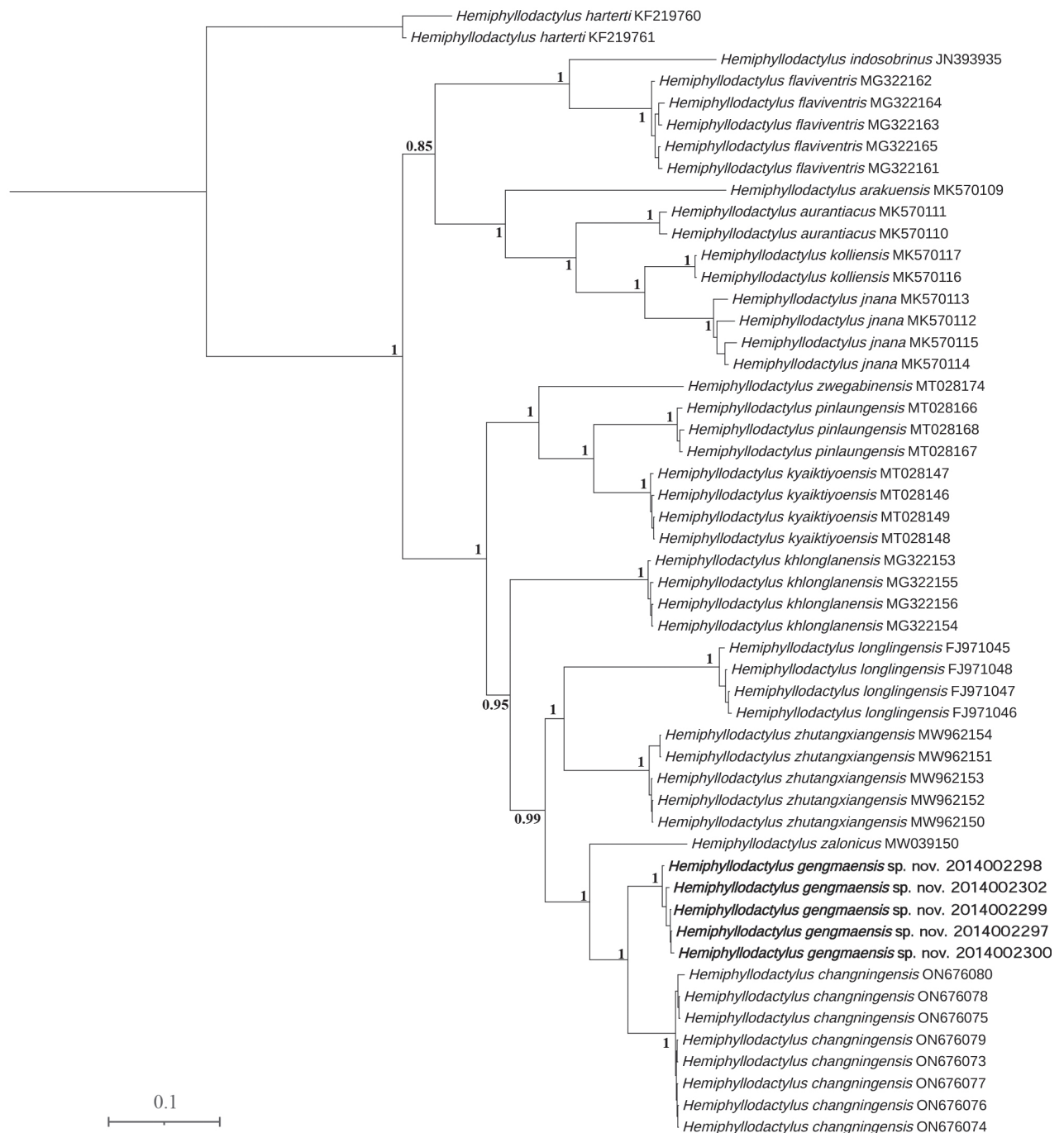


Figure 3. Phylogenetic tree by Bayesian inference based on 1038 bp mitochondrial ND2 gene. Numbers by the nodes indicate posterior probability values of the BI.

Taxonomic account

Hemiphyllodactylus gengmaensis sp. nov.

<https://zoobank.org/16760DC6-5331-4742-A5FE-FD3F6E42DAC8>

Figs 4, 5

Material. Holotype. 2014002302, adult female, collected by Hong Hui on 15 May 2014 from Banxing Village, Gengma Dai and Wa Autonomous County, Yunnan, China (23.517°N, 98.925°E, at an elevation of 664 m).

Table 2. The mean percentage of the uncorrected *p*-distance among the *Hemiphyllodactylus* species studied based on mitochondrial ND2 gene fragments.

Species name (n)	1	2	3	4	5	6	7	8	9	10	11	12	13	14
1. <i>H. longlingensis</i> (4)	–													
2. <i>H. khlonglanensis</i> (4)	25.0	–												
3. <i>H. flaviventris</i> (5)	41.7	34.9	–											
4. <i>H. arakuentris</i> (1)	35.4	35.2	33.1	–										
5. <i>H. aurantiacus</i> (2)	37.3	33.9	30.6	26.9	–									
6. <i>H. jnana</i> (4)	36.6	35.1	30.1	20.4	17.1	–								
7. <i>H. kolliensis</i> (2)	34.1	34.5	30.4	21.8	16.5	10.0	–							
8. <i>H. kyaiktiyoensis</i> (4)	27.3	20.3	36.3	41.3	39.2	35.0	36.7	–						
9. <i>H. pinlaungensis</i> (3)	28.7	23.1	44.4	44.1	38.1	36.6	37.7	13.1	–					
10. <i>H. zwegabinensis</i> (1)	25.6	23.1	39.9	42.5	37.9	37.1	36.0	17.7	21.6	–				
11. <i>H. zalonicus</i> (1)	16.1	17.8	40.2	29.3	35.0	32.8	32.7	22.0	25.2	25.7	–			
12. <i>H. zhutangxiangensis</i> (5)	21.9	19.2	38.8	30.2	33.4	31.0	28.2	24.9	26.4	26.9	16.6	–		
13. <i>H. changningensis</i> (8)	23.3	23.0	38.5	35.1	36.3	35.4	34.4	25.8	28.3	27.0	14.5	22.2	–	
14. <i>H. gengmaensis</i> sp. nov. (5)	19.8	22.7	37.3	32.2	31.2	32.2	34.5	24.5	26.3	24.7	11.5	19.1	9.7	0.3

Paratypes. 2014002297, 2014002298, 2014002299, adult females, 2014002300, 2014002301, adult males, collected at the same locality as the holotype on 15 May 2014.

Diagnosis. *Hemiphyllodactylus gengmaensis* sp. nov. can be distinguished from its congeners by the combination of the following characters: maximum SVL of 43.24 mm; 8–9 chin scales; enlarged postmentals; 6 circumnasal scales; 2–3 internasal scales; 9–11 supralabial scales; 8–9 infralabial scales; 11–18 dorsal scales; 8–10 ventral scales; a manual lamellar formula of 5–5–5–4 or 5–6–5–4 and a pedal lamellar formula of 5–5–6–5; 20–25 preloacal and femoral pore-bearing scales contiguous in males. dark postorbital stripes or striping on body; dark dorsal transverse blotches; and a brown postsacral mark bearing anteriorly projecting arms.

Description of holotype. Adult female, SVL 38.52 mm; head triangular in dorsal profile, depressed, distinct from neck (HL 10.80 mm; HW 7.36 mm); lores flat; snout short (SnEye 3.94 mm; SnEye/HL 36%), narrow (SnW 1.78 mm; SnW/HW 24%); eye large (ED 2.12 mm; ED/HL 20%); rostral scale wider than high, bordered posteriorly by two large supranasals and three internasals (IS); nares bordered anteriorly by rostral scale, ventrally by first and second supralabial scale, dorsally by supranasal scale, posteriorly by three postnasals; supralabials square, 10/9 (left/right), tapering from rostral to a point in line with posterior margin of orbit (SL); infralabials square, 9/9 (left/right), tapering from mental to a point in line with posterior margin of orbit (IL); scales on head small, rounded, largest on rostrum; mental triangular, eight chin scales touching internal edges of infralabials from juncture of the second and the third on left and right and mental scale (Chin); scales in gular region rounded, non-overlapping, becoming larger and more ovoid on venter. Robust body type and small, (TrunkL/SVL 45%), dorsoventrally compressed; dorsal body scales small, granular, 18 dorsal scales at midbody contained within one eye diameter; ventral body scales smooth and flat, much larger than dorsal scales, subimbricate, 10 ventral

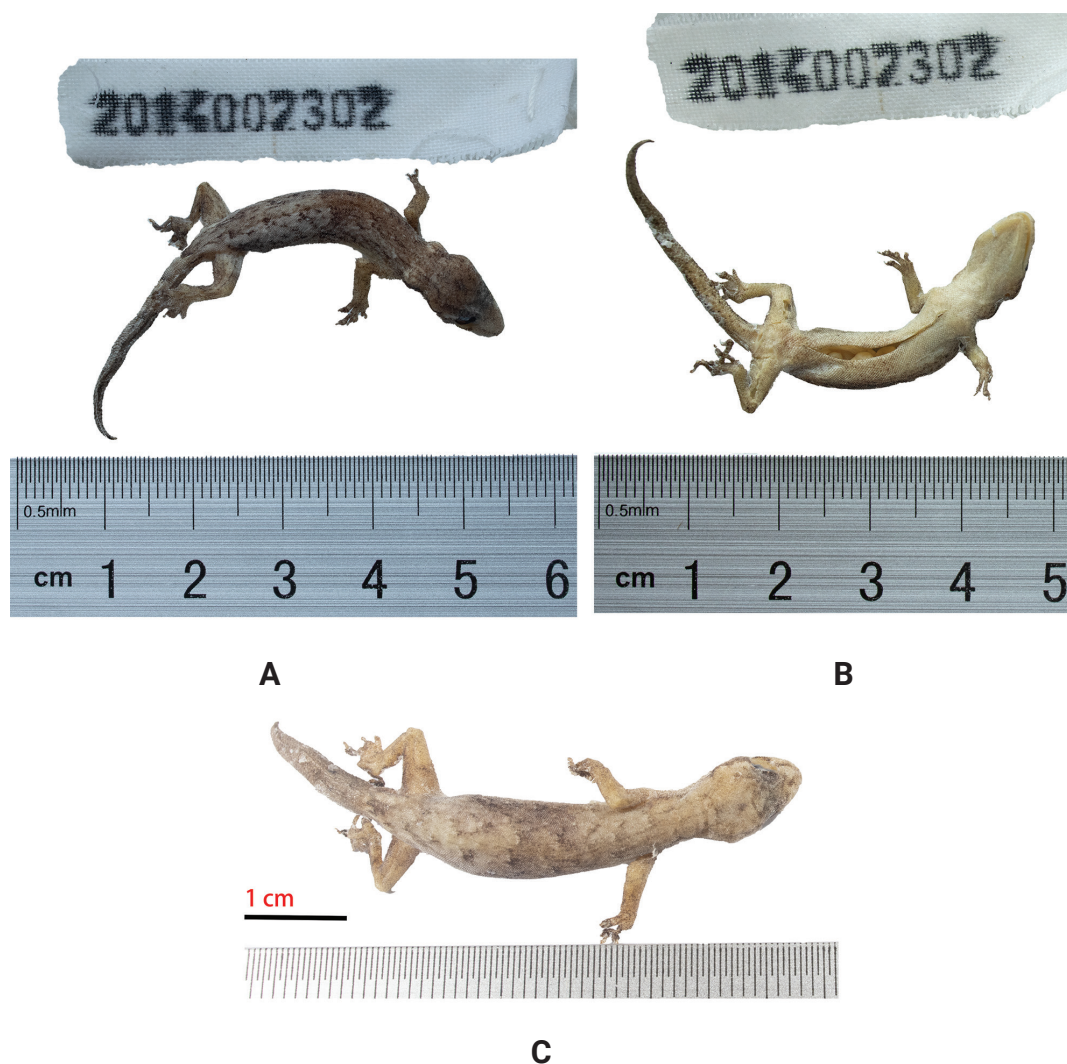


Figure 4. *Hemiphyllodactylus gengmaensis* sp. nov. **A** holotype, 2014002302, dorsal view in alcohol **B** holotype, 2014002302, ventral view in alcohol **C** paratype, 2014002301, dorsal view in alcohol.

scales at midbody contained within one eye diameter; granular scales on the limbs; finger I is vestigial, clawless, and with rectangular subdigital lamellae, while fingers II–V are well developed; the proximal subdigital lamellae are undivided and rectangular, while the distal subdigital lamellae are divided, angular, U-shaped, except for the terminal lamellae, which are rounded and undivided; the forefoot and hindfoot digital formulae are unidentifiable; white cloacal spur present, one on each side. Tail length (TL/SVL = 73%), with dorsal scales on the tail larger than those on the body and head, but smaller than the subcaudals. The ventral scales are large and flat.

Coloration in ethanol. The dorsal surface of head and body is light brown; dark brown stripes extend from the posterior corner of the eye socket to the neck; the back is covered with irregular, dark-brown stripes that interconnect to form a net-like pattern; the dorsal surfaces of the limbs are brown, with irregular, dark-brown stripes; the tail is brown, with several dark-brown, transverse stripes; the regenerated tail is gray and without transverse stripes; the ventral surfaces of the head and limbs are cream-grey.

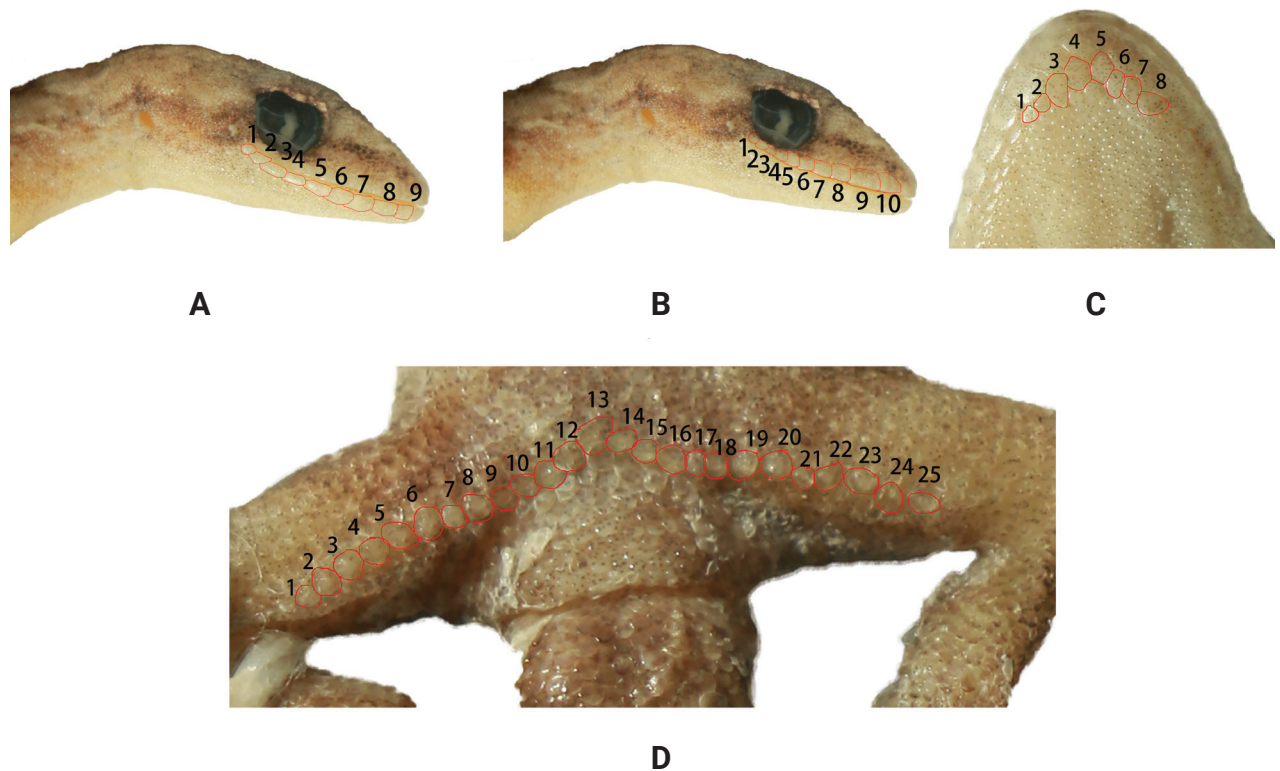


Figure 5. Paratype (2014002301) of *Hemiphyllodactylus gengmaensis* sp. nov. **A, B** lateral views of head, red lines indicate IL and SL, respectively **C** ventral view, red lines indicate chin scales **D** ventral view, red lines indicate femoropreloacal pores.

Variation. Variation of mensural and meristic data are presented in Table 3. Dark dorsal transverse blotches on the body of this species are relatively small, with those of two specimens (2014002302, 2014002300) being indistinct and fragmented. Furthermore, females are slightly larger than males. The post-sacral mark, bearing anteriorly projecting arms, of one individual (2014002300) is indistinct, possibly due to prolonged preservation.

Distribution. This species is currently known to be distributed at the type locality Banxing Village, Gengma Dai and Wa Autonomous County of Yunnan Province in China (Fig. 1).

Natural History. *Hemiphyllodactylus gengmaensis* sp. nov. was found at an elevation of 664 m a.s.l., around 21:00. The specimens were found on a restaurant's wall, which was rough and with crevices. When illuminated with a flashlight, the animals quickly crawled into the crevices.

Etymology. The scientific name “*gengmaensis*” is derived from its type locality Gengma Dai and Wa Autonomous County in Yunnan province. We suggest Gengma Slender Gecko in English and “耿马半叶趾虎 (Gěng Mǎ Bàn Yè Zhǐ Hǔ)” in Chinese.

Comparisons. We compared the morphology of the new species against its closely related species, specifically species from clade 3, as inferred from the phylogeny we constructed (Table 4). In terms of body proportions, *H. gengmaensis* sp. nov. has a longer head which separates it from *H. longlingensis*, *H. zalonicus*, *H. changningensis*, and *H. zhutangxiangensis* (HL/SVL = 0.26–0.31 versus 0.22–0.24, 0.22–0.23, 0.22–0.25, 0.17–0.20, respectively); greater SnW distance (SnW/HW = 0.22–0.33 versus 0.15–0.18, 0.21, 0.16–0.20, 0.16–0.21, respectively); the new species has a shorter SnEye distance which separates it

from *H. longlingensis*, *H. changningensis*, and *H. zhutangxiangensis* (SnEye/HL = 0.36–0.41 versus 0.42–0.45, 0.41–0.49, 0.53–0.60, respectively); shorter head width (HW/HL = 0.64–0.74 versus 0.75–0.80, 0.72–0.80, 1.03–1.13, respectively); it has a shorter NarEye compared to *H. changningensis* and *H. zhutangxiangensis* (NarEye/HL = 0.24–0.30 versus 0.30–0.37, 0.39–0.4, respectively); smaller eyes compared to *H. zalonicus* and *H. zhutangxiangensis* (ED/HL = 0.20–0.24 versus 0.23–0.30, 0.30–0.36, respectively). In terms of scalation, the new species has more CN can be distinguished from *H. longlingensis*, *H. zalonicus*, *H. changningensis*, and *H. zhutangxiangensis* (CN = 6 versus 4–5, 5, 3–4, 5, respectively); more VS compared to *H. longlingensis*, *H. changningensis*, and *H. zhutangxiangensis* (VS = 8–10 versus 6–7, 6–8, 5–7, respectively); the new species has more femoroprecloacal pores which separates it from *H. zalonicus*, *H. changningensis*, and *H. zhutangxiangensis* (20–25 versus 16–20, 19–22, 20–23, respectively). For the lamellar and coloration, the new species differs from *H. longlingensis*, *H. zalonicus*, and *H. changningensis* by having more lamellae on the hand (5–5(6)–5–4 versus 3–4–4–4(3), 3–3(4)–3(4)–3(4) and 3–3(4)–3(4)–3, respectively); differs from *H. zalonicus*, *H. changningensis*, and *H. zhutangxiangensis* by having more lamellae on first fingers (SL1T = 6 versus 4, 3–4, 4–5, respectively). Furthermore, *H. gengmaensis* sp. nov. has dark transverse blotches on the dorsum, which *H. zalonicus* does not have. The new species has a dark, reticulate dorsal pattern, which *H. zalonicus* and *H. zhutangxiangensis* do not have. It has a postsacral marking with anteriorly projecting arms, which is absent in *H. zalonicus* and *H. changningensis*.

Table 3. Mensural (in mm), meristic, color pattern, and proportions of the type series of *Hemiphyllodactylus gengmaensis* sp. nov. (–) = data unavailable. (*) = regenerated tail.

Character	Holotype	Paratypes				
	2014002302	2014002300	2014002299	2014002297	2014002298	2014002301
Sex	Female	Male	Female	Female	Female	Male
SVL	38.52	35.24	36.5	40.86	43.24	39.45
TL	28.22	–	9.18*	–	–	15.34*
TrunkL	17.46	17.54	17.6	21.6	23.22	18.82
HL	10.80	10.80	10.24	11.24	11.14	11.24
HW	7.36	6.94	6.88	7.86	8.2	7.74
ED	2.12	2.56	2.16	2.62	2.6	2.34
SnEye	3.94	3.88	4.02	4.5	4.52	4.3
NarEye	2.78	2.74	2.96	3.04	3.32	2.72
SnW	1.78	1.78	1.6	1.84	2.72	1.7
TrunkL/SVL	0.45	0.50	0.48	0.53	0.54	0.48
HL/SVL	0.28	0.31	0.28	0.28	0.26	0.28
HW/SVL	0.19	0.20	0.19	0.19	0.19	0.20
HW/HL	0.68	0.64	0.67	0.70	0.74	0.69
SnEye/HL	0.36	0.36	0.39	0.40	0.41	0.38
NarEye/HL	0.26	0.25	0.29	0.27	0.30	0.24
ED/HL	0.20	0.24	0.21	0.23	0.23	0.21
SnW/HL	0.16	0.16	0.16	0.16	0.24	0.15
ED/NarEye	0.76	0.93	0.73	0.86	0.78	0.86
Snw/HW	0.24	0.26	0.23	0.23	0.33	0.22
Chin	8	9	8	9	9	8

Character	Holotype	Paratypes				
	2014002302	2014002300	2014002299	2014002297	2014002298	2014002301
CN	6	6	6	6	6	6
IS	3	2	2	3	3	2
SL (left/right)	10/9	10/10	10/11	10/9	10/9	10/10
IL (left/right)	9/9	9/9	8/8	9/9	9/9	9/9
VS	10	9	9	8	8	9
DS	18	14	11	15	15	16
Lamellar formulae hands II–V (left)	–	–	–	–	5–5–5–4	–
Lamellar formulae hands II–V (right)	–	–	–	–	5–6–5–4	–
Lamellar formulae foot II–V (left)	–	–	–	–	5–5–6–5	–
Lamellar formulae foot II–V (right)	–	–	–	–	5–5–6–5	–
SL1F	–	–	–	–	5	–
SL1T	–	–	–	–	6	–
Precloacal and femoral pore series separate (1) or continuous (0)	–	0	–	–	–	0
Total femoroprecloacal pores	0	20	0	0	0	25
CloacS on each side	1	1	1	1	2	1
Subcaudals enlarged, plate-like	No	No	No	No	No	No
Dark postorbital stripe	Yes	Yes	Yes	Yes	Yes	Yes
Dorsolateral light-colored spots on trunk	No	No	No	No	No	No
Dark dorsolateral stripe on trunk	No	No	No	No	No	No
Dark ventrolateral stripe on trunk	No	No	No	No	No	No
Dark dorsal transverse blotches	Indistinct	Indistinct	Yes	Yes	Yes	Yes
Dark reticulate pattern on dorsum	Indistinct	Yes	Yes	Indistinct	Yes	Yes
Postsacral marking anteriorly projecting arms	Yes	indistinct	Yes	Yes	Yes	Yes

Table 4. Diagnostic characters separating *Hemiphyllodactylus gengmaensis* sp. nov. from other nominal taxa of *Hemiphyllodactylus* within clade 3 of Agung et al. (2022). (–) = data unavailable. Mensural characters are in mm. Data for *H. zalonicus* and *H. longlingensis* were obtained from Grismer et al. (2020a). Data for *H. changningensis* were obtained from Guo et al. (2015). Data for *H. zhutangxiangensis* were obtained from Agung et al. (2021).

Character	<i>H. gengmaensis</i> sp. nov.	<i>H. longlingensis</i>	<i>H. zalonicus</i>	<i>H. changningensis</i>	<i>H. zhutangxiangensis</i>
Max SVL	43.24	45.7	37.7	43.8	44.42
<i>n</i>	6	–	2	10	13
TrunkL	17.46–23.22	–	18.1–18.9	17.4–22.5	16.1–23.1
HL	10.8–11.24	–	8.4–8.5	8.2–10.1	6.2–7.6
HW	6.88–8.2	–	5.7–5.8	6.1–7.5	6.5–8.2

Character	<i>H. gengmaensis</i> sp. nov.	<i>H. longlingensis</i>	<i>H. zalonicus</i>	<i>H. changningensis</i>	<i>H. zhutangxiangensis</i>
ED	2.12–2.62	–	2.0–2.6	1.7–2.3	2.1–2.7
SnEye	3.88–4.52	–	3.4–3.5	3.5–4.5	3.4–4.4
NarEye	2.72–3.32	–	2.4–2.7	2.8–3.4	2.6–3.2
SnW	1.6–2.72	–	1.2	1.1–1.4	1.3–1.6
TrunkL/SVL	0.45–0.54	0.47–0.52	0.49–0.50	0.46–0.51	0.48–0.52
HL/SVL	0.26–0.31	0.22–0.24	0.22–0.23	0.22–0.25	0.17–0.20
HW/SVL	0.19–0.2	0.17–0.19	0.15	0.17–0.18	0.18–0.20
HW/HL	0.64–0.74	0.75–0.80	0.68	0.72–0.80	1.03–1.13
SnEye/HL	0.36–0.41	0.42–0.45	0.40–0.42	0.41–0.49	0.53–0.60
NarEye/HL	0.24–0.30	0.29–0.34	0.28–0.31	0.30–0.37	0.39–0.44
ED/HL	0.20–0.24	0.22–0.25	0.23–0.30	0.21–0.25	0.30–0.36
SnW/HL	0.15–0.24	0.12–0.14	0.14	0.12–0.16	0.19–0.22
ED/NarEye	0.73–0.94	0.66–0.82	0.74–1.08	0.61–0.77	0.70–0.91
Snw/HW	0.22–0.33	0.15–0.18	0.21	0.16–0.20	0.16–0.21
Chin	8–9	7–9	8–10	7–8	7–9
CN	6	4–5	5	3–4	5
IS	2–3	1–3	3–4	2–3	2–4
SL	9–11	9–10	10	8–11	8–11
IL	8–9	8–10	8–9	8–10	8–11
VS	8–10	6–7	9–10	6–8	5–7
DS	11–18	10–14	17–18	11–15	11–15
Lamellar formulae hands II–V	5–5(6)–5–4	3–4–4–4(3) 4–4–4(5)–4	3–3–3–3	3–3(4)–3(4)–3	(3–5)–(4–6)–(4 or 5)–(4 or 5)
Lamellar formulae feet II–V	5–5–6–5	4–4(5)–4(5)–4	3–4–4–4	3–3–3–3 3–4–4–4	(4 or 5)–(4 or 5)–(4–6)–(4 or 5)
SL1F	5	4–5	3	3–4	4–5
SL1T	6	4–6	4	3–4	4–5
Precloacal and femoral pore series separate (1) or continuous (0)	0	0	0	0	0
Total femoroprecloacal pores	20–25	16–27	16–20	19–22	20–23
CloacS on each side	1 or 2	1 or 2	1	1 or 2	1 or 2
Subcaudals enlarged, plate-like	No	No	No	No	No
Dark postorbital stripe	Yes	Yes	Yes	Yes	Yes
Dorsolateral light-colored spots on trunk	No	No	No	No	No
Dark dorsolateral stripe on trunk	No	No	No	No	No
Dark ventrolateral stripe on trunk	No	No	No	No	No
Dark dorsal transverse blotches	Yes or indistinct	Variable	No	Yes	Yes
Dark reticulate pattern on dorsum	Yes or indistinct	Variable	No	Yes	No
Postsacral marking anteriorly projecting arms	Yes or indistinct	Pale colored	Indistinct or not	No	Fork-like, dark colored

Discussion

Our research supports the recognition of the *Hemiphyllodactylus gengmaensis* sp. nov. as a new species, belonging to clade 3 of Agung et al. (2021). It is sister taxa to *H. longlingensis*, *H. zalonicus*, *H. changningensis*, and *H. zhutangxiangensis*. Except for *H. zalonicus*, all species of clade 3 occur in China. Considering the 292 km of unexplored area between *H. zalonicus* and its closest distance species (*H. longlingensis*), there may be numerous undescribed species in northern Myanmar and Dehong Dai and Jingpo Autonomous Prefecture, Yunnan Province, China. The 56 km distance between *H. gengmaensis* sp. nov. and *H. changningensis*, along with recent new species discoveries (Grismer et al. 2013; Guo et al. 2015; Che et al. 2020; Agung et al. 2021, 2022), suggests a high diversity of this genus within Yunnan. The border area of Dali Bai Autonomous Prefecture, Pu'er City, and Lincang City in southern Yunnan Province could be a key area for future research.

Our study increases the number of recognized species in the *Hemiphyllodactylus* in China to 15. Apart from *H. typus*, *H. dupanglingensis*, and *H. hongkongensis*, all other species in the genus *Hemiphyllodactylus* are montane species. *Hemiphyllodactylus gengmaensis* sp. nov. was found at an elevation of 664 m a.s.l. The discovery of the new species may represent an intermediate elevation type given by the known ranges, suggesting that species in the *Hemiphyllodactylus* may have a wide distribution range in southern China, spanning elevations from 120 m (Sung et al. 2018) to 2,169 m (unpublished data). Additionally, Grismer et al. (2018b) discovered 12 new gecko species within two weeks in a single study of karsts in Myanmar, with similar climatic and habitat conditions likely to exist in southern China. Moreover, some populations previously considered as *H. yunnanensis* in China have also been described as new species (Deng et al. 1998; Shi et al. 2011; Che et al. 2020; Zhang B et al. 2020). Therefore, it is possible that there are still numerous undiscovered cryptic species in southern China.

Acknowledgements

We thank Hong Hui for assistance in the field. We also thank the editors and reviews for their comments on the manuscript.

Additional information

Conflict of interest

The authors have declared that no competing interests exist.

Ethical statement

No ethical statement was reported.

Funding

This work was supported by Science Technology Basic Condition Platform from the Ministry of Science and Technology of the People's Republic of China (grant no. 2005DKA21402), National Natural Science Foundation Project: Investigation and Classificatory and Phylogenetic Studies on the Lizards of Gekkonidae of China (grant no. NSFC-31970404).

Author contributions

Funding acquisition: DR. Visualization: HZ, ZS, SL. Writing – original draft: HZ. Writing – review and editing: DR, SL.

Author ORCIDs

Hongxin Zhou  <https://orcid.org/0009-0004-9801-8811>

Shuo Liu  <https://orcid.org/0000-0001-7825-3006>

Data availability

All of the data that support the findings of this study are available in the main text.

References

- Agarwal I, Khandekar A, Giri VB, Ramakrishnan U, Karanth KP (2019) The hills are alive with geckos! A radiation of a dozen species on sky islands across peninsular India (Squamata: Gekkonidae, *Hemiphyllodactylus*) with the description of three new species. *Organisms, Diversity & Evolution* 19(2): 341–361. <https://doi.org/10.1007/s13127-019-00392-5>
- Agung AP, Grismer LL, Grismer JL, Quah ES, Chornelia A, Lu JM, Hughes LC (2021) A new species of *Hemiphyllodactylus* Bleeker (Squamata: Gekkonidae) from Yunnan, China and its phylogenetic relationship to other congeners. *Zootaxa* 4980(1): 1–27. <https://doi.org/10.11646/zootaxa.4980.1.1>
- Agung AP, Chornelia A, Grismer LL, Grismer JL, Quah ESH, Lu J, Tomlinson KW, Hughes AC (2022) Description of two new species of *Hemiphyllodactylus* (Reptilia: Gekkonidae) from karst landscapes in Yunnan, China, highlights complex conservation needs. *Zoological Research* 43(5): 767–786. <https://doi.org/10.24272/j.issn.2095-8137.2022.105>
- Che J, Jiang K, Yan F, Zhang Y (2020) Amphibians and Reptiles in Tibet – Diversity and Evolution. Science Press, Beijing, 803 pp.
- Deng XJ, Ye YY, Yang DD (1998) Two reptile records new to Hunan Province. *Sichuan Journal of Zoology* 17(2): 53. [In Chinese]
- Eliades SJ, Phimmachak S, Sivongxay N, Siler CD, Stuart BL (2019) Two new species of *Hemiphyllodactylus* (Reptilia: Gekkonidae) from Laos. *Zootaxa* 4577(1): 131–147. <https://doi.org/10.11646/zootaxa.4577.1.8>
- Grismer LL, Wood Jr PL, Anuar S, Muin MA, Quah ES, McGuire JA, Brown RM, Ngo TV, Hong Thai P (2013) Integrative taxonomy uncovers high levels of cryptic species diversity in *Hemiphyllodactylus* Bleeker, 1860 (Squamata: Gekkonidae) and the description of a new species from Peninsular Malaysia. *Zoological Journal of the Linnean Society* 169(4): 849–880. <https://doi.org/10.1111/zoj.12064>
- Grismer LL, Riyanto A, Djoko IT, McGuire JA (2014a) A new species of *Hemiphyllodactylus* Bleeker, 1860 (Squamata: Gekkonidae) from Pulau Enggano, southwestern Sumatra, Indonesia. *Zootaxa* 3821(4): 485–495. <https://doi.org/10.11646/zootaxa.3821.4.7>
- Grismer LL, Wood Jr PL, Cota M (2014b) A new species of *Hemiphyllodactylus* Bleeker, 1860 (Squamata: Gekkonidae) from northwestern Thailand. *Zootaxa* 3760(1): 67–68. <https://doi.org/10.11646/zootaxa.3760.1.4>
- Grismer LL, Wood Jr PL, Thura MK, Zin T, Quah ESH, Murdoch ML, Grismer MS, Li A, Kyaw H, Ngwe L (2017) Phylogenetic taxonomy of *Hemiphyllodactylus* Bleeker, 1860 (Squamata: Gekkonidae) with descriptions of three new species from Myanmar. *Journal of Natural History* 52(13–16): 881–915. <https://doi.org/10.1080/00222933.2017.1367045>

- Grismer LL, Wood Jr PL, Zug GR, Thura MK, Grismer MS, Murdoch ML, Quah EH, Lin A (2018a) Two more new species of *Hemiphyllodactylus* Bleeker (Squamata: Gekkonidae) from the Shan Hills of eastern Myanmar (Burma). *Zootaxa* 4483(2): 295–316. <https://doi.org/10.11646/zootaxa.4483.2.4>
- Grismer LL, Wood Jr PL, Thura MK, Zin T, Quah ES, Murdoch ML, Grismer MS, Lin A, Kyaw H, Lwin N (2018b) Twelve new species of *Cyrtodactylus* Gray (Squamata: Gekkonidae) from isolated limestone habitats in east-central and southern Myanmar demonstrate high localized diversity and unprecedented microendemism. *Zoological Journal of the Linnean Society* 182(4): 862–959. <https://doi.org/10.1093/zoolinnean/zlx057>
- Grismer LL, Chit MT, Pawangkhanant P, Nazarov RA, Zaw T, Poyarkov NA (2020a) The phylogeny of *Hemiphyllodactylus* Bleeker, 1860 (Squamata: Gekkonidae) with a description of a new species from the Mangin Range, Sagaing Region, northern Myanmar. *Journal of Natural History* 54(29–30): 1913–1931. <https://doi.org/10.1080/00222933.2020.1833095>
- Grismer LL, Yushchenko PV, Pawangkhanant P, Naiduangchan M, Nazarov RA, Orlova VF, Suwannapoom C, Poyarkov NA (2020b) A new species of *Hemiphyllodactylus* Bleeker (Squamata; Gekkonidae) from Peninsular Thailand that converges in morphology and color pattern on *Pseudogekko smaragdinus* (Taylor) from the Philippines. *Zootaxa* 4816(2): 171–190. <https://doi.org/10.11646/zootaxa.4816.2.2>
- Guo W, Zhou K, Yan J, Li P (2015) A new species of *Hemiphyllodactylus* Bleeker, 1860 (Squamata: Gekkonidae) from western Yunnan, China. *Zootaxa* 3974(3): 377–390. <https://doi.org/10.11646/zootaxa.3974.3.5>
- Huelsenbeck JP, Ronquist F, Nielsen R, Bollback JP (2001) Bayesian inference of phylogeny and its impact on evolutionary biology. *Science* 294(5550): 2310–2314. <https://doi.org/10.1126/science.1065889>
- Kalyaanamoorthy S, Minh BQ, Wong TK, Von Haeseler A, Jermini LS (2017) ModelFinder: Fast model selection for accurate phylogenetic estimates. *Nature Methods* 14(6): 587–589. <https://doi.org/10.1038/nmeth.4285>
- Kumar S, Stecher G, Tamura K (2016) MEGA7: Molecular evolutionary genetics analysis version 7.0 for bigger datasets. *Molecular Biology and Evolution* 33(7): 1870–1874. <https://doi.org/10.1093/molbev/msw054>
- Macey JJ, Larson A, Ananjeva NB, Fang Z, Papenfuss TJ (1997) Two novel gene orders and the role of light-strand replication in rearrangement of the vertebrate mitochondrial genome. *Molecular Biology and Evolution* 14(1): 91–104. <https://doi.org/10.1093/oxfordjournals.molbev.a025706>
- Minh BQ, Nguyen MA, von Haeseler A (2013) Ultrafast approximation for phylogenetic bootstrap. *Molecular Biology and Evolution* 30(5): 1188–1195. <https://doi.org/10.1093/molbev/mst024>
- Ngo VT, Grismer LL, Pham HT, Wood Jr PL (2014) A new species of *Hemiphyllodactylus* Bleeker, 1860 (Squamata: Gekkonidae) from Ba Na–Nui Chua Nature Reserve, Central Vietnam. *Zootaxa* 3760(4): 539–552. <https://doi.org/10.11646/zootaxa.3760.4.3>
- Nguyen LT, Schmidt HA, von Haeseler A, Minh BQ (2015) IQ-TREE: A fast and effective stochastic algorithm for estimating maximum likelihood phylogenies. *Molecular Biology and Evolution* 32(1): 268–274. <https://doi.org/10.1093/molbev/msu300>
- Ronquist F, Teslenko M, van der Mark P, Ayres DL, Darling A, Höhna S, Larget B, Liu L, Suchard MA, Huelsenbeck JP (2012) MrBayes 3.2: Efficient Bayesian phylogenetic inference and model choice across a large model space. *Systematic Biology* 61(3): 539–542. <https://doi.org/10.1093/sysbio/sys029>

- Shi L, Lin XL, Zhao H (2011) New records of *Hemiphyllodactylus yunnanensis* to Xizang Autonomous Region, China. *Chinensis Journal of Zoology* 46(1): 131–133. [in Chinese] <https://doi.org/10.13859/j.cjz.2011.01.022>
- Sung YH, Lee WH, Ng HN, Zhang Y, Yang JH (2018) A new species of *Hemiphyllodactylus* (Squamata: Gekkonidae) from Hong Kong. *Zootaxa* 4392(2): 361–373. <https://doi.org/10.11646/zootaxa.4392.2.8>
- Talavera G, Castresana J (2007) Improvement of phylogenies after removing divergent and ambiguously aligned blocks from protein sequence alignments. *Systematic Biology* 56(4): 564–577. <https://doi.org/10.1080/10635150701472164>
- Thompson JD, Higgins DG, Gibson TJ (1994) CLUSTAL W: Improving the sensitivity of progressive multiple sequence alignment through sequence weighting, position-specific gap penalties and weight matrix choice. *Nucleic Acids Research* 22(22): 4673–4680. <https://doi.org/10.1093/nar/22.22.4673>
- Uetz P, Freed P, Aguilar R, Reyes F, Hošek J [Eds] (2023) The Reptile Database. <http://www.reptile-database.org> [Accessed 2 May 2023]
- Wilcox TP, Zwickl DJ, Heath TA, Hillis DM (2002) Phylogenetic relationships of the Dwarf Boas and a comparison of Bayesian and bootstrap measures of phylogenetic support. *Molecular Phylogenetics and Evolution* 25(2): 361–371. [https://doi.org/10.1016/S1055-7903\(02\)00244-0](https://doi.org/10.1016/S1055-7903(02)00244-0)
- Xiang CY, Gao F, Jakovlić I, Lei HP, Hu Y, Zhang H, Zou H, Wang GT, Zhang D (2023) Using PhyloSuite for molecular phylogeny and tree-based analyses. *iMeta* 2(1): e87. <https://doi.org/10.1002/imt2.87>
- Zhang B, Qian T, Jiang X, Cai B, Deng X, Yang DD (2020) A new species of *Hemiphyllodactylus* Bleeker, 1860 (Reptilia: Squamata) from Hunan Province, China. *Asian Herpetological Research* 11(3): 183–193. <https://doi.org/10.16373/j.cnki.ahr.190066>
- Zhang D, Gao F, Jakovlić I, Zou H, Zhang J, Li WX, Wang GT (2020) PhyloSuite: An integrated and scalable desktop platform for streamlined molecular sequence data management and evolutionary phylogenetics studies. *Molecular Ecology Resources* 20(1): 348–355. <https://doi.org/10.1111/1755-0998.13096>
- Zhou KY, Liu YZ, Yang GP (1981) Three new subspecies of *Hemiphyllodactylus yunnanensis* (Boulenger) from China (Lacertiformes: Gekkonidae). *Dong Wu Fen Lei Xue Bao* 6(2): 202–209. [In Chinese, English translation by H. Ota (1996) in *Smithsonian Herpetological Information Service*, 110, 1–8, 1 pl.]
- Zug GR (2010) Speciation and dispersal in a low diversity taxon: The slender geckos *Hemiphyllodactylus* (Reptilia, Gekkonidae). *Smithsonian Contributions to Zoology* 631(631): 1–70. <https://doi.org/10.5479/si.00810282.631>

New species and other new records of the family Mycetophilidae (Insecta, Diptera) from Morocco

Mohamed Amin El Mouden¹, Peter J. Chandler², Ouafaa Driauach^{1,3}, Ouarda Banamar¹,
Imane Saidoun¹, Abdellatif Akarid¹, Khalid Aattouch¹, Boutaina Belqat¹

¹ LESCOB URL/CNRST N°18, Faculty of Sciences, Abdelmalek Essaâdi University, Tétouan, Morocco

² 606B Berryfield Lane, Melksham, Wilts SN12 6EL, UK

³ Biotechnology, Environmental Technology and Valorization of Bio-Resources Team, Department of Biology, Laboratory of Research and Development in Engineering Sciences Faculty of Sciences and Techniques Al-Hoceima, Abdelmalek Essaadi University, Tétouan, Morocco

Corresponding author: Boutaina Belqat (bbelqat@uae.ac.ma)

Abstract

Twelve species in nine genera of Mycetophilidae are newly recorded from Morocco and from North Africa. Five species are described as new to science: *Rymosia ebejeri* **sp. nov.**, *Leia arcana* **sp. nov.**, *Megophthalmidia amsemlii* **sp. nov.**, *Mycomya mira* **sp. nov.**, and *Phthinia snibbypinsae* **sp. nov.** Three species are newly recorded from Gibraltar.

Key words: Fungus gnats, Moroccan endemism, North Africa



Academic editor: Vladimir Blagoderov

Received: 9 January 2024

Accepted: 15 March 2024

Published: 17 April 2024

ZooBank: <https://zoobank.org/5956A253-60AD-476F-BB52-94E3F52FE6B2>

Citation: El Mouden MA, Chandler PJ, Driauach O, Banamar O, Saidoun I, Akarid A, Aattouch K, Belqat B (2024) New species and other new records of the family Mycetophilidae (Insecta, Diptera) from Morocco. ZooKeys 1197: 215–236. <https://doi.org/10.3897/zookeys.1197.118503>

Copyright: © Mohamed Amin El Mouden et al. This is an open access article distributed under terms of the Creative Commons Attribution License ([Attribution 4.0 International – CC BY 4.0](https://creativecommons.org/licenses/by/4.0/)).

Introduction

Banamar et al. (2020) included Moroccan records of 64 species of Mycetophilidae, of which 54 were newly recorded, but they noted that most of the species recorded are widespread in the Mediterranean region and more widely in Europe and the Palaearctic Region. However, also found were some species that were new to science. These and some other species identified after that publication are treated here. Results are presented in the same taxonomic order as by Banamar et al. (2020) and Kettani et al. (2022) in the Catalogue of Moroccan Diptera, except that *Docosia* Winnertz, 1864 is placed in subfamily Gnoristinae rather than Leiinae following recent phylogenetic studies using molecular methods (e.g. Kaspřák et al. 2019).

Materials and methods

Most of the material totalling 148 specimens (122 males and 26 females) was collected using diverse techniques such as sweeping and rearing, by B. Belqat, O. Driauach, and M.A. El Mouden between 12 December 2013 and 28 February 2022 in 31 of 33 sites in the Rif and Middle Atlas Mountains, and on the Atlantic plain (Fig. 1; Table 1). Additional materials were collected in the Middle Atlas (8 May 2012) and the Rif (12 June 2013) were provided by Dr Martin Ebejer, who kindly permitted us to publish his new records.

Table 1. Sampling sites (in alphabetical order) hosting the species collected in the Rif and Middle Atlas Mountains and on the Atlantic plain, with localities, altitudes, and geographic coordinates. PNTLS = National Park of Talassemtane; PPNB = Bouhachem Natural Park Project; PNTZK = National Park of Tazekka.

Site	Locality	Elevation (m)	Latitude
Rif			
1. Aïn El Ma Bared	Bouzthate, Parc Bab El Karne	1267	35°00.333'N, 5°12.105'W
2. Aïn El Maounzil	PNTLS	1106	35°04.577'N, 5°10.406'W
3. Aïn Sidi Brahim Ben Arrif	PPNB	897	35°20.398'N, 5°32.712'W
4. Akchour	PNTLS	600	35°14.203'N, 5°10.145'W
5. Bab El Karne	Douar Tamakoute, Parc Bab El Karne	1248	34°58.510'N, 5°11.838'W
6. Bab Rouida	PNTLS	1678	35°06.881'N, 5°08.270'W
7. Daya Amsemlil	Jbel Bouhachem, PPNB	1059	35°15.596'N, 5°25.917'W
8. Daya avant Taïda	Taïda, PPNB	436	35°22.426'N, 5°31.662'W
9. Daya Mtahen	Jbel Bouhachem, PPNB	966	35°16.195'N, 5°26.158'W
10. Douar Bni Leit	Bni Leit, PPNB	836	35°17.382'N, 5°23.558'W
11. Faculté des Sciences	Université Abdelmalek Essaâdi, Tétouan	7	35°33.413'N, 5°21.464'W
12. Forêt Adayourha	PPNB	794	35°14.599'N, 5°24.001'W
13. Forêt Aïn Lahcen	Aïn Lahcen	186	35°32.532'N, 5°33.378'W
14. Forêt Azilane	Azilane, PNTLS	1291	35°10.354'N, 5°12.053'W
15. Forêt Bab Hajara	PPNB	1203	35°15.292'N, 5°26.258'W
16. Forêt Bni Leit	Bni Leit, PPNB	826	35°17.564'N, 5°23.527'W
17. Forêt Bouhachem st.1	PPNB	1016	35°16.119'N, 5°26.144'W
18. Forêt Jbel Lekrâa	PNTLS	1541	35°06.825'N, 5°08.077'W
19. Forêt Malâab Tizimezzan	PNTLS	1452	35°06.562'N, 5°08.197'W
20. Forêt Sed Nakhla	Barrage Nakhla, PPNB	414	35°26.110'N, 5°24.407'W
21. Khandek Melouka	Aïn Lahcen	287	35°33.326'N, 5°34.597'W
22. Maison forestière Bouhachem	PPNB	1048	35°15.040'N, 5°25.240'W
23. Maison forestière Talassemtane	PNTLS	1674	35°08.076'N, 5°08.262'W
24. Marabout Abou Bnar	Abou Bnar, PNTLS	1247	35°10.812'N, 5°07.500'W
25. Oued Ferda	Akoumi, PNTLS	420	35°14.350'N, 5°10.46'W
26. Oued Majjou	Majjou Village, PNTLS	799	35°06.186'N, 5°10.935'W
27. Oued Majjou avant source	Majjou Village, PNTLS	1055	35°06.105'N, 5°10.502'W
28. Pont Imezzane	Imezzane, PNTLS	1181	35°10.391'N, 5°09.353'W
29. Route vers Abou Bnar	Abou Bnar, PNTLS	1410	35°10.398'N, 5°08.234'W
30. Tissemlal	PNTLS	1187	35°10.458'N, 5°14.587'W
Atlantic plain			
31. Sidi Yahya El Gharb	Sidi Yahya El Gharb	25	34°18.552'N, 6°17.532'W
Middle Atlas			
32. Forêt-3.5 km S. Azrou	Azrou	1450	33°25.491'N, 5°12.393'W
33. Oued Taourirt	PNTZK	1343	34°04.225'N, 4°07.508'W

The holotypes of the newly described species and M.J. Ebejer collection will be deposited at the Natural History Museum, London, UK (**NHMUK**). Paratypes and additional studied materials will be deposited in our Diptera collection, in the Department of Biology, Faculty of Sciences of Tétouan, Abdelmalek Essaâdi University, Morocco (**UAE-FST**).

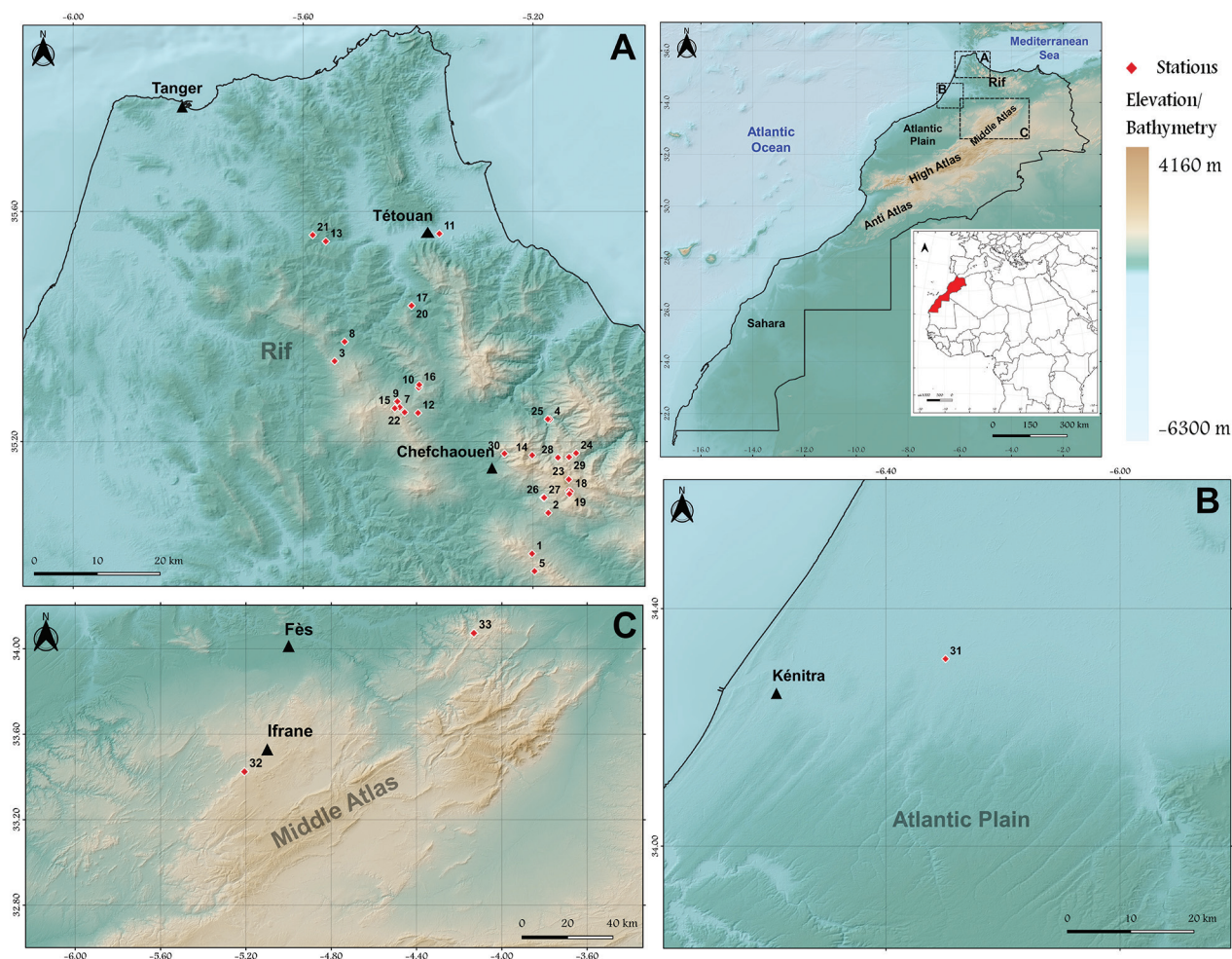


Figure 1. Maps showing all sampling localities for Mycetophilidae in the current study; numbers correspond to those in Table 1.

Taxonomy

Subfamily Mycetophilinae Newman, 1834

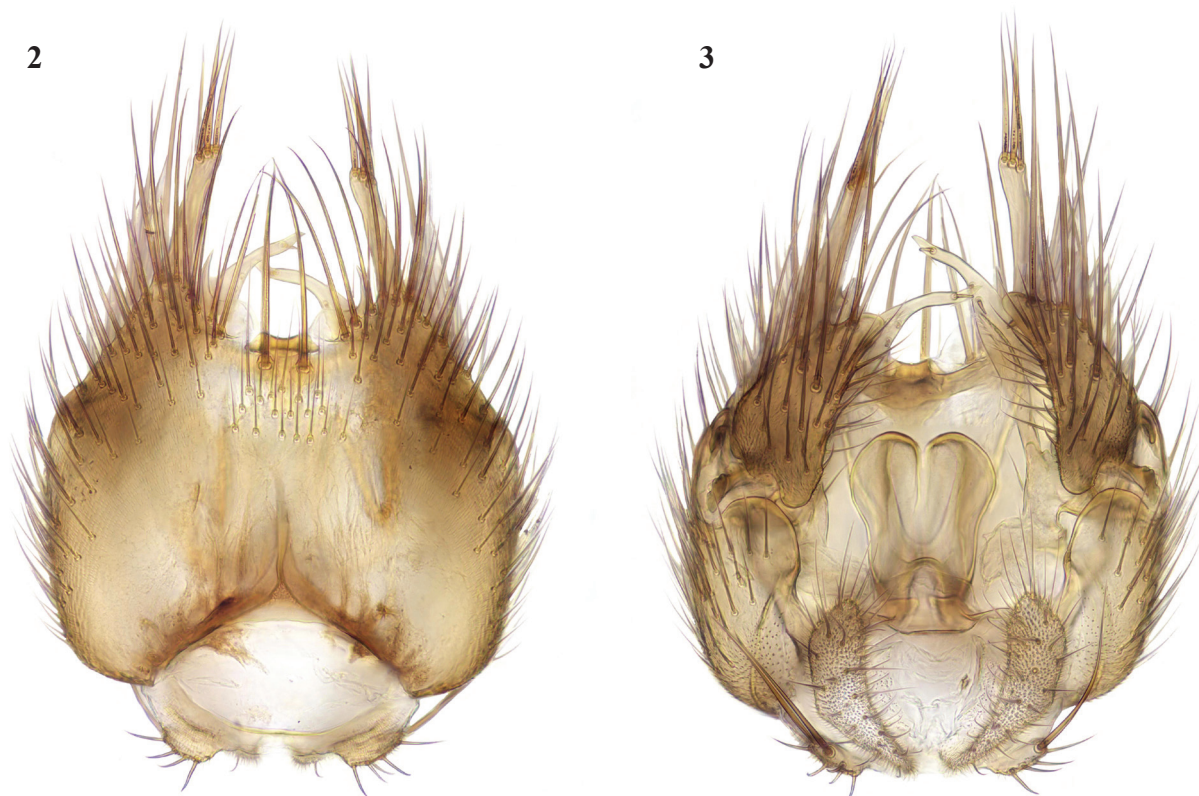
Tribe Exechiini Edwards, 1925

Genus *Exechia* Winnertz, 1864

Exechia repandoides Caspers, 1984

New record. MOROCCO – Rif Region • 2♂♂, 6♀♀; Faculté des Sciences; 14–28/II/2022; A. Akarid leg; reared from fungus *Cyclocybe aegerita*; UAE-FST R22/2441.

Comments. This species belongs to the *Exechia parva* Lundström, 1909 group, which was revised by Lindemann et al. (2021). The Moroccan males are similar in structure of their terminalia (Figs 2, 3) to *E. repandoides*, which is widespread in central and northern Europe and is also recorded from Corsica. These Moroccan males differ in coloration from European specimens, which have the abdomen dark coloured apart from the yellow terminalia. The Moroccan males have the abdomen brown dorsally, but broadly yellow laterally on tergites 2 and 3; sternites 1–3 are yellow, while tergites and sternites 4–6 are brown. The female has not been previously associated for *E.*



Figures 2, 3. *Exechia repandoides* Caspers, male terminalia 2 ventral view 3 dorsal view.



Figure 4. *Exechia repandoides* Caspers, lateral view of female abdomen.

repandoides. The Moroccan females are more brightly coloured than European females of this group; the abdomen (Fig. 4) is broadly yellow laterally, with brown dorsal markings on tergites 2–6 often not quite reaching fore margins, while tergite 7, the ovipositor, and all sternites are yellow. New to North Africa.

Genus *Exechiopsis* Tuomikoski, 1966

***Exechiopsis corona* Chandler & Ribeiro, 1995**

New record. MOROCCO – Rif Region • 1♂; Maison forestière, Talassemrane; 13/II/2020; B. Belqat and O. Driauch leg; collected using sweep net; UAE-FST R20/2442.

Comments. This species was described from two males, respectively from Tenerife, Canary Islands and the Greek island of Naxos (Chandler and Ribeiro 1995). It has otherwise only been recorded from Cyprus (Chandler et al. 2006). New to North Africa.

Genus *Rymosia* Winnertz, 1864

Rymosia ebejeri Chandler & Belqat, sp. nov.

<https://zoobank.org/7E574E63-8756-4B7B-AB24-F62930656AF1>

Type material. Holotype. MOROCCO – Rif Region • ♂ (mounted in DMHF); Forêt Jbel Lekraa; 12/VI/2013; M.J. Ebejer leg; collected using sweep net; NHMUK.

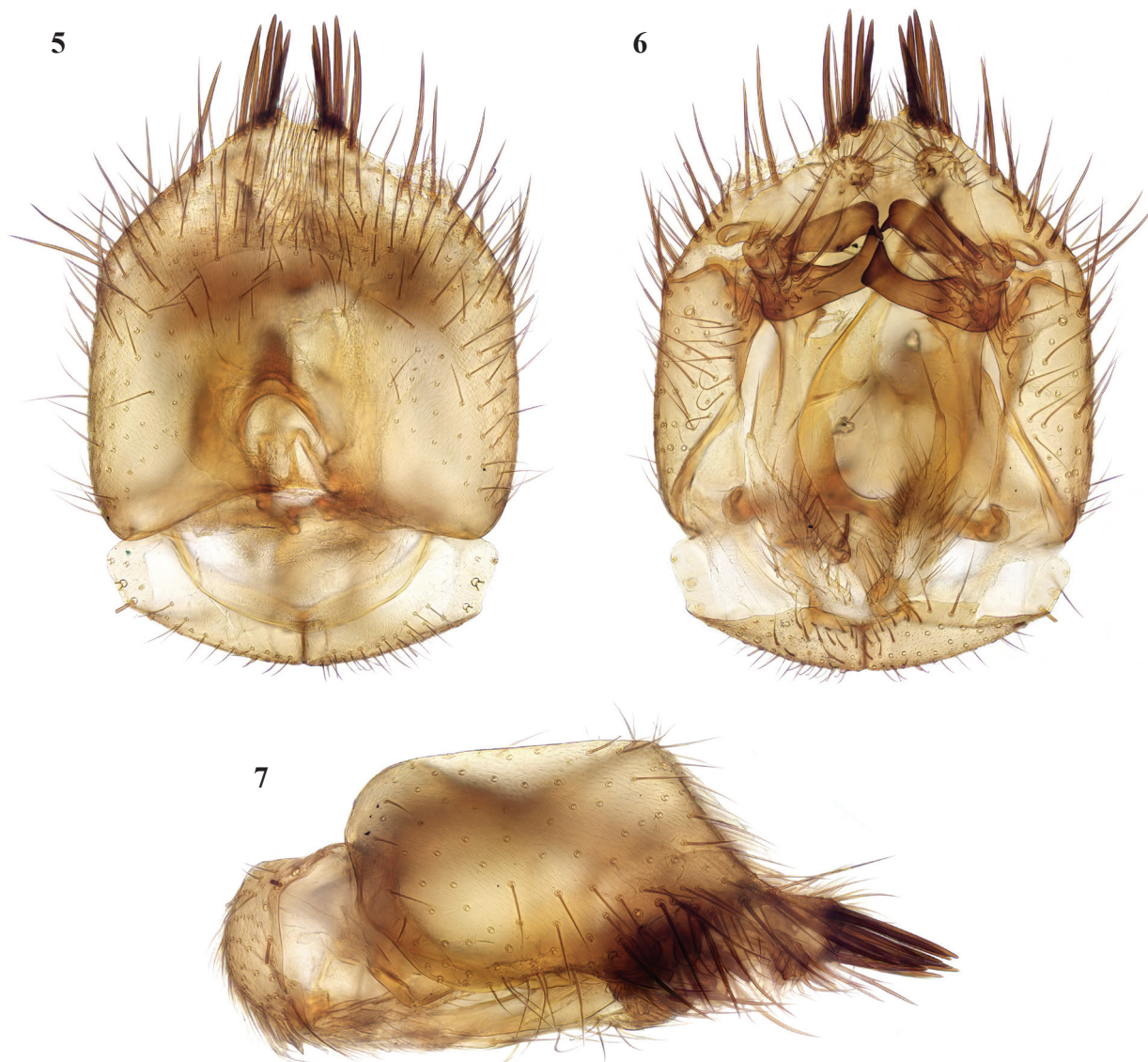
Paratypes. MOROCCO – Rif Region • 1♂; Oued Majjou; 5/II/2019; B. Belqat and O. Driauach leg; collected using sweep net; UAE-FST R19/2425 • 3♂♂; Tissemlal; 3/II/2020; B. Belqat and O. Driauach leg; collected using sweep net; UAE-FST R20/2426 • 1♂; Bab Rouida; 13/II/2020; B. Belqat and O. Driauach leg; collected using sweep net; UAE-FST R202427.

The species has been found mostly in the PNTLS, at high altitudes, in the large expanse of a cedar forest, in the environment of the Majjou River and in/and around the depression in a rock, resembling a small cave in the Bab Rouida site.

Diagnosis. This belongs among those *Rymosia* species without any spinules on the male fore tarsi. It is very distinct from other species in the structure of its male terminalia. The produced apical margin of the gonocoxites, bearing strong apical setae, is an especially unusual feature. This and the gonostylus concealed within the gonocoxites in ventral view distinguish it from the other three *Rymosia* species recorded from Morocco, *R. affinis* Winnertz, 1864, *R. beaucournui* Matile, 1963, and *R. pseudocretensis* Burghel-Balacesco, 1966 (Banamar et al. 2020).

Description. Male. Wing length 4–4,5 mm. **Coloration.** Head brown, with face yellowish. Antenna with basal segments and base of first flagellomere yellow, flagellum otherwise brownish. Palpus yellow. Thorax yellowish brown; mesonotum with three more or less fused

brown stripes, leaving humeral area and sides yellowish. Legs all yellow. Wing clear yellowish. Abdomen yellow with apical half of tergites 2–5 brown, each of these markings extended forwards as a dorsal triangle almost reaching fore margin and as a rounded extension laterally on each side; tergite 6 all brown. Terminalia yellow. **Head.** Antenna longer than head and thorax together, with flagellomeres progressively longer, from 3–4× to 6× as long as broad. Palpus elongate. **Thorax.** Mesonotum with long, dark setae in dorsocentral rows, near the side margins, and on pronotum; one long dark proepisternal seta; anepisternum covered with short setae; laterotergite with several long setae medially. **Legs.** Without any modification of tarsi (found in some species of this genus); hind tibial spurs about a third as long as hind tarsomere 1; tibial setae short, not longer than width of tibia. **Wing.** Vein Sc short, ending free. Crossvein r-m 2–3× as long as stem of median fork. Base of posterior fork at or before level of base of median stem; false vein extends to level of about half length of posterior fork, vein CuP reaches to level of about a third of fork. **Terminalia** (Figs 5–7). Gonocoxites produced medially with a group of 4 or 5 short but strong spines on each side of a small median emargination, and a row of strong



Figures 5–7. *Rymosia ebejeri* sp. nov., male terminalia 5 ventral view 6 dorsal view 7 lateral view.

setae on the apical margin external to the spines; gonostylus with ventral lobe short, not extending beyond margin of gonocoxites, rounded and densely setose apically; median and dorsal lobes with long setae basally and an apically bare sclerotised portion adjacent to ventral lobe, dorsal lobe with long basal extension bare except for preapical spine.

Female. Unknown.

Etymology. Named for Dr Martin Ebejer, who collected the first known specimen.

Subfamily Leinae Edwards, 1925

Genus *Leia* Meigen, 1818

With the species added here, four *Leia* species are known to occur in Morocco. Two of them, *L. beckeri* Landrock, 1940 and *L. arsona* Hutson, 1978 have a mainly Mediterranean distribution, and both have a dark marking over the r-m

crossvein, and one behind the posterior fork, in addition to a preapical wing band; *L. arsona* differs from other species in having a dark knob to the halteres. *Leia bimaculata* (Meigen, 1804) is widespread in the Palearctic Region; it has a preapical wing band but lacks any central marking. It is very variable in body coloration, from a largely black thorax and abdomen to being largely pale, but with bands on the abdominal tergites that are usually broader in the middle than at the sides. Moroccan specimens of *L. bimaculata* are generally lighter coloured, and it became apparent that some darker coloured Moroccan specimens also had differences in the male terminalia from typical *bimaculata*; we conclude here that these represent a distinct species that may have been overlooked elsewhere within the range of *L. bimaculata*. Polevoi and Salmela (2016) described and figured some variation in European specimens of *L. bimaculata*, with some specimens from Finland and Russia differing in details of the male terminalia including lack of a dorsal projection at the base of the gonostylus; they showed similar variation in body coloration to typical *L. bimaculata* but had unmarked wings. Further study of *L. bimaculata* across its range is necessary to establish whether more species may have been overlooked under this name.

***Leia arcana* Chandler, Belqat & Driauach, sp. nov.**

<https://zoobank.org/46D501E8-0AEA-4D5E-841A-0A40BC967CFB>

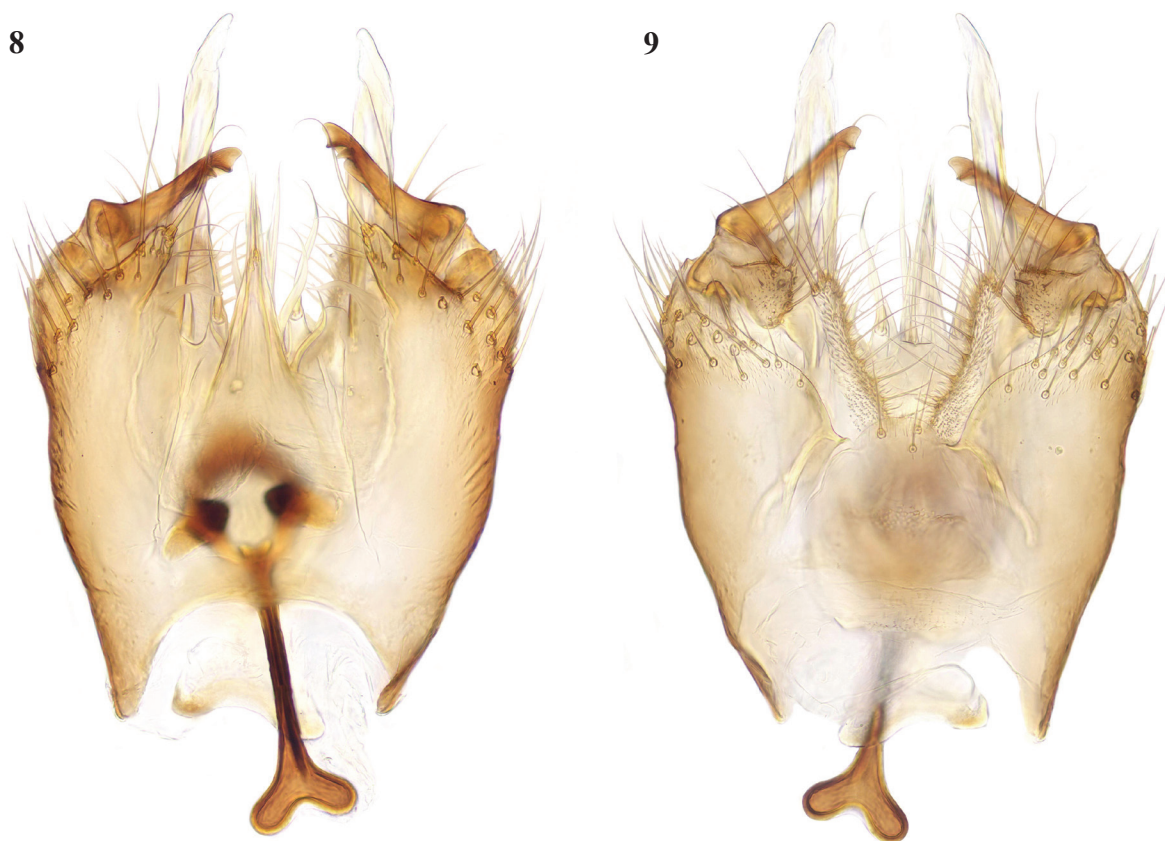
Type material. Holotype. MOROCCO – **Rif Region** • ♂ (mounted in DMHF from alcohol, terminalia on a slide); Aïn El Maounzil; 3/II/2020; B. Belqat and O. Driauach leg; collected using sweep net; NHMUK. **Paratypes.** MOROCCO – **Rif Region** • 3♂♂; Aïn Sidi Brahim Ben Arrif; 25/IV/2014. B. Belqat and O. Driauach leg; collected using sweep net; UAE-FST R14/2401 • 1♂; Maison forestière, Talassemrane; 17/VI/2014; B. Belqat and O. Driauach leg; collected using sweep net; UAE-FST R142402 • 1♂; Aïn El Ma Bared; 25/XII/2015; B. Belqat and O. Driauach leg; collected using sweep net; UAE-FST R15/2403 • 1♂; Bab El Karne; 25/XII/2015; B. Belqat and O. Driauach leg; collected using sweep net; UAE-FST R15/2404 • 1♂; Daya Mtahen; 23/III/2021; B. Belqat and O. Driauach leg; collected using sweep net; UAE-FST R21/2405.

Other material. MOROCCO – **Rif Region** • 1♀; Aïn Sidi Brahim Ben Arrif; 25/IV/2014; B. Belqat and O. Driauach leg; collected using sweep net; UAE-FST R14/2406. – **Middle Atlas Region** • 1♀; Forêt–3.5 km S. Azrou; cedar forest; 8/V/2012; M.J. Ebejer leg; collected using sweep net; NHMUK.

This species was collected mostly in environments of aquatic ecosystems such as springs (Aïn) and ponds (Daya), but also in forest environments.

Diagnosis. The most obvious differences in the male terminalia from *L. bimaculata* (Figs 10, 13, 16) are that the apical part of the gonostylus is shorter and thicker, and the adjacent ventral lobe of the gonocoxites is broader basally (arrowed in Fig. 15 of *L. arcana* and in Fig. 16 of *L. bimaculata* for comparison). In these respects, *L. arcana* resembles these structures in the figures of *L. montanosilvatica* Zaitzev, 1994, described from Kyrgyzstan (Zaitzev 1994). However, *L. montanosilvatica* is said to have unmarked wings, so *L. arcana* is considered a distinct species pending further revision of this genus.

Leia beckeri is similar in colour to *L. arcana*; in examined specimens of *L. beckeri*, the dark-brown thoracic stripes are more sharply contrasted with

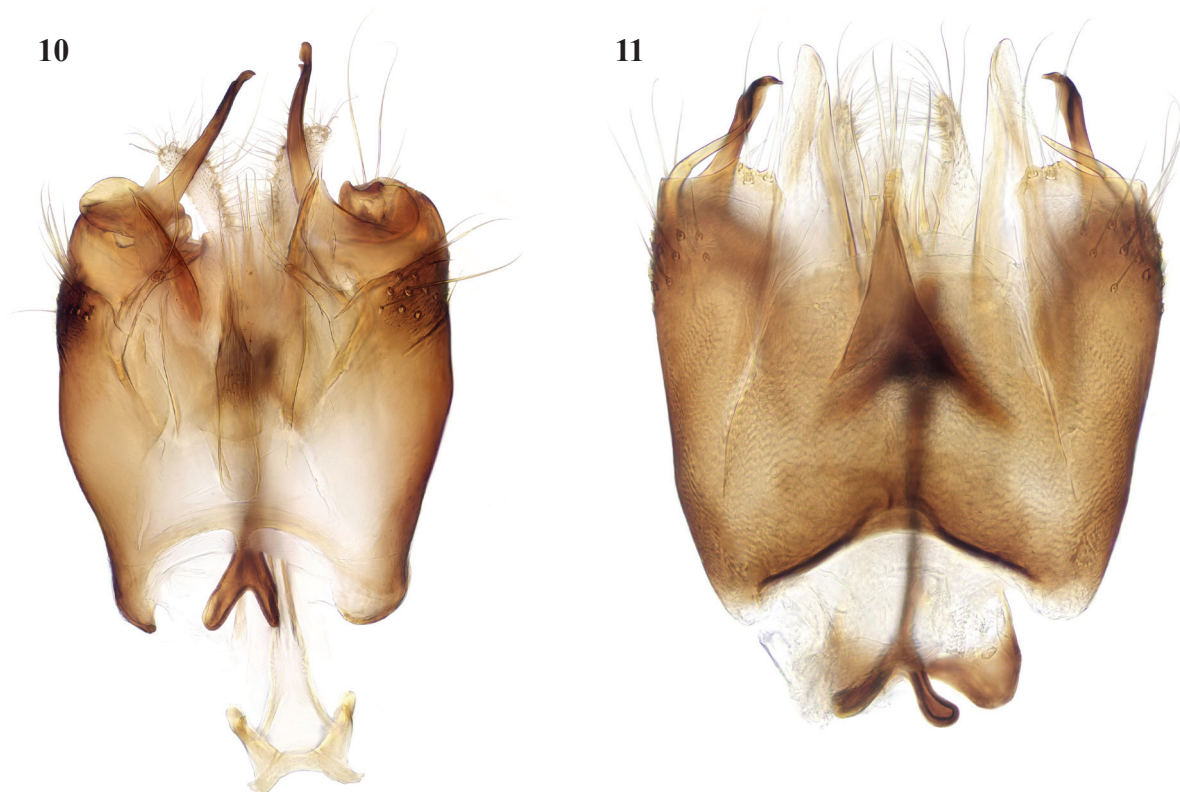


Figures 8, 9. *Leia arcana* sp. nov., male terminalia 8 ventral view 9 dorsal view.

the yellow sides and humeral area of the mesonotum than in *L. arcana*, and the pleura and abdomen are all dark brown. The marking over r-m may sometimes be faint in *L. beckeri*, but it differs in the preapical wing marking being situated closer to the tip of vein R_1 than in the other Moroccan species and well before the tip of cell r_1 . The male terminalia of *L. beckeri* (Figs 11, 14, 17) are also similar to this group of the genus; the gonostylus is constructed similar to *L. bimaculata* and *L. arcana*, with the apical part intermediate in thickness between these species, but there is a slender tapered process ventral and external to the gonostylus (arrowed in Fig. 17), and the ventral lobe of the gonocoxites is broadly rounded and not apically produced as in these other species.

The females of these three species are similar in the structure of the ovipositor (Figs 18–20), but they evidently differ in the form in lateral view of the upper margin of sternite 8, which is more rounded in *L. bimaculata*, straighter and slightly emarginate in *L. arcana*, and with a more distinct emargination in *L. beckeri*.

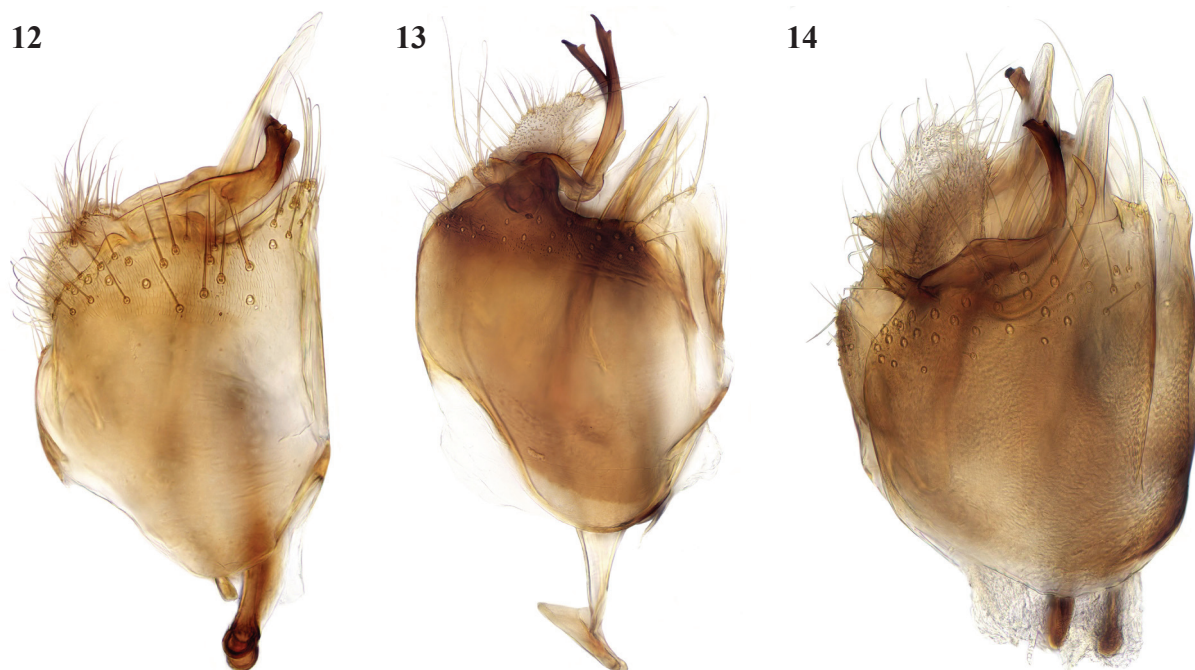
Description. Male. Wing length 4–4.5 mm. **Coloration.** Mainly shining black or dark brown with yellow markings. Head black; antenna with scape and pedicel yellow, flagellum dark brown. Mesonotum bearing three almost fused shining dark brown stripes (separated by narrow yellow dorsocentral stripes), leaving the humeral area and sides yellow; scutellum dark brown dorsally, sometimes more or less yellowish at sides; propleura brownish yellow; pleura otherwise and mediotergite all dark brown. Legs yellow except for narrow dark tips to coxae and trochanters and apical eighth of hind femur. Wing clear yellowish except for brown preapical patch that extends from fore margin (including tip of cell r_1)



Figures 10, 11. *Leia* species, male terminalia, ventral view 10 *L. bimaculata* (Meigen, 1804) 11 *L. beckeri* Landrock, 1940.

over the median fork. Haltere yellowish white. Abdomen dark brown with hind margins of tergites 2–4 and fore margins (basal third) of tergites 3–5 narrowly yellow; sternites similarly coloured or with more yellow. Terminalia yellow. **Head.** Antenna about 1.5× as long as head and thorax, with flagellomeres more than 2× as long as broad. **Thorax.** Mesonotum and scutellum with long yellow setae; laterotergite setose. **Legs.** Tibiae 2 and 3 with long yellow apical spurs, more than half as long as tarsomere 1; setulae on femora pale, on rest of legs dark; dark tibial setae, mostly longer than width of tibia: mid tibia with 2–3 d, 1 a-d, 3 a, and 2 a-v setae; hind tibia with 3–4 d and 3–4 a-d setae. **Wing.** Vein Sc ends in costa near to level of base of posterior fork, with crossvein sc-r at about its apical third. Vein R_1 a third to half the length of crossvein r-m, which is longer than the stem of median fork. Median fork complete. Posterior fork arises before level of base of stem of median fork, its anterior branch (M_4) narrowly interrupted at its extreme base. CuP stops short beyond level of base of posterior fork. A short dark streak at base of fork of axillary veins (as in *L. bimaculata*). **Terminalia** (Figs 8, 9, 12, 15). Gonostylus comprising a single lobe, curved medially and with a small preapical incision; gonocoxites with a setose ventral lobe basal to each gonostylus that is tapered to a bluntly rounded tip (arrowed in Fig. 15).

Female. Coloration. Similar to male, with scape and pedicel yellow, flagellum dark. Abdomen with segments 2–6 yellow on apical quarter; ovipositor with cerci narrow, brownish. **Head.** Antenna distinctly shorter than in male, less than length of thorax. **Legs.** Mid tibia with 3 d, 1 a-d, 3 v, and 3 p-v setae; hind tibia with 4 d, 3 a-d setae. **Ovipositor** (Fig. 18). Sternite 8 with dorsal margin in lateral view straight and cerci narrow.



Figures 12–14. *Leia* species, male terminalia, lateral view 12 *L. arcana* sp. nov. 13 *L. bimaculata* (Meigen) 14 *L. beckeri* Landrock.



Figures 15–17. *Leia* species, male terminalia, ventral view of medial lobe of gonocoxite (arrowed in 15 and 16) and gonostylus 15 *L. arcana* sp. nov. 16 *L. bimaculata* (Meigen) 17 *L. beckeri* Landrock (additional process from base of gonostylus arrowed, absent in other two species; medial lobe of gonocoxites broadly rounded).

Etymology. From Latin *arcanus*, meaning secret as the separation of this species was previously hidden.

Comments. The male from Ain El Ma Bared and the female from Azrou were listed under *L. bimaculata* by Banamar et al. (2020). The female (Fig. 18) is considered conspecific with *L. arcana* on basis of its coloration.

Genus *Megophthalmidia* Dziedzicki, 1889

This genus was recognised to have a greater diversity in southern Europe than previously appreciated when six species, five of them newly described, were



Figures 18–20. *Leia* species females, lateral view of ovipositor 18 *L. arcana* 19 *L. bimaculata* 20 *L. beckeri*.

recorded from Greece by Chandler et al. (2006). Two of these species were recorded from Sardinia by Chandler (2009) and one of them, *M. illyrica* Chandler, Bechev & Caspers, 2006 is newly recorded here from Gibraltar (Governor's lookout, Upper Rock, 1♂, 28/II/2010, coll. K. Bensusan and R. Gwillem). As there is also a species of this genus, *M. decora* (Santos Abreu, 1920), in the Canary Islands and Madeira the occurrence of the genus in Morocco was expected.

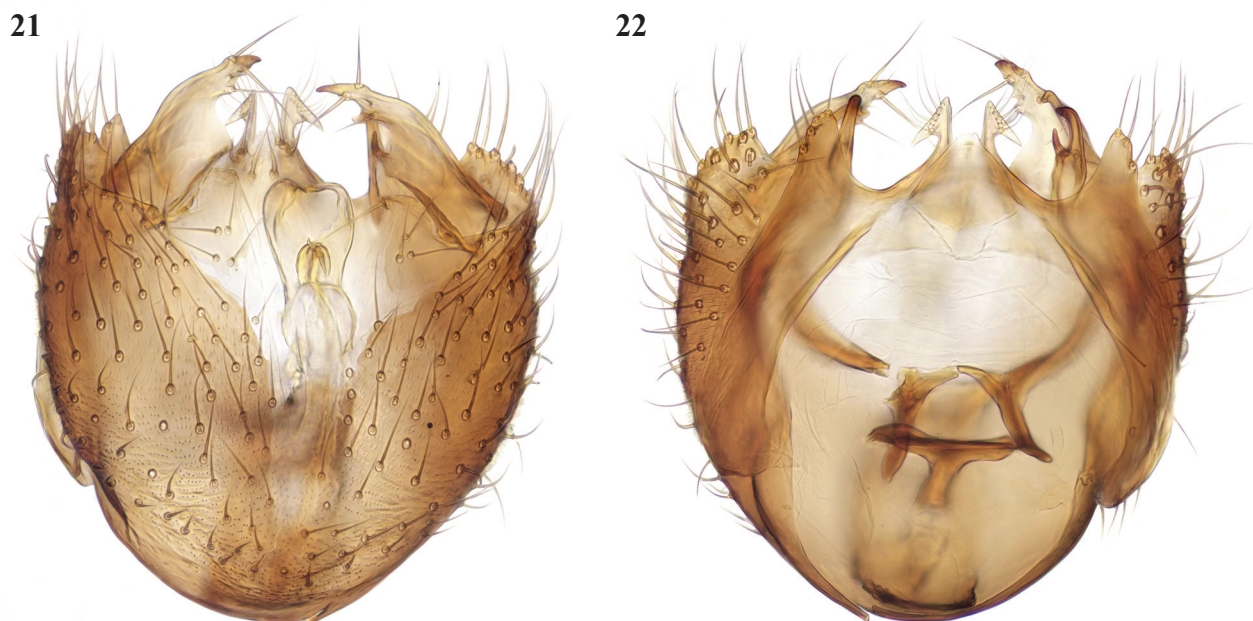
***Megophthalmidia amsemlii* Chandler, Belqat & Banamar, sp. nov.**

<https://zoobank.org/C4EF93E3-83ED-4461-86B7-CD09F33CD522>

Type material. Holotype. MOROCCO – **Rif Region** • ♂ (mounted in DMHF, terminalia on slide); Marabout Abou Bnar; 18/V/2014; B. Belqat and O. Driauach leg; collected using sweep net; NHMUK. **Paratypes.** MOROCCO – **Rif Region** • 1♂; Daya Amsemliil; 26/III/2016; B. Belqat and O. Driauach leg; collected using sweep net; UAE-FST R16/2407 • 1♂; Forêt Malâab Tizimezzan; 12/V/2022; M.A. El Mouden leg; collected using sweep net; UAE-FST R22/2408 • 1♂; Pont Imezzane; 12/V/2022; M.A. El Mouden leg; collected using sweep net; UAE-FST R22/2409 • 1♂; Route vers Abou Bnar; 12/V/2022; M.A. El Mouden leg; collected using sweep net; UAE-FST R22/2410 • 1♂; Forêt Azilane; 13/V/2022; M.A. El Mouden leg; collected using sweep net; UAE-FST R22/2411 • 1♂; Daya Mtahen; 5/VI/2022; B. Belqat, M.A. El Mouden and O. Driauach leg; collected using sweep net; UAE-FST R22/2412. – **Middle Atlas Region** • 1♂; Oued Taourirt; 20/V/2022; M.A. El Mouden leg; collected using sweep net; UAE-FST MA22/2401. **Other material.** MOROCCO – **Rif Region** • 1♀; Daya Amsemliil; 23/IV/2016; B. Belqat and O. Driauach leg; collected using sweep net; UAE-FST R16/2413. – **Atlantic Plain Region** • 1♀; Sidi Yahya El Gharb; 25/IV/2015; B. Belqat and O. Driauach leg; collected using sweep net; UAE-FST AP15/2401.

Found in environments of protected areas (National Park of Talassemrane and Bouhachem Natural Park Project), around aquatic systems (rivers and ponds) but also in developed as well as inhabited areas.

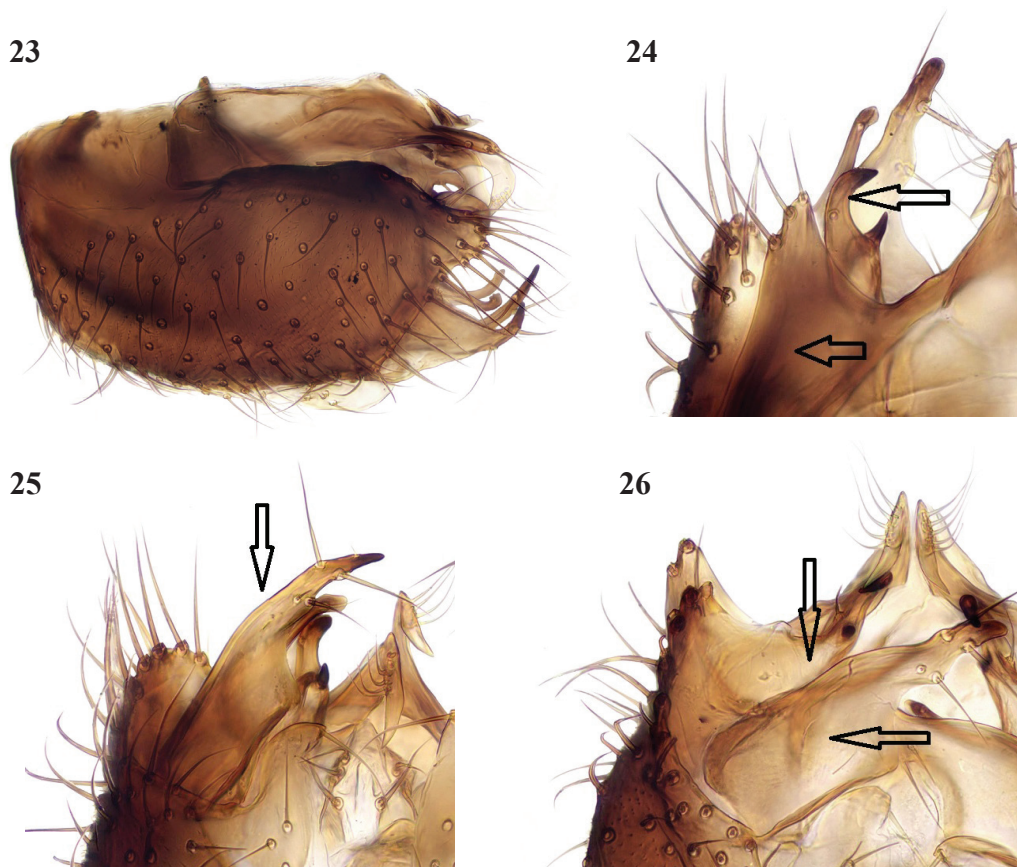
Diagnosis. This species is similar in coloration to *M. illyrica*, and the male tergite 9 is also similar in form to that species. The structure of the terminalia is otherwise quite distinct with the gonocoxites more deeply excavated ventrally and the gonostylus differing in form, broader basally and more angular apically. Specimens examined vary in the extent to which the gonostylus is extended in situ, giving a differing appearance which might suggest that more than one



Figures 21, 22. *Megophthalmidia amsemlili* sp. nov., male terminalia, paratype from Pont Imezzane **21** ventral view **22** dorsal view.

species is involved but their structural details are in common as described below. To take this apparent variation in form into account three specimens have contributed to the figures as indicated.

Description. Male. Wing about 2 mm. **Coloration.** Body nearly all black, with yellowish apical margins to tergites 2–4, interrupted dorsally, and there may also be very narrow yellow basal margins to tergites 3–5; sternites 2–4 all yellow. Antenna black. Palpus black at base, otherwise yellow. Legs with mid and hind coxae brownish externally, otherwise all yellow. Wing clear yellowish. Terminalia dark coloured. **Head.** Antenna a little longer than head and thorax together, with flagellomeres at least as long as broad: flagellomeres 1 and 2 quadrate, other flagellomeres a little longer than broad. **Legs.** [Only one fore leg, femur, and part of tibia of one mid leg, and both hind legs are present in the holotype; paratypes are all missing one or more legs]. Mid tibia and hind tibia with rows of anterior and dorsal setae, all shorter than tibial width, the dorsal setae on hind tibia denser and occupying most of its length. Tibial spurs 1: 2: 2, yellow, the longer spurs on each about two-thirds length of first tarsomere. **Wing.** Radial veins and crossvein r-m with setulae, fork veins and their stems bare. Vein R_1 a little longer than r-m, median stem about twice length of r-m. Base of posterior fork level with or just beyond base of stem of median fork, its branches widely divergent from base. Costa extends about 0.6 distance from R_{4+5} to M_1 . **Terminalia** (Figs 21–26). Small. Tergite 9 comprising apically pointed lateral lobes, connected by a narrow bridge to a prominent bilobed median process bearing cerci; each cercus with a ventrally directed tapered lobe with a row of long setae; gonocoxites with broad and deep medial excavation ventrally, dorsally produced medially on each side into a bifid process (arrowed in Figs 24, 26) with each lobe with a short terminal spine. Gonostylus (arrowed in Figs 25, 26) broad and bare basally, sharply narrowed to an angular apical part bearing some long setae and a short terminal tooth-like spine.



Figures 23–26. *Megophthalmidia amsemlii* sp. nov., male terminalia **23** lateral view **24** dorsal view with tergite 9 (lower arrow) and gonocoxal margin (upper arrow) **25** ventral view, gonostylus (arrowed) extended posteriorly **26** ventral view, gonostylus (lower arrow) deflected internally, gonocoxal margin upper arrow **23–25** paratype from Oued Taourirt **26** holotype.

Female. Those listed under other material, with coloration as in male, and with flagellomeres similar to male, are considered likely to be conspecific.

Etymology. Named for the locality Daya Amsemliil, where both *Megophthalmidia* species recorded here and the new species of *Mycomya* described below were collected.

Comments. This is evidently a widespread species in Morocco.

***Megophthalmidia ionica* Chandler, Bechev & Caspers, 2006**

New records. MOROCCO – **Rif Region** • 1♂; Daya Amsemliil; 28/II/2015; B. Belqat and O. Driauach leg; collected using sweep net; UAE-FST R15/2443 • 1♂; Forêt Bouhachem st. 1; 5/V/2022; B. Belqat, M.A. El Mouden and O. Driauach leg; collected using sweep net; UAE-FST R22/2444 • 1♂; Daya Mtahen; 5/VI/2022; B. Belqat, M.A. El Mouden and O. Driauach leg; collected using sweep net; UAE-FST R22/2445.

Comments. This species was described from Greece (Chandler et al. 2006), later recorded from Sardinia (Chandler 2009), and has most recently been identified from Corsica. It is similar in coloration and most structural characters to *M. amsemlii* and *M. illyrica*. The terminalia (Figs 27–29) are, however, quite distinct in structure. The antenna is shorter than in *M. amsemlii* and *M. illyrica*; the



Figures 27–29. *Megophthalmidia ionica* Chandler, Bechev & Caspers, male terminalia 27 ventral view 28 dorsal view 29 lateral view.

flagellomeres, except the terminal one, are distinctly shorter than broad, and this character also enables females to be separated from those of *M. amsemlili* and *M. illyrica*. New to North Africa.

Subfamily Gnoristinae Edwards, 1925

Genus *Docosia* Winnertz, 1864

Species in this genus mostly have a uniform appearance of black body, mainly yellow legs and unmarked wings, specific characters being in small details of the structure of the male terminalia. Ševčík et al. (2020) noted that 57 species were now known from the Palaearctic region; of these about 20 have been recorded from around the Mediterranean, many of them little known apart from

their original description. When the previous account of Moroccan Mycetophilidae (Banamar et al. 2020) was prepared, the material of *Docosia* had not yet been fully investigated, only the distinctive species *D. gilvipes* (Haliday in Walker, 1856) then being recorded. Although a larger number might be anticipated, so far five further species have been recognised in the available material, two of which are recorded here; the others are apparently previously undescribed and will be treated elsewhere. Females taken with males might be assumed to be conspecific but cannot be recognised for most species.

***Docosia melita* Chandler & Gatt, 2000**

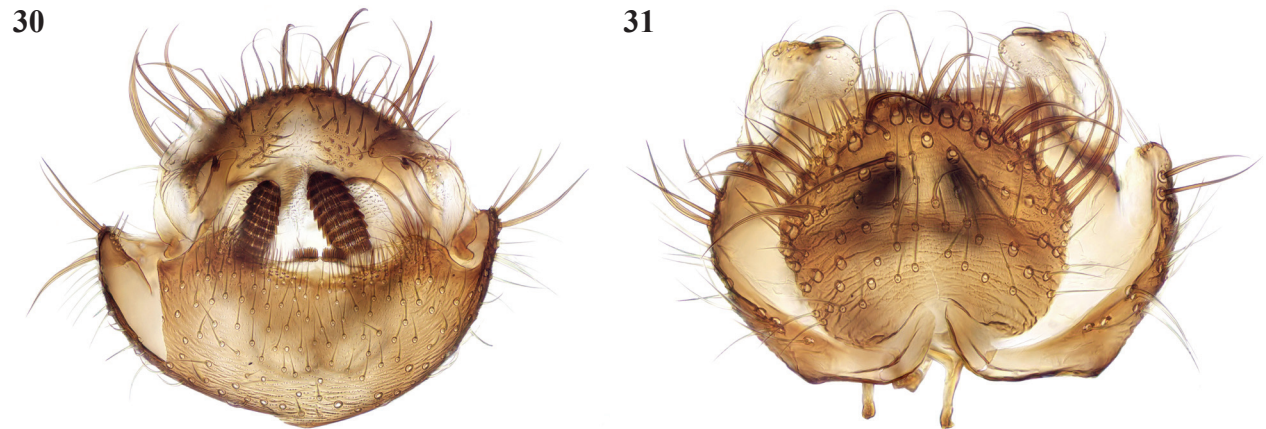
New records. MOROCCO – Rif Region • 1♂; Oued Ferda; 13/II/2013; B. Belqat and O. Driauach leg; collected using sweep net; UAE-FST R13/2434 • 1♂; Oued Majjou avant source; 9/IV/2013; B. Belqat and O. Driauach leg; collected using sweep net; UAE-FST R13/2435 • 6♂♂; Maison forestière, Talassemrane; 17/VI/2014; B. Belqat and O. Driauach leg; collected using sweep net; UAE-FST R14/2436 • 2♂♂; Akchour; 16/IV/2016; B. Belqat and O. Driauach leg; collected using sweep net; UAE-FST R16/2437 • 1♂; Oued Majjou; 5/II/2019; B. Belqat and O. Driauach leg; collected using sweep net; UAE-FST R19/2438 • 2♂♂; Maison forestière, Talassemrane; 13/II/2021; B. Belqat and O. Driauach leg; collected using sweep net; UAE-FST R21/2439 • 3♂♂; Oued Majjou; 6/II/2022; B. Belqat and O. Driauach leg; collected using sweep net; UAE-FST R22/2440.

Comments. This species was described from Malta and has been recorded from Greece (Chandler et al. 2006) and Sardinia (Chandler 2009). It can also be newly recorded from Gibraltar (Mediterranean steps, maquis, 1♂, 23/III/2010; Camp Bay, ruderal vegetation, 1♂, 21/III/2010, both coll. M.J. Ebejer). New to North Africa. The male terminalia of a Moroccan specimen are shown here (Figs 30, 31); the female cannot be distinguished from allied species.

***Docosia flavicoxa* Strobl, 1900**

New records. MOROCCO – Rif Region • 1♂; Oued Ferda; 13/II/2013; B. Belqat and O. Driauach leg; collected using sweep net; UAE-FST R13/2428 • 2♀; Oued Majjou avant source; 9/IV/2013; B. Belqat and O. Driauach leg; collected using sweep net; UAE-FST R13/2429 • 1♂; Daya avant Taïda; 20/IV/2018; B. Belqat and O. Driauach leg; collected using sweep net; UAE-FST R18/2430 • 1♂; Oued Majjou; 5/II/2019; B. Belqat and O. Driauach leg; collected using sweep net; UAE-FST R19/2431 • 2♀♀; Oued Majjou; 6/II/2022; B. Belqat and O. Driauach leg; collected using sweep net; UAE-FST R22/2432 • 1♂; Oued Majjou; 20/II/2022; B. Belqat and O. Driauach leg; collected using sweep net; UAE-FST R22/2433.

Comments. This is a widespread Palaearctic species, distinguished by its entirely yellow legs from the other Moroccan species which have the bases of the mid and hind coxae more or less darkened, and also by its setose laterotergite which is bare in the other Moroccan species examined. It is also newly recorded from Gibraltar (Upper Rock, meadow in woodland, 1♂, 1♀, 21/III/2010, coll. K. Bensusan). New to North Africa. The terminalia of a Moroccan specimen are shown here (Figs 32, 33).



Figures 30, 31. *Docosia melita* Chandler & Gatt, male terminalia 30 ventral view 31 dorsal view.



Figures 32, 33. *Docosia flavicoxa* Strobl, male terminalia 32 posteroventral view 33 dorsal view.

Subfamily Mycomyinae Edwards, 1925

Genus *Mycomya* Rondani, 1856

***Mycomya mira* Chandler, Belqat & Banamar, sp. nov.**

<https://zoobank.org/BBE4B953-B1BF-4B5D-9292-48843474873B>

Type material. Holotype. MOROCCO – Rif Region • ♂ (mounted in DMHF); Forêt Adayourha; 1/II/2020; B. Belqat and O. Driauach leg; collected using sweep net; NHMUK. **Paratypes.** MOROCCO – Rif Region • 2♂♂; Forêt Bab Hajara; 14/VII/2013; B. Belqat and O. Driauach leg; collected using sweep net; UAE-FST R13/2414 • 1♂; Aïn Sidi Brahim Ben Arrif; 25/IV/2014; B. Belqat and O. Driauach leg; collected using sweep net; UAE-FST R14/2415 • 5♂♂, 2♀♀; Forêt Bab Hajara; 28/II/2015; B. Belqat and O. Driauach leg; collected using sweep net; UAE-FST R15/2416 • 32♂♂; Daya Amsemlil; 1/I/2020; B. Belqat and O. Driauach leg; collected using sweep net; UAE-FST R20/2417 • 19♂♂, 4♀♀; Forêt Adayourha; 1/II/2020; B. Belqat and O. Driauach leg; collected using sweep net; UAE-FST R20/2418 • 5♀♀; Maison forestière Bouhachem; 1/II/2020; B. Belqat

and O. Driaouach leg; collected using sweep net; UAE-FST R20/2419 • 7♂♂, 1♀; Forêt Sed Nakhla; 10/II/2020; B. Belqat and O. Driaouach leg; collected using sweep net; UAE-FST R20/2420 • 1♂; Forêt Azilane; 13/II/2020; B. Belqat and O. Driaouach leg; collected using sweep net; UAE-FST R20/2421 • 1♂; Forêt Bni Leit; 10/I/2021; B. Belqat and O. Driaouach leg; collected using sweep net; UAE-FST R21/2422 • 1♂; Douar Bni Leit; 10–16/I/2021; B. Belqat and O. Driaouach leg; reared; UAE-FST R21/2423.

This species inhabits the diverse landscape of the Bouhachem Natural Parc Project, particularly including wetlands, which present a typology from sphagnum peat bogs to temporary ponds to springs, spring streams, and headwaters of three river systems, as well as in forests.

Diagnosis. This species belongs to the subgenus *Mycomya* sensu stricto and differs from other species in the following combination of male characters: legs simple except for short mid-coxal spur; tergite 9 with neither a medial process nor lateral appendages, medially emarginate and with short internal spinose setae subapically. It runs to couplet 75 in the key by Väisänen (1984), where it is between the two options in that the base of the posterior fork is usually level with the base of the stem of the median fork. It fits the first option in the structure of tergite 9 and in couplet 76 it agrees with the western Nearctic *M. fuscipalpis* van Duzee, 1928 in the form of the gonostylus. Thus, it could be assigned to the species group of which *M. fuscipalpis* was the only member. The most obvious difference from *M. fuscipalpis* is that there are separate submedian appendages of the gonocoxites, while in *M. fuscipalpis* these are fused medially.

Description. Male. Wing length 4–4.5 mm. **Coloration.** Body entirely dark greyish brown. Head and antennae uniformly dark; palpi yellowish. Coxae brown, legs otherwise entirely yellow. Terminalia dark grey. **Head.** Antenna slender, about 3 mm long, longer than abdomen, with flagellomeres about 6× as long as broad. **Legs.** Long and slender. Fore coxa unmodified; mid coxa with anteriorly directed slender spur, straight for most of its length, then slightly curved apically, relatively short, about half length of coxa. Fore tarsomere 1 a little shorter than its tibia. Vein Sc ending in R at middle of radial cell, often with anterior spur, more or less extended to costa (may vary between the wings of a specimen). Base of posterior fork at or just beyond level of base of stem of median fork. **Terminalia** (Figs 34, 35). Short. Tergite 9 with a median emargination between broad rounded setose lobes, with a pair of internal submedian lobes each bearing a slender curved spine laterally and a row of 5–7 short blunt spines (cones of Väisänen 1984) apically. Gonocoxites with short broad submedian appendages that are bluntly rounded apically. Gonostylus reflexed within gonocoxites, thick and angular basally and sharply narrowed to a slender curved and pointed apical part which has a small blunt tooth at its base.

Female. Wing length range as in male. **Coloration.** As in male; ovipositor yellowish. **Head.** Antenna relatively shorter than in male, about 1.5× head and thorax together; flagellomeres about 4× as long as broad. **Legs.** Simple, without mid-coxal spur. **Ovipositor** (Fig. 36). Sternite 8 with a pair of tapered apically rounded setose lobes. Cercus with elongate basal segment and small rounded apical segment bearing short setae.

Etymology. From Latin *mirus*, to note the astonishing discovery of this species.

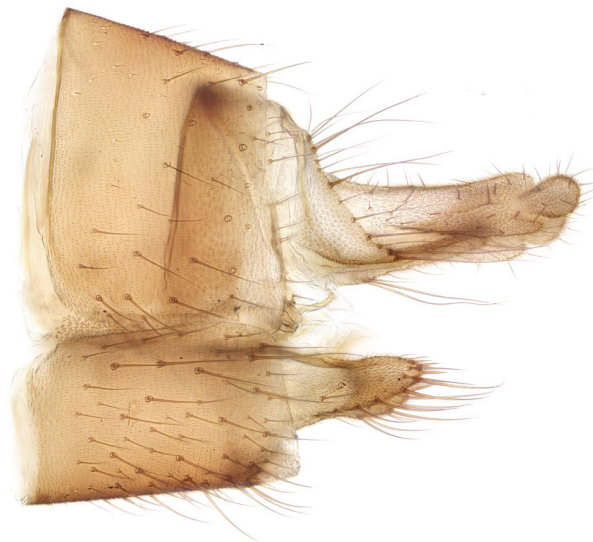
34



35



Figures 34, 35. *Mycomya mira* sp. nov., male terminalia 34 ventral view 35 dorsal view.



Figures 36. *Mycomya mira* sp. nov., female, lateral view of ovipositor.

Comments. This is a very distinct species, which is evidently frequent and widespread in Morocco.

***Mycomya prominens* (Lundström, 1913)**

New records. MOROCCO – Rif Region • 1♂; Daya Mtahen; 23/III/2021; B. Belqat and O. Driauach leg; collected using sweep net; UAE-FST R21/2448.

Comments. This is a common and widespread European species, with previous records in the Mediterranean region from Israel and Greece (Chandler 1994; Chandler et al. 2006). It has also been recorded from Madeira (Chandler and Ribeiro 1995). New to North Africa.

Subfamily Sciophilinae Rondani, 1840

Genus *Monoclona* Mik, 1886

***Monoclona rufilatera* (Walker, 1837)**

New records. MOROCCO – **Rif Region** • 1♂; Forêt Aïn Lahcen; 15/I/2020; B. Belqat and O. Driauach leg; collected using sweep net; UAE-FST R20/2446 • 1♂; Khandek Melouka; 10/IV/2021; B. Belqat and O. Driauach leg; collected using sweep net; UAE-FST R21/24467.

Comments. This is a Holarctic species, which is widespread in Europe. New to North Africa.

Genus *Phthinia* Winnertz, 1864

This is a small genus, but with a diversity of structure of the male terminalia. Zaitzev (1994) included 10 Palaearctic species, of which four occur in Europe, one (*P. hyrcanica* Zaitzev, 1984) occurs in Azerbaijan, and the rest live in the Eastern Palaearctic. Three more European species have since been described (Plassmann 1984, 1990; Zaitzev 2001). A male and a female, collected at the same locality in Morocco, have been examined; both specimens are in poor condition, but the structure of the male terminalia is distinct from any previously known species of the genus.

***Phthinia snibbypinsae* Chandler, Belqat & Driauach, sp. nov.**

<https://zoobank.org/C90346E3-F2FF-40A7-8F37-092DD7421877>

Type material. Holotype. MOROCCO – **Rif Region** • ♂ (mounted in DMHF, terminalia on slide); Khandek Melouka; 10/IV/2021; B. Belqat and O. Driauach leg; collected using sweep net; NHMUK. **Paratype.** ♀; same data as for holotype; UAE-FST R21/2424.

The type locality is in the environment (forest and cultivated fields) of Aïn Lahcen, a rural commune whose name (Aïn) is taken from a spring that flows through it.

Diagnosis. This is a slender bodied species with small male terminalia, similar in this respect to *P. winnertzi* Mik, 1869 and allied species. Among Palaearctic species, it most closely resembles *P. hyrcanica* in the apically bilobed gonostylus situated within the broadly rounded gonocoxites. It differs from that species in the lobes of the gonostylus being short and blunt and in the dense short setae on the margins of the gonocoxites.

Description. Male. Body 7 mm, of which about 6 mm is length of abdomen.

Coloration. Head brown. Antenna with short basal segments and base of first flagellomere yellow, remainder brown. Palpi yellow. Thorax yellowish brown, darker brown on disc of mesonotum and scutellum. Legs yellow. Wings clear grey, presumed to be unmarked as in female. Haltere brown. Abdomen entirely dark brown. Terminalia yellow. **Head.** Both antennae incomplete (11 and 5 flagellomeres present). **Legs.** Missing apart from one fore femur and one hind leg. **Wing.** Both wings are represented only by short stubs. **Abdomen.** Long, slender.

37



38



Figures 37, 38. *Phthinia snibbypinsae* sp. nov., male terminalia 37 ventral view 38 dorsal view.

Terminalia (Figs 37, 38). Small. Gonocoxites rounded laterally, with deep medial excavation bordered by short, dense setae; gonostylus enclosed by gonocoxites, short and with two short, blunt apical lobes.

Female. Body 6 mm, of which around 5 mm is length of abdomen. **Coloration.** As in male; wings clear greyish. Ovipositor brownish yellow. **Legs.** Fore legs missing but mid and hind legs complete, long, slender, about 9 mm long. **Wing.** Both wings are represented only by stubs, but more of the right wing is present, including the bases of fork veins. Vein Sc ends in costa before level of base of Rs. Crossvein r-m about 3× as long as stem of median fork. Base of posterior fork beyond that of median fork, with posterior branch (vein CuA) downturned; false vein also downturned, parallel with it. Vein CuP stops short before level of base of posterior fork. **Abdomen.** Slender, relatively shorter than in male. Ovipositor short and small, with cerci short ovoid and covered with short setae.

Etymology. The name commemorates Snibby Pins, erstwhile companion of Benjamin Bottom, after whom the Sardinian gnat *Sciophila benjaminbottomi* Chandler, 2009 was named.

Comments. This is the first record of this genus from North Africa, and this species is evidently rare. *Phthinia* species are usually found around rotten wood, and they develop in encrusting fungi.

Discussion

The new findings presented in this study increase the number of Mycetophilidae of Morocco to 76 species, so enriching the biodiversity of the Mycetophilidae fauna of the whole North Africa region. The fauna of other parts of North Afri-

ca is poorly known, with only 23 species of Mycetophilidae presently recorded from Algeria and 27 species from Tunisia, with a combined total including unpublished records of 45 species, of which 26 are in common with Morocco; this comparison will be discussed further elsewhere. The five newly described species allow us to consider for the first time endemic mycetophilids in Morocco, of which three are specifically endemic to the occidental Rif region. More fieldwork in this region and elsewhere in Morocco will probably find more new species.

Acknowledgements

We are grateful to Dr Martin Ebejer who kindly provided material that he collected in Morocco and for permitting us to publish his new records. Jostein Kjærandsen and Olavi Kurina provided helpful comments on the terminalia photographs of the new species and confirmation that they were likely to represent previously undescribed species. We are indebted to Janet Graham who, assisted by her brother Andrew, took all the photographs illustrating this paper.

Additional information

Conflict of interest

The authors have declared that no competing interests exist.

Ethical statement

No ethical statement was reported.

Funding

No funding was reported.

Author contributions

All authors have contributed equally.

Author ORCIDs

Mohamed Amin El Mouden  <https://orcid.org/0009-0002-6085-924X>

Peter J. Chandler  <https://orcid.org/0009-0000-4789-3596>

Ouafaa Driauach  <https://orcid.org/0000-0002-9748-2450>

Ouarda Banamar  <https://orcid.org/0000-0002-7838-1080>

Imane Saidoun  <https://orcid.org/0009-0005-2809-5384>

Abdellatif Akarid  <https://orcid.org/0000-0003-3823-1229>

Khalid Aattouch  <https://orcid.org/0009-0001-0680-4822>

Boutaina Belqat  <https://orcid.org/0000-0003-2857-7699>

Data availability



All of the data that support the findings of this study are available in the main text.

References

- Banamar O, Chandler PJ, Driauach O, Belqat B (2020) New faunistic records of the family Mycetophilidae (Insecta, Diptera) from Morocco. *ZooKeys* 934: 93–110. <https://doi.org/10.3897/zookeys.934.49157>

- Chandler PJ (1994) Fungus gnats of Israel (Diptera: Sciaroidea, excluding Sciaridae). *Israel Journal of Entomology* 28: 1–100.
- Chandler PJ (2009) The fungus gnats (Diptera: Bolitophilidae, Keroplatidae, Mycetophilidae) of Sardinia, with description of six new species. *Zootaxa* 2318(1): 450–506. <https://doi.org/10.11646/zootaxa.2318.1.19>
- Chandler PJ, Gatt P (2000) Fungus Gnats (Diptera, Bolitophilidae, Keroplatidae and Mycetophilidae) from the Maltese Islands. *Studia Dipterologica* 7: 69–81.
- Chandler PJ, Ribeiro E (1995) The Sciaroidea (Diptera) (excluding Sciaridae) of the Atlantic Islands (Canary Islands, Madeira and the Azores). *Boletim do Museu Municipal do Funchal* 3: 1–170. [Historia Natural]
- Chandler PJ, Bechev DN, Caspers N (2006) The Fungus Gnats (Diptera: Bolitophilidae, Diadocidiidae, Ditomyiidae, Keroplatidae and Mycetophilidae) of Greece, its islands and Cyprus. *Studia Dipterologica* 12(2005): 255–314.
- Kaspřák D, Kerr P, Sýkora V, Tóthová A, Ševčík J (2019) Molecular phylogeny of the fungus gnat subfamilies Gnoristinae and Mycomyinae, and their position within Mycetophilidae (Diptera). *Systematic Entomology* 44(1): 128–138. <https://doi.org/10.1111/syen.12312>
- Kettani K, Ebejer MJ, Ackland DM, Bächli G, Barraclough D, Barták M, Carles-Tolrá M, Černý M, Cerretti P, Chandler P, Dakki M, Dageron C, De Jong H, Dils J, Disney H, Droz B, Evenhuis N, Gatt P, Graciolli G, Grichanov IY, Haenni J-P, Hauser M, Himmi O, Macgowan I, Mathieu B, Mouna M, Munari L, Nartshuk EP, Negrobov OP, Oosterbroek P, Pape T, Pont AC, Popov GV, Rognes K, Skuhrová M, Skuhrová V, Speight M, Tomasovic G, Trari B, Tschorsnig H-P, Vala J-C, von Tschirnhaus M, Wagner R, Whitmore D, Woźnica AJ, Zatwarnicki T, Zwick P (2022) Catalogue of the Diptera (Insecta) of Morocco – An annotated checklist, with distributions and a bibliography. *ZooKeys* 1094: 1–466. <https://doi.org/10.3897/zookeys.1094.62644>
- Lindemann JP, Søli G, Kjærandsen J (2021) Revision of the *Exechia parva* group (Diptera: Mycetophilidae). *Biodiversity Data Journal* 9: e67134. <https://doi.org/10.3897/BDJ.9.e67134>
- Plassmann E (1984) Sechs neue Pilzmücken aus Schweden, Österreich, Griechenland und Brasilien (Diptera, Nematocera, Mycetophilidae). *Nachrichtenblatt der Bayerischen Entomologen* 33: 44–49.
- Plassmann E (1990) Fünf neue Pilzmücken aus Schweden. *Nachrichtenblatt der Bayerischen Entomologen* 39(2): 61–64.
- Polevoi A, Salmela J (2016) New data on poorly known species of the genus *Leia* Meigen (Diptera, Mycetophilidae) from the Palaearctic region. *Zootaxa* 4103(5): 487–500. <https://doi.org/10.11646/zootaxa.4103.5.7>
- Ševčík J, Burdíková N, Kaspřák D, Kurina O (2020) Five new Palaearctic species of *Docosia* (Diptera: Mycetophilidae), with updated molecular phylogeny of the genus. *European Journal of Taxonomy* 717: 3–26. <https://doi.org/10.5852/ejt.2020.717.1095>
- Väisänen R (1984) A monograph of the genus *Mycomya* Rondani in the Holarctic Region (Diptera, Mycetophilidae). *Acta Zoologica Fennica* 177: 1–346.
- Zaitzev AI (1994) Fungus Gnats of the Fauna of Russia and Adjacent Regions –Part 1, Moscow, 288 pp. [In Russian]
- Zaitzev AI (2001) New species of fungus gnats from Russia and Italy (Diptera: Mycetophilidae). *Zoosystematica Rossica* 9: 453–458.

Taxonomic position of holothurian *Eupentacta fraudatrix* (Echinodermata, Holothuroidea)

Sergei V. Turanov^{1,2}, Alexey V. Smirnov³, Yuri Ph. Kartavtsev¹

1 A.V. Zhirmunsky National Scientific Center of Marine Biology, Russian Academy of Sciences, Vladivostok, Russia

2 Far Eastern State Technical Fisheries University, Vladivostok, Russia

3 Zoological Institute of Russian Academy of Sciences, St. Petersburg, Russia

Corresponding author: Yuri Ph. Kartavtsev (yuri.kartavtsev48@hotmail.com)

Abstract

Samples of the holothurian *Eupentacta fraudatrix* (Djakonov & Baranova in Djakonov, Baranova & Saveljeva, 1958) from the Sea of Japan were studied and the relationships of the genera *Eupentacta* and *Sclerodactyla*, as well as related taxa, were evaluated on the basis of phylogenetic analysis of the mitochondrial DNA COI and 16S rRNA genes. Using three methods, phylogenetic trees were constructed, and the degree of reliability of topological reconstructions was estimated by means of a nonparametric bootstrap test for the neighbor joining (NJ) and maximum likelihood (ML) techniques, as well as by a posteriori probability for Bayesian inference (BI) analysis. Genetic data confirm the validity of the assignment of *Cucumaria fraudatrix* to the genus *Eupentacta* Deichmann, 1938. The study of sequences obtained from the holothurian specimens collected in Russian waters, near the city of Vladivostok, and determined by morphological characters clearly indicate that these specimens belong to the genus *Eupentacta* and are assigned as *E. fraudatrix*. The specimens from China in GenBank named as *Sclerodactyla multipes* and used in the present study, were likely misidentified, and after re-examination they may be assigned to the genus *Eupentacta*, either as *E. fraudatrix* or another taxon. Analyses of morphological characters of *S. multipes* unequivocally affirm that this species must be excluded from *Sclerodactyla* Ayres, 1851 and is provisionally assigned to the genus *Sclerothyone* Thandar, 1989 based on the external morphological characters and the body wall ossicles.

Key words: 16S rRNA, COI, mitochondrial DNA, mtDNA, molecular phylogeny, *Sclerodactyla*, *Sclerothyone*, Sea of Japan, taxonomy



Academic editor: Sabine Stöhr

Received: 25 December 2023

Accepted: 14 March 2024

Published: 18 April 2024

ZooBank: <https://zoobank.org/58301587-72BB-4BA0-9A20-D1445FB7AB72>

Citation: Turanov SV, Smirnov AV, Kartavtsev YuPh (2024) Taxonomic position of holothurian *Eupentacta fraudatrix* (Echinodermata, Holothuroidea). ZooKeys 1197: 237–248. <https://doi.org/10.3897/zookeys.1197.117752>

Copyright: © Sergei V. Turanov et al. This is an open access article distributed under terms of the Creative Commons Attribution License ([Attribution 4.0 International – CC BY 4.0](https://creativecommons.org/licenses/by/4.0/)).

Introduction

The holothurian *Eupentacta fraudatrix* (Djakonov & Baranova in Djakonov, Baranova & Saveljeva, 1958) is currently used as a model species in numerous studies on biology, anatomy, histology, embryology, regeneration, biochemistry, chemistry of natural compounds, etc. A complete bibliography of studies conducted on *E. fraudatrix* up to 2015 was provided by Panina (2015).

The genus *Eupentacta* was erected by Deichmann (1938) to include the type species *Cucumaria quinquesemita* Selenka, 1867 and a new species that

she described, *Eupentacta pseudoquinquesemita* Deichmann, 1938. Panning (1949) established the family Sclerodactylidae and placed the genus *Eupentacta* in it. Unfortunately, he did not provide support for this decision, and subsequent researchers did not provide the dedicated considerations of the genus *Eupentacta* in their taxonomic studies. In the World Register of Marine Species (WoRMS 2024a, *Eupentacta* Deichmann, 1938; <https://www.marinespecies.org/aphia.php?p=taxdetails&id=528610>), the genus *Eupentacta* is included in the family Sclerodactylidae with the following species assigned to it: *Eupentacta quinquesemita* (with *Cucumaria chronhjelmi* Théel, 1886 as a synonym), *E. pseudoquinquesemita*, *E. fraudatrix*, and *E. exigua* (Ludwig, 1875) (WoRMS 2024a; *Eupentacta* Deichmann, 1938; <https://www.marinespecies.org/aphia.php?p=taxdetails&id=528610>).

Eupentacta fraudatrix is very common in bays of Primorsky Krai, southwestern Sakhalin, and in the southern Kuril Islands at depths of 0–40 m, but mostly at 0–10 m. Morphology, anatomy, skeletal elements, and distribution of this species were described by Djakonov et al. (1958), Baranova (1971), Stukova and Levin (1990), Levin and Bekova (2005), and Panina (2015). This species was initially described in *Cucumaria* de Blainville, 1830 (Djakonov et al. 1958). Baranova (1979) placed this species in *Eupentacta* without providing evidence to support her viewpoint, but this placement was accepted by subsequent researchers without comment, and this species is currently considered to belong to that genus (WoRMS 2024a; <https://www.marinespecies.org/aphia.php?p=taxdetails&id=528610>).

The type species of *Eupentacta*, *E. quinquesemita* (Selenka, 1867), inhabits waters off the Pacific coast of North America from Kodiak Island and Baranof Island (Alaska) to southern California and Mexico at depths from 0 to 55 m. *Cucumaria chronhjelmi*, which was described from Vancouver Island, was synonymized to *E. quinquesemita* by Deichmann (1938: 110). Lambert (1997) gave information on the biology of *E. quinquesemita* and the similar species *E. pseudoquinquesemita* and provided a list of publications including these species as model organisms off the west coast of Canada.

Eupentacta pseudoquinquesemita has been found near the Commander and Aleutian Islands and along the North American Pacific coast from Kodiak Island to Puget Sound at depths from 0 to 228 m. A brief description of its morphology and skeletal elements was made available by Deichmann (1938) and Lambert (1997).

Sclerodactyla Ayres, 1851 had been considered a synonym of *Thyone* Oken, 1815 for many years. Panning (1949) restored it as an independent genus and designated it as the type genus of the family Sclerodactylidae, which he established. The type species of *Sclerodactyla* is *Holothuria briareus* Lesueur, 1824 by original designation. Panning (1949) also placed *Cucumaria longipeda* Semper, 1867 (now *Phyllophorella longipeda*, family Phyllophoridae) and *Cucumaria multipes* Théel, 1886 in *Sclerodactyla*, but without discussion. Since Panning (1949), *Sclerodactyla* has not been the subject of dedicated taxonomic research. In WoRMS (2024c <https://www.marinespecies.org/aphia.php?p=taxdetails&id=158531>), two species are assigned to *Sclerodactyla*: *Sclerodactyla briareus* (Lesueur, 1824) and *S. multipes* (Théel, 1886).

Sclerodactyla briareus lives in waters off the North American Atlantic coast from Nova Scotia to Florida, and in the Gulf of Mexico and off Venezuela. The species

has been recorded from habitats at depths from 0 to 183 m (Hendler et al. 1995). The external morphology, anatomy, and structure of skeletal elements were described by Clark (1902), Coe (1912), Deichmann (1930), and Hendler et al. (1995). Information on this species' biology and a brief overview of studies on *S. briareus* and its utility for biological research are provided by Hendler et al. (1995).

Sclerodactyla multipes was described from a single, fragmented specimen from Yokohama, Japan (Théel 1886). Later, specimens identified as *Cucumaria multipes* (= *Sclerodactyla multipes*) were collected off the Japanese coast, including at Yokohama and along the Sea of Okhotsk coast of Hokkaido Island (Mitsukuri 1912), in the Yellow Sea in Chinese waters, Chefoo Harbour (Chang 1948), and in the Korea Strait (Rho and Shin 1984; Shin and Rho 1996). These articles provide descriptions and drawings of the external morphology, the calcareous ring, ossicles from the body wall, introvert, podia, and tentacles.

Because the taxonomic position of *E. fraudatrix* has not been well established, we performed additional research on this species. In the last decade, molecular genetics methods have been regularly used taxonomy, including in the class Holothuroidea (e.g. Arndt et al. 1996; Miller et al. 2017). To clarify the systematic position of *E. fraudatrix*, we analyzed ribosomal RNA (rRNA) sequences in the 16S rRNA gene region and mitochondrial DNA (mtDNA) in the cytochrome c oxidase (COI) gene. We also used data from GenBank for a comparative analysis (<https://www.ncbi.nlm.nih.gov/>) with subsequent verification using the MIDORI server (Leray et al. 2018). 16S rRNA and COI mtDNA sequences were obtained from *E. quinquesemita*, the type species of the genus *Eupentacta*, and *E. pseudoquinquesemita*. Sequence data were also collected for the following species of *Sclerodactyla*, the type genus of the family Sclerodactylidae: *S. briareus*, the type species of the genus, and *S. multipes*. Unfortunately, sequences of Chinese specimens treated as *S. multipes* in GenBank and used in the current study have not been published, nor is their identity supported by morphological data; obviously they cannot be attributed with certainty to *S. multipes*. In other words, the possibility of misnamed specimens (as sometimes happens with GenBank records) cannot be ruled out. Despite this, we use the name "*S. multipes*" to refer to these specimens, as they appear in GenBank.

Materials and methods

Three individuals of *Eupentacta fraudatrix* were collected from a depth of 1–4 m in Patrokl Cove, Peter the Great Bay, Sea of Japan (43.1619°N, 131.9164°E) in June 2021. From these individuals, tissue specimens were fixed in 95% ethyl alcohol. DNA was extracted from muscle tissue using a K-Sorb kit (Syntol LLC, Moscow). A PCR was performed using the primers 16Sar/16Sbr (Palumbi 1996) and LCO1490/HC02198 (Folmer et al. 1994), respectively, with a 20 µL cocktail including 10 µL AmpliTaq Gold 360 Master Mix (ThermoFisher Scientific, USA), 0.5 µL of each (forward and reverse) primer (10 µM), 0.16 µL bovine serum albumin, 1 ng DNA, and deionized water for the remaining volume. The PCR algorithm for both fragments consisted of preheating at 94 °C for 2 min and then 35 cycles with denaturation at 94 °C for 30 s, annealing at 42 °C for 40 s, and elongation at 72 °C for 1 min; the final stage of elongation lasted 10 min. Amplicons were verified using electrophoresis in a 1% agarose gel (Helicon, Russia; <https://www.helicon.ru/>), visualized with ethidium bromide under transmitted UV light.

The alcohol-purified amplicons were used for forward and reverse stepping sequencing with appropriate primers (see above) and a BrightDye™ Terminator Cycle Sequencing Kit v. 3.1 (NimaGen, The Netherlands). Capillary electrophoresis was performed on an ABI Prism 3500 DNA sequencer. The obtained chromatograms were edited in Geneious (Kearse et al. 2012). The sequences were deposited in GenBank (Benson et al. 2018) under accession nos. OR288149–OR288151 (COI) and OR289514–OR289515 (16S rRNA). Original specimens of fixed animals are at the NSCMB FEB RAS in the personal collection of S.V. Turanov.

We accessed 21 COI mtDNA and 11 16S rRNA sequences from GenBank for comparison. Alignment was carried out separately for each marker in the MEGA 7 software package (Kumar et al. 2016) by the Muscle algorithm (Edgar 2004). Estimation of genetic distances, *p*-distances, was also performed in MEGA 7 (Nei and Kumar 2000). External indels were encoded as missing data (“?”). Selection of models for nucleotide substitutions and phylogenetic analysis of sequences by the neighbor-joining (NJ) and maximum-likelihood (ML) techniques with evaluation of the stability of topologies by the nonparametric bootstrap test was carried out using a set of respective functions in the phangorn (Schliep 2011) and ape packages (Paradis et al. 2004) of the R environment (R Core Team 2021). Bayesian-inference (BI) phylogeny was inferred in the MrBayes 3.2.7 software (Ronquist et al. 2012). A complex simultaneous selection of an optimal model for nucleotide substitutions implemented in MrBayes and gene partitions that that were taken into account (COI sequences) and were not taken into account (16S rRNA sequences) was made on the basis of AIC value in the PartitionFinder 2.0 software (Guindon et al. 2010; Lanfear et al. 2012, 2014). The search for tree topology and marginal values of *a posteriori* probability was performed by running four Markov chains for $n = 10^6$ generations. The rate of sampling topologies and parameters by the metropolis algorithm was 1 per 100 generations. The first 25% of the trees corresponding to the burn-in step were discarded as suboptimal. A consensus tree was constructed based on the remaining $n = 15,002$ topologies. The convergence indices (ESS, PSRF) indicated a sufficient sample for all parameters. Combined visualization of the topologies was obtained by the *cophylo* function in the phytools package (Revell 2023). The NJ topology comprises the basic tree for comparison and two others used for illustrative needs (Fig. 1).

Results and discussion

The length of the COI sequences matrix after alignment was 888 base pairs (bp). Of these, 267 sites were variable, including 162 parsimony informative and 103 singleton sites. The 16S rRNA sequence matrix after alignment consisted of 569 bp, of which 186 were variable, including 97 parsimony informative and 88 singleton ones. In the COI phylogenetic tree (Fig. 1), a branch with significant support was formed that combined two deeply divergent groups consisting of the sequences of *Eupentacta pseudoquinquesemita* and *E. quinquesemita* (group 1, with high support scores of 99/96/99% for the three techniques used, consequently), and also *S. multipes* and *E. fraudatrix* (group 2, with support scores of 99/88/90%). *Eupentacta pseudoquinquesemita* and *E. quinquesemita* were well-supported sisters, as were *S. multipes* and *E. fraudatrix*. The divergence between members of these two groups have a *p*-distance of 0.06–0.07, and 0.05 between *E. pseudoquinquesemita*–*E. quinquesemita* and 0.03 between

S. multipes–*E. fraudatrix*. Intraspecific *p*-distances were all ≤ 0.01 . *Sclerodactyla* was paraphyletic. However, in view of the possible mislabeling of five specimens from China, we have to raise a question about the presence of a new taxon in the area and will send a note to GenBank with the suggestion of relabeling these five specimens. The rank of this taxon is subspecies–species, as we clarify below.

The 16S rRNA-based tree showed less comparative material, but the relationships of the genera *Eupentacta* and *Sclerodactyla*, similarly, is paraphyletic and certain tree topologies are unresolved. The main branch is well supported, but represented by a large number of taxa, including *Pentamera* Ayres, 1852, whose species diverged from other representatives with the *p*-distance of 0.08–0.11 (mean 0.09 ± 0.01). The interspecific *p*-distance in this genus was 0.05. In the *Eupentacta*–*Sclerodactyla* branch, which is also highly supported, the closest branch comprised only of *E. fraudatrix* sequences. *Eupentacta quinquesemita* took a basal position here. The interspecific divergence ranged from 0.03 (*E. fraudatrix*–*S. multipes*) to 0.07 (*E. fraudatrix*–*E. quinquesemita*). The intraspecific variability was as above ≤ 0.01 . The order of species, depending on distance from the main branch, was as follows: *Pachythyone rubra* (Clark, 1901) (divergence with respect to *E. fraudatrix*, 0.21) and *Sclerodactyla briareus* (0.22). Representatives of the genus *Pentactella* Verrill, 1876 formed a clear outgroup in this topology.

In this paper, we combined information on 20 specimens for COI and seven specimens for 16S rRNA from the genus *Eupentacta* (Fig. 1). Five specimens from one area of China (unfortunately, no precise information was given on the sample location by the submitters of sequences to GenBank, but provisionally the samples were collected near Qingdao City) are obviously not a comprehensive sample. We are going to expand our research in the future, but for this paper, the present samples appear suitable for a valid conclusion. Thus, the divergence between specimens from Russia and China is close to 3%, as it is given above. However, this amount of divergence cannot be explained by the intraspecific variability, e.g., even our own dataset presented above and the one comprised of COI and 16S rRNA sequences provide supportive information. The divergence between members of two groups of *S. multipes* and *E. fraudatrix* in the *p*-distance value was 0.06–0.07 (6–7%) with a mean of 0.065 ± 0.005 . The divergence within the groups was 0.05 (*E. pseudoquinquesemita*–*E. quinquesemita*) and 0.03 (*S. multipes*–*E. fraudatrix*). The intraspecific *p*-distances in all the above-listed species were not greater than 0.01 (1%). Looking at a comprehensive review of over 20,000 invertebrate and vertebrate specimens, the score of genetic distances estimated at different taxon levels could explain the matter (e.g. Kartavtsev 2011, 2013). The distance data revealed increasing levels of genetic divergence of the sequences of the two genes, cytochrome b (Cyt-b) and COI, in the five groups compared: (i) populations within a species; (ii) subspecies, semi-species, or/and sibling species; (iii) species within a genus; (iv) species from different genera within a family; and (v) species from separate families within an order. The mean unweighted scores of *p*-distances (%) for these five groups for Cyt-b were as follows: (i) 1.38 ± 0.30 ; (ii) 5.10 ± 0.91 ; (iii) 10.31 ± 0.93 ; (iv) 17.86 ± 1.36 ; and (v) 26.36 ± 3.88 , respectively; and for COI, the scores were the following: (i) 0.89 ± 0.16 ; (ii) 3.78 ± 1.18 ; (iii) 11.06 ± 0.53 ; (iv) 16.60 ± 0.69 ; and (v) 20.57 ± 0.40 . Evidently, the intraspecific level for these two gene markers is approximately 1%, i.e., that is the exact value we had in our *multipes* and *fraudatrix* data for the two analyzed genes.

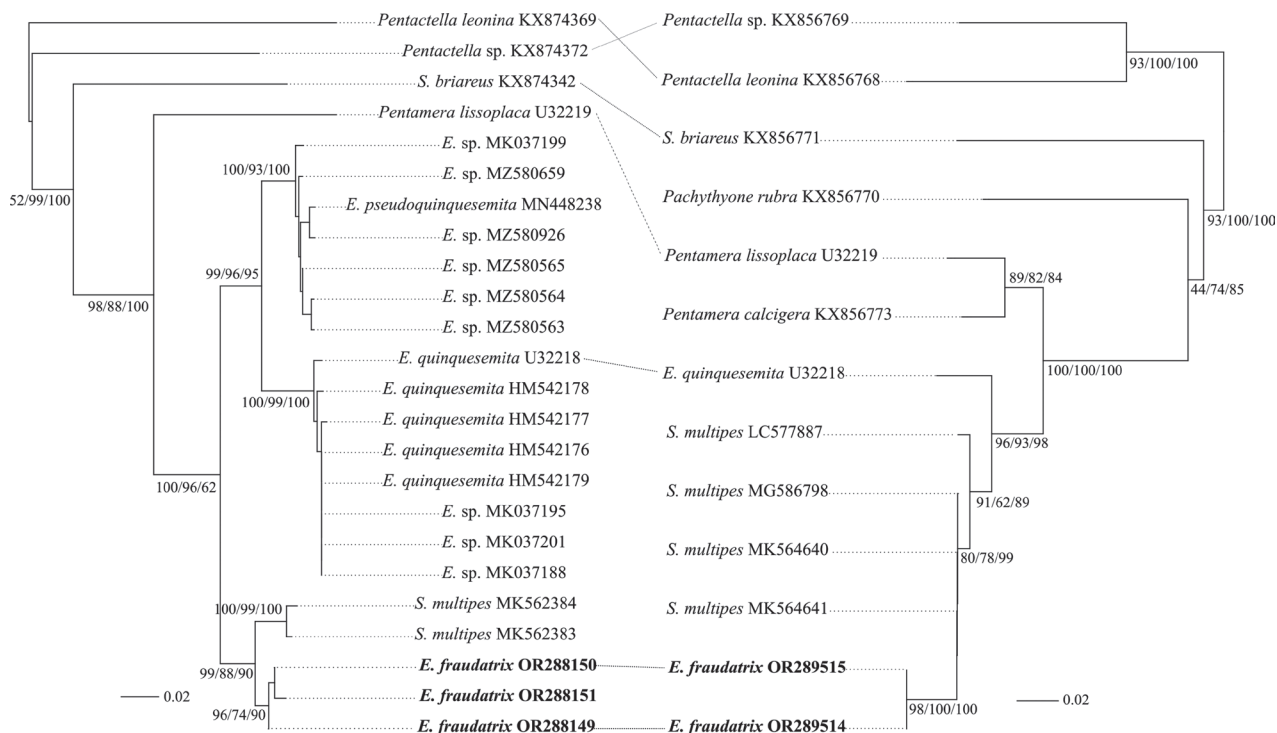


Figure 1. Co-phylogram plot showing relationships of the genera *Eupentacta* and *Sclerodactyla*, with related holothurians, as inferred from a phylogenetic analysis of the COI (left) and 16S rRNA (right) gene sequences. The trees were rooted at a midpoint. The numerals at the nodes are nonparametric bootstrap test (NJ, ML) and *a posteriori* probability (BI, %) values (the order is NJ/ML/BI). The dotted line connects the identifiers of the sequences from the same specimen. The sequences obtained in the present study are indicated with bold letters. The scale on the left and right bottom shows the relative length of branches in two gene trees.

We also must consider whether *S. multipes* from China is a separate taxon. The topology of the gene trees for COI and 16S rRNA may be even more important, and this allows us to place the Chinese samples jointly with other *Eupentacta* species, i.e., the topology in that part of the whole tree combines “*multipes*” and “*fraudatrix*”. The two trees show high support for the integrity of each of the two datasets by the three techniques of tree building (Fig. 1; 99/88/90% for COI and 80/78/99% for 16S rRNA). Thus, molecular genetics alone give good support to the Chinese samples as an independent taxon at the subspecies/semi-species level and place it, with the reservations made in the Introduction, definitely near the genus *Eupentacta*. DNA barcoding considers a 2–4% difference the threshold for the intraspecies/species discrimination (Ward 2009; Turanov and Kartavtsev 2014).

A comparison of the morphological traits of *S. briareus* and *S. multipes* clearly indicates that these species do not belong to the same genus. In *S. briareus*, tube feet are located all over the body, while in *S. multipes* they are bounded only by radii, as in *Eupentacta*. In *S. briareus*, the radial and interradial plates of the calcareous ring are connected for two-thirds of their length (Clark 1902: pl. 13, fig. 95; Panning 1949: 459); in *S. multipes*, the structure of the calcareous ring in the holotype is unknown, but in the specimens that were subsequently identified as *S. multipes*, the calcareous ring plates are connected only in the lower part (Chang 1948: 77, fig. 20j; Shin and Rho 1996: 541, fig. 136). The close similarity of Chinese sequences to *E. fraudatrix* sequences raises doubts that Chinese researchers correctly identified the studied specimens, since the structure and composition of

the ossicles vary greatly between *E. fraudatrix* and *S. multipes*. It is possible that these workers were not dealing with *S. multipes*, but instead with a close relative of *E. fraudatrix*, although neither *E. fraudatrix* nor forms close to this species had previously been recorded off the Chinese coast. The taxonomic morphological characters of *S. briareus* and *S. multipes* clearly indicate that *S. multipes* must be excluded from *Sclerodactyla*. *Sclerodactyla multipes* should provisionally be placed in the genus *Sclerothyone* Thandar, 1989 based on the structure of the ossicles of the body wall. This placement is supported by the fact that the closely related *Havelockia nozawai* (Mitsukuri, 1912), described from Japanese waters and considered a possible synonym of *Sclerodactyla multipes* by Chang (1948: 76), was recently placed in *Sclerothyone* by Thandar (2021: 509–511).

Conclusions

The obtained molecular genetics data confirm the assignment of *Cucumaria fraudatrix* from Russian waters to the genus *Eupentacta*. *Sclerodactyla multipes* unequivocally cannot remain in the genus *Sclerodactyla* and, based on morphological characters, should provisionally be placed in *Sclerothyone*. In the diagnosis of *Eupentacta*, the molecular data and morphology of the calcareous ring structure are considered. The diagnosis is given below.

The position of the genus *Eupentacta* in the system of the order Dendrochirotida remains poorly resolved. Based on the calcareous ring structure, *Eupentacta* does not fit well in the family Sclerodactylidae. In the description of *Eupentacta* (Deichmann 1938: 110), it was noted that it is intermediate in position between the genera *Pentamera* (family Thyonidae) and *Pentacta* Goldfuss, 1820 (family Cucumariidae). Our analysis of molecular data indicates the proximity of *Eupentacta* to *Pentamera* (Fig. 1). Our study supports the need for a revision of the order Dendrochirotida, based on both molecular genetics and morpho-anatomical data collected by modern methods. Until the families Sclerodactylidae, Sclerothyonidae, and Thyonidae are revised, we temporarily leave *Eupentacta* in the Sclerodactylidae. Below is an updated diagnosis of the genus *Eupentacta*.

Figs 2, 3 (a drawing and an SEM photomicrograph) illustrate the key morphological characters of the genus *Eupentacta*.

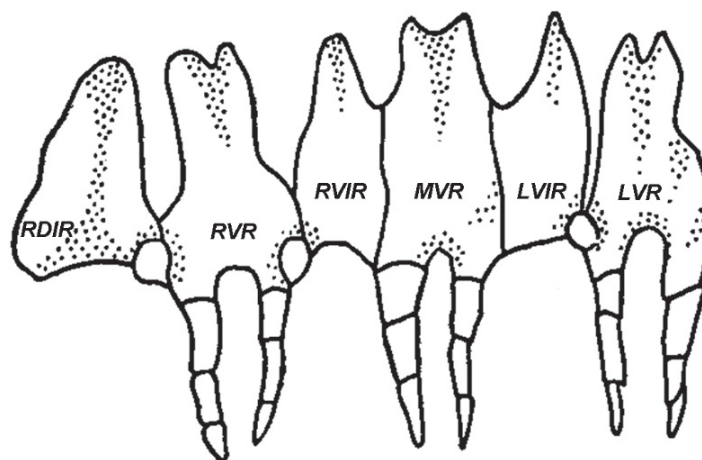


Figure 2. Part of the calcareous ring of *Eupentacta fraudatrix*. RDIR, right dorsal interradial plate; RVR, right ventral radial plate; RVIR, right ventral interradial plate; MVR, medioventral radial plate; LVIR, left ventral interradial plate; LVR, left ventral radial plate (from Baranova 1971).

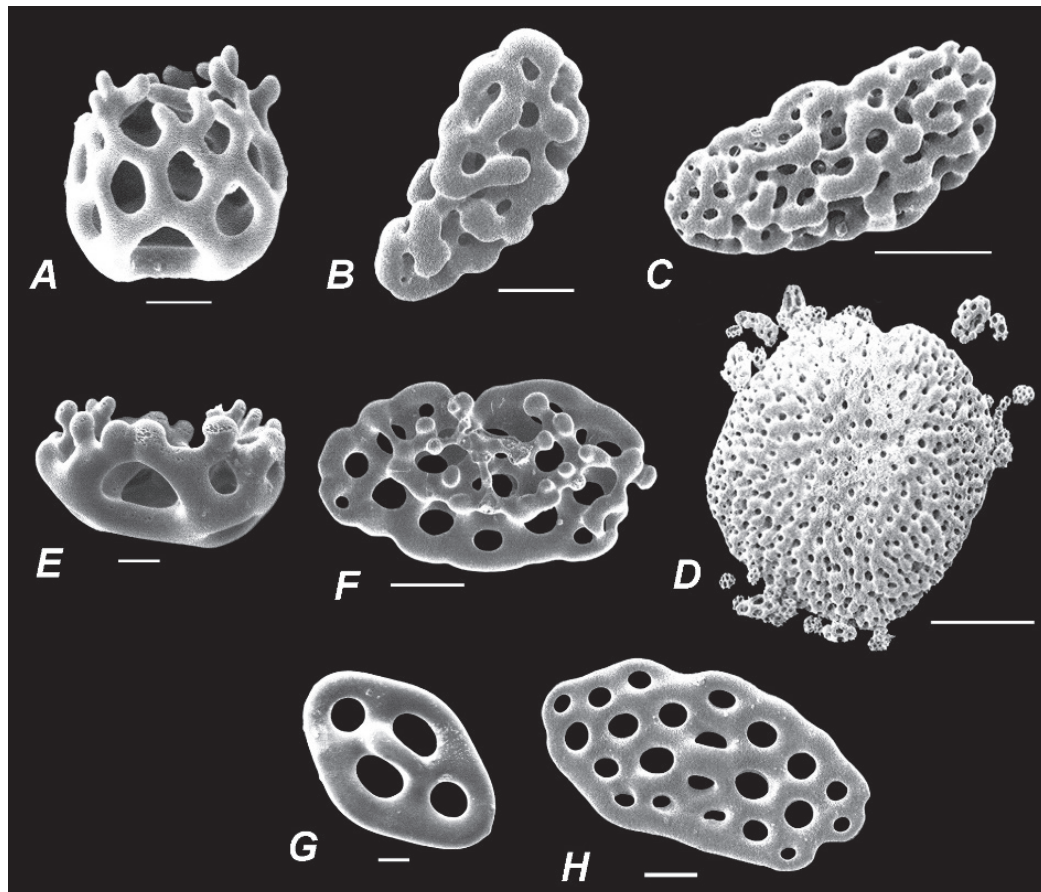


Figure 3. SEM photomicrographs of the body wall ossicles of *Eupentacta* species **A–D** *E. quinquesemita*, Mendocino, California (holotype, Museum of Comparative Zoology at Harvard University) **A** basket **B** knobbed plate **C** fenestrated hollow ellipsoid **D** very large scale-like multilayer plate **E, F** *E. pseudoquinquesemita*, Kodiak Island, Shelikof Strait, Uyak Bay, Heard of Larson's Inlet, Alaska (paralectotype, United States National Museum E2288) **E** basket **F** irregular plate with tubercles rising above **G, H** *E. fraudatrix*, Peter the Great Bay, Vostok Bay, Russia **G** plate with oval disk with four holes and a handle-like arch between the two holes in the longitudinal axis (underdeveloped table with modified 2-pillared spire?) **H** plate with small elevation in the center. Scale bars: 10 μm (**A, B, E, G**); 30 μm (**F, H**); 100 μm (**C, D**).

Emended, updated diagnosis

Genus *Eupentacta* Deichmann, 1930

Medium-sized holothurians, with cylindrical body and rounded posterior end. Tube feet confined to ambulacra; 10 tentacles, two ventral tentacles smaller than others; anus surrounded by five small anal papillae. Radial plates of calcareous ring with fairly short posterior processes smaller in length than plate height; posterior processes consisting of 2–3 pieces; anterior part of radial plates narrowed toward anterior margin; small notch present on anterior margin; interradial plates triangular, pointed anteriorly, without posterior processes; medioventral radial plate and two adjacent interradial plates fused together in the lower and middle parts for approximately $\frac{2}{3}$ of plate height into single plate; other radial and interradial plates separate and articulate with each other only in their lower part. Body wall ossicles: in outer layer of body wall in form of baskets; in deeper layers of body wall different ossicles specific to each species present: large knobbed plates, fenestrated hollow ellipsoids and very large scale-like multilayer plates (in *E. quinquesemita*); irregular plates with tubercles rising above (in *E. pseudo-*

quinquesemita); plates usually with oval disk with four or sometimes more holes and a handle-like arch between the two holes in the longitudinal axis in the middle layer (underdeveloped tables with modified 2-pillared spire?), and different plates with 4–6 and more holes up to large massive plates with numerous holes with small elevation in the center in the deep layer (in *E. fraudatrix*). Tube feet ossicles supporting tables with elongated narrow base and small column or with reduced column in form of bridge, and large, well-developed, rounded end plate. Tentacle ossicles elongated rods with small holes.

Type species. *Cucumaria quinquesemita* Selenka, 1867.

Other species included. *Eupentacta pseudoquinquesemita* Deichmann, 1938; *Cucumaria fraudatrix* Djakonov & Baranova in Djakonov, Baranova & Saveljeva, 1958, and in question *Cucumaria exigua* Ludwig, 1875.

Eupentacta differs from other genera of Sclerodactylidae and Thyonidae in the structure of the calcareous ring: the medioventral radial plate is fused with the adjacent interradial plates. *Eupentacta* also differs from *Sclerodactyla* Ayres, 1851 and *Pachythyone* Deichmann, 1941 (Sclerodactylidae) in having the podia restricted to radia, scattered over the whole body in *Sclerodactyla*, settled along the radii and numerous in the interradia in *Pachythyone*, and strictly located along the radii in *Eupentacta*; from the genus *Sclerothyone* (Sclerothyonidae) it differs by the presence of baskets in the surface layer of the body wall, and the absence of tables with well-developed 2-pillared spires in the body wall. It differs from *Pentamera* Ayres, 1852 (Thyonidae) by body shape: curved upwards and gradually tapering posteriorly in *Pentamera* and cylindrical with rounded posterior end in *Eupentacta*.

Acknowledgements

Authors are very thankful to Dr Igor Yu. Dolmatov for the idea of molecular genetic validation of the holothurian *Eupentacta fraudatrix* and sharing the animal specimens. We also would like to extend our thanks to Evgeny P. Shvetsov and Anastasia D. Chera for their careful translation of the manuscript into English and the proofreading of the revised paper.

Additional information

Conflict of interest

The authors have declared that no competing interests exist.

Ethical statement

This study does not require ethical approval because no procedures were performed on live animals, and the tissue samples used were collected from dead specimens.

Funding

This work was supported by the A.V. Zhirmunsky National Scientific Center of Marine Biology, Far Eastern Branch of Russian Academy of Sciences (1021062912508-7).

Author contributions

Conceptualization: YPK. Data curation: YPK, AVS, SVT. Funding acquisition: YPK. Methodology: YPK, AVS, SVT. Project administration: YPK. Software: SVT. Supervision: YPK. Visualization: SVT. Writing - original draft: AVS, YPK, SVT. Writing - review and editing: YPK.

Author ORCIDs

Sergei V. Turanov  <https://orcid.org/0000-0003-4829-9729>

Alexey V. Smirnov  <https://orcid.org/0000-0002-7350-9276>

Yuri Ph. Kartavtsev  <https://orcid.org/0000-0002-0436-4763>

Data availability

The gene sequence data of this study are openly available in GenBank of NCBI at (<https://www.ncbi.nlm.nih.gov/>) under the accession nos.: OR288149–OR288151 (COI) and OR289514–OR289515 (16S rRNA). Other options could be requested from the authors.

References

- Arndt A, Marquez C, Lambert P, Smith MJ (1996) Molecular phylogeny of eastern Pacific sea cucumbers (Echinodermata: Holothuroidea) based on mitochondrial DNA sequence. *Molecular Phylogenetics and Evolution* 6(3): 425–437. <https://doi.org/10.1006/mpev.1996.0091>
- Baranova ZI (1971) Echinoderms from the Possjet Bay of the Sea of Japan. *Explorations of the fauna of the seas* 8(16): 242–264. [In Russian]
- Baranova ZI (1979) Composition and distribution of holothurians (Echinodermata, Holothuroidea) on the shelf of the North-Western Pacific. In: Zhirmunsky AV (Ed.) XIV Pacific Science Congress. USSR, Khabarovsk, August 1979. Committee for marine sciences. Section F II. Marine biology. Section F II. a. Biology of shelf. Abstracts of papers. Pacific Sciences Association, Moscow, 76–77.
- Benson DA, Cavanaugh M, Clark K, Karsch-Mizrachi I, Ostell J, Pruitt KD, Sayers EW (2018) GenBank. *Nucleic Acids Research* 46(D1): D41–D47. <https://doi.org/10.1093/nar/gkx1094>
- Chang F-Y (1948) Echinoderms of Tsingtao. *Contributions from the Institute of Zoology National Academy of Peiping* 4(2): 33–104. [pls 1–11]
- Clark HL (1901) Echinoderms from Puget Sound: observations made on the Echinoderms collected by the parties from Columbia University, in Puget Sound in 1896 and 1897. *Proceedings Boston Society Natural History* 29(15): 323–337. [pls 1–4]
- Clark HL (1902) The echinoderms of the Woods Hole Region. *Bulletin of the United States Fish Commission* 22: 547–576. [pls 1–14]
- Coe WR (1912) Echinoderms of Connecticut. *State geological and natural History Survey, Bulletin* 19: 1–152. [pls 1–32] <https://doi.org/10.5962/bhl.title.56252>
- Deichmann E (1930) The Holothurians of the western part of the Atlantic Ocean. *Bulletin of the Museum of Comparative Zoology at Harvard College* 71(3): 43–226. [pls 1–24]
- Deichmann E (1938) New holothurians from the western coast of North America and some remarks on the genus *Caudina*. *Proceedings New England Zoological Club* 16: 103–115.
- Djakonov AM, Baranova ZI, Saveljeva TS (1958) Note on holothurians (Holothuroidea) of the region of southern Sakhalin and the southern Kuril Islands. *Research of the Far Eastern Seas of the USSR* 5: 358–380. [In Russian]
- Edgar RC (2004) MUSCLE: Multiple sequence alignment with high accuracy and high throughput. *Nucleic Acids Research* 32(5): 1792–1797. <https://doi.org/10.1093/nar/gkh340>
- Folmer O, Black M, Hoeh W, Lutz R, Vrijenhoek R (1994) DNA primers for amplification of mitochondrial cytochrome c oxidase subunit I from diverse metazoan invertebrates. *Molecular Marine Biology and Biotechnology* 3(5): 294–299.

- Guindon S, Dufayard JF, Lefort V, Anisimova M, Hordijk W, Gascuel O (2010) New algorithms and methods to estimate maximum-likelihood phylogenies: Assessing the performance of PhyML 3.0. *Systematic Biology* 59(3): 307–321. <https://doi.org/10.1093/sysbio/syq010>
- Hendler G, Miller JE, Pawson DL, Kier PM (1995) *Sea Stars, Sea Urchins, and Allies Echinoderms of Florida and the Caribbean*. Smithsonian Institution Press, Washington DC, [xii +] 390 pp.
- Kartavtsev YP (2011) Sequence divergence at Co-1 and Cyt-b mtDNA on different taxonomic levels and genetics of speciation in animals. *Mitochondrial DNA* 2: 55–65. <https://doi.org/10.3109/19401736.2011.588215>
- Kartavtsev YP (2013) Genetic divergence of species and other taxa. Geographical speciation and the genetic paradigm of Neo-Darwinism in action. *Uspekhi Sovremennoi Biologii* 5: 419–451.
- Kearse M, Moir R, Wilson A, Stones-Havas S, Cheung M, Sturrock S, Buxton S, Cooper A, Markowitz S, Duran C, Thierer T, Ashton B, Meintjes P, Drummond A (2012) Geneious Basic: An integrated and extendable desktop software platform for the organization and analysis of sequence data. *Bioinformatics (Oxford, England)* 28(12): 1647–1649. <https://doi.org/10.1093/bioinformatics/bts199>
- Kumar S, Stecher G, Tamura K (2016) MEGA7: Molecular evolutionary genetics analysis version 7.0 for bigger datasets. *Molecular Biology and Evolution* 33(7): 1870–1874. <https://doi.org/10.1093/molbev/msw054>
- Lambert P (1997) *Sea cucumbers of British Columbia, Southeast Alaska and Puget Sound*. Royal British Columbia Museum Handbook. UBC Press, Vancouver, 166 pp. [16 pls]
- Lanfear R, Calcott B, Ho SYW, Guindon S (2012) PartitionFinder: Combined selection of partitioning schemes and substitution models for phylogenetic analyses. *Molecular Biology and Evolution* 29(6): 1695–1701. <https://doi.org/10.1093/molbev/mss020>
- Lanfear R, Calcott B, Kainer D, Mayer C, Stamatakis A (2014) Selecting optimal partitioning schemes for phylogenomic datasets. *BMC Evolutionary Biology* 14(1): 82. <https://doi.org/10.1186/1471-2148-14-82>
- Leray M, Ho SL, Lin IJ, Machida RJ (2018) MIDORI server: A webserver for taxonomic assignment of unknown metazoan mitochondrial-encoded sequences using a curated database. *Bioinformatics (Oxford, England)* 34(21): 3753–3754. <https://doi.org/10.1093/bioinformatics/bty454>
- Levin VS, Bekova NV (2005) Dendrochirotida holothurians of the Far Eastern Seas by the collections of TINRO-center. *Izvestiâ Tihookeanskogo naučno-issledovatel'skogo rybohozâjstvennogo centra* 142: 310–322. [In Russian]
- Miller AK, Kerr AM, Paulay G, Reich M, Wilson NG, Carvajal JI, Rouse GW (2017) Molecular phylogeny of extant Holothuroidea (Echinodermata). *Molecular Phylogenetics and Evolution* 111: 110–131. <https://doi.org/10.1016/j.ympev.2017.02.014>
- Mitsukuri K (1912) Studies on Actinopodous Holothuroidea. *Journal of the College of Science, Imperial University of Tokyo* 29(2): 1–284. [pls 1–8] <https://doi.org/10.5962/bhl.title.37880>
- Nei M, Kumar S (2000) *Molecular Evolution and Phylogenetics*. Oxford University Press, Oxford and New York, [xiv +] 333 pp.
- Ohshima H (1918) Northwestern Pacific holothurians collected by the U.S. Fisheries Steamer “Albatross”. *Dobutsugaku zasshi [Zoological Magazine]* 30: 177–182. [In Japanese]
- Palumbi S (1996) Nucleic acids II: The polymerase chain reaction. In: Hillis D, Moritz C, Mable B (Eds) *Molecular Systematics*. Sinauer & Associates, Sunderland, Massachusetts, 205–247.

- Panina EG (2015) List of species of the sea cucumbers (Holothuroidea) in the Far-Eastern seas of Russia, IV. Families Sclerodactylidae, Thyonidae, Ypsilorthuriidae and Thyonidiidae (Echinodermata: Holothuroidea: Dendrochirotida). Bulletin of Kamchatka State Technical University 33: 37–53. [In Russian] <https://doi.org/10.17217/2079-0333-2015-33-37-53>
- Panning A (1949) Versuch einer Neuordnung der Familie Cucumariidae (Holothuroidea, Dendrochirota). Zoologische Jahrbücher. Abteilung für Systematik, Ökologie und Geographie der Tiere 78(4): 403–470.
- Paradis E, Claude J, Strimmer K (2004) APE: Analyses of phylogenetics and evolution in R language. Bioinformatics (Oxford, England) 20(2): 289–290. <https://doi.org/10.1093/bioinformatics/btg412>
- R Core Team (2021) R: a language and environment for statistical computing. R Foundation for Statistical Computing, Vienna, Austria. <https://www.R-project.org/>
- Revell LJ (2023) phytools 2.0: an updated R ecosystem for phylogenetic comparative methods (and other things). BioRxiv 2023-03. <https://doi.org/10.1101/2023.03.08.531791>
- Rho BG, Shin S (1984) A systematic study on the Holothuroidea in Korea. 1 Dendrochirotida. Bulletin of Institute of Littoral Biota Mokpo National College 1(1): 43–55.
- Ronquist F, Teslenko M, Van Der Mark P, Ayres DL, Darling A, Höhna S, Larget B, Liu L, Suchard MA, Huelsenbeck JP (2012) MrBayes 3.2: Efficient bayesian phylogenetic inference and model choice across a large model space. Systematic Biology 61(3): 539–542. <https://doi.org/10.1093/sysbio/sys029>
- Schliep KP (2011) phangorn: Phylogenetic analysis in R. Bioinformatics (Oxford, England) 27(4): 592–593. <https://doi.org/10.1093/bioinformatics/btq706>
- Selenka E (1867) Beiträge zur Anatomie und Systematik der Holothurien. Zeitschrift für wissenschaftliche Zoologie 17: 291–374. [pls 18–20]
- Shin S, Rho BG (1996) Illustrated Encyclopedia of Fauna and Flora of Korea. Vol. 36. Echinodermata. Ministry of Education, Seoul, 780 pp. [in Korean]
- Stukova TV, Levin VS (1990) Age-related changes in the spicules of holothurian *Eupentacta fraudatrix*. Vladivostok. Manuscript deposited in VINITI on 09/20/1990, No. 5109 B90, 17 pp. [In Russian]
- Thandar A (2021) Nomenclatural changes in some sea cucumbers with the erection of a new genus and description of a *Thyone?* juvenile (?n. sp.) from the Gulf of California (Echinodermata: Holothuroidea: Dendrochirotida). Zootaxa 5026(4): 507–526. <https://doi.org/10.11646/zootaxa.5026.4.3>
- Théel H (1886) Report on the Holothuroidea dredged by HMS *Challenger*, during the years 1873–1876. Part II. Scientific Results of the HMS *Challenger* during the years 1873–1876. Zoology 14(39): 1–290. [pls 1–16]
- Turanov SV, Kartavtsev YP (2014) Taxonomic Composition and Distribution of Sand Lances from the Genus *Ammodytes* (Perciformes: Ammodytidae) in the North Pacific. Russian Journal of Marine Biology 40(6): 447–454. <https://doi.org/10.1134/S1063074014060212>
- Ward RD (2009) DNA barcode divergence among species and genera of birds and fishes. Molecular Ecology Resources 4(4): 1077–1085. <https://doi.org/10.1111/j.1755-0998.2009.02541.x>
- WoRMS (2024a) *Eupentacta* Deichmann, 1938. <https://www.marinespecies.org/aphia.php?p=taxdetails&id=528610> [Accessed on 2023-10-10]
- WoRMS (2024b) *Eupentacta fraudatrix* (D'yakonov & Baranova in D'yakonov, Baranova & Savel'eva, 1958). <https://www.marinespecies.org/aphia.php?p=taxdetails&id=529482> [Accessed on 2024-03-29]
- WoRMS (2024c) *Sclerodactyla* Ayres, 1851. <https://marinespecies.org/aphia.php?p=taxdetails&id=158531> [Accessed on 2024-03-29]

A new genus and three new species of Hahniidae (Araneae) from China

Lu-Yu Wang¹, Zhi-Sheng Zhang¹

¹ Key Laboratory of Eco-environments in Three Gorges Reservoir Region (Ministry of Education), School of Life Sciences, Southwest University, Chongqing 400715, China

Corresponding author: Zhi-Sheng Zhang (zhangzs327@qq.com)

Abstract

A new genus of comb-tailed spider (Hahniidae), *Sinahahnia* **gen. nov.**, is described based on three new species from the high-altitude areas of China: *Sinahahnia eyu* **sp. nov.** (♂♀, Chongqing and Hubei), *S. fanjingshan* **sp. nov.** (♂♀, Guizhou), and *S. yintiaoling* **sp. nov.** (♀, Chongqing). Digital images, illustrations, and a distribution map are provided.

Key words: Comb-tailed spider, description, morphology, taxonomy, Wuling Mountains

Introduction

The family Hahniidae is distinguishable from other spider families by its transversely oriented spinnerets. Although it is a widely distributed group, only 28 genera and 236 species have been described globally (WSC 2024). Most hahniid genera have limited distributions, with the exception of the type genus, *Hahnia* C.L. Koch, 1841, which is found throughout Africa, Europe, Asia, and North America.

Recently, several local studies have shown that the diversity of Hahniidae is still not completely explored. For example, Dupérré and Tapia (2024) recently recorded Hahniidae from Ecuador, describing for the first time three new genera and 13 new species. A study on Chinese Hahniidae revealed four new genera and 11 new species from southwest China and adjacent Southeast Asian countries (Chu et al. 2023).

Here, we describe a new genus and three new species of Hahniidae from Wuling Mountains area (Shennongjia in Hubei, Yintiaoling in Chongqing, and Fanjinshan in Guizhou). The most closely related hahniid genus is *Troglohnia* Lin & Li, 2023, which is known from the caves of the Yunnan-Guizhou Plateau, in the western Wuling Mountains.

Materials and methods

All specimens are preserved in 75% ethanol and were examined, illustrated, photographed, and measured using a Leica M205A stereomicroscope equipped with a drawing tube, a Leica DFC450 Camera, and LAS v. 4.6 software. Male palps and epigynes were examined and illustrated after they were dissected. Epigynes



Academic editor: Francesco Ballarin

Received: 31 January 2024

Accepted: 21 March 2024

Published: 18 April 2024

ZooBank: <https://zoobank.org/36DCFD36-CD52-41B1-AB5D-73A00BDF7A76>

Citation: Wang L-Y, Zhang Z-S (2024)

A new genus and three new species of Hahniidae (Araneae) from China.

ZooKeys 1197: 249–259. <https://doi.org/10.3897/zookeys.1197.119935>

Copyright: © Lu-Yu Wang & Zhi-Sheng Zhang. This is an open access article distributed under terms of the Creative Commons Attribution License ([Attribution 4.0 International – CC BY 4.0](https://creativecommons.org/licenses/by/4.0/)).

were cleared by immersing them in pancreatin for about 1 h (Álvarez-Padilla and Hormiga 2007). Eye sizes were measured as the maximum dorsal diameter. Leg measurements are shown as: total length (femur, patella and tibia, metatarsus, tarsus). All measurements are in millimetres. Specimens examined here are deposited in the Collection of Spiders, School of Life Sciences, Southwest University, Chongqing, China (SWUC). Terminology follows Zhang and Zhang (2013).

Abbreviations used in the text: **ALE**—anterior lateral eye; **AME**—anterior median eye; **PLE**—posterior lateral eye; **PME**—posterior median eye; **RTA**—retrolateral tibial apophysis.

Taxonomy

Family Hahniidae Bertkau, 1878

Sinahahnia gen. nov.

<https://zoobank.org/28AEBFCF1-E818-49C4-9C8B-B4CEAF08C6D2>

Type species. *Sinahahnia eyu* sp. nov.

Etymology. The generic name is a compound noun derived from the Latin *sinae* (= the Chinese) and '-Hahnia'.

Diagnosis. Species of *Sinahahnia* gen. nov. resemble those of *Troglohnia* in having a similar slender embolus, large and membranous median apophysis, short and strong patellar apophysis, and long, spiral copulatory ducts, but they differ by the long embolus originating at a 6-o'clock position (vs 3-o'clock in *Troglohnia*), the large membranous median apophysis originating from the prolateral part of the tegulum (vs retrolateral in *Troglohnia*), RTA not bifurcated (vs bifurcated in *Troglohnia*) (Figs 2A–C, 3C–E, 5A–C, 6C–E cf. Chu et al. 2023: figs 3C, 10A, B, 12A, B, 15A, B), and the peanut-shaped or spherical spermathecae of the epigyne (vs oval in *Troglohnia*) (Figs 2E, 3G, 4C, 5E, 6G, 7B, 8C cf. Chu et al. 2023: figs 11B, 13B, 14B, 16B).

Description. Small size (male: 1.65–1.94, female: 1.39–2.27). Carapace yellowish brown. Eight eyes. Fovea vertical. Cervical groove and radial furrows distinct. Chelicerae, yellowish brown. Labium yellowish brown, wider than long. Endites yellowish brown, longer than wide. Sternum yellowish brown and scutellate with sparse black hairs. Chelicera with 1–3 promarginal and 5 retromarginal teeth. Legs yellowish brown. Leg formula: 4123. Opisthosoma oval, dorsum yellowish brown, dorsally with five light chevrons, venter yellowish brown.

Male palp patella with 1 or 2 apophyses. RTA curved, short, as long as tibia. Cymbial furrow as long as cymbium. Tegulum spherical, about 1/3 of length of cymbium. Median apophysis large and membranous, arc-shaped, originating from the prolateral part of the tegulum. Embolus originating at approximately 6-o'clock position (retrolateral part at 3:30 o'clock), long, slender, curved along bulb, with its tip staying in cymbial furrow near embolic base.

Epigyne: epigynal plate wider than long. Copulatory openings small, conspicuous, located mid-ventrally on epigynal plate, not touching each other. Copulatory ducts thin, long, strongly coiled. Secondary spermathecae small, spherical, located anteriorly. Spermathecae peanut-shaped or spherical.

Composition. *Sinahahnia eyu* sp. nov., *S. fanjingshan* sp. nov., and *S. yintiaoling* sp. nov.

Distribution. China (Hubei, Chongqing, Guizhou) (Fig. 9).

***Sinahahnia eyu* sp. nov.**

<https://zoobank.org/ADA60175-515D-4C96-8508-891D21B46501>

Figs 1–4, 9

Type material. *Holotype* ♂ (SWUC-T-HA-10-01), **CHINA**, Hubei Prov., Shiyan City, Zhushan Co., Liulin Township, Duheyuan Nature Reserve, 31°31'50"N, 110°0'29"E, elev. 1678 m, 19 September 2023, L.Y. Wang, et al. leg. **Paratypes:**



Figure 1. Living male specimen of *Sinahahnia eyu* sp. nov. (photo by Qian-Le Lu).

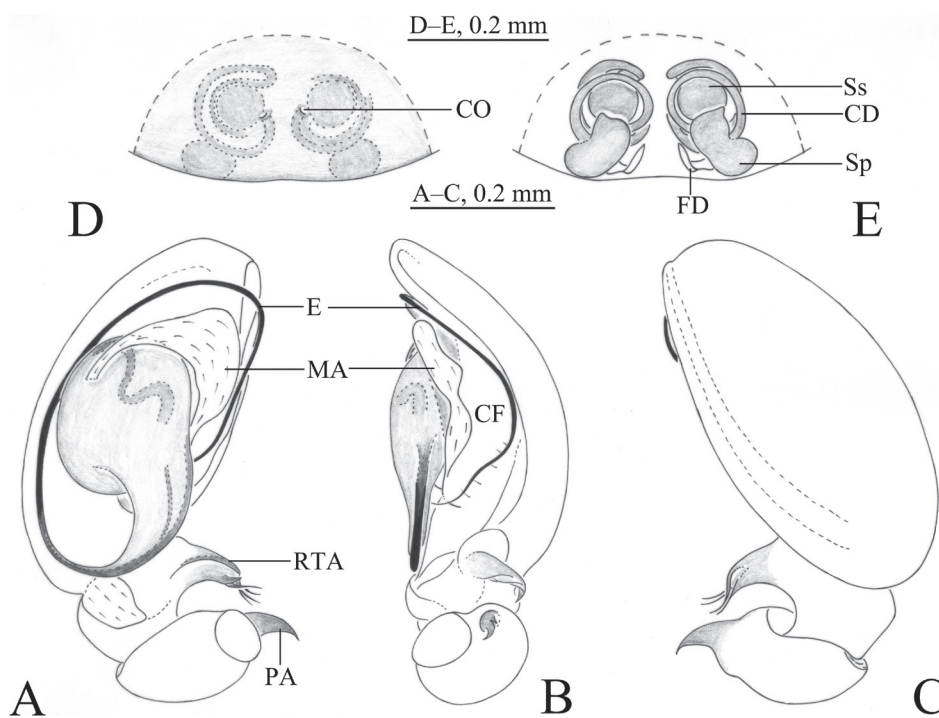


Figure 2. *Sinahahnia eyu* sp. nov. **A–C** holotype male **D, E** paratype female **A** left male palp, ventral view **B** same, retrolateral view **C** same, dorsal view **D** epigyne, ventral view **E** vulva, dorsal view. Abbreviations: CD = copulatory duct; CF = cymbial furrow; CO = copulatory opening; E = embolus; FD = fertilization duct; MA = median apophysis; PA = patellar apophysis; RTA = retrolateral tibial apophysis; Sp = spermatheca; Ss = secondary spermatheca.

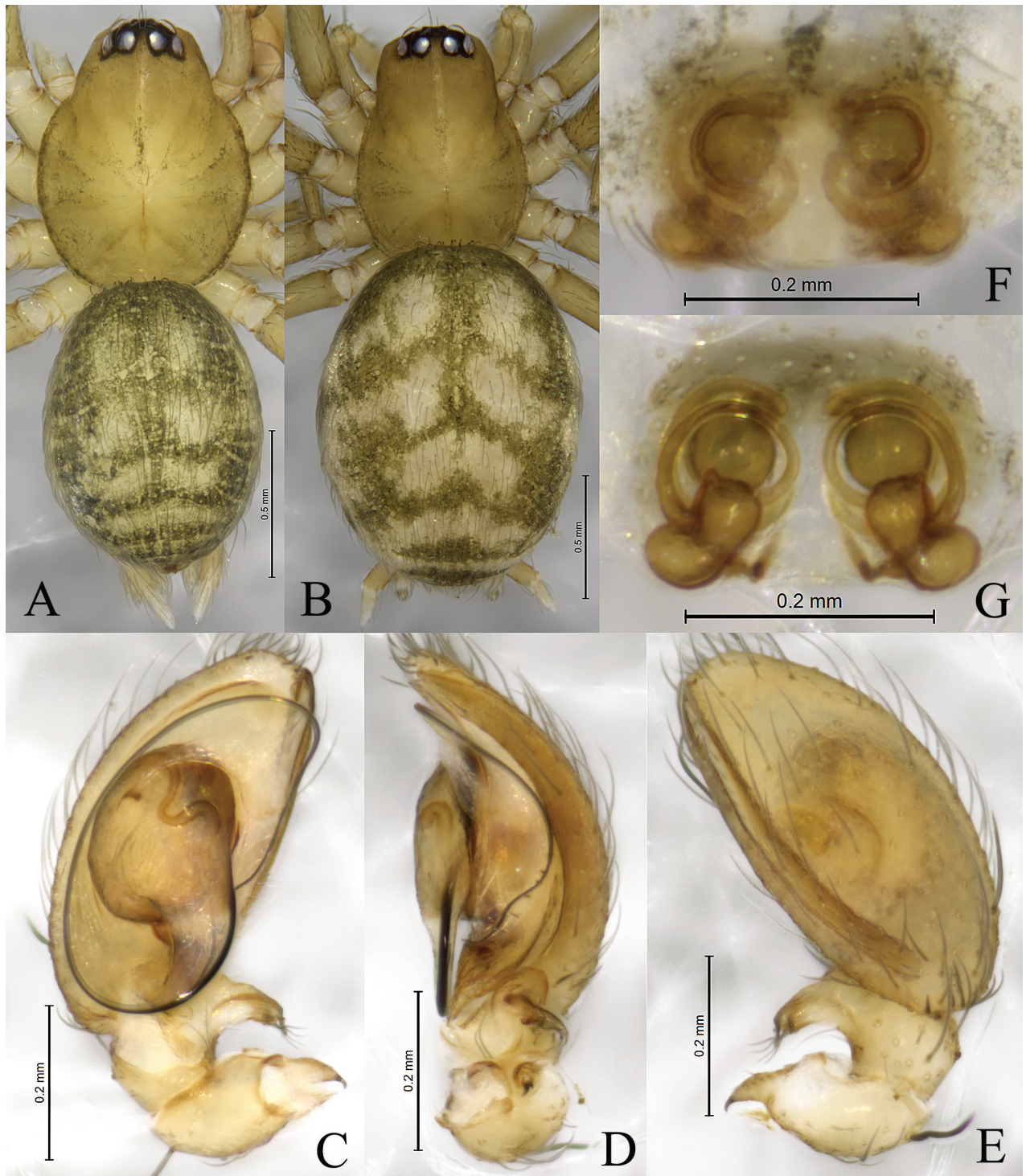


Figure 3. *Sinahahnia eyu* sp. nov. **A, C–E** holotype male **B, F, G** paratype female **A** male habitus, dorsal view **B** female habitus, dorsal view **C** left male palp, ventral view **D** same, retrolateral view **E** same, dorsal view **F** epigyne, ventral view **G** same, dorsal view.

1♂ 4♀ (SWUC-T-HA-10-02~06), same data as for holotype • 1♀ (SWUC-T-HA-10-07), Chongqing City, Wuxi Co., Yintiaoling Nature Reserve, Linkouzi, Fenshuihe, 31°29'47"N, 109°55'33"E, elev. 1796 m, 13 April 2022, LY. Wang leg.

Etymology. The specific name is derived from the Chinese word 'e' and 'yu', E is an abbreviated name for Hubei and Yu is an abbreviated name for Chongqing.

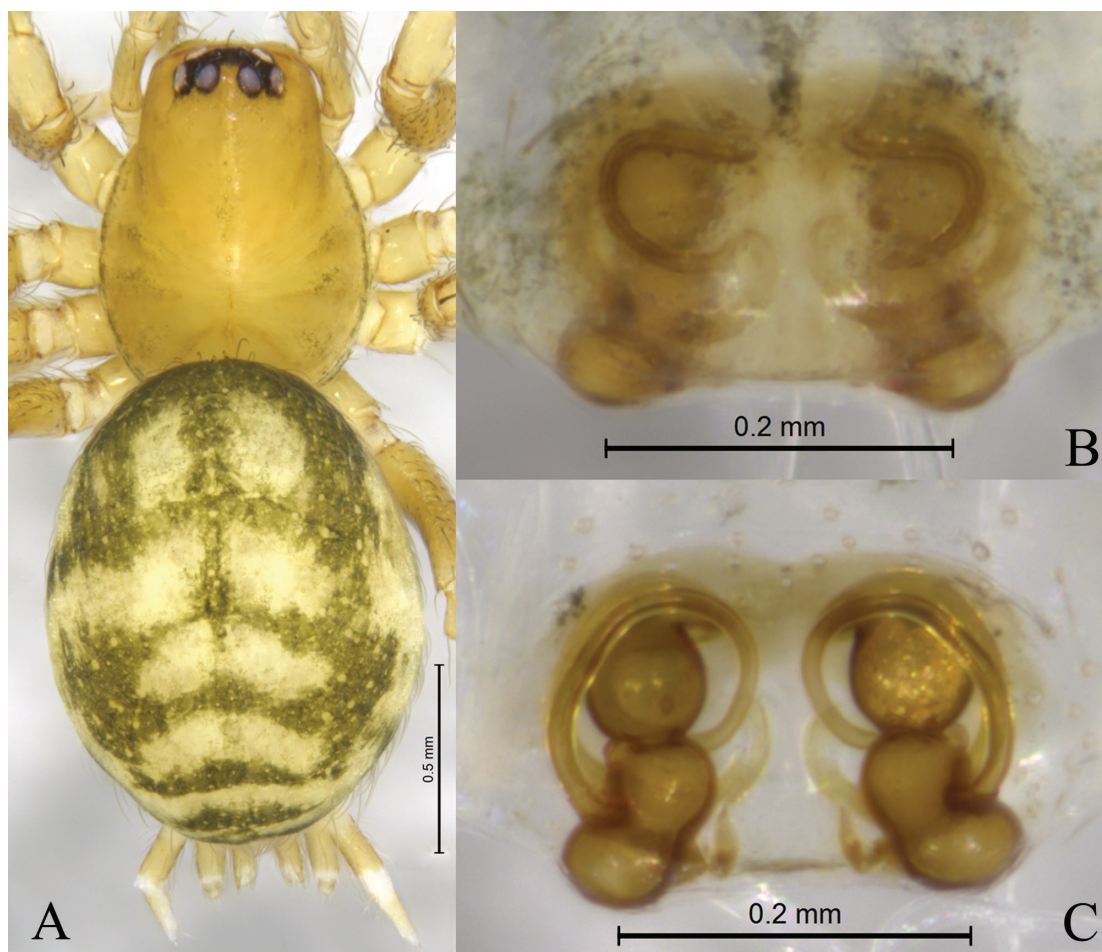


Figure 4. *Sinahahnia eyu* sp. nov., paratype female (SWUC-T-HA-10-07) **A** female habitus, dorsal view **B** epigyne, ventral view **C** same, dorsal view.

Diagnosis. The new species resembles *S. fanjingshan* sp. nov. (Figs 5, 6 cf. Figs 2–4) in having a long, slender embolus, a large, membranous median apophysis, and long, spiral copulatory ducts, but the new species differs from the latter by the twisted RTA with small thorns (vs curved and without thorn in *S. fanjingshan* sp. nov.), the single patellar apophysis (vs two in *S. fanjingshan* sp. nov.) (Figs 2A–C, 3C–E cf. Figs 5A–C, 6C–E), the reniform spermathecae (Figs 2E, 3G, 4C cf. Figs 5E, 6G) (vs peanut-shaped in *S. fanjingshan* sp. nov.).

Description. Male holotype (Fig. 3A) total length 1.88. Carapace 0.92 long, 0.73 wide; opisthosoma 0.99 long, 0.76 wide. Eye sizes and interdistances: AME 0.03, ALE 0.06, PME 0.06, PLE 0.07; AME–AME 0.02, AME–ALE 0.01, PME–PME 0.04, PME–PLE 0.02, ALE–PLE 0.02. MOA 0.14 long, anterior width 0.09, posterior width 0.17. Clypeus height 0.09. Chelicerae with 2 promarginal and 5 retromarginal teeth. Leg measurements: I 2.49 (0.70, 0.78, 0.55, 0.46); II 2.29 (0.65, 0.78, 0.49, 0.37); III 1.92 (0.52, 0.56, 0.45, 0.39); IV 2.51 (0.75, 0.75, 0.56, 0.45).

Palp (Figs 2A–C, 3C–E). Patellar apophysis curved, short, about 1/3 length of patella, with sharp tip. RTA spiral, with some small thorns. Cymbial furrow as long as cymbium. Median apophysis membranous. Embolus originating at approximately 6-o’clock position, slender, curved along with bulb, its tip staying in cymbial furrow near embolic base.

One of the paratypes (SWUC-T-HA-10-02, Fig. 3B) total length 2.27. Carapace 0.97 long, 0.70 wide; opisthosoma 1.38 long, 1.08 wide. Eye sizes and interdistances: AME 0.04, ALE 0.08, PME 0.07, PLE, 0.08; AME–AME 0.03, AME–ALE 0.01, PME–PME 0.05, PME–PLE 0.02, ALE–PLE 0.01. MOA 0.15 long, anterior width 0.11, posterior width 0.19. Clypeus height 0.07. Leg measurements: I 2.08 (0.57, 0.71, 0.42, 0.38); II 2.01 (0.60, 0.64, 0.39, 0.38); III 1.76 (0.51, 0.56, 0.36, 0.33); IV 2.33 (0.63, 0.76, 0.52, 0.42).

Epigyne and vulva (Figs 2D–E, 3F, G, 4B, C). Epigynal plate wider than long. Copulatory openings small, located mid-ventrally on epigynal plate. Copulatory ducts thin, long, wrapped three times around secondary spermathecae. Secondary spermathecae small, located anteriorly. Spermathecae reniform, more than twice as large as secondary spermathecae. Fertilization ducts spiral and hook-like.

Variation. Males ($n = 2$) total length 1.76–1.88; females ($n = 5$) total length 1.86–2.27.

Distribution. China (Chongqing, Hubei) (Fig. 9).

***Sinahahnia fanjingshan* sp. nov.**

<https://zoobank.org/D59809F3-05ED-4387-813B-8809A9E55739>

Figs 5, 6, 9

Type material. Holotype ♂ (SWUC-T-HA-11-01), **CHINA**, Guizhou Prov., Tongren City, Songtao Co., Wuluo Town, Fanjingshan Nature Reserve, near Maxi'ao Tunnel, 28°01'09"N, 108°45'24"E, elev. 1239 m, 11 October 2013, L.Y. Wang, D. Wang and X.K. Jiang leg. **Paratypes:** 1♂ 2♀ (SWUC-T-HA-11-02~04), with same data as for holotype • 12♀ (SWUC-T-HA-11-05~16), Fanjingshan Nature Reserve, Jinding, 27°54'29"N, 108°41'52"E, elev. 2214 m, 29 September 2013, L.Y. Wang, D. Wang and X.K. Jiang leg. • 1♀ (SWUC-T-HA-11-17), Fanjingshan Nature Reserve, Mianxuling, 27°54'32"N, 108°39'49"E, elev. 1974m, 30 September 2013, L.Y. Wang, D. Wang and X.K. Jiang leg. • 1♂ 2♀ (SWUC-T-HA-11-18~20), same data as for holotype except date, 5 October 2013.

Etymology. The specific name is derived from the type locality; it is a noun in apposition.

Diagnosis. The new species resembles *S. eyu* sp. nov. (Figs 2–4 cf. Figs 5, 6) in having a long, slender embolus, a large, membranous median apophysis, and long, spiral copulatory ducts, but the new species differs from the latter in having a curved RTA (vs twisted and with small thorns in *S. eyu* sp. nov.), a bifurcated patellar apophysis (vs single in *S. eyu* sp. nov.), a finger-shaped retrolateral patellar apophysis (vs absent in *S. eyu* sp. nov.) (Figs 5A–C, 6C–E cf. 2A–C, 3C–E), and a peanut-shaped spermathecae (vs reniform in *S. eyu* sp. nov.) (Figs 5E, 6G cf. 2E, 3G, 4C).

Description. Male holotype (Fig. 6A) total length 1.65. Carapace 0.81 long, 0.57 wide; opisthosoma 0.77 long, 0.56 wide. Eye sizes and interdistances: AME 0.02, ALE 0.06, PME 0.05, PLE 0.06; AME–AME 0.02, AME–ALE 0.01, PME–PME 0.04, PME–PLE 0.02, ALE–PLE 0.01. MOA 0.11 long, anterior width 0.04, posterior width 0.16. Clypeus height 0.12. Chelicerae with 1 promarginal and 5 retromarginal teeth. Leg measurements: I 2.19 (0.62, 0.72, 0.46, 0.39); II 1.96 (0.57, 0.62, 0.40, 0.37); III 1.80 (0.52, 0.56, 0.39, 0.33); IV 2.25 (0.63, 0.73, 0.50, 0.39).

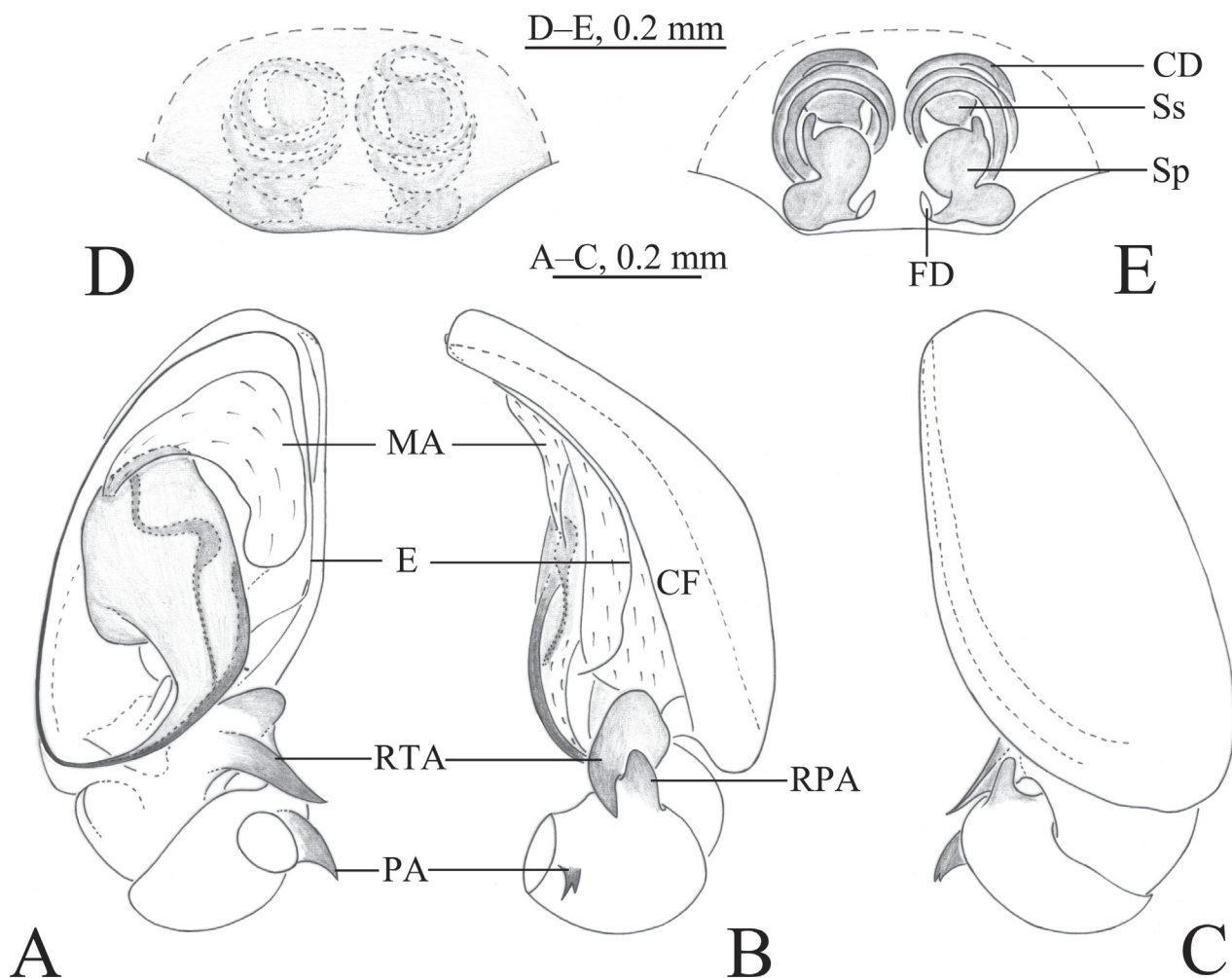


Figure 5. *Sinahahnia fanjingshan* sp. nov. **A–C** holotype male **D, E** paratype female **A** left male palp, ventral view **B** same, retrolateral view **C** same, dorsal view **D** epigyne, ventral view **E** vulva, dorsal view. Abbreviations: CD = copulatory duct; CF = cymbial furrow; CO = copulatory opening; E = embolus; FD = fertilization duct; MA = median apophysis; PA = patellar apophysis; RPA = retrolateral patellar apophysis; RTA = retrolateral tibial apophysis; Sp = spermatheca; Ss = secondary spermatheca.

Palp (Figs 5A–C, 6C–E). Patellar apophysis curved, short, about 1/3 length of patella, with a bifurcated end. Retrolateral patellar apophysis finger-shaped. RTA curved, as long as tibia. Cymbial furrow as long as cymbium. Median apophysis membranous. Embolus originating at approximately 6-o’clock position, slender, curved along with bulb, its tip staying in the cymbial furrow near embolic base.

One of the paratypes (SWUC-T-HA-11-02, Fig. 6B) total length 1.39. Carapace 0.69 long, 0.50 wide; opisthosoma 0.72 long, 0.53 wide. Eye sizes and interdistances: AME 0.02, ALE 0.04, PME 0.04, PLE, 0.06; AME–AME 0.01, AME–ALE 0.01, PME–PME 0.05, PME–PLE 0.02, ALE–PLE 0.01. MOA 0.09 long, anterior width 0.05, posterior width 0.15. Clypeus height 0.08. Leg measurements: I 1.59 (0.48, 0.51, 0.31, 0.29); II 1.46 (0.45, 0.46, 0.29, 0.26); III 1.33 (0.38, 0.42, 0.28, 0.25); IV 1.72 (0.53, 0.53, 0.37, 0.29).

Epigyne and vulva (Figs 5D, E, 6F, G). Epigynal plate wider than long. Copulatory ducts thin and long, wrapped three times around secondary spermathecae. Secondary spermathecae small, anteriorly located. Spermathecae peanut-shaped, more than twice as large as secondary spermathecae. Fertilization ducts small, hook-like.

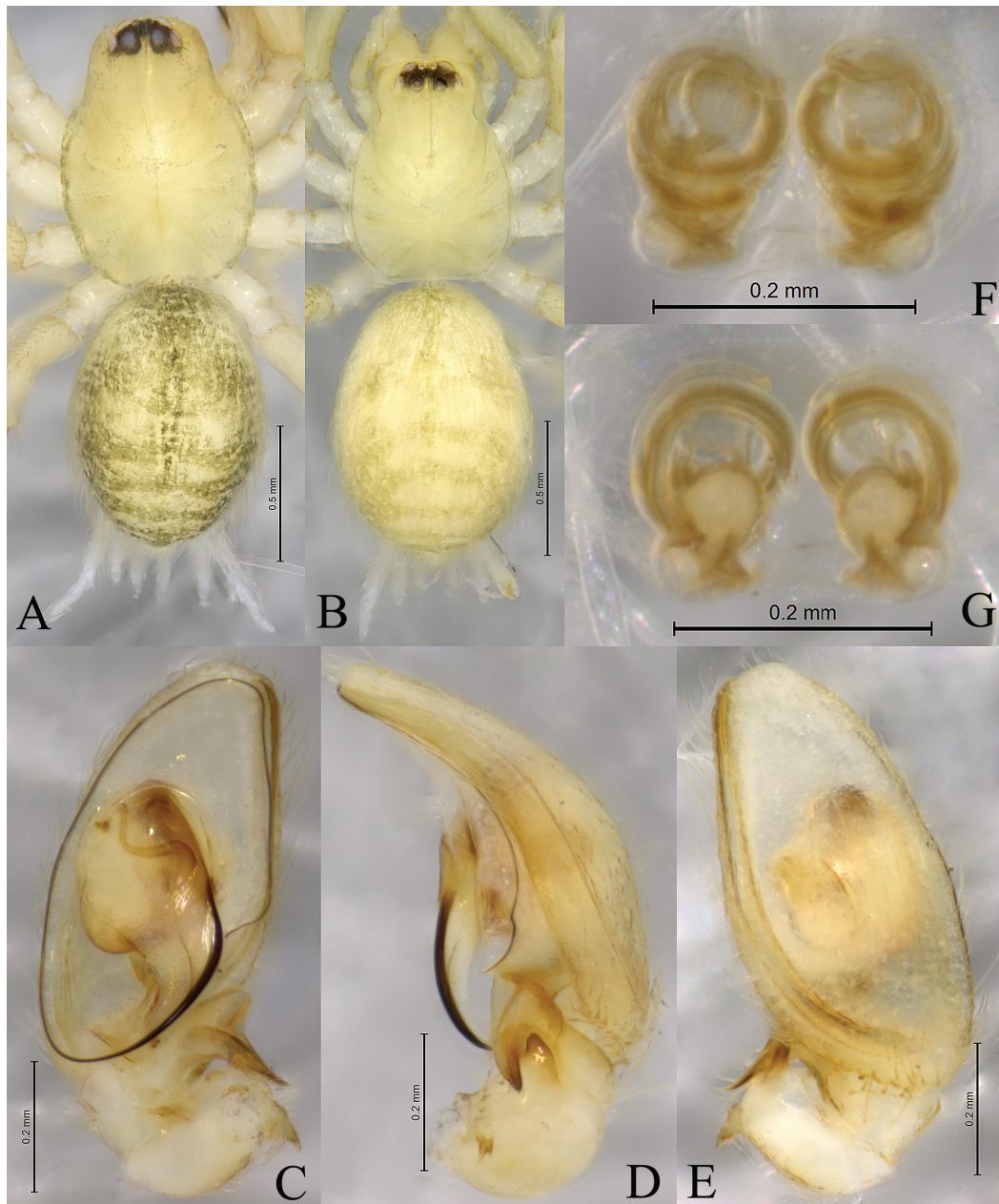


Figure 6. *Sinahahnia fanjingshan* sp. nov. **A, C–E** holotype male **B, F, G** paratype female **A** male habitus, dorsal view **B** female habitus, dorsal view **C** left male palp, ventral view **D** same, retrolateral view **E** same, dorsal view **F** epigyne, ventral view **G** same, dorsal view.

Variation. Males ($n=3$) total length 1.65–1.94; females ($n=17$) total length 1.39–1.83.

Distribution. Known only from the type locality in Guizhou, China (Fig. 9).

***Sinahahnia yintiaoling* sp. nov.**

<https://zoobank.org/663B4C66-F4DB-474D-8D6A-E20DEEE56931>

Figs 7–9

Type material. *Holotype* ♀ (SWUC-T-HA-12-01), **CHINA**, Chongqing City, Wuxi Co., Yintiaoling Nature Reserve, Guanshan, Shizhuzi, 31°32'15"N, 109°41'49"E,

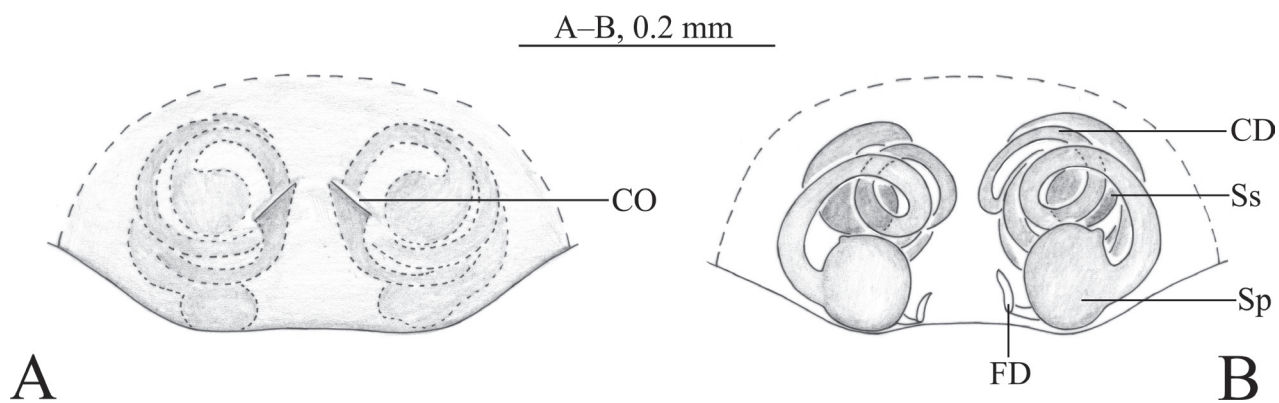


Figure 7. *Sinahahnia yintiaoling* sp. nov., holotype female **A** epigyne, ventral view **B** vulva, dorsal view. Abbreviations: CD = copulatory duct; CO = copulatory opening; FD = fertilization duct; Sp = spermatheca; Ss = secondary spermatheca.

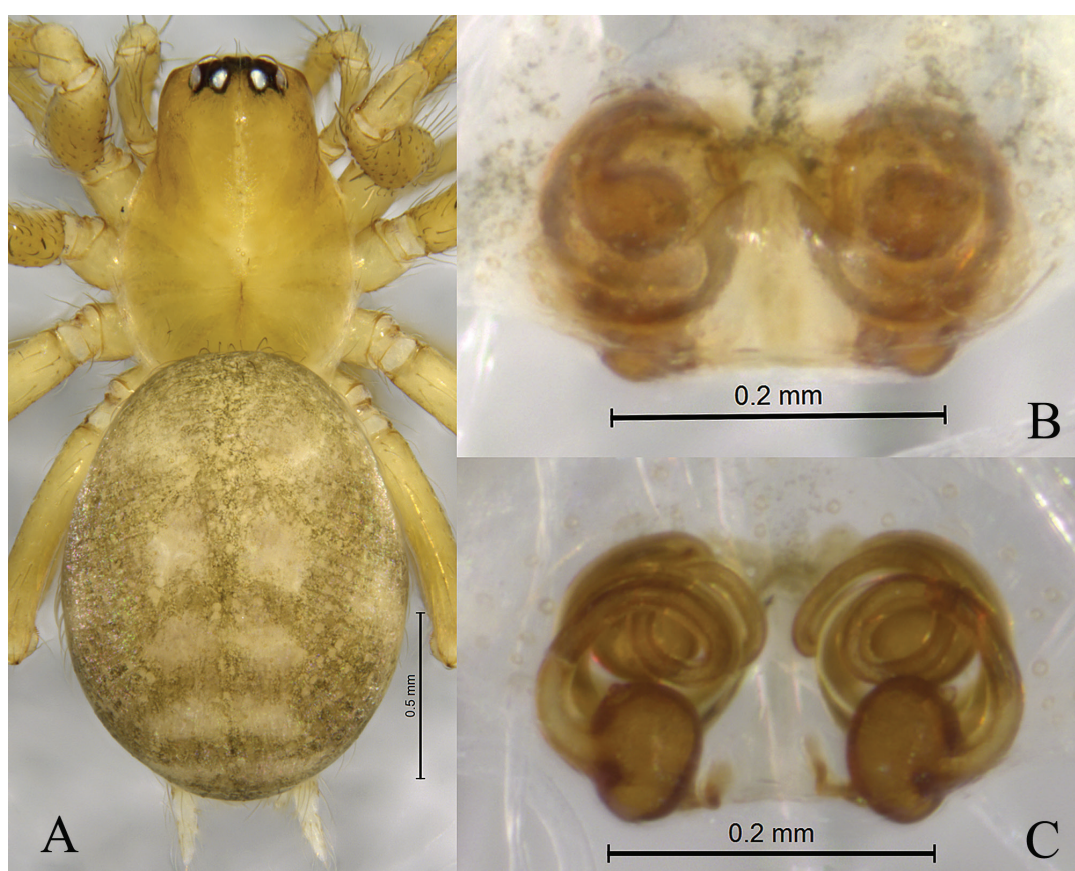


Figure 8. *Sinahahnia yintiaoling* sp. nov., holotype female **A** female habitus, dorsal view **C** epigyne, ventral view **D** same, dorsal view.

elev. 2147 m, 1 September 2020, Z.S. Zhang, L.Y. Wang, Y. Zhang and P. Liu leg.

Paratypes: 8♀ (SWUC-T-HA-12-02~09), with same data as for holotype.

Etymology. The specific name is derived from the type locality; it is a noun in apposition.

Diagnosis. The new species resembles *S. eyu* sp. nov. (Figs 2–4 cf. Figs 7, 8) in having long and spiral copulatory ducts, but the new species differs from the latter in the large copulatory openings and the spherical spermathecae (vs small copulatory openings and reniform spermathecae in *S. eyu* sp. nov.) (Figs 7, 8B, C cf. Figs 2D–E, 3F, G, 4B, C).

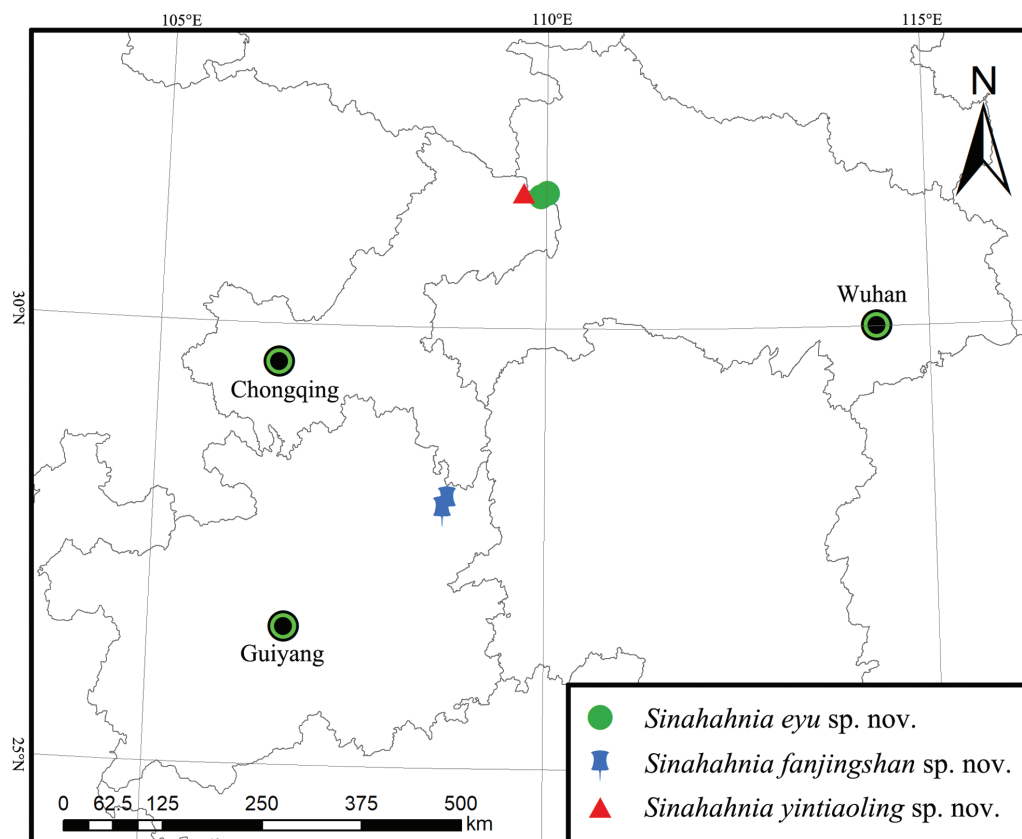


Figure 9. Distribution of *Sinahahnia* in China.

Description. Female holotype (Fig. 8A) total length 2.23. Carapace 1.01 long, 0.74 wide; opisthosoma 1.35 long, 1.04 wide. Eye sizes and interdistances: AME 0.03, ALE 0.06, PME 0.07, PLE 0.08; AME–AME 0.02, AME–ALE 0.01, PME–PME 0.06, PME–PLE 0.03, ALE–PLE 0.01. MOA 0.17 long, anterior width 0.10, posterior width 0.18. Clypeus height 0.09. Chelicerae with 3 promarginal and 5 retromarginal teeth. Leg measurements: I 2.23 (0.66, 0.75, 0.43, 0.39); II 2.09 (0.65, 0.65, 0.42, 0.37); III 2.00 (0.58, 0.62, 0.41, 0.39); IV 2.51 (0.72, 0.81, 0.57, 0.41).

Epigyne and vulva (Figs 7A, B, 8B, C). Epigynal plate wider than long. Copulatory openings small, located mid-ventrally on epigynal plate. Copulatory ducts thin, long, wrapped four times around secondary spermathecae. Secondary spermathecae small, anteriorly located. Spermathecae spherical, more than twice as large as secondary spermathecae. Fertilization ducts small, hook-like.

Male unknown.

Variation. Females ($n=9$) total length 2.06–2.23.

Distribution. Known only from the type locality in Chongqing, China (Fig. 9).

Acknowledgements

We give great thanks to two reviewers (Y. Marusik and an anonymous reviewer) and the subject editor (Francesco Ballarin) for their constructive comments. Many thanks are given to Mr Yu Zhang, Xuan-Kong Jiang, Xu-Long Chen (SWUC), Qian-Le Lu (Shenzhen) and Ms Piao Liu, Yu-Jun Cai, and Xiang-Yun Zhang for their assistance during the fieldwork and collection.

Additional information

Conflict of interest

The authors have declared that no competing interests exist.

Ethical statement

No ethical statement was reported.

Funding


This research was supported by the Science & Technology Fundamental Resources Investigation Program (grant no. 2022FY202100) and the Science Foundation of School of Life Sciences SWU (20212020110501).

Author contributions

All authors have contributed equally.

Author ORCIDs

Lu-Yu Wang  <https://orcid.org/0000-0002-5250-3473>

Zhi-Sheng Zhang  <https://orcid.org/0000-0002-9304-1789>

Data availability

All of the data that support the findings of this study are available in the main text.

References

- Álvarez-Padilla F, Hormiga G (2007) A protocol for digesting internal soft tissues and mounting spiders for scanning electron microscopy. *The Journal of Arachnology* 35(3): 538–542. <https://doi.org/10.1636/Sh06-55.1>
- Chu C, Lin YJ, Li SQ (2023) New genera and new species of Hahniidae (Araneae) from China, Laos, Myanmar, and Vietnam. *ZooKeys* 1187: 91–134. <https://doi.org/10.3897/zookeys.1187.112936>
- Dupérré N, Tapia E (2024) First record of the family Hahniidae in Ecuador with description of thirteen new species and three new genera (Araneae: Hahniidae). *Taxonomy* 4(1): 53–111. <https://doi.org/10.3390/taxonomy4010005>
- World Spider Catalog (2024) World Spider Catalog. Version 25.0. Natural History Museum Bern. [<http://wsc.nmbe.ch>] [Accessed on: 2024-01-23] <https://doi.org/10.24436/2>
- Zhang ZS, Zhang YG (2013) Synonymy and misidentification of three *Hahnia* species (Araneae: Hahniidae) from China. *Zootaxa* 3682(4): 521–533. <https://doi.org/10.11646/zootaxa.3682.4.3>

A new species of *Habrophorula* from Vietnam and an updated key to species of the genus (Hymenoptera, Apidae)

Ngat Thi Tran¹, Michael S. Engel^{2,3,4}, Lien Thi Phuong Nguyen¹

1 Institute of Ecology and Biological Resources, Vietnam Academy of Science and Technology, 18 Hoang Quoc Viet Road, Nghia Do, Cau Giay, Hanoi, Vietnam

2 Division of Invertebrate Zoology, American Museum of Natural History, Central Park West at 79th Street, New York, New York 10024, USA

3 Facultad de Ciencias Biológicas, Universidad Nacional Mayor de San Marcos, Lima, Peru

4 Departamento de Entomología, Museo de Historia Natural, Universidad Nacional Mayor de San Marcos, Avenida Antonio Álvarez de Arenales 1256 Jesús María, Lima 14, Peru

Corresponding authors: Ngat Thi Tran (tranthingat1012@gmail.com); Michael S. Engel (mengel@amnh.org)

Abstract

The rare bee genus *Habrophorula* Lieftinck, 1974 is recorded for the first time from Vietnam. The genus is represented by a new species, *Habrophorula belladeceptrix* Tran, Engel & Nguyen, **sp. nov.**, from Cao Bang Province and can be most easily confused with *H. nigripes* Wu from China. The species is most easily differentiated by the unique form of the male terminalia but can also be distinguished by differences in integumental and setal coloration. A revised key is provided to the species of the genus. Females of the new species were collected at flowers of *Saurauia roxburghii* Wall. and *Saurauia napaulensis* DC. (Actinidiaceae); males were collected at flowers of *Lantana camara* L. (Verbenaceae).

Abstract in Vietnamese

Một giống ong hiếm có tên *Habrophorula* Lieftinck lần đầu tiên được ghi nhận ở Việt Nam. Trong giống này, *Habrophorula belladeceptrix* Tran, Engel, & Nguyen, **sp. nov.** được phát hiện ở tỉnh Cao Bằng và loài này rất dễ nhầm lẫn với loài *H. nigripes* Wu từng được ghi nhận tại Trung Quốc. Chúng khác với các loài *Habrophorula* còn lại ở hình dạng đực đáo của bộ phận sinh dục đực, màu sắc của các đốt bụng và lông. Khóa định loại đến loài của giống này được cập nhật. Cá thể cái của loài ong này được thu thập trên hoa của loài Nóng roxburgh *Saurauia roxburghii* Wall. và Nóng hoa nhọn *Saurauia napaulensis* DC. thuộc họ Dương đào (Actinidiaceae), cá thể đực được ghi nhận trên hoa của loài Bông ổi *Lantana camara* L. thuộc họ Cỏ roi ngựa (Verbenaceae).

Key words: Anthophorini, Apoidea, morphology, new record, systematics, taxonomy, Vietnam

Introduction

The uncommon southern Asian bee genus *Habrophorula* Lieftinck, 1974 belongs to the small *Elaphropoda*-group of the subfamily Anthophorinae (Michener 2007; Engel 2018; Orr et al. 2022). The genus is distinguished from others in this group by the following features: clypeus not greatly protuberant, extending



Academic editor: Thorleif Dörfel

Received: 2 January 2024

Accepted: 28 March 2024

Published: 18 April 2024

ZooBank: <https://zoobank.org/4D6195BA-B5AB-40D8-861C-4057EBB53CE4>

Citation: Tran NT, Engel MS, Nguyen LTP (2024) A new species of *Habrophorula* from Vietnam and an updated key to species of the genus (Hymenoptera, Apidae). ZooKeys 1197: 261–272. <https://doi.org/10.3897/zookeys.1197.118126>

Copyright: © Ngat Thi Tran et al.

This is an open access article distributed under terms of the Creative Commons Attribution License ([Attribution 4.0 International – CC BY 4.0](https://creativecommons.org/licenses/by/4.0/)).

anteriorly by about one-half compound eye width or less in profile; mandible tridentate; third submarginal cell about as wide on anterior margin as on posterior margin; hind leg of male not enlarged, metatrochanter lacking rounded projection; metasomal tergum VII and sternum VI of male not attenuate, apex of tergum VI nearly always bidentate or with emarginate apical truncation; sternum VII of male transverse, disc much broader than long, without apical process (Lieftinck 1974; Michener 2007). Individuals of *Habrophorula* are collected infrequently, and hitherto there have been only four species known, all from southern China (Wu 1991, 2000).

Here, *Habrophorula* is newly recorded for the first time from Vietnam, based on a series of females and males of a new species. We provided a description and figures for the new species along with a revised key for the identification of taxa in the genus.

Materials and methods

Specimens examined in this study are deposited in the collection of Hymenoptera of the Institute of Ecology and Biological Resources (IEBR), Hanoi, Vietnam, and in the Division of Invertebrate Zoology, American Museum of Natural History, New York, New York (AMNH). Adult morphological and color characters were examined with a Nikon SMZ745 stereomicroscope, while images were photographed with a Nikon SMZ800N digital stereomicroscope, and with an attached ILCE-5000L/WAP2 digital camera. Stacked focus images were prepared using Helicon Focus 7. Lastly, all files were processed with Adobe Photoshop CS6. Male terminalia were dissected from relaxed specimens and then treated with Proteinase K so as to remove tissue and partially clear the integument. The morphological terminology used in the descriptions follows Engel (2001) and Michener (2007), with the following body metrics in mm (as used in Tran et al. 2022, 2023): **body length**: measured from the base of the antennal torulus to the metasomal apex (in dorsal view), **head length**: measured from the medioapical margin of the clypeus to the upper margin of the vertex (in facial view), **head width**: measured at the widest point of the head across the compound eyes (in facial view), **eye width**: the greatest width of the compound eye (in profile), **genal width**: the greatest width of the gena (in profile), **intertegular distance**: measured between the inner rims of the tegulae (in dorsal view). The abbreviations F, S, and T (followed by Arabic numerals) refer to numbered flagellomeres, metasomal sterna, and metasomal terga, respectively.

Systematics

Genus *Habrophorula* Lieftinck, 1974

Habrophorula Lieftinck, 1974: 217. Type species: *Habropoda nubilipennis* Cockerell, 1930, original designation.

Note. This is an uncommon genus that superficially resembles the more widely distributed *Elaphropoda* Lieftinck, species which are often more reddish in color. Unlike *Elaphropoda* the third submarginal cell is about as wide anteriorly as it is posteriorly (the cell is wider posteriorly in *Elaphropoda*); the clypeus

is only moderately convex and not greatly protuberant, extending only about one-half the compound eye width, or less, in front of the compound eye when viewed in profile (except in the new species); male hind leg unmodified, metatrochanter lacking a rounded projection (hind leg of male enlarged, metatrochanter with broadly rounded projection in *Elaphropoda*); and tergum VII and sternum VI of the male not attenuate, apex of tergum VI of male with apical truncation weakly emarginate medially, and sternum VII of male with disc broader than long and lacking an apical process (tergum VII and sternum VI somewhat attenuate, tergum VI not emarginate, and sternum VII slightly broader than long and with apical process present in *Elaphropoda*) (Michener 2007; Engel 2018). Table 1 gives a summary of species currently included in *Habrophorula*, including species treated in this study, and with information on the known sexes and distribution.

Table 1. Summary of species currently in the genus *Habrophorula* Lieftinck (Anthophorini).

Species	Sexes known	Distribution
<i>Habrophorula belladeceptrix</i> sp. nov.	♀♂	Vietnam (Cao Bang)
<i>Habrophorula ferruginipes</i> Wu, 1991	♂	China (Guangxi)
<i>Habrophorula nigripes</i> Wu, 1991	♀♂	China (Guizhou)
<i>Habrophorula nubilipennis</i> (Cockerell, 1930)	♀♂	China (Fujian, Hunan)
<i>Habrophorula rubigolabralis</i> Wu, 2000	♀	China (Jiangxi)

Recently, Orr et al. (2022) treated the monotypic *Varthemapistra* Engel, 2008 as a synonym of *Habrophorula*. However, such a decision seems ill-advised at present, especially given that representatives of all anthophorine genera were included in the analysis with the exception of *Varthemapistra*, the sole specimen of which was also never examined by the authors. Engel (2018) did note that *Varthemapistra* might eventually be considered a subgenus of *Habrophorula* but in the absence of cladistic evidence for its placement as within or sister to *Habrophorula* or even a more inclusive clade of *Habrophorula* and other genera, any decision regarding its ultimate classification should await the discovery of additional specimens, particularly the currently unknown male. The simple female mandible of *Varthemapistra edentata* Engel, 2018 is not the result of wear as is easily evident from the holotype (which also does not show other signs of usual wear) and that both mandibles are identical (refer to Engel 2018: fig. 4 and discussion therein). The simple mandible is unique among anthophorines and, as such, while distinctive, is an autapomorphy. *Varthemapistra* was distinguished from *Habrophorula* and other anthophorines not only on the autapomorphic absence of mandibular teeth but also characters of the clypeus, metatibia, and especially forewing. It therefore seems groundless and unwarranted to place *V. edentata* in *Habrophorula* without cladistic evidence indicating the former renders the latter paraphyletic. Thus, given its unique suite of characters, its unique biogeographic occurrence relative to species of *Habrophorula*, and the possibility that it may be sister to *Habrophorula* (in which case its recognition as a genus or a distinctive subgenus serves to emphasize its unique characters and distribution), we retain the genus as distinct from *Habrophorula*.

***Habrophorula belladeceptrix* Tran, Engel & Nguyen, sp. nov.**

<https://zoobank.org/70DFD59A-1C27-4BF9-9097-30988B462051>

Figs 1–26

Diagnosis. This species can be distinguished from among its congeners by the clypeus and supraclypeal area rather convex, extending in front of the compound eye almost as much as the compound eye width in profile, in this respect resembling the genus *Elaphropoda* (but can be distinguished from this genus by all of the other aforementioned characters). It could be easily confused with other species of *Habrophorula*, if ignoring the more protuberant clypeus, which have black legs and black apical margins of the metasomal terga, but differs in the fine clypeal markings of the female, the setal coloration of the male, and the male terminalia (Figs 18–21). Males could be confused with *H. nigripes* Wu except for the clypeal markings and setal coloration (*vide* key, *infra*) and, most notably, in the differences of the terminalia (*cf.* Wu 2000: fig. 186), particularly the forms of the hidden sterna. The terminalia somewhat resemble those of *H. nubilipennis* except in the new species sternum VII is narrower, sternum VIII is deeply concave medioapically, and the gonostylar setae are denser and more elongate.

Type material. Holotype. VIETNAM: ♀, Cao Bang, Nguyen Binh, Phan Thanh, Salmon Station 2, Phia Oac–Phia Den National Park, 22°35'28"N, 105°51'20"E, alt. 1046 m, 2.vi.2023 [2 June 2023], NT Tran leg. (IEBR). **Paratypes.** VIETNAM: 23♀♀, same data as holotype (IEBR, 2♀♀ AMNH); 2.vii.2022 [2 July 2022]; 1♀, Cao Bang, Nguyen Binh, Phan Thanh, Phia Oac–Phia Den NP, 22°35'03"N, 105°51'40"E, alt. 944 m, 9.vi.2020 [9 June 2020], LX Truong, LTP Nguyen, CQ Nguyen, HD Nguyen, NT Tran, TV Mai, UTP Tran leg.; 8♂♂, Nguyen Binh, Phan Thanh, Ca My Station of Resources Protection, Phia Oac–Phia Den National Park, 22°38'30"N, 105°50'59"E, alt. 1009 m, 7.vi.2020 [7 June 2020], LX Truong, LTP Nguyen, CQ Nguyen, HD Nguyen, NT Tran, TV Mai, UTP Tran leg. (IEBR, 2♂♂ AMNH); 18♂♂, alt. 1009 m, 3.vi.2023 [3 June 2023], NT Tran leg.

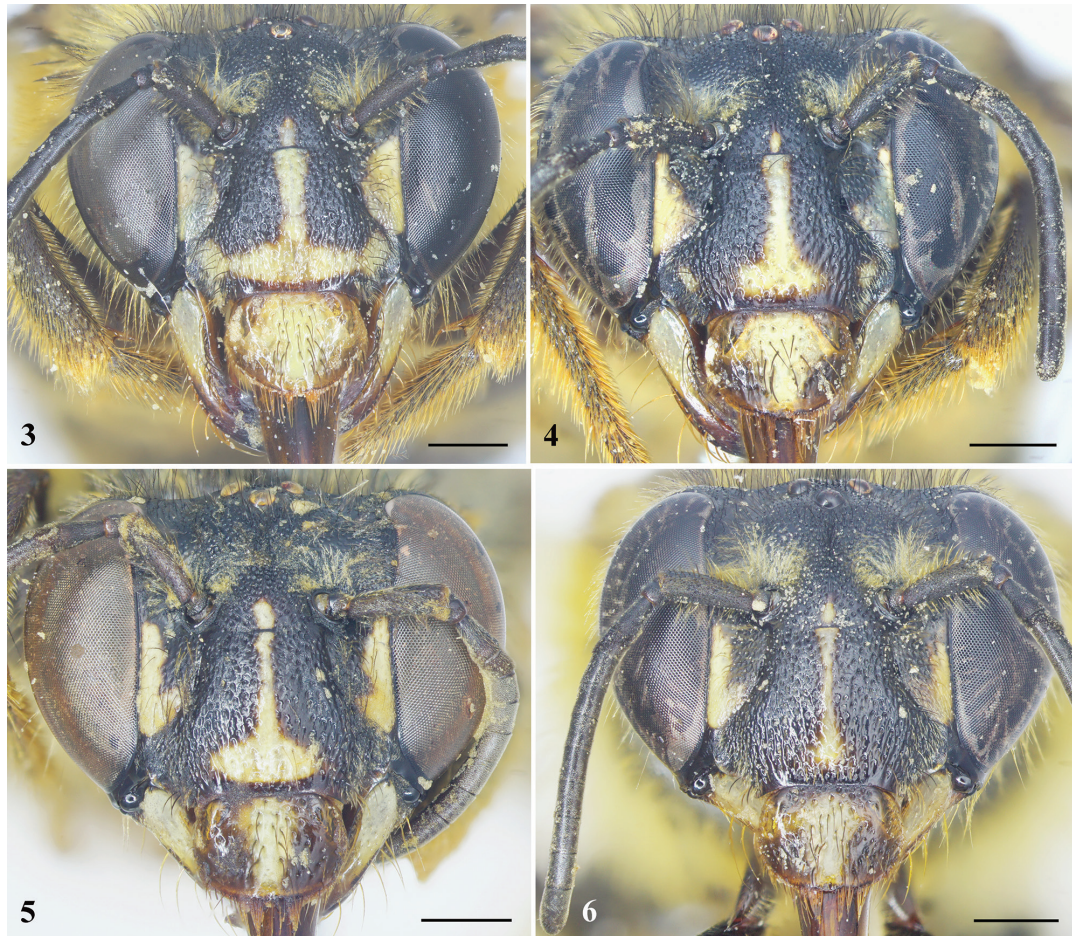
Description. ♀: Total body length 12 mm, forewing length 9 mm.

Structure. Head broader than long, about 1.4× as broad as long, head length 3.1 mm, width 4.4 mm (Fig. 3); compound eyes about 2× genal width; mandible with three teeth (as preserved, teeth relatively worn apically, and preapical tooth nearly completely worn) (Fig. 7); clypeus broader than long, about 1.5× as broad as long; clypeus and supraclypeal area rather convex, extending in front of compound eye almost as much as compound eye width in profile (unique to genus); labrum apically with small median emargination; scape slender, about 3.5× as long as broad, pedicel approximately 1.1× as broad as long and about 0.4× length of F1, F1 longer than broad and approximately 2× length of F2, F3–9 ascending in length, F3–5, F6–7, and F8–9 subequal in length, F10 longest flagellomere, about 1.4× as long as broad (Fig. 8). Mesosoma approximately as broad as long; mesoscutellum short and with apical margin rounded, not overhanging metanotum (Fig. 2). Forewing with three submarginal cells, first and third submarginal cells broader than second submarginal cell, 1m-cu entering near apex of second marginal cell (Fig. 9). Metabasitibial plate large (Fig. 1). Metasoma rather heart-shaped (Fig. 2); pygidial plate large, rounded apically (Fig. 10).

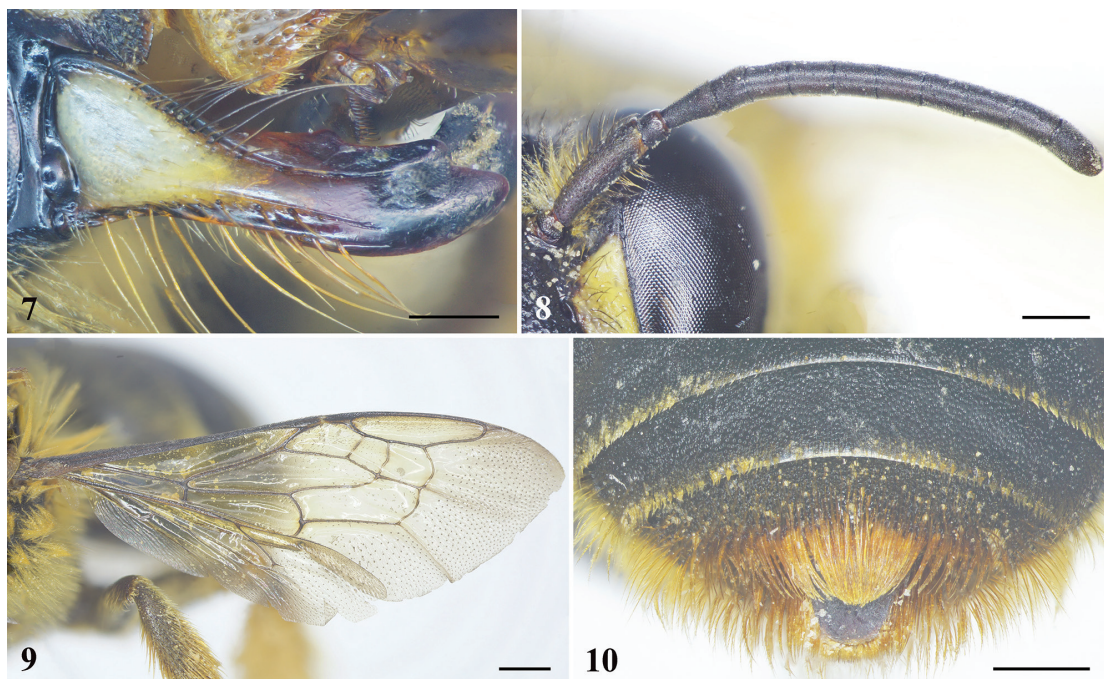


Figures 1, 2. *Habrophorula belladeceptrix* sp. nov., female **1** habitus, lateral view **2** habitus, dorsal view. Scale bars: 1 mm.

Sculpturing and texture. Clypeus and supraclypeal area with dense, coarse punctures, such punctures becoming elongate apically to give surface a wrinkled appearance (Fig. 3); paraocular area below antennal torulus with punctures similar to elongate punctures of clypeus except shallow and more spaced; frons and vertex with small, round, dense punctures separated by less than a puncture width, such punctures in ocellular area becoming sparse, integument between punctures smooth; gena with dense, elongate punctures. Mesoscutum and mesoscutellum with large, round, dense punctures separated by much less than a puncture width; metanotum with punctures similar to mesoscutellum



Figures 3–6. Facial marks variation of *Habrophorula belladeceptrix* sp. nov., female 3 holotype 4–6 paratypes. Scale bars: 1 mm.

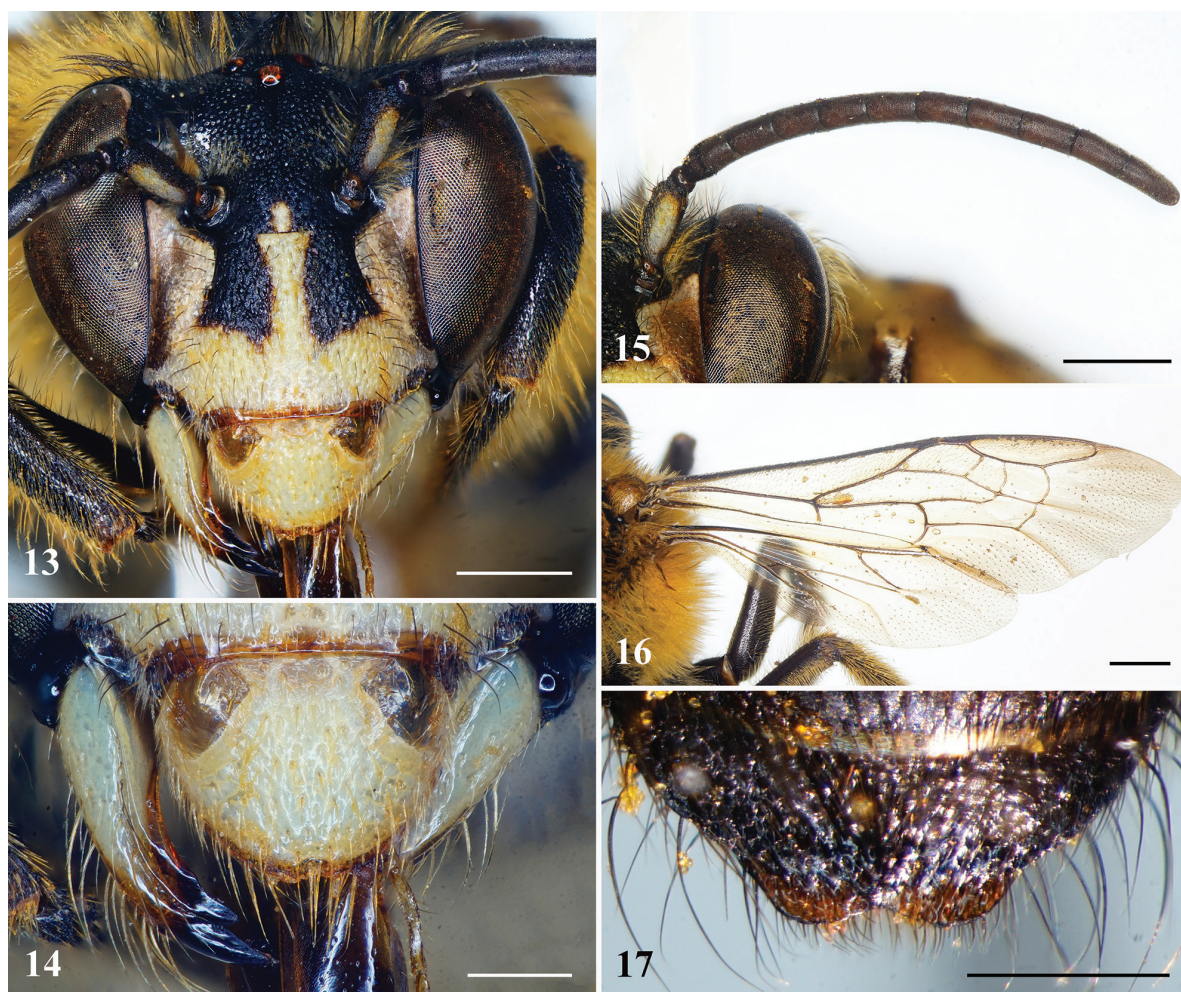


Figures 7–10. *Habrophorula belladeceptrix* sp. nov., female 7 mandible, latero-dorsal view 8 left antenna 9 left forewing 10 pygidial plate, dorsal view. Scale bars: 0.5 mm (7, 8); 1 mm (9, 10).



Figures 11, 12. *Habrophorula belladeceptrix* sp. nov., male **11** habitus, lateral view **12** habitus, dorsal view. Scale bars: 1 mm.

except smaller, such punctures becoming fainter mesally and integument more imbricate; pleura with punctures similar to mesoscutum except contiguous; basal area of propodeum wholly vertical, scarcely differentiated from posterior surface, with punctures similar to mesoscutellum on basal area and lateral and posterior surfaces. Metasomal terga with small, round, punctures separated by a puncture width, integument between smooth and matte, such punctures denser in apical marginal zones and progressively so laterally on each tergum and on more apical terga; sterna with coarser punctures than those of terga,



Figures 13–17. *Habrophorula belladeceptrix* sp. nov., male **13** head, facial view **14** labrum and mandible, dorsal view **15** left antenna. **16** right forewing **17** metasomal tergum VII, dorsal view. Scale bars: 0.5 mm (**14**, **17**); 1 mm (**13**, **15**, **16**).

separated by less than a puncture width, smaller and denser toward apical marginal zones, narrow apical margins impunctate, pregradular surfaces impunctate and imbricate.

Color. Labrum brown, except yellowish mark medially (Fig. 3); mandible with yellow mark basally, then brown to black on remainder (Fig. 7); paraocular area with yellowish marking extending along inner margin to level of antennal toruli, except black spot on upper side of clypeus; clypeus black, except inverted yellowish T-shaped mark medially and apically, and brown mark apically; supraclypeal area with small yellowish mark medially (Fig. 3). Yellowish marks of labrum, clypeus and paraocular area variety in paratypes (Figs 4–6). Remainder of integument black.

Pubescence. Clypeus with some short, yellowish setae intermixed with black setae latero-apically; paraocular area with short, yellowish setae intermixed with sparse black setae; scape with long, brownish black setae; face above antennal torulus with yellowish tuft of setae (Fig. 3); vertex with long, blackish setae; occiput with long, yellowish, dense setae. Mesosoma with long, dense, yellowish setae intermixed with blackish setae anteriorly and yellowish setae laterally (Figs 1, 2), such setae sparse to absent on disc. Coxae and trochanters with dense, yellowish setal tufts ventrally; outer surface of mesotibia and mesobasitarsus with long, yellowish-orange setae, inner surface of mesobasitarsus with short, dense,



Figures 18–21. *Habrophorula belladeceptrix* sp. nov., male terminalia **18** metasomal sternum VII **19** metasomal sternum VIII **20** genitalia, dorsal view **21** genitalia, ventral view. Scale bars: 0.5 mm.

orange setae; outer surface of metatibia and metabasitarsus with yellowish-orange scopal setae. Apical margins of metasomal T1–3 with short, yellowish setal bands, interrupted medially; T4 with short setal band apically; T5 with long, dense, orange setae (Fig. 2); T6 covered with orange setae lateral to pygidial plate (Fig. 10); S2–4 apical margins with long, sparse, yellowish-orange setae; S5 apical margin with long, dense, orange setae; S6 apically with orange setal tufts.

♂: Total body length about 10 mm, forewing length 9 mm. Head in facial view with yellowish marks as in Figs 13–15; mandible with three teeth, prominent preapical tooth and two long apical teeth (Fig. 14); antenna with scape about 2.5× as long as broad, F1 approximately 0.8× length of F2, F3–10 subequal in length, F11 longest flagellomere (Fig. 15); forewing as in Fig. 16; T7 with apical margin concave medially to form short, broad, paramedial lobes (Fig. 17). Male terminalia as in Figs 18–21.

Sculpturing as described for female (*vide supra*) except coarse punctures of sterna sparser.

Integument black except mandible largely yellow with black apex, labrum yellow with basolateral ovals of semitranslucent brown; clypeus with large, inverted-T-shaped

yellow marking; paraocular area below antennal torulus pale yellow to off-white, somewhat diaphanous; venter of scape with yellow longitudinal stripe.

Metasomal T1 basally and laterally with relatively long, yellowish-orange setae; T1–T5 apically with short, yellowish-orange to yellowish setal bands, broadly interrupted medially (Figs 11, 12).

Etymology. The specific epithet is a combination of the Latin adjectives *bellā*, meaning, “beautiful”, and *dēceptrix*, meaning, “she who deceives”.

Remarks. This species was collected exclusively from Phia Oac-Phia Den National Park, Cao Bang Province (Figs 22, 25). Females were collected from flowers of *Saurauia roxburghii* Wall. (Fig. 23) and *Saurauia napaulensis* DC. (Actinidiaceae) (Fig. 24), which are relatively common on the sides of roads. Its associated sex was recorded from flowers of *Lantana camara* L. (Verbenaceae) (Fig. 26).

Revised key to species of *Habrophorula*

The following key is expanded and revised from that presented by Wu (2000). Characteristics for the key were extracted from the original descriptions of the species (Lieftinck 1974; Wu 1991, 2000), and the examination of identified species in the Division of Entomology, University of Kansas Natural History Museum. The male of *H. rubigolabralis* and the female of *H. ferruginipes* remain unknown.

- 1 Females.....2
- Males.....5
- 2(1) Metasomal T1–4 with apical margins black; body lengths 10.5–13 mm....3
- Metasomal T1–4 with apical margins broadly reddish brown; body lengths 13–14 mm *H. nubilipennis* (Cockerell)
- 3(2) Legs black; clypeus variable, but markings never reddish brown, instead yellow4
- Legs brown; clypeus black with reddish brown inverted T-shaped mark medially and apically, apical portion long and with mountain-peak-shaped extensions on either side of middle stripe (see Wu 2000: fig. 187); body length 10.5 mm *H. rubigolabralis* Wu
- 4(3) Clypeus black with thin, yellow inverted T-shaped mark medially and apically; body length 12 mm *H. belladeceptrix* sp. nov.
- Clypeus largely yellow, with large extensions of black basolaterally and extending to about two-thirds length (see Wu 2000: fig. 186g); body lengths 12–13 mm *H. nigripes* Wu
- 5(1) Legs yellow to testaceous or reddish brown; clypeus with yellow markings; mesosoma with yellow or griseous setae6
- Legs black; clypeus with yellow or cream white markings; mesosoma covered with yellow or tawny setae; body length 10 mm7
- 6(5) Legs and tegula reddish brown, antenna reddish brown; mesosoma covered with griseous setae; body length 12 mm *H. nubilipennis* (Cockerell)
- Legs and tegula yellow, antenna dark brown; mesosoma covered with yellow setae; body length 10 mm..... *H. ferruginipes* Wu
- 7(5) Clypeus with yellow markings; mesosoma with yellow setae except more tawny on pleura and propodeum..... *H. belladeceptrix* sp. nov.
- Clypeus with cream white markings; mesosoma with yellow setae..... *H. nigripes* Wu



Figures 22–26. Habitat and floral associations of *Habrophorula belladeceptrix* sp. nov. in Vietnam **22** habitat where females were found **23** flowers of *Saurauia roxburghii* Wall. (Actinidiaceae) at which females were collecting **24** flowers of *Saurauia napaulensis* DC. (Actinidiaceae) at which females were collected **25** habitat where males were found **26** flowers of *Lantana camara* L. (Verbenaceae).

Acknowledgements

The authors are grateful to Dr Quang Hong Bui (Department of Botany, IEBR) for the identification of plant species, and to Michael Orr for an earlier review that inspired us to collect more extensively, work that ultimately revealed that the Vietnamese *Habrophorula* were representative an undescribed species.

Additional information

Conflict of interest

The authors have declared that no competing interests exist.

Ethical statement

No ethical statement was reported.


Funding


M.S.E. was supported by CONCYTEC through the PROCIENCIA program “Interinstitutional Alliances for Doctorate Programs” (contract PE501084299-2023-PROCIENCIA-BM). This work was funded by the Vietnam Academy of Science and Technology under grant number CSCL09.03/24-25.

Author contributions

All authors have contributed equally.

Author ORCIDs

Ngat Thi Tran  <https://orcid.org/0000-0002-7057-4638>

Michael S. Engel  <https://orcid.org/0000-0003-3067-077X>

Lien Thi Phuong Nguyen  <https://orcid.org/0000-0003-3527-9577>

Data availability

All of the data that support the findings of this study are available in the main text.

References

- Cockerell TDA (1930) Descriptions and records of bees – CXXIV. *Annals & Magazine of Natural History* 6(31): 48–57. <https://doi.org/10.1080/00222933008673186>
- Engel MS (2001) A monograph of the Baltic amber bees and evolution of the Apoidea (Hymenoptera). *Bulletin of the American Museum of Natural History* 259: 1–192. [https://doi.org/10.1206/0003-0090\(2001\)259<0001:AMOTBA>2.0.CO;2](https://doi.org/10.1206/0003-0090(2001)259<0001:AMOTBA>2.0.CO;2)
- Engel MS (2018) A new genus of anthophorine bees from Brunei (Hymenoptera: Apidae). *Journal of Melittology* 78(78): 1–13. <https://doi.org/10.17161/jom.v0i78.7488>
- Lieftinck MA (1974) A review of the central and east Asiatic *Habropoda* F. Smith, with *Habrophorula*, a new genus from China (Hymenoptera, Anthophoridae). *Tijdschrift voor Entomologie* 117(5): 217–224.
- Michener CD (2007) *The Bees of the World* [2nd edn.]. Johns Hopkins University Press; Baltimore, MD, [xvi + [i] +] 953 pp. [+20 pls]
- Orr MC, Branstetter MG, Straka J, Yuan F, Leijs R, Zhang D, Zhou Q, Zhu CD (2022) Phylogenomic interrogation revives an overlooked hypothesis for the early evolution of the bee family Apidae (Hymenoptera: Apoidea), with a focus on the subfamily Anthophorinae. *Insect Systematics and Diversity* 6(4): 1–15. <https://doi.org/10.1093/isd/ixac022>
- Tran NT, Engel MS, Truong LX, Nguyen LTP (2022) First occurrence of the little-known genus *Noteriades* (Hymenoptera, Megachilidae) from Vietnam: Discovery of a new species and a key to the Southeast Asian fauna. *ZooKeys* 1102: 191–200. <https://doi.org/10.3897/zookeys.1102.82466>
- Tran NT, Engel MS, Nguyen CQ, Tran DD, Nguyen LTP (2023) The bee genus *Anthidiellum* in Vietnam: Descriptions of five new species and the first male of *Anthidiellum coronum* (Hymenoptera, Megachilidae). *ZooKeys* 1144: 171–196. <https://doi.org/10.3897/zookeys.1144.98644>
- Wu YR (1991) Studies on Chinese Habropodini with descriptions of new species (Apoidea: Anthophoridae). In: Zhang G-X (Ed.) *Scientific Treatise on Systematic and Evolution Biology* [Volume 1]: 215–233. Science and Technology Press, Beijing, 239 pp. [+4 pls] [In Chinese, with English summary]
- Wu YR (2000) *Fauna Sinica. Insecta. Volume 20. Hymenoptera. Melittidae, Apidae*. Science Press, Beijing, [xiv+]442 pp. [+9 pls] [In Chinese, with English summary]